Earthquake Engineering

Challenges and Trends

HONORING

LUIS ESTEVA

Editor

J. J. Pérez-Gavilán E.

September 2006

Symposium Committee
J J Pérez-Gavilán E (coordination)
Sergio Alcocer
Mario Ordaz

Edition technical support
Maximino Reséndiz

Technical Secretariat
Ing. Javier Palomas

Promotion and linking secretariat
Lic. Maria Olvido

Earthquake Engineering Challenges and Trends
J. J. Pérez-Gavilán (Ed.)

www.iingen.unam.mx

Printed by Impresión Offset Express
Published September 2006

ISBN: 970-32-3699-5

PRINTED IN MEXICO

Dr. Luis Esteva

Luis Esteva's award

The upcoming curved plates represent the two vital aspects of Dr. Luis Esteva: human and intellectual values, respectively. The plates terminate in an ascending curve to signify that his value as human and scientist keeps on growing. Each of the seven transverse horizontal irregular plates represents ten years of his life, the irregularity meaning that life is not smooth or planar. The shaky aspects of the lamina represent an earthquake. All the structure comes out from earth.

Foreword

When a person has an enviable academic record, full of fruitful activities and of relevant contributions to a discipline, the idea to honor this person is by all means appropriate and rewarding. However, when such an individual also outstands for his/her generosity and friendship, a commemoration becomes mandatory.

In the case of Professor Luis Esteva, it was the occasion of his seventieth birthday, on January 31, 2005, the perfect time to commemorate his active and fruitful career.

In contrast, the year 2005 was also marked by the very sad memories of the people that lost their lives in and of all the damage inflicted by the 1985 Mexico earthquakes. Therefore, 20 years after was a good time for discussion and meditation of the needed actions to accelerate the reduction of seismic risk.

With both senses of joy and meditation, the Institute of Engineering at the National University of Mexico, UNAM, decided to organize a tribute symposium. To discuss about the needs and possible strategies for coping with the increase in seismic risk in the world, a selected group of long-time colleagues and friends of Luis was invited for this occasion. Distinguished researchers and practitioners in the field of earthquake engineering attended from all over the world, presenting their thoughts and state-of-the art reports on the subject.

It is the aim of this book to present the thoughtful contributions of the symposium participants. Also included are some of the papers of Luis Esteva which help to understand different topics of the discipline. The book is intended for both practicing and research specialists on earthquake engineering.

We are deeply indebted to the authors who accepted the invitation to attend the symposium, wrote thoughtful papers, presented them at the symposium,
chaired the sessions, and participated in lively discussions.

Mexico City
August, 2006

Sergio M. Alcocer
Director
Institute of Engineering
National University of Mexico,
UNAM

Preface

This book is about earthquake engineering science. It was set up with selected contributions, past and recent, of Prof. Luis Esteva and the contributions of distinguished researchers around the world.

In September 2005, long-time friends and colleagues of Luis were gathered by the Institute of Engineering at UNAM, in a symposium to honor Dr. Esteva, for his long and productive career, and for his many contributions to earthquake engineering in Mexico and the world.

The book is organized into two parts. In the first part the bibliography of Luis Esteva is compiled, including research reports, chapters in books and journal papers but not including conference papers. The bibliography is followed by the transcription of selected contributions of Luis Esteva. The collection includes two renowned general manuscripts regarding seismicity (1976) and earthquake design (1977), which are a splendid introduction to earthquake engineering. The rest of Luis Esteva's contributions cover a wide spectrum of themes spreading in time from 1989 up to 2002. The second part of the book includes the contributions of some of the most distinguished researchers in earthquake engineering around the world, all colleagues and friends, some former students of Luis Esteva , which together give and exceptional view of earthquake engineering state of the art. Each contribution is preceded by some words of the author that relates him to Luis Esteva, as colleague, friend or teacher. These contributions give a clear picture of the relevance of Luis Esteva as a scientist but also as a human being.

We give many thanks to all authors for the excellent quality of their contributions and for their enthusiasm in coming to México to honor Luis Esteva. Special thanks to Prof. Tom Paulay and Prof. Rodolfo Saragoni, whom although could not come to México for the symposium, sent their contributions with the most kind regrets for missing the event.

México City,
August 2006

Juan José Pérez Gavilán E.
Applied Mechanics
Institute of Engineering, CU,
National Autonomous University of México

CONTENTS

Part1: Selected contributions of Luis Esteva

Part2: Invited contributions

Part 1

Selected contributions of LUIS ESTEVA

BIBLIOGRAPHY

Journal papers

1 "A semi-empirical model for site effects on realistic acceleration time-histories at soft soil sites, Part 1: formulation and development", with A. Bárcena; *Earthquake Engineering and Structural Dynamics*, 33, 11 (2004) 1165-1186.

2 "Comparing the adequacy of alternative ground motion intensity measures for the estimation of structural responses", with P. Giovenale and C. A. Cornell, *Earthquake Engineering and Structural Dynamics*, 8, 10 (2004) 951-979.

3 "Optimal maintenance strategies for structures in seismic zones", with R. Montes and E. Heredia; *Earthquake Engineering and Structural Dynamics*, 32 (2003) 245-264.

4 "Life-cycle optimization in the establishment of performance-acceptance parameters for seismic design", with O. Díaz-López, J. García-Pérez, G. Sierra and E. Ismael, Proc.ICOSSAR 2001, Newport Beach, California (2001); an enhanced version was published in *Structural Safety*, 24 (2002) 187- 204 (special volume).

5 "Simulating earthquake ground motion at a site, for given intensity and uncertain source location", with J. Alamilla, J. García and O. Díaz, *Journal of Seismology*, 5 (2001) 475-485.

6 "Evolutionary properties of stochastic models of earthquake ground motion: their dependence on magnitude and distance", with J. Alamilla, J. García and O. Díaz, *Journal of Seismology*, 5 (2001) 1-21.

7 "Reliability functions for earthquake resistant design", with O. Díaz-López and J. García-Pérez, to be published in Reliability Oriented Structural Design, special issue of *Reliability Engineering and Systems Safety*, 73 (2001) 239-262.

8 "Performance-based earthquake resistant design: trends and challenges" (in Spanish) *Ingeniería Sísmica*, 63 (2000) 31-54.

9 "Theoretical models and recorded response in the estimation of cumulative seismic damage on nonlinear structures", with E. Heredia and E. Zevallos, *Earthquake Engineering and Structural Dynamics*, 29, 12 (2000) 1779-1796.

10 "Life-cycle optimization and practical considerations for earthquake resistant design of structures with energy-dissipating devices", with L. Veras and V. Díaz, Proc. Asia Pacific Workshop on Earthquake Resistant Design and Structural Retrofitting (Taipei, 1998). Published also in *Earthquake Engineering and Engineering Seismology*, 1, 1 (1999) 13-26.

11 "Accounting for source location errors in the analysis of seismicity and seismic hazard", with O. Díaz, J. García and S. K. Singh, *Journal of Seismology*, 3 (1999) 153-166.

12 "Optimal instrumentation of structural systems on flexible base for system identification", with E. Heredia and R. Montes, *Earthquake Engineering and Structural Dynamics*, 28, 12 (1999) 1471-1482.

13 "Stochastic seismic performance evaluation of tuned liquid column dampers", discussion to an article by A. Y. J. Won, J. A. Pires and M. A. Haroun, with S. E. Ruiz, *Earthquake Engineering and Structural Dynamics*, 26, 8 (1997) 875-876.

14 "Cumulative damage functions in seismic safety decisions", with O. Díaz, in special volume *Safety and Reliability of Structural Systems*, Elsevier (1996)

15 "Seismic hazard and seismic design response spectra for Mexico" (in Spanish), with M. Ordaz, *Revista del Colegio de Ingenieros Civiles de México* (1995)

16 “Seismic ductility demands predicted by alternate models of building frames”, with O. Díaz and E. Mendoza, *Earthquake Spectra*, 10, 3 (1994), 465-488
17 “Seismic nonlinear response of building models” (in Spanish), *Ingeniería Sísmica*, 46
18 “Seismic ductility demands predicted by alternate models of building frames”, with O. Díaz and E. Mendoza, *Earthquake Spectra* (1993) (January-April 1994), 1-22, Mexico
19 “Comparison of simplified and detailed models to estimate the reliability of structures subjected to earthquakes”, with O. Díaz (in Spanish), *Sismodinámica*, 3, 15-38 (1992)
20 “Nonlinear seismic response of soft-first-story buildings subjected to narrow-band accelerograms”, *Earthquake Spectra*, 8, 3 (1992). Published also in Spanish as Report 544 of the Institute of Engineering, National
21 “Nonlinear seismic response of different models of buildings”, with O. Díaz and E. Mendoza (in Spanish), submitted for publication in the *Journal of the Mexican Society for Earthquake Engineering* (1992)
22 “In-situ determination of soil damping in the lake deposit area of Mexico City, with J. C. S. Yang, G. Z. Qi, V. Pavlin and A. Durelli, *Soil Dynamic and Earthquake Engineering*, 8, 1, 43-52 (1989)
23 “Probabilistic analysis of earthquake damage risk in constructions in Mexico”, in Catastrophes and Society, special volume, *MAPFRE Foundation*, Madrid (1989)
24 “Seismic failure rates of multi-story frames”, with S. E. Ruiz, *Journal of the Structural Division, ASCE*, 115, 2 (1989)
25 “The Mexico earthquakes of September 1985: consequences, lessons and impact on research and practice”, *Earthquake Spectra*, 4, 3 (1988)
26 “Earthquake engineering research and practice in Mexico after the 1985 earthquakes”, *Bull. New Zealand National Society for Earthquake Engineering*, 20, 3 (1987)
27 “Empirical Bayes estimation of seismicity parameters”, with A.M. Hasofer, *Structural Safety* 2, 3 (Jan. 1985)
28 “Statics of small earthquakes and frequency of large earthquakes along the Mexican subduction zone”, with S. K. Sing and M. Rodríguez, *Bull. Seism. Soc. A.*, 73, 1979-1996 (1983)
29 “Influence on the seismic response of a bridge of the phase differences in the motion of its supports”, with S. E. Ruiz and D. de León, *Rev. Soc. Mex. de Ing. Sísmica*, 24 (Aug. 1981)
30 “Expected Earthquake Magnitude from a Fault”, with E. Bazán and S. Singh, *Bull. Seism. Soc. of America*, 70, 3, (Jun. 1980)
31 “Ductility and seismic design”, *Bol. Soc. Mex. de Ing. Sísmica*, 16 (1976)
32 “Amplification of Rayleigh waves”, with S. E. Ruiz, *Bol. Soc. Mex. de Ing. Sísmica*, 16 (1976)
33 “Bonus and penalty in acceptance criteria for concrete”, with E. Rosenblueth and J. Damy, *Journal American Concrete Institute*, 71, 9, 466-472 (1974)
34 “Seismic hazard in the balsas river basin”, with J. L. Trigos, *Rev. Soc. Mex. de Ing. Sísmica*, 8 (Sep. 1972)
35 “Reliability basis of some Mexican codes”, with E. Rosenblueth, *ACI Special Publication*, 31 1-41 (1972)
36 “Test of structural models of the Palace of Sports”, with R. Meli and A. Olivares, *Ingeniería*, (Oct. 1968)

37 Discussion of “Analysis of tall building frames by distribution of deformations”, *Rev. Soc. Mex. de Ing. Sísmica* (1966)

38 “The Lima Earthquake of 17 October, 1966”, with J. A. Nieto, *Rev. Soc. Mex. de Ing. Sísmica*, 4, 2 (1966)

39 “Research in the solution of the housing problem”, Rev. Mex. de Construcción (Nov. 1965)

40 Spectra of earthquakes at long and moderate distances”, with E. Rosenblueth, Primeras Jornadas Chilenas de Sismología e Ingeniería Antisísmica (Jul. 1963), *Bol. Soc. Mex. de Ing. Sísmica*, 2 (Mar. 1964)

41 “Elastic Analysis of buildings with slender shear walls”, Primeras Jornadas Chilenas de Sismología e Ingeniería Antisísmica, Santiago de Chile (Jul. 1963), *Bol. Soc. Mexicana de Ing. Sísmica*, 2, 1 (Dec. 1964)

42 “Transient response of elastic systems to out of phase disturbances”, with E. Rosenblueth and O. A. Rascón, *Bol. Soc. Mex. de Ing. Sísmica*, 2 (Mar. 1964)

43 “Seismic Zoning of Mexico”, *Bol. Soc. Mex. de Ing. Sísmica*, 1 (Jul. 1963)

44 “Coefficients for design of slabs with free edges”, *Ingeniería* (Jul. 1963)

45 “Assessment of probable damage caused by earthquakes on structures”, *Bol. Soc. Mex. de Ing. Sísmica*, 1, 1 (Jul. 1963)

46 “The Acapulco earthquake of May 1962), Primeras Jornadas Chilenas de Sismología e Ingeniería Antisísmica, Santiago de Chile (Jul. 1963). *Bol. Soc. Mex. de Ing. Sísmica*, 1, 2

Research reports

1 “A Methodological Guideline for the Formulation of a Risk Atlas” (in Spanish), coauthor and editor, *CENAPRED: National Center for Disaster Prevention*, Mexico City (2003).

2 “Evaluation of seismic safety of earth dams of the National Water Commission, with V. Taboada, M. Romo, J. Alamilla, J. García and O. Díaz (in Spanish), Report *Institute of Engineering, UNAM*, to National Water Commission (1997)

3 “Mechanics of Structures”, General Report, Proc. of Seventh International Conference on Applications of Statistics and Probability in Civil Engineering, International Association for Civil Engineering Reliability and Risk Analysis (Paris, 1995)

4 “Seismic hazard at the construction site of “La Parota Hydroelectric Plant”, with O Díaz, J García and S K Singh (in Spanish), Report *Institute of Engineering, UNAM* to the Federal Commission of Electricity, Mexico (1995)

5 “Preliminary evaluation of the seismic safety of six dams of the Federal Commission for Electricity”. With M. Ordaz and M. P. Romo (in Spanish), *Institute of Engineering, UNAM* (1993)

6 “Comments about the expected costs of damage in Mexico City, due to the occurrence of a large earthquake in the Guerrero gap”, with M. Ordaz and O. Díaz (in Spanish), *Institute of Engineering, UNAM* (1993)

7 “Maximum expected losses due to earthquake in Mexico City”, with O. Díaz and M. Ordaz (in Spanish), *Institute of Engineering, UNAM* (1993)

8 “Expected costs of damage in Mexico City, produced by a large subduction earthquake along the coast of Guerrero”, with M. Ordaz and O. Díaz (in Spanish), *Institute of Engineering, UNAM* (1992)

9 Dynamic response of nonlinear soft-story shear buildings subjected to the SCT accelerogram of the Mexico earthquake of 19 September 1985”, with E. Blasco, Special publication 89.02, *Earthquake Engineering Research Institute*, El Cerrito, California (1989)

10 “Influence of soil-structure interaction on the nonlinear seismic response of buildings”, with E. Mendoza, Research report to the *Technical Committee on Structural Safety of the Federal District*, Mexico, (in Spanish, 1989)

11 “Comparison of seismic non-linear responses of frame and shear-beam systems”, with O. Díaz, E. Mendoza and O. Flores, *Institute of Engineering, UNAM* (May, 1989)

12 “Revision of insurance rates for earthquake damage”, with O. Díaz and A. Terán, Report *Institute of Engineering, UNAM* to the Mexican Association of Research Institutions (in Spanish, 1988)

13 “Development of a predictive model for the transport and deposit of volcanic ashes in the valley of Mexico”, with J. L. Sánchez and O. Fuentes, *Institute of Engineering, UNAM*, Report 525 (1988)

14 “Analysis of seismic response of school buildings reinforced with bracing cables”, with E. Lira, *Institute of Engineering*, *UNAM* to CAPFCE (1988)

15 “Evaluation of probable damage cost caused by earthquakes on structures”, with O. Díaz, J. García and A. Terán, Report *Institute of Engineering, UNAM* to Mexican Association of Insurance Institutions (1988)

16 “Seismic hazard at Zimapán, Hidalgo”, with J. García Report *Institute of Engineering, UNAM* to Federal Commission of Electricity (1987)

17 “Seismic hazard at Zimapán, Hidalgo”, with J. García Report *Institute of Engineering, UNAM* to Federal Commission of Electricity (1987)

18 “Seismic hazard in Lázaro Cárdenas”, with S. E. Ruiz, R- Paredes and E. Mendoza, Report Institute of Engineering, UNAM to Federal Commission of Electricity (1987)

19 “Revision of seismic safety of railway-bridges. Out-of-phase ground motion”, Institute of Engineering to Secretariat of Communication and Transportation, (1984)

20 “Seismicity and seismic hazard at several sites along the Santiago River”, with M. Chavez, H. Galviz and J. Road, Institute of Engineering, UNAM (1984)

21 “On research and practice in structural engineering in Mexico”, Meeting on National Priorities and Scientific, Technical and Cultural Dependence of Mexico, National University of Mexico (Aug. 1982)

22 “Preliminary design spectra including the influence of local conditions for Lázaro Cárdenas and Laguna del Ostión”, with M. Chávez (Feb. 1982)

23 “Seismicity and seismic risk for Lázaro Cárdenas industrial harbor”, with M. Chavez and D. de León, Institute of Engineering, UNAM (1981)

24 “Seismicity and seismic hazard studies for Laguna del Ostión Industrial harbor”, with M. Chávez and D. de León, Institute of Engineering, UNAM (1981)

25 “Seismic design recommendations for Cerro Prieto thermo-electric plant”, with M. Chávez and D. de Léon, Institute of Engineering, UNAM (1981)

26 “Basic concepts for seismic codes”, document proposed to an ad hoc committee of the International Association for Earthquake Engineering and approved for publication by the latter (1981)

27 “Influence on the seismic response of the bridge Coatzacoalcos II of the pahse differences in the motion of its supports, Second part: Influence of nonlinear response”. With D. De León, Institute of Engineering, UNAM (1981)
28 “Reliability Analysis of offshore structures”, Institute of Engineering, UNAM (Jan. 1981)
29 “System reliability analysis for static lateral loads”, with C. Ferregut, F. Téllez and M. Chávez, Institute of Engineering, UNAM (Jan. 1981)
30 “Reliability of structures subjected to fluctuating loads”, with M. Chávez and F. Téllez, Institute of Engineering, UNAM (Jan. 1981)
31 “Reliability analysis of pile foundations subjected to static lateral loads”, Institute of Engineering, UNAM (Jan. 1981)
32 “Probabilistic analysis of the seismic response of multi-support structures on soft ground”, with S. E. Ruiz, Report 432, Institute of Engineering, UNAM (1980)
33 “Probable seismic response of multi-support structures subjected to non-stationary out of phase random excitation”, with S. E. Ruiz, Institute of Engineering, UNAM (1980)
34 “Preliminary studies for the optimum seismic design of the curtain of El Caracol dam”, with A. Reyes and G. López, Institute of Engineering, UNAM (1979)
35 “Analysis of seismic hazard with incomplete information. Application to hydroelectric project of San Roque, Filipinas”, with R. Guerra, Institute of Engineering, UNAM (1979)
36 “Seismic response of large, extended structures”, with C. Ramos, Institute of Engineering, UNAM (1979)
37 “Probabilistic analysis of the seismic response of long bridges on soft soils”, with S. E. Ruiz, Institute of Engineering, UNAM (1979)
38 “Seismic design spectra in Paraíso, Tab., and Ciudad del Carmen, Campeche”, with R. Guerra, Report to Proyectos Marinos (1978)
39 “Seismic design spectra for Paraíso, Tab. and Ciudad del Carmen, Camp.”, with R-Guerra Institute of Engineering, UNAM (Jan. 1978)
40 “Amlification of Rayleigh waves for different topographies”, with H. Cuadros and S. E. Ruiz, Institute of Engineering, UNAM (Mar. 1978)
41 “Effect of topography on ground motion produced by plane P and S V waves”, with S. E. Ruiz, Institute of Engineering, UNAM (Mar. 1978)
42 “Seismic hazard in El Caracol”, with E. Bazán, Institute of Engineering, UNAM (Mar. 1978)
43 “Analysis of continuous foundations on soft ground, Incremental methods”, with J. Damy and R. Guerra, Institute of Engineering (Sep. 1977)
44 “Successive approximations for the analysis of continuous foundations on soft soil”, with R. Guerra and I. Barrandas, Institute of Engineering, UNAM (Sep. 1977)
45 “Estimation of the maximum probable damage produced by a seismic event in Mexico”, with R. Guerra, Institute of Engineering, UNAM (1976)
46 “Probable costs of damage caused by earthquakes in constructions”, with R. Villaverde, Report of Institute of Engineering, UNAM (1974)
47 “Seismic response of earth and rockfill dams”, with V. Porras and R. Cervantes, Report Institute of Engineering, UNAM to Federal Commission of Electricity (Jan. 1974)

48 "Seismic hazard in Managua", with J. L. Trigos, Technical studies carried out for the Government of Nicaragua under sponsorship of the Mexican Ministry of Public Works (Aug. 1973)
49 "Seismic hazard in El Sumidero, Chiapas", with J. L. Trigos, Report of Institute of Engineering, UNAM to Federal Commission of Electricity (Aug. 1973)
50 "Seismic hazard in Las Truchas, Michoacán", with J. L. Trigos, Report of Institute of Engineering, UNAM to SICARTSA (Aug. 1973)
51 "Seismic hazard in Punta Limón, Veracruz", with J. L. Trigos, Report of Institute of Engineering, UNAM to Federal Commission of Electricity (Jan. 1973)
52 "Planning and design of tall buildings", Structural Safety, Summary Report, Technical Committee No. 10 Structural Safety and Probability Methods, ASCE-IABSE Joint Committee on Planning and Design of Tall Buildings, Lehigh University, Bethlehem, Pa. (1972)
53 "Seismic hazard on stratified formations", with R. Cervantes and A. Alducin, Report of Institute of Engineering, UNAM to Federal Commission of Electricity (Oct. 1972)
54 "Seismic risk study for Las Piedras dam", with R. Cervantes, Report of Institute of Engineering, UNAM to Secretaría de Recursos Hidráulicos (Jul. 1972)
55 "Design of foundation on soft ground, Numerical methods and design aids", with A. Flores, Institute of Engineering, UNAM (1970)
56 "Practical consideration on bayesian assessment of seismic risk", Report 248, Institute of Engineering, UNAM (1969)
57 "Seismic Zoning of Mexico for Engineering Purposes", Report 246, Institute of Engineering, UNAM (1969)
58 "Reliability analysis of Tepuxtepec dam under the action of earthquakes", with J. Elorduy and J. Salvador, Institute of Engineering, UNAM (1969)
59 "Effects of wind forces on flexible bridges. Studies on models of Metlac and Fernando Espinoza bridges", Report 206, Institute of Engineering, UNAM (Jan. 1969)
60 "Analysis and design of foundations on soft soil", with A. Flores and F. Téllez, Institute of Engineering, UNAM (Oct. 1968)
61 "Criteria for the Construction of Seismic Design Spectra", Report 198, Institute of Engineering, UNAM (Oct. 1968)
62 "Bases for the formulation of seismic design decisions", Report 182, Institute of Engineering, UNAM (Aug. 1968)
63 "The Caracas earthquake of July 29, 1967", Institute of Engineering, UNAM (Apr. 1968)
64 "Design for earthquake and wind", Recommendations for the Design and Construction of Civil Works"; Institute of Engineering, UNAM to Federal Commission of Electricity (1967)
65 "Response of elastic systems to transient disturbances out of phase", with E. Rosenblueth, Institute of Engineering, UNAM (1963)
66 "Analysis of tall buildings under lateral forces", Report for Committee 442, Lateral Loads, of American Concrete Institute (1963)
67 "Considerations on earthquake resistant design of earth and rockfill dams", with E. Rosenblueth and R. Sánchez Trejo, Institute of Engineering, UNAM (Apr. 1961)

Chapters in books

1 "Earthquake resistant design at the end of the twentieth century: recent experiences and immediate challenges", Introductory chapter to the special volume Earthquake resistant design: regulations and criteria used in Venezuela (in Spanish), Academy of Physical, Mathematical and Natural Sciences of Venezuela (Caracas, 1997)

2 "Seismic hazard and earthquake engineering in Mexico", Chapter in the special volume “”Towards the third millenium" (in Spanish), Colegio Nacional, Mexico (1995)

3 "Seismicity", chapter 6 of the book Risk and Engineering Decisions, edited by C. Lomnitz and E. Rosenblueth , Elsevier, Amsterdam (1976)

4 "Design: general", Chap. 3 of the book , Chap 3 of the book Earthquake Resistant Design, Edited by E. Rosenblueth, Pentech Press, London (1977)

SEISMICITY[1]

1. On seismicity models

Rational formulation of engineering decisions in seismic areas requires quantitative descriptions of seismicity. These descriptions should conform with their intended applications: in some instances, simultaneous intensities during each earthquake have to be predicted at several locations, while in others it suffices to make independent evaluations of the probable effects of earthquakes at each of those locations.

The second model is adequate for the selection of design parameters of individual components of a regional system (the structures in a region or country) when no significant interaction exists between response or damage of several such individual components, or between any of them and the system as a whole. In other words, it applies when the damage -or negative utility- inflicted upon the system by an earthquake can be taken simply as the addition of the losses in the individual components.

The linearity between monetary values and utilities implied in the second model is not always applicable. Such is the case, for instance, when a significant portion of the national wealth or of the production system is concentrated in a relatively narrow area, or when failure of life-line components may disrupt emergency and relief actions just after an earthquake. Evaluation of risk for the whole regional system has then to be based on seismicity models of the first type, that is, models that predict simultaneous intensities at several locations during each event; for the purpose of decision making, nonlinearity between monetary values and utilities can be accounted for by means of adequate scale transformations. These models are also of interest to insurance companies, when the probability distribution of the maximum loss in a given region during a given time interval is to be estimated.

Whatever the category to which a seismic risk problem belongs, it requires the prediction of probability distributions of certain ground motion characteristics (such as peak ground acceleration or velocity, spectral density, response or Fourier spectra, duration) at a given site during a single shock or of maximum values of some of those characteristics in earthquakes occurring during given time intervals. When the reference interval tends to infinity, the probability distribution of the maximum value of a given characteristic approaches that of its maximum *possible* value. Because different systems or subsystems are sensitive to different ground motion characteristics, the term *intensity characteristic* will be used throughout this chapter to mean a particular parameter or set of parameters of an earthquake motion, in terms of which the response is to be predicted. Thus, when dealing with the failure probability of a structure, intensity can be alternatively measured —with different degrees of correlation with structural response— by the ordinate of the response spectrum for the corresponding period and damping, the peak ground acceleration, or the peak ground velocity.

In general, local instrumental information does not suffice for estimating the probability distributions of maximum intensity characteristics, and use has to be made of data on subjective measures of intensities of past earthquakes, of models of *local seismicity,* and of expressions relating characteristics with magnitude and site-to-source distance. Models of local seismicity consist, at least, of expressions relating magnitudes

---

[1] First published as Chapter 6 in Seismic Risk and Engineering Decisions, Eds. C. Lomnitz and E. Rosenblueth, *Elsevier*, Amsterdam (1976)

of earthquakes generated in given volumes of the earth's crust with their return periods. More often than not, a more detailed description of local seismicity is required, including estimates of the maximum magnitude that can be generated in these volumes, as well as probabilistic (stochastic process) models of the possible histories of seismic events (defined by magnitudes and coordinates).

This chapter deals with the various steps to be followed in the evaluation of seismic risk at sites where information other than direct instrumental records of intensities has to be used: identifying potential sources of activity near the site, formulating mathematical models of local seismicity for each source, obtaining the contribution of each source to seismic risk at the site and adding up contributions of the various sources and combining information obtained from local seismicity of sources near the site with data on instrumental or subjective intensities observed at the site.

The foregoing steps consider use of information stemming from sources of different nature. Quantitative values derived there from are ordinarily tied to wide uncertainty margins. Hence they demand probabilistic evaluation, even though they cannot always be interpreted in terms of relative frequencies of outcomes of given experiments. Thus, geologists talk of the maximum magnitude that can be generated in a given area, assessed by looking at the dimensions of the geological accidents and by extrapolating the observations of other regions which available evidence allows to brand as similar to the one of interest; the estimates produced are obviously uncertain, and the degree of uncertainty should be expressed together with the most probable value. Following nearly parallel lines, some geophysicists estimate the energy that can be liberated by a single shock in a given area by making quantitative assumptions about source dimensions, dislocation amplitude and stress drop, consistent with tectonic models of the region and, again, with comparisons with areas of similar tectonic characteristics.

Uncertainties attached to estimates of the type just described are in general extremely large: some studies relating fault rupture area, stress drop, and magnitude (Brune, 1968) show that, considering not unusually high stress drops, it does not take very large source dimensions to get magnitudes 8.0 and greater, and those studies are practically restricted to the simplest types of fault displacement. It is not clear, therefore, that realistic bounds can always be assigned to potential magnitudes in given areas or that, when this is feasible, those bounds are sufficiently low, so that designing structures to withstand the corresponding intensities is economically sound, particularly when occurrence of those intensities is not very likely in the near future. Because uncertainties in maximum feasible magnitudes and in other parameters defining magnitude-recurrence laws can be as significant as their mean values when trying to make rational seismic design decisions, those uncertainties have to be explicitly recognized and accounted for by means of adequate probabilistic criteria. A corollary is that geophysical based estimates of seismicity parameters should be accompanied with corresponding uncertainty measures.

Seismic risk estimates are often based only on statistical information (observed magnitudes and hypocentral coordinates). When this is done, a wealth of relevant geophysical information is neglected, while the probabilistic prediction of the future is made to rely on a sample that is often small and of little value, particularly if the sampling period is short as compared with the desirable return period of the events capable of severely damaging a given system.

The criterion advocated here intends to unify the foregoing approaches and rationally to assimilate the corresponding pieces of information. Its philosophy consists in using the geological, geophysical, and all other available non-statistical evidence for producing a set of alternate assumptions concerning a mathematical (stochastic process) model of seismicity in a given source area. An initial probability distribution is assigned to the set of hypotheses, and the statistical information is then used to improve that probability assignment. The criterion is based on application of *Bayes theorem,* also called the *theorem of the probabilities of hypotheses.* Since estimates of risk depend largely on conceptual models of the geophysical processes involved, and these are known with different degrees of uncertainty in different zones of the earth's crust, those estimates will be derived from stochastic process models with uncertain forms or parameters. The degree to which these uncertainties can be reduced depends on the limitations of the state of the art of geophysical sciences and on the effort that can be put into compilation and interpretation of geophysical and statistical information. This is an economical problem that should be handled, formally or informally, by the criteria of decision making under uncertainty.

2. Intensity attenuation

Available criteria for the evaluation of the contribution of potential seismic sources to the risk at a site make use of *intensity attenuation* expressions that relate intensity characteristics with magnitude and distance from site to source. Depending on the application envisaged, the intensity characteristic to be predicted can be expressed in a number of manners, ranging from a subjective index, such as the *Modified Mercalli intensity,* to a combination of one or more quantitative measures of ground shaking (see Chapter 1).

A number of expressions for attenuation of various intensity characteristics with distance have been developed, but there is little agreement among most of them (Ambraseys, 1973). This is due in part to discrepancies in the definitions of some parameters, in the ranges of values analyzed, in the actual wave propagation properties of the geological formations lying between source and site, in the dominating shock mechanisms, and in the forms of the analytical expressions adopted a priori.

Most intensity-attenuation studies concern the prediction of earthquake characteristics on rock or firm ground, and assume that these characteristics, properly modified in terms of frequency-dependent soil amplification factors, should constitute the basis for estimating their counterparts on soft ground. Observations about the influence of soil properties on earthquake damage support the assumption of a strong correlation between types of local ground and. intensity in a given shock. Attempts to analytically predict the characteristics of motions on soil given those on firm ground or on bedrock have not been too successful, however (Crouse, 1973; Hudson and Udwadia, 1973; Salt, 1974), with the exception of some peculiar cases, like Mexico City (Herrera et al., 1965), where local conditions favor the fulfillment of the assumptions implied by usual analytical models. The following paragraphs concentrate on prediction on intensities on firm ground; the influence of local soil is discussed in Chapter 4.

2.1 Intensity attenuation on firm ground

When isoseismals (lines joining sites showing equal intensity) of a given shock are based only on intensities observed on homogeneous ground conditions, such as *firm ground* (compact soils) or bedrock, they are roughly elliptical and the orientations of the corresponding axes are often correlated with local or regional geological trends (Figs. 1-3). In some regions -for instance near major faults in the western United States- those trends are well defined and the correlations are clear enough as to permit prediction of intensity in the near and far fields in terms of magnitude and distance to the generating fault or to the centroid of the energy liberating volume. In other regions, such as the eastern United States and most of Mexico, isoseismals seem to elongate systematically in a direction that is a function of the epicentral coordinates (Bollinger, 1973; Figueroa, 1963). In that case, intensity should be expressed as a function of magnitude and coordinates of source and site. For most areas in the world, intensity has to be predicted in terms of simple -and cruder- expressions that depend only on magnitude and distance from site to instrumental hypocenter. This stems from inadequate knowledge of geotectonic conditions and from limited information concerning the volume where energy is liberated in each shock.

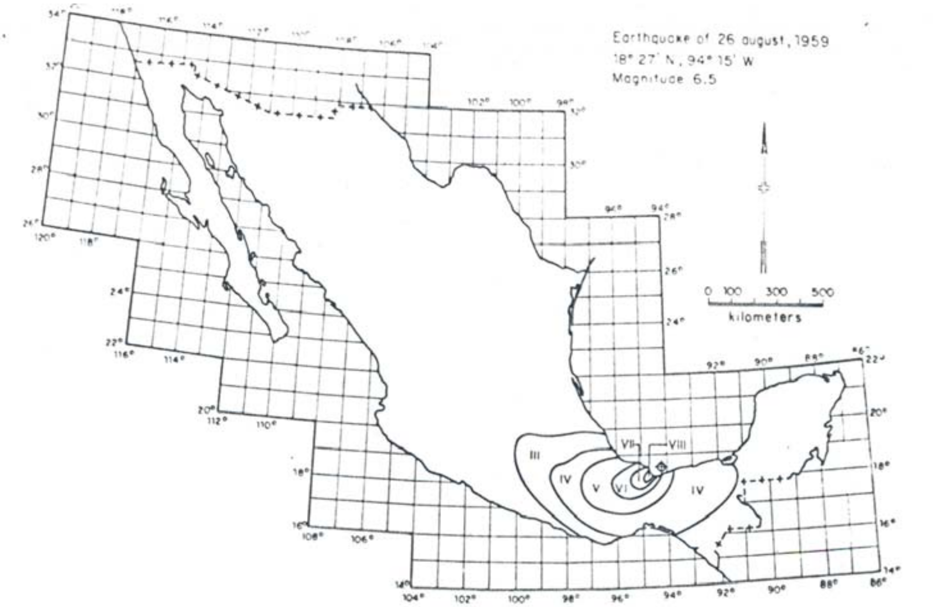

Figure 1. Isoseismals of an earthquake in Mexico. (After Figueroa, 1963)

A comparison of the rates of attenuation of intensities on firm ground for shocks on western and eastern North America has disclosed systematic differences between those rates (Milne and Davenport, 1969). This is the source of a basic, but often unavoidable, weakness of most intensity-attenuation expressions, because they are based on heterogeneous data, recorded in different zones, and the very nature of their applications implies that the less is known about possible systematic deviations in a given zone, as a consequence of the meagerness of local information, the greater weight is given to predictions with respect to observations.

2.1.1 Modified Mercalli intensities

An analysis of the Modified Mercalli intensities on firm ground reported for earthquakes occurring in Mexico in the last few decades leads to the following expression relating magnitude M, hypocentral distance R (in kilometers) and intensity I (Esteva, 1968):

$$I = 1.45M - 5.7\log_{10} R + 7.9 \tag{1}$$

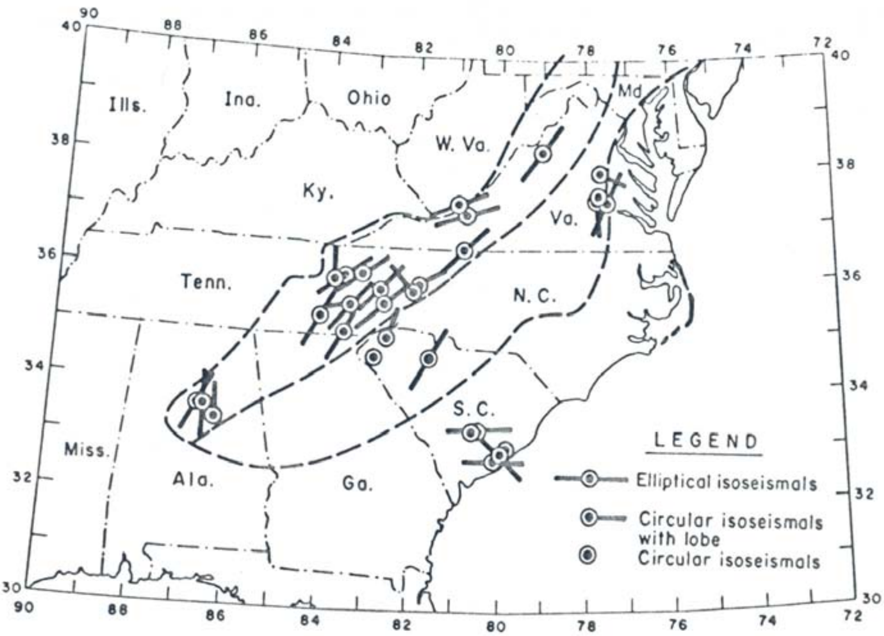

Figure 2. Elongation of isoseismals in the southeastern United States. (After Bollinger, 1973)

The prediction error, defined as the difference between observed and computed intensity, is roughly normally distributed, with a standard deviation of 2.04, which means that there is a probability of 60 % that an observed intensity is more than one degree greater or smaller than its predicted value.

2.1.2 Peak ground accelerations and velocities

A few of the available expressions will be described. Their comparison will show how cautiously a designer intending to use them should proceed.

Housner studied the attenuation of peak ground accelerations in several regions of the United States and presented his results graphically (1969) in terms of fault length (in turn a function of magnitude), shapes of isoseismals and areas experiencing intensities greater than given values (Fig. 4 and 5).

He showed that intensities attenuate faster with distance on the west coast than in the rest of the country. This comparison is in agreement with Milne and Davenport (1969), who performed a similar analysis for Canada. From observations of strong earthquakes in California and in British Columbia, they developed the following expression for *a*, the peak ground acceleration, as a fraction of gravity:

$$a/g = 0.0069\,\mathrm{e}^{1.6M} / (1.1\mathrm{e}^{1.1M} + R^2) \qquad (2)$$

Here, *R* is epicentral distance in kilometers. The acceleration varies roughly as $\mathrm{e}^{1.64M} R^{-2}$ for large *R*, and as $\mathrm{e}^{O.54M}$ where *R* approaches zero. This reflects to some extent the fact that energy is released not at *a* single point but from a finite volume. A later study by Davenport (1972) led him to propose the expression:

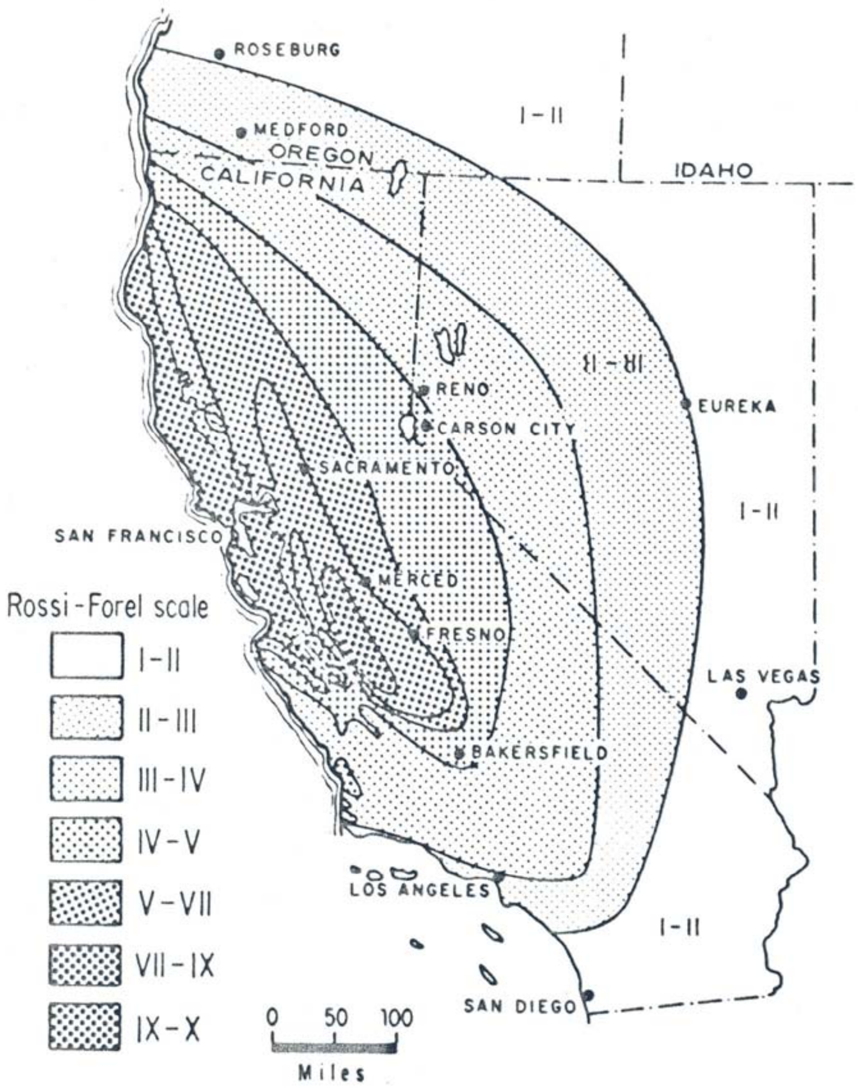

Figure 3. Isoseismals in California. (After Bolt, 1970)

$$a/g = 0.279\,\mathrm{e}^{0.8M} \;/\; R^{1.64} \tag{3}$$

The statistical error of this equation was studied by fitting a lognormal probability distribution to the ratios of observed to computed accelerations. A standard deviation of 0.74 was found in the natural logarithms of those ratios.

Esteva and Villaverde (1973), on the basis of accelerations reported by Hudson (1971, 1972a,b), derived expressions for peak ground accelerations and velocities, as follows:

$$a/g = 5.7\,\mathrm{e}^{0.8M} \;/(R+40)^2 \tag{4}$$

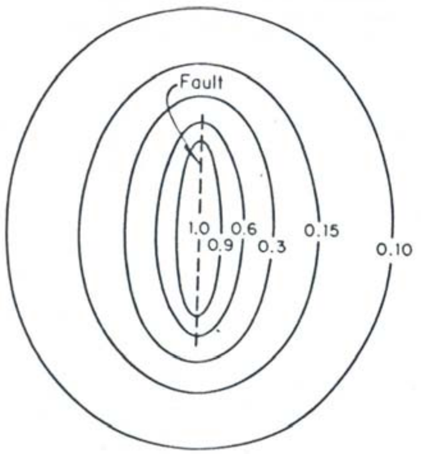

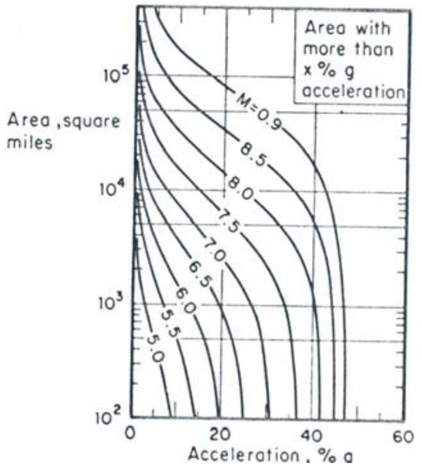

Figure 4. Idealized contour lines of intensity of ground shaking. (After Housner, 1969)

Figure 5. Area in square miles experiencing shaking of x *%* g *or greater for shocks of different magnitudes*. (After Housner, 1969.)

$$v = 32\,\mathrm{e}^{M}\ /(R+25)^{1.7} \qquad (5)$$

Here v is peak ground velocity in cm/sec and the other symbols mean the same as above. The standard deviation of the natural logarithm of the ratio of observed to predicted intensity is 0.64 for accelerations and 0.74 for velocities. If judged by this parameter, eqs. 3 and 4 seem equally reliable. However, as shown by Fig. 6, their mean values differ significantly in some ranges.

With the exception of eq. 2, all the foregoing attenuation expressions are products of a function of R and a function of M. This form, which is acceptable when the dimensions of the energy-liberating source are small compared with R, is inadequate when dealing with earthquake sources whose dimensions are of the order of moderate hypocentral distances, and often greater than them. Although equation errors (probability distributions of the ratio of observed to predicted intensities) have been evaluated by Davenport (1972) and Esteva and Villaverde (1973), their dependence on M and R has not been analyzed. Because seismic risk estimates are very sensitive to the attenuation expressions in the range of large magnitudes and short distances, more detailed studies should be undertaken, aiming at improving those expressions in the mentioned range, and at evaluating the influence of M and R on equation error. Information on strong-motion records will probably be scanty for those studies, and hence they will have to be largely based on analytical or physical models of the generation and propagation of seismic waves. Although significant progress has been lately attained in this direction (Trifunac, 1973) the results from such models have hardly influenced the practice of seismic risk estimation because they have remained either unknown to or imperfectly appreciated by engineers in charge of the corresponding decisions.

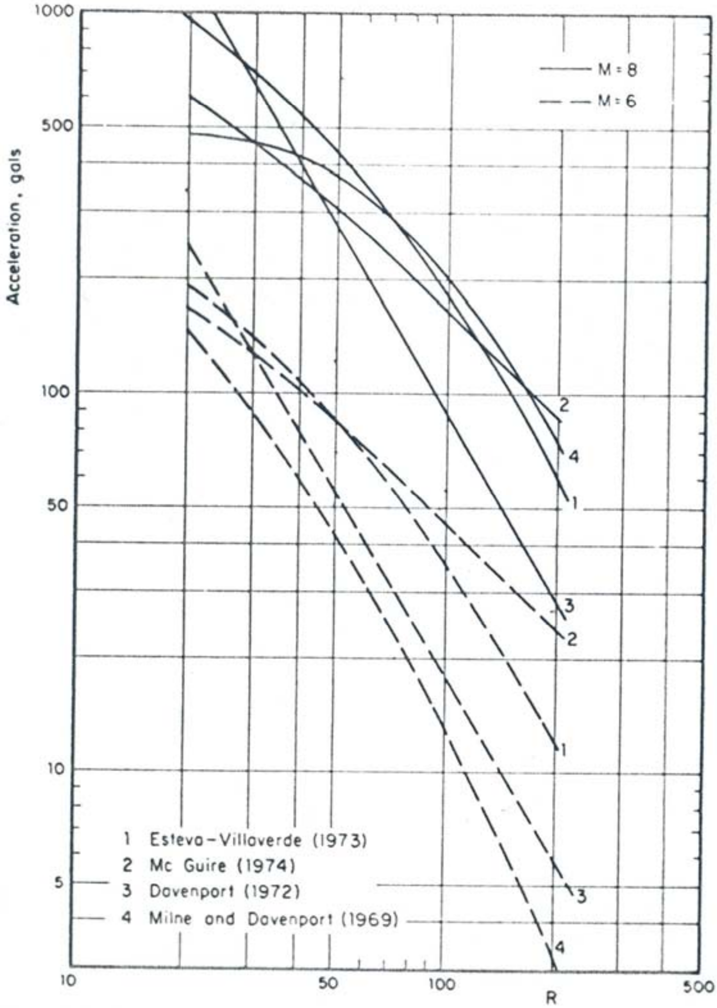

Figure 6. Comparison of several attenuation expressions

2.1.3 Response spectra

Peak ground acceleration and displacement are fairly good indicators of the response of structures possessing respectively very high and very small natural frequencies. Peak velocity is correlated with the response of intermediate-period systems, but the correlation is less precise than that tying the former parameters; hence, it is natural to formulate seismic risk evaluation and engineering design criteria in terms of spectral ordinates.

Response spectrum prediction for given magnitude and hypocentral or site-to-fault distance usually entails a two-step process, according to which peak ground acceleration, velocity and displacement are initially estimated and then used as reference values for prediction of the ordinates of the response spectrum. Let the second step in the process be represented by the operation $y_s = \alpha y_g$, where y_s is an ordinate of the response spectrum for a given natural period and damping ratio, and y_g is a parameter (such as peak

TABLE 1

McGuire's attenuation expressions $y = b_1\, 10^{b_2 M}(R + 25)^{-b_3}$

y	b_1	b_2	b_3	$V(y)$ = coeff. of var. of y
a gals	472.3	0.278	1.301	0.548
v cm/sec	5.64	0.401	1.202	0.696
d cm	0.393	0.434	0.885	0.883
Undamped spectral pseudovelocities				
T = 0.1 sec	11.0	0.278	1.346	0.941
0.5	3.05	0.391	1.001	0.636
1.0	0.631	0.378	0.549	0.768
2.0	0.0768	0.469	0.419	0.989
5.0	0.0834	0.564	0.897	1.344
5% damped spectral pseudovelocities				
T = 0.1 sec	10.09	0.233	1.341	0.651
0.5	5.74	0.356	1.197	0.591
1.0	0.432	0.399	0.704	0.703
2.0	0.122	0.466	0.675	0.941
5.0	0.0706	0.557	0.938	1.193

ground acceleration or velocity) that can be directly obtained from the time history record of a given shock regardless of the dynamic properties of the systems whose response is to be predicted. For given M and R, y_g is random and so is $y_s / y_g = \alpha$; the mean and standard deviation of y_s depend on those of y_g and α and on the coefficient of correlation of the latter variables. As shown above, y_g can only be predicted within wide uncertainty limits, often wider than those tied to y_s (Esteva and Villaverde, 1973). The coefficient of variation of y_s given M and R can be smaller than that of y_g only if α and y_g are negatively correlated, which is often the case: the greater the deviation of an observed value of y_g with respect to its expectation for given M and R, the lower is likely to be α. In other words, it seems that in the intermediate range of natural periods the expected values of spectral ordinates for given damping ratios can be predicted directly in terms of magnitude and focal distance with narrower (or at most equal) margins of uncertainty than those tied to predicted peak ground velocities. For the ranges of very short or very long natural periods, peak amplitudes of ground motion and spectral ordinates approach each other and their standard errors are therefore nearly equal.

McGuire (1974) has derived attenuation expressions for the conditional values (given M and R) of the mean and of various percentiles of the probability distributions of the ordinates of the response spectra for given natural periods and damping ratios. Those expressions have the same form as eqs. 4 and 5, but their parameters show that the rates of attenuation of spectral ordinates differ significantly from those of peak ground accelerations or velocities. For instance, McGuire finds that peak ground velocity attenuates in proportion to $(R + 25)^{-1.20}$, while the mean of the pseudovelocity for a natural period of 1 sec and a damping ratio of 2 % attenuates in proportion to $(R + 25)^{-0.59}$. These results stem from the way that frequency content changes with R and lead to the conclusion that the ratio of spectral velocity should be taken as a function of M and R.

Table 1 summarizes McGuire's attenuation expressions and their coefficients of variation for ordinates of the pseudovelocity spectra and for peak ground acceleration, velocity and displacement. Similar expressions were derived by Esteva and Villaverde (1973), but they are intended to predict only the maxima of the expected acceleration and velocity spectra, regardless of the periods associated with those maxima. No analysis has been performed of the relative validity of McGuire's and Esteva and Villaverde's expressions for various ranges of M and R.

3. Local seismicity

The term *local seismicity* will be used here to designate the degree of seismic activity in a given volume of the earth's crust; it can be quantitatively described according to various criteria, each providing a different amount of information. Most usual criteria are based on upper bounds to the magnitudes of earthquakes that can originate in a given seismic source, on the amount of energy liberated by shocks per unit volume and per unit time or on more detailed statistical descriptions of the process.

3.1 Magnitude-recurrence expressions

Gutenberg and Richter (1954) obtained expressions relating earthquake magnitudes with their rates of occurrence for several zones of the earth. Their results can be put in the form:

$$\lambda = \alpha \, \mathrm{e}^{-\beta M} \tag{6}$$

where λ is the mean number of earthquakes per unit volume and per unit time having magnitude greater than M and α and β are zone-dependent constants; α varies widely from point to point, as evidenced by the map of epicenters shown in Fig. 7, while β remains within a relatively narrow range, as shown in Fig. 8. Equation 6 implies a distribution of the energy liberated per shock which is very similar to that observed in the process of microfracturing of laboratory specimens of several types of rock subjected to gradually increasing compressive or bending strain (Mogi, 1962; Scholz, 1968). The values of β determined in the laboratory are of the same order as those obtained from seismic events, and have been shown to depend on the heterogeneity of the specimens and on their ability to yield locally. Thus, in heterogeneous specimens made of brittle materials many small shocks precede a major fracture, while in homogeneous or plastic materials the number of small shocks is relatively small. These cases correspond to large and small β-values, respectively. No general relationship is known to the writer between β and geotectonic features of seismic provinces: complexity of crustal structure and of stress gradients precludes extrapolation of laboratory results; and statistical records for relatively small zones of the earth are not, as a rule, adequate for establishing local values of β. Figure 8 shows that for very high magnitudes the observed frequency of events is lower than predicted by eq. 6. In addition, Rosenblueth (1969) has shown that β cannot be sm.aller than 3.46, since that would imply an infinite amount of energy liberated per unit time. However, Fig. 8 shows that the values of β which result from fitting expressions of the form 6 to observed data are smaller than 3.46; hence, for very high values of M (above 7, approximately) the curve should bend down, in accordance with statistical evidence.

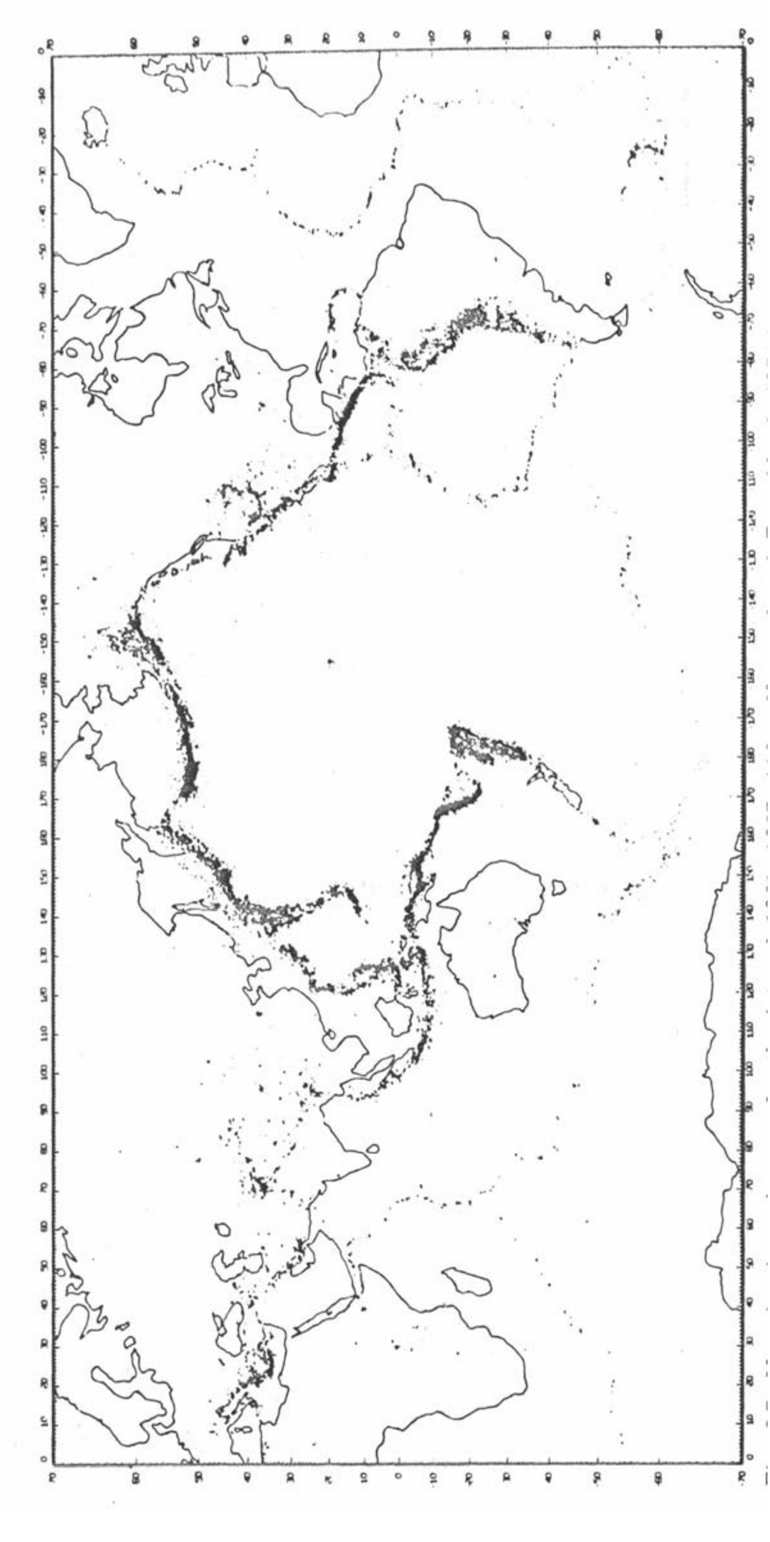

Figure.7. Map showing epicenters for the interval 1961-1967. (After Newmark and Rosenblueth, 1971)

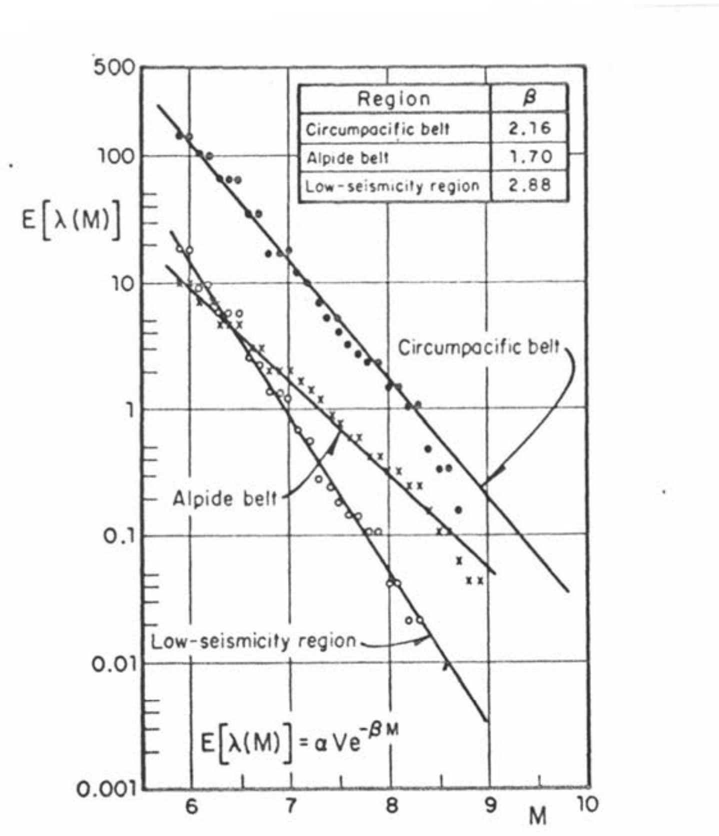

Figure 8. Seismicity of macrozones. (After Esteva, 1968)

Expressions alternative to eq. 6 have been proposed, attempting to represent more adequately the observed magnitude-recurrence data (Rosenblueth, 1964; Merz and Cornell, 1973). Most of these expressions also fail to recognize the existence of an upper bound to the magnitude that can be generated in a given source. Although no precise estimates of this upper bound can yet be obtained, recognition of its existence and of its dependence on the geotectonic characteristics of the source is inescapable. Indeed, the practice of seismic zoning in the Soviet Union has been based on this concept (Gzovsky, 1962; Ananiin et al., 1968) and in many countries design spectra for very important structures, such as nuclear reactors or large dams, are usually derived from the assumption of a maximum credible intensity at a site; that intensity is ordinarily obtained by taking the maximum of the intensities that result at the site when at each of the potential sources an earthquake with magnitude equal to the maximum feasible value for that source is generated at the most unfavourable location within the same source. When this criterion is applied no attention is usually paid to the uncertainty in the maximum feasible magnitude nor to the probability that an earthquake with that magnitude will occur during a given time period. The need to formulate seismic-risk-related decisions that account both for upper bounds to magnitudes and for their probabilities of occurrence suggests adoption of magnitude recurrence expressions of the form:

$$\begin{aligned} \lambda &= \lambda_L\, G^*(M) && \text{for } M_L \le M \le M_U \\ &= \lambda_L && \text{for } M < M_L \\ &= 0 && \text{for } M > M_U \end{aligned} \tag{7}$$

where M_L = lowest magnitude whose contribution to risk is significant, M_U = maximum feasible magnitude, and $G^*(M)$ = complementary cumulative probability distribution of magnitudes every time that an event ($M \ge M_L$) occurs. A particular form of $G^*(M)$ that lends itself to analytical derivations is:

$$G^*(M) = A_0 + A_1 \exp(-\beta M) - A_2 \exp[-(\beta - \beta_1)M] \tag{8}$$

where

$$\begin{aligned} A_0 &= A\beta_1 \exp\left[-\beta\left(M_U - M_L\right)\right] \\ A_1 &= A\left(\beta - \beta_1\right)\exp\left(\beta M_L\right) \\ A_2 &= A_\beta \exp\left(-\beta_1 M_U + \beta M_L\right) \\ A &= \left[\beta\left\{1 - \exp\left[-\beta_1\left(M_U - M_L\right)\right]\right\} - \beta_1\left\{1 - \exp\left[-\beta\left(M_U - M_L\right)\right]\right\}\right]^{-1} \end{aligned}$$

As M tends to M_L from above, eq. 7 approaches eq. 6. Adoption of adequate values of M_U and β_1 permits satisfying two additional conditions: the maximum feasible magnitude and the rate of variation of λ in its vicinity. When $\beta_1 \to \infty$, eq. 8 tends to an expression proposed by Cornell and Vanmarcke (1969).

Yegulalp and Kuo (1974) have applied the theory of extreme values to estimating the probabilities that given magnitudes are exceeded in given time intervals. They assume those probabilities to fit an extreme type-III distribution given by:

$$\begin{aligned} F_{M_{\max}}(M \mid t) &= \exp\left[-C\left(M_U - M\right)^k t\right] && \text{for } M \le M_U \\ &= 0 && \text{for } M > M_U \end{aligned} \tag{9}$$

Here $F_{M_{\max}}(M \mid t)$ indicates the probability that the maximum magnitude observed in t years is smaller than M, M_U has the same meaning as above, and C and K are zone dependent parameters. This distribution is consistent with the assumption that earthquakes with magnitudes greater than M take place in accordance with a Poisson process with mean rate λ equal to $C\,(M_U - M)^k$. Equation 9 produces magnitude recurrence curves that fit closely the statistical data on which they are based for magnitudes above 5.2 and return periods from 1 to 50 years, even though the values of M_U that result from pure statistical analysis are not reliable measures of the upper bound to magnitudes, since in many cases they turn out inadmissibly high.

For low magnitudes, only a fraction of the number of shocks that take place is detected. As a consequence, λ-values based on statistical information lie below those computed according to eqs. 6 and 8 for M smaller than about 5.5. In addition, Fig. 9, taken from Yegulalp and Kuo (1974), shows that the numbers of detected shocks fit the extreme type III in eq. 9 better than the extreme type-I distribution implied by eq. 6, coupled with the assumption of Poisson distribution of the number of events. It is not clear what portion of the deviation from the extreme type-I distribution is due to the low the low values of the detectability levels and what portion comes from differences between the actual form of variation of λ with M and that given by eq. 6.

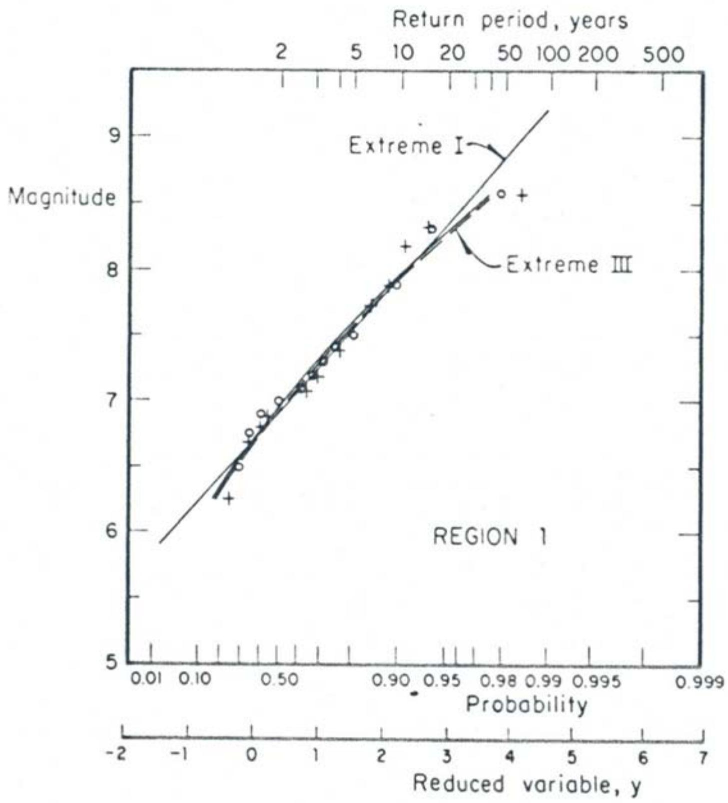

Figure 9. Magnitude statistics in the Aleutian Islands region.
(After Yegulalp and Kuo, 1974)

The problem deserves attention because estimates of expected losses due to non-structural damage may be sensitive to the values of λ for small magnitudes (say below 5.5) and because the evaluation of the level of seismic activity in a region is often made to depend on the recorded numbers of small magnitude shocks and on assumed detectability levels, i.e. of ratios of numbers of detected and occurred earthquakes (Kaila and Narain 1971; Kaila et al., 1972, 1974).

None of the expressions for λ presented in this chapter possess the desirable property that its applicability over a number of non-overlapping regions of the earth's crust implies the validity of an expression of the same form over the addition of those regions, unless some restrictions are imposed on the parameters of each λ. For instance, the addition of expressions like 6 gives place to an expression of the same form only if β is the same for all terms in the sum. Similar objections can be made to eq. 8. In what follows these forms will be preserved, however, as their accuracy is consistent with the amount of available information and their adoption offers significant advantages in the evaluation of regional seismicity, as shown later.

3.2 Variation with depth

Depth of prevailing seismic activity in a region depends on its tectonic structure. For instance, most of the activity in the western coast of the United States and Canada consists of shocks with hypocentral depths in the range of 20-30 km. In other areas, such as the southern coast of Mexico, seismic events can be grouped into two ensembles: one of small shallow shocks and one of earthquakes with magnitudes comprised in a wide range, and with depths whose mean value increases with distance from the shoreline (Fig. 10). Figure 11 shows the depth distribution of earthquakes with magnitude above 5.9 for the whole circum-Pacific belt.

3.3 Stochastic models of earthquake occurrence

Mean exceedance rates of given magnitudes are expected averages during long time intervals. For decision-making purposes the times of earthquake occurrence are also significant. At present those times can only be predicted within a probabilistic context.

Let t_i (i = 1,..., n) be the unknown times of occurrence of earthquakes generated in a given volume of the earth's crust during a given time interval, and let M_i be the corresponding magnitudes. For the moment it will be assumed that the risk is uniformly distributed throughout the given volume, and hence no attention will be paid to the focal coordinates of each shock.

Classical methods of time-series analysis have been applied by different researchers attempting to devise analytical models for random earthquake sequences. The following approaches are often found in the literature:

a) Plotting of histograms of waiting times between shocks (Knopoff, 1964; Aki, 1963).
b) Evaluation of Poisson's index of dispersion, that is of the ratio of the sample variance of the number of shocks to its expected value (Vere-Jones, 1970; Shlien and Toksöz, 1970). This index equals unity for Poisson processes, is smaller for nearly periodic sequences, and is greater than one when events tend to cluster.
c) Determination of autocovariance functions, that is, of functions representing the covariance of the numbers of events observed in given time intervals, expressed in terms of the time elapsed between those intervals (Vere-Jones, 1970; Shlien and Toksöz, 1970). The autocovariance function of a Poisson process is a Dirac delta function. This feature is characteristic for the Poisson model since it does not hold for any other stochastic process.
d) The hazard function $h(t)$, defined so that $h(t)$ dt is the conditional probability that an event will take place in the interval (t, t + dt) given that no events have occurred before t. If $F(t)$ is the cumulative probability distribution of the time between events:

$$h(t) = f(t)/[1 - F(t)] \tag{10}$$

where

$$f(t) = \partial F(t)/\partial t \, .$$

For the Poisson model, $h(t)$ is a constant equal to the mean rate of the process.

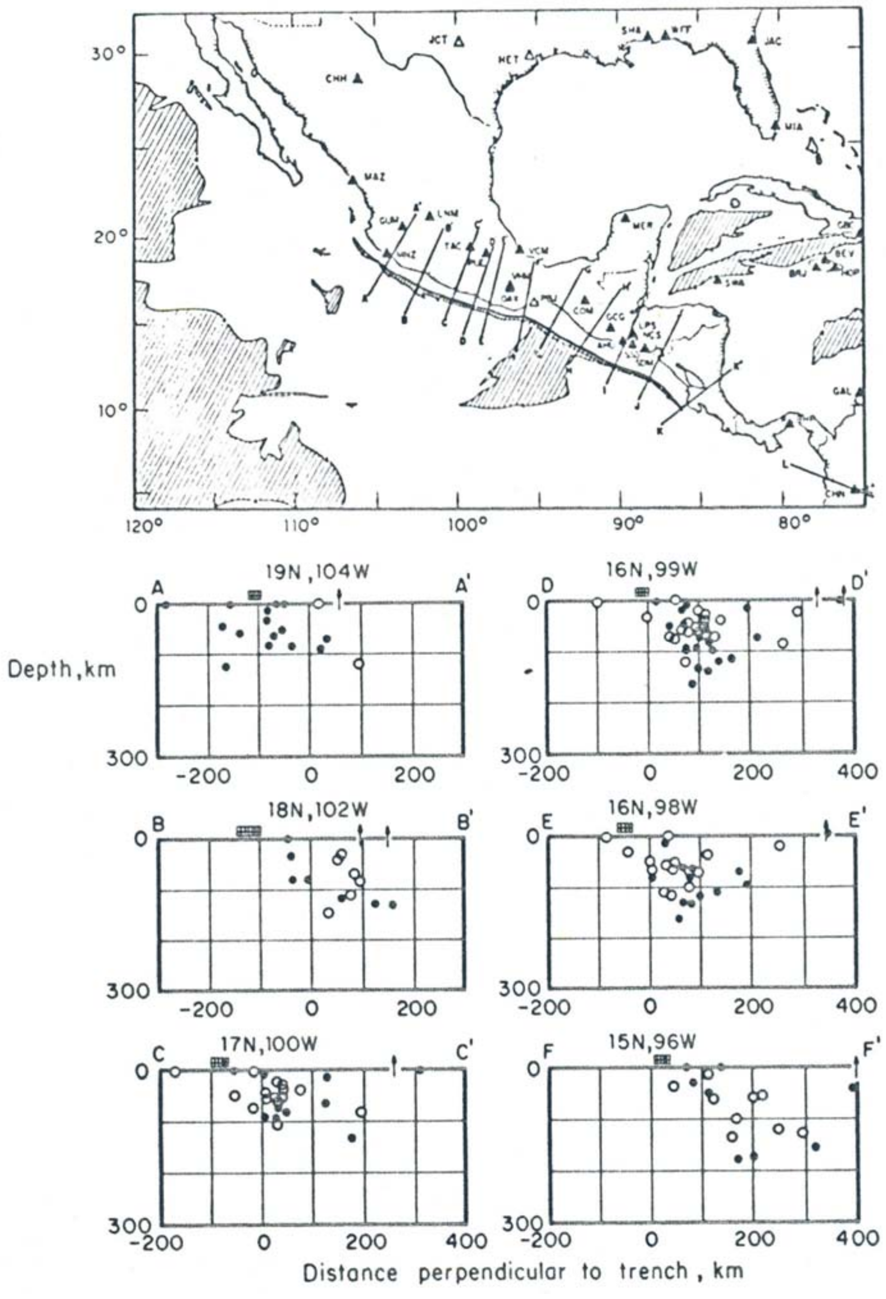

Figure 10. Earthquake hypocenters projected onto a series of vertical sections through Mexico (After Molnar and Sykes, 1969)

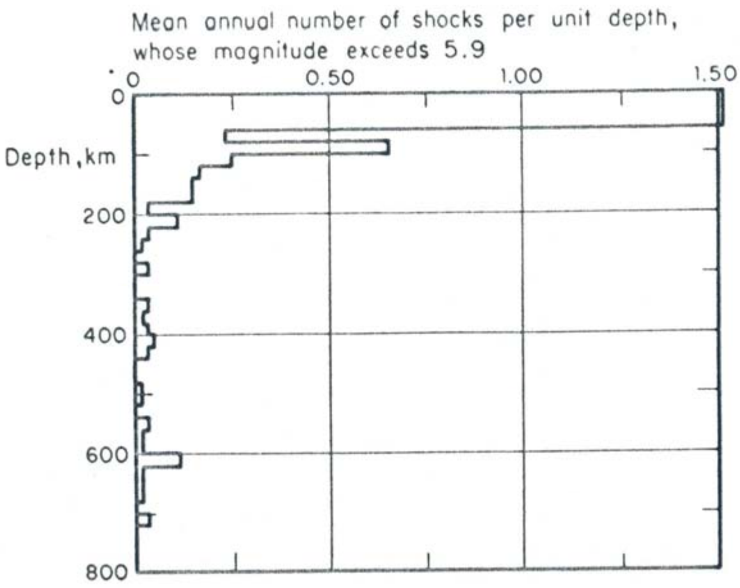

Figure 11. Variation of seismicity with depth. Circum-Pacific Belt
(After Newmark and Rosenblueth, 1971)

3.3.1 Poisson model

Most commonly applied stochastic models of seismicity assume that the events of earthquake occurrence constitute a Poisson process and that the M_i's are independent and identically distributed. This assumption implies that the probability of having N earthquakes with magnitude exceeding M during time interval (0, t) equals:

$$p_N = [\exp(-v_M t)(v_M t)^N] / N! \tag{11}$$

where v_M is the mean rate of exceedance of magnitude M in the given volume. If N is taken equal to zero in eq. 11, one obtains that the probability distribution of the maximum magnitude during time interval t is equal to exp($-v_M$ t). If v_M is given by eq. 6, the extreme type-I distribution is obtained.

Some weaknesses of this model become evident in the light of statistical information and of an analysis of the physical processes involved: the Poisson assumption implies that the distribution of the waiting time to the next event is not modified by the knowledge of the time elapsed since the last one, while physical models of gradually accumulated and suddenly released energy call for a more general renewal process such that, unlike what happens in the Poisson process, the expected time to the next event decreases as time goes on (Esteva, 1974). Statistical data show that the Poisson assumption may be acceptable when dealing with large shocks throughout the world (Ben-Menahem, 1960), implying lack of correlation between seismicities of different regions; however, when considering small volumes of the earth, of the order of those that can significantly contribute to seismic risk at a site, data often contradict Poisson's model, usually because of clustering of earthquakes in time: the observed numbers of short intervals between events are significantly higher than predicted by the exponential distribution, and values of Poisson's index of dispersion are well above unity (Figs. 12 and 13). In some instances, however, deviations in the opposite direction have been observed: waiting times tend to be more nearly periodic, Poisson's index of dispersion is smaller than one, and the process can be represented by a renewal model. This condition has been reported, for instance, in the southern coast of Mexico (Esteva, 1974), and in the Karmchatka and Pamir-Hindu Kush regions (Gaisky, 1966 and 1967). The models under discussion also fail to account for clustering in space (Tsuboi, 1958; Gajardo and Lomnitz, 1960), for the evolution of seismicity with time, and for the systematic shifting of active sources along geologic accidents (Allen, Chapter 3 of this book). On account of its simplicity, however, the Poisson process model provides a valuable tool for the formulation of some seismic-risk-related decisions, particularly of those that are sensitive only to magnitudes of events having very long return periods.

3.3.2 Trigger models

Statistical analysis of waiting times between earthquakes does not favor the adoption of the Poisson model or of other forms of renewal processes, such as those that assume that waiting times are mutually independent with lognormal or gamma distributions (Shlien and Toksöz, 1970). Alternative models have been developed, most of them of the 'trigger type' (Vere-Jones, 1970), i.e. the overall process of earthquake generation is considered as the superposition of a number of time series, each having a different origin, where the origin times are the events of a Poisson process. In general, let N be the number of events that take place during time interval (0, t), τ_m = origin time of the mth series, W_m (t, τ_m) the corresponding number of events up to instant t_1 and n_t the random number of time series initiated in the interval (0, t). The total number of events that occur before instant t is then:

$$N = \sum_{m}^{n_t} W_m\left(t, \tau_m\right) \tag{12}$$

If origin times are distributed according to a homogeneous Poisson process with mean rate v, and all W_m's are identically distributed stochastic processes with respect to (t - τ_m), it can be shown (Parzen, 1962) that the mean and variance of N can be obtained from:

$$E(N) = v\int_0^t E[W(t,\tau)]\,\mathrm{d}\tau \tag{13}$$

$$\mathrm{var}(N) = v\int_0^t E\left[W^2(t,\tau)\right]\mathrm{d}\tau \tag{14}$$

Parzen (1962) gives also an expression for the probability generating function ψ_N (Z; t) of the distribution of N in terms of ψ_W (Z; t, τ), the generating function of each of the component processes:

$$\psi_N(Z\,;t) = \exp\left[-vt + v\int_0^t \psi_W(Z\,;\,t,\tau)\,\mathrm{d}\tau\right] \tag{15}$$

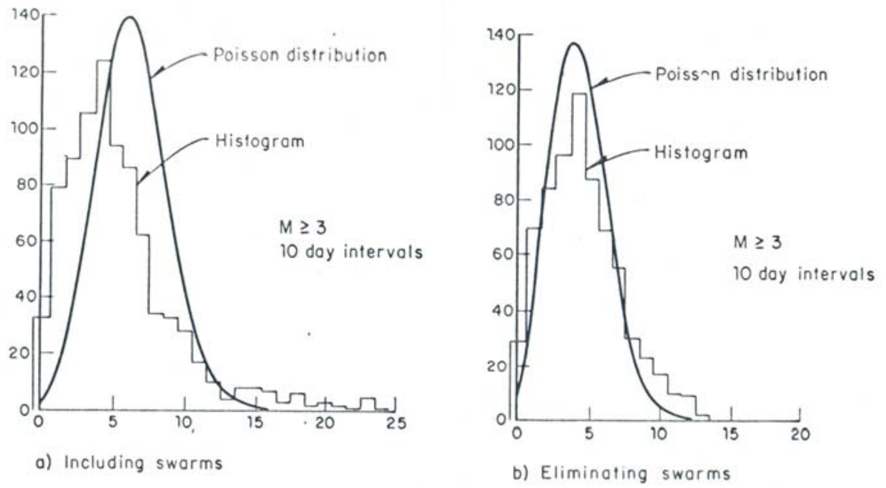

Figure 12. Evaluation of Poisson process assumption. (After Knopoff, 1964)

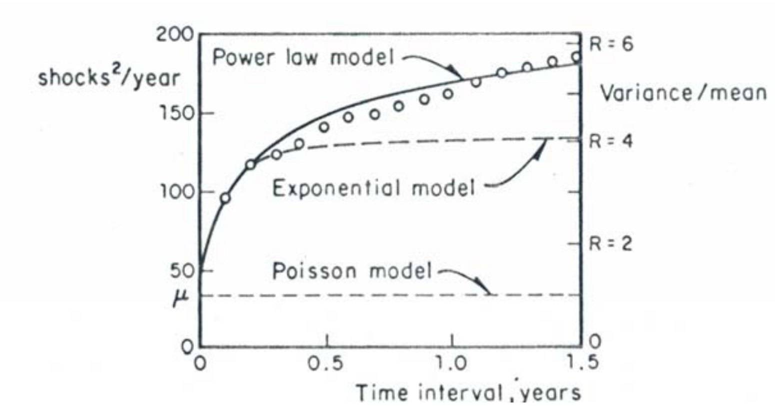

Figure 13. Variance-time curve for New Zealand shallow shocks.
(After Vere-Jones, 1966)

where:

$$\psi_W(Z;t,\tau)=\sum_{n=0}^{\infty} Z^n P\{W(t,\tau)=n\} \tag{16}$$

and the probability mass function of N can be obtained from $\psi_N(Z;t)$ by recalling that:

$$\psi_N(Z;t)=\sum_{n=0}^{\infty} Z^n P\{N=n\}$$

expanding ψ_N in power series of Z, and taking $P\{N=n\}$ equal to the coefficient of Z^n in that expansion. For instance, if it is of interest to compute $P\{N=0\}$, expansion of $\psi_N(Z;t)$ in a Taylor's series with respect to $Z=0$ leads to:

$$\psi_N(Z;t) = \psi_N(0;t) + Z\psi'_N\ (0;t) + \frac{Z^2}{2!}\psi''_N\ (0;t) + \ldots \qquad (17)$$

where the prime signifies derivative with respect to *Z*. From the definition of ψ_N, $P\{N = 0\} = \psi_N\,(0;\,t)$.

Because the component processes of 'trigger'-type time series appear overlapped in sample histories, their analytical representation usually entails study of a number of alternative models, estimation of their parameters, and comparison of model and sample properties -often second order properties (Cox and Lewis, 1966).

Vere-Jones models. Applicability of some general 'trigger' models to represent local seismicity processes was discussed in a comprehensive paper by Vere-Jones (1970), who calibrated them mainly against records of seismic activity in New Zealand. In addition to simple and compound Poisson processes (Parzen, 1962), he considered Neyman-Scott and Bartlett-Lewis models, both of which assume that earthquakes occur in clusters and that the number of events in each cluster is stocastically independent of its origin time. In the Neyman-Scott model, the process of clusters is assumed stationary and Poisson, and each cluster is defined by p_N, the probability mass function of its number of events, and $\Lambda(t)$, the cumulative distribution function of the time of an event corresponding to a given cluster, measured from the cluster origin. The Bartlett-Lewis model is a special case of the former, where each cluster is a renewal process that ends after a finite number of renewals. In these models the conditional probability of an event taking place during the interval (t, t + dt), given that the cluster consists of *N* shocks, is equal to $N\lambda(t)\mathrm{d}t$, where $\lambda(t) = \partial\Lambda(t)/\,\partial t$.

Because clusters overlap in time they cannot easily be identified and separated. Estimation of process parameters is accomplished by assuming different sets of those parameters and evaluating the corresponding goodness of fit with observed data.

Various alternative forms of Neyman-Scott's model were compared by Vere-Jones with observed data on the basis of first and second order statistics: hazard functions, interval distributions (in the form of power spectra) and variance time curves.

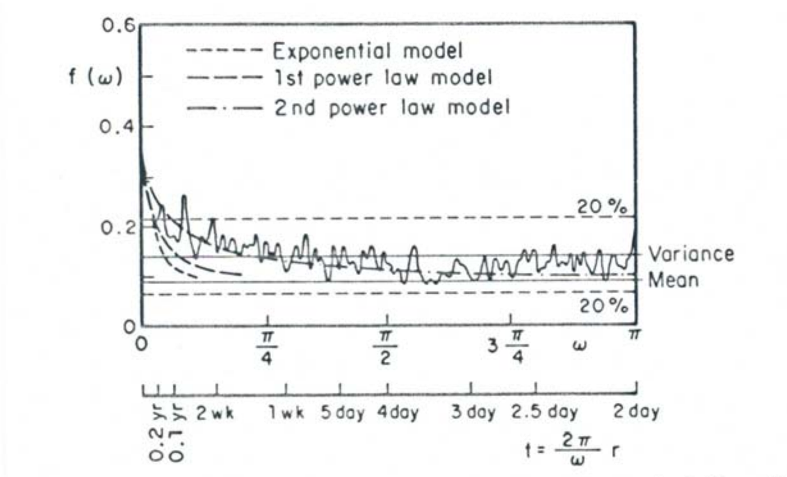

Figure 14. Smoothed periodogram for New Zealand shallow shocks.
(After Vere-Jones, 1966)

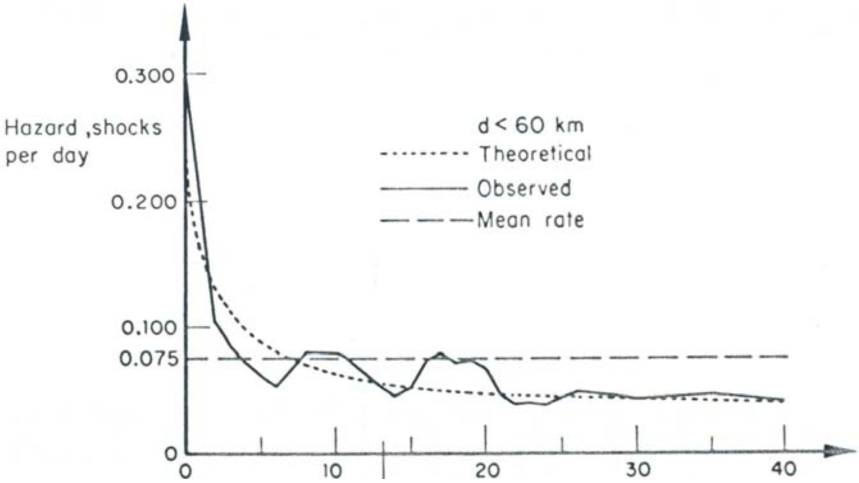

Figure 15. Hazard function for New Zealand shallow shocks. (After Vere-Jones, 1970)

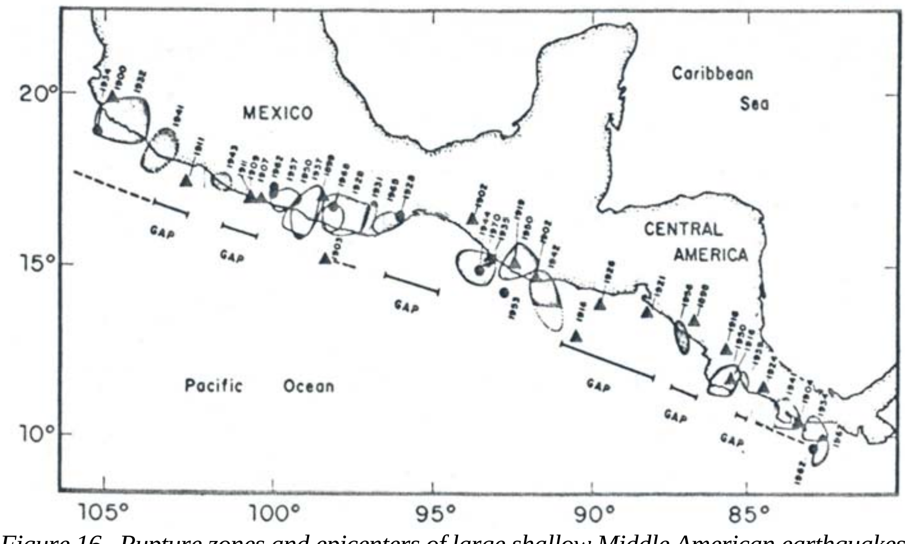

Figure 16. Rupture zones and epicenters of large shallow Middle American earthquakes of this century. (After Kelleher et al. 1973)

The statistical record comprises about one thousand New Zealand earthquakes with magnitudes greater than 4.5, recorded from 1942 to 1961. Figures 13-15 show results of the analysis for shallow New Zealand shocks as well as the comparison of observed data with several alternative models. The process of cluster origins is Poisson in all cases, but the distributions of cluster sizes (N) and of times of events within clusters differ among the various instances: in the Poisson model no clustering takes place (the distribution of N is a Dirac delta function centered at $N = 1$) while in the exponential and in the power-law models the distribution of N is extremely skewed towards $N = 1$, and $\Lambda(t)$ is taken respectively as $1 - e^{-\lambda t}$ and $1 - [c/(c + t)]^{\delta}$ for $t \geq 0$, and as zero for $t < 0$, where λ, c, and δ are positive parameters. In Figs. 13-15, $\delta = 0.25$, $c = 2.3$ days, and $\lambda = 0.061$ shocks/day. The significance of clustering is evidenced by the high value of Poisson's dispersion index in Fig. 13, while no significant periodicity can be inferred from Fig. 14. Both figures show that the power-law model provides the best fit to the statistics of the samples. A similar analysis for New Zealand's deep shocks shows much less clustering: Poisson's dispersion index equals 2, and the hazard function is nearly constant with time.

Still, data reported by Gaisky (1967) have hazard functions that suggest models where the cluster origins as well as the clusters themselves may be represented by renewal processes. Mean return periods are of the order of several months, and hence these processes do not correspond, at least in the time scale, to the process of alternate periods of activity and quiescense of some geological structures cited by Kelleher et al. (1973), which have led to the concept of 'temporal seismic gaps', discussed below.

Simplified trigger models. Shlien and Toksöz (1970) proposed a simple particular case of the Neyman-Scott process; they lumped together all earthquakes taking place during non-overlapping time intervals of a given length and defined them as clusters for which $\lambda(t)$ was a Dirac delta function. Working with one-day intervals, they assumed the number of events per cluster to be distributed in accordance with the discrete Pareto law and applied a maximum-likelihood criterion to the information consisting of 35 000 earthquakes reported by the USCGS from January 1971 to August 1968. The model proposed represents reasonably well both the distribution of the number of earthquakes in one-day intervals and the dispersion index. However, owing to the assumption that no cluster lasts more than one day, the model fails to represent the autocorrelation function of the daily numbers of shocks for small time lags. The degree of clustering is shown to be a regional function, and to diminish with the magnitude threshold value and with the focal depth.

Aftershock sequences. The trigger processes described have been branded as reasonable representations of regional seismic activity, even when aftershock sequences and earthquake swarms are suppressed from statistical records, however arbitrary that suppression may be. The most significant instances of clustering are related, however, to aftershock sequences which often follow shallow shocks and only rarely intermediate and deep events. Persistence of large numbers of aftershocks for a few days or weeks has propitiated the detailed statistical analysis of those sequences since last century. Omori (1894) pointed out the decay in the mean rate of aftershock occurrence with t, the time elapsed since the main shock; he expressed that rate as inversely proportional to $t + q$, where q is an empirical constant. Utsu (1961) proposed a more general expression, proportional to $(t + c)^{-\zeta}$ where ζ is a constant; Utsu's proposal is consistent with the power-law expression for $\Lambda(t)$ presented above.

Lomnitz and Hax (1966) proposed a clustering model to represent aftershock sequences; it is a modified version of Neyman and Scott's model, where the process of cluster origins is non-homogeneous Poisson with mean rate decaying in accordance with Omori's law, the number of events in each cluster has a Poisson distribution, and $\Lambda(t)$ is exponential. All the results and methods of analysis described by Vere-Jones (1970) for the stationary process of cluster origins can be applied to the nonstationary case through a transformation of the time scale. Fitting of parameters to four aftershock sequences was accomplished through use of the second-order information of the sample defined on a transformed time scale. By applying this criterion to earthquake sets having magnitudes above different threshold values it was noticed that the degree of clustering decreases as the threshold value increases.

The magnitude of the main shock influences the number of aftershocks and the distribution of their magnitudes and, although the rate of activity decreases with time, the distribution of magnitudes remains stable throughout each sequence (Lomnitz, 1966; Utsu, 1962; Drakopoulos, 1971). Equation 6 represents fairly well the distribution of magnitudes observed in most aftershock sequences. Values of β range from 0.9 to 3.9 and decrease as the depth increases. Since values of β for regular (main) earthquakes are usually estimated from relatively small numbers of shocks generated throughout crust volumes much wider than those active during aftershock sequences, no relation has been established among β-values for series of both types of events. The parameters of Utsu's expression for the decay of aftershock activity with time have been estimated for several sequences, for instance those following the Aleutian earthquake of March 9, 1957, the Central Alaska earthquake of April 7, 1958, and the Southeastern Alaska earthquake of July 10, 1958 (Utsu, 1962), with magnitudes equal to 8.3, 7.3, and 7.9, respectively; c (in days) was 0.37, 0.40, and 0.01, while ζ was 1.05, 1.05 and 1.13, respectively. The relationship of the total number of aftershocks whose magnitude exceeds a given value with the magnitude of the main shock was studied by Drakopoulos (1971) for 140 aftershock sequences in Greece from 1912 to 1968. His results can be expressed by $N(M) = A \exp(-\beta M)$, where $N(M)$ is the total number of aftershocks with magnitude greater than M, and A is a function of M_0, the magnitude of the main shock:

$$A = \exp\left(3.62\,\beta + 1.1 M_0 - 3.46\right) \tag{18}$$

Formulation of stochastic process models for given earthquake sequences is feasible once this relationship and the activity decay law are available for the source of interest. For seismic-risk estimation at a given site the spatial distribution of aftershocks may be as significant as the distribution of magnitudes and the time variation of activity, particularly for sources of relatively large dimensions.

3.3.3 Renewal process models

The trigger models described are based on information about earthquakes with magnitudes above relatively low thresholds recorded during time intervals of at most ten years. The degrees of clustering observed and the distributions of times between clusters cannot be extrapolated to higher magnitude thresholds and longer time intervals without further study.

Available information shows beyond doubt that significant clustering is the rule, at least when dealing with shallow shocks. However, there is considerable ground for discussion on the nature of the process of cluster origins during intervals of the order of one century or longer. While lack of statistical data hinders the formulation of seismicity models valid over long time intervals, qualitative consideration of the physical processes of earthquake generation may point to models which at least are consistent with the state of knowledge of geophysical sciences. Thus, if strain energy stored in a region grows in a more or less systematic manner, the hazard function should grow with the time elapsed since the last event, and not remain constant as the Poisson assumption implies. The concept of a growing hazard function is consistent with the conclusions of Kelleher et al. (1973) concerning the theory of periodic activation of *seismic gaps.* This theory is partially supported by results of nearly qualitative analysis of the migration of seismic activity along a number of geological structures. An instance is provided by the southern coast of Mexico, one of the most active regions in the world. Large shallow shocks are generated probably by the interaction of the continental mass and the subductive oceanic Cocos plate that underthrusts it and by compressive or flexural failure of the latter (Chapter 2). Seismological data show significant gaps of activity along the coast during the present century and not much is known about previous history (Fig. 16). Along these gaps, seismic-risk estimates based solely on observed intensities are quite low, although no significant difference is evident in the geological structure of these regions with respect to the rest of the coast, save some transverse faults which divide the continental formation into several blocks. Without looking at the statistical records a geophysicist would assign equal risk throughout the area. On the basis of seismicity data, Kelleher et al. have concluded that activity migrates along the region, in such a manner that large earthquakes tend to occur at seismic gaps, thus implying that the hazard function grows with time since the last earthquake. Similar phenomena have been observed in other regions; of particular interest is the North Anatolian fault where activity has shifted systematically along it from east to west during the last forty years (Allen, 1969).

Conclusions relative to activation of seismic gaps are controversial because the observation periods have not exceeded one cycle of each process. Nevertheless, those conclusions point to the formulation of stochastic models of seismicity that reflect plausible features of the geophysical processes.

These considerations suggest the use of renewal-process models to represent sequences of individual shocks or of clusters. Such models are characterized because times between events are independent and identically distributed. The Poisson process is a particular renewal model for which the distribution of the waiting time is exponential. Wider generality is achieved, without much loss of mathematical tractability, if inter-event times are supposed to be distributed in accordance with a gamma function:

$$f_T(t) = \frac{\nu}{(k-1)!}(\nu t)^{k-1} \mathrm{e}^{-\nu t} \tag{19}$$

which becomes the exponential distribution when $k = 1$. If $k < 1$, short intervals are more frequent and the coefficient of variation is greater than in the Poisson model; if $k > 1$, the reverse is true. Shlien and Toksöz (1970) found that gamma models were unable to represent the sequences of individual shocks they analyzed; but these authors handled time intervals at least an order of magnitude shorter than those referred to in this section.

On the basis of hazard function estimated from sequences of small shocks in the Hindu-Kush, Vere-Jones (1970) deduces the validity of 'branching renewal process' models, in which the intervals between cluster centers, as well as those between cluster members, constitute renewal processes.

Owing to the scarcity of statistical information, reliable comparisons between alternate models will have to rest partially on simulation of the process of storage and liberation of strain energy (Burridge and Knopoff, 1967; Veneziano and Cornell, 1973).

3.4 Influence of the seismicity model on seismic risk

Nominal values of investments made at a given instant increase with time when placing them at compound interest rates, i.e. when capitalizing them. Their real value -and not only the nominal one- will also grow, provided the interest rate overshadows inflation. Conversely, for the purpose of making design decisions, nominal values of expected utilities and costs inflicted upon in the future have to be converted into present or actualized values, which can be directly compared with initial expenditures. Descriptions of seismic risk at a site are insufficient for that purpose unless the probability distributions of the times of occurrence of different intensities -or magnitudes at neighbouring sources- are stipulated; this entails more than simple magnitude-recurrence graphs or even than maximum feasible magnitude estimates.

Immediately after the occurrence of a large earthquake, seismic risk is abnormally high due to aftershock activity and to the probability that damage inflicted by the main shock may have weakened natural or man-made structures if emergency measures are not taken in time. When aftershock activity has ceased and damaged systems have been repaired, a normal risk level is attained, which depends on the probability-density functions of the waiting times to the ensuing damaging earthquakes.

For the purpose of illustration, let it be assumed that a fixed and deterministically known damage D_0 occurs whenever a magnitude above a given value is generated at a given source. If *f(t)* is the probability-density function of the waiting time to the occurrence of the damaging event, and if the risk level is sufficiently low that only the first failure is of concern, the expected value of the actualized cost of damage is (see Chapter 9):

$$\bar{D} = D_0 \int_0^{\infty} \mathrm{e}^{-\gamma t} f(t)\,\mathrm{d}t \qquad (20)$$

where γ is the discount (or compound interest) coefficient and the overbar denotes expectation. If the process is Poisson with mean rate v, then $f(t)$ is exponential and $\bar{D} \cong D_0\, v/\gamma$; however, if damaging events take place in clusters and most of the damage produced by each cluster corresponds to its first event, the computation of $\bar{D}$ should make use of the mean rate v corresponding to the clusters, instead of that applicable to individual events. Table 2 shows a comparison of seismic risk determined under the alternative assumptions of a Poisson and a gamma model (k = 2), both with the same mean return period, k/v (Esteva, 1974).

TABLE 2

Comparison of Poisson and gamma processes

$t_0\, v/k$	$\bar{T}_1\ v/k$	Poisson process, k = 1		hk/v	$T_1\ v/k$	Gamma process, k = 2		hk/v
		D/D_0				D/D_0		
		$\gamma k/v$ = 10	$\gamma k/v$ = 100			$\gamma k/v$ = 10	bk/v = 100	
0					1.0	0.0278	0.0004	0
0.1					0.92	0.0511	0.0036	0.367
0.2					0.86	0.0675	0.0059	0.667
0.5					0.75	0.0973	0.0100	1.333
1	1.0	0.0909	0.0099	1.0	0.67	0.120	0.0132	2.000
2					0.60	0.139	0.0158	2.667
5					0.54	0.154	0.0179	3.333
10					0.52	0.160	00187	3.633
					0.50	0.167	0.0196	4.000

Three descriptions of risk are presented as functions of the time t_0 elapsed since the last damaging event: T_1, the expected time to the next event, measured from instant

t_0; the expected value of the present cost of failure computed from eq. 20, and the hazard function (or mean failure rate). Since clustering is neglected, risk of aftershock occurrence must be either included in D_0 or superimposed on that displayed in the table.

This table shows very significant differences among risk levels for both processes. At small values of t_0, risk is lower for the gamma process, but it grows with time, until it outrides that for the Poisson process, which remains constant. The differences shown clearly affect engineering decisions.

4. Assesment of local seismicity

Only exceptionally can magnitude-recurrence relations for small volumes of the earth's crust and statistical correlation functions of the process of earthquake generation be derived exclusively from statistical analysis of recorded shocks. In most cases this information is too limited for that purpose and it does not always reflect geological evidence. Since the latter, as well as its connection with seismicity, is beset with wide uncertainty margins, information of different nature has to be evaluated, its uncertainty analyzed, and conclusions reached consistent with all pieces of information. A probabilistic criterion that accomplishes this is presented here: on the basis of geotectonic data and of conceptual models of the physical processes involved, a set of alternate assumptions can be made concerning the functions in question (magnitude recurrence, time, and space correlation) and an initial probability distribution assigned thereto; statistical information is used to judge the likelihood of each assumption, and a posterior probability distribution is obtained. How statistical information contributes to the posterior probabilities of the alternate assumptions depends on the extent of that information and on the degree of uncertainty implied by the initial probabilities. Thus, if geological evidence supports confidence in a particular assumption or range of assumptions, statistical information should not greatly modify the initial probabilities. If, on the other hand, a long and reliable statistical record is available, it practically determines the form and parameters of the mathematical model selected to represent local seismicity.

4.1 Bayesian estimation of seismicity

Bayesian statistics provide a framework for probabilistic inference that accounts for prior probabilities assigned to a set of alternate hypothetical models of a given phenomenon as well as for statistical samples of events related to that phenomenon. Unlike conventional methods of statistical inference, Bayesian methods give weight to probability measures obtained from samples or from other sources; numbers, coordinates and magnitudes of earthquakes observed in given time intervals serve to ascertain the probable validity of each of the alternative models of local seismicity that can be postulated on the grounds of geological evidence. Any criterion intended to weigh information of different nature and different degrees of uncertainty should lead to probabilistic conclusions consistent with the degree of confidence attached to each source of information. This is accomplished by Bayesian methods.

Let H_i (i = 1, ..., n) be a comprehensive set of mutually exclusive assumptions concerning a given, imperfectly known phenomenon and let A be the observed outcome of such a phenomenon. Before observing outcome A we assign an initial probability $P(H_i)$ to each hypothesis. If $P(A/H_i)$ is the probability of A in case hypothesis H_i is true, then Bayes' theorem (Raiffa and Schlaifer, 1968) states that:

$$P(H_i \mid A) = P(H_i) \frac{P(A \mid H_i)}{\sum_j P(H_i) P(A \mid H_j)} \tag{21}$$

The first member in this equation is the (posterior) probability that assumption H_i is true, given the observed outcome *A*.

In the evaluation of seismic risk, Bayes' theorem can be used to improve initial estimates of $\lambda(M)$ and its variation with depth in a given area as well as those of the parameters that define the shape of $\lambda(M)$ or, equivalently, the conditional distribution of magnitudes given the occurrence of an earthquake. For that purpose, take $\lambda(M)$ as the product of a rate function $\lambda_L = A(M_L)$ by a shape function $G^*(M, B)$, equal to the conditional complementary distribution of magnitudes given the occurrence of an earthquake with $M \geq M_L$, where M_L is the magnitude thereshold of the set of statistical data used in the estimation, and *B* is the vector of (uncertain) parameters $B,\ldots, B_r$ that define the shape of $\lambda(M)$. For instance, if $\lambda(M)$ is taken as given by eq. 8, *B* is a vector of three elements equal respectively to β, β_1, and M_U; if eq. 9 is adopted, *B* is defined by *k* and M_U.

The initial distribution of seismicity is in this case expressed by the initial joint probability density function of λ_L and *B*: $f'(\lambda_L, B)$. The observed out come *A* can be expressed by the magnitudes of all earthquakes generated in a given source during a given time interval. For instance, suppose that *N* earthquakes were observed during time interval *t* and that their magnitudes were $m_1, \ldots m_2, \ldots, m_N$. Bayes' expression takes the form:

$$f''(\lambda_L, B \mid m_1,\ldots,m_N;t) = f'(\lambda_L, B) \frac{P[m_1, m_2,\ldots,m_N;t \mid \lambda_L, B]}{\iint P[m_1, m_2,\ldots,m_N;t \mid l,b]\, f'(l,b)\,\mathrm{d}l\,\mathrm{d}b} \tag{22}$$

where $f''(.)$ is the posterior probability density function, and *l* and *b* are dummy variables that stand for all values that may be taken by λ_L and *B*, respectively. Estimation of λ_L can usually be formulated independently of that of the other parameters. The observed fact is then expressed by N_L, the number of earthquakes with magnitude above M_L during time *t*, and the following expression is obtained, as a first step in the estimation of $\lambda(M)$:

$$f''(\lambda_L \mid N_L;t) = f'(\lambda_L) \frac{P(N_L;t \mid \lambda_L)}{\int P(N_L;t \mid l)\, f'(l)\,\mathrm{d}l} \tag{23}$$

4.1.1 Initial probabilities of hypothetical models

Where statistical information is scarce, seismicity estimates will be very sensitive to initial probabilities assigned to alternative hypothetical models; the opinions of geologists and geophysicists about probable models, about the parameters of these models, and the corresponding margins of uncertainty should be adequately interpreted and expressed in terms of a function f', as required by equations similar to 22 and 23. Ideally, these opinions should be based on the formulation of potential earthquake sources and on their comparison with possibly similar geotectonic structures. This is usually done by geologists, more qualitatively than quantitatively, when they estimate M_U. Initial estimates of λ_L are seldom made, despite the significance of this parameter for the design of moderately important structures (see Chapter 9).

Analysis of geological information must consider local details as well as general structure and evolution. In some areas it is clear that all potential earthquake sources can be identified by surface faults, and their displacements in recent geological times measured. When mean displacements per unit time can be estimated, the order of magnitude of creep and of energy liberated by shocks and hence of the recurrence intervals of given magnitudes can be established (Wallace, 1970; Davies and Brune, 1971), the corresponding uncertainty evaluated, and an initial probability distribution assigned. The fact that magnitude-recurrence relations are only weakly correlated with the size of recent displacements is reflected in large uncertainties (Petrushevsky, 1966).

Application of the criterion described in the foregoing paragraph can be unfeasible or inadequate in many problems, as in areas where the abundance of faults of different sizes, ages, and activity, and the insufficient accuracy with which focal coordinates are determined preclude a differentiation of all sources. Regional seismicity may then be evaluated under the assumption that at least part of the seismic activity is distributed in a given volume rather than concentrated in faults of different importance. The same situation would be faced when dealing with active zones where there is no surface evidence of motions. Hence, consideration of the overall behavior of complex geological structures is often more significant than the study of local details.

Not much work has been done in the analysis of the overall behavior of large geological structures with respect to the energy that can be expected to be liberated per unit volume and per unit time in given portions of those structures. Important research and applications should be expected, however, since, as a result of the contribution of plate-tectonics theory to the understanding of large-scale tectonic processes, the numerical values of some of the variables correlated with energy liberation are being determined, and can be used at least to obtain orders of magnitude of expected activity along plate boundaries. Far less well understood are the occurrences of shocks in apparently inactive regions of continental shields and the behavior of complex continental blocks or regions of intense folding, but even there some progress is expected in the study of accumulation of stresses in the crust.

Knowledge of the geological structure can serve to formulate initial probability distributions of seismicity even when quantitative use of geophysical information seems beyond reach. Initial probability distributions of local seismicity parameters λ_L, B in the small volumes of the earth's crust that contribute significantly to seismic risk at a site, can be assigned by comparison with the average seismicity observed in wider areas of similar tectonic characteristics, or where the extent and completeness of statistical information warrant reliable estimates of magnitude-recurrence curves (Esteva, 1969). In this manner we can, for instance, use the information about the average distribution of the depths of earthquakes of different magnitudes throughout a seismic province to estimate the corresponding distribution in an area of that province, where activity has been low during the observation interval, even though there might be no apparent geophysical reason to account for the difference. Similarly, the expected value and coefficient of variation of λ_L in a given area of moderate or low seismicity (as a continental shield) can be obtained from the statistics of the motions originated at all the supposedly stable or aseismic regions in the world.

The significance of initial probabilities in seismic risk estimates, against the weight given to purely statistical information, becomes evident in the example of Fig. 16: if Kelleher's theory about activation of seismic gaps is true, risk is greater at the gaps than anywhere else along the coast; if Poisson models are deemed representative of the process of energy liberation, the extent of statistical information is enough to substantiate the hypothesis of reduced risk at gaps. Because both models are still controversial, and represent at most two extreme positions concerning the properties of the actual process, risk estimates will necessarily reflect subjective opinions.

4.1.2 Significance of statistical information

Estimation of λ_L. Application of eq. 23 to estimate λ_L independently of other parameters will be first discussed, because it is a relatively simple problem and because λ_L is usually more uncertain than M_U and much more so than β.

A model as defined by eq. 19 will be assumed to apply. If the possible assumptions concerning the values of λ_L constitute a continuous interval, the initial probabilities of the alternative hypotheses can be expressed in terms of a probability-density function of λ_L. If, in addition, a certain assumption is made concerning the form of this probability-density function, only the initial values of $E(\lambda_L)$ and $V(\lambda_L)$ have to be assumed. It is advantageous to assign to $v = k/E(T)$ a gamma distribution. Then, if ρ and μ are the parameters of this initial distribution of v, if k is assumed to be known, and if the observed outcome is expressed as the time t_n elapsed during $n + 1$ consecutive events (earthquakes with magnitude $\geq M_L$), application of eq. 23 leads to the conclusion that the posterior probability function of v is also gamma, now with parameters $\rho + nk$ and $\mu + t_n$. The initial and the posterior expected values of v are respectively equal to ρ/μ, and to $(\rho + nk)/(\mu + t_n)$. When initial uncertainty about v is small, ρ and μ will be large and the initial and the posterior expected values of v will not differ greatly. On the other hand, if only statistical information were deemed significant, ρ and μ should be given very small values in the initial distribution, and $E(v)$, and hence λ_L, will be practically defined by n, k, and t_n. This means that the initial estimates of geologists should not only include expected or most probable values of the different parameters, but also statements about ranges of possible values and degrees of confidence attached to each.

In the case studied above only a portion of the statistical information was used. In most cases, especially if seismic activity has been low during the observation interval, significant information is provided by the durations of the intervals elapsed from the initiation of observations to the first of the $n + 1$ events considered, and from the last of these events until the end of the observation period. Here, application of eq. 23 leads to expressions slightly more complicated than those obtained when only information about t_n is used.

The particular case when the statistical record reports no events during *at least* an interval $(0, t_0)$ comes up frequently in practical problems. The probability-density function of the time T_1 from t_0 to the occurrence of the first event must account for the corresponding shifting of the time axis. Furthermore, if the time of occurrence of the last event before the origin is unknown, the distribution of the waiting time from $t = 0$ to the first event coincides with that of the *excess life* in a renewal process at an arbitrary value of t that approaches infinity (Parzen, 1962). For the particular case when the waiting times constitute a gamma process, T_1 is measured from $t = 0$, T is the waiting time between consecutive events, and it is known that $T_1 \geq t_0$, the conditional density function of $\tau_1 = (T_1 - t_0)/E(T)$ is given by eq. 24 (Esteva, 1974), where $\mu_0 = t_0/E(T)$:

$$f_{\tau_1}(u \mid T_1 \geq t_0) = \frac{\sum_{m=1}^{k} \frac{k}{(m-1)!}[k(u+u_0)]^{m-1}}{\sum_{m=1}^{k}\sum_{n=1}^{m} \frac{1}{(n-1)!}(ku_0)^{n-1}} \mathrm{e}^{-ku} \tag{24}$$

Consider now the implications of Bayesian analysis when applied to one of the seismic gaps in Fig. 16, under the conditions implicit in eq. 24. An initial set of assumptions and corresponding probabilities was adopted as described in the following. From previous studies referring to all the southern coast of Mexico, local seismicity in the gap area (measured in terms of λ for $M \geq 6.5$) was represented by a gamma process with $k = 2$. An initial probability density function for v was adopted such that the expected value of $\lambda(6.5)$ for the region coincided with its average throughout the complete seismic province. Two values of ρ were considered: 2 and 10, which correspond to coefficients of variation of 0.71 and 0.32, respectively. Values in Table 3 were obtained for the ratio of the final to the initial expected values of v, in terms of μ_0.

The last two columns in the table contain the ratios of the computed values of $E''(T_1)$ and $E'(T)$ when v is taken as equal respectively to its initial or to its posterior expected value. This table shows that, for $\rho = 10$, that is, when uncertainty attached to the geologically based assumptions is low, the expected value of the time to the next event keeps decreasing, in accordance with the conclusions of Kelleher et al. (1973). However, as time goes on and no events occur, the statistical evidence leads to a reduction in the estimated risk, which shows in the increased conditional expected values of T_1, For $\rho = 2$, the geological evidence is less significant and risk estimates decrease at a faster rate.

4.1.3 Bayesian estimation of jointly distributed parameters

In the general case, estimation of B will consist in the determination of the posterior Bayesian joint probability function of its components, taking as statistical evidence the relative frequencies of observed magnitudes. Thus, if event A is described as the occurrence of N shocks, with magnitudes m_1, ..., m_N, and b_i (i = 1, ..., r) are values that may be adopted by the components of vector B being estimated, eq. 21 becomes:

$$f''_B(b_1,...,b_r \mid A) = \frac{f'_B(b_1,...,b_r)P(A \mid b_1,...,b_r)}{\int ... \int f'_B(u_1,...,u_r)P(A \mid u_1,...,u_r)\,\mathrm{d}u_1,...,\mathrm{d}u_r} \tag{25}$$

where $P(A \mid u_1, \ldots, u_r)$ is proportional to:

$$\prod_{i=1}^{N} \mathrm{g}(m_i \mid u_1,...,u_r)$$

and $g(m) = -\partial G^*(m) / \partial m$.

Closed-form solutions for f'' as given by eq. 25 are not feasible in general. For the purpose of evaluating risk, however, estimates of the posterior first and second moments of f'' can be obtained from eq. 25, making use of available first-order approximations (Benjamin and Cornell, 1970; Rosenblueth, 1975). Thus, the posterior expected value of B_i is given by $\int f''_{B_i}.(u)\, u\, \mathrm{d}u$, where $f''_{B_i}(u_i) = \int ... \int f''_B(u_1,..., u_r)\, \mathrm{d}u_1,..., \mathrm{d}u_n$ and the multiple integral is of order r - 1, because it is not extended to the dominion of B_i.

Hence:

$$E''(B_i) = \frac{E'_B[B_i P(A \mid B_1,..., B_r)]}{E'_B[P(A \mid B_1,..., B_r)]} \tag{26}$$

TABLE 3

Bayesian estimates of seismicity in one seismic gap

$u_0 = t_0/ E'(T)$	$E''(\nu)/E'(\nu)$		$E''(T_1 \mid T_1 \geq t_0)/E'(T)$	
	$\rho = 2$	$\rho = 10$	$\rho = 2$	$\rho = 10$
0	1.0	1.0	0.75	0.75
0.1	0.95	0.99	0.76	0.74
0.5	0.75	0.94	0.91	0.71
1	0.58	0.87	1.14	0.73
5	0.20	0.54	3.11	1.05
10	0.11	0.36	5.47	1.55
20	0.06	0.22	10.50	2.48

where E' and E'' stand for initial and posterior expectation, and subscript B means that expectation is taken with respect to all the components of B. Likewise, the following *posterior moments* can be obtained:

Covariance of B_i and B_j

$$\mathrm{Cov}''(B_i, B_j) = \frac{E'_B\,[B_i B_j P(A \mid B_1,\ldots,B_r)]}{E'_B\,[P(A \mid B_1,\ldots,B_r)]} - E''(B_i)E''(B_j) \tag{27}$$

Expected value of $\lambda(M)$

$$\begin{aligned} E''[\lambda(M)] &= E''(\lambda_1)E''[G^*(M;B)] \\ &= E''(\lambda_1)\frac{E'_B\,[G^*(M;B)P(A \mid B_1,\ldots,B_r)]}{E'_B\,[P(A \mid B_1,\ldots,B_r)]} \end{aligned} \tag{28}$$

Marginal distributions. The posterior expectation of $\lambda(M)$ is in some cases all that is required to describe seismicity for decision-making purposes. Often, however, uncertainty in $\lambda(M)$ must also be acounted for. For instance, the probability of exceedance of a given magnitude during a given time interval has to be obtained as the expectation of the corresponding probabilities over all alternative hypotheses concerning $\lambda(M)$. In this manner it can be shown that, if the occurrence of earthquakes is a Poisson process and the Bayesian distribution of λ_L is gamma with mean $\bar{\lambda}_L$ and coefficient of variation V_L, the marginal distribution of the number of earthquakes is negative binomial with mean $\bar{\lambda}_L$. In particular, the marginal probability of zero events during time interval t —equivalently, the complementary distribution function of the waiting time between events— is equal to $(1 + t/t'')^{-r''}$, where $r'' = V_L^{-2}$ and $t'' = r''/\bar{\lambda}_L$. The marginal probability-density function of the waiting time, that should be substituted in eq. 20, is $\bar{\lambda}_L\ (1 + t/t'')^{-r''-1}$, which tends to the exponential probability function as r'' and t'' tend to infinity (and $V_L \to 0$) while their ratio remains equal to $\bar{\lambda}_L$.

Bayesian uncertainty tied to the joint distribution of all seismicity parameters (λ_L, B_1, ..., B_r) can be included in the computation of the probability of occurrence of a given event Z by taking the expectation of that probability with respect to all parameters:

$$P(Z) = E_{\lambda_L, B}[P(Z); \lambda_L, B_1, \ldots, B_r)] \quad (29)$$

When the joint distribution of λ_L, B stems from Bayesian analysis of an initial distribution and an observed event, A, this equation adopts the form:

$$P''(Z) = \frac{E'_{\lambda_L, B}[P(Z \mid \lambda_L, B) P(A \mid \lambda_L, B)]}{E'_{\lambda_L, B}[P(A \mid \lambda_L, B)]} \quad (30)$$

where ' and " stand for initial and posterior, respectively.

Spatial variability. Figure 17 shows a map of geotectonic provinces of Mexico, according to F. Mooser. Each province is characterized by the large-scale features of its tectonic structure, but significant local perturbations to the overall patterns can be identified. Take for instance zone 1, whose seismotectonic features were described above, and are schematically shown in Fig. 18 (Singh, 1975): the Pacific plate underthrusts the continental block and is thought to break into several blocks, separated by faults transverse to the coast, that dip at different angles. The continental mass is also made up of several large blocks. Seismic activity at the underthrusting plate or at its interface with the continental mass is characterized by magnitudes that may reach very high values and by the increase of mean hypocentral depth with distance from the coast; small and moderate shallow shocks are generated at the blocks themselves. Variability of statistical data along the whole tectonic system was discussed above and is apparent in Fig. 10.

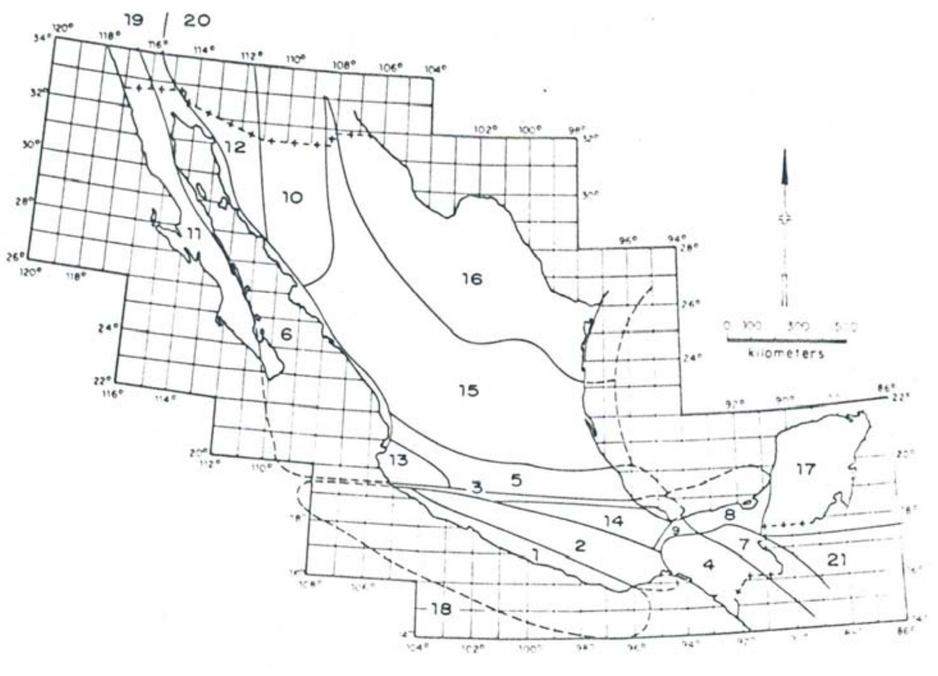

Figure 17. Seismotectonic provinces of Mexico. (After F. Mooser)

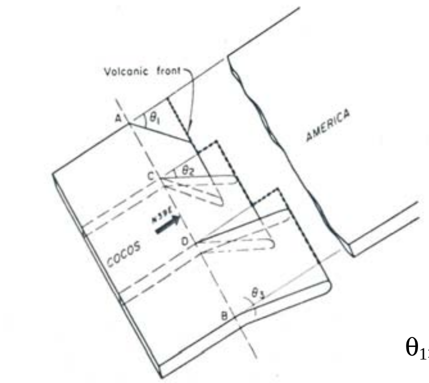

$\theta_1 > \theta_2 > \theta_3$

Figure 18. Schematic drawing of the segmenting of Cocos plate as it subducts below American plate. (After Singh, 1974)

Bayesian estimation of local seismicity averaged throughout the system is a matter of applying eq. 21 or any of its special forms (eqs. 22 and 23), taking as statistical evidence the information corresponding to the whole system. However, seismic risk estimates are sensitive to values of local seismicity averaged over much smaller volumes of the earth's crust; hence the need to develop criteria for probabilistic inference of possible patterns of space variability of seismicity along tectonically homogeneous zones.

On the basis of seismotectonic information, the system under consideration can first be subdivided into the underthrusting plate and the subsystem of shallow sources; each subsystem can then be separately analyzed. Take for instance the underthrusting plate and subdivide it into s sufficiently small equal-volume subzones. Let v_L be the rate of exceedance of magnitude M_L throughout the main system, v_{L_i} the corresponding rate at each subzone, and define p_i as v_L/v_L, with p_i independent of v_L (p_i is equal to the probability that an earthquake known to have been generated in the overall system originated at subzone i). Initial information about possible space variability of v_{L_i} can be expressed in terms of an initial probability distribution of p_i and of the correlation among p_i and p_j for any i and j. Because $\sum v_{L_i} = v_L$, one obtains $\sum p_i = 1$. This imposes two restrictions on the initial joint probability distribution of the p_i's: $E'(p_i) = 1$, var' $\sum p_i = 0$. If all p_i's are assigned equal expectations and all pairs p_i, p_j, $i \neq j$ are assumed to possess the same correlation coefficient $\rho_{ij} = \rho'$, the restrictions mentioned lead to $E'(p_i) = 1/s$ and $\rho' = -1/(s - 1)$. Posterior values of $E(p_i)$ and ρ_{ij} are obtained according to the same principles that led to eqs. 25-28. Statistical evidence is in this case described by N, the total number of earthquakes generated in the system, and n_i (i = 1, ..., s) the corresponding numbers for the subzones. Given the p_i's, the probability of this event is the multinomial distribution:

$$P[A \mid p_1,..., p_s] = \frac{N!}{n_1!,...,n_s!}\, p_1^{n_1} ... p_s^{n_s} \tag{31}$$

If the correlation coefficients among seismicities of the various subzones can be neglected, each p_i can be separately estimated. Because p_i has to be comprised between 0 and 1, it is natural to assign it a beta initial probability distribution, defined by its parameters n'_i and N'_i, such that $E'(p_i) = n'_i/N'_i$ and var'$(p_i) = n'_i (N'_i - n'_i)/[N'^2_i (N'_i + 1)]$ (Raiffa and Schlaifer, 1968). The parameters of the posterior distribution will be:

$$n'' = n'_i + n_i \ , \qquad N''_i = N'_i + N$$

Take for instance a zone whose prior distribution of λ_L is assumed gamma with expected value l'_L and coefficient of variation V'_L. Suppose that, on the basis of geological evidence and of the dimensions involved, it is decided to subdivide the zone into four subzones of equal dimensions; a-priori considerations lead to the assignment of expected values and coefficients of variation of p_i for those subzones, say $E'(p_i) = 0.25$, $V'(p_i) = 0.25$ ($i = 1,..., 4$). From previous considerations for $s = 4$ take $\rho'_{ij} = -1/3$ for $i \neq j$. Suppose now that, during a given time interval t, ten earthquakes were observed in the zone, of which 0, 1, 3, and 6 occurred respectively in each subzone. If the Poisson process model is adopted, λ'_L and V'_L can be expressed in terms of a fictitious number of events $n' = V'^{-2}_L$ occurred during a fictitious time interval $t' = n'/\bar{\lambda}'_L$; after observing n earthquakes during an interval t, the Bayesian mean and coefficient of variation of λ_L will be $\bar{\lambda}''_L = (n' + n) / (t' + t)$, $V''_L = (n' + n)^{-1/2}$ (Esteva, 1968). Hence:

$$\lambda''_L = (V'^{-2}_L + 10) / (V'^{-2}_L \, \bar{\lambda}'^{-1}_L + t), \qquad V''_L = (V'^{-2}_L + 10)^{-1/2}$$

Local deviations of seismicity in each subzone with respect to the average λ_L can be analyzed in terms of p_i ($i = 1, ..., 4$); Bayesian analysis of the proportion in which the ten earthquakes were distributed among the subzones proceeds according to:

$$E''(p_i \mid A) = \frac{E'[p_i P(A \mid p_i, ..., p_4)]}{E'[P(A \mid p_i, ..., p_4)]} \tag{32}$$

The expectations that appear in this equation have to be computed with respect to the initial joint distribution of the p'_is. In practice, adequate approximations are required. For instance, Benjamin and Cornells' (1970) first-order approximation leads to $E''(p_1) = 0.226$, $E''(p_4) = 0.294$.

If correlation among subzone seismicities is neglected, and statistical information of each subzone is independently analyzed, when the p'_is are assigned beta probability-density functions with means and coefficients of variation as defined above, one obtains $E''(p_1) = 0.206$, $E''(p_4) = 0.311$, which are not very different from those formerly obtained; however, when $E'(p_i) = 0.25$ and $V'(p_i) = 0.5$, the first criterion leads to $E''(p_i) = 0.206$, $E''(p_4) = 0.314$, while the second produces 0.131 and 0.416, respectively. Part of the difference may be due to neglect of ρ'_{ij}, but probably a significant part stems from inaccuracies of the first-order approximation to the expectations that appear in eq. 32; alternate approximations are therefore desirable.

Incomplete data. Statistical information is known to be fairly reliable only for magnitudes above threshold values that depend on the region considered, its level of activity, and the quality of local and nearby seismic instrumentation. Even incomplete statistical records may be significant when evaluating some seismicity parameters; their use has to be accompanied by estimates of detectability values, that is, of ratios of the numbers of events recorded to total numbers of events in given ranges (Esteva, 1970; Kaila and Narain, 1971).

5. Regional seismicity

The final goal of local seismicity assessment is the estimation of regional seismicity, that is, of probability distributions of intensities at given sites, and of probabilistic correlations among them. These functions are obtained by integrating the contributions of local seismicities of nearby sources, and hence their estimates reflect Bayesian uncertainties tied to those seismicities. In the following, regional seismicity will be expressed in terms of mean rates of exceedance of given intensities; more detailed probabilistic descriptions would entail adoption of specific hypotheses concerning space and time correlations of earthquake generation.

5.1 Intensity-recurrence curves

The case when uncertainty in seismicity parameters is neglected will be discussed first. Consider an elementary seismic source with volume dV and local seismicity $\lambda(M)$ per unit volume, distant R from a site S, where intensity-recurrence functions are to be estimated. Every time that a magnitude M shock is generated at that source, the intensity at S equals:

$$Y = \varepsilon Y_p = \varepsilon b_1 \exp(b_2 M) g(R) \tag{33}$$

(see eqs. 4 and 5), where ε is a random factor and Y and Y_p stand for actual and predicted intensities, b_1 and b_2 are given constants, and $g(R)$ is a function of hypocentral distance. The probability that an earthquake originating at the source will have an intensity greater than y is equal to the probability that $\varepsilon Y_p > y$. If Y_p is expressed in terms of M and randomness in ε is accounted for, one obtains:

$$\nu(y) = \int_{\alpha_u}^{\alpha_L} \nu_p(y/u) f_\varepsilon(u)\,\mathrm{d}u \tag{34}$$

where v and v_p are respectively mean rates at which actual and predicted intensities exceed given values, $\alpha_U = y/y_U$, $\alpha_L = y/y_L$, y_U, and y_L are the predicted intensities that correspond to M_U and M_L, and f_ε the probability-density function of ε. If eq. 33 is assumed to hold:

$$v_p(y) = K_0 + K_1 y^{-r_1} - K_2 y^{-r_2} \tag{35}$$

where:

$$K_i = [b_1 g(R)]^{r_i} A_i \lambda_L \,\mathrm{d}V \qquad (i = 0,1,2) \tag{36}$$

$$r_0 = 0, \quad r_1 = \beta / b_2, \qquad r_2 = (\beta - \beta_1)/b_2 \tag{37}$$

Substitution of eq. 35 into 34, coupled with the assumption that ln ε is normally distributed with mean m and standard deviation σ leads to:

$$\nu(y) = c_0 K_0 + c_1 K_1 y^{-r_1} - c_2 K_2 y^{-r_2} \tag{38}$$

where

$$c_i = \exp(Q_i)\left[\phi\left(\frac{\ln \alpha_L - u_i}{\sigma}\right) - \phi\left(\frac{\ln \alpha_U - u_i}{\sigma}\right)\right] \tag{39}$$

ϕ is the standard normal cumulative distribution function, Q_i = 1/2 $a^2 r_i^2 + m r_i$, and $u_i = m + \sigma^2 r_i$. Similar expressions have been presented by Merz and Cornell (1973) for the special case of eq. 8 when $\beta_1 \rightarrow \infty$ and for a quadratic form of the relation between magnitude and logarithm of exceedance rate. Closed-form solutions in terms of incomplete gamma functions are obtained when magnitudes are assumed to possess extreme type-III distributions (eq. 9).

Intensity-recurrence curves at given sites are obtained by integration of the contributions of all significant sources. Uncertainties in local seismicities can be handled by describing regional seismicity in terms of means and variances of $v(y)$ and estimating these moments from eq. 34 and suitable first- and second-moment approximations. Influence of these uncertainties in design decisions has been discussed by Rosenblueth (in preparation).

5.2 Seismic probability maps

When intensity-recurrence functions are determined for a number of sites with uniform local ground conditions the results are conveniently represented by sets of seismic probability maps, each map showing contours of intensities that correspond to a given return period. For instance, Figs. 19 and 20 show peak ground velocities and accelerations that correspond to 100 years return period on firm ground in Mexico. These maps form part of a set that was obtained through application of the criteria described in this chapter. Because the ratio of peak ground accelerations and velocities does not remain constant throughout a region, the corresponding design spectra will not only vary in scale but also in shape (frequency content); in other words, seismic risk will usually have to be expressed in terms of at least the values of two parameters (for instance, as in this case, peak ground accelerations and velocities that correspond to various risk levels (return periods)).

5.3 Microzoning

Implicit in the above criteria for evaluation of regional seismicity is the adoption of intensity attenuation expressions valid on firm ground. Scatter of actual intensities with respect to predicted values was ascribed to differences in source mechanisms. propagation paths, and local site conditions; at least the latter group of variables can introduce systematic deviations in the ratio of actual to predicted intensities; and geological details may significantly alter local seismicity in a small region, as well as energy radiation patterns, and hence regional seismicity in the neighbourhood. These systematic deviations are the matter of microzoning, that is, of local modification of risk maps similar to Figs. 19 and 20.

Most of the effort invested in microzoning has been devoted to study of the influence of local soil stratigraphy on the intensity and frequency content of earthquakes (see Chapter 4). Analytical models have been practically limited to response analysis of stratified formations of linear or nonlinear soils to vertically traveling shear waves. The results of comparing observed and predicted behavior have ranged from satisfactory (Herrera et al., 1965) to poor (Hudson and Udwadia, 1972).

Topographic irregularities, as hills or slopes of firm ground formations underlying sediments, may introduce significant systematic perturbations in the surface motion, as a consequence of wave focusing or dynamic amplification. The latter effect was probably responsible for the exceptionally high accelerations recorded at the abutment of Pacoima dam during the 1971 San Fernando earthquake.

Present practice of microzoning determines seismic intensities or design parameters in two steps. First the values of those parameters on firm ground are estimated by

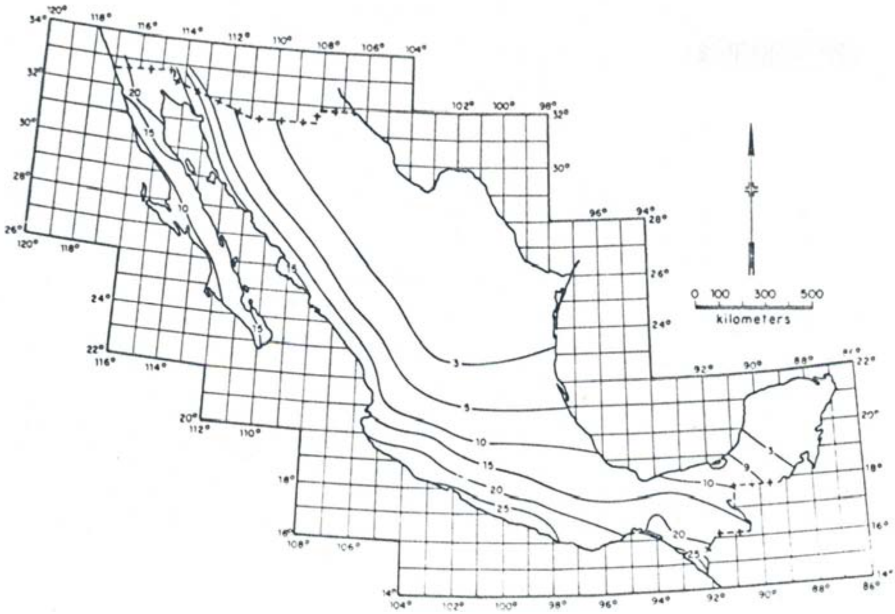

Figure 19. Peak ground velocities with return period of 100 years (cm/sec)

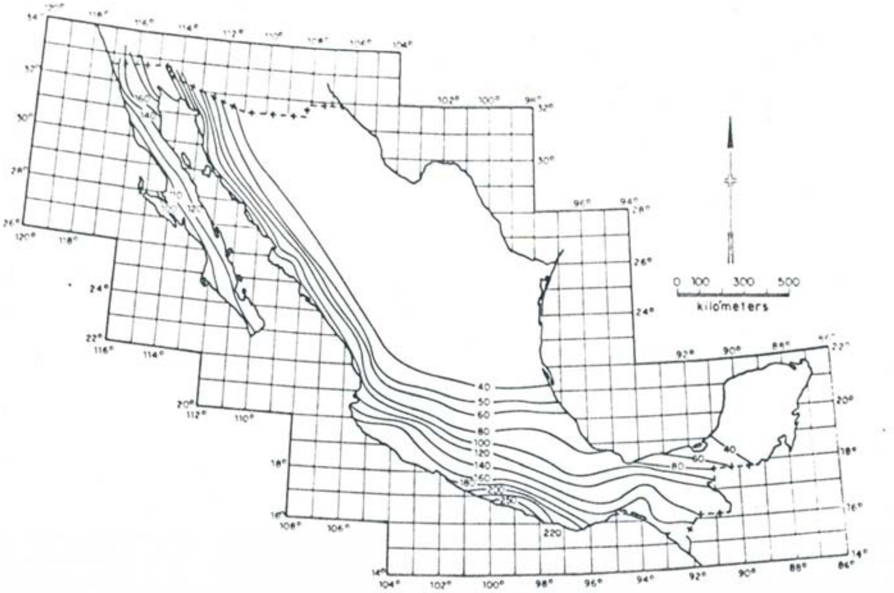

Figure 20. Peak ground accelerations with return period of 100 years (cm/sec^2)

means of suitable attenuation expressions and then they are amplified according to the properties of local soil; but this implies an arbitrary decision to which seismic risk is very sensitive: selecting the boundary between soil and firm ground. A specially difficult problem stems when trying to fix that boundary for the purpose of predicting the motion at the top of a hill or the slope stability of a high cliff (Rukos, 1974).

It can be concluded that rational formulation of microzoning for seismic risk is still in its infancy and that new criteria will appear that will probably require intensity attenuation models which include the influence of local systematic perturbations. Whether these models are available or the two-step process described above is acceptable, intensity-recurrence expressions can be obtained as for the unperturbated case, after multiplying the second member of eq. 34 by an adequate intensity-dependent corrective factor.

References

Aki, K., 1963. *Some Problems in Statistical Seismology*. University of Tokyo, Geophysical Institute.

Allen, C.R., 1969. Active faulting in northern Turkey. *Calif. Inst. Tech., Div. Geol. Sci., Contrib.* 1577.

Allen, C.R., St. Amand, P., Richter, C.F. and Nordquist, J.M., 1965. Relationship between seismicity and geologic structure in the southern California region. *Bull. Seismol. Soc. Am.*, 55 (4): 753-797.

Ambraseys, N.N., 1973. Dynamics and response of foundation materials in epicentral regions of strong earthquakes. *Proc. 5th World Conf. Earthquake Eng., Rome.*

Ananiin, I.V., Bune, V.I., Vvedenskaia, N.A., Kirillova, I.V., Reisner, G.1. and Sholpo, V.N., 1968. *Methods of Compiling a Map of Seismic Regionalization on the Example of the Caucasus.* C. Yu. Schmidt Institute of the Physics of the Earth, Academy of Sciences of the USSR, Moscow.

Benjamin, J.R. and Cornell, C.A., 1970. *Probability, Statistics and Decision for Civil Engineers.* McGraw-Hill, New York.

Ben-Menahem, *A.,* 1960. Some consequences of earthquake statistics for the years 1918-1955. *Gerlands Beitr. Geophys.,* 69: 68-72

Bollinger, G.A., 1973. Seismicity of the southeastern United States. *Bull. Seismol. Soc. Am.,* 63: 1785-1808.

Bolt, B.A., 1970. Causes of earthquakes. In: R.L. Wiegel (editor), *Earthquake Engineering.* Prentice-Hall, Englewood Cliffs.

Brune, J.N., 1968. Seismic moment, seismicity and rate of slip along major fault zones. *J. Geophys. Res.,* 73: 777-784.

Burridge, R. and Knopoff, L., 1967. Model and theoretical seismicity. *Bull. Seismol. Soc. Am.,* 57: 341-371.

Cornell, C.A. and Vanmarcke, E.H., 1969. The major influences on seismic risk. *Proc. 4th World Conf. Earthquake Eng. Santiago.*

Crouse, C.B., 1973. Engineering studies of the San Fernando earthquake. *Calif. Inst. Technol., Earthquake Eng. Res. Lab.* Rep. 73-04.

Cox, D.F. and Lewis, P.A.W., 1966. *The Statistieal Ana/ysis of Series of Euents.* Methuen, London.

Davenport, A.G., 1972. A statistical relationship between shock amplitude, magnitude and epicentral distance and its application lo seismic zoning. *Univ. Western Ontario, Faculty Eng. Sci.,* BLWT-4-72.

Davies, G.F. and Brune, J.N., 1971. Regional and global fault slip rates from seismicity. *Nature,* 229: 101-107.

Drakopoulos, J.C., 1971. A statistical model on the occurrence of aftershocks in the area of Greece. *Bull. Int. Inst. Seismol. Earthquake Eng.,* 8: 17-39.

Esteva, L., 1968. Bases para la formulación de decisiones de diseño sísmico. *Natl. Univ. Mexico, Inst. Eng. Rep.* 182.

Esteva, L., 1969, Seismicity prediction: a bayesian approach. *Proc. 4th World Conf. Earthquake Eng. Santiago.*

Esteva, L., 1970. Consideraciones prácticas en la estimación bayesiana de riesgo sísmico. *Natl. Univ. Mexico, Inst. Eng., Rep.* 248.

Esteva, L., 1974. Geology and probability in the assessment of seismic risk. *Proc. 2nd Int. Congr. Int. Assoc. Eng. Geol., Sao Paulo.*

Esteva, L. and VilIaverde, R., 1973. Seismic risk, design spectra and structural reliability. *Proc. 5th World Conf. Earthquake Eng., Rome,* pp. 2586-2597.

Figueroa, J., 1963. lsosistas de macrosismos mexicanos. *Ingeniería,* 33 (1): 45-68.

Gaisky, V.N., 1966. The time distribution of large, deep earthquakes from the Pamir Hindu-Kush. *Dokl. Akad. Nauk Tadjik S.S.R.,* 9 (8): 18-21.

Gaisky, V.N., 1967. On similarity between collections of earthquakes, the connections between them, and their tendency to periodicity. *Fiz. Zemli,* 7: 20-28 (English transl., pp. 432-437).

Gajardo, E. and Lomnitz, C., 1960. Seismic provinces of Chile. *Proc. 2nd World Conf. Earthquake Eng., Tokyo,* pp. 1529-1540.

Gutenberg, B. and Richter, C.F., 1954. *Seismicity of the Earth.* Princeton University Press, Princeton.

Gzovsky, M.G., 1962. Tectonophysics and earthquake forecasting. *Bull. Seismol. Soc. Am.,* 52 (3): 485-505.

Herrera, l., Rosenblueth, E. and Rascón, O.A., 1965. Earthquake spectrum prediction for the Valley of Mexico. *Proc. 3rd Int. Conf. Earthquake Eng., Auckland and Wellington,* 1: 61-74.

Housner, G.W., 1969. Engineering estimates of ground shaking and maximum earthquake magnitude. *Proc. 4th World Conf. Earthquake Eng., Santiago.*

Hudson, D.E., 1971. *Strong Motion Instrumental Data on the San Fernando Earthquake of February 9,* 1971. California Institute of Technology, Earthquake Engineering Research Laboratory.

Hudson, D.E., 1972a. Local distributions of strong earthquake ground shaking. *Bull. Seismol. Soc. Am.,* 62 (6).

Hudson, D.E., 1972b. *Analysis of Strong Motion Earthquake Accelerograms, III, Response Spectra, Part A.* California Institute of Technology, Earthquake Engineering Research Laboratory.

Hudson, D.E. and Vdwadia, F.E., 1973. Local distribution of strong earthquake ground motions. *Proc. 5th World Conf. Earthquake Eng., Rome,* pp. 691-700.

Kaila, K.L. and Narain, H., 1971. A new approach for preparation of quantitative seismicity maps as applied to Alpide Belt-Sunda Arc and adjoining areas. *Bull. Seismol. Soc. Am.,* 61 (5): 1275-1291.

Kaila, K.L., Gaur, V.K. and Narain, H., 1972. Quantitative seismicity maps of India. *Bull. Seismol. Soc. Am.,* 62 (5): 1119-1132.

Kaila, K.L., Rao, N.M. and Narain, H., 1974. Seismotectonic maps of southwest Asia region comprising eastern Turkey, Caucasus, Persian Plateau, Afghanistan and Hindu-kush. *Bull. Seismol. Soc. Am.,* 64 (3): 657-669.

Kelleher, J., Sykes, L. and Oliver, J., 1973. Possible criteria for predicting earthquake locations and their application to major plate boundaries of the Pacific and the Caribbean. J. *Geophys. Res.,* 78 (14): 2547-2585.

Knopoff, L., 1964. The statistics of earthquakes in southern California. *Bull. Seismol. Soc. Am.,* 54: 1871-1873.

Lomnitz, C., 1966. Magnitude stability in earthquake sequences. *Bull. Seismol. Soc. Am.,* 56: 247-249.

Lomnitz, C. and Hax, A., 1966. Clustering in aftershock sequences. In: J.S. Steinhart and T. Jefferson Smith (editors). *The Earth Beneath the Continents.* Am. Geophys. Union, pp. 502-508.

McGuire, R.K., 1974. Seismic structural response risk analysis incorporating peak response regressions on earthquake magnitude and distance. *Mass. Inst. Technol., Dep. Civ. Eng.,* R74-51.

Merz, H.A. and Camell, C.A., 1973. Seismic risk analysis based on a quadratic magnitude-frequency law. *Bull. Seismol. Soc. Am.,* 63 (6): 1999-2006.

Milne, W.G. and Davenport, A.G., 1969. Earthquake probability. *Proc. 4th World Conf. Earthquake Eng., Santiago.*

Mogi, K., 1962. Study of elastic shocks caused by the fracture of heterogeneous materials and its relations to earthquake phenomena. *Bull. Earthquake Res. Inst. Tokyo,* 40: 125-173.

Molnar, P. and Sykes, L.R., 1969. Tectonics of the Caribbean and Middle America regions from focal mechanisms and seismicity. *Geol. Soc. Am. Bull.,* 80: 1639.

Newark, N.M. and Rosenblueth, E., 1971. *Fundamentals of Earthquake Engineering.* Prentice-HaIl, Englewood Cliffs.

Omori, F., 1894. On the aftershocks of earthquakes. J. *Coll. Sci. Imp. Univ. Tokyo,* 7: 111-200.

Parzen, E., 1962. *Stochastic Processes.* Holden Day, San Francisco.

Petrushevsky, B.A., 1966. *The Geological Fundamentals of Seismic Zoning.* Scientific Translation Service, order 5032, Ann Arbor, USA.

Raiffa, H. and Schlaifer, R., 1968. *Applied Statistical Decision Theory,* MIT Press.

Rosenblueth, E., 1964. Probabilistic design to resist earthquakes. *Am. Soc. Civ. Eng.,* J. *Eng. Mech. Div.,* 90 (EM5): 189-249.

Rosenblueth, E., 1969. Seismicity and earthquake simulation. *Rep. NSF-UCEER Conf. Earthquake Eng. Res., Pasadena,* pp. 47-64.

Rosenblueth, E., 1975. *Point Estimates for Probability Moments.* National University of Mexico, lnstitute of Engineering, Mexico City.

Rosenblueth, E., in preparation. Optimum design for infrequent disturbances.

Rukos, E., 1974. *Análisis dinámico de la margen izquierda de Chicoasén.* National University of Mexico, Institute of Engineering, Mexico City.

Salt, P.E., 1974. Seismic site response. *Bull. N. Z. Natl. Soc. Earthquake Eng.,* 7 (2): 63-77.

Scholz, C.H., 1968. The frequency-magnitude relation of microfracturing and its relation to earthquakes. *Bull. Seismol. Soc. Am.,* 58: 399-417.

Shlien, S. and Toksöz, M.N., 1970. A clustering model for earthquake occurrences. *Bull. Seismol. Soc. Am.,* 60 (6): 1765-1787.

Singh, S.K., 1975. *Mexican Volcanic Belt: Some Comments on a Model Proposed by F. Mooser.* National University of Mexico, Institute of Engineering, Mexico City.

Trifunac, M.D., 1973. Characterization of response spectra by parameters governing the gross nature of earthquake source mechanisms. *Proc. 5th World Conf. Earthquake Eng.*, Rome, pp. 701-704.

Tsuboi, C., 1958. Earthquake province. Domain of sympathetic seismic activities. *J. Phys. Earth.*, 6 (1): 35-49.

Utsu, T., 1961. A statistical study on the occurrence of aftershocks. *Geophys. Mag., Tokyo*, 30: 521-605.

Utsu, T., 1962. On the nature of three Alaska aftershock sequences of 1957 and 1958. *Bull. Seismol. Soc. Am.*, 52: 179-297.

Veneziano, D. and Cornell, C.A., 1973. Earthquake models with spatial and temporal memory for engineering seismic risk analysis. *Mass. Inst. Technol., Dep. Civ. Eng.*

Vere-Jones, D., 1970. Stochastic models for earthquake occurrence. *J. R. Stat. Soc.*, 32 (1): 1-45.

Wallace, R.E., 1970. Earthquake recurrence intervals on the San Andreas Fault. *Geol. Soc. Am. Bull.*, 81: 2875-2890.

Yegulalp, T.M. and Kuo, J.T., 1974. Statistical prediction of the occurrences of maximum magnitude earthquakes. *Bull. Seismol. Soc. Am.*, 64 (2): 393-414. I

DESIGN: GENERAL[1]

1. Nature and objectives of earthquake resistant design

Engineering design is rooted in society's need to optimize. It implies considering alternate lines of action, assessing their consequences and making the best choice. In earthquake engineering, every alternate line of action includes the adoption of both a structural system and a seismic design criterion, while assessing consequences implies estimating structural response and hence the expected cost of damage. The choice is based on comparison of initial, maintenance and repair costs for the various alternatives. However obvious these concepts may appear to the authors of design codes, they are often not explicit in those codes and hence they are not always present in the minds of those who apply design prescriptions to practical problems. Equally concealed within the regulations of seismic design codes are the approximations implicit in conventional criteria for the prediction of structural response: the accuracy of their predictions is often strongly dependent on the type of structural system considered. Base shear coefficients and design response spectra are taken as measures of response parameters, as the latter are usually expressed in terms of accelerations and equivalent lateral forces acting on linear systems. But these variables are no more than indirect measures of system performance during earthquakes: they serve to control the values of more significant variables, such as lateral deflections of actual nonlinear systems, global and local ductilities, and safety margins with respect to instability failure (second-order effects). Because the relations of control variables to actual response are affected by the type and features of the structural system, better designs will be obtained if these relations are understood and accounted for, in contrast with blindly applying codified recommendations. In seismic design more than in any other field of engineering, it is easy to fall on a strict —but blind— application of the most advanced regulations and yet to produce a structure bound to perform poorly. This chapter does not intend to summarize modern design specifications; it aims, instead, at discussing the main concepts on which they are based, analyzing their virtues and their weaknesses, and stating the conditions for which acceptable results are to be expected.

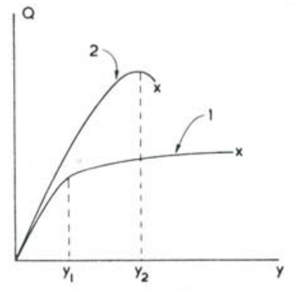

Figure 1. Ductile and brittle systems

Codified values of design intensities and of allowable values of response control variables stem from formal or informal cost-benefit studies. As implicit in these studies,

[1] First published in Chapter 3 of Earthquake Resistant Design, editor Rosenblueth., *Pentech Press*, London (1977).

the general goal of optimization can be expressed in terms of direct, particular objectives: seismic design aims at providing adequate safety levels with respect to collapse in the face of exceptionally intense earthquakes, as well as with respect to damage to adjacent constructions; it also seeks to protect structures against excessive material damage under the action of moderate intensity earthquakes, to ensure simplicity of the required repair, reconstruction or strengthening works in case damage takes place, and to provide protection against the accumulation of structural damage during series of earthquakes. Finally, safety and comfort of occupants and of public in general is to be preserved by ensuring that structural response during moderate intensity earthquakes will not exceed given tolerance levels and that panic will not occur during earthquakes of moderate and high intensity, particularly in buildings where frequent gathering of people is expected.

Achievement of the foregoing objectives requires much more than dimensioning structural members for given internal forces. It implies explicit consideration of those objectives and of the problems related with nonlinear structural response and with the behavior of materials, members, and connections when subjected to several cycles of high-load reversals. It implies as well identifying serviceability conditions and formulating acceptance criteria with respect to them.

2. Structural response and control variables

2.1 Ductility and strength

A structural system is said to be ductile if it is capable of undergoing substantial deformations at nearly constant load, without suffering excessive damage or loss of strength in face of subsequent load applications. Curves 1 and 2 in Figure 1 show typical load Q vs. deflection y relations for first load application in ductile and brittle systems, respectively. Curve 1 corresponds to the response under lateral load of an adequately detailed reinforced concrete frame where slenderness effects are not significant; curve 2 is typical of weakly reinforced hollow block masonry. But when the effect of several loading cycles has to be considered, ductile behavior cannot be inferred from looking only at curves such as these for first load application: damage produced during the first cycles may impair the system's energy absorption capacity for subsequent cycles, and stiffness can degrade, as in Figure 2b, typical of plain masonry shear walls confined by reinforced concrete frames[1]. In this case, stiffness degradation is associated with diagonal tension cracking of the infilling wall panel and the ensuing residual strains. Practically stable hysteretic cycles found for structural steel joints[2] as shown in Figure 2a are synonymous with negligible damage.

As shown in Section 2.2, the ability of structural systems to respond to dynamic excitations according to load deflection curves similar to Figure 2a provides support to conventional seismic design criteria, which require structures to sustain only a fraction of the lateral forces they should have to resist would they be demanded to remain within their linear range of behavior during strong earthquakes. Thus, safety against collapse can be provided by making a structure strong, by making it ductile, or by designing it for an economic combination of both properties. For some types of materials and structural members, ductility is difficult to achieve, and economy dictates designing for relatively high lateral forces; for others, providing ductility is much cheaper than providing lateral capacity, and design practice reflects this. But material ductility does not necessarily imply system ductility, as P-Δ effects (that is, interaction between lateral deflections and internal forces produced by gravity loads acting on the deformed structure)

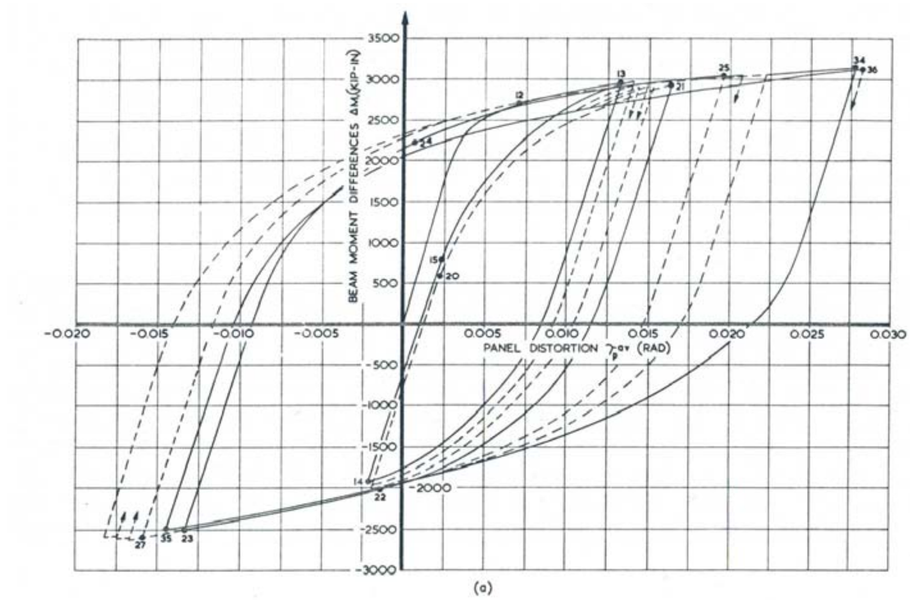

Figure 2a. Non degrading stiffness (after Krawinkler et al.[2])

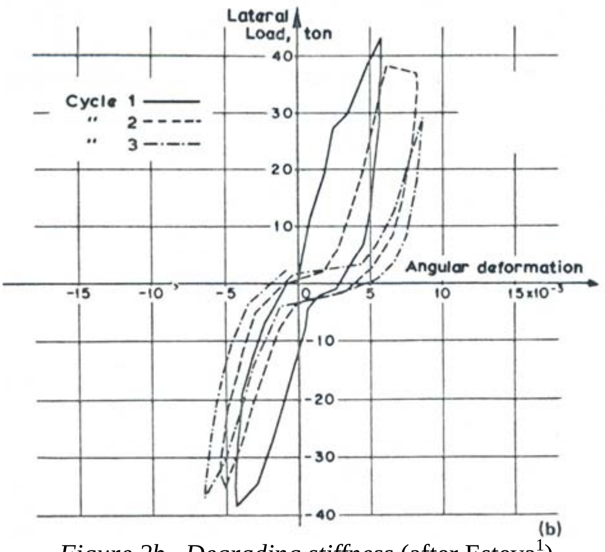

Figure 2b. Degrading stiffness (after Esteva[1])

can lead to instability failure when the effective lateral stiffness is too low (see Figure 3).

Nonlinear ductile behavior of complex systems usually stems as a consequence of *local* or *concentrated* ductile deformations that take place at those particular sections of a given structure where yielding strains are reached (Figure 4). Numerically, local ductility can be expressed either as the ratio of total to yield-limit curvatures at a given section or as the ratio of total to yield-limit rotation at a member end[3]. *Global* or *overall* ductility is a property of a load-deformation curve expressed in terms of the resultant of

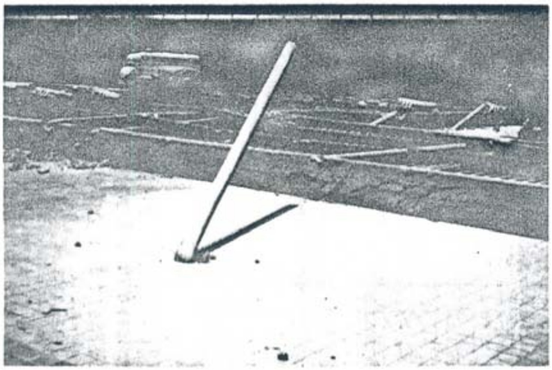

Figure 3. Instability failure

external loads acting on a large portion of a given system. For instance, building frames are often dealt with as shear systems for the purpose of estimating their dynamic nonlinear response to seismic excitation. Global or overall ductilities can then be expressed in terms of the curves tying shear forces with lateral distortions. Numerical values of local ductilities determined by the above alternate criteria do not coincide among themselves, nor does overall ductility at a given story idealized as a segment of a shear beam coincide with the values of concentrated ductilities developed at the corresponding locations of the story, as overall ductility is a function of the ratio of the contributions to story distortion of concentrated ductile deformations and distributed elastic strains. Because beams are usually capable of developing larger ductilities than columns subjected to significant compressive loads, many building frames are designed under the 'strong column-weak girder' criterion, according to which different load factors are adopted for different internal forces so as to make yielding much more likely at beam- than at column-ends. Under these conditions, significant coupling is introduced between nonlinear deformations of adjacent stories, and the shear-beam model may cease to apply. Whether the model in question strictly applies or not, nominal story ductilities are only indicators of their local values, and features contributing to ductility concentrations have to be held in mind while designing. The relation between local and overall ductility is illustrated for a simple frame in Figure 4. Figure 4b shows the ideal case where moment-curvature graphs at critical sections are elasto-plastic and yielding is reached simultaneously at the four column-ends. If the frame is forced to undergo additional

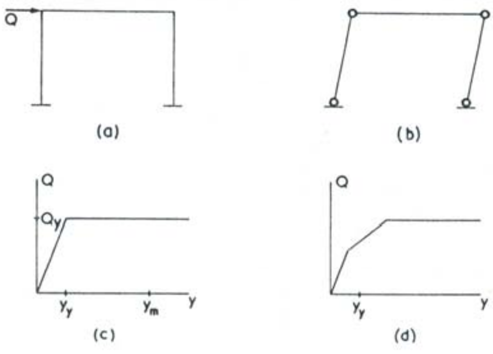

Figure 4. Local and general ductility under lateral loads: (*a*) *loads*, (*b*) *failure mechanism*, (*c*) *simultaneous yielding*, (*d*) *sequential yielding*

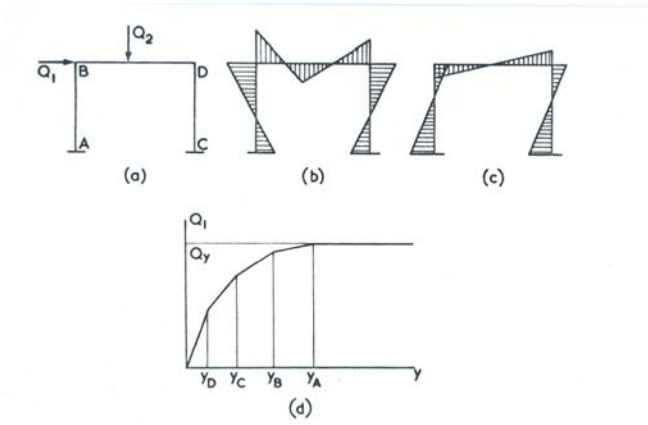

Figure 5. Inelastic behaviour under vertical and lateral loads: (*a*) *loads*, (*b*) *vertical-load moments*, (*c*) *lateral load moments*, (*d*) *resulting load deflection curve*

deformations at constant load, local curvatures at the yielding locations will increase and the lateral deflection of the frame will grow from y_y to y_m (Figure 4c).

Local ductility can be measured by the ratio of the final and yielding values of the curvatures mentioned. Overall ductility is given by y_m/y_y and is a function of local ductility and of the lengths of the member segments along which curvatures will be greater than their values at yielding. Those lengths are functions of the type of material, the local details and the relative variation of bending moment ordinates and structural section strength.

Consider now a frame subjected to a constant system of vertical loads Q_2 (Figure 5) that produce an initial state of internal forces. If a system Q_1 of lateral loads is gradually applied, the ordinates of bending moment diagrams (b) and (c) will be additive at some locations and subtractive at others. Yielding will occur sequentially, say in the order DCBA, giving place to the load-deflection curve shown in Figure 5d. Local ductilities will differ at the mentioned locations; they will depend, among other things, on the order in which they reached their yield moments. Where axial loads are important, they can have a significant influence on these moments.

The following sections describe the quantitative relationships tying ductility demands with strength and stiffness in simple structural systems, as well as some problems found when trying to extrapolate those relationships to complex systems, representative of those encountered by engineers in their design practice.

Dynamic response of simple non linear systems. A usual idealization of ductile structures is the elastoplastic system with load-deflection curve as shown in Figure 6b, with stiffness k in the linear range of behavior, coefficient of viscous damping c, and top mass m. When the system responds to a strong earthquake, the maximum relative displacement D will exceed the yield deformation y_y, while the maximum lateral force will remain at the yield value Q_y if P-Δ. effects are neglected. Failure is said to occur if the ductility demand D/y_y is greater than the available ductility μ. Figure 7 is a plot of yield deformations required to make ductility demands equal to available ductility for different values of this parameter, for the range of natural periods (computed in terms of the initial tangent stiffness of the elastoplastic system) most significant in practice, and for damping ratio $\zeta = 0.5c\ (km)^{-1/2}$ equal to 0.02. Pseudos accelerations kD/m can be read on the proper scale in the same plot. Inspection of these curves shows that, provided the

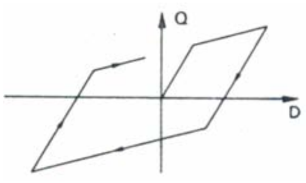

(a) Bilinear

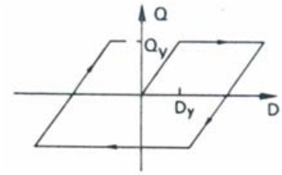

(b) Symmetric elastoplastic

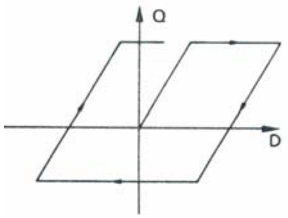

(c) Asymmetric elastoplastic

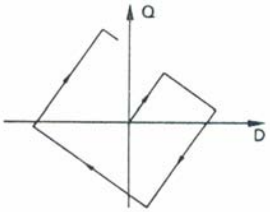

(d) Ustable

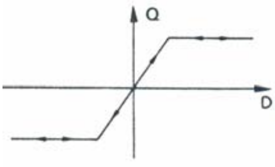

(e) Yielding elastic

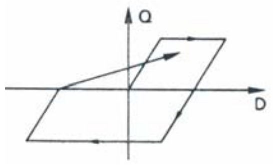

(f) Degrading

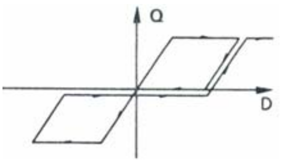

(g) Slip type

Figure 6. Models of nonlinear behaviour

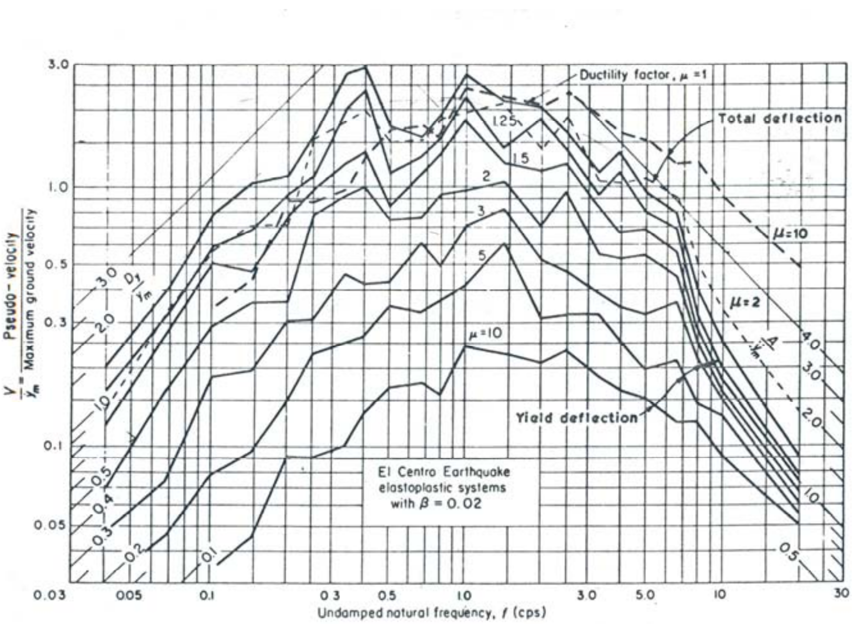

Figure 7. Deformation spectra for elastoplastic systems with 2% critical damping subjected to the 1940 El Centro earthquake (after Newmark[33])

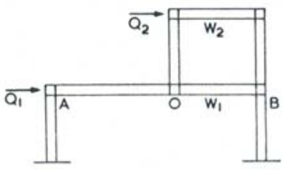

Figure 8. Structure with asymmetric load deflection curve

natural period is not too short, required yield deformations —and hence required base shear coefficients— vary inversely with ductility.

The same conclusion is reached if one reads along the scale of spectral pseudo accelerations. But this favorable influence of ductility in reducing the required base-shear coefficient is less pronounced in the range of short natural periods, say shorter than $2\pi v/a$, where v and a are peak values of ground velocity and acceleration, respectively: as the system becomes stiffer, T tends to zero and spectral pseudo acceleration tends to a, regardless of μ, assuming that μ has to remain bounded. Actual values of lateral relative displacements are equal to μy_y, which means that, for moderate and long natural periods, those displacements are nearly insensitive to μ, while for very short natural periods they tend to be proportional to μ. The results just described can be expressed as follows: if a simple elastoplastic system with initial natural period T is to develop a ductility factor μ during an earthquake, the required base shear coefficient can be obtained by applying a reduction factor to the corresponding spectral value for an elastic system having equal natural period and damping; for moderate and long values of T, the reduction factor is approximately equal to μ^{-1}, while for short natural periods it will be comprised between μ^{-1} and 1. Relative displacements will equal μ times those of an elastic system subjected to the reduced base shear; that is, they will be approximately equal to those of the elastic system subjected to the actual, unreduced earthquake, if T is not too short, or to μ times the latter values if T is nearly zero. This is shown by a comparison of the dashed and full lines in Figure 7.

Similar conclusions have been derived from other earthquake records obtained on firm ground. Although these conclusions can be expected to be qualitatively valid for soft soil conditions, corresponding approximate quantitative rules are still to be derived.

The foregoing conclusions have to be modified when considering systems whose response cannot be idealized as elastoplastic. Other usual idealizations are depicted in Figures 6e-f. Lateral strengths required for not exceeding given ductility demands in these systems are as a rule greater in 10 to 50% than those valid for the conventional elastoplastic system[5-9]. In the asymmetric elastoplastic case, yield strength is different for each direction of load application. It occurs, for instance, as a consequence of gravity loads giving place to increased or decreased lateral capacity of the second story of the system shown in Figure 8, depending on whether the vertical reaction to force Q_2, transmitted to beam AB at O, is directed upwards or downwards. Slip-type curves (Figure 9) usually stem as a result of lateral loads being carried by elements such as cross-braces or tie-cables, which can only carry tensile stresses. Yielding elastic curves are close approximations to the behavior of some prestressed concrete beams, subjected to antisymmetric end moments: these curves are often characterized by very narrow hysteretic loops. Degrading curves are frequently found in systems where a significant portion of the lateral capacity is due to members built with brittle materials and where no special precautions have been taken to prevent excessive damage in each cycle of

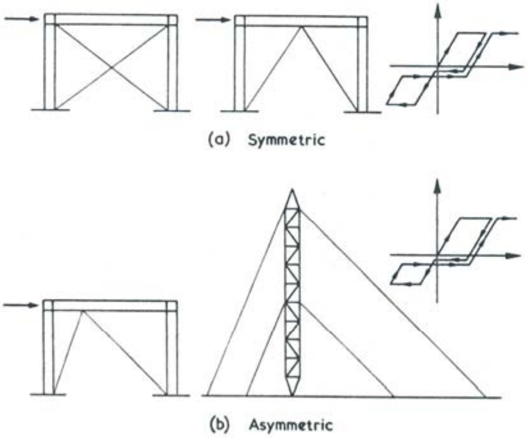

Figure 9. Slip-type systems

load application. Such is the case, for instance, in masonry shear diaphragms or poorly detailed reinforced concrete frames.

Unstable curves (Figure 6d are produced by the influence of significant vertical loads acting on the displacements of the deformed structure. The influence of instability effects on ductility demands and on safety against collapse can be much more drastic than that associated with the features of the curves previously discussed, and is usually controlled in design practice by the specification of amplification factors for lateral deflections and internal forces that account for increments associated with second-order effects.

Ductility demands in complex systems. Local ductility demands vary from point to point. Their distribution depends on that of local strength throughout the system, with significant interaction taking place between energy dissipation at different sections. The general patterns of ductility demands in complex systems have been studied almost exclusively in building frames, idealized either as shear beams or as assemblages of beams and columns where yielding is restricted to occur at plastic hinges located at the bar ends. Some results are plotted in Figures 10 and 11 for shear beams and frame systems, respectively. Each set of results corresponds to a different set of simulated earthquakes with frequency content similar to that observed under normal conditions on firm ground in the western coast of the United States. Structures were designed for the average ordinates, with respect to each set of motions, of the elastoplastic response spectrum corresponding to a ductility factor of 4. The systems in Figure 10 were designed for the contribution of the fundamental mode of vibration alone, while that in Figure 11 was designed for the superposition of its four natural modes, in accordance with the criterion of square root of sum of squares advocated in Ref. 10. The load factor was in all cases taken as unity. Ductilities were expressed in terms of story sway for the shear beams and of local curvature at hinges for the framed system; thus, their absolute values cannot be compared. Their variability throughout the building is evident; however, as is the occurrence of large ductilities at the upper portion of systems for which the response associated with higher natural modes was neglected.

More pronounced variability in ductility demands has been observed in some shear systems with fundamental periods shorter than the dominant period of the ground motion, and in those whose safety factors with respect to design story shears vary

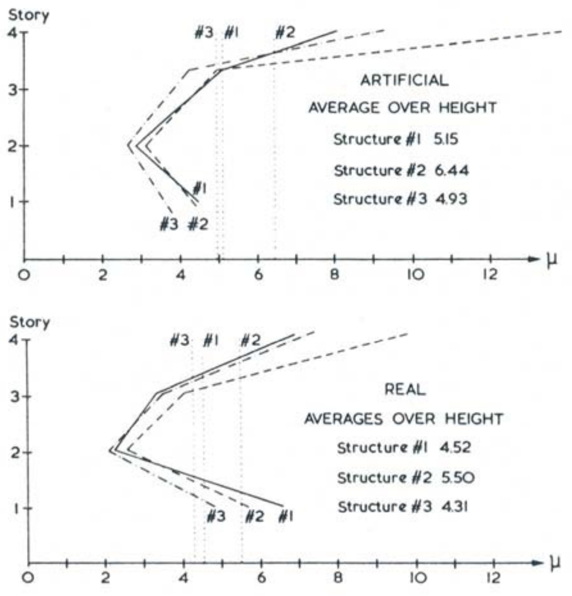

Figure 10. Ductility demands in shear systems subjected to simulated and real earthquakes (after Frank et al.[3])

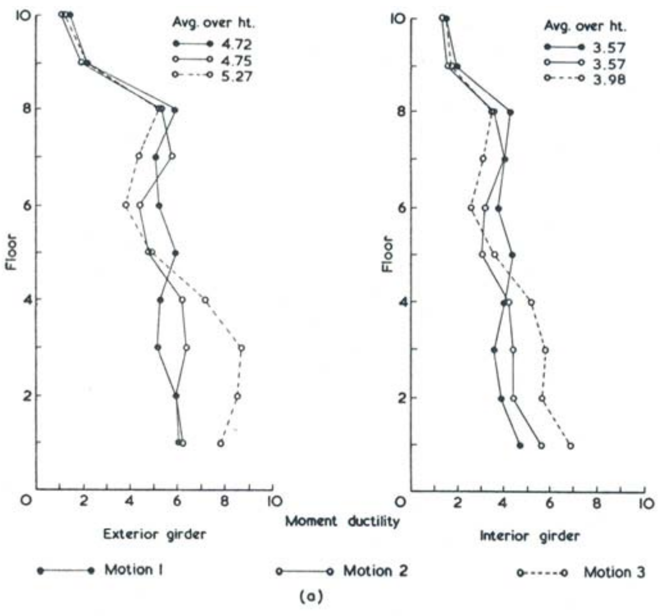

Figure 11a. Maximum girder ductility factors for gravity and earthquake design

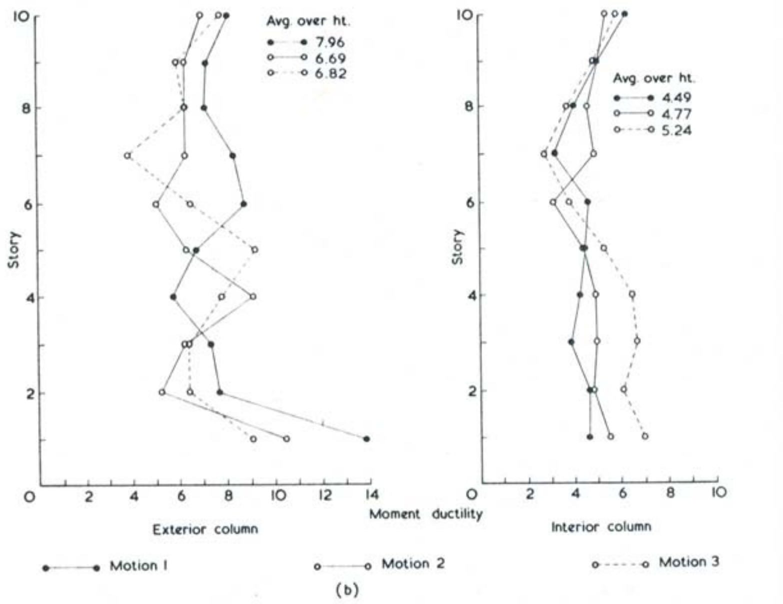

Figure 11b. Maximum column ductility factors for gravity and earthquake design

significantly through the building height[11]. Such variability may be a consequence of architectural requirements, which often lead to some stories possessing elements stronger than they need to be in order to comply with the seismic coefficient adopted. When this happens, the relative contribution of each story to the hysteretic dissipation of kinetic energy changes, and those stories possessing the smallest safety factors are subjected to higher ductility demands than if the safety factor were uniform throughout the structure. When these increased ductility demands cannot be met with adequate yielding capacity, the lateral force coefficient has to be raised. Because of the large displacements implied, slenderness effects may become especially significant.

2.2 Stiffness and deformations

Structural stiffness controls natural period and hence seismic forces. The latter are lower for longer periods, that is, for small stiffnesses, but then displacements and deformations may become excessive. In addition to ensuring adequate safety factors against collapse, seismic criteria should aim at controlling deformations, because they are directly responsible for damage to nonstructural elements, impact with adjacent structures, panic and discomfort.

Stiffness is also the main variable controlling safety against instability. Lateral displacements and internal forces produced by horizontal ground motion are amplified by interaction between gravity loads and the displacements mentioned. The amplification function varies in a nonlinear fashion with respect to lateral stiffness and reaches very high values when the latter variable approaches a certain critical value. In ductile structures, safety against instability failure is a function of effective stiffness, that is, of the slope of the line joining the origin of the force-deflection graph with the point representing the maximum deflection and the corresponding lateral force (in elastoplastic

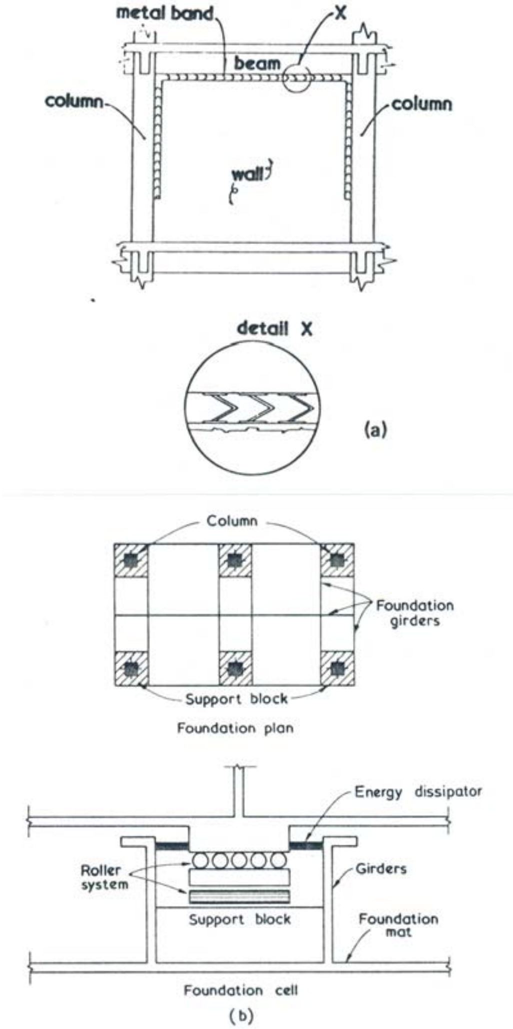

Figure 12. *Energy-absorbing and shock-isolating devices.* (a) *Metal band to protect partitions* (*after Newmark and Rosenblueth*[10]). (b) *Roller support* (after Ruiz, et al.[15])

systems, this is the same as the value of the tangent initial stiffness divided by the ductility factor). The increasing rate of variation of the amplification function mentioned with respect to lateral stiffness when the latter is made to approach its critical value hinders the possibility of designing for very small lateral forces through the construction of very ductile structures (Figure 3).

2.3 Damage and energy absorption

Ductile hysteretic response provides a manner of transforming and dissipating the kinetic energy imparted to a structure through its base. Such response usually implies some degree of damage, and possibly the deterioration of the system to withstand future severe earthquakes. Damage may accumulate during successive events, and the system's capacity may be seriously impaired. Decisions concerning the extent and level of damage that it is advisable to admit are mostly of an economic nature. In general, the degree of structural damage and its harmful effects on future performance can be controlled at some cost through selection of adequate materials and construction details, as described in Chapter 8. Damage to nonstructural members can be prevented through their isolation from the deformations of the structure. However, economy may dictate taking advantage of energy dissipation associated with damage. Architectural elements or ad hoc devices can be used for this purpose (Figure 12). In either case, considerations on facility of repair or replacement should form part of design.

The use of metal bands around partitions as shown in Figure 12a may serve the purposes of limiting the lateral forces that the structure will transmit to the partitions and at the same time taking advantage of the capacity of the partitions to resist such forces and making use of the energy absorbing capacity of the bands[10]. In other cases, designing for significant damage on partitions may prove to be attractive.

Anchor bolts that yield during severe ground motion can provide protection to slender chimney stacks against local buckling or overall bending failure[12], at the expense of nonrecoverable elongations. Adequate performance of anchor bolts during sequences of earthquakes demands adjusting nuts after each event and replacing those bolts for which the sum of previous residual elongations is excessive. (See Section 4.8).

Large concentrated deformations are frequent at spandrel beams connecting coupled shear-walls (Figure l6b) or at the ends of beams meeting shear-wall edges, and hence constitute adequate locations for energy-absorbing devices.

Partial isolation of building foundations from the ground motion has been advocated as a means to control structural response and nonstructural damage[13-15]. Isolating systems may consist of pads of very flexible material, assemblages of rollers or the like. Relative displacements between foundation and ground can be controlled by means of passive energy absorbing devices located at the ground-foundation interface (Figure l2b).

3. Design principles

3.1 Design requirements and basic priciples

The art of designing for eartbquakes does not consist in producing structures capable of withstanding given sets of lateral forces, although that capability is part of a sound design. It involves producing systems characterized by an optimum combination of properties such as strength, stiffness, energy-absorption, and ductile-deformation capacities that will enable them to respond to frequent, moderate earthquakes without suffering significant damage and to exceptional, severe earthquakes without endangering their own stability, their contents, or human life and limb. Achievment of this purpose means much more than application of codified rules; it demands understanding of the basic factors that determine the seismic response of structures, as well as ingenuity to produce systems with the required properties.

Codified requirements set optimum design levels in accordance with implicit cost-benefit analyses that balance initial construction costs with expected costs of damage and failure. They also recommend criteria and algorithms deemed adequate for the evaluation of the design actions tied to the optimum design levels. These recommendations serve the purpose of implementing sufficiently simple design criteria at the expense of narrowing the range of conditions where they give place to accurate predictions of response. It is the role of the engineer to recognize the possible deviations and to apply basic principles before trying to extrapolate general requirements to the particular problem at hand.

Static criteria of seismic design are stated in terms of the coefficients by which the masses of each structure have to be multiplied in order to produce the set of lateral forces to be designed for; but in most cases those coefficients stem from the dynamic response of linear shear beams possessing approximately uniform distributions of mass and stiffness. The meaning of the mentioned lateral forces must be clearly understood: they aim at providing a diagram of story shears that correspond to consistent safety levels; but they fail to predict other significant effects. Thus, reduction factors for overturning moment are required to account for the fact that maximum story shears do not occur simultaneously, and special algorithms have to be used to determine local effects, such as response of appendages and diaphragm stresses in floor systems, corresponding to safety levels consistent with those intended for story shear.

Dynamic criteria of design usually require performing a modal analysis, and hence variability in masses and stiffnesses is accounted for in the computation of the lateral force coefficients. Modal analysis however fails to predict the influence of nonlinear behavior except for some simple cases in which hysteretic dissipation or energy is distributed uniformly throughout the system and it is uncapable of predicting ductility-demand concentrations and nonlinear interactions for the simultaneous action of several ground motion components. Whatever design criterion is adopted, departures of actual conditions from those leading to uniform energy dissipation have to be recognized and their possible influence on behavior evaluated.

Given a set of design requirements and response control variables, a criterion of structural analysis capable of predicting with sufficient accuracy those variables must be applied to determine internal forces and deformed configuration. Simultaneous action of the significant components of ground motion has to be considered, including a scaling factor applied to each component in order to account for its probable value when the maximum absolute value of their combination takes place (see Chapter 2). The criterion of structural analysis adopted must be such as to recognize the possible concentrations of nonlinear behavior and to attain a sufficiently low probability that they occur at undesirable locations, as a consequence of inaccuracies of that criterion. This means that prediction of displacements and internal forces must account for stiffness and continuity, including all significant deformations; in particular, P–Δ effects must be considered at least by means of an approximate analysis intended to define the desirability of more refined studies. Some building code regulations state simple rules for deciding when P–Δ effects can be disregarded[16]. The contribution of the so-called nonstructural elements to stiffness should not be neglected, unless those elements are properly isolated from the structure or it is shown that they can not be harmful to its behavior.

Attention should be given to inertia forces associated with all significant components of local acceleration, namely angular acceleration (rotational inertia) of umbrella-like canopies or segments of stacks and vertical accelerations of long-span girders in bridges or industrial bents. Both types of acceleration are produced by horizontal, vertical, or rotational ground motion.

Adequate stress paths must be provided in order to guarantee that design forces can be transmitted down to the foundation. Deformability of the substructure and of the ground underlying it must be considered when defining the stiffness matrix of the whole system or the support conditions of the superstructure on the foundation. Distribution of contact pressures between ground and substructure should be computed on the bases that no tensile stresses can be transmitted at the interface, unless special provisions are taken, such as the construction of anchors or tension bearing piles.

Safety of structural and nonstructural elements to withstand the effects of local accelerations should be studied; in particular, overturning of walls and parapets produced by forces normal to their planes must be prevented by adequate reinforcement and anchorage.

3.2 Framing systems

Decisions concerning the selection of a framing system are influenced by many factors; Basic criteria are best illustrated by discussing some typical problems, as done in what follows.

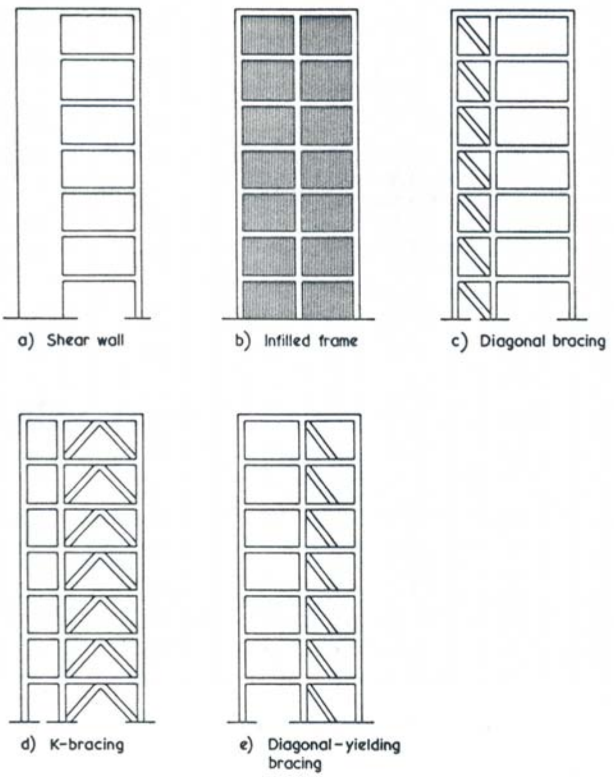

Figure 13. Stiffening elements

Stiffening elements. Continuous frames can usually resist seismic forces by developing rather uniform stress paths. Their main asset is that they can easily be designed and built so as to withstand large ductility demands. However, their efficiency, based on the bending capacity of beams and columns, is lower than that of systems that base their strength on that of elements subjected to simple shear or axial forces. Besides permitting the development of larger lateral capacities without excessive costs, stiffening systems can be decisive in the control of damage associated with lateral distortions. But economic and architectural considerations may preclude the use of these elements in some instances, and they may show significant technical disadvantages in others. In tall build

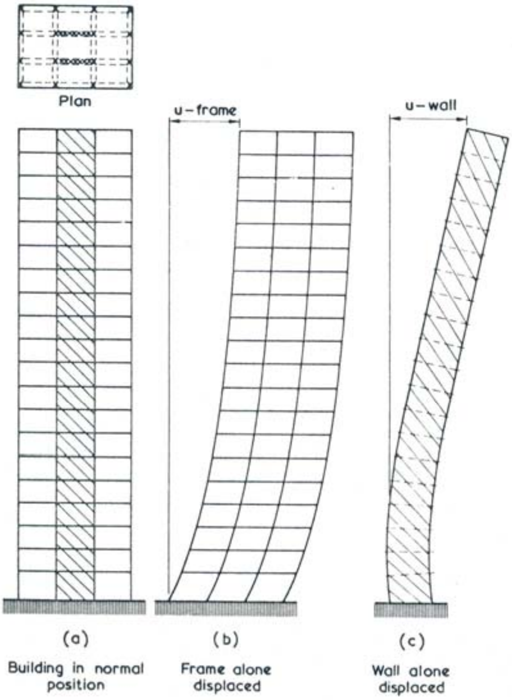

Figure 14. Lateral load response of shear walls and frames (after Newmark[33])

ings, enhanced stiffness is usually provided by diaphragms and cross braces; the former built in reinforced concrete or masonry, the latter in reinforced concrete or steel (Figure 13). Use of cross bracing is usually to be preferred over that of diaphragms in low buildings and industrial bents, except in those instances where the diaphragms are required for architectural reasons. In intermediate and tall buildings the reverse is usually trae, mainly on account of the large cross-sectional dimensions that would be required for the bracing members and of the serious problems posed by their anchorage, particularly in reinforced concrete structures.

The efficiency of cross-braced bays and shear walls is reduced as their aspect ratio (height-to-width ratio) increases. The reason for this can be understood from Figure 14, which compares the deflected shapes of a braced bay or a wall acting as a flexural beam fixed at its base and a continuous frame acting essentially as a shear beam when both are subjected to a system of lateral forces. For equal top deflections, near the bottom the slopes of the flexural beam will be much smaller than those of the shear beam, but near the top the reverse will be true. The greater the aspect ratio of the flexural beam, the more important will be this effect. It follows that, when a system of lateral forces is resisted by the combination of a continuous frame and a slender wall, the latter will take a significant portion of the total story shear in the lower stories, but will fail to do so in the upper ones, as there the wall will tend to lean on the frame, instead of helping it to withstand the total story shear. The occurrence of large rotations of the wall horizontal sections gives place to excessive local deformations and ductility demands at the ends of beams connected to the wall edges. These problems can be aggravated by the occurrence of significant displacements associated with the flexibility of the foundation at the base of the wall.

Figure 15. Efficient shear wall sections

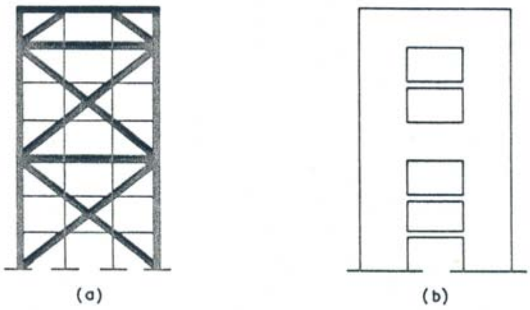

Figure 16. Efficient use of stiffening elements; (a) *cross braces,* (b) *shear walls and spandrel beams*

Adoption of cross sections as shown in Figure 15 can significantly enhance the efficiency of slender shear walls by increasing their flexural stiffness; but the most effective manner of reducing overall bending deflections is to get as wide a portion of a given bay to contribute to overall bending stiffness. In braced systems, this can be accomplished by adopting configurations as shown in Figure l6a. Where architectural requirements force the adoption of a number of separate walls in the same plane, one solution consists in coupling several of them and making them act together by means of sufficiently stiff and strong spandrel beams (Figure 16b); then stems the problem of attaining ductile behavior in these beams (see Chapler 5).

Use of stiffening elements may bring about other problems: the nexibility of the foundation and that of the floor diaphragms may be significant in comparison with that of the stiffening elements and have to be accounted for when obtaining the distribution of internal forces. In-plane deformability of horizontal diaphragms may become very important in buildings long in plan where lateral forces are resisted by shear walls located near the ends of the building plan. Not only stiffness, but also strength of the floor diaphragms in their own plane becomes then a relevant variable.

Symmetry. The distressing influence of asymmetry in structural behavior has been recognized, and perhaps over-emphasized. Efforts to avoid its effects have concentrated on the problem of adjusting stiffnesses so as to avoid torsional eccentricities; but even if computed eccentricities are negligible, important torques can develop, for instance, when high stiffnesses of certain structural members on one end of the building plan are balanced by very dissimilar elements on the other, as the relative values of the computed stiffnesses may be little reliable. In addition, eccentricities of variable magnitude may occur as a consequence of nonlinear behavior, even in those cases where conventional linear analysis predicts no torsional stresses. For this reason, it is desirable that structures be symmetric not only with respect to stiffnesses, but also to types of structural members.

Uniformity. Adoption of very different spans in a given frame gives place to high shears and bending moments in the girders covering the shortest spans. These internal forces may reach excessive values in tall buildings, and even give place to objectionable variations on the axial loads of the adjacent columns; those variations can in turn affect foundation design. In low rise buildings these effects may be insignificant; the degree of uniformity which may be desirable in tall buildings may thus be objectionable in the lower ones, if it prevents taking advantage of the irregularly located points put forward by the architect. For instance, in the reinforced concrete frame structure whose floor plan is shown in Figure 17a, the arrangement of service walls permits locating columns al points A, B, C, D. Such columns would reduce beam spans, and hence they would be desirable in a two- to five-story building; probably, they would be objectionable in a building having more than eight or ten stories. Nevertheless, it may in some cases be advantageous to locate columns at points that imply marked discrepancies between the spans of a tall building. It is then advisable to decrease the stiffnesses of the girders connecting those columns, mainly by reducing their depth, as shown in Figure 17b.

As a consequence of vertical displacements produced by lengthening and shortening of columns, problems derived from excessive stiffness of short span beams tend to augment. Stiffness reduction called for by a good design for lateral loads might then be inconvenient because of limitations related with vertical load deflections. It is then advisable to project plastic hinges at the ends of the elements under consideration.

Buildings having irregular plans that inelude two or more main sections interconnected by narrow corridors (Figure 18) pose special problems of analysis and design: excessive stresses in the corridor diaphragms and significant twisting forces in the building sections can result as a consequence of interaction among those sections. Evaluation of these effects is in general a difficult task including explicit consideration of diaphragm deformability. The problem can be successfully handled by means of properly located and carefully detailed vertical construction joints.

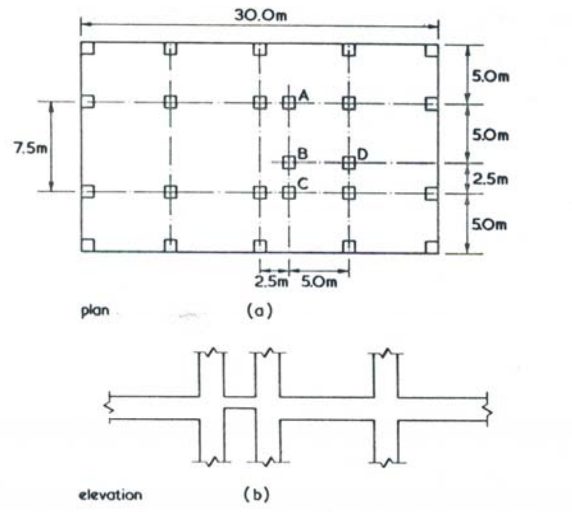

Figure 17. Structural solution for building with uneven spans
(after Newmark and Rosenblueth[10])

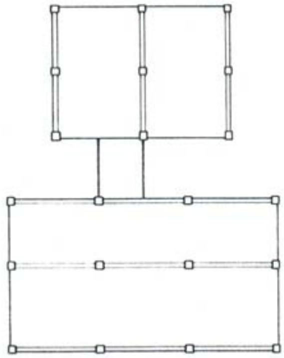

Figure 18. Building sections interconnected by narrow corridors

Staggered lines of defense. A large number of buildings base their lateral strength on the contribution of brittle elements that crack while they absorb energy during the strongest phases of a shock. Design of such buildings is often done assuming no reduction in the elastic spectral ordinates on account of ductility, as cracking may be tantamount to collapse. Their performance is greatly improved, and the design forces for a given reliability sharply reduced, however, if the system is provided with a second line of defense, capable of developing a fraction of the lateral strength of the brittle elements and of showing ductile behavior after cracking of the first, stronger and usually stiffer system. This property has been recognized by some building codes[16,20], which specify nearly equal ductilities for moment resisting structural frames as for dual systems that resist lateral forces by a combination of vertical bracing trusses, reinforced concrete or reinforced masonry shear walls and ductile moment resisting frames, provided the frames take at least 25%:) of the prescribed seismic forces.

3.3 Design for ductility and energy absorption

Neither local nor global ductilities can be ensured by use of a ductile material: both properties depend as well on the types of potential failure modes and on the relative values of the safety factors with respect to each of them. Thus, onset of instability precluded taking full advantage of the ductility inherent in the material used in the structure of Figure 3. While the stress-strain law for the material can be represented by Figure 6b, the relationship between lateral force and displacement is better described by Figure 6d, and this non-ductile curve will dominate system behavior unless the lateral stiffness is increased or the vertical load decreased; only the first of these actions is ordinarily feasible. Likewise, premature local buckling of a beam-flange may prevent the development of a ductile plastic hinge at the same cross section.

In order to attain ductile behavior, one must identify potential failure modes, determine those characterized by ductile behavior, and adopt a set of safety factors leading to a sufficiently low probability for the event that limit states with respect to brittle modes of behavior will be reached before those associated with ductile modes. For instance, reduction factors for lateral forces specified by Mexico City Building Code[16] for ordinary moment resisting reinforced concrete frames correspond to an assumed ductility of 4, but the code permits that parameter to be taken as 6 if some special requirements are satisfied. Among those requirements, load factors of 1.4 are specified for brittle-failure limit states, such as those associated with shear force, torsion and buckling, for the superposition of permanent loads and earthquake, instead of 1.1, applicable to ductile limit states.

Details and connections. Because global ductility of usual structures depends as a rule on local ductilities of small regions, careful design and detailing of those regions is mandatory. In building frames, yielding is usually restricted to occur at plastic hinges located at the sections where the ratios of capacity to action are lowest. As a rule, it is feasible and convenient to have those sections at the member ends. Chapters 4 and 5 deal with the specific design criteria intended to ensure that sufficiently ductile plastic hinges will form at predetermined locations.

Brittle modes of behavior are often the consequence of exceedance of structural capacity at some particular regions where drastic changes in mechanical properties of the structural members take place. As a rule, brittleness of behavior can in those cases be ascribed to local nonlinear buckling or to stress concentrations usually unaccounted for in ordinary design. Typical among the vulnerable regions are connections between structural members. In steel structures, local brittle behavior usually results from local buckling or welding failure, while in reinforced concrete, problems of bond, diagonal tension, and stress transfer between reinforcement of different members dominate. On account of the complexity of the stress patterns usually involved, the problem is in general not only one of brittleness but also one of ignorance or carelessness in the evaluation of the structural capacity of the joint. Practical recommendations for evaluation of this capacity are provided in Chapters 4 and 5. The condition that the probability of brittle failure is sufficiently smaller than that of ductile failure is attained by adopting larger safety factors with respect to capacity of the joint than to that of the members it connects; but often the difference in safety factors is insufficient to override the wide uncertainties associated with joint behavior.

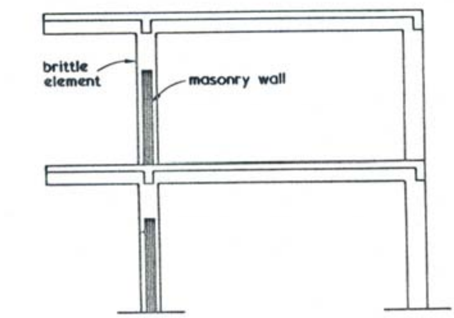

Figure 19. Low ductility structure

Ductility of members and subsystems. In members and subsystems, ratios of safety factors with respect to brittle and ductile modes depend on the capacities of critical sections with respect to various combinations of internal forces and on the ratios between those internal forces when the member or subsystem deforms beyond the failure limit states of the critical sections. Thus, a reinforced concrete beam acted on its ends by moments M_1 and M_2 produced by permanent loads and by seismic couples M'_1 and M'_2 which grow from zero to their final values, will attain its bending capacity if either $M_1 + M'_1$ or $M_2 + M'_2$ reach the corresponding strength. Failure will be ductile if the beam is under-reinforced, i.e. if tensile bending failure governs. Brittle failure will take place if the member is over-reinforced or if development of the bending capacity is precluded by premature failure in diagonal tension. As couples M'_1 and M'_2 grow, end shears vary as $[V = V_0 \pm (M'_1 + M'_2)/L]$, where V_0 is the effect of permanent loads and L is the member span, and the member fails prematurely in diagonal tension if the shear at either end reaches the beam capacity before moments $M_1 + M'_1$ and $M_2 + M'_2$ reach the corresponding bending strengths.

Large values of L imply small values of the shear force for given values of M'_1; and M'_2, and bending failure is likely to dominate; ductile behavior will take place at ordinary under-reinforced members. For small values of L the opposite will be the case: brittle-type diagonal tension failure will be reached before bending failure, unless special precautions are taken to ensure that the safety factor with respect to the former mode is greater than that applicable to the latter.

The condition is often encountered in buildings with irregular plan, as shown in Figure 17a; adoption of a smaller beam depth can lead to a ratio of shear to bending strengths capable of ensuring ductile behavior. The same problem is characteristic of the structural system shown in Figure19, typical of school buildings in some countries: the clear height of some columns is reduced by their interaction with masonry panels lower than the story height. This leads on one hand to shear concentrations and torsional response, and on the other to large ratios of shear force to bending moments, and hence to brittle failure, under usual conditions. All these problems can be avoided if the columns are liberated from restrictions throughout the full story height, either by placing a flexible joint between wall panels and columns, or by locating frame and wall on different, parallel planes. Alternatively, ductile behavior can be accomplished in this case by designing the free-standing portion of a given column for a shear capacity equal to or larger than the sum of the bending capacities at the ends of the mentioned portion divided by its height. Interaction with axial forces must not be forgotten. In the extreme case of very short spandrel beams used for providing coupled action of adjacent shear walls (Figure 20), special reinforcement has to be furnished in order to attain ductile behavior under diagonal tension.

Axial loads reduce available ductility at columns ends; the larger the axial stress, the larger the reduction, as shown in Figure 21 for a reinforced concrete column of given characteristics. Hence the criterion that suggests that plastic hinges occur at the end of beams, rather than of columns; this can be accomplished with reasonable reliability

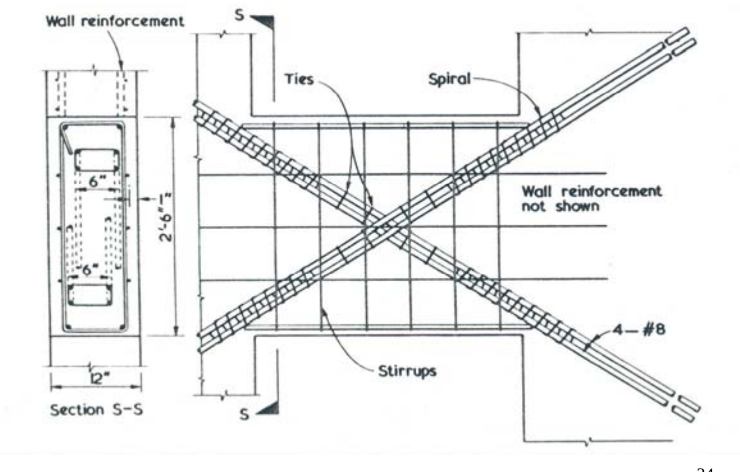

Figure 20. Suggested reinforcement for coupling beam (after Paulay[34])

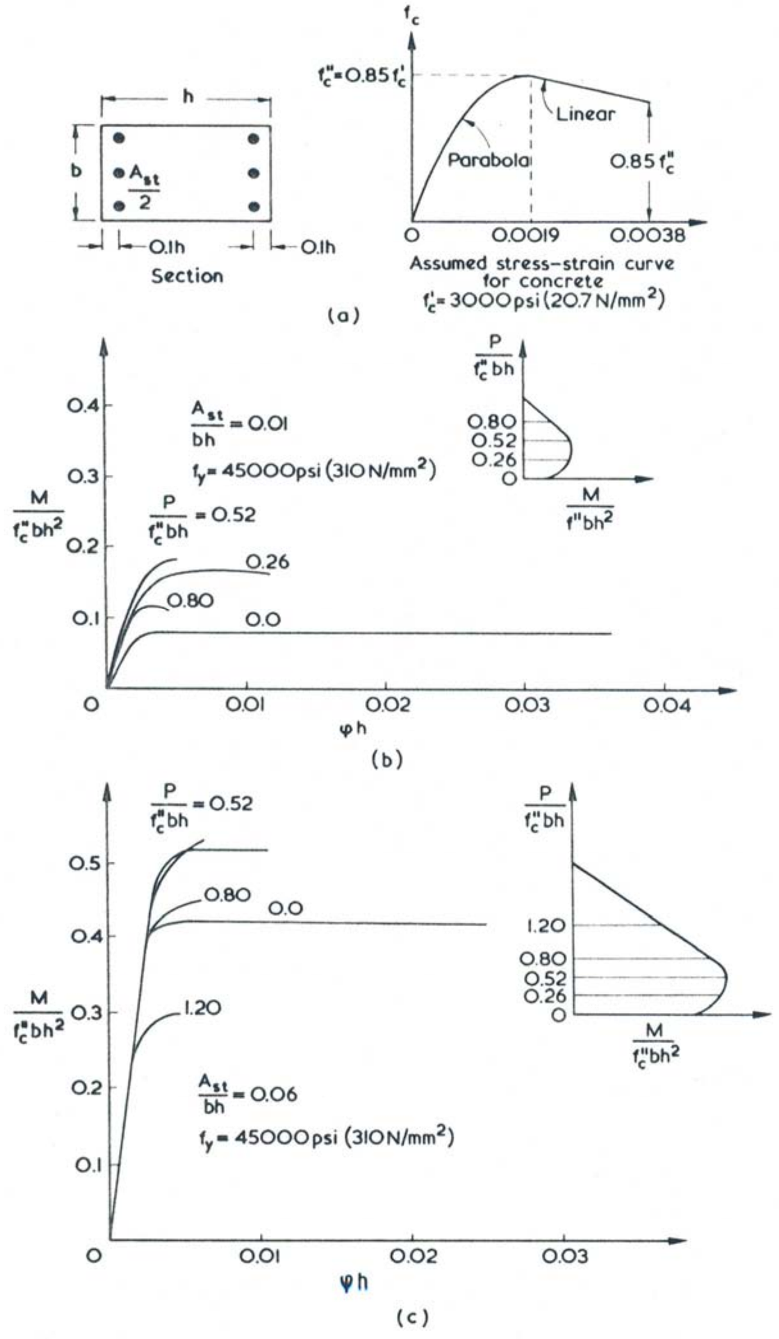

Figure 21. Influence of axial load on column ductility (after Park and Paulay[35])

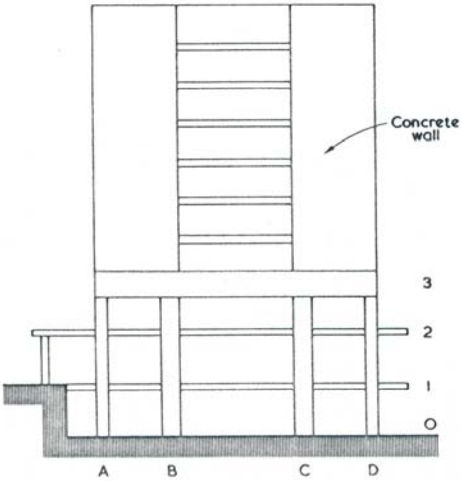

Figure 22. Schematic cross-section of building damaged during Caracas 1967 earthquake[17]

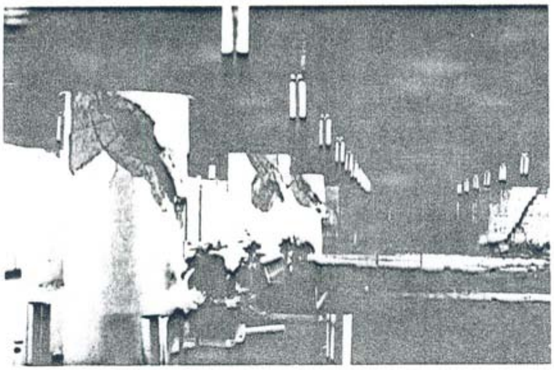

Figure 23. Failure of reinforced concrete columns

reliability by adopting slightly higher load factors (say 10 or 20%) for column than for beam design.

The consequences of designing exclusively for strength, with neglect of ductility considerations, can be as serious as displayed in Figure 23, which shows the brittle failure of a large number of columns of a building having the cross section shown in Figure 22, during the Caracas earthquake of 1967[17]. Axial loads due to gravity forces and to seismic response impaired the capacity of the otherwise strong columns to develop sufficient ductility; the situation may have been aggravated because the upper stories, being much stronger in shear than the lower ones, must have given place to the occurrence of specially higher ductility demands at the columns under consideration.

4. Safety criteria

4.1 Structural safety

Uncertainty and safety in seismic design. Neither loads acting on buildings nor strengths of structural members can be predicted with sufficient accuracy that uncertainty can be neglected in design. Nomina1 values of loads and strengths are most unfavorable values only in the sense that the probability that those loads and strengths adopt values more dangerous for the performance of a given system is sufficiently small. If the actual value of the internal force acting on a critical section or subassemblage of a structure exceeds the actual value of the corresponding strength, failure occurs. Structural safety is measured by the probability of survival, that is, that failure does not take place. When only a single load application is contemplated the probability of survival is determined by the probability distributions of load and strength at the instant when the load is applied, provided the safety margin, i.e. the difference between strength and load does not decrease with time. Seismic excitation however consists of a random number of events of random intensities taking place at random instants in time, and seismic safety cannot be described by a single probability of survival under a given load application, but rather by a time-dependent reliability function $L(t)$, equal to the probability that the structure survives all combinations of dead, live and seismic actions that affect it during an interval of length t starting at the same time as construction.

Limitation of material losses and other forms of damage is as important an aim of earthquake resistant design as is safety against collapse. For the sake of simplicity, these two objectives are usually pursued by design codes through the specification of a design earthquake for which collapse safety and deformation restrictions have to be verified. Some special structures are analyzed for two different design earthquakes safety requirements with respect to collapse limit states are established for an extreme intensity event, while limitation of non-structura1 damage is aimed for through the control of stresses and deformations for shocks of moderate intensity, likely to be exceeded several times during the structure's life.

Complying with collapse safety design conditions does not mean that failure probability is annulled: it is rarely possible to set sufficiently low upper bounds to seismic intensity at a site or to structural response that designing for them will be economical or even feasible. Besides, neither structural strength nor performance for a given intensity can be predicted with certainty. Establishment of design conditions follows cost-benefit studies, where the initial costs required to provide given safety levels and degrees of protection with respect to material losses are compared with the present value of the expected consequences of structural behavior. This is obtained by adding up the costs of failure and damage that may occur during given time intervals, multiplied by their corresponding probabilities and by actualization factors that convert monetary values at arbitrary instants in the future into equivalent values at the moment of making the initial investment.

Evaluation of failure and damage probabilities implies an analysis of the uncertainties associated with structural parameters, such as mass, strength, stiffness and damping[18], and with those defining seismic excitation, such as motion intensity and relation of the latter to the ordinates of the response spectra for given periods and damping values, or to other variables closely correlated with structural response. Conversely, attainment of given safety levels and degrees of protection for material losses is accomplished through the specification of nominal values of design parameters used to compute structural capacity and response and of safety factors that must relate the latter variables.

Optimum safety. The formal application of cost-benefit studies to decision making in earthquake engineering is often hindered by problems that arise in the evaluation of expected performance of structures. Prominent among them is the difficulty to express different types of failure consequences in the same unit or, more specifically, to assign monetary values to concepts such as panic, injury, death and even loss of prestige of designers, contractors or regulating agencies responsible for safety policies. Those difficulties can be overcome through adoption of decision-making models that account for uncertainty in the mentioned concepts and of policies for assessing that uncertainty. An important asset of decision oriented cost-benefit studies, however informal they may be, is their providing of insight into the relevant variables and the manner in which optimum design intensities and safety factors should vary with respect to those variables. Thus, it is concluded that optimum design intensity is an increasing function of the ratio of the derivative of initial cost with respect to capacity to the expected cost of failure, and is a decreasing function of seismic activity at a site.

The latter conclusion means that the higher the activity the higher the optimum level of risk to be accepted in design[19]. This is often neglected, as it contradicts the widely extended concept that in seismic design consistent safety means design for intensities having a given return period, regardless of initial costs.

The benefits of adopting safety levels that depend on the consequences of failure have been recognized in some modern design regulations. For instance, structures are classified in Mexico City Building Code[16] in three categories according to their usage, namely provisional, ordinary and especially important. The second category includes apartment and office buildings, and the third includes structures the failure of which would have especially important consequences, the good performance of which is critical just after an earthquake (hospitals, fire stations), or the contents of which are very valuable (museums). Structures in the first category do not require formal earthquake resistant design, while those in the third category are designed for 1.3 times the spectral ordinates specified for the second group.

In the recently proposed Recommended Comprehensive Seismic Design Provisions for Buildings[20], structures are classified into three main groups according to their seismic hazard exposure, that is, the relative hazard to the public based on the intended use of the building. In decreasing order of importance, these groups include, respectively, buildings housing critical facilities which are necessary to post-disaster recovery, those which have a high density of occupancy or which restrict the movements of occupants, and other structures. Seismic design spectra are based in all seismic regions on intensities that may be exceeded with 10% probability in 50 years. Differences in the optimum safety levels for different building usages are not recognized in the adoption of different seismic coefficients, but only in the restrictions concerning height and types of structural systems and in the refinement of the criteria for structural analysis and design, which are made to depend on the seismic zone and the seismic hazard exposure.

4.2 Design values

Nominal values of design variables and safety factors –and hence of implicit safety levels– have been traditionally established by trial and error and engineering judgement. Although explicit optimization as described above seems the ideal framework for design, its direct application by designers is at present impractical, with the exception, perhaps, of extremely expensive structures, such as nuclear reactors, or structures built in large numbers from the same design, such as offshore drilling platforms. Design values specified in a building code should be based on optimization studies covering the types of structures contemplated by that code, and optimization should be referred to the expected population of those structures. The fact that explicit optimization is not directly applied to each individual structure implies that we are dealing with suboptimization, that is, optimization within given restrictions: design formats must be kept simple, and the number of relevant variables small. As a consequence, what is optimum for a population of structures may not be optimum for every individual member.

Nevertheless, the theory of structural reliability has provided the framework for recent attempts to attain consistency between those rules and to extrapolate them to more general conditions; simplified formulations derived from the basic concepts have led to design criteria that approach consistency while not departing from the simplicity required for practical applications[21, 24]. Nominal values of the design variables are chosen such that the probability that each variable will adopt a more unfavorable value does not exceed a certain limit; often, the probability limit specification is substituted with a criterion stating a number of standard deviations above or below the mean value of each variable. Consistent safety levels based on cost-benefit studies are approached through proper handling of load factors and strength reduction factors[25].

Permanent loads. Dead and live loads affect seismic design conditions in various manners: they give place to internal forces produced by gravity –thus reducing capacity available to resist seismic forces– and they influence seismic response, both with regard to the structure's vibration periods and to the relation between mass, acceleration and force. The inf1uence on natural periods is usually disregarded when specifying design loads, but can be accounted for by stating probable ranges of variation of those periods with respect to their computed values. Because dead loads are essentially constant in time, their design values for the combination of permanent and accidental loads coincide with those valid for the action of the former alone. Design values for live loads to be used in combination with earthquake must be obtained from the probability distributions of their value at an arbitrary instant in time, rather than of their maximum during a relatively long interval; the fact that the cost of failure in case it occurs is a function of the acting live load has been accounted for in some recent cost-benefit studies[26]. These considerations substantiate the requirements of some design codes that state different design live loads for their combination with permanent and accidental loads or with permanent loads alone[16].

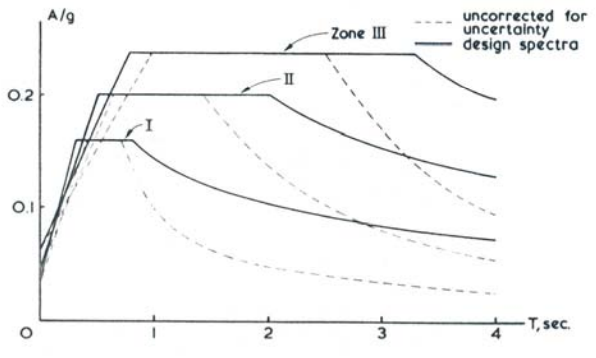

Figure 24. Design spectra corrected for uncertainty in natural period

Natural periods. Uncertainty in natural periods stems from that associated with mass and stiffness as well as with soil-structure interaction; its significance arises from the sensitivity of spectral ordinates to this parameter. That uncertainty can be taken into account by adopting unfavorable values derived either by applying corrective factors to those computed in terms of nominal values of the relevant parameters or by covering those uncertainties by means of suitable modifications to the ordinates of the nominal design spectra. As a rule, corrective factors greater than unity are applied to periods lying on the ascending branch of the acceleration spectrum, and values smaller than unity are applied otherwise. For instance, Figure 24 shows design spectra for three microzones in Mexico City both for deterministically known and uncertain natural periods[16]. For multidegree of freedom systems this criterion errs on the safe side, as it neglects probabilistic correlation among natural periods.

Design spectra. Detailed characteristics of earthquakes are only approximately specified when a design intensity is adopted. Specification of design spectra for linear systems involves making decisions with respect to the design intensity and to the probability of exceedance of the proposed spectral ordinates given that intensity. Because the frequency content of ground motion varies with magnitude, focal mechanism, and site-to-source distance, earthquake intensity by itself does not determine the probability distribution of spectral ordinates for all ranges of natural periods. Unless seismic risk at a site can be ascribed exclusively to shocks that may generate at the same source, design spectra can not be made to correspond to the 'worst probable earthquake' to be expected at the site; rather, they should be obtained from the probability distributions of maximum response for different natural periods, regardless of the seismic source where every particular shock may have originated.

As a rule, the probability distributions of maximum spectral ordinates referred to in the foregoing paragraphs cannot be directly inferred from strong-motion records obtained at the site of interest, as only exceptionally is a large enough sample of those records available for the site. Instead, those distributions are usually generated from stochastic process models of local seismicity in the near-by seismic sources and the transformation of magnitudes and source locations into intensities at the site by means of attenuation laws that relate the pertinent variables with site-to-source distance[27, 28]. Spectral ordinates corresponding to given probabilities of exceedance for a given magnitude and distance are shown in Figure 25, obtained from Ref. 29. If peak ground acceleration and velocity are given, *mean* values of design spectra or values corresponding to given exceedance probabilities for different damping ratios can be readily estimated, as shown in Figure 2.1.

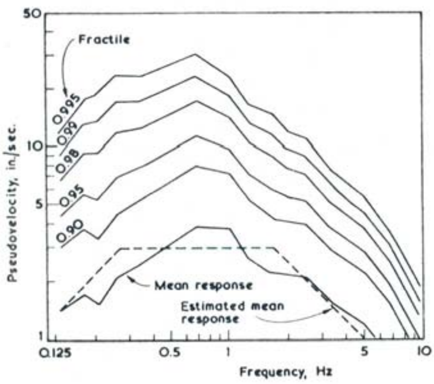

Figure 25. Response spectra for different excedance probabilities (after McGuire[29])

Use of elastic spectra on firm ground as the basis for constructing inelastic design spectra is illustrated in Figure 2.3. The solid line represents an elastic design spectrum constructed according to the criterion of Ref. 30; ordinates are pseudovelocities and abscissas are natural frequencies, and both scales are logarithmic. The dashed line represents the nonlinear spectrum for the same damping as the elastic spectrum and a ductility factor μ; spectral accelerations can be directly read from the dashed-line plot by referring it to an adequate system of straight lines sloping down from the left, and total displacements of the inelastic system are obtained by multiplying those corresponding to the dashed line by the ductility factor μ (dash-point line). The relation between the various segments of the reduced acceleration spectrum D'V'A'A'$_0$ and their counterparts for the elastic case is as follows[30]. The extreme right-hand portion of the spectrum, where the response is governed by the maximum ground acceleration, remains at the same acceleration level as for the elastic case, and therefore at a corresponding increased total displacement level; the ordinates of segments D and V in the small and intermediate frequency ranges, respectively, are divided by μ, and the ordinates of segment A are reduced according to an equal-energy criterion, which for elasto-plastic systems is tantamount to dividing by $(2\mu - 1)^{1/2}$

The accelerograms of some earthquakes recorded on the surface of thick sediments of soft soil are characterized by their long duration and by their nearly harmonic nature. These properties are reflected in their linear response spectra, which show very narrow and pronounced peaks at one or more dominant periods (Figure 26). The validity of the foregoing rules for transforming linear spectra into their nonlinear counterparts has not been assessed yet, but some significant features have been qualitatively applied in the formulation of design spectra for the soft soil region in Mexico City. As Figure 26 shows, the design spectra uncorrected for uncertainty in natural period shows a wide plateau of constant ordinates, which is intended to cover the tendency of structures possessing natural periods shorter than those dominant in the ground motion to show increased responses as their effective periods grow as a consequence of nonlinear behavior.

Figure 26 also shows a correction for uncertainty in natural periods on both sides of the region of maximum ordinates; it also shows that on the long period side, specified ordinates are made to decay at a significantly slower rate than in the recorded spectrum. The latter requirement stand s for the convenience of covering the decrease in reliability due to the possibility of occurrence of a large number of failure modes, and of providing additional protection with respect to unfavorable behavior caused by phenomena typical of long period structures and not normally considered in analysis, such as some forms of soil-structure interaction, concentrations of ductility demand, and slenderness effects in excess of computed values.

Dumping and ductility. The recommendations of some modern building codes[16, 20] are formulated as though design spectra were actually based on linear response spectra for 5 to 10% viscous damping, with correction factors intended to account for ductilities in the approximate range of 1 to 6. But structural damping at small strains is much smaller than openly recognized in design specifications. Thus, while linear response spectra that provide the basis for the recommendations of Ref. 16 correspond to a damping ratio of 0.05 of critical, tests on actual structures subjected to small amplitude vibration show that this value should not exceed 2 to 3% for reinforced concrete structures or 0.5 to 1% for welded steel structures with low density of nonstructural elements. Apparent inconsistencies are rather a matter of tradition and of nomenclature than of actual safety, as most damping, even at low strains, must be ascribed to nonlinear response and

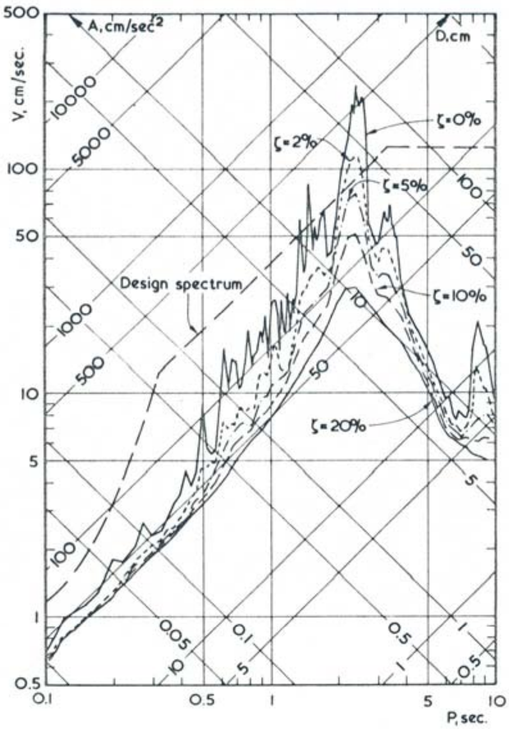

Figure 26. Typical response spectra on soft clay in Mexico City

deterioration rather than to viscous, non-damaging behavior. Nominal ductile capacity for given structures has not been derived from probabilistic analysis of the measured ductilities developed by various structural systems subjected to dynamic excitation, but rather by semi-empirical adjustment of design coefficients based on engineering judgement, economic considerations, and study of the observed response of structures of known properties to severe ground shaking.

4.3 Reliability analysis in seismic design

As mentioned above, the reliability function of a system in a given environment is the probability that the system survives all the actions exerted upon it by the environment during a given time interval. Its computation is based on the probability distribution of the minimum safety margin during the given interval, and this probability is in turn dependent on the probability distributions of system strength and environment action at every instant within the interval. In seismic reliability problems the environment is described by stochastic models of dead, live and seismic loads, while system strength is described by probabilities of occurrence of given failure modes for given combinations of the mentioned loads. Uncertainty in seismic loads arises from randomness in earthquake origin, magnitude, rupture mechanism and wave propagation path, as well as from uncertainty in dynamic response for a given earthquake intensity. A brief description of the basic concepts of seismic reliability analysis is presented in the following, with the intention that it will provide a conceptual framework for the rational determination of safety levels and hence of pertinent design values and safety factors. More complete studies can be found in Refs. 21, 27 and 31.

Seismicity. Let Y be earthquake intensity, expressed in terms of a set of parameters (such as peak ground acceleration or velocity, spectral response for given period and damping) that can be directly correlated with structural response or performance. Seismicity will be described by the stochastic process of occurrence of significant events, that is earthquakes having at the site of interest an intensity sufficiently high as to affect engineering structures, and by the conditional probability distribution of intensity given the occurrence of an event. Let T be the interval between occurrence of successive significant events, T_1 the time from the instant observations are started to the first event, and $f(t)$, $f_1(t)$ the respective probability density functions. The probability density function of the time to the rth significant event is obtained recursively as follows:

$$f_r(t) = \int_0^t f_{r-1}(t-\tau)\, f(\tau)\, \mathrm{d}\tau, \qquad r > 1 \tag{1}$$

thus, the probability density function of the time to first exceedance of intensity y equals

$$g_1(t) = \sum_{r=1}^{\infty} f_r(t) P Q^{r-1} \tag{2}$$

where $Q(y)$ (assumed independent of t and r) is the conditional cumulative probability distribution of intensity given that a significant event has occurred, and $P = 1 - Q$. The probability density function of the time to failure for a structure having a deterministically known strength Y_R, can be obtained by means of Equation 2, making $Q = Q(Y_R)$.

Different expressions have been proposed for f_T and f_{T_1}[28]. The simplest of them, although not the most realistic, assumes significant events to take place in accordance with a Poisson process, that is,

$$f_{T_1}(t) = f_T(t) = \nu \exp(-\nu t)$$

where ν is the mean rate of occurrence of the mentioned events. Under this assumption, Equation 2 leads to

$$g_1(t) = \nu\, P\, \mathrm{e}^{-\nu P t} \tag{3}$$

The discussion that follows will be confined to this assumption. A more general treatment can be found in Ref. 31.

Structural response. Let D be the cost of damage caused by an earthquake on a structure. It can vary between 0 and $D_0 + A$, where D_0 is the total cost of the structure and A that of its contents, as well as all other consequences (such as loss of human lives and indirect effects) expressed in monetary terms, diminished by the salvage value. A probability density function of D conditional to every possible value of intensity can be established[32]. If that function is denoted by $f_{D|Y}(d|y)$, the probability density function of D every time a significant event takes place is

$$f_D(d) = \int \frac{dQ(y)}{dy} f_{D|\mathrm{Y}}(d|y)\, \mathrm{d}y \tag{4}$$

It may be advantageous to express the domain of possible damage levels of a given structure by a set of potential failure modes. If $p_i(y)$ is the probability of failure in mode i given an intensity equal to y, and D_i is the corresponding cost of damage, then the marginal probability of failure in mode i given the occurrence of a significant event is

$$\bar{p}_i = \int \frac{\mathrm{d}Q(y)}{\mathrm{d}y}\, p_i(y)\,\mathrm{d}y \tag{5}$$

and the expected cost of damage for each event is

$$\overline{D} = \sum_i D_i \bar{p}_i \tag{6}$$

the $\bar{p}_i$'s are functions of acting permanent loads, design parameters, and safety factors with respect to all relevant failure modes. By changing relative values of those safety factors it is possible to make failure modes with the highest consequences (in general, brittle modes) much less likely than those leading to lower damage levels. Thus, adoption of higher load factors for column than for beam bending moments may be advisable when significant axial loads hinder the development of enough ductile capacity at column ends; or it may be advantageous to make a structure safer with respect to overturning moment than to lateral yielding. Quantitative assessment of adequate increments of load factors can be established from economic considerations within the cost-benefit framework advocated in the sequel.

Optimum design. Let $C(x_1, \ldots, x_n)$ be the initial cost of a given structure, and $x_1, \ldots, x_n$ a set of design parameters (resistances, stiffnesses, ductilities). Optimal values of those parameters are those maximizing the function

$$V = B - C - Z \tag{7}$$

where B and Z, also functions of the set of design parameters, are present values of the expected benefits and failure consequences, respectively. In other words; if $b(t)$ is the expected value of benefits at time t derived from performance of the structure, and γ is a discount rate such that present values of future losses or benefits can be obtained through multiplication of the latter by exp $(-\gamma t)$, then

$$B = \int_0^\infty b(t)\,\mathrm{e}^{-\gamma t} L(t)\,\mathrm{d}t \tag{8}$$

and

$$Z = \int_0^\infty \nu\,\overline{D}\,\mathrm{e}^{-\gamma t} L(t)\,\mathrm{d}t \tag{9}$$

where $L(t)$ is the reliability function defined above. The meaning of $L(t)$ in Equations 8 and 9 is that production of benefits and losses is subjected to the condition that the structure has survived all previous loads. For the case of deterministically known strength Y_R, Equation 3 leads to

$$L(t) = \exp\left(-\nu P_R t\right) \tag{10}$$

where $P_R = \mathrm{P}(Y_R)$.

From Equations 8, 10 and the assumption that $b(t) = b$ is constant.

$$B = \frac{b}{\gamma + \nu P_R} \tag{11}$$

Likewise, from Equation 9,

$$Z = \frac{\nu \bar{D}}{\gamma + \nu P_R} \tag{12}$$

and the expression for utility becomes

$$U = \frac{b}{\gamma + \nu P_R} - C - \frac{\nu \bar{D}}{\gamma + \nu P_R} \tag{13}$$

If Y_0 is the minimum intensity of significant events, that is, an intensity below which no damage can occur, thcn ν can be approximately expressed as KY_0^{-r}, where K and r depend on the activity of seismic sources near the site[28]. Under these conditions, $P_R = (Y_0/Y_R)^r$.

Expressing b, P_R, C and D in terms of the set of design parameters and differentiating with respect to them, a system of equations is obtained from which optimum values of those parameters can be determined.

If structural strength for a given set of design parameters is uncertain, Equations 10 and 13 become respectively

$$L(t) = E\left[\exp\left(-\nu P_R t\right)\right] \tag{14}$$

$$U = E\left[\frac{b}{\gamma + \nu P_R} - C - \frac{\nu \bar{D}}{\gamma + \nu P_R}\right] \tag{15}$$

The expectations in the above equations are taken with respect to the probability density functions of structural strength Y_R.

Different expressions for U can be obtained, depending on the policy adopted *a priori* with regard to repair and reconstruction measures to be taken after every damaging event[31]. Optimum design parameters may be strongly influenced by that policy.

Specification of safety in codified design. According to the optimization criteria described above, determination of design resistances, stiffnesses and ductilities is not based on the expected response to a single event, defined by a given spectrum and assumed to correspond to a given return period. Instead, design parameters are optimum in the sense that they lead to the best investment of resources taking into account long term expected behavior under the action of a random number of random loads. However, by comparison with safety requirements for permanent loads, it is usually advantageous to specify seismic safety in terms of a design earthquake, assumed to correspond to a given return period, a set of rules to define minimum probable resistances from their expected values and variation coefficients, and a set of load factors. Safety under the action of the design earthquake is not significant by itself, but because it is an indirect measure of the reliability function $L(t)$,

Member and system reliability. In the applications of the theory of structural reliability to the formulation of consistent safety design criteria for a single load application, nominal capacities of members or critical sections are often defined by either of the following expressions[21, 22]

$$R^* = \bar{R}\exp\left(-\alpha V_R\right) \tag{16}$$

$$R^* = \bar{R}/(1 + \alpha V_R) \tag{17}$$

Here, R^* denotes nominal value of the random strength R, $\bar{R}$ its expected value, V_R its coefficient of variation and α a constant that depends on the probability that R is smaller than its nominal value. It is clear that the ratio $R^*/\bar{R}$ is smal1er than unity and decreases when V_R increases.

The capacity with respect to some failure modes in ductile systems can be expressed as the sum of the contributions of the capacities of a number of critical sections. Take for instance the shear capacity of a given story of a frame building and consider that capacity to be made up of the contributions of the moment capacities at all column ends. The coefficient of variation of the story shear capacity is equal to

$$V = \frac{\left(\sum_i \sum_j \rho_{ij} V_i V_j \bar{R}_i \bar{R}_j \right)^{1/2}}{\sum_i \bar{R}_i}$$

where R_i is the strength at the ith critical section, $\bar{R}_i$ and V_i respectively its expected value and coefficient of variation and ρ_{ij} the correlation coefficient between R_i and R_j. If the latter variables are stochastically independent,

$$V = \frac{\left\{ \sum_i (V_i \bar{R}_i)^2 \right\}^{1/2}}{\sum_i \bar{R}_i}$$

and if all V_i's are equal to v,

$$V = v\left(\sum_i \bar{R}_i^2 \right)^{1/2} V = \frac{v\left(\sum_i \bar{R}_i^2 \right)^{1/2}}{\sum_i \bar{R}_i}$$

hence, $V \leqq v$ and the nominal value of R that would be obtained by direct application of Equation 17 with the adequate value of V will exceed that obtained by simple addition of the nominal values R_i^* of the contributions of all critical sections. This result is an analytical way of expressing an often intuitively derived principle: that under similar safety conditions for individual critical sections the reliability of ductile systems with respect to failure modes that require the development of the capacity of n critical sections decreases with decreasing n. Because design criteria for the revision of safety conditions are usual1y stated in terms of the ratio of structural capacity to internal load at each individual critical section, the effect under study has to be accounted for by making required safety factors vary with the number of critical sections involved in a failure mode. This is the basis for the prescription in the 1976 Mexico City Building Code stating that the generalized force acting on every shear wall or column that takes up more than 20% of the story generalized force (shear, torque or overturning moment) be increased 20%; or by the prescription concerning nonredundant systems in ATC recommendations[20] stating that when a building system is designed or constructed so that the failure of a single member, connection or component would endanger the stability of the building, that member, connection or component should be provided with a strength at least 50% greater than otherwise required.

Superposition of modal contributions. Maximum contributions of all natural modes to a given response –internal force at a critical section, displacement or deformation– do not take place simultaneously. The design value of a response parameter is assumed proportional to its standard deviation at the end of the earthquake. After some simplifications[10], this criterion leads to the following expression:

$$S = \left(\sum_i \sum_j \frac{S_i S_j}{1+\varepsilon_{ij}^2} \right)^{1/2} \tag{18}$$

in which

$$\varepsilon_{ij} = \frac{\omega'_i - \omega'_j}{\xi'_i \, \omega_i + \xi'_j \, \omega_j} \tag{19}$$

and S_i is the maximum absolute value of the contribution of the *i*th mode to the response of interest; it is to be taken with the sign adopted by the unit impulse response function of the response of interest to a ground velocity step-increment when the mentioned function attains its maximum numerical value.

In Equation 19, ω_i = undamped circular frequency of *i*th natural mode, $\omega'_i = \omega_i \left(1- \zeta'^2_i\right)^{1/2}$ = damped circular frequency of *i*th natural mode, $\zeta'_i = \zeta_i + 2/\omega_i s$, ζ_i = damping ratio of *i*th natural mode (assumed equal to 0.05 unless a different value is justified), and s = duration of segment of stationary white noise equivalent to the family of actual design earthquakes; s may range from 15 to 40 seconds for ground conditions ranging from firm ground to thick deposits of very soft material. The influence of stochastic correlation between the instants when the response associated with each mode reaches its maximum is reflected in Equation 18 through the participation of ε_{ij}: when ω_j' differs significantly from ω_j', ε_{ij} is large and S^2 approaches the sum of the squares of the individual mode contributions, $\sum_i S_i^2$. However, when ω_i' is close to ω_j', ε_{ij} tends to zero and the cross-product terms $S_i S_j$, for $i \neq *j$, become significant. The fact that each of these terms can be either positive or negative accounts for the possibilities of strongly correlated modal responses taking place with phase angles close to either 0 or 180.

In buildings, cross-product terms are usually negligible. Exceptions occur, for instance, in the modal analysis of buildings possessing small torsional eccentricities, when torsional degrees of freedom are taken into account, or in the analysis of any type of structure when the response of an appendage (portion characterized by a mass much smaller than the others into which the system has been discretized) is taken as a degree of freedom in the computation of modal shapes and frequencies[16].

Superposition of ground motion components. It has been customary to design structures so that they resist the envelope of effects of the various components of earthquake motion as though these components acted one at a time. There is growing consciousness that design should recognize the simultaneous action of all the components, as a number of conditions have been identified where superposition of those components significantly affects safety. Take, for instance, a building possessing continuous frames in two orthogonal directions, another with an asymmetrical plan, and a long continuous bridge with several supports. If the columns in the first structure are built in reinforced concrete and possess a square cross section, the most unfavorable direction of application of seismic forces will be along their diagonal, rather than parallel to either system of orthogonal frames. In addition, if the nonlinear response of the structure is analyzed and substantial ductility is developed at the column ends, effective stiffnesses of the frames in one direction will depend at any instant on the simultaneous state of deformation of the other system of frames; in other words, significant interaction will exist between ductility demands in both directions. Frames normal to the direction of asymmetry in the second case are subjected to the effects of direct shear produced by the horizontal ground component parallel to them, and to the torsional effects associated with the other horizontal component. Out of phase motion of the various supports in the third structure affect qualitatively and quantitatively the distribution of internal forces.

An approximate criterion to account for the foregoing effects has been recently developed; it evolved from a simplification of a second moment formulation of structural safety[36], and consists of the following[37]:

1) Compute the responses to gravity loads and to the components of ground motion regarded as potentially significant. Let those responses be arranged into vectors $R = R_0$ and R_i respectively, with $i = 1,2, \ldots, n$.
2) Obtain vectors

$$R = R_0 + \sum_{i=1} \alpha_i R_i \ ,$$

   assigning plus and minus signs to $\alpha_i R_i$, ordering the R_i's in all possible permutations, and giving the α_i's the values in Table 1.
3) If the problem is one of analysis, find out whether all points fall within the failure surface. If the problem is one of design, assign the design parameters such values that the safe domain will contain all the points.

In the analysis and design of towers and chimney stacks it is advisable to take α_i equal to 0.5 instead of 0.3 for $i \geqq 2$. This recommendation stems from two considerations: in towers having square or rectangular plan, supported on four equal columns, application of the foregoing criterion with $\alpha_2 = 0.3$ to safety checking with respect to axial stresses produced by overturning moment leads to systematic errors on the unsafe side; and in structures nominally having radial symmetry, such as chimney stacks, an apparently ¡nsignificant asymmetry causes an appreciable degree of coupling between modes of vibration involving orthogonal horizontal displacements. (See Sections 1.10 and 2.7.4.)

4.4 Repair and strengthening of existing structures

Historical monuments, damaged structures and those to be remodeled or the use of which is modified, often pose the problem of deciding about adequate safety levels and compliance with current building codes. In some regions, large portions of important buildings have been designed and built according to standards that were afterwards deemed insufficiently strict, and there are large numbers of unengineered dwelling units. Adoption of standards applicable to new structures is cumbersome and expensive in most cases mentioned above. The situation must be coped with having in mind that the objective of engineering design is to optimize for society. Decision models dealing with these cases have recently been developed[32].

TABLE 1.

Values of α_i and maximum errors in amplilude of seismic-response vector (after Ref. 27)

i or n	α_i	*max. error* (%)	α_i	*Max. error safe side* (%)	*Max. error unsafe side* (%)
1	1.000	0.0	1.0	0.0	0.0
2	0.336	5.5	0.3	4.4	8.1
3	0.250	8.4	0.3	8.6	7.6
4	0.206	10.4	0.3	12.7	5.0
5	0.179	11.8	0.3	16.6	1.6
6	0.160	13.0	0.3	20.4	- 2.1
7	0.146	13.9	0.3	24.1	- 5.8
8	0.135	14.7	0.3	27.7	- 9.6
9	0.126	15.4	0.3	31.1	-13.3
10	0.118	16.0	0.3	34.5	-17.0

References

1. Esteva, L., 'Behavior Under Alternating Loads of Masonry Diaphragms Framed by Reinforced Concrete Members'. *Proc. International Symposium on the Effects of Repeated Loading of Materials and Structures*, RILEM, Mexico City (1966)
2. Krawinkler, H., Bertero, V. V. and Popov, E. P., 'Inelastic Behavior of Steel Beam-to Column Subassemblages', *Earthquake Engineering Research Center, Collage of Engineering, Univ. California*, EERC 71 7, Berkeley. Cal. (1971)
3. Frank, R. A., Anagnostopoulos, S. A., Biggs, J. M. and Vanmarcke, E. H., 'Variability of Structural Response Due to Real and Artificial Ground Motions', MIT Department of Civil Engineering, *Research Report R*76-6 (1976)
4. Havilane, R. W., Biggs, J. M. and Anagnostopoulos, S. A., 'Inelastic Response Spectrum Design Procedures for Steel Frames', MIT Department of Civil Engineering, *Research Report R*76-40 (1976)
5. Veletsos, A. S., 'Maximum Deformations of Certain Nonlinear Systems', *Proc. Fourth World Conference on Earthquake Engineering*, Santiago, Chile (1969)
6. Bielak, J., 'Dynamic Response of Single-Degree-of-Freedom Bilinear Systems', Master's Thesis, Rice University, Houston, Tex. (1966)
7. Spencer, R. A., 'The Nonlinear Response of Multistory Prestressed Concrete Structures to Earthquake Excitation', *Proc. Fourth World Conference on Earthquake Engineering*, Santiago, Chile (1969)
8. Penzien, J. and Liu, S. C., 'Nondeterministic Analysis of Nonlinear Structures Subjected to Earthquake Excitations', *Proc. Fourth World Conference on Earthquake Engineering*, Santiago, Chile (1969)
9. Ramírez, J., 'Efectos de Inestabilidad en la Respuesta Sísmica de Estructuras de Cortante Inelásticas', Master's Thesis, *Faculty of Engineering, National University of Mexico* (1977¡
10. Newmark, N. M. and Rosenblueth, E., 'Fundamentals of Earthquake Engineering', Prentice-Hall, Englewood Clifrs, N.J. (1971)

11. Guerra, O. R. and Esteva, L., 'Equivalent Properties and Ductility Requirements in Seismic Dynamic Analysis of Nonlinear Systems', *Proc. Sixth World Conference on Earthquake Engineering*, New Delhi, India (1977)
12. Rosenblueth, E., 'Temblores Chilenos de Mayo 1970: Sus Efectos en Estructuras Civiles', Ingeniería, **31**, 1, México, D.F. (1961)
13. González-Flores, M., 'Sistema para Elimar los Esfuerzos Peligrosos que los Temblores Causan en las Estructuras', Quinto Congreso Mexicano de la Industria de la Construcción, México, D.F. (1964)
14. Skinner, R. l., Kelly, J. M. and Heine, A. J., 'Energy Absorption Devices for Earthquake Resistant Structures', *Proc. Fifth World Conference on Earthquake Engineering*, Rome, Italy (1973)
15. Ruiz, S. E., Esteva, L. and Guerra, O. R., 'Desarrollo y Evaluación de Sistemas para Limitar las Acciones Sísmicas sobre Edificios', Ingeniería, **47**, 2, México, D.F. (1977)
16. 'Diseno estructural', Mexico City Building Code, México, D.F. (1977)
17. Esteva, L., Díaz de Cossío, R. and Elorduy, J., 'El Temblor de Caracas, Julio de 1967', Ingeniería, **38**, 3, México, D.F. (1968)
18. Haviland, R., 'A Study of the Uncertainties in the Fundamental Translational Periods and Damping Values for Real Buildings', MIT, Department of Civil Engineering, *Research Report R*76-12 (1976)
19. Esteva, L., 'Seismic Risk and Seismic Design Decisions', *Seminar on Seismic Design of Nuclear Power Plants*, MIT Press, Cambridge, Mass (1969)
20. *'Recommended Comprehensive Seismic Design Provisions for Buildings'*, Applied Technology Council, Palo Alto, Calif. (1977)
21. Rosenblueth, E. and Esteva, L., 'Reliability Basis for Some Mexican Codes', American Concrete Institute, *Special Publication* 31 (1971)
22. Meli, R., 'Bases para los Criterios de Diseno Estructural del Proyecto del Reglamento de Construcciones para el Distrito Federal', *Institute of Engineering, National University of Mexico*, Report 375 (1976)
23. Esteva, L., 'Regionalización Sísmica de México para Fines de Ingeniería, Institute of Engineering, National University of Mexico, *Report* 246 (1070)
24. Rosenblueth, E., 'Code Specification of Safety and Serviceability', State of Art Report 2, Technical Committee 10: Structural Safety and Probabilistic Methods, *ASCE-IABSE Joint Committee on Planning and Design of Tall Buildings*, Fritz Engineering Laboratory, Lehigh University, Bethlehem, Pa. (1972)
25. Lind, N. C., 'Deterministic Format for the Probabilistic Design of Structures', in *An Introduction to Structural Optimization*, Solid Mechanics Division, Univ. Waterloo, Waterloo, Ont., Canada, SM Study 1 (1969)
26. Rosenblueth, E. and Mendoza, E., 'Optimum Seismic Design of Auditoriums', *Proc. Fifth World Conference on Earthquake Engineering*, 2, Rome, Italy (1973)
27. Esteva, L., 'Criterios para la Construcción de Espectros de Diseño Sísmico', Institute of Engineering, National University of Mexico, Report 178 (1968)
28. Esteva, L., 'Seismicity', Chapter 6 of *Seismic Risk and Engineering Decisions* (Edited by C. Lomnitz and E. Rosenblueth), Elsevier, Amsterdam (1976)
29. McGuire, R. K., 'Seismic Structural Response Risk Analysis, lncorporating Peak Response Regressions on Earthquake Magnitude and Distance', Ph.D. Thesis, *MIT, Department of Civil Engineering* (1974)

30. Newmark, N. M. and Hall, W. J., 'Procedures and Criteria for Earthquake Resistant Design', *Building Practices for Disaster Mitigation*, *Building Science Series* 46, National Bureau of Standards, Washington, D.C. (1973)
31. Rosenblueth, E., 'Optimum Design for Infrequent Disturbances', Proc. Am. Soc. Civ. Engrs, **102**, ST9 (Sept. 1976)
32. Rosenblueth, E., 'Decisiones Óptimas para Estructuras Existentes en Zona Sísmica. Primera Etapa', Institute of Engineering, National University of Mexico (in press)
33. Newmark, N. M., 'Current Trends in the Seismic Analysis and Design of High-Rise Structure', in *Earthquake Engineering* (Edited by R. Wiegel), Prentice Hall, Englewood Cliffs, N.J. (1970)
34. Paulay, T., 'Coupling Beams of Reinforced Concrete Shear Walls', *Proc. Am. Soc. Civ. Engrs*, **97**, ST3 (March, 1971)
35. Park, R. and Paulay, T., 'Reinforced Concrete Structures', John Wiley and Sons, New York (1975)
36. Hasofer, A. M. and Lind. N. C. 'Exact and Invariant Second-Moment Code Format', *Proc. Am. Soc. Civ. Engrs,* **100**, EM1 (1974)
37. Rosenblueth, E. and Contreras, H., 'Approximate Design for Multicomponent Earthquakes', Submitted for publication in *J. Engng Mech. Div. Am. Soc. Civ. Engrs*

SEISMIC FAILURE RATES OF MULTISTORY FRAMES[1]

ABSTRACT

A general approach is presented for the estimation of expected failure rates of structures per unit time, which accounts for uncertainties about mechanical and geometrical properties, as well as about live load and seismic excitation. Such an approach is applied to one-, three-, and nine-story frames with nonlinear behavior, subjected to random sequences of simulated accelerograms corresponding to soft and hard types of ground. Conclusions are reached concerning the influence of several concepts on the probability of failure of the structures analyzed, including: (1) The influence of the spatial statistical correlation among the mechanical properties of the structural members is relatively small as compared to that of other variables; (2) the number of degrees of freedom has a great influence on the probability of failure; (3) for small coefficients of variation of the available ductility, the probabilities of structural failure for a given intensity are higher than those corresponding to greater coefficients of variation (this is a consequence of the assumed relation between expected and nominal values of this variable); and (4) the structural failure rate decreases when the design ductility factors increase. It is pointed out that these conclusions are not valid if the safety factors with respect to local brittle failure modes are small as compared with those associated with ductile modes.

Introduction

Basic criteria and algorithms for selecting seismic design coefficients and spectra on the basis of optimizing present values of expected uti1ities, including uncertainties about both structural properties and seismic excitations, have been avai1ab1e for a 1ong time (Esteva 1967, 1968, 1969, 1976; Rosenblueth 1976). These highly developed algorithms cover cases in which the occurrence of earthquakes of different intensities at a site is modeled either by a Poisson process or by a renewal process. In addition to the probabilistic descriptions of the seismic-activity process, the algorithms make use of concepts such as the probability distribution of the ground-motion intensity at which a structure of interest fails and the probability of failure for a given intensity or, more generally, the probability distribution of the Cost of damage for that intensity.

Both the relevance and the complexity tied to the analysis of the seismic process have been recognized for many years; therefore, large efforts have been devoted to defining adequate probabilistic models and to formulating criteria for estimating their parameters (Cornell 1972; Esteva 1976; Rosenblueth 1986). Much less attention has been paid to the study of the probability distributions of the intensities resisted by given structures and to the distributions of damage for given intensities. One reason for this neglect is the frequently used argument that uncertainties tied to structural parameters, i.e., response and performance, are very small as compared to those attached to the nature and parameters of the seismic processes. In most cases, this argument justifies

[1] First Published in:
Luis Esteva & Sonia E. Ruiz, Sesimic failure rates of multi-storey frames, *Journal of the Structural Division, ASCE*, **115**, 2 (1989) 268-284

replacing an uncertain structural strength with its expected value when performing studies about the reliability of a structure in a seismic environment. However, the problems still remain of determining the ratio of the excepted value of the earthquake intensity resisted by a structure to the nominal value used to express safety-related specifications, and of obtaining $E\,(v_F)$, the expected rate of failure per unit time of a structure with uncertain mechanical properties, in terms of $v_Y\,(y^*)$, the rate of occurrence of intensities greater than y^*, the nominal value of the design intensity.

The problems that hinder the determination of accurate values of $E\,(v_F)$ given $v_Y\,(y^*)$ range from insufficient knowledge about the mechanical properties and failure mechanisms of structural members and systems to the wide complexity of the mathematical models needed to represent the joint probability distributions of the variables that determine seismic response and performance, i.e., ground-motion history, gravity loads, constitutive laws of structural materials and members, and failure mechanisms and conditions.

The studies reported in this article aim at assessing the influence of a number of structural parameters on computed failure probabilities of systems designed with the same safety factors for the same nominal intensities. For this purpose, it is assumed that building frames fail in a ductile manner by the formation of plastic hinges at those member sections where the acting bending moment reaches the local bending capacity and that a brittle failure limit state is reached when the ductility demand at any given story, expressed in terms of lateral deformations of that story, reaches the available capacity of ductile deformation. The analytical difficulties implied by the mathematical models adopted are circumvented by applying a Monte Carlo simulation.

Problem formulation

The following approach and assumptions will be adopted:

1. Seismic hazard at the site of interest is expressed in mathematical terms by a known function, $v_Y\,(y)$, representing the mean number of times per unit time (year) that an intensity greater than y occurs at the site.
2. Under the action of an earthquake of intensity y, the structure may fail in n different modes; for instance, each failure mode may correspond to exceedance of the capacity for ductile deformation at a given story. R_i will designate the structural capacity to resist the ith failure mode, and S_i will be used to denote the maximum amplitude of the response variable governing the occurrence of the ith failure mode. The ratio S_i/R_i is the reciprocal of a random safety factor and will be denoted by Q_i. Failure in the ith mode occurs if $Q_i \geq 1$. It is also assumed that failure occurs precisely in the ith mode and not in any other, provided that $Q_i \geq Q_j$ for all $j = 1, ..., n$. This means that if we have two modes, i and j, such that $Q_i \geq Q_j \geq 1$, failure will be assumed to take place precisely in the ith mode, in spite of the fact that during the response process the condition $Q_j \geq 1$ may be reached before the condition $Q_i \geq 1$. This assumption is introduced for simplicity and does not have any practical implication if it is assumed that the consequences of failure are independent of the failure mode leading to it.

   From these assumptions, the probability of failure for a given intensity equals the probability that the maximum of all the values of Q_i exceeds unity. Thus, if that maximum is called Q, then

$$p_F\,(y) = P\,(Q \geq 1 | y) \tag{1}$$

where $P_F(y)$ = the probability of structural failure under the action of an earthquake with intensity y.

3. The rate of failure of a structure with deterministically known properties (vector **R**) is

$$\nu_F(\mathbf{R}) = \int_0^\infty -\frac{\partial \nu_Y(u)}{\partial u} P_F(u|\mathbf{R})\,\mathrm{d}u \tag{2}$$

where $\nu_F(u)$ = the rate of occurrence of an intensity in excess of u, and $P_F(u)$ is given by Eq. 1. If **R** is a vector of uncertain structural properties, then the expected value of ν_F can be obtained by weighing the value given by Eq. 2 with respect to the joint p.d.f. of **R**. Denoting by $f_{\mathbf{R}}(r)$ this p.d.f., the expected va1ue of ν_F can be obtained as follows:

$$E(\nu_F) = \int_0^\infty f_{\mathbf{R}}(r) \int_0^\infty -\frac{\partial \nu_Y(u)}{\partial u} P_F(u|\,r)\,\mathrm{d}u\,\mathrm{d}r \tag{3}$$

The first integral appearing in this equation must be understood as a multiple integral, with a number of dimensions equal to the order of **R**. Changing the order of integrations, Eq. 4 is obtained:

$$E(\nu_F) = \int_0^\infty -\frac{\partial \nu_Y(u)}{\partial u} \int_0^\infty P_F(u|\,r)\, f_{\mathbf{R}}(\mathrm{r})\,\mathrm{d}r\,\mathrm{d}u \tag{4}$$

This order of performing the integrations lends itself better than Eq. 3 to the calculation of $E(\nu_F)$ by the algorithm that will be proposed later. The interior integral in Eq. 4 is the failure probability of a system with uncertain properties subjected to an earthquake with intensity $Y = u$.

Basic Models and Assumptions

Seismic Hazard Function

For the purpose of calculating $p_F(y)$, as given by Eq. 1, it is convenient to express y as the value of a parameter of the ground-motion time-history, which can then be used by engineers to estimate maximum values of structural responses. Examples of such parameters are peak ground accelerations or velocities, ordinates of response spectra for given period and damping, and expected values of these ordinates. If one of these parameters is used to measure intensity, then the expected rate of occurrence of earthquakes with intensities higher than a given value y is known. It can be expressed by a function of the form

$$\nu(y) = Ky^{-r}\left[1 - \left(\frac{y}{y_M}\right)^{\epsilon}\right], \quad \text{for} \quad y \le y_M \tag{5a}$$

$$\nu(y) = 0, \qquad\qquad \text{for} \;\; y \ge y_M \tag{5b}$$

where y_M = an upper bound to the intensities that may occur at the site of interest; r and $\in$ = parameters defining the shape of the distribution of intensities; and K = a scaling factor. For the applications that follow, y and y_M are measured by peak ground acceleration at the site during an earthquake, and the parameters in Eq. 5 are assumed to take the values K = 129.5, r = 1.6, $\in$ = 1, and Y_M = 1,125 cm/s^2 for the analysis of cases 1-13. This means that accelerations in excess of 200 and 500 cm/s^2 occur, respectively, every

45 and 285 years on the average. For case 14, K = 80 and Y_M = 500 cm/s^2. Although Eq. 5 is deemed adequate for engineering applications, it is not acceptable for small values of y, as it leads to unbounded values of $v(y)$ as y tends to zero.

Ground-Motion Time-Histories

Two sets of simulated ground-motion time-histories were used; one based on the statistical properties of the NS component of the record obtained in 1940 in El Centro, California, and the other represents the most intense portion of the EW component obtained at the parking lot of the SCT building in Mexico City during the earthquake of September 19, 1985 (Mena 1986). 20 sample records belonging to the first set and nine belonging to the second one were generated by means of the algorithm described by Ruiz, Paredes-López, and Galarza (1986) and Ruiz and Lira (1987). For the first case, the simulated records have a duration of 30 sec and for the second, 82 sec.

The algorithm used to generate the simulated accelerograms takes into account the variation in time of ground-motion intensity, as well as the distribution of energy content among frequencies. Briefly, it may be described as a sequence of three operations: first, the duration of the record to be simulated is divided into several segments, and the frequency content and intensity of the ground motion included within each segment is obtained; second, unit-intensity segments of samples of Gaussian processes with the corresponding spectral densities are generated for each segment defined in the first step; and, finally, the simulated segments are put together, and each resulting record is modulated by a deterministic time function.

Structures Studied

The studies reported herein cover three families of single-bay frames with one, three, and nine stories, respectively. Their nominal dimensions are shown in Fig. 1. The computed values of the fundamental periods resulting from their member sections and from the nominal values of their material properties are given in Table 1, as well as the ductility-related reduction factors adopted for design and the corresponding seismic design coefficient. Each of the latter resulted from dividing by the corresponding reduction factor the average ordinates of the linear response spectra of each set of simulated records for the computed fundamental period of the structure of interest. This way of transforming the ordinates of a linear response spectrum to those of the corresponding elasto-plastic response spectrum for a specified ductility demand was deemed reasonably approximate because the fundamental natural periods are not too short as compared to the dominant periods of the ground-motion records.

As previously mentioned, failure is assumed to occur when the ductility demand at any given story reaches the available capacity of ductile deformation of that story. This capacity is taken as uncertain, and several assumptions about its variation coefficient were considered, as shown in the fifth column of Table 1.

The probability distributions of member strengths and stiffnesses were not directly obtained, but, as explained in the following, random values of these properties were generated by Monte Carlo simulation of the material properties and cross-section dimensions, followed by application of conventional expressions of structural mechanics.

The parameters and the assumed forms of the statistical distributions of these properties are given in Table 2, which also includes values corresponding to live loads. Those parameters are: concrete strength f_c; steel yield stress f_y; reinforcement cover in girders and columns r; width and depth, b and h; and live load W_L. The expected capacity

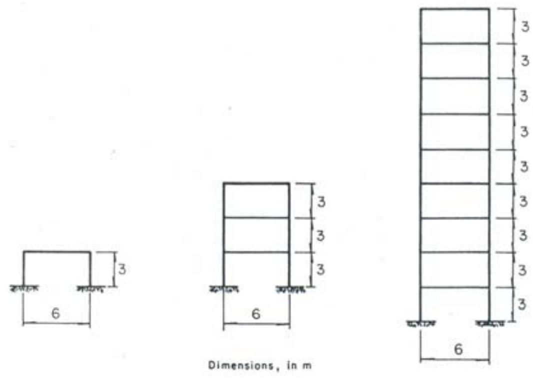

Figure 1. Overall Dimensions of Cases Studied

of ductile deformation $\bar{\mu}$ at a given story is related to its nominal value μ^* through the equation $\bar{\mu} = \mu^* \exp(0.55 \times 3 \times V_\mu)$, where V_μ = the coefficient of variation of the available ductility. The probability distribution of the latter variable was obtained by defining a new variable, $w = \mu - 1$, assumed to possess log-normal distribution. Symbols HC and LC in the sixth column of Table 1 mean "high correlation" and "low correlation". In the first case, each material property or cross-section dimension is assumed to be perfectly correlated throughout the structure, but the different variables at a given member are stochastically independent. In the second case, each material property or cross-

TABLE 1. Cases Studied

Case number	Number of stories	Fundamental period (sec)	Ductility design factor	Ductility coefficient of variation	Spatial correlation[a]	Seismic design coefficient	Excitation[b]
(1)	(2)	(3)	(4)	(5)	(6)	(7)	(8)
1	1	0.36	1	0.3	HC	0.69	EC
2	1	0.36	1	0.5	HC	0.69	EC
3	1	0.36	2	0.3	HC	0.35	EC
4	1	0.36	2	0.5	HC	0.35	EC
5	1	0.36	4	0.3	HC	0.17	EC
6	1	0.36	4	0.5	HC	0:17	EC
7	1	0.36	6	0.3	HC	0.12	EC
8	1	0.36	6	0.5	HC	0.12	EC
9	3	0.85	2	0.3	LC	0.25	EC
10	3	0.85	4	0.3	LC	0.12	EC
11	3	0.36	4	0.3	LC	0.17	EC
12	3	0.36	4	0.3	HC	0.17	EC
13	3	0.36	4	0.6	HC	0.17	EC
14	9	1.32	2.5	0.3	LC	0.115	SCT

[a] HC = High correlation between structural member properties; LC = low correlation between structural member properties.

[b] EC = El Centro, 1940, NS component; SCT = SCT, Mexico City, 1985, EW component.

TABLE 2. Statistical Parameters of Distributions of Material Properties and Loads

Variable (1)	Assumed probability function (2)	Nominal value (kPa) (3)	Mean value (kPa) (4)	Coefficient of variation (5)
W_L	Gamma	0.88	0.69	0.480
f_c (field)	Gaussian	17,600	19,800	0.195
f_y	Gaussian	411,600	458,600	0.096
b, h, r	Gaussian	—[a]	—[a]	—[a]

[a] Similar to those given by Mirza (1979)

TABLE 3. Correlation Coefficients for Cases with Low Correlation (LC) between Mechanical Properties

Variable (1)	Correlation coefficient, ρ (2)
f_c	0.6
f_y	0.8
b	0.8
h	0.8
r	0.8

section dimension at a given member-end is correlated with its counterpart at any other member-end in accordance with the correlation coefficients of Table 3, and there is no correlation between the values of the different variables.

All systems studied were assumed to possess a viscous damping of 5% of critical.

Algorithms Used

Failure Probabilities for Given Intensities

Trying to obtain failure probabilities in analytic terms is intractable by present means, and trying to generate them by Monte Carlo simulation requires an excessively large number of samples if we are interested in the ranges of very low values of these probabilities. Because our interest is focused on obtaining rates of failure of structures subjected to earthquakes of random intensities, and because the uncertainties about the latter are much larger than those concerning the properties of a structure, it is acceptable to limit our efforts to estimating second moments of Q, the reciprocal of the safety factor, and assuming a reasonable form for its probability density function. This is the approach adopted in this paper. According to it, the following procedure was applied:

1. Artificial accelerograms were simulated and scaled to the intensity of interest. This variable was measured by the peak ground acceleration.
2. A structure was designed in accordance with the design coefficients in Table 1. These coefficients correspond to intensities (expected peak ground accelerations) of 0.283 g and 0.176 g, i.e., to return intervals of 84 and 32 years, according to Eq. 5 and its parameters adopted previously.
3. On the basis of the statistical parameters and distribution forms in Tables 1-3, the mechanical properties of a sample of structures were obtained by Monte Carlo simulation in correspondence with each structure designed as described in the previous paragraph.
4. The simulated structures were excited by randomly selected members of the population of simulated accelerograms. In order to keep within acceptable limits, the computational effort involved, and the sample of the combinations of simulated

structures and ground-motion time-histories, was integrated as follows: (1) A set of intensities was chosen, with values covering the interval of interest in engineering, from a sufficiently small lower bound to the maximum feasible intensity y_M; (2) for each of these intensities, one member was randomly selected from the population of simulated records, and it was scaled to the corresponding intensity; and (3) for each intensity, a sample structure was simulated.

5. The response of each structure was obtained by step-by-step integration, and the corresponding value of Q (maximum value of S_i/R_i for all the potential failure modes) was obtained. For this purpose, S_i = the peak value of the relative displacement of the ith story; and R_i = its capacity for ductile deformation. The latter value is obtained by multiplying the story yield displacement resulting from the simulated stiffnesses and strengths by the simulated ductility factor. In order to determine story yield displacements, nonlinear shear-displacement curves were obtained for each story by means of elasto-plastic static analysis of the response of the frame to a gradually increasing force pattern, with amplitudes proportional to the elevation with respect to the bottom ends of the first-story columns, using an algorithm similar to that proposed by Moehle and Alarcón (1985). At each story, the yield displacement was taken as that corresponding to the intersection of the tangent to the shear-deformation curve at the origin with the tangent to the branch corresponding to very large deformations.
6. The values of Q are plotted against the corresponding intensities for each structural type and each design coefficient. Then, curves relating expected values of Q, intensities, and nominal ductility-related reduction factors are fitted to the result, and the variances of the differences between individual and expected values are estimated. Thus, for each structural type and reduction factor the conditional mean value and standard deviation of Q, given the ground-motion intensity, will be known. They are denoted in the sequel by $E(Q|y)$ and $\sigma_{Q|y}$ respectively.
7. The conditional probability density function of Q, given that the intensity equals y, was arbitrarily taken as log-normal, with the first two moments as given in the preceding paragraph. Computing $p_F(y)$ according to Eq. 1 is immediate. The ordinates of the log-normal probability distribution function were obtained by an elementary transformation of an expression proposed by Rosenblueth (1986).

Response Analysis

Frame members were modeled as simple one-dimensional bending elements. Nonlinear behavior of the members was assumed to be concentrated at plastic hinges at their ends. These hinges were assumed to possess bilinear hysteretic stiffness-degrading moment-rotation curves with plastic hardening characteristics, such that the slope of the plastic branch is 2 % of the initial tangent stiffness for small deformations. The damping matrix was taken as a linear combination of the initial-stiffness and mass matrices.

The equations of motion were integrated by means of a constant-acceleration step-by-step algorithm included in computer program DRAIN-2D (Kanaan and Powell 1973).

Results of Simulations

Single-Story Frames

Values of Q in terms of peak ground accelerations and nominal design ductilities μ^* for these cases are plotted in Figs. 2 and 3 for a natural period of 0.36 sec and variation coefficients of the available ductility μ of 0.3 and 0.5, respectively. The figures also

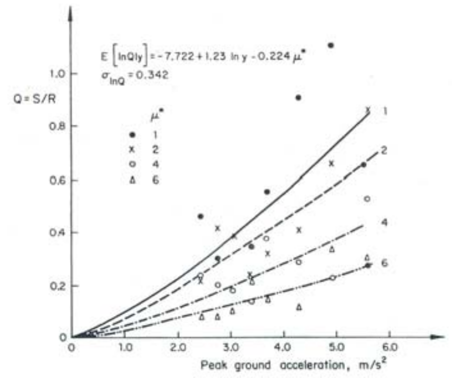

Fig 2. Normalized Response of Single-Story Frames (T = 0.36 s and V_μ = 0.3)

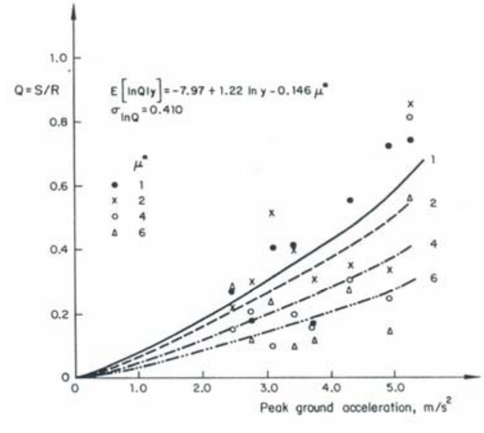

Fig 3. Normalized Response of Single-Story Frames (T = 0.36 s and V_μ = 0.5)

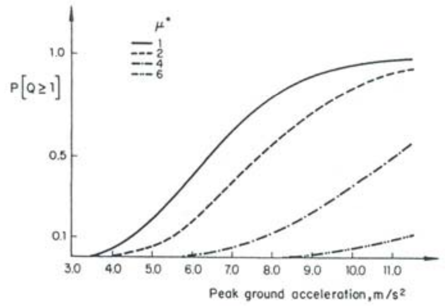

Fig 4. Failure Probabilities of Single-Story Frames Designed for Different Ductility Factors (V_μ = 0.3)

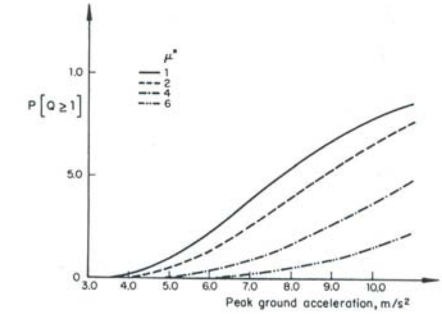

Fig 5. Failure Probabilities of Single-Story Frames Designed for Different Ductility Factors (V_μ = 0.5)

show the curves fitted to the expected values of Q, as well as the corresponding mathematical expression for the expected value of the natural logarithm of Q and the standard deviation of that logarithm. These figures show that the expected values of Q grow for decreasing variation coefficients of μ, as well as for decreasing values of nominal design ductilities μ^*. The first of these trends is related to the fact that, according to the manner in which mean and nominal values of available ductilities are assumed to be associated, if μ^* is kept fixed, the mean value of μ grows with V_μ. The second trend arises from the fact that the frames being studied are continuous at their joint and possess a lateral strength even though they are not specifically designed to resist lateral forces. The contribution of this strength to that necessary to satisfy the design requirements for the superposition of gravity and seismic forces is more significant for high design ductilities than for low values of them. The results in Figs. 4 and 5, showing failure probabilities in terms of intensities and design ductilities, are consistent with these trends.

Three-Story Frames

One objective of the studies on three-story frames was that of assessing the influence of spatial correlation of mechanical properties on the distribution of Q, as well as on the probabilities of failure. The results in Figs. 6 and 7 make comparisons of both variables for cases 11 and 12 of Table 1, i.e., for T = 0.36 sec, V_μ = 0.3, and μ^* = 4; these cases differ in the degree of spatial correlation assumed. For this case, no significant influence of that correlation was found on any of the variables studied: probabilistic moments of ln Q and failure probabilities. This low sensitivity of Q to the correlation coefficients is probably due to the fact that uncertainties related to the detailed ground-motion characteristics for a given intensity are much greater than those concerning the mechanical properties of the structure.

The influence of V_μ on the expected values of ln Q and failure probabilities for given intensities is shown in Figs. 8 and 9 for T = 0.36 sec, μ^* = 4, and high spatial correlation. The trends that may be observed are similar to those discussed in connection with single-story frames.

Finally, Fig. 10, obtained for T = 0.85 sec, V_μ = 0.3, and low spatial correlation, shows that expected values of Q grow with decreasing values in the design ductilities.

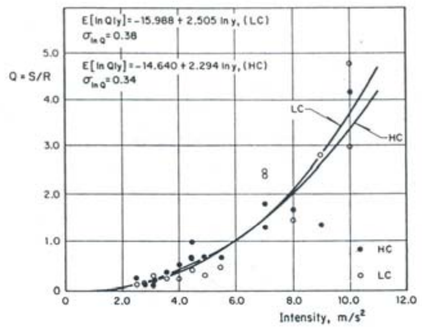

Fig 6. *Normalized Response of Three-Story Frames* (T = 0.3 s, $\mu*$ = 4, and V_μ = 0.3) High (HC) and Low (LC) Spatial Correlation

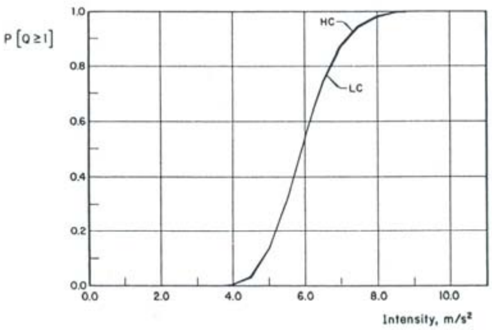

Fig 7. *Failure Probabilities of Three-Story Frames* (T = 0.36 s, $\mu*$ = 4; and V_μ = 0.3); High (HC) and Low (LC) Spatial Correlation

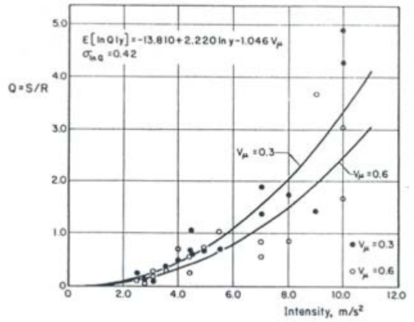

Fig 8. *Normalized Response of Three-Story Frames* (T = 0.36 s, $\mu*$ = 4, and V_μ = 0.3 and 0.6) High Spatial Correlation

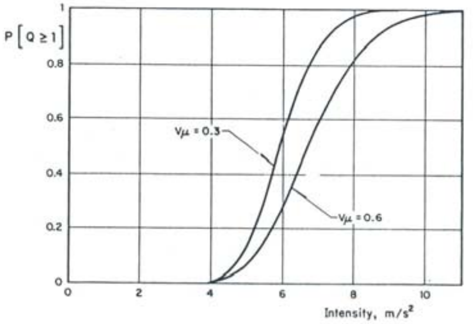

Fig 9. *Failure Probabilities of Three-Story Frames* (T = 0.36 s, $\mu*$ = 4; and V_μ = 0.3 and 0.6); High Spatial Correlation

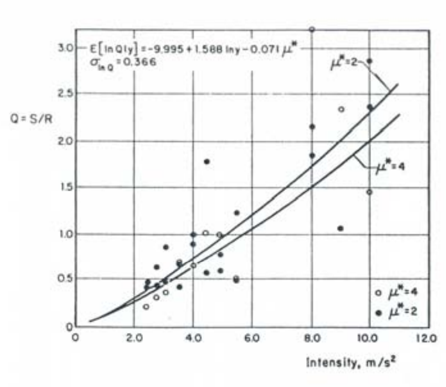

Fig 10. Normalized Response of Three-Story Frames (T = 0.85 s, μ^* = 2 and 4, and V_μ = 0.3) Low Spatial Correlation

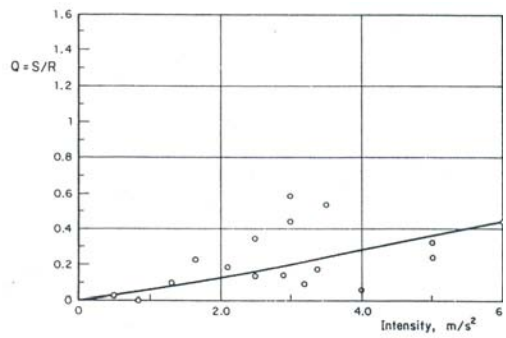

Fig 11. Normalized Response of Nine-Story Frames (T = 1.33 s, V_μ = 0.3, and μ^* = 2.5); Low Spatial Correlation

Failure probabilities were found to behave in the same manner. Again, these trends are consistent with those observed for single-story frames.

Nine-Story Frames

Only one case was studied. The natural period is equal to 1.33 sec, the variation coefficient of the available story ductilities is 0.3, and the nominal design ductility is 2.5. Spatial correlation of mechanical properties is low. Unlike the previous cases, the simulated ground-motion records belong to the same population as the EW component of the SCT record of September 19, 1985, in Mexico City. The results are shown in Fig. 11.

Because the yield moments at column ends depend on the axial forces acting on them, they are sensitive to the overturning moment, which is a function of time. At any given instant, the axial forces due to overturning are of positive sign on the columns on one side of the neutral axis of the building plan and of negative sign on those lying on the other side. Therefore, the decrements in the yield moments produced at some column ends at a given story will be approximately compensated by the increments taking-place at the other column ends in the same story. Consequently, the response analyses carried out in this study were based on the simplifying assumption that column yield moments are constant and equal to the values that result when column axial forces equal their design values for the condition of ordinary gravity loads.

In order to explore the possible influence of the uncertainty about structural parameters on failure probabilities, two sets of five structures were analyzed under the action of randomly chosen ground-motion records with peak ground accelerations equal to 2.5 m/s^2. The mechanical properties of the structure were taken as deterministically equal to their expected values in one set of structures and as uncertain in the other. Sample means and variation coefficients of Q were obtained for both cases. The resulting failure probabilities, assuming log-normal distribution of Q, were 1.7×10^{-4} and 4.8×10^{-4}, respectively, for the deterministic and uncertain systems. However, if the ln Q is taken as normally distributed, and sample values of it are used to obtain its mean and standard deviation, the resulting failure probabilities are 1.8×10^{-2} and 1.3×10^{-3}, respectively. The large discrepancies between the results arising from the different approaches in analyzing the sample statistics may originate from the small sample size and from the possible inadequacy of the assumption regarding the form of the distribution of Q. Thus, the significance of the uncertainty about structural properties on failure probabilities remains an open question.

The nine-story frame of Fig. 1 was also used for the study of the possible role of the large uncertainties about the excitation on explaining the small differences noted in Figs. 6 and 7 between failure probabilities of systems characterized by high or low statistical correlations between mechanical properties of different members. For this purpose, one set of five simulated frames with lowly correlated mechanical properties and another corresponding to perfectly correlated properties were subjected to the same time-history of ground acceleration (SCT record, normalized to a peak ground acceleration of 250 cm/s^2). In three cases in the first group, the maximum Q-value was attained at the first story, and in the other two, the maximum occurred at the ninth story. In the second group the maximum appeared four times at the first story and once at the third story. However, failure probabilities were not very different: 0.085 and 0.111, respectively.

Expected Failure Rates

Expected failure rates for the different cases considered were obtained in accordance with Eq. 4, using for the interior integral the failure probability curves in terms of intensities, similar to those shown in Figs. 4, 5, 7, and 9. These failure rates are shown as $E(\nu_F)$ in Table 4, which also indicates values of $\nu(y^*)$, the rates of occurrence of intensities higher than the value assumed for seismic design, as well as the ratios $E(\nu_F)/\nu(y^*)$. The latter ratios are seen to vary over very wide intervals. They are lower for high design ductilities than for low values of this parameter. The reason for this trend is similar to that mentioned in connection with the forms of variation of expected ductility demand and failure probabilities in terms of intensities. Asterisks in the last columns of Table 4 serve to identify cases where some reinforced concrete members have reinforcement ratios higher than those strictly necessary

TABLE 4. Expected Failure Rates

Case number (1)	Number of stories (2)	$E(\nu_F) \times 10^3$ (one/yr) (3)	$\nu(y^*) \times 10^3$ (one/yr) (4)	Ratio, $E(\nu_F)/\nu(y^*)$ (5)
1	1	2.550	12.00	0.213
2	1	1.456	12.00	0.121
3	1	1.342	12.00	0.112 (*)
4	1	1.007	12.00	0.084 (*)
5	1	0.332	12.00	0.028 (*)
6	1	0.420	12.00	0.035 (*)
7	1	0.036	12.00	0.003 (*)
8	1	0.137	12.00	0.011 (*)
9	3	2.609	12.00	0.217
10	3	2.060	12.00	0.172 (*)
11	3	2.426	12.00	0.202
12	3	2.527	12.00	0.211
13	3	1.794	12.00	0.150
14	9	0.213	13.70	0.0155

to provide the strengths resulting from the seismic analysis. These higher ratios were adopted for the purpose of complying with minimum re-inforcement ratios required for temperature and shrinkage effects. Thus, part of the decrease in the ratio $E(v_F)/v(y^*)$ for these cases must be ascribed to their being on average stronger than was assumed when adopting a design intensity.

Failure rates of three-story frames are in general higher than those of single-story frames. Two main causes have been identified as possibly leading to this systematic discrepancy: (1) Minimum reinforcement ratios are not found to govern design as often in three-story frames as in the lower ones; and (2) because of the irregularity of the ground motion and the contribution of higher vibration modes to the response, the probability that the latter exceeds a given ductility value at any story is higher for three-story structures.

The failure rate obtained in case 14 cannot easily be compared with those of the previous cases, as it corresponds to a widely different family of strong-motion records and to a different seismic design criterion. The low failure rate obtained can be partly explained by the application of a reduction factor of 0.8 to the nominal value of the available ductility factor considered in design.

Conclusions

A general approach toward evaluating expected failure rates of structures per unit time has been presented; which accounts for uncertainties about mechanical and geometrical properties, as well as about seismic excitation and live load.

Such an approach was applied to one-, three-, and nine-story frames under simulated accelerograms, which were associated with soft and hard types of ground. From the cases analyzed the following was concluded:

l. Among the mechanical properties of the structural members on the probability of failure, the influence of the spatial statistical correlation is relatively small as compared to the influence of other variables.
2. The number of degrees of freedom has a great influence on the probability of failure of structures subjected to earthquakes.
3. The structural failure rate was observed to decrease when the design ductility factors increased. This can be explained in terms of the contribution of the available lateral load capacity that any continuous frame has even if it has not been specifically designed for that type of load. The higher the capacity of the structure to take ductile deformations, the lower the additional lateral strength required to resist a specified set of lateral forces; therefore, the higher the design ductility, the higher, in proportion, is the contribution of the member resistances needed for vertical loads to the lateral strength required to take an earthquake of given intensity, and the higher are the earthquake intensities that may be resisted by the strength reserves due to the differences between expected and nominal values of member resistances.
4. Due to the form of the assumed relation between the expected and the nominal values of the available ductility, as a function of the variation coefficient of that variable, the probabilities of failure for a given intensity are greater for the cases for which that variation coefficient is lower.
5. The seismic hazard function used in this study was arbitrarily chosen. Obviously, other ratios $E(\mathrm{v}_F)/v(y^*)$ would be obtained for other hazard functions. Thus, the values presented in the last column of Table 4 are only general indicators of the signifi-

cance of the variables studied and should not be blindly used to make design decisions.

6. It must be remembered that most systems considered in this study are assumed to develop significant local yielding at several critical sections before a failure limit state is reached. Neither the results reported herein nor the conclusions reached are valid if the safety factors with respect to local brittle failure modes are not sufficiently high with respect to those associated to ductile modes as to prevent the occurrence of the former.
7. Finally, the variability of the failure probabilities obtained for the few cases studied is significant enough as to justify the development of new studies designed to gain greater understanding of it. Future investigations should not only widen the ranges of cases studied, but they should also explore better representations of the mechanical behavior of structural members and systems.

Acknowledments

The writers express their sincere recognition to R. Paredes-López, C. Esguerra, N. Quiroz, and J. E. Ramírez for their invaluable assistance. This project was sponsored by the National Science and Technology Council of Mexico.

Appendix l. References

Cornell, C. A. (1972). "Bayesian statistical decision theory and reliability based design." *Proc., Int. Conf. on Structural Safety and Reliability,* A. M. Freudenthal, ed., Pergamon Press, Oxford, U.K.

Esteva, L. (1967). "Criterios para la construcción de espectros de diseño sísmico". *Tercer Simposio Panamericano de Estructuras,* Universidad Central de Venezuela, Caracas, Venezuela (in Spanish).

Esteva, L. (1968). "Bases para la formulación de decisiones de diseño sísmico", *Report 182,* Institute of Engineering, UNAM, Mexico City, Mexico (in Spanish).

Esteva, L. (1969). "Seismic risk and seismic design decisions". *Proc., Seminar on Seismic Design of Nuclear Power Plants,* R. Hansen, ed., M.I.T., Cambridge, Mass.

Esteva, L. (1976). "Seismicity". *Seismic risk and engineering decisions,* C. Lomnitz and E. Rosenblueth, eds., Elsevier, Amsterdam, The Netherlands.

Kanaan, A. E., and Powell, G. H. (1973). "DRAIN-2D, a general purpose program for dynamic analysis of inelastic plane structures". *Reports No. 73-6 and No. 73-22*, Earthquake Engineering Research Center, University of California, Berkeley, Calif.

Mena, E., et al. (1986). "Catálogo de acelerogramas para terreno blando", *Report 497*, Institute of Engineering, UNAM, Mexico City, Mexico (in Spanish).

Mirza, S. A., and McGregor, J. (1979). "Variation in dimensions of reinforcement concrete members". *J. Struct. Div.,* ASCE, 105(ST4), 751-766.

Moehle, J. P., and Alarcón, L. F. (1985). "Seismic analysis methods for irregular buildings". *J. of Struct. Engrg.,* ASCE, 112(6), 35-52.

Rosenblueth, E. (1976). "Optimum design for infrequent disturbances". *J. Struct. Div.,* ASCE, 102(ST9), 1807-1825.

Rosenblueth, E. (1985). "On computing normal reliabilities". *Struct. Safety*, 2,165-167.

Rosenblueth, E. (1986). "Use of statistical data in assessing local seismicity". *Earthquake Engrg. Struct. Dyn.*, 14(3), 325-338.
Ruiz, S. E., and Lira, E. (1987). "Simulación de acelerogramas para terreno blando". *Report of Project* 5745, Institute of Engineering, UNAM, Mexico City, Mexico.
Ruiz, S. E., Paredes-López, R., and Galarza, V. (1986). "Reliability of structures". *Proc., Eighth European Conf. on Earthquake Engineering*, Vol. 1, 2.4/63-2.4/70.

Appendix II. Notation

The following symbols are used in this paper:

b = width of girders and columns;
EC = El Centro, 1940, NS component;
$E(v_F)$ = expected rate of structural failure per unit time;
f_c = concrete strength;
$f_{\mathbf{R}}(r)$ = probability density function of **R**;
f_y = steel yield resistance;
HC = high spatial correlation;
h = depth of girders and columns;
$K, \in, y_M$ = parameters defining shape of distribution of intensities;
LC = low spatial correlation;
$p_F(y)$ = probability of structural failure under action of earthquake with intensity y;
Q = reciprocal of safety factor, $Q_i = S_i/R_i$;
R_i = structural capacity to resist ith failure mode;
r = cover of reinforcement in girders and columns;
S_i = maximum amplitude of response governing occurrence of ith failure mode;
SCT = SCT, Mexico City, 1985, EW component;
T = fundamental period of structure;
V_x = coefficient of variation of x;
V_μ = coefficient of variation of available ductility;
W_L = live load;
$\underline{X}$ = mean value of x;
y = intensity;
y^* = nominal value of design intensity;
μ = ductility factor;
$v(y^*)$ = rate of occurrence of intensities greater than y^*;
ρ = correlation coefficient; and
$\sigma_{Q/y}$ = standard deviation of Q for given value of y.

Superscripts

* = nominal value.

Subscripts

F = failure.

NONLINEAR SEISMIC RESPONSE OF SOFT-FIRST-STORY BUILDINGS SUBJECTED TO NARROW-BAND ACCELEROGRAMS[1]

The nonlinear dynamic response of shear systems representative of buildings with excess stiffness and strength at all stories above the first one is studied. Variables covered were number of stories, fundamental period, along-height form of variation of story stiffness, ratio of post-yield to initial stiffness, in addition to the variable of primary interest: the factor **r**, expressing the ratio of the average value of the safety factor for lateral shear at the upper stories to that at the bottom story. The lateral strength at the latter was taken as equal to the nominal value of the corresponding story shear computed by conventional modal dynamic analysis for the design spectrum specified by Mexico City seismic design regulations of 1987 for a seismic behavior (ductility) reduction coefficient of 4.0. The excitation was in some cases the EW component of the accelerogram recorded at the parking lot of the Ministry of Communications and Transport in the same city during the destructive earthquake of September 19, 1985, and in some other cases an ensemble of artificial accelerograms with similar statistical properties. It is conc1uded that the nonlinear seismic response of shear buildings whose upper stories have lateral strengths and stiffnesses which correspond to safety factors larger than those applied to the first story is very sensitive to the relation between the average of the over-strength factors at the upper stories and that at the first one, as well as to the ratio of post-yield to initial stiffnesses. The nature and magnitude of the influence of **r** on the maximum ductility demands at the first story depend on the low-strain fundamental natural period of the system. The ductility demands computed for elastoplastic systems may in some cases be extremely large. Accounting for P-delta effects leads to an enhancement of the sensitivity of the response with respect to **r**.

Introduction

It is widely recognized that to a large extent the high rate of destruction caused on the constructions in Mexico City by the earthquake of September 19, 1985, was due to the high intensity of that event as compared to that considered in the seismic design regulations in force at that time. However, the variation of the average damage ratio for different structural types brought to the surface some limitations of modern conventional design criteria to prevent some widely observed damage patterns, particularly in structures characterized by irregular distributions of geometric and mechanical properties. Those limitations arise from the unfitness of the linear methods (both static and dynamic) of response analysis to produce accurate estimates of the distributions of local strains on members and regions of structures —in particular on irregular structures— when they respond to high-intensity earthquakes, capable of giving place to wide incursions of the response into the nonlinear range of behavior.

---

[1] First published in:
Luis Esteva, Nonlinear sesimic response of soft-first-story buildings subjected to narrow-band accelerograms, *Earthquake Spectra*, **8**, 3, (1992)

An important number of the buildings which suffered collapse or extreme damage in 1985 belonged to the type herein designated as "soft-first-story" (SFS), characterized by significantly lower amount of partitions or walls (either designed as structural elements or not) in any one of two orthogonal directions in the first story, as compared to that of the upper stories. As a consequence of this *irregular* distribution of walls, the strengths of the stories above the first one are significantly greater than that of the latter. A quantitative measure of this irregularity is the ratio of the mean of the over-strength factors at the upper stories to that corresponding to the first story. The high rates of damage suffered by structural systems of this type may be largely ascribed to the peculiarities of their nonlinear response and to the uncertainties tied to the prediction of this response, enhanced as a result of the drastic variations of safety factors. However, in many cases the high damage rates may also be due to the plain fact that the first-story lateral strength was too low, regardless of its relation to the strengths of the stories above. On the other hand, the high proportion in which these types of structural systems occur in the total number of cases of collapse or severe damage largely reflects the high percentage of these constructions as related to the total number of tall buildings in the city. The above comments point at the necessity of understanding a) the extent to which the behavior of SFS building s may be more unfavorable than that of buildings with along-height uniform or slowly varying stiffnesses and values of the safety factor (ratio of actual shear strength to computed acting shear), designed for the same seismic coefficients and spectra, and b) how the design criteria applicable to the SFS building s should be adjusted, in order to obtain safety levels comparable to those of the latter.

Several exploratory research programs on the topic are described by Esteva (1987). In the first of those programs a systematic study is made of a number of two-degrees-of-freedom shear-beam systems, the properties of which were selected in such a way that in each case the linear dynamic response of the first story is equal to that corresponding to the fundamental mode of a multi-degree shear system, representative of a typical tall building having the same period as the equivalent two-degree system. In another series of studies, the emphasis is placed on the details of the response histories of a set of five- and twelve-story in-filled frame systems (Ruiz and Diederich, 1989).

Some of the 2 d.o.f. systems mentioned above are representative of building structures designed as frame systems with uniform safety factors along their height, built in such a way that the first story remains free from shear walls, while the upper stories are (unintentionally) strengthened and stiffened by partitions originally not intended to act as structural walls, but in fact bound to act so, as a consequence of not being properly isolated from the structural frames. Thus, the first stories of these structures have lateral strengths consistent with those assumed by the structural designer, but the upper stories are significantly stronger and stiffer than those considered in the project. Therefore, the actual vibration periods are significantly shorter than the calculated ones. Other cases correspond to systems where the lateral stiffnesses of both the first story and the upper ones (or their equivalent, in systems represented with two masses), are determined so as to lead to specified values of the fundamental period and of the ratios of stiffnesses of lowest and upper stories.

In some cases studied, the degree of irregularity of the system was represented by the ratio of the mean of the ratios of actual to required strength at the upper stories to its value at the first story, while in others the basic independent variable was the ratio of the strength increment applied to all the stories above the first one and the strength of the latter. Lateral stiffnesses were incremented in quantities proportional to the increments of strength. In all cases it was concluded that the sensitivity of the first story's lateral deformations to the degree of irregularity grows with the yield ratio, that is, the quotient between the maximum linear —response seismic shear at the first story and the lateral strength of that story, and that for values of the yield ratio of the order of those to be found in conventional structures subjected to moderate— or high-intensity earthquake ground motion the degree of irregularity may show a considerable influence on the mentioned lateral deformations. In addition, it was observed that the influence of the irregularities under study may in some instances lead to reductions of the response of the first story, and in others to increments of that response.

This article presents a summary of previous results, followed by a parametric study on the influence of the presence of a soft first story on the nonlinear dynamic response of shear-beam systems representative of buildings characterized by different numbers of stories and natural periods. For the latter, the ranges of values considered were restricted to those corresponding to the story-stiffnesses that comply with the upper bound to the acceptable deformation established in the 1987 Mexico City earthquake resistant design regulations (Normas Técnicas Complementarias para Diseño Sísmico del Reglamento de Construcciones para el Distrito Federal RDF87 in the following). The study includes cases of stories with hysteretic bilinear behavior, both including and neglecting P-delta effects.

Previous results

The shear-beam systems described by Esteva (1987) were designed in accordance with the Emergency Seismic Design Code of 1985 for the Federal District (Mexico City) with a safety factor equal to unity, and were subjected to the EW component of the record obtained at the parking lot of the Ministry of Communications and Transport (Secretaría de Comunicaciones y Transportes) on September 19, 1985 (record SCT850919EW). Three families of 2 d.o.f. systems were selected, equivalent to building s with 7, 12, and 25 stories and natural periods of 0.7, 1.4, and 2.0 sec., respectively. Equivalence was defined as the equality of fundamental periods, participation factors, and over-strength factors for shear at the first story and those above it.

Among others, a set of elastoplastic shear structures was defined so that in each case the story stiffnesses were proportional to their corresponding safety factors for shear (Fig. 1). The absolute values of the required stiffnesses were determined by consistency with the specified natural periods, but a few of the structures defined in this manner do not comply with the requirement relative to maximum allowable story sways for the design lateral forces. From Figure 1 it is concluded that the ductility demands on the first story are very sensitive to the ratio of the safety factors in the upper and bottom portions of each structure, as well as to its low-strain natural period. It is also observed that the most unfavorable effects occur for intermediate values of the ratio of safety factors.

Other studies considered a set of 2 d.o.f. shear systems, representative of buildings with their first story free of structural walls, designed as rigid frame systems with homogeneous safety factors along their height, but built in such a way that the infill walls placed at the upper stories are not properly isolated from the structure, thus violating the project specifications. Under these circumstances the strength and stiffness of the first story coincide with those assumed in the project, but in the upper stories the values of those properties may be significantly greater than specified. In order to study these cases, two basic systems with uniform safety factors were adopted, each having a different form of variation of story stiffnesses along its height (Fig. 2). A new set of systems was generated from each basic system by increasing its strengths and stiffnesses. For each case the increments were constant; they were applied to every story, with the exception of the first one. The ratio $\delta = \Delta K/K_1$ of the stiffness increment at the upper stories to the first-story stiffness was taken equal to the ratio $\Delta R/R_1$ of the strength increment at the upper stories to the first-story strength. (The condition $\delta = 0$ corresponds to the cases when the over-strength factors are uniform along the height of the building, and the stiffnesses are those corresponding to the structural members needed to supply the required design shear strength). As a consequence of the increment on stiffnesses, for the case of constant-along-height initial stiffness the fundamental periods of the systems studied dropped to 0.54, 0.58, and 0.68 of those corresponding to the basic, unmodified systems for 25, 14, and 7 stories, respectively. The design values of the first-story lateral displacement suffered slight changes (Esteva, 1987). For each system, a companion 2 d.o.f. e1astoplastic equivalent (in the sense defined above) system was defined and its nonlinear dynamic response was computed neglecting P-delta effects. The results are shown in Figure 2, taken from the same reference. These results are qualitatively similar to those in Figure 1.

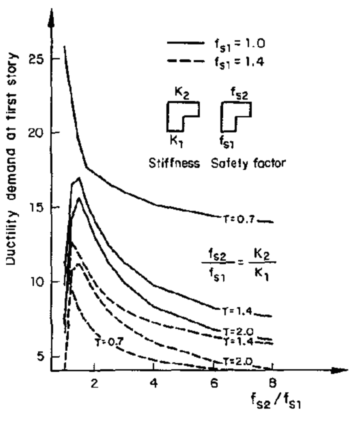

Figure 1. Ductility demands for constant natural periods

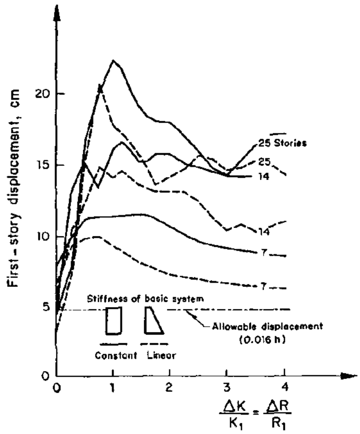

Figure 2. Structural response of systems with modified natural period

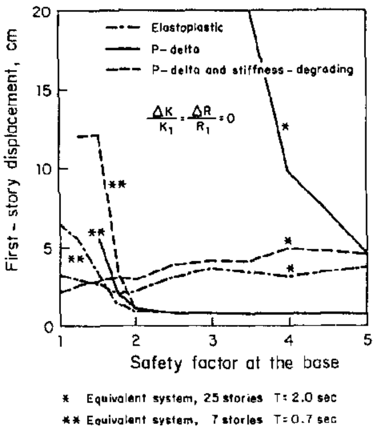

Figure 3. Influence of P-delta and stiffness-degrading effects

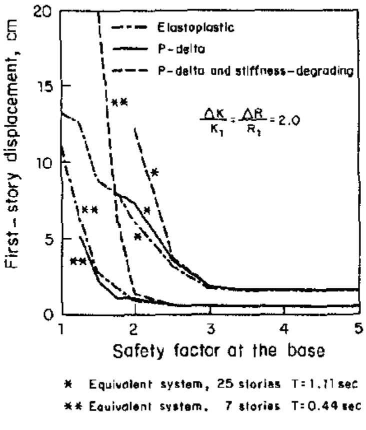

Figure 4. Influence of P-delta and stiffness-degrading effects

Figures 3 and 4, taken also from Esteva (1987), show the sensitivity of the response to P-delta and stiffness-degrading effects. Figure 3 corresponds to uniform systems, and Figure 4 to cases where the stiffnesses and safety factors of all the stories, with the exception of the first one, have been multiplied by 3. The horizontal axis represents the safety factor applied at the first story, while the vertical axis corresponds to lateral deformations. Stiffness-degrading was represented by means of Takeda's model. As seen in Figure 3, this phenomenon can be a determining factor to control the response of some systems with significant P-delta effects. These results contribute to make evident the wide uncertainties which affect the prediction of the dynamic response of real structures, arising from our imperfect knowledge of the forms and parameters of the load-deformation curves under the action of high-intensity alternating loads.

Elastoplastic Systems Without P-Delta Effects

This section presents some results derived from the nonlinear dynamic response analysis of systems representative of buildings with 7, 14, and 20 stories. The behavior of each story is represented by an elastoplastic shear element. All masses were assumed concentrated at the floor levels. The weight of each floor mass was taken as 880 kips (400 metric tons). On the basis of information derived from the properties of some actual buildings, the story stiffnesses of the basic systems (that is, excluding any stiffening element) were assumed to vary linearly along the height of each building, so that the stiffness at the top story was equal to that at the lowest story divided by $n^{2/3}$, where n is the number of stories. The absolute values of the stiffnesses adopted for each system were those required to produce the specified natural period, in accordance with the following table.

TABLE 1

n = number of stories	Natural periods		
7	0.4,	0.7,	1.0
14	1.1,	1.4,	1.5
20	1.8,	2.0	

The story strengths (that is, the ordinates of the horizontal branch of the load-deformation curve) were taken equal to the nominal design values (affected in each case by the applicable load factor) obtained by modal dynamic analysis for the seismic design spectrum specified by the Federal District (Mexico City) Building Code of 1987 (RDF-87, according to its Spanish initials).

The acceleration design spectrum for an inelastic response reduction factor of 4 has maximum values lying along a plateau between 0.6 and 3.9 sec. In addition, attention was paid to complying with the upper bound of 0.012 imposed by the building code considered on the maximum allowable story angular deformations for the design seismic loads. This restriction is satisfied by the stiffnesses which correspond to the natural periods 1isted in Table 1.

Starting from each basic system as described in the foregoing paragraph, a set of modified SFS systems was defined, having the periods listed in Tab1e 1 and story stiffnesses given as follows (Fig. 5):

$$K_1 = \alpha K_{10} \tag{1}$$

$$K_i = \alpha(1+\beta)K_{io}, \qquad i > 1 \tag{2}$$

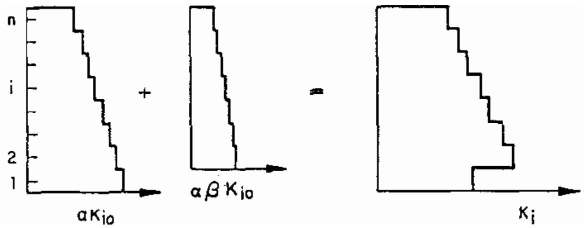

Figure 5. Distribution of lateral stiffness in shear buildings with soft first story

Here, K_{io} is the lateral stiffness of the i-th story of the basic system, K_i that corresponding to a modified SFS system, β the over-stiffness factor at the upper stories, and α a scalar used to adjust the natural period of the modified system to the desired va1ue. It was also assumed that in each modified system the story shear strengths vary in accordance with the following equation.

$$R_i = \frac{K_i}{K_{io}} R_{io} \tag{3}$$

Hence, β may also be defined as an over-strength factor. This variable was assigned values within the interval (0, 2). 1t was verified that for such va1ues the systems whose properties were defined in accordance with the above paragraphs comp1y with the codified restrictions re1ative to allowab1e story deformations. Then a step-by-step integration procedure was app1ied to computing the dynamic response of each system to the record SCT850919EW. P-delta effects were neglected in this part of the study. The response was expressed in each case in terms of the maximum ductility demand (ratio between maximum and yield deformations) at the first story.

The design spectra proposed for various inelastic response reduction factors by RDF-87, adopted in this study, are compared in Figure 6 with those computed from the accelerogram SCT850919EW for various ductility factors. From the comparison it is concluded that for va1ues of the seismic behavior factor between 2 and 4 the ordinates of the design spectrum generally coincide with those corresponding to the mentioned accelerogram for a ductility factor numerically equal to the response reduction factor. However, for short vibration periods the ordinates of the spectra derived from the recorded ground motion are slightly greater than those specified by the design spectra.

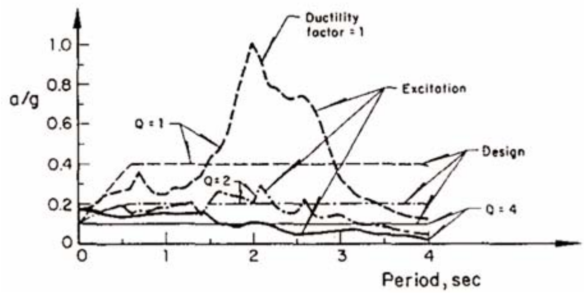

Figure 6. Response spectra for excitation and for nominal design conditions

The results of the response analyses are shown in Figures 7-9. There it may be observed that the computed first-story ductility demands are very large for short natural periods. This may be ascribed to the discrepancies between the design-spectrum ordinates and those obtained from the recorded acce1erogram for a response reduction factor of 4. With the purpose of supporting this assumption and trying to discard the possibility of significant numerical errors in the dynamic response computations as the main cause for the high values of the ductility demands, the same numerical integration program was applied to determine the dynamic response of a hysteretic elastoplastic 1 d.o.f. system with a natural period equal to 1.4 sec, designed for a base shear coefficient of 0.1532, which corresponds to the ordinate of the elastoplastic response spectrum of the accelerogram SCT850919EW for a response reduction factor equa1 to 4. The computed ductility demand was 3.56. The same system, designed for a base shear coefficient of 0.10, specified by RDF-87 for the vibration period of interest for a seismic behavior coefficient of 4, responded with a ductility demand of 5.8. These results support the assumption formulated above, although they do not constitute a conclusive proof thereof. Another concept which contributes to the large values of the first-story nonlinear response is the difference between the nominal seismic design coefficient (0.10) and the ratio of the first-story lateral strength and the weight of the building. In those cases whose results are shown in Figure 8 for $\beta = 0$ and periods between 1.1 and 1.5 sec, this ratio equals 0.0758. Its discrepancy with the nominal seismic design coefficient is due to the introduction of modal participation factors in conventional linear dynamic analysis. Differences like these are often associated with excessive ductility demands at the bottom stories of multi-degree-of-freedom shear systems (Esteva, 1980).

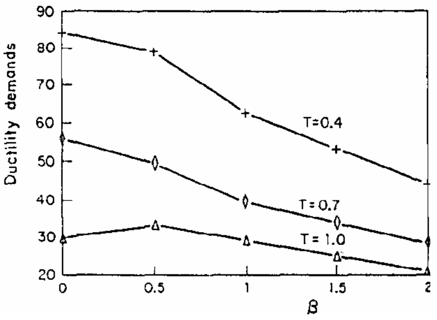

Figure 7. Response of seven-story systemas without P-delta effects

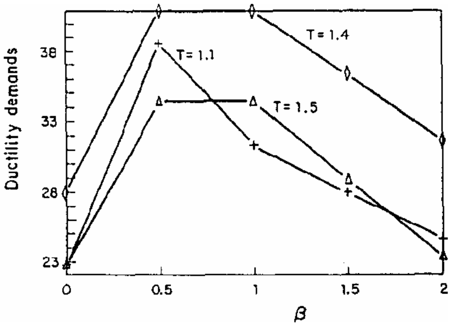

Figure 8. Response of fourteen-story systems without P-delta effects

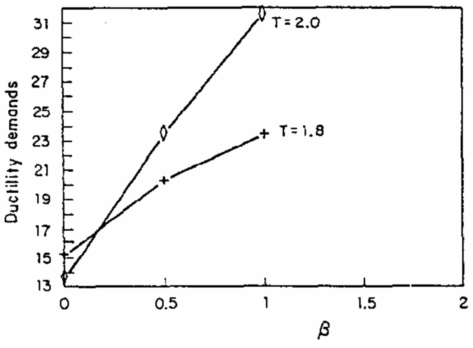

Figure 9. Response of twenty-story systems without P-delta effects

Figures 7-9 also show that for short-period systems ductility demands decrease while β grows, while for moderate and long periods those demands show an initial increase up to a maximum and then start decreasing for large values of β. These results are consistent with those derived from the previous studies described above (Esteva, 1987; Ruiz and Diederich, 1989).

Bilinear Systems With P-Delta Effects

Two series of studies were undertaken. The first one was devoted to obtaining the responses of the structures described in the preceding section subjected to the same accelerogram, that is SCT850919EW. Because for some structures collapse by instability was reached before the end of the ground motion, it was decided to present the results as in Figures 10-17, in terms of the safety factors (ratios of story strengths to acting shear forces) applied in the design of the shear systems, as well as of the coefficient β of over-strength of the upper stories. The figures show that for the chosen design and excitations safety factors as high as 2.0 or more are required to keep ductility demands of short period structures within reasonable limits. For structures with long natural periods the required safety factors may lie around 5.0. On the other hand, the same figures show that for short period structures ductility demands at the first story decrease when β grows, while for long period structures the inverse effect takes place.

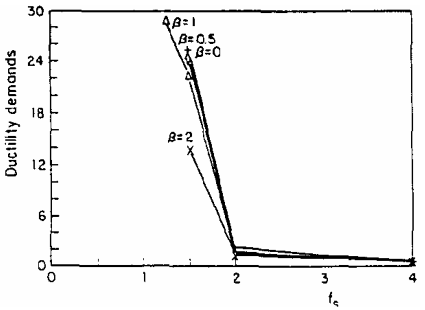

Figure 10. Response of systems with P-delta effects to SCT850919 EW. 7 stories, T=0.4 sec

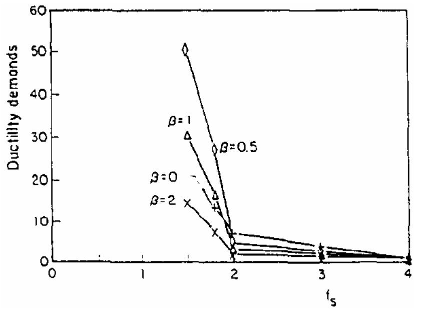

Figure 11. Response of systems with P-delta effects to SCT850919 EW. 7 stories, T=0.7 sec

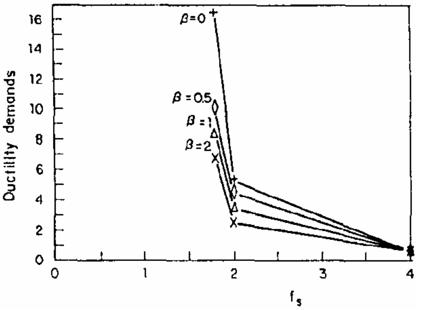

Figure 12. Response of systems with P-delta effects to SCT850919 EW. 7 stories, T=1.0 sec

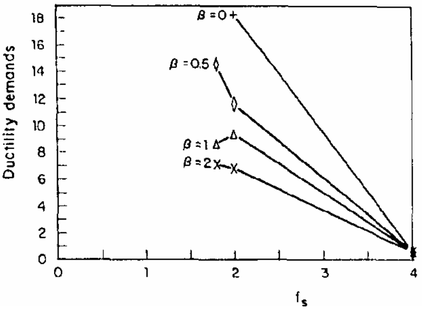

Figure 13. Response of systems with P-delta effects to SCT850919 EW. 7 stories, T=1.1 sec

This difference in behavior may be explained as the result of the superposition of two effects: the concentration of ductility demands at the weakest story and the variation of the response spectrum ordinate in terms of the effective vibration period of the nonlinear response of the structure. In some cases both effects are additive, while in other cases, such as short period structures, the reduction of the response spectrum ordinate associated with the shortening of the effective natural period overshadows the concentration of ductility demands.

The second series of studies dealt with structures having stories with initial stiffnesses and yield capacities equal to those of the first series. However, three different alternate forms of the force-deflection curves for a given story were considered: one elastoplastic and two bilinear. These curves were defined in terms of k_1, the initial stiffness, corresponding to small deformations in the linear range of behavior, and k_2, the post-yield stiffness. Thus, three different values of the ratio k_2/k_1 were considered for each story. The response of each system was computed for a set of artificial accelerograms having statistical properties equal to those of SCT8509l9EW (Grigoriu et al, 1988). The results were represented in terms of the minimum safety factor required to avoid in each case the collapse by dynamic instability. Such minimum factors were estimated from the responses of systems with various safety factors by means of the algorithm described in the Appendix.

Figures 18-21 show the response to each accelerogram of some of the systems studied, as well as the points joining the mean values of the responses with respect to the set of accelerograms. Besides the considerable dispersion of the results, other trends become evident. They are studied in detail by means of Figures 22-32, which show the mean values obtained for al1 the cases studied. The groups of Figures 22-24, 25-27, and 31-32 respective1y correspond to 7, 14, and 20 stories. Each figure refers to a va1ue of the system's fundamental period and includes three curves, one for each value of the ratio k_2/k_1. The group 28-30 corresponds to 14-story buildings, but un1ike group 25-27 each figure corresponds to a given va1ue of k_2/k_1 and contains curves associated with various natural periods.

Figures 22-24 show that for short natural periods (T = 0.4, 0.7) the required safety factors decrease as β increases. For these cases the influence of k_2/k_1 is significant, practically equal for the two values of k_2/k_1 studied, that is, 0.01 and 0.10. It can be observed that this variable contributes to reducing the sensitivity of the response with respect to β.

For moderate periods (T = 1.0, N = 7, Fig. 24, T = 1.1, N = 14, Fig. 25) the required safety factors are not very sensitive to β. Besides, the influence of k_2/k_1 is more gradual than that occurring in short period systems.

For natural periods equal or greater than 1.4 sec the required safety factors grow significantly and systematically with β (Figs. 26-32). The influence of k_2/k_1 is low for small values of this variable, but for k_2/k_1 = 0.10 it is of the same order as that affecting structures with short and moderate natural periods.

From Figures 22-32 it is also concluded that for the design and excitation conditions described above (RDF-87, artificial accelerograms with statistical properties equal to those of SCT850919EW) the mean values of the required safety factors for elastoplastic systems vary from 1.9 to 1.6 for short period systems (0.4 and 0.7 sec), remain between 1.8 and 2.1 for periods of 1.0 and 1.1 sec, grow with β from 2.5 to 3.4 sec for structures with periods of 1.4 and 1.5 sec and reach values between 4.3 and 6.3 for periods of 1.8 and 2.0 sec.

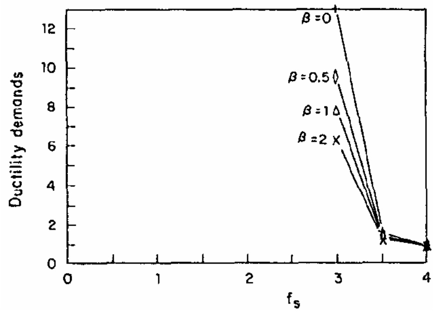

Figure 14. Response of systems with P-delta effects to SCT850919 EW. 14 stories, T=1.4 sec

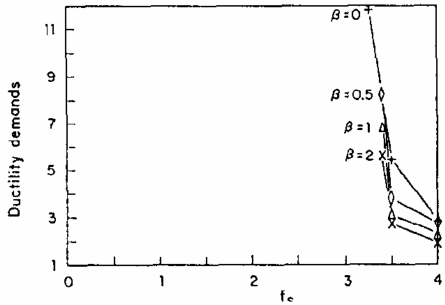

Figure 15. Response of systems with P-delta effects to SCT850919 EW. 14 stories, T=1.5 sec

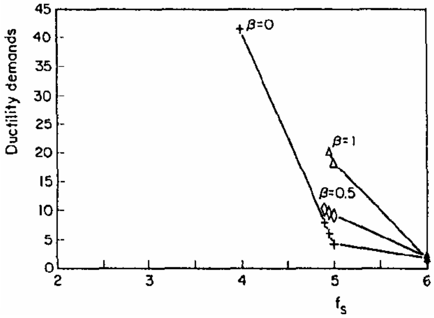

Figure 16. Response of systems with P-delta effects to SCT850919 EW. 20 stories, T=1.9 sec

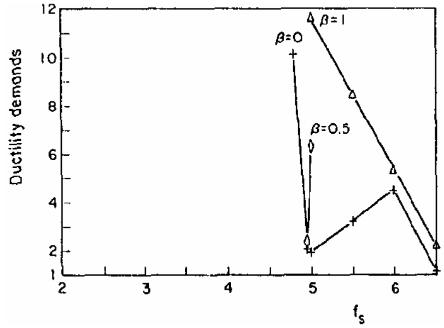

Figure 17. Response of systems with P-delta effects to SCT850919 EW. 20 stories, T=2.0 sec

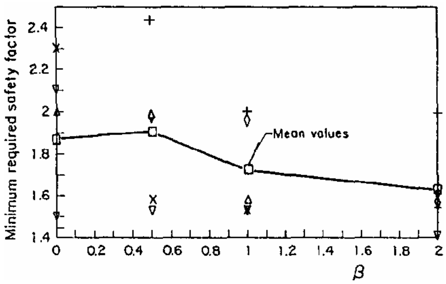

Figure 18. Response of bilinear structures with P-delta effects to artificial accelerograms . 7 stories, T=0.4 sec. k_2/k_1=0

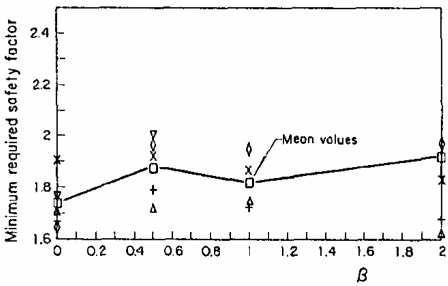

Figure 19. Response of bilinear structures with P-delta effects to artificial accelerograms. 7 stories, T=1.0 sec, .k_2/k_1=0.1

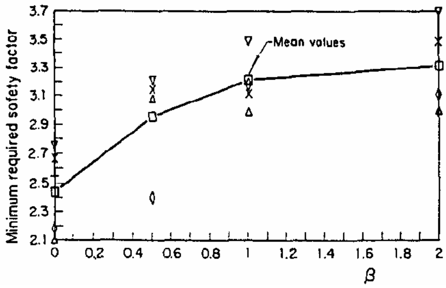

Figure 20. Response of bilinear structures with P-delta effects to artificial accelerograms. 14 stories, T=1.5 sec. k_2/k_1=0

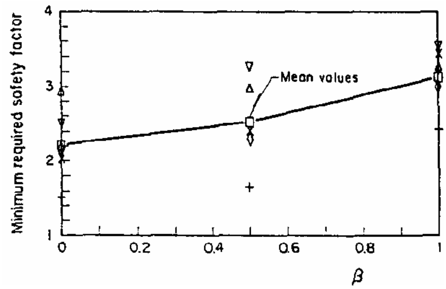

Figure 21. Response of bilinear structures with P-delta effects to artificial accelerograms. 20 stories, T=2.0 sec, .k_2/k_1=0.1

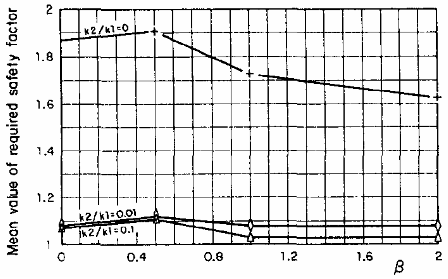

Figure 22. Shear systems with P-delta effects. Artificial accelerograms. 7 stories, T=0.4 sec.

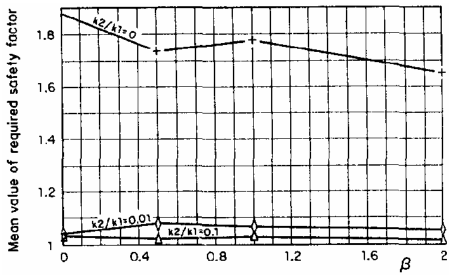

Figure 23. Shear systems with P-delta effects. Artificial accelerograms. 7 stories, T=0.7 sec.

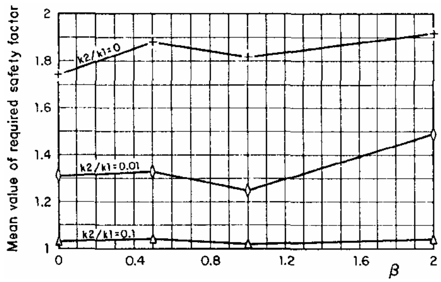

Figure 24. Shear systems with P-delta effects. Artificial accelerograms. 7 stories, T=1.0 sec.

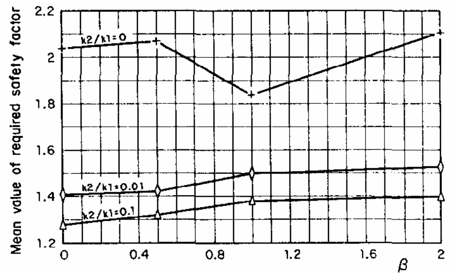

Figure 25. Shear systems with P-delta effects. Artificial accelerograms. 14 stories, T=1.1 sec.

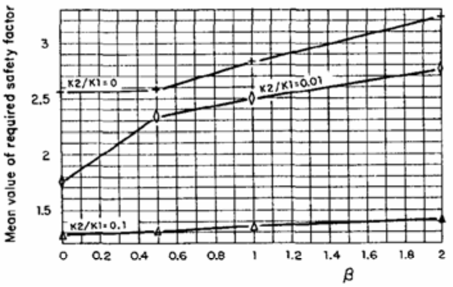

Figure 26. Shear systems with P-delta effects. Artificial accelerograms. 14 stories, T=1.4 sec.

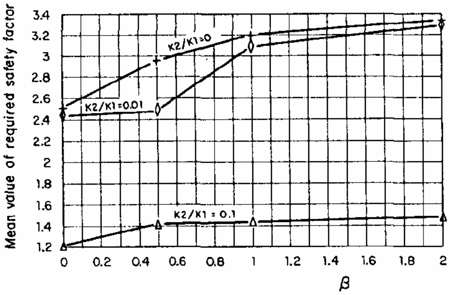

Figure 27. Shear systems with P-delta effects. Artificial accelerograms. 14 stories, T=1.5 sec.

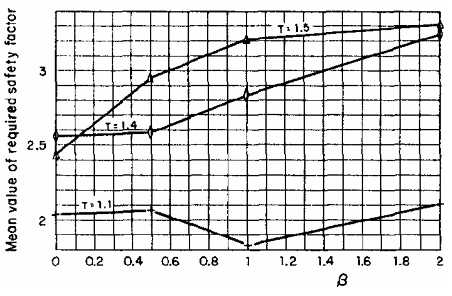

Figure 28. Shear systems with P-delta effects. Artificial accelerograms. 14 stories, k_2/k_1=0.0

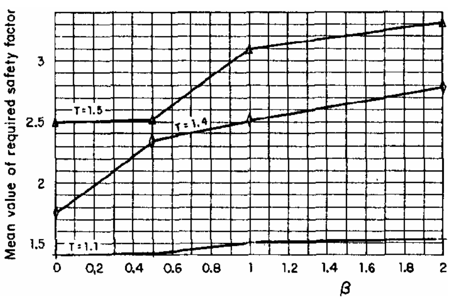

Figure 29. Shear systems with P-delta effects. Artificial accelerograms. 14 stories, k_2/k_1=0.01

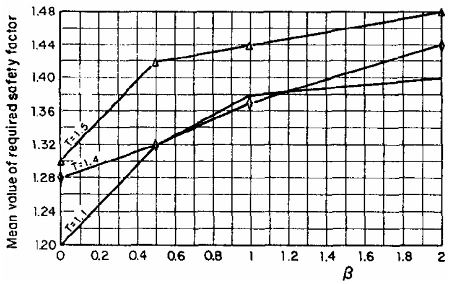

Figure 30. Shear systems with P-delta effects. Artificial accelerograms. 14 stories, k_2/k_1=0.10

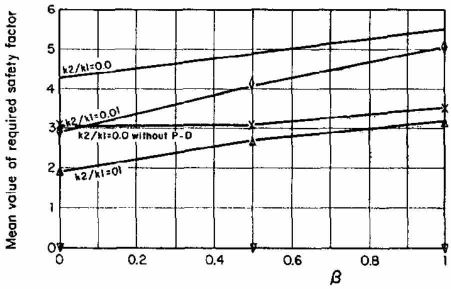

Figure 31. Shear systems with P-delta effects. Artificial accelerograms. 20 stories, T=1.8 sec.

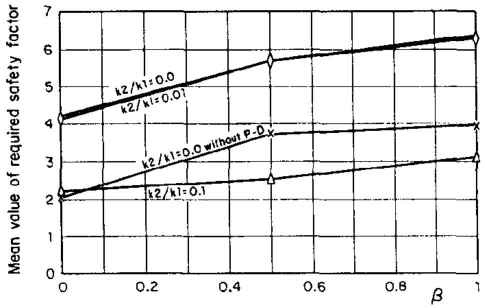

Figure 32. Shear systems with P-delta effects. Artificial accelerograms. 20 stories, T=2.0 sec.

Figures 31 and 32 show also curves corresponding to responses calculated neglecting P-delta effects. Here, the failure criterion was expressed by the condition that the story ductility exceeded 4.0. Under these circumstances the required safety factors fluctuate between 3.0 and 3.6 for T = 1.8 sec and between 2.3 and 3.1 for T = 2.0 sec.

Conclusions

From previous studies and those presented in this work the following conclusions are reached, applicable to ground motion histories having durations and frequency contents similar to those of SCT850919EW, and to buildings with stiffness and strength distributions similar to those described above.

1. The nonlinear seismic response of shear buildings (that is, systems such that the lateral deformation of each story depends only on the mechanical properties of that story and the shear force acting on it) whose upper stories have lateral strengths and stiffnesses which correspond to over-strength factors larger than those applied to the first story is very sensitive to the ratios between the over-strength factors at the upper and bottom stories.
2. The nature and magnitude of the influence of the ratio r = 1 + β of the average over-strength factor at the upper stories to the over-strength factor at the first story on the maximum ductility demands at the latter depend on the low-strain fundamental natural period of the system. For very short natural periods (0.4 sec) those ductility demands may be reduced in about 30 percent when **r** grows from 1.0 to 3.0. For intermediate periods (T = 1.0), ductility demands are little sensitive to **r,** but for longer periods they may reach increments of 50 to 100 percent while r varies within

the mentioned interval. For períods between 1.1 and 1.5 sec the maximum amplifications occur for r values between 1.5 and 2.0, while for periods of 1.8 and 2.0 sec ductility demands grow monotonically with r within the interval of values considered (1.0 - 2.0).

3. The ductility demands computed for elastoplastíc shear systems with periods ranging from 1.1 to 2.0 sec are extremely large, even in those cases where the amplification due to the sharp variation of safety factors is not present.
4. The influence of **r** on the response of the first story is strongly enhanced if P-delta effects are taken into account. For elastoplastic systems, when **r** varies from 1.0 to 2.0 the mean values of the safety factors at the first story required to avoid collapse by dynamic instability under an ensemble of accelerograms representative of SCT850919EW vary from 1.87 to 1.63 for periods of 004 and 0.7 sec, between 1.74 and 1.92 for periods of 1.0 sec, between 2.57 and 3.24 for periods near 1.4 sec and between 4.3 and 6.4 for 2.0 sec.
5. The above mentioned effects suffer qualitatively similar variations for bilinear hysteretic systems with post-yield stiffness greater than zero. However, those variations are less pronounced than for elastoplastic systems.
6. The results described above may serve as guidelines for applications by structural designers and code writers. However, it appears convenient to widen the scope of this contribution by means of additional studies, covering the following concepts, among others:
   a) Accelerograms with various durations and frequency contents;
   b) Systematic study of the influence of post-yielding stiffness, as well as stiffness and strength degradation;
   c) Probabilistic response analyses, incorporating uncertainties tied to mechanical properties of the systems;
   d) Response of frame systems with infilled panels; and
   e) Systems whose response may be significantly sensitive to soil-structure interaction.

Appendix: Estimation of the minimum safety factor required to prevent collapse

From Figures 10-17 it is concluded that a possible way of determining the lower bound to the safety factor required to prevent collapse consists in extending the curve of responses μ vs over-strength factors f_s as far to the left as possible, in order to determine with sufficient accuracy the abscisa of the vertical asymptote to that curve. This may require computing the dynamic response for too many values of the safety factor in the neighborhood of the lower value to be determined. One way of cutting down the numerical work without undue loss of accuracy consists in plotting along the vertical axis the reciprocal of the ductility demand. The resulting curve intersects the horizontal axis at $f_s = f_{so}$, which is the desired lower bound (Fig. Al). On the basis of the values of $1/\mu$ and f_s for three conveniently located points, f_{so} may be estimated by fitting a curve through those points. If at least one of them lies near the intersection f_{so}, the form adopted for the curve under consideration is not too important, provided it satisfies the conditions at the ends. One form which satisfies this criterion is the following.

$$1/\mu = af_s - b\exp[-cf_s] \tag{A1}$$

Here, a, b, and c are parameters to be determined by curve fitting through three points chosen as follows (Fig. Al).

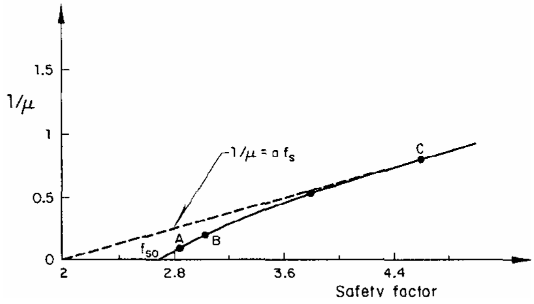

Figure A1. Estimation of f_{so}

1. Point C corresponds to a very large f_s, thus permitting an immediate, accurate estimation of a.
2. Point A is chosen on the basis of previous experience, so that $1/\mu$ is not greater than 0.1.
3. Point B is selected in accordance with the criterion that the corresponding value of af_s - $1/\mu$ is of the order of one half of that for point A.

Given a, b, and c, f_{so} may be obtained by applying Newton-Raphston's method to Equation 1, with $1/\mu = 0$.

References

Esteva, L. (1987), "Earthquake Engineering Research and Practice in Mexico after the 1985 Earthquake", *Bull. New Zealand National Society for Earthquake Engineering.* 20 (no. 3): 159-200.

Ruiz, S.E. and Diederich, R. (1989), "The Seismic Performance of Buildings with Weak First Story", *Earthquake Spectra* 5 (no. 1): 89-102 (Feb. 1989).

RDF87, "Normas Técnicas Complementarias para Diseño Sísmico del Reglamento de Construcciones del Distrito Federal", México, D.F.

Esteva, L. (1980), "Design: General", Chapter 3 of *Design of Earthquake Resistant Structures.* edited by E. Rosenblueth, Pentech Press, London.

Grigoriu, M., Ruiz, S.E. and Rosenblueth, E. (1988), "Nonstationary Models of Seismic Ground Acceleration", *Earthquake Spectra* 4 (no. 3): 551-568 (Aug. 1988).

SEISMIC DUCTILITY DEMANDS PREDICTED BY ALTERNATE MODELS OF BUILDING FRAMES[1]

Peak values of story ductility demands produced by earthquakes on several models of multistory rigid frames are evaluated by means of step-by-step nonlinear dynamic analysis of structural response to simulated ground motion time histories. The models studied include the basic rigid frame model with nonlinear behavior concentrated at plastic hinges eventually forming at the ends of beams and columns, as well as two approximations, the conventional shear-beam system and a shear-frame system constituted by ordinary reinforced concrete columns and infinitely stiff and strong beams. Two families of models were studied, including seven-story and fourteen-story systems, respectively. The contributions of soil-structure interaction, stiffness-degradation and P-delta effects were analyzed. The equivalent shear-beam model produced results clearly different from those of its rigid frame counterpart: while peak values of story ductility demands vary gradually along the height of rigid frames, they concentrate at the bottom story of shear-beam systems, where they are significantly greater than for the corresponding rigid frame. The responses of both, shear-beam and shear-frame systems, displayed a more pronounced sensitivity to variations in the lateral strengths of structural members than that observed in rigid frames.

Introduction

Among the wide diversity of structural models used to estimate the nonlinear seismic response of building frames, the shear-beam is the one most frequently adopted. It has been shown, however, that this model predicts excessive ductility demands in the lowest stories, as compared with those resulting from the use of the more refined, and more accurate, rigid frame model (1, 2). These differences in the response have been ascribed to the differences in the capabilities of both types of systems to redistribute the ductility demands acting at a given story by transforming them into smaller demands acting at the adjacent stories. While this capability is significant in building frames designed in accordance with the strong-column-weak-beam concept, it does not exist in multistory shear systems. Another limitation of the conventional shear model is its inability to represent many details of structural behavior, such as the local failure of element cross sections, the influence of axial force on column behavior and the deterioration of stiffness and strength of the individual members. In spite of these drawbacks, shear-beam models are widely used to study the seismic response of multistory buildings, because of their simplicity and their low computer time consumption, thus permitting the performance of ample parametric studies.

This article presents a study about the nonlinear seismic response of two buildings, each represented by three different models: rigid frame, equivalent shear-beam system and equivalent shear-frame. (The latter case corresponds to a rigid frame with infinitely stiff and strong girders.) The study also covers the influence on the response of these

[1] First published in:
Orlando Díaz, Enrique Mendoza, and Luis Esteva, Seismic Ductility Demands Predicted by Alternate Models of Building Frames, *Earthquake Spectra*, **10**, 3, 465-487, 1994.

models of diverse effects such as soil-structure interaction, P-delta effects and hysteretic behavior of structural members. Comparisons are made between the responses predicted by the various models and possible explanations for the discrepancies are found.

The buildings studied are assumed to be founded on compressible soil with mechanical properties similar to those of Mexico City clay.

Buildings Studied

Two idealized buildings were studied. They were respectively seven and fourteen stories high and possessed the following general characteristics.

a) Aspect ratio (height/width ratio) greater than 2.5.
b) Approximately linear variation of lateral stiffness along the building height.
c) Uniform distribution of mass along building height.

The seven-story building has a 22 m height and a 8 m by 8 m plan. Its structure consists of three rigid frames in each of two orthogonal directions (fig. 1). The fourteen-story building is 43.2 m high, has a 14 m by 14 m plan, and its structure consists of three rigid frames in each direction and continuous secondary beams supported at midspan of the main girders (fig. 2). In both cases the resulting dead load acting on each floor is equal to 7063 Pa (147 psf); the maximum live load, w, is 2453 Pa (51 psf), and the instantaneous live load, w, is 1766 Pa (37 psf). In order to obtain a linear variation of the lateral stiffness along the building height, in both building models the height of the first story was assumed to be greater than that of the other stories. This configuration is typical of actual buildings. In addition, it was assumed that the bottom ends of the columns of the fourteen-story building were not fixed at the foundation, but connected to a foundation girder with finite stiffness (fig. 2).

The lateral stiffnesses of all the stories were computed on the basis of the assumed cross-sections of the structural members. The resulting values are presented in Table 1. For the purpose of taking into account soil-structure interaction effects, the foundation of the seven-story building was assumed to consist of a partial-load-compensation system: a reinforced concrete hollow box, stiffened by a grid of foundation girders (fig. 3).

The fourteen-story building was considered to be supported on friction piles (fig. 4). For the design of the foundations, the mechanical properties of the soil were taken as equal to those corresponding to the SCT site (Spanish initials for the Ministry of Communications and Transport) in the soft soil area in Mexico City (4). The criteria adopted for the design of the foundations were those specified in the 1987 revision of Mexico City Building Code (5), for both, failure and serviceability limit states. Figures 3 and 4 show the data assumed for design purposes.

Models Studied

It was assumed that the seismic response of a building along a given direction could be approximated by that of the central frame, isolated from the rest of the structure.

The effects of gravitational loads on the internal forces acting on the sections of beams and columns of that frame were obtained by the conventional methods of structural analysis, taking into account the corresponding tributary areas. However, for the purpose of computing seismic response, the mass associated to each floor level of the frame was taken equal to one third of the corresponding mass for the whole building at the same floor level.

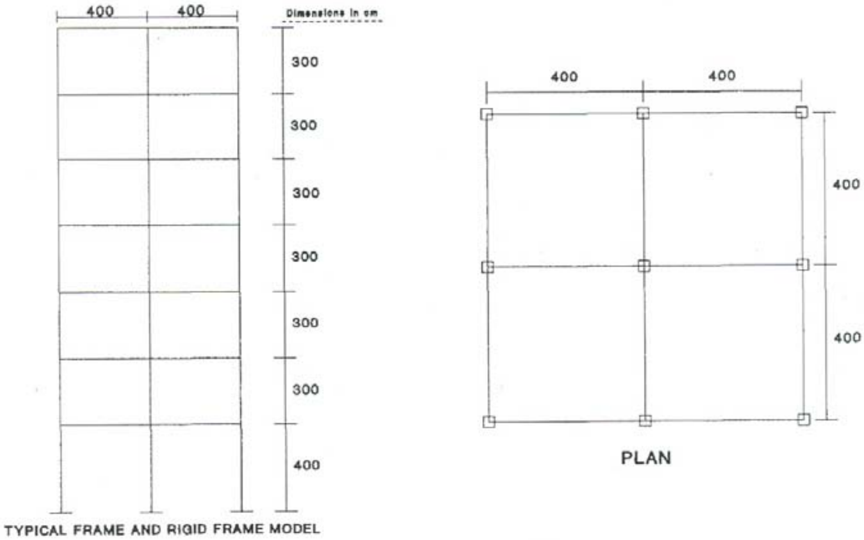

Figure 1. Seven-story building

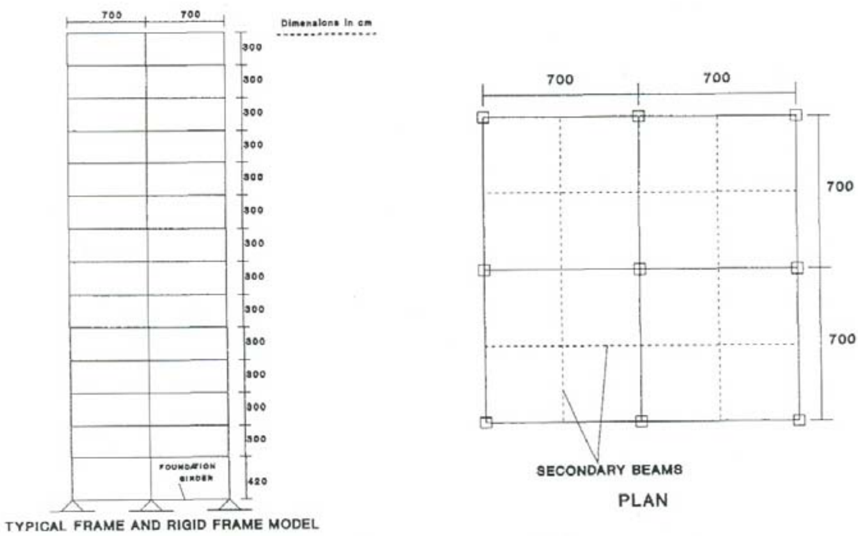

Figure 2. Fourteen-story building

TABLE 1

Story Stiffnesses of the Buildings Studied

	STIFFNESS (kips/in)	
STORY	SEVEN-STORY	FOURTEEN-STORY
1	501	1971
2	457	1839
3	424	1600
4	346	1476
5	324	1368
6	215	1303
7	196	1218
8		1169
9		1074
10		1030
11		901
12		859
13		748
14		632

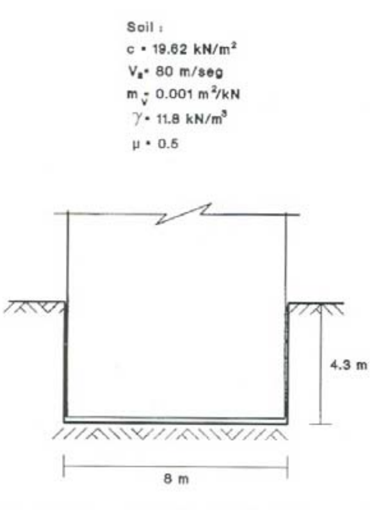

Figure 3. Foundation of seven-story building

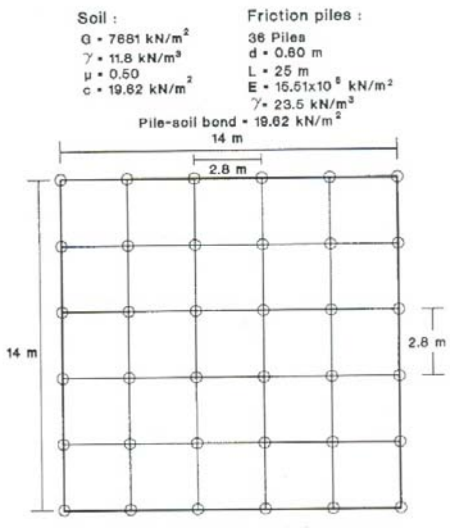

Figure 4. Foundation of fourteen-story building

Three alternative models were used to estimate the response of each building: a) rigid frame, b) equivalent shear-beam, and c) equivalent "shear-frame". The details are explained in the following.

a) Rigid Frame

This model corresponds to the conventional representation of an assemblage of beams and columns with finite stiffnesses and resistances, and with the connections between structural members free to rotate as infinitely rigid elements. The structural analysis and design were carried out in accordance with the 1987 Mexico City Building Code (RDF87) (6), for the conditions corresponding to building resting on the soft clay formation (zone III, according to the code), for a reduction factor (to account for nonlinear ductile behavior) of 4. In order to simplify the design process, it was assumed that all columns in a given story would have the same cross section and reinforcement, which would correspond to the highest requirements for all the column cross sections in the story. Reference 3 includes a detailed description of the analysis and design of all frames studied, as well as of the geometrical and mechanical properties of all structural members.

As it is well known, the values of forces and structural member resistances used in the design equations result from multiplying the nominal values of those forces and resistances by adequate load factors or strength reduction factors.

The criteria applied for the determination of the nominal values of loads and resistances, as well as the associated load factors and strength reduction factors, aim at attaining sufficiently small failure probabilities. As a consequence, the design values of those variables correspond to conservative values of them. Because an objective of this article is to estimate the response of structures designed and built in accordance with a given set of requirements and specifications, it is convenient to work with the most likely values of the design variables or with their expected values, rather than with their design values. The latter approach was preferred in this article instead of the more rigorous, but more demanding, approach of incorporating the influence of the uncertainties about loads and mechanical properties on the failure probabilities of the system through Monte Carlo simulation. Reference 2 presents a detailed analysis of the estimation of the expected values of the design variables. According to that study, the expected and the design values of these variables are related as follows: $m_s = S_d /1.24$, $m_R = 1.406\ R_d$ for beams, and $m_R = 2.108\ R_d$ for columns. In these equations, m_s is the expected value of a load effect resulting from the action of gravitational loads and S_d the corresponding design value; m_R is the expected resistance of a given member cross section, and R_d its design value.

b) Equivalent shear-beam

This model corresponds to a system of masses, springs and dampers, the properties of which are defined as follows:

i) The system is an assemblage of structural members connected along horizontal interfaces, which coincide with the floor levels and, therefore, with the levels where the building mass is assumed to be concentrated. These members suffer only shear deformations when subjected to lateral forces (fig. 5).

ii) The lateral stiffness of the structural element used to represent the mechanical properties of a given story is equal to the lateral stiffness of that story, computed on the basis of adequate assumptions regarding the deformed shape of the original frame.

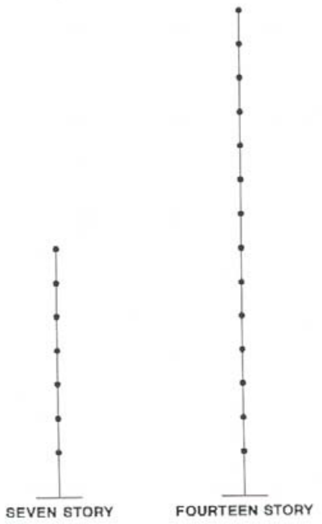

Figure 5. Equivalent shear-beam model

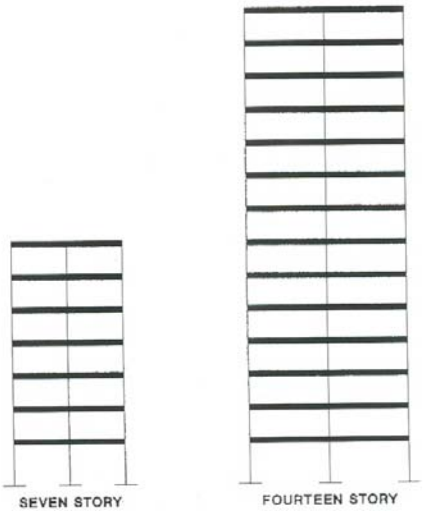

Figure 6. Equivalent shear-frame model

iii) The expected values of the gravitational loads acting on the frame are taken into account for the purpose of determining P-delta effects on the seismic response.
iv) The yield strengths of the stories are determined on the basis of the seismic responses of the rigid frames, computed by means of nonlinear dynamic response studies. For those stories whose computed response does not reach their yield strengths, the estimation of the latter has to be done by a different procedure. An alternative approach, presented in Ref. 2, consists in applying to the original frame a configuration of lateral deformations which are made to increase proportionally up to the point when the stories of interest reach their yield capacities. Reference 3 presents the values of the lateral yield strengths used for the response analysis studied herein.

c) Equivalent shear-frame

The general geometry of this model is similar to that of the conventional rigid frame (equal numbers of stories and spans and equal story heights), but differs from it in the mechanical properties of its members: the columns have very large axial stiffnesses and the beams have very large flexural strengths and stiffnesses (fig. 6). As a consequence of these properties, the lateral response of the shear-frame is similar to that of a shear-beam, but the flexural strengths of the columns are influenced by the axial forces on the columns induced by both gravitational and seismic actions. The model is defined in accordance with the following concepts:

i) The mass concentrated at each floor level is equal to one third of the mass at the same floor level for the whole building.
ii) All the columns in a given story have equal cross sections, such that the lateral story stiffness of the model is equal to the story stiffness of the central frame of the building.
iii) The joints are free to rotate and to displace in the vertical and in the horizontal directions in the plane of the frame.

iv) Axial forces on the columns resulting from gravitational loads are distributed as the reactions of a continuous beam.

v) The frame is analyzed and designed following the same criteria and methods as the conventional rigid frame, but the beams are assumed to be infinitely strong. It is also assumed that all the columns in a given story have a strength equal to that of the column requiring the largest reinforcement area in the story. Steel percentages adopted were in all cases directly obtained from the design equations, in spite of the fact that in some cases those percentages were greater than the maximum allowable values established by the design code adopted (Mexico City 1987 code).

This type of system was studied only for the case of the fourteen-story building.

Models for Response Analysis

In the studies of dynamic response, due consideration was given to the influence of soil-structure interaction, P-delta effects and stiffness degradation of beams subjected to cyclic loading. This gave place to the following cases of analysis:

1. Elastoplastic behavior of beams and columns, neglecting soil-structure interaction and P-delta effects.
2. Elastoplastic behavior of beams and columns, including soil-structure
3. Elastoplastic behavior of beams and columns, including soil-structure interaction and P-delta effects.
4. Elastoplastic columns, stiffness-degrading beams (Takeda-type), including soil-structure interaction and P-delta effects. This type of analysis was applied only to the rigid frame systems.

Soil–Structure Interaction

The influence of soil-structure interaction is studied with the aid of the model described in Reference 1. That model accounts separately for two modes of interaction (fig. 7):

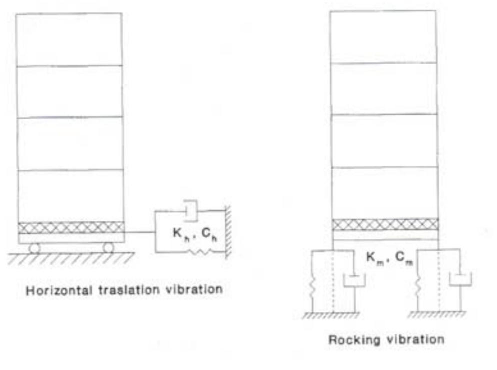

Figure 7. Soil-structure interaction model

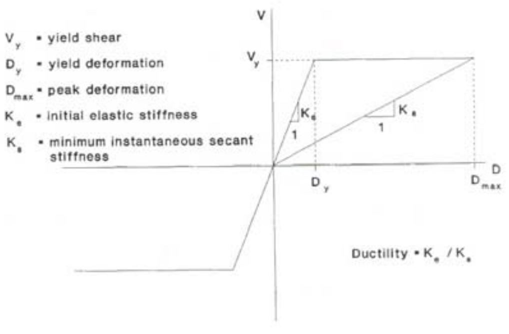

Figure 8. Peak story-displacement ductility

a) A translational mode, represented by a linear-behavior spring and a linear-viscosity damper, both referred to the horizontal degree of freedom of the base of the structure.
b) A rocking mode, represented by a linear-behavior rotational spring and a linear-viscosity rotational damper, both referred to the angular degree of freedom of the base of the structure.

The values of the parameters associated to both springs and dampers were calculated for each building studied, on the basis of the characteristics of its corresponding foundation. For the seven-story building, the values of stiffness and damping were based on the assumption of a foundation mat resting directly on the ground, at a given embedment depth (3). For the fourteen-story building, a friction pile foundation was assumed; the mechanical properties of the elements representing soil-structure interaction were determined accordingly, using the method described in Reference 1. The values resulting for both cases are displayed in Table 2. One third of the stiffness and damping shown was assigned to the central frame of each building studied.

TABLE 2

Stiffness and Damping Constants for the Soil-Structure Interaction Model

BUILDING	LATERAL MODE		ROCKING MODE	
	K_h (kp/in)	C_h (kp.s/in)	K_m (kp.ft/rad)	C_m (kp.ft.s/rad)
7 STORIES	1782	148	6.49×10^6	2.46×10^5
14 STORIES	5546	252	9.77×10^7	1.92×10^6

In the design of the models studied considering soil-structure interaction, no attention was paid to the requirements contained in the Appendix of Reference 8, relative to the adoption of site-specific response spectra.

Ground Motion Time Histories

For the cases studied, the structural response was obtained for five simulated ground motion records, statistically similar to the EW component of the accelerogram recorded at the Ministry of Communications and Transport, Mexico City, on September 19, 1992 (9). The first and the last portions of each "record" were eliminated, in order to keep only its most intense portion, comprised between 2 and 98 percent of the accumulated energy. For the interval (0, t), the latter is defined as $\int_0^t a^2(t)\mathrm{d}t$, where $a(t)$ is the ground acceleration (10).

Results

The seismic response for each member of the selected sample of simulated records was calculated for each of the three structural models of each building considered. In all cases a viscous damping ratio of 5 percent of critical was assumed. The step-by-step response analysis was carried out employing the program DRAIN-2D (11). A modified version (DRAINTER) was used to account for soil-structure interaction according to the spring-dashpot system described above (12).

The results of the structural response studies were expressed in terms of the maximum instantaneous value, throughout the response duration, of the displacement ductility demands at each story; this value was estimated as the ratio of the initial tangent stiffness to the minimum instantaneous secant stiffness (Fig. 8). The latter is obtained dividing the story shear force by the story deformation.

a) Seven-story building

Figure 9 shows mean values of peak story ductilities for the rigid frame model. It may be observed that, for all the cases studied, mean peak ductilities are almost constant for the lowest five stories, and they decrease for the uppermost two. Soil-structure interaction causes mean ductilities to increase 20 percent with respect to those of case 1. Inclusion of P-delta effects (case 3) does not lead to significant increments in response. Stiffness degradation of beams (case 4) leads to considerable increments in mean peak ductilities of all stories, with the exception of the last one, with respect to the three previous cases. Although not shown in this article, it was concluded that in general terms the influence on structural response of the various concepts studied here is very similar for all records considered (3).

Figure 10 shows the results for the equivalent shear-beam model. Maximum mean peak ductilities for case 1 occur at the first story; they are significantly smaller at the upper stories. In this model, soil-structure interaction (case 2) gives place to small increments of mean peak ductilities at stories 1 to 4, and does not have a significant effect on the three uppermost stories. P-delta effects (case 3) are very important in these cases, leading in some cases to three-fold increments of mean peak ductilities at the first three stories, but the effects almost vanish at other locations.

A comparison of the results of the two models studied for this building shows that for cases 1 and 2 (figs. 11 and 12) the equivalent shear-beam model demands much higher ductilities at the first story than the corresponding rigid frame, while at the other stories the ductility demands of the equivalent shear-beam model are smaller as a rule. For case 3 (fig. 13), the discrepancies at the lowest three stories are accentuated.

The foregoing results show that ductility demands in the rigid frame model are nearly uniformly distributed along the building height, while in the shear-beam model these demands are concentrated at a few stories, generally at the lowest one, with considerably lower values at the others.

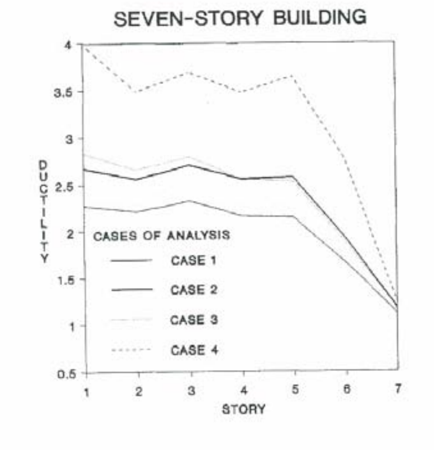

Figure 9. Rigid frame model

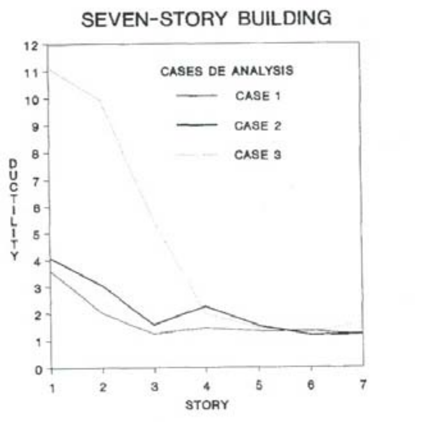

Figure 10. Shear-beam model

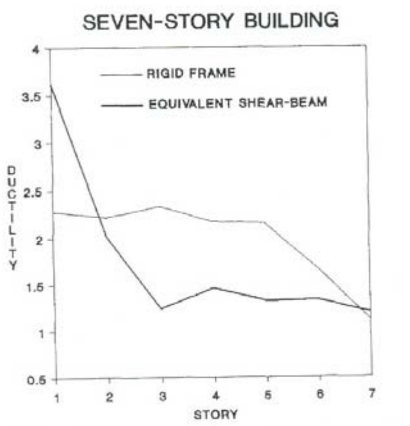

Figure 11. Comparison of alternate assumptions for case 1

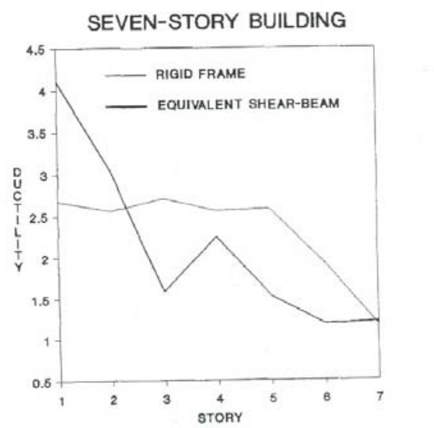

Figure 12. Comparison of alternate assumptions for case 2

b) Fourteen-story building

Figure 14 shows the results for the rigid frame model. Mean peak ductilities for cases 1, 2 and 3 are large at the lowest story with values of 3 to 4. They decrease rapidly from the first to the second story. From the second up to the ninth story the decrease is gradual, and above them the rate of decrease is large again, until the system reaches a linear response at the fourteenth story.

Increments associated to soil-structure interaction are of 15 percent at most; their influence is largest at stories 6 to 9. Including P-delta effects (case 3) does not significantly alter the results, particularly at the top stories. Stiffness degradation at the beams (case 4) provokes a noticeable increase of story ductilities, particularly at stories 6 to 11, but its effect at the last three stories is small.

For the equivalent shear-beam model, the overall behavior is similar for the three cases studied. (Fig. 15 illustrates cases 1 and 2.) The results show that mean peak ductilities are very large at the first story and decrease fast upwards, with linear elastic response of the top story. The effect of soil-structure interaction (case 2) is an increase of up to 30 percent at the first story, with respect to case 1. Case 3 deserves special mention. It includes P-delta effects, as for this case the structure collapsed for several of the ground motion record s applied (in this context, "collapse" means that lateral deformations of one or more stories were excessively high, leading to instability of the numerical solution); hence, no mean peak ductilities are presented for this case in Figure 15.

Figure 16 corresponds to the equivalent shear-frame, which is characterized by a very peculiar behavior, as compared with that of the other two models studied. The results show that, for the three cases studied (1 to 3), the structure develops large ductilities at the first story, has an almost linear behavior at the intermediate stories, and shows an appreciable increase of ductilities at the upper stories (stories 11 to 14 for cases 1 and 2, and 10 to 14 for case 3). The influence of soil-structure interaction (case 2) is important at the first story, as well as at stories 11 to 14, with increments of the mean peak ductilities of these stories of as much as 75 percent with respect to case 1.

When P-delta effects are inc1uded (case 3), ductilities are considerably increased at the first story, and reach even larger values at the upper end of the building. By comparing the results obtained with the three models studied above, it is found that for case 1 (fig. 17) the distribution of story ductilities in the rigid frame model differs significantly from that obtained with the other two models, in particular with those corresponding to the equivalent shear-frame. These differences in behavior are similar to those observed in the other two cases (figs. 18 and 19).

c) Additional results

The equivalent shear-frame model deserves some additional comments. Its response is quite different from that of both, the rigid frame and the equivalent shear-beam. The maximum ductility demands occur at the first story, just like in the other two models; but in the equivalent shear-frame, unlike in the other models, those demands decrease sharply for stories 2 to 9 or 10 (according to the type of analysis), and show a

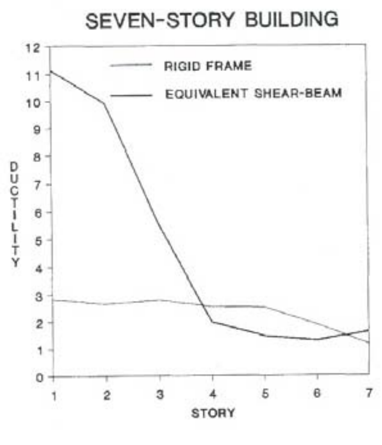

Figure 13. Comparison of alternate assumptions for case 3

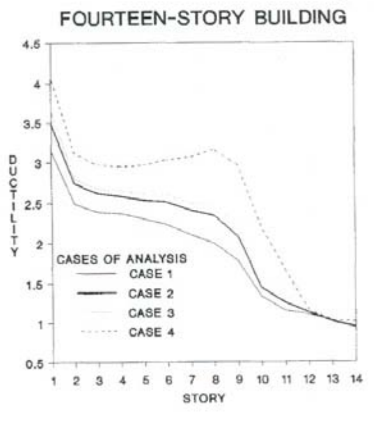

Figure 14. Rigid frame model

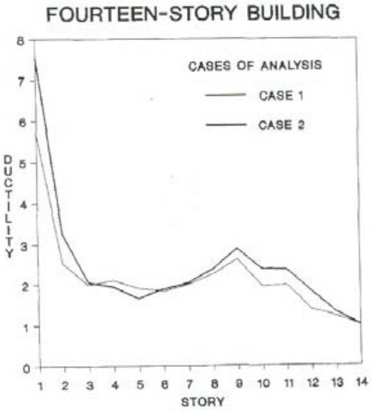

Figure 15. Shear-beam model

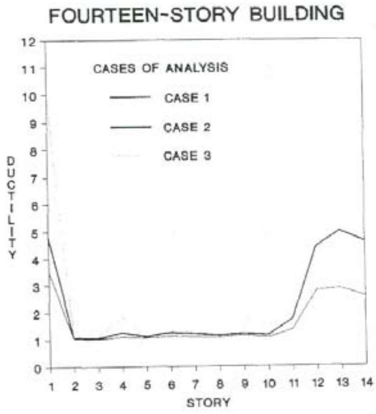

Figure 16. Shear-frame model

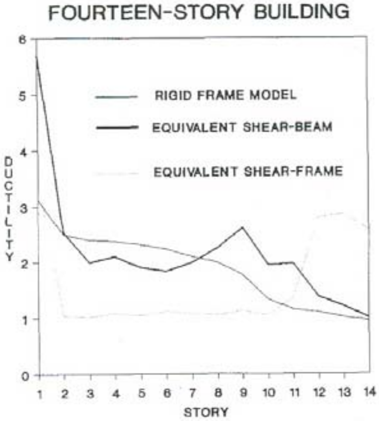

Figure 17. Comparison of alternate assumptions for case 1

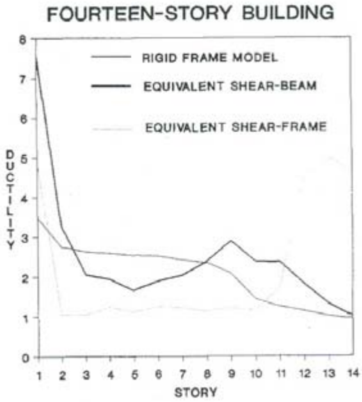

Figure 18. Comparison of alternate assumptions for case 2

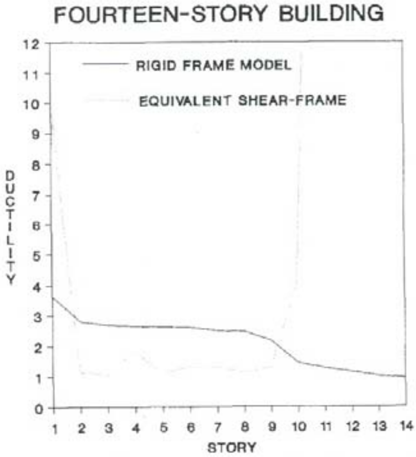

Figure 19. Comparison of alternate assumptions for case 3

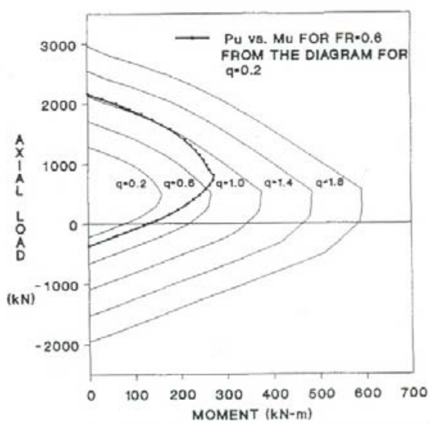

Figure 20. Interaction diagrams

considerable increase at the top stories (fig. 16). Some additional studies were carried out in order to understand this behavior.

When the story shear capacities of the rigid frame model (obtained as described in concept iv, section b) of the chapter on MODELS STUDIED) for analysis type 1 and artificial accelerogram 1 are compared with those calculated for the equivalent shear-frame, it is found that the latter shows shear capacities significantly higher than those calculated for the rigid frame (Table 3). This difference is larger for stories 1 to 10, and decreases from the eleventh story to the top, where small values result.

An explanation for the overstrength observed in the lower and intermediate stories of the shear-frame is presented in the following. A fraction of that overstrength may be ascribed to the assumption that all the columns at a given story have a strength equal to that required by the one subjected to the severest load conditions. This criterion was applied also for the structural design of the columns of the associated rigid frame, but in this case the resulting local overstrength did not lead to a significant story overstrength, as a consequence of the prevalence of the strong-column-weak-beam failure mechanism: column hinges formed only at the bottom ends of the first story and at a few locations at intermediate stories. In the equivalent shear-frame, hinges can form only at column ends.

When each of the columns at a given story of the equivalent shear-frame is individually designed for its own acting forces, the story shear capacity decreases slightly (Table 3), but a relatively high value of shear capacity still remains at the bottom stories. When checking the structural design of the mentioned frame (3), it was observed that for all columns of stories 1 to 11, as well as for the middle column of the twelfth story, failure is governed by concrete crushing. According to the design criterion employed, a strength-reduction factor φ, equal to 0.6, must be applied to the computed nominal capacity of the column (7), to avoid crushing.

Figure 20 shows the P-M interaction diagrams for a given column cross section, prior to the application of any strength-reduction factor. The bold-faced line was obtained dividing by 0.6 the loads and moments of the interaction diagram corresponding to q = 0.2 (where $q = p\, f_y/f'_c$; p is the reinforcement ratio; f_y is the steel reinforcement yield stress, and f'_c is the reduced nominal concrete compression strength). Referred to the interaction diagrams, that line represents the values of q that must be supplied to a column for which the nominal required interaction diagram is that corresponding to q = 0.2; the discrepancies account for the strength-reduction factor of 0.6. The figure also shows that the increments of q with respect to the values required when no strength-reductions factors are applied are proportionately greater for columns where failure is governed by compression than for those where tensile stresses are critical. This behavior explains why a proportionately higher strength margin occurs on the columns of stories 1 to 11 and on the middle column of the twelfth story than on any other.

For comparison, Figure 21 shows column designs for stories 1, 7 and 14, for both the basic rigid frame and the equivalent shear-frame. Table 4 shows the design values of axial forces and moments for those columns, as well as the corresponding cross-section dimensions. It can be observed in the figure that for the rigid frame columns failure was governed by tension, while for the equivalent shear-frame compressive failure governs at columns of stories 1 and 7, and tension failure governs at the fourteenth story. Prevalence of compression failures for the cases mentioned is due to the combination of their axial load design values and their dimensions, which are responsible for the larger overstrength factors at the corresponding stories. This condition does not take place in the columns of the rigid frame.

TABLE 3

Story Yield Shears for Rigid Frame and Equivalent Shear Frame, kp (Case 1, Record 1)

STORY	RIGID FRAME	EQUIVALENT SHEAR FRAME EQUAL COLUMNS	EQUIVALENT SHEAR FRAME DIFFERENT COLUMNS
14	57.6	53.1	50.6
13	91.7	103.7	99.4
12	121.4	161.4	153.1
11	130.0	235.2	207.3
10	158.7	298.6	253.2
9	188.4	361.8	308.5
8	214.3	410.3	351.7
7	236.1	451.9	389.7
6	255.4	490.4	422.9
5	273.2	521.9	450.4
4	288.5	545.9	475.3
3	301.5	565.0	492.6
2	308.3	607.8	518.9
1	297.5	558.3	475.5

TABLE 4

Design Axial Load and Moment, and Cross Section of
Columns of Rigid Frame and Equivalent Shear-Frame

FRAME	STORY	COLUMN	AXIAL LOAD Pu (kp)	MOMENT Mu (kp-ft)	WIDTH b (in)	DEPTH h (in)
RIGID	1	CENTRAL	1728	1252	37.4	37.4
	7	CENTRAL	454	311	27.6	27.6
	14	LATERAL	35	137	17.7	17.7
SHEAR	1	CENTRAL	1112	456	23.6	23.6
	7	CENTRAL	635	261	16.1	16.1
	14	CENTRAL	79	45	13.8	13.8

In order to verify the validity of the foregoing interpretation, several alternate criteria were applied to the design of the columns of the equivalent shear-frame, and the resulting story shear capacities were evaluated. The criteria applied are described in the following.

a) Columns are designed for a strength-reduction factor of 0.6, and all columns at a given story are assigned the dimensions corresponding to the most unfavorable case. Expected values of strengths and loads (instead of nominal, or design, values) are assumed for dynamic response studies.
b) Each column is assigned the dimensions resulting from its design for a strength reduction factor of 0.6. Expected values of strengths and loads are assumed for dynamic response studies.
c) Design is carried out as in paragraph b), but nominal design capacities and loads are assumed for dynamic response studies.

d) Each column is assigned the dimensions resulting from its design for a strength factor of 1.0. Expected values of strengths and loads are assumed for dynamic response studies.
e) Design is carried out as in paragraph d), but nominal design capacities and loads are assumed for dynamic response studies.

Table 5 shows strength values for some columns of the frame under study, as wel1 as the loads assumed for the seismic response studies, for the different design criteria adopted. The influence of those criteria on seismic response is summarized in Figure 22, which shows the peak ductility demand at each story for one of the artificial records considered in the study (case 1, record 1). Structures designed and analyzed in accordance with criteria a), b) and c) show some general similarities in behavior. In these cases, ductilities at the upper stories are larger than at intermediate ones. Results obtained for structures designed and analyzed as described in d) and e) resemble more closely the behavior of the rigid frame, where ductilities are largest at the bottom stories and decrease gradually along the building height, although ductilities exhibit a trend to increase at the upper portions of the structure but finally decrease at the top two stories. In these cases the first story shows an overstrength, which is responsible for the shifting of the largest ductility demands up to the second story.

TABLE 5

Strengths and Acting Axial Forces on Central Columns of Equivalent Shear-Frame

DESIGN	STORY	P_y (kp)	P_t (kp)	M_y (kp.ft)	P_b (kp)	M_b (kp.ft)	LOAD (psf)
(a)	1	3596	1809	1441	827	1571	149
	7	2601	1862	804	364	812	149
	14	759	180	81	235	134	149
(b)	1	3596	1890	1441	827	1571	149
	7	2601	1862	804	364	812	149
	14	726	145	66	239	123	149
(c)	1	2842	1495	1140	654	1242	184
	7	2056	1472	635	288	642	184
	14	574	114	53	189	97	184
(d)	1	2230	468	403	780	717	149
	7	1587	806	381	349	426	149
	14	726	145	66	239	123	149
(e)	1	1763	370	319	617	567	184
	7	1255	637	301	276	337	184
	14	574	114	53	189	97	184

Figure 23 shows yield shear capacities for the stories of the different structures studied. They result from the design and analysis criteria described above.

The nominal values of the design shears are also shown, for comparison. The ratios of the resulting story capacity to the nominal design value for each case studied are shown in figure 24. It is observed that the overstrength ratios corresponding to criteria a), b) and c) are larger for the lowest and intermediate stories (1 to 11) than for the upper ones (12 to 14). Slight differences persist for criteria d) and e), but the overstrength ratios are more uniform along the building height.

The foregoing results clearly demonstrate the decisive influence of the design criterion adopted for the columns of the equivalent shear-frame on its calculated seismic response. Significant discrepancies between the responses of conventional rigid frames and equivalent shear-frames are obtained, even when criteria d) and e) are applied. These discrepancies include, for instance, the larger response of the second story, and of some stories near the upper part of the building, for the shear-frame case. Similar discrepancies might be associated to inclusion in the design requirements of some additional specifications, such as the minimum allowable value of the design eccentricity and the form of idealizing the P-M interaction diagram when computing the dynamic response.

The results also show the great influence that the distribution of the story shear capacity along the height of the building may have on the dynamic response of shear systems.

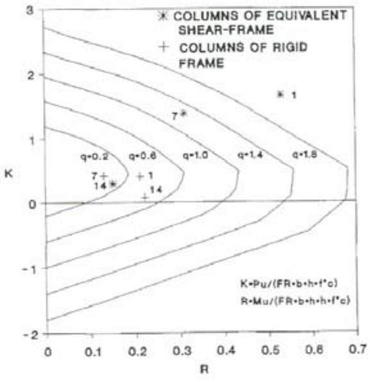

Figure 21. Design of columns

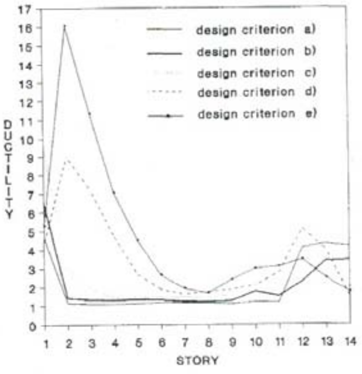

Figure 22. Peak story ductilities

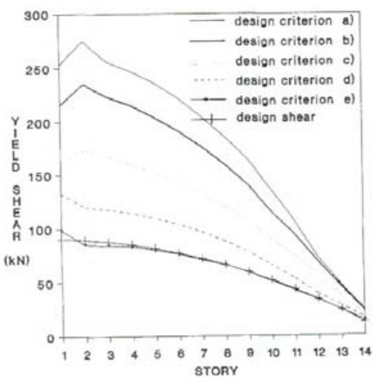

Figure 23. Yield shears

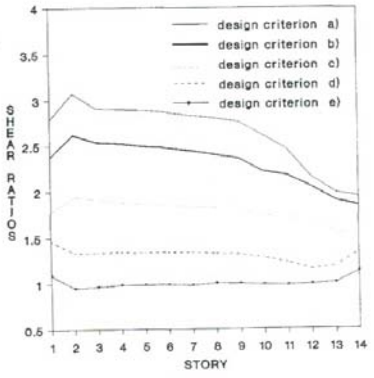

Figure 24. Shear ratios

Conclusions

From the results described above it may be concluded that, for the two buildings considered, the effects studied (soil-structure interaction, P-delta, and stiffness degradation) contribute, to a larger or lesser extent, to enhanced ductility demands for the stories of rigid frames. In particular, soil-structure interaction may increase ductility demands at stories, although for the cases studied and the types of foundation considered the influence was not substantial; neither did it give place to qua1itative differences in response or behavior (such as, for instance, excessive effects of rocking at the top stories, or unexpected concentrations of ductility demands at individual stories).

The analyses also show that P-delta effects have only a minor influence on the structural performance for this type of model, represented by a slight increase of story ductility demands. This app1ies to both, the seven-story and the fourteen-story buildings.

Stiffness degradation of beams gave place to more important effects, particulary for seven-story buildings, which experienced larger increases (in proportion) in the mean peak ductilities of stories than those observed in fourteen-story buildings. The latter were characterized by larger increases (also in proportion) of ductility demands at the intermediate and upper stories than at the others.

The equivalent shear-beam model produced results clearly different from those of its rigid frame counterpart. In the former, large ductility demands occur at the first story, much larger than those occurring at the first story of the corresponding rigid frame. At stories above the first one, the situation is reversed: the ductility demands for the shear-beam model are significantly smaller than both, those at the first story of the same structure and those corresponding to the rigid frame structure. This difference is more pronounced for the seven-story buildings. Similar comments apply to all effects studied. For the shear-beam model, P-delta effects provoke large ductility demands at the first story of the structures; in some cases they may lead to collapse due to instability.

The peculiar behavior experienced by the equivalent shear-frame used to represent the fourteen-story building has been explained in detail above. The results found with this model point at the extreme precaution that must be exerted when a similar system is used to model the behavior of a conventional building: the manner in which the strength of its members is defined may introduce non-uniform strength- excesses at several stories, which may significantly influence dynamic response. This model was utilized to represent a building with structural properties unusual under practical conditions. Also, some complementary design requirements were ignored when defining its properties. Nonetheless, the results found give a hint about the types of problems to be faced in structures with very strong and stiff beams. In addition to the well known disadvantages of the weak-column failure mechanism, these systems are affected by the possibility of large concentrations of story ductility demands which may be associated to minor variations of available story strengths with respect to those required by conventional design.

The main practical implications of the foregoing comments may be summarized as follows:

1. The results provide additional arguments in support of the strong-column-weak-beam design philosophy: in addition to avoiding the low-ductility failure modes typical of members subjected to bending and compression, this philosophy prevents the concentration of ductility demands at the lowest stories of buildings
2. Overstrength for shear at some stories may cause concentrations of ductility demands at others. These concentrations are more pronounced for shear systems than

for rigid frames, and can also be prevented by careful application of the strong-column-weak-beam philosophy.

3. Results of nonlinear dynamic response studies carried out on shear-beam models of buildings subjected to earthquake may be misleading, as they to do not consider the distribution of inelastic behavior among the members of adjacent stories. This limitation points at the convenience of replacing the shear-beam models that are typically used in parametric studies of nonlinear response with single-bay or half-bay models, capable of accounting for the rotation of column ends as well as for the occurrence of nonlinear behavior at both column and beam ends.

References

1. Esteva, L. and Mendoza, E., "Influencia de la interacción suelo-estructura en la respuesta sísmica in elástica de edificios", Internal report, *Institute of Engineering, National University of Mexico*, 1989.
2. Díaz, O., Esteva, L., Mendoza, E. and Flores, O., "Comparación entre las respuestas sísmicas no lineales de marcos y sistemas de cortante", Internal report, *Institute of Engineering, National University of Mexico*, 1989.
3. Mendoza, B., Díaz, O. and Esteva, L., "Respuesta sísmica inelástica de sistemas estructurales considerando interacción suelo-estructura", Internal report, *Institute of Engineering, National University of Mexico*, 1991.
4. Jaime, A., "Geotecnia y sismicidad en e1 valle de México", *Institute of Engineering, National University of Mexico*, Report D-29, 1988.
5. Complementary Technical Regulations for Mexico City Building Code: Design and Construction of Foundations, 1987.
6. Mexico City Building Code, 1987.
7. Complementary Technical Regulations for Mexico City Building Code: Design and Construction of Reinforced Concrete Structures, 1987.
8. Complementary Technical Regulations for Mexico City Building Code: Earthquake Resistant Design, 1987.
9. Grigoriu, M., Ruiz, S. E. and Rosenblueth, E., "Nonstationary models of seismic ground acceleration", *Earthquake Spectra*, Vol. 4. No. 3, 1988.
10. Arias, A., "A measure of earthquake intensity", in Seismic Design for Nuclear Power Plants (Edited by R. Hansen), *MIT Press*, Cambridge, Mass, 1970
11. Powell, H. G., "DRAIN-2D User's Guide", *Earthquake Engineering Research Center, University of California*, Berkeley, California, 1973.
12. Mendoza, E., "Programa de computadora para el análisis sísmico inelástico de marcos planos con interacción suelo-estructura", Internal report, *Institute of Engineering, National University of Mexico*, 1991.

OPTIMAL INSTRUMENTATION OF UNCERTAIN STRUCTURAL SYSTEMS SUBJECT TO EARTHQUAKE GROUND MOTIONS[1]

SUMMARY

A criterion is proposed for making decisions regarding the optimal location of a given number of sensors to record the seismic response of a structure for identification purposes. The optimal location of the sensors is selected so that the expected value of a Bayesian loss function, expressed in terms of the Fisher information in the recordings, is minimized. The criterion is applied to the case of multi-degree-of-freedom systems with uncertain structural properties subjected to earthquake ground motions modelled as stationary stochastic processes. The use and capabilities of the criterion are thoroughly illustrated by means of an example. Results are used to assess the influence of record duration, recording noise, and ground motion frequency content and amplitude, on the optimal location of accelerometers as well as on the reduction of prior uncertainty about the structural parameters.

KEY WORDS: sensor location; optimal instrumentation; Fisher information; system identification; random vibration; seismic response

Introduction

Our interest in the identification of the mechanical properties of civil engineering structures subjected to seismic ground motion of different intensities has several sources. The information provided by records of the dynamic response of full-size structures under the action of real earthquakes is of great value in the development of our capability to predict the expected response of new structures while they are in the design stage; and a collection of records obtained on a structure during a sequence of earthquakes can help us to evaluate the influence of damage accumulation on the mecha nical properties of that structure.

Due to the limitations of the mathematical models used to represent the behaviour of real, complex systems, and because of the limited number of records that can be obtained simultaneously during a seismic event, which in usual cases is much smaller than the number of degrees of freedom of the structure of interest, the mechanical properties estimated from the analysis of the recorded responses are usually tied to significant uncertainties. Hence, our interest in the study of the concepts that affect those uncertainties, as well as in the development of optimum instrumentation schemes, i.e. selection of the locations of the recording instruments on a structure that lead to the smallest probabilistic deviations of the values estimated for the system's properties from the real ones.

Some research has been carried out to develop methodologies for selecting the optimal location of sensors for identification of dynamic systems (see e.g. Reference 1). Criteria for locating recording instruments to assure global convergence and uniqueness

---

[1] First published in:
Ernesto Heredia-Zavoni and Luis Esteva, Optimal Instrumentation of Uncertain Structural Systems Subject to Earthquake Ground Motions, *Earthquake Engng. Struct. Dyn.* **27**, 343-362 (1998)

of the inverse problem associated with parameter identification have also been established.[2, 3] More recently, a methodology has been formulated by Udwadia[4] to solve the optimum sensor location problem. It is advantageous in that the optimization is uncoupled from the identification problem through the concept of efficient estimation. The criterion presented here also makes use of efficient estimators but explicitly takes into account the uncertainty about the structural parameters and the seismic ground motion excitation; in this sense it could be thought of as an extension of the methodology developed by Udwadia. Current knowledge on the structural parameters to be identified from recordings is considered to be summarized by prior probability density functions and the ground motion at the base of the structural systems is described in terms of spectral density functions. The paper first proposes a criterion for selecting optimal locations of a given number of recording instruments based on minimizing an expected loss function. Through the use of efficient estimation theory, the loss function is related to the Fisher information associated with the responses to be recorded. Expressions for applying such criterion are then rigorously derived for the case of linear stochastic structural response. The paper then goes on to show a detailed example for illustration of the use and features of the formulation proposed. Results are thoroughly discussed and conclusions and recommendations are given at the end.

Optimizing Criterion

Consider the case where a vector $\Theta = \{\theta_1, \theta_2, ..., \theta_K\}$ uncertain parameters θ_i, $i = 1, 2, ..., K$, is to be estimated based on the observation of a set of random vectors $Y_0 = \{\mathbf{Y}_1, \mathbf{Y}_2, ... , \mathbf{Y}_N\}$. Suppose that given certain constraints on the number of vectors that can be observed, a subset Y of M vectors out of the N vectors in Y_0 has to be chosen for the estimation of Θ. It is desirable to select for observation the M vectors that would yield the 'best' estimate of the parameter vector Θ.

Let $f(y\,|\,\theta)$ denote the conditional joint probability density function of the random vectors Y. An unbiased estimator $\hat{\Theta}(Y)$ of Θ, $E_{Y|\Theta}[\hat{\Theta}(Y)] = \Theta$, is said to be efficient if its conditional covariance matrix $\mathrm{Cov}(\hat{\Theta}(Y)|\Theta)$ is given by

$$\mathrm{Cov}\left(\hat{\Theta}(Y)\,|\,\Theta\right) = M_\Theta^{-1} \tag{1}$$

In equation (1), M_Θ is the Fisher information matrix defined as

$$M_\Theta = E_{Y|\Theta}\left[\left\{\frac{\partial}{\partial\Theta}\ln f\left(Y\,|\,\Theta\right)\right\}\left\{\frac{\partial}{\partial\Theta}\ln f\left(Y\,|\,\Theta\right)\right\}^T\right] \tag{2}$$

where $\partial \ln f(Y|\Theta)/\partial\Theta$ is the vector

$$\frac{\partial}{\partial\Theta}\ln f\left(Y\,|\,\Theta\right) = \left\{\frac{\partial}{\partial\theta_i}\ln f\left(Y\,|\,\Theta\right)\right\}, \qquad i = 1, 2, ..., K \tag{3}$$

and the superscript 'T' denotes vector transpose. The inverse of the Fisher information matrix (FIM) is the Cramer-Rao lower bound and represents the minimum covariance that an unbiased estimator can achieve. Equation (1) suggests that the greater the size of the FIM, as measured by suitable norms of the matrix, the smaller the size of the estimator covariance matrix. The size of the FIM gets larger as the random function $f(Y|\Theta)$ becomes more sensitive to changes in the values of the parameters in Θ.

Suppose now that we can assign to Θ a prior distribution which summarizes the information and knowledge that one has on the likelihood of the possible values of Θ before Y is observed. Each subset Y of M vectors is a collection of observations from a possible 'instrumentation' for the estimation of Θ. In order to compare between different instrumentation alternatives, a measure of the goodness of each alternative —related to the expected accuracy of the parameter estimates to be obtained from the observed Y —is required. A suitable measure of goodness can be defined in terms of a Bayesian loss function $L(\Theta, \hat{\Theta}(Y))$ for which the expectation $E[L(\Theta, \hat{\Theta}(Y))]$ is to be minimized. Based on a Taylor series expansion of $L(\Theta, \hat{\Theta}(Y))$ about Θ it may be shown that [4]

$$E\left[L\left(\Theta, \hat{\Theta}(Y)\right)\right] \approx \frac{1}{2} E_{\Theta}\left[\operatorname{tr} \frac{\partial^2 L}{\partial \hat{\Theta}^2} \operatorname{Cov}\left(\hat{\Theta}(Y) \mid \Theta\right)\right] \tag{4}$$

and since $\hat{\Theta}(Y)$ is an efficient estimator, it follows from equation (1) that

$$E\left[L\left(\Theta, \hat{\Theta}(Y)\right)\right] \approx \frac{1}{2} E_{\Theta}\left[\operatorname{tr} \frac{\partial^2 L}{\partial \hat{\Theta}^2} M_{\Theta}^{-1}\right] \tag{5}$$

The expectations on the left-hand side of equations (4) and (5) are taken over Y and Θ jointly. A commonly used loss function is the so-called squared error loss function,

$$L\left(\Theta, \hat{\Theta}(Y)\right) = \left(\hat{\Theta} - \Theta\right)^T \left(\hat{\Theta} - \Theta\right) \tag{6}$$

For the squared error loss function, the second derivative of L with respect to Θ is equal to two times the identity matrix and equation (5) becomes an equality; thus,

$$E\left(\left(\hat{\Theta} - \Theta\right)^T \left(\hat{\Theta} - \Theta\right)\right) = E_{\Theta}\left[\operatorname{tr} M_{\Theta}^{-1}\right] \tag{7}$$

The criterion to select the optimal instrumentation alternative is then to choose for observation the subset Y for which the expected loss in equation (7) is a minimum. The expected value on the right-hand side of equation (7) is taken with respect to Θ, i.e. with respect to the prior distribution of Θ. Therefore, selecting the optimal alternative involves the prior knowledge that one has about the properties of the system. Notice that whereas the criterion proposed by Udwadia [4] maximizes the size of the Fisher information matrix, the one proposed here is based on minimizing the expected value of the Bayesian loss function.

Optimal Instrumentation of MDOF Structural Systems

Let $\mathbf{Y}_1$, $\mathbf{Y}_2$, ... , $\mathbf{Y}_N$ be M-dimensional, independent, Gaussian, zero-mean, random vectors. Let θ_k be any uncertain parameter in Θ; then the partial derivative of the logarithm of the conditional joint density function $f(Y \mid \Theta) = f(\mathbf{Y}_1, \mathbf{Y}_2, ..., \mathbf{Y}_N \mid \Theta)$ can be written as

$$\frac{\partial \ln f(Y \mid \Theta)}{\partial \theta_k} = -\frac{1}{2} \sum_{i=1}^{N} \left\{ \frac{\partial \ln \Delta_i}{\partial \theta_k} + \mathbf{Y}_i^T \frac{\partial \mathbf{C}_i^{-1}}{\partial \theta_k} \mathbf{Y}_i \right\} \tag{8}$$

where $\mathbf{C}_i = E_{Y\,|\,\Theta}\,[\mathbf{Y}_i\mathbf{Y}^T_i]$ is a covariance matrix and Δ_i denotes its determinant. If M_{kl} denotes an element in the kth row and lth column of the Fisher information matrix, then by definition

$$\begin{aligned} M_{kl} &= E_{Y|\Theta}\left[\frac{\partial \ln f\left(Y\mid\Theta\right)}{\partial\theta_k}\frac{\partial \ln f\left(Y\mid\Theta\right)}{\partial\theta_l}\right]= \\ &= \frac{1}{4}E_{Y|\Theta}\left[\sum_{i=1}^{N}\sum_{j=1}^{N}\left\{\frac{\partial \ln \Delta_i}{\partial\theta_k}+\mathbf{Y}_i^T\frac{\partial \mathbf{C}_i^{-1}}{\partial\theta_k}\mathbf{Y}_i\right\}\left\{\frac{\partial \ln \Delta_j}{\partial\theta_l}+\mathbf{Y}_j^T\frac{\partial \mathbf{C}_j^{-1}}{\partial\theta_l}\mathbf{Y}_j\right\}\right] \end{aligned} \tag{9}$$

It can be shown (see Appendix I) that

$$E_{Y|\Theta}\left[\frac{\partial \ln \Delta_i}{\partial\theta_k}+\mathbf{Y}_i^T\frac{\partial \mathbf{C}_i^{-1}}{\partial\theta_k}\mathbf{Y}_i\right]=0 \tag{10}$$

Thus, using equation (10) and given that $\mathbf{Y}_i$ and $\mathbf{Y}_j$ are statistically independent for $i \neq j$, equation (9) can be written as follows:

$$M_{kl} = \frac{1}{4}E_{Y|\Theta}\left[\sum_{i=1}^{N}\left\{\frac{\partial \ln \Delta_i}{\partial\theta_k}+\mathbf{Y}_i^T\frac{\partial \mathbf{C}_i^{-1}}{\partial\theta_k}\mathbf{Y}_i\right\}\left\{\frac{\partial \ln \Delta_i}{\partial\theta_l}+\mathbf{Y}_i^T\frac{\partial \mathbf{C}_i^{-1}}{\partial\theta_l}\mathbf{Y}_i\right\}\right] \tag{11}$$

The expected values in equation (11) involve fourth-order moments which can be obtained from the second order ones provided that $\mathbf{Y}_i$ is a Gaussian vector. In Appendix II it is shown that

$$E_{Y|\Theta}\left[\mathbf{Y}_i^T\frac{\partial \mathbf{C}_i^{-1}}{\partial\theta_l}\mathbf{Y}_i\mathbf{Y}_i^T\frac{\partial \mathbf{C}_i^{-1}}{\partial\theta_l}\mathbf{Y}_i\right]=2\mathbf{C}_i^{-1}\frac{\partial \mathbf{C}_i}{\partial\theta_k}\cdot\frac{\partial \mathbf{C}_i}{\partial\theta_l}\mathbf{C}_i^{-1}+\frac{\partial \ln \Delta_i}{\partial\theta_k}\frac{\partial \ln \Delta_i}{\partial\theta_l} \tag{12}$$

where the dot in equation (12) denotes a scalar matrix product. Substituting equation (12) into equation (11) and making use of equation (10), one obtains for M_{kl}:

$$M_{kl} = \frac{1}{2}\sum_{i=1}^{N}\mathbf{C}_i^{-1}\frac{\partial \mathbf{C}_i}{\partial\theta_k}\cdot\frac{\partial \mathbf{C}_i}{\partial\theta_l}\mathbf{C}_i^{-1} \tag{13}$$

Consider now a linear structural system with Q degrees of freedom subjected to an earthquake ground motion modelled as a zero-mean stationary Gaussian stochastic process. Suppose there are $M < Q$ recording instruments available to record the system response. Let the process $Y_i(t_n)$, $i = 1,2, \ldots , M$, denote the ith recorded response at discrete times $t_n = (n - 1)\Delta t$, $n = 1, 2, \ldots, N$. Under the assumption of mean-square continuity, $Y_i\,(t_n)$ can be expressed as a sum of independent frequency-specific processes in consecutive constant-size frequency intervals as follows[5]:

$$Y_i\left(t_n\right)=\sum_{k=1}^{N}A_{ik}\cos\left(\omega_k t_n\right)+B_{ik}\sin\left(\omega_k t_n\right) \tag{14}$$

where the Fourier coefficients A_{ik}, B_{ik}, corresponding to frequency $\omega_k = (k - 1)\,2\pi/N\Delta t$, are random variables. The coefficients A_{ik}, B_{ik}, are related to $Y_i\,(t_n)$ through the discrete Fourier transform:

$$A_{ik} = \frac{1}{N}\sum_{n=1}^{N} Y_i(t_n)\cos\left(\frac{2\pi(k-1)(n-1)}{N}\right)$$
$$B_{ik} = \frac{1}{N}\sum_{n=1}^{N} Y_i(t_n)\sin\left(\frac{2\pi(k-1)(n-1)}{N}\right) \tag{15}$$

Notice that the recorded response $Y_i(t_n)$ is a periodic stationary stochastic process with physical length $L = (N - 1)\,\Delta t$ and period $T = N\,\Delta t$. In this modelling, we could think of L as the record duration.

Let A_{jk}, B_{jk}, denote the Fourier coefficients of the jth recorded response $Y_j(t_n)$. The covariance between coefficients $A_{ik}\,B_{ik}$ and $A_{jk}\,B_{jk}$ can be obtained using the expressions in equation (15):[6, 7]

$$E\left[A_{ik}A_{jk}\right] = \begin{cases} \tfrac{1}{2}R_{ij}(\omega_k)\Delta\omega & \text{for } k = 1 \\ \tfrac{1}{4}\left\{R_{ij}(\omega_k) + R_{ij}(\omega_{N-k+2})\right\}\Delta\omega & \text{for } k = 2,\ldots,N/2 \\ R_{ij}(\omega_k)\Delta\omega & \text{for } k = 1 + N/2 \end{cases} \tag{16}$$

$$E\left[A_{ik}A_{jk}\right] = \begin{cases} \tfrac{1}{4}\left\{Q_{ij}(\omega_k) - Q_{ij}(\omega_{N-k+2})\right\}\Delta\omega & \text{for } k = 2,\ldots,N/2 \\ 0 & \text{for } k = 1, 1 + N/2 \end{cases} \tag{17}$$

and $E[B_{ik}\,B_{jk}] = E[A_{ik}\,A_{jk}]$ for $k = 2, 3, \ldots, N/2$, $E[B_{ik}\,B_{jk}] = 0$ for $k = 1,\ 1 + N/2$; when $k = 1 + N/2$, ω_k is the Nyquist frequency. In equations (16) and (17), $R_{ij}(\omega_k)$ and $Q_{ij}(\omega_k)$ are the real and imaginary parts of the cross-spectral density function of recorded responses Y_i and Y_j, $SY_{ij}(\omega_k)$, respectively,

$$SY_{ij}(\omega_k) = R_{ij}(\omega_k) + \imath\, Q_{ij}(\omega_k), \qquad \imath = \sqrt{-1} \tag{18}$$

The recorded response $Y_i(t_n)$ can be expressed in terms of the system response $X_i(t_n)$ and a recording noise $N_i(t_n)$ as follows:

$$Y_i(t_n) = X_i(t_n) + N_i(t_n) \tag{19}$$

where the system response is a zero-mean stationary Gaussian process and the recording noises are modelled as independent, zero-mean, Gaussian, stationary, white noise processes with spectral density amplitude N_0.

From equation (19) it follows that $SY_{ij}(\omega_k)$ can be written as

$$SY_{ij}(\omega_k) = S_{ij}(\omega_k) + N_0\delta_{ij} \tag{20}$$

where $S_{ij}(\omega_k)$ is the complex cross-spectral density function of system responses $X_i(t_n)$ and $X_j(t_n)$, N_0 is the recording noise spectral density function and δ_{ij} is the Kronecker delta. Notice that $SY_{ij}(\omega_k) = S_{ij}(\omega_k)$ for $i \neq j$; the presence of noise in the recordings affects the spectral density functions only, thus

$$SY_{ii}(\omega_k) = S_{ii}(\omega_k) + N_0 \tag{21}$$

Let $\mathbf{F}^{T}_{k} = \{\mathbf{A}_k, \mathbf{B}_k\}^{T}$ denote the (1 x 2M) vector of recorded response Fourier coefficients at the M recording points corresponding to frequency ω_k, where $\mathbf{A}_k = \{A_{1k}, A_{2k}, \ldots, A_{Mk},\}$, $\mathbf{B}_k = \{B_{1k}, B_{2k}, \ldots, B_{Mk}\}$. The Fourier coefficients $\mathbf{F}_1, \mathbf{F}_2, \ldots, \mathbf{F}_N$ are independent, zero-mean, Gaussian random vectors. Using the expressions in equations (16) and (17), the (2M x 2M) covariance matrix $\mathbf{C}_k = E[\mathbf{F}_k\mathbf{F}^{T}_{k}]$ can be assembled as follows:

$$\mathbf{C}_k = \begin{bmatrix} \mathbf{C}_{AA} & \mathbf{C}_{AB} \\ \mathbf{C}_{AB}^T & \mathbf{C}_{BB} \end{bmatrix} \tag{22}$$

where matrices $\mathbf{C}_{AA} = E\,[\mathbf{A}_k\mathbf{A}^{\mathrm{T}}{}_k]$, $\mathbf{C}_{AB} = E\,[\mathbf{A}_k\mathbf{B}^{\mathrm{T}}{}_k]$, $\mathbf{C}_{BB} = \mathrm{E}[\mathbf{B}_k\mathbf{B}^{\mathrm{T}}{}_k]$ for each frequency ω_k, $k = 1, 2, \ldots, N$.

Once the covariance matrices $\mathbf{C}_k$, $k = 1, 2, \ldots, N$, for the Fourier coefficients are obtained, equation (13) for a set of independent Gaussian random vectors can be used to evaluate the elements of the Fisher information matrix,

$$M_{pq} = \frac{1}{2}\sum_{k=1}^{N} \mathbf{C}_k^{-1}\frac{\partial \mathbf{C}_k}{\partial \theta_p}\cdot\frac{\partial \mathbf{C}_k}{\partial \theta_q}\mathbf{C}_k^{-1} \tag{23}$$

where θ_p and θ_q are two of the uncertain structural parameters, N is the number of discrete points in the records, $\mathbf{C}_k$ are covariance matrices of order ($2M$ x $2M$), and M is the number of available recording instruments. Equation (23) shows that the Fisher information matrix depends on the degrees of correlation between recorded responses, as measured by the covariance matrices, and on the sensitivity of such degrees of correlation to the uncertain structural parameters, as accounted for by the partial derivatives of the covariance matrices. The FIM can be thought of as a weighted combination of the sensitivities of the degrees of correlation between recorded responses, with the weights being the inverse covariance matrices of such responses. Conceptually, since the objective is to maximize the size of the FIM, more weight is given in equation (23) to those responses that are more correlated and whose covariances are more sensitive to small changes in the parameters to be estimated.

In order to select the optimal instrumentation alternative one then proceeds as follows. First, for each instrumentation alternative of the MDOF structural system, i.e. for each possible combination of recorded responses Y_i, $i = 1, 2, \ldots, M$, the corresponding Fisher information matrix is assembled based on equation (23). As stated earlier, the elements in the FIM will in general depend on the uncertain parameters in Θ. The trace of the FIM inverse is obtained next and its expected value with respect to the prior distribution of Θ is computed. According to the criterion proposed here, the optimal instrumentation alternative will then be the set of M recorded responses Y_i for which such expected value is a minimum.

Stochastic Structural Response

Next, we turn to the evaluation of the cross-spectral density function of a pair of system responses, $S_{ij}(\omega)$, Consider two response components X_i and X_j of a linear structural system with Q degrees of freedom, mass and stiffness matrices **M** and **K**, modal frequencies and critical damping ratios ω_q, ξ_q, and mode shapes ϕ_q, $q = 1, 2, \ldots, Q$. The cross-spectral density function of the response components X_i and X_j, $S_{ij}(\omega)$ is given by[8]

$$\begin{aligned} S_{ij}(\omega) = S_{UU}(\omega) + \sum_{q=1}^{Q} c_q^j H_q^*(\omega) S_{U\ddot{U}}(\omega) + \sum_{q=1}^{Q} c_q^i H_q(\omega)\, S_{\ddot{U}U}(\omega) \\ + \sum_{q=1}^{Q} \alpha_q^{ij} \left|H_q(\omega)\right|^2 S_{\ddot{U}\ddot{U}}(\omega) \end{aligned} \tag{24}$$

where S_{UU} and $S_{\ddot{U}\ddot{U}}$ are the ground displacement and acceleration spectral density functions, respectively, $S_{U\ddot{U}}(\omega)$ is the cross-spectrum between ground displacement U and ground acceleration $\ddot{U}$, $H_q(\omega)$ is the modal transfer function

$$H_q(\omega) = \frac{1}{\omega_q^2 - \omega^2 + 2\imath\xi_q\omega_q\omega}, \qquad \imath = \sqrt{-1} \tag{25}$$

and $H^*_q(\omega)$ is the complex conjugate. The first term on the right-hand side of equation (24) corresponds to the contribution from the pseudo-static response; the fourth term corresponds to that from the dynamic response, whereas the second and third terms represent the contribution from the cross-correlation between them. In equation (24), c^i_q is an effective modal participation factor associated with response X_i,

$$c_q^i = -\mathbf{r}_i^T \phi_q \frac{\phi_q^T \mathbf{MJ}}{\phi_q^T \mathbf{M} \phi_q} \tag{26}$$

and $\mathbf{r}_i$ denotes a response transfer vector which relates the response component X_i with the system response displacements $\mathbf{x}$ along degrees of freedom, $\mathbf{x} = \{x_1, x_2, \ldots, x_Q\}$, $X_i = \mathbf{r}^T{}_i\, \mathbf{x}$; $\mathbf{J}$ is a column vector of ones. The coefficients α^{ij}_q in equation (24) are equal to[6]

$$\alpha_q^{ij} = c_q^i c_q^j + \frac{1}{2} \sum_{k=1,k\neq q}^{Q} \left(c_q^i c_k^j + c_k^i c_q^j \right) \mathscr{A}_{qk} \tag{27}$$

The factor $\mathscr{A}_{qk}$ in equation (27) depends only on the modal frequencies and dampings associated with the qth and kth modes, and takes into account the contribution to the system response from the cross-correlation between them. For a system with well-spaced modal frequencies or light modal dampings, $\mathscr{A}_{qk}$ is approximately zero and can be neglected in equation (27).

If response components X_i and X_j are total displacements along the response degrees of freedom of the structural system, the effective modal participation factors in equation (26) are equal to

$$\begin{aligned} c_q^i &= -\phi_{iq} \frac{\phi_q^T \mathbf{MJ}}{\phi_q^T \mathbf{M} \phi_q} \\ c_q^j &= -\phi_{jq} \frac{\phi_q^T \mathbf{MJ}}{\phi_q^T \mathbf{M} \phi_q} \end{aligned} \tag{28}$$

where ϕ_{iq} denotes the ith component of the modal shape vector ϕ_q.

It is usually the case that the recorded response components are total accelerations along the response degrees of freedom. In such a case, the cross-spectral density function of total accelerations can be obtained from equation (24) using the relations for the cross-spectrum of a derivative process,

$$\begin{aligned} S_{ij}(\omega) = \omega^4 \Bigg[& S_{UU}(\omega) + \sum_{q=1}^{Q} c_q^j H_q^*(\omega) S_{U\ddot{U}}(\omega) \\ & + \sum_{q=1}^{Q} c_q^i H_q(\omega) S_{\ddot{U}U}(\omega) + \sum_{q=1}^{Q} \alpha_q^{ij} \left| H_q(\omega) \right|^2 S_{\ddot{U}\ddot{U}}(\omega) \Bigg] \end{aligned} \tag{29}$$

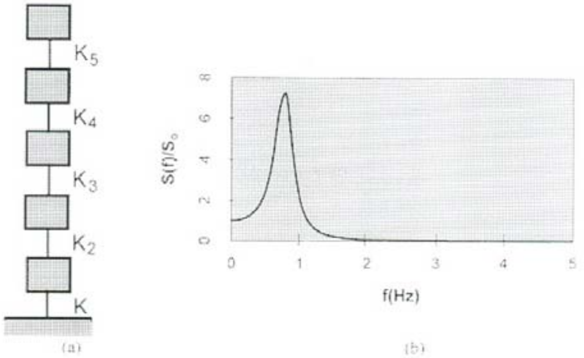

Figure 1. (a) Five degree-of-freedom structural system; (b) earthquake ground motion spectral density function. $\omega_g = 0.8$ *Hz,* $\xi_g = 0.20$

Notice though that in equation (29), the factors c^i_q, c^j_q are as given in equation (28) for displacement response components. Taking into account that $S_{\ddot{U}\ddot{U}}(\omega) = \omega^4 S_{UU}$, $S_{\ddot{U}\ddot{U}}(\omega) = -\omega^2 S_{U\ddot{U}}(\omega)$, equation (29) can be rewritten as

$$S_{ij}(\omega) = S_{\ddot{U}\ddot{U}}(\omega)\left[1 - \sum_{q=1}^{Q} c_q^j \omega^2 H_q^*(\omega) - \sum_{q=1}^{Q} c_q^i \omega^2 H_q(\omega) + \sum_{q=1}^{Q} \alpha_q^{ij} \left|\omega^2 H_q(\omega)\right|^2\right] \tag{30}$$

Expression (30) is used in equation (20) for computing the covariances between Fourier coefficients given by equations (16) and (17). It is also used to obtain the co-variance matrix derivatives in equation (23) for the evaluation of the Fisher information matrix.

Examples

Consider the five degree-of-freedom shear building shown in Figure 1 (a) having uncertain lateral inter-storey stiffnesses. Masses at the floor levels are taken equal to 1 K sec^2/in and a critical damping ratio of 2 per cent is considered for all modes. The system is subjected to a Gaussian ground acceleration with the Kanai-Tajimi spectral density function shown in Figure l(b); the characteristic soil frequency, ω_g, and critical damping ratio, ξ_g, for the Kanai-Tajimi model are equal to 0.8 Hz and 0.20, respectively. Let K denote the uncertain lateral stiffness of the first inter-storey and K_i, i = 2, ... , 5 denote the stiffnesses of the upper inter-storeys. For the purpose of illustration, results will be given for the case of perfectly correlated lateral stiffnesses, i.e. $K_i = c_i K$ where c_i, i = 2, ... , 5 are constants. It should be noticed, however, that the formulation developed above is of a general nature and is not restricted to the case of perfectly correlated structural parameters.

In order to compute the Fisher information according to equation (23), it is necessary to evaluate the partial derivatives of the covariance matrices $\mathbf{C}_k$ given in equation (22). The elements of these covariance matrices depend on the cross-spectral density functions of system responses, $S_{ij}(\omega)$, as shown in equations (16)-(20). Suppose that the recording instruments available are accelerometers that will record total accelerations along the response degrees of freedom of the structure. One needs to evaluate the partial derivative of $S_{ij}(\omega)$ in equation (30) with respect to the uncertain first-storey lateral stiffness K:

$$\begin{aligned}\frac{\partial S_{ij}(\omega)}{\partial K} = S_{\ddot{U}\ddot{U}}(\omega)\Bigg[& -\sum_{q=1}^{Q}\frac{\partial c_q^j}{\partial K}\omega^2 H_q^*(\omega) - \sum_{q=1}^{Q} c_q^j\omega^2\frac{\partial H_q^*(\omega)}{\partial K} - \sum_{q=1}^{Q}\frac{\partial c_q^i}{\partial K}\omega^2 H_q(\omega) - \\ & -\sum_{q=1}^{Q} c_q^i\omega^2\frac{\partial H_q(\omega)}{\partial K} + \sum_{q=1}^{Q}\frac{\partial \alpha_q^{ij}}{\partial K}\left|\omega^2 H_q(\omega)\right|^2 + \sum_{q=1}^{Q}\alpha_q^{ij}\frac{\partial\left|\omega^2 H_q(\omega)\right|^2}{\partial K}\Bigg]\end{aligned} \qquad (31)$$

The partial derivatives on the right-hand side of equation (31) are obtained as follows:

(a) From equation (25) for the modal transfer functions $H_q(\omega)$,

$$\begin{aligned}\frac{\partial H_q(\omega)}{\partial K} = & \left|H_q(\omega)\right|^2\left\{\frac{\partial w_q^2}{\partial K} - 2\iota\xi_q\omega\frac{\partial\omega_q}{\partial K}\right\} - \left\{\left(\omega_q^2-\omega^2\right) - 2\iota\xi_q\omega_q\omega\right\}2\left(\omega_q^2-\omega^2\right) + \\ & + 4\xi_q^2\omega^2\left|H_q(\omega)\right|^4\frac{\partial\omega_q^2}{\partial K}\end{aligned} \qquad (32)$$

$$\frac{\partial\left|\omega^2 H_q(\omega)\right|^2}{\partial K} = -\omega^4\frac{2\left(\omega_q^2-\omega^2\right)+4\xi_q^2\omega^2}{\left[\left(\omega_q^2-\omega^2\right)^2+4\xi_q^2\omega_q^2\omega^2\right]^2}\frac{\partial\omega_q^2}{\partial K} \qquad (33)$$

(b) From equation (27) for the modal coefficients α^{ij}_q,

$$\frac{\partial\alpha_q^{ij}}{\partial K} = \frac{\partial c_q^i}{\partial K}c_q^j + c_q^i\frac{\partial c_q^j}{\partial K} \qquad (34)$$

(c) From equation (28) for the effective modal participation factors c^i_q,

$$\begin{aligned}\frac{\partial c_q^i}{\partial K} & = -\frac{\partial\phi_{iq}}{\partial K}\frac{\phi_q^T\mathbf{MJ}}{\phi_q^T\mathbf{M}\phi_q} - \phi_{iq}\frac{\partial}{\partial K}\left\{\frac{\phi_q^T\mathbf{MJ}}{\phi_q^T\mathbf{M}\phi_q}\right\} \\ & = -\frac{\partial\phi_{iq}}{\partial K}\frac{\phi_q^T\mathbf{MJ}}{\phi_q^T\mathbf{M}\phi_q} - \phi_{iq}\left\{\frac{\partial\phi_q^T}{\partial K}\right\}\frac{\mathbf{MJ}}{\phi_q^T\mathbf{M}\phi_q} + 2\phi_{iq}\frac{\phi_q^T\mathbf{MJ}}{\left\{\phi_q^T\mathbf{M}\phi_q\right\}^2}\left\{\frac{\partial\phi_q^T}{\partial K}\mathbf{M}\phi_q\right\}\end{aligned} \qquad (35)$$

Equations (32)-(35) depend on the derivatives of squared modal frequencies, $\partial\omega^2_q/\partial K$, and mode shapes, $\partial\phi^T_q/\partial K$, with respect to stiffness K. The reader is referred to Appendix III where expressions are given for the computation of such derivatives. Based on equations (31)-(35), the partial derivatives of the covariances between Fourier coefficients given in equations (16) and (17) can be evaluated and then the covariance matrix derivatives $\partial C_k/\partial K$ can be assembled.

The stiffness K was assumed to have a prior lognormal probability density function. A prior mean μ_k = 3000 K/in was considered for the stiffness. Two values were used for the prior coefficient of variation of the stiffness, COV = 0.15 and 0.30. The corresponding prior lognormal distributions for K have parameters $\mu_{\ln K}$ = 7.99, ($\sigma_{\ln K}$ = 0.15 and $\mu_{\ln K}$ = 7.96, $\sigma_{\ln K}$ = 0.29, respectively, The stiffness constants for the upper storeys c_i were taken all equal to 1.0 and therefore the distribution of mean stiffness with height is uniform. Records were assumed to have a sampling frequency of 50 Hz and a 10 sec duration.

Consider now the case where only one accelerometer is available and we want to choose its optimum location to best identify the stiffness K. The computation of the loss function expected value was carried out by means of Monte-Carlo simulations based on 3000 sample sets for K and K_i, $i = 2, \ldots, 5$. For each sample set and each possible location of the accelerometer, we proceed as follows: (1) solve the eigenvalue problem (equation (68) in Appendix III); (2) evaluate the modal transfer functions given in equation (25); (3) assemble the covariance matrices in equation (22) for the recorded response using equations (16) and (17), and computer their inverse; (4) evaluate the partial derivatives of squared modal frequencies and mode shape vectors solving the system of linear equations (71) in Appendix III; (5) evaluate the partial derivatives of modal transfer functions, modal coefficients and participation factors using equations (32)-(35); (6) assemble the covariance matrix partial derivatives; and (7) compute the Fisher information according to equation (23); in this example, the Fisher information is a scalar given that there is only one uncertain structural parameter. Once steps 1-7 have been repeated for all the stiffness sample sets, the inverse of the Fisher information values are averaged to obtain the expected loss function.

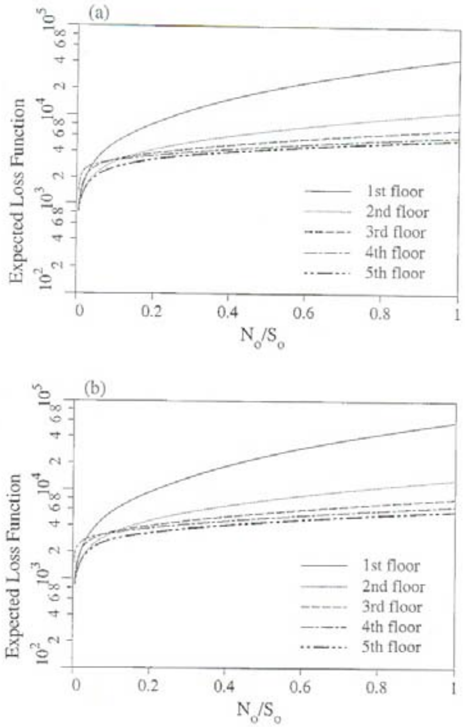

Figure 2. Expected loss function versus normalized noise:
(a) COV = *0.15; (b)* COV = *0.30*

Figure 2 shows the variation of the expected loss function, for each possible location of the accelerometer, versus a nomalized noise amplitude N_0/S_0, where N_0 and S_0 are the white noise amplitudes of the recording noise and of the seismic motion at baserock level, respectively. The results shown in Figure 2(a) were obtained for a stiffness prior coefficient of variation COV = 0.15. For all values considered of the normalized noise, the expected loss function has a minimum value when the accelerometer is placed at the fifth floor, although there is no significant difference from that corresponding to the fourth one. If the location of the accelerometer is moved downwards from the top, the expected loss function values become larger; hence, when comparing any two floors, a better location for the accelerometer is that of the floor that is atop. The expected loss function decreases with decreasing values of the normalized noise, i.e. for small expected recording noise amplitudes relative to those of the ground motion or, *vice versa*, for large expected ground motion amplitudes compared to those of the recording noise, as determined by the values of N_0 and S_0. As the normalized noise amplitude decreases towards zero, the expected loss functions for the recorded responses approach similar values; in the case of noise-free recordings, the accelerometer could be placed at any of the floor levels. Figure 2(b) shows results for the case of a stiffness prior coefficient of variation COV = 0.30. Results are similar to those shown in Figure 2(a) for COV = 0.15. The COV in the prior distribution of K did not have an effect on the optimal location of the accelerometer; however, as discussed below, it did influence the reduction of prior uncertainty about K when the response is recorded.

The results shown in Figure 2 may be used to assess the amount of prior uncertainty about K that can be reduced by recording a response acceleration. Let $\mathrm{Var}(K|Y{=}y)$ denote the posterior variance of K when the values y are measured for response Y. Prior to the observation of Y, $\mathrm{Var}(K|Y)$ is an uncertain variable. The posterior variance of K, averaged over all possible values of the response Y is then $E[\mathrm{Var}(K|Y)]$. It is worth pointing out that $E[\mathrm{Var}(K|Y)]$ is the posterior variance associated with the process of recording Y and then estimating K, *before* any particular value $Y = y$ has been observed. Thus, if response Y is recorded for estimating K, the reduction in the uncertainty about K is then $\mathrm{Var}(K) - E[\mathrm{Var}(K|Y)]$, where $\mathrm{Var}(K)$ is the prior variance of K. Given that the Bayesian loss function used here is the squared error function, $L(K, \hat{K}) = \{K - \hat{K}(Y)\}^2$, the estimator $\hat{K}(Y)$ is equal to the conditional mean of K given the response Y, i.e. $\hat{K}(Y) = E[K|Y]$. Hence,

$$
\begin{aligned}
E[\mathrm{Var}(K \mid Y)] &= E_Y E_{K|Y}\left(\left\{K - \hat{K}(Y)\right\}^2\right) \\
&= E\left[L\left(K, \hat{K}\right)\right] \\
&= E_K M_K^{-1}
\end{aligned}
\tag{36}
$$

where M_K is the Fisher information in Y about K. As seen in equation (36), the Fisher information may be used to evaluate the posterior variance of K and, therefore, to assess the reduction of prior uncertainty associated with the process of recording response Y for the estimation of K. In fact, if an instrumentation program is to be useful, a reduction of prior uncertainty about the structural parameters should be achieved based on the information contained in the recordings.

Figure 2 thus shows that the posterior stiffness variance increases with increasing values of the normalized noise; the larger the noise amplitudes the lower the reduction of prior uncertainty. For relatively large recording noise amplitudes or for low to moderate ground motion intensities, the most accurate estimates of the stiffness can be expected if the accelerometer is placed at the fifth floor to record the response. On the other hand, Figure 2 also shows that for small values of the normalized noise, say $N_0/S_0 \leq 0.05$, i.e. for noise-free recordings or large ground motion intensities, there is not a significant difference in the posterior stiffness variances, thus implying, as stated before, that the accelerometer could be placed at any of the five floors. However, taking into account that: (1) the ground motion white noise intensity S_0 of future earthquakes is uncertain, and (2) once the accelerometer has been placed on the structure one would expect the recordings obtained during any future event (even if it corresponds to a low to moderate intensity S_0) to be useful for reducing as much of the prior uncertainty as possible, then the optimal location for the accelerometer is that of the fifth floor.

One should keep in mind that these results depend not only on the expected ground motion amplitudes, as measured by S_0, but also on its dominant or characteristic frequency. Figure 3 shows results for the same example structure but subjected to a random earthquake ground motion excitation with characteristic soil frequency ω_g = 2.47 Hz and critical damping ratio ξ_g = 0.20 in the Kanai-Tajimi spectral density function. The characteristic frequency ω_g was chosen to match the mean first modal frequency of the structural system so that the contribution of the first mode to the total response was dominant. The results in Figure 3 show that when the structure tends to respond in its first fundamental mode, there will not be much of a difference in the expected loss function values associated with the possible locations of the accelerometer. Hence, it should be just as useful in this case to place the accelerometer at any of the floor levels. These results suggest that when excited in the fundamental mode, response amplitudes are much larger than those of noise. It is also interesting to point out that a lower posterior uncertainty about K can be expected when records are obtained from the structure responding in its fundamental mode. In the following, the characteristic frequency in the Kanai-Tajimi spectral density is kept equal to 0.8 Hz as assumed first.

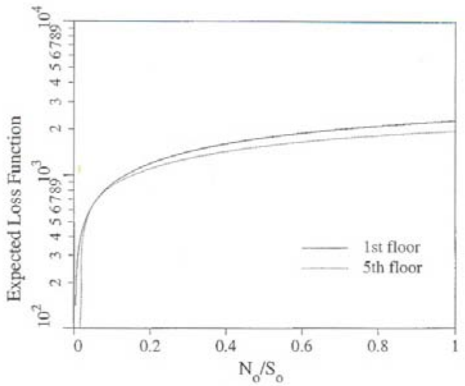

Figure 3. Expected loss function versus normalized noise, ω_g = 2.47 Hz, COV = *0.15*

Consider now an uncertainty reduction index (URI) defined as the portion of the prior coefficient of variation that can be reduced by means of an instrumentation program,

$$\mathrm{URI} = \frac{\mathrm{COV} - \mathrm{COV}_f}{\mathrm{COV}} \tag{37}$$

where COV_f is the posterior coefficient of variation of the stiffness K. The larger the URI, the more efficient the instrumentation is regarding the reduction of prior uncertainty about K. Optimally, the URI should be as close to one as possible. Figure 4(a) shows plots of the URI versus the normalized noise amplitudes, when the accelerometer is placed at the first floor and for both prior coefficients of variation COV = 0.15 and 0.30. It can be seen that a greater uncertainty reduction can be achieved when the prior uncertainty is higher. Similar results are shown in Figure 4(b) when the accelerometer is placed at the fifth floor. It is interesting to notice that a very small posterior uncertainty about K remains once recordings from the fifth floor are obtained for the estimation of K. Hence, one can expect to be able to estimate, with great certainty, the lateral stiffness from records of the structure considered in this example. Different results in terms of optimal accelerometer location and uncertainty reduction might be obtained for the case of partially correlated lateral stiffnesses or for the case where other structural parameters, such as masses and dampings, were to be estimated from a response recording. Moreover, other locations could be found to be optimal if considerations of uniqueness in the solution of the inverse problem for identification of the lateral stiffness were taken into account. [3, 4]

The criterion proposed in this paper can be used to assess the influence of the duration of the recordings on the reduction of prior uncertainty. Following the same procedure indicated before for the computation of the expected loss function, results were obtained for different recording durations. Figure 5 shows the variation of the URI as a function of the record durations for a normalized noise amplitude of 0.20 and for prior coefficients of variation COV = 0.15 and 0.30. As expected, the URI increases with longer record durations. Take, for instance, the case where the accelerometer is placed at the fifth floor and COV = 0.15 (Figure 5(a)): the URI increases from values of about 60 per cent for a record duration equal to 2 sec, up to values of about 85 per cent for record durations equal to 10 sec. These curves indicate the minimum duration that record s should have in order to obtain a significant reduction of prior uncertainty. For instance, for a prior COV = 0.15 and a 2 sec record duration, the URI would be equal to about 25 per cent if the accelerometer had been placed at the first floor. Given the noise amplitude considered, records with shorter durations would not be useful for identifying the lateral stiffness. Between 2 and 10 sec, the increase in the URI is significant. For a target uncertainty reduction, say 80 per cent, acceleration records from the first floor should have a duration of at least 10 sec.

The capabilities of the criterion were also tested against cases in which the distribution of mean lateral stiffness with height is not uniform. Four cases with different sets of values for the stiffness constants c_i were used to obtain structures with different configurations of mean stiffness with height: Case I: $c_2 = 100$, $c_3 = 1$, $c_4 = 1$, $c_5 = 100$; Case II: $c_2 = 100$, $c_3 = 100$, $c_4 = 1$, $c_5 = 1$; Case III: $c_2 = 100$, $c_3 = 100$, $c_4 = 100$, $c_5 = 100$; Case IV: $c_2 = 1$, $c_3 = 0.01$, $c_4 = 1$, $c_5 = 1$. The expected loss functions were computed assuming a prior COV = 0.15, a normalized noise $N_0/S_0 = 0.20$ and a record duration equal to 10 sec.

Results are listed in Table I and Figure 6 shows the optimal location of the accelerometer for each of the four cases. In Case I ($K_2 = 100\,K$, $K_3 = K$, $K_4 = K$, $K_5 = 100\,K$), the second and fifth inter-storeys are stiff compared to the other ones. Due to its relative large stiffness, response accelerations along the degrees of freedom at the fourth and fifth floors are highly correlated and the results show that the expected loss function values when the accelerometer is placed at any of these floors are consequently very close. The same argument can be stated for the response acceleration at the first and second floors. The results show that either the fourth or the fifth floor is optimal location for the accelerometer, implying that their responses are more sensitive to the lateral stiffness than those of the first and second floors. In Case II ($K_2 = 100\,K$, $K_3 = 100\,K$, $K_4 = K$, $K_5 = K$), response accelerations along the degrees of freedom at the first, second and third floor levels are highly correlated; hence, the computed expected loss functions when the accelerometer is placed at any of these floors are similar to each other.

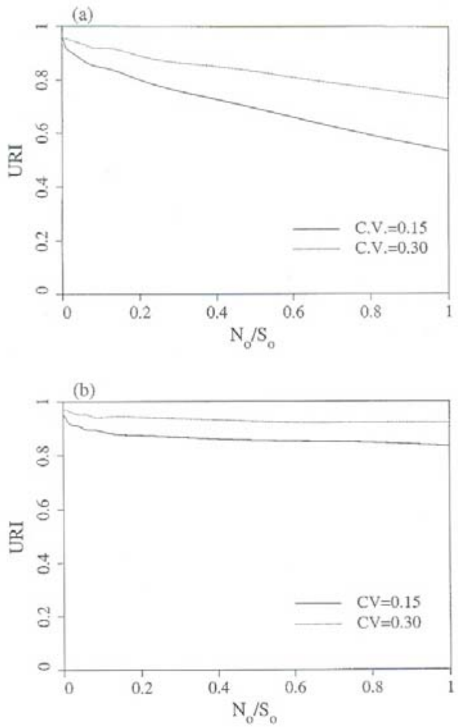

Figure 4. Uncertainty reduction index versus normalized noise for accelerometer located at (a) first floor: (b) fifth floor.

As in the case of uniform mean stiffness with height, the optimal location for the accelerometer is the fifth floor. In Case III (K_2 = 100 K, K_3 = 100 K, K_4 = 100 K, K_5 = 100 K), the four upper storeys tend to respond as a rigid block. Although the expected loss function when the accelerometer is placed at the fifth floor is the minimum, as a consequence of its being more sensitive to K, it is seen that values of the loss function at the other floor levels are close to that corresponding to the fifth one. Case IV yields a different optimal location for the accelerometer. In Case IV ($K_2 = K$, $K_3 = 0.01K$, $K_4 = K$, $K_5 = K$), the third inter-storey is very flexible compared to the stiffness of the other inter-storeys. Due to such flexibility, a small portion of the ground motion energy input excites the responses of the upper three storeys, which are highly correlated as indicated by the values of the corresponding expected loss functions. The response acceleration along the second and first floor degrees of freedom are less correlated compared to those of the upper storeys. The minimum expected loss function corresponds to an accelerometer placed at the second floor which becomes the optimal location and suggests that such response is more sensitive to changes in K than that of the first floor.

In the case of the example structure with known masses and damping, and equal mean inter-storey stiffnesses, that has been discussed here, the prior uncertainty about K can be reduced significantly if just one accelerometer is placed on the structure. However, just for the sake of completeness and illustration of the criterion capabilities, results are given now for the cases in which more than one accelerometer was available. Figure 7 (a) shows the optimal location for different numbers of accelerometers considering a normalized noise equal to 0.20, a 10 sec record duration and COV = 0.15. It is seen that if one accelerometer were added at a time to the array of instruments, it should

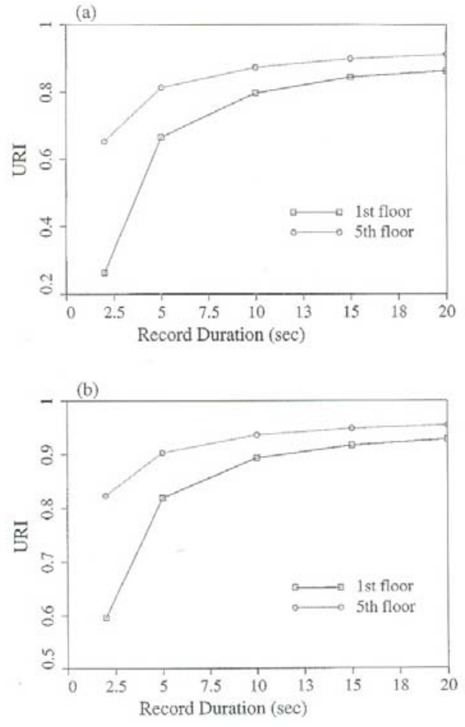

Figure 5. Uncertainty reduction index versus record duration:
(a) COV = *0.15;* COV = *0.30*

TABLE 1

Expected loss functions for a structure with variation of mean stiffness with height

Storey level	Case I	Case II	Case III	Case IV
1st	5172	4400	3411	6001
2nd	5122	4362	3388	3079
3rd	3629	4335	3371	14 066
4th	3071	3155	3359	14 081
5th	3068	2720	3354	14 087

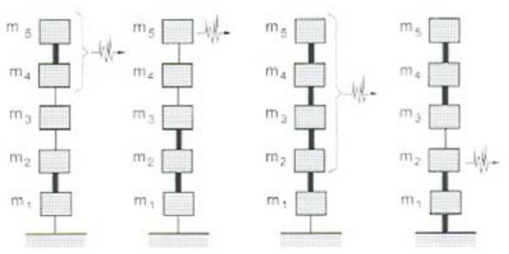

Figure 6. Optimal location of accelerometer for different distributions of mean stiffness with height; COV = *0.15*

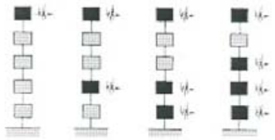

a)

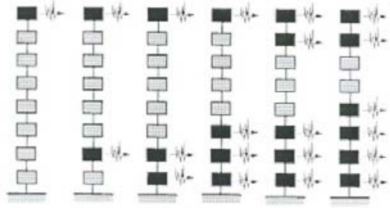

b)

Figure 7. Optimal arrays of accelerometers: (a) 5-DOF system; (b) 8-DOF system

be placed on the structure in the following order: first at the second floor, then at the first one and finally at the third one. The case of a similar eight-storey shear building subjected to the same ground motion excitation was also analysed. Masses concentrated at the floor levels were taken all equal to 1 K sec^2/in, critical damping ratios of 2 per cent were given for all modes, a prior stiffness COV = 0.15 was considered, and the distribution of mean lateral stiffness with height was assumed uniform, $c_i = 1$, $i = 2, \ldots, 8$. A normalized noise amplitude equal to 0.20 and a 10 sec record duration were also considered. The optimal locations for different number of accelerometers are shown in Figure 7(b). As in the case of the five-degree-of-freedom building, the top floor is the optimal location for a single accelerometer. Next optimal locations are the second, first and third floors. From then on, the results suggest that further accelerometers should be placed starting from the top and lower storeys moving downwards and upwards, respectively. Similar results have also been obtained for systems with a greater number of degrees of freedom.

Conclusions

A criterion has been proposed for selecting the optimal location of a given number of sensors to record the seismic response of a structural system for identification purposes. The optimal sensor locations are selected so that the expected value of a Bayesian loss function is minimized. Assuming that efficient estimators are used for the structural parameters, the expected loss function is then given in terms of the expected size of the Fisher information matrix associated with the responses to be recorded. The criterion has been applied to the case of linear systems with uncertain structural properties subjected to random earthquake ground motions. By means of a discrete Fourier transform, responses were expressed in terms of their Fourier coefficients and the problem formulated in the frequency domain. Thus, an efficient use can be made of the statistical independence between response Fourier coefficients and of the stochastic solution for the structural response in terms of cross-spectral density functions. Expressions have been derived for computing the Fisher information matrix associated with a set of recorded responses. The formulation clearly shows that the Fisher information matrix is a weighted combination of the covariances between recorded responses and the sensitivity of such covariances to changes in the uncertain structural parameters. Thus, the relative weights of the covariances between responses and of the sensitivities of such covariances to the structural parameters to be identified can be accounted for in the selection of the optimal locations of the recording instruments, which is a fundamental contribution of the paper.

A thorough example has been given to illustrate the use and features of the proposed formulation. Results in terms of optimal locations of recording instruments and reduction of uncertainty about the structural properties, have been used to assess the influence of the recording noise, the ground-motion-dominant frequencies and expected amplitudes, the record durations, the prior uncertainty in the knowledge of the structural properties and the correlation structure of the recorded responses. In the case of shear buildings where the uncertain lateral stiffnesses may be considered to be perfectly correlated, the optimal location for a single accelerometer is that of the top storey. Much of the prior uncertainty is found to be reduced by recordings from a single accelerometer. However, different conclusions may be drawn in those cases where other structural properties are to be identified instead, or when the assumption of perfect correlation could not hold. In its present form, the formulation proposed here can be used to analyze such cases which are left as the topic of future studies by the authors. Optimal arrays for a number of accelerometers have also been proposed. The results suggest that if several accelerometers are available, they should be placed starting at the top and bottom floors, and then progress with the instrumentation towards the middle ones.

Appendix I

Here we will show that

$$E_{Y|\Theta}\left[\mathbf{Y}_i^T \frac{\partial \mathbf{C}_i^{-1}}{\partial \theta_k}\mathbf{Y}_i\right] = -\frac{\partial \ln \mathit{\Delta}_i}{\partial \theta_\mathrm{k}} \tag{38}$$

For the simplicity of notation in the proof that follows, the subscript '*i*' will be dropped from the terms in equation (38). Thus, let $\mathbf{C}$ denote the conditional covariance matrix of a random vector $\mathbf{Y}$, $\mathbf{C} = E_{Y|\Theta}[\mathbf{Y}\mathbf{Y}^T]$, and let $\mathit{\Delta}$ denote its determinant. By the chain rule of differentiation, and using indicial notation, we have that

$$\frac{\partial \ln \Delta}{\partial \theta_k} = \frac{\partial \ln \Delta}{\partial C_{ij}}\frac{\partial C_{ij}}{\partial \theta_k} \tag{39}$$

where C_{ij} is the element in the *i*th row and *j*th column of the covariance matrix $\mathbf{C}$. If matrix $\overline{\mathbf{C}}$ denotes the adjoint of $\mathbf{C}$, the inverse matrix $\mathbf{C}^{-1}$ is given by

$$\mathbf{C}^{-1} = \frac{\overline{\mathbf{C}}}{\mathit{\Delta}} \tag{40}$$

Since the product $\mathbf{C}\mathbf{C}^{-1}$ equals the identity matrix $\mathbf{I}$**,** then

$$\mathit{\Delta}\mathbf{I} = \mathbf{C}\overline{\mathbf{C}} \tag{41}$$

Considering the *i*th element in the diagonal of matrix $\Delta\mathbf{I}$, and using incidal notation, it follows from equation (41) that the determinant Δ can be expressed as

$$\Delta = C_{ik}\overline{C}_{ki} \tag{42}$$

where $\overline{C}_{ki}$ is an element in matrix $\overline{\mathbf{C}}$. Equation (42) can be used to obtain the partial derivative

$$\frac{\partial \ln \Delta}{\partial C_{ij}} = \frac{1}{\Delta}\left\{\frac{\partial C_{ik}}{\partial C_{ij}}\overline{C}_{ki} + C_{ik}\frac{\partial \overline{C}_{ki}}{\partial C_{ij}}\right\} \tag{43}$$

Taking into account that (1) $\partial C_{ik}/\partial C_{ij}$ equals the Kronecker δ_{jk}, and (2) $\partial \overline{C}_{ki}/\partial C_{ij} = 0$ since by definition of adjoint matrix, element $\overline{C}_{ki}$ does not depend on the elements in the *i*th row of **C**, then equation (43) reduces to

$$\frac{\partial \ln \Delta}{\partial C_{ij}} = \frac{1}{\Delta}\overline{C}_{ji} \tag{44}$$

Noting that, by definition of inverse matrix, the right-hand side of equation (44) is the *ji*th element of matrix $\mathbf{C}^{-1}$ and given the symmetry of covariance matrix **C**, then

$$\frac{\partial \ln \mathit{\Delta}}{\partial C_{ij}} = C_{ij}^{-1} \tag{45}$$

and substituting equation (45) back into equation (39),

$$\frac{\partial \ln \mathit{\Delta}}{\partial \theta_k} = C_{ij}^{-1}\frac{\partial C_{ij}}{\partial \theta_k} \tag{46}$$

According to indicial notation, the product in equation (46) represents a dot product between matrices $\mathbf{C}^{-1}$ and $\partial \mathbf{C}/\partial \theta_k$,

$$\frac{\partial \ln \mathit{\Delta}}{\partial \theta_k} = \mathbf{C}^{-1}\cdot \partial \mathbf{C}/\partial \theta_k$$

Consider now the expected value in equation (38) expressed in indicial notation,

$$E_{Y|\Theta}\left[\mathbf{Y}^T\frac{\partial \mathbf{C}^{-1}}{\partial \theta_k}\mathbf{Y}\right] = E_{Y|\Theta}\left[Y_m\frac{\partial C_{mn}^{-1}}{\partial \theta_k}Y_n\right] \tag{47}$$

As stated above, the subscript has been dropped for simplicity on the left-hand side of equation (47). Given that the expectation is taken conditionally on Θ, equation (47) can be written as follows:

$$\begin{aligned} E_{Y|\Theta}\left[\mathbf{Y}^T\frac{\partial \mathbf{C}^{-1}}{\partial \theta_k}\mathbf{Y}\right] &= \frac{\partial C_{mn}^{-1}}{\partial \theta_k}E_{Y|\Theta}\left[Y_mY_n\right] \\ &= \frac{\partial C_{mn}^{-1}}{\partial \theta_k}C_{mn} \end{aligned} \tag{48}$$

where the last equality in equation (48) follows from the definition of covariance, $E_{Y|\Theta}[Y_m\ Y_n] = C_{mn}$. From the chain rule for the derivative of a product, the right-hand side in equation (48) can be expressed as

$$\frac{\partial C_{mn}^{-1}}{\partial \theta_k} C_{mn} = \frac{\partial}{\partial \theta_k} \left\{ C_{mn}^{-1} C_{mn} \right\} - C_{mn}^{-1} \frac{\partial C_{mn}}{\partial \theta_k} \tag{49}$$

The first partial derivative on the right-hand side of equation (49) is equal to zero since the term $C^{-1}_{mn}C_{mn}$ represents the trace of the identity matrix **I**,

$$\begin{aligned} C_{mn}^{-1} C_{mn} &= C_{mn}^{-1} C_{nm} \\ &= I_{mm} \\ &= \operatorname{tr} \mathbf{I} \end{aligned} \tag{50}$$

Thus,

$$\frac{\partial C_{mn}^{-1}}{\partial \theta_k} C_{mn} = - C_{mn}^{-1} \frac{\partial C_{mn}}{\partial \theta_k} \tag{51}$$

Substituting equation (51) into equation (48) one obtains

$$E_{Y|\Theta} \left[\mathbf{Y}^T \frac{\partial \mathbf{C}^{-1}}{\partial \theta_k} \mathbf{Y} \right] = -C_{mn}^{-1} \frac{\partial C_{mn}}{\partial \theta_k} \tag{52}$$

and from equation (46) it follows that

$$E_{Y|\Theta} \left[\mathbf{Y}^T \frac{\partial \mathbf{C}^{-1}}{\partial \theta_k} \mathbf{Y} \right] = - \frac{\partial \ln \mathit{\Delta}}{\partial \theta_{\mathrm{k}}} \tag{53}$$

which proves expression (10) used in this paper.

Appendix II

Here we prove the following expression used in equation (12):

$$E_{Y|\Theta} \left[\mathbf{Y}^T \frac{\partial \mathbf{C}^{-1}}{\partial \theta_k} \mathbf{Y} \, \mathbf{Y}^T \frac{\partial \mathbf{C}^{-1}}{\partial \theta_l} \mathbf{Y} \right] = 2 \mathbf{C}^{-1} \frac{\partial \mathbf{C}}{\partial \theta_k} \cdot \frac{\partial \mathbf{C}}{\partial \theta_l} \mathbf{C}^{-1} + \frac{\partial \ln \mathit{\Delta}}{\partial \theta_k} \frac{\partial \ln \mathit{\Delta}}{\partial \theta_l} \tag{54}$$

In equation (54), **C**, **Y** and $\mathit{\Delta}$ are defined as in Appendix I. Using indicial notation and denoting by K_{qm} and L_{np} the elements in matrices $\partial \mathbf{C}^{-1}/\partial \theta_k$ and $\partial \mathbf{C}^{-1}/\partial \theta_l$, respectively, equation (54) can be expressed as

$$E_{Y|\Theta} \left[\mathbf{Y}^T \frac{\partial \mathbf{C}^{-1}}{\partial \theta_k} \mathbf{Y} \mathbf{Y}^T \frac{\partial \mathbf{C}^{-1}}{\partial \theta_l} \mathbf{Y} \right] = E_{Y|\Theta} \left[Y_q K_{qm} Y_m Y_n L_{np} Y_p \right] \tag{55}$$

The expected value in equation (55) involves fourth-order moments that can be obtained based on second-order moments provided **Y** is a Gaussian random vector as follows:

$$\begin{aligned} E_{Y|\Theta} \left[\mathbf{Y}^T \frac{\partial \mathbf{C}^{-1}}{\partial \theta_k} \mathbf{Y} \, \mathbf{Y}^T \frac{\partial \mathbf{C}^{-1}}{\partial \theta_l} \mathbf{Y} \right] &= K_{qm} L_{np} E_{Y|\Theta} \left[Y_q Y_m Y_n Y_p \right] \\ &= K_{qm} L_{np} \left\{ C_{qm} C_{np} + C_{qn} C_{mp} + C_{qp} C_{mn} \right\} \end{aligned} \tag{56}$$

where $C_{ij} = E_{Y|\Theta}[Y_i\, Y_j]$ is an element of covariance matrix $\mathbf{C} = E_{Y|\Theta}[\mathbf{YY}^{\mathrm{T}}]$. Since $C_{ij} = C_{ji}$ and $L_{np} = L_{pn}$, because of symmetry, equation (56) is then equal to

$$E_{Y|\Theta}\left[\mathbf{Y}^T \frac{\partial \mathbf{C}^{-1}}{\partial \theta_k} \mathbf{Y}\, \mathbf{Y}^T \frac{\partial \mathbf{C}^{-1}}{\partial \theta_l} \mathbf{Y}\right] = K_{qm} C_{qm} L_{np} C_{np} + \\ + K_{qm} C_{qn} L_{np} C_{pm} + K_{qm} C_{qp} L_{pn} C_{nm} \tag{57}$$

Notice that the matrix products $C_{qn}L_{np}C_{pm}$ and $C_{qp}L_{pn}C_{nm}$ are equal to each other; thus equation (57) reduces to

$$E_{Y|\Theta}\left[\mathbf{Y}^T \frac{\partial \mathbf{C}^{-1}}{\partial \theta_k} \mathbf{Y}\, \mathbf{Y}^T \frac{\partial \mathbf{C}^{-1}}{\partial \theta_l} \mathbf{Y}\right] = K_{qm} C_{qm} L_{np} C_{np} + 2 K_{qm} C_{qn} L_{np} C_{pm} \tag{58}$$

Recalling that K_{qm} and L_{np} denote elements of matrices $\partial \mathbf{C}^{-1}/\partial \theta_k$, $\partial \mathbf{C}^{-1}/\partial \theta_l$, respectively, the first term on the right-hand side of equation (58) is equal to

$$K_{qm} C_{qm} L_{np} C_{np} = \frac{\partial C_{qm}^{-1}}{\partial \theta_k} C_{qm} \frac{\partial C_{np}^{-1}}{\partial \theta_l} C_{np} \tag{59}$$

It follows from equations (46) and (51) in Appendix I that

$$\frac{\partial \ln \Delta}{\partial \theta_k} = C_{ij}^{-1} \frac{\partial C_{ij}}{\partial \theta_k} = -\frac{\partial C_{ij}^{-1}}{\partial \theta_k} C_{ij} \tag{60}$$

Thus, equation (59) becomes

$$K_{qm} C_{qm} L_{np} C_{np} = \frac{\partial \ln \Delta}{\partial \theta_k} \frac{\partial \ln \Delta}{\partial \theta_l} \tag{61}$$

Consider now the term $L_{np}C_{pm}$ on the right-hand side of equation (58); it can be written as

$$L_{np} C_{pm} = \frac{\partial C_{np}^{-1}}{\partial \theta_l} C_{pm} \tag{62}$$

and according to the derivative of a product,

$$\begin{aligned} L_{np} C_{pm} &= \frac{\partial}{\partial \theta_l}\left\{C_{np}^{-1} C_{pm}\right\} - C_{np}^{-1} \frac{\partial C_{pm}}{\partial \theta_l} \\ &= -C_{np}^{-1} \frac{\partial C_{pm}}{\partial \theta_l} \end{aligned} \tag{63}$$

given that $C^{-1}_{np}C_{pm} = \delta_{nm}$, δ_{nm} being the Kronecker delta. In the same way, it can be shown that

$$K_{qm} C_{qn} = -C_{mq}^{-1} \frac{\partial C_{qn}}{\partial \theta_k} \tag{64}$$

Using equations (63) and (64), the term $K_{qm}C_{qn}L_{np}C_{pm}$ on the right-hand side of equation (58) is given by

$$K_{qm}C_{qn}L_{np}C_{pm} = C_{mq}^{-1}\,\frac{\partial C_{qn}}{\partial \theta_k}\,C_{np}^{-1}\,\frac{\partial C_{pm}}{\partial \theta_l} \tag{65}$$

The expression in indicial notation in equation (65) represents the following matrix product:

$$K_{qm}C_{qn}L_{np}C_{pm} = \mathbf{C}^{-1}\,\frac{\partial \mathbf{C}}{\partial \theta_k}\cdot\left\{\mathbf{C}^{-1}\,\frac{\partial \mathbf{C}}{\partial \theta_l}\right\}^T = \mathbf{C}^{-1}\,\frac{\partial \mathbf{C}}{\partial \theta_k}\cdot\frac{\partial \mathbf{C}}{\partial \theta_l}\,\mathbf{C}^{-1} \tag{66}$$

Therefore, substituting equations (61) and (66) into equation (58), one obtains

$$E_{Y|\Theta}\left[\mathbf{Y}^T\,\frac{\partial \mathbf{C}^{-1}}{\partial \theta_k}\,\mathbf{Y}\;\mathbf{Y}^T\,\frac{\partial \mathbf{C}^{-1}}{\partial \theta_l}\,\mathbf{Y}\right] = 2\mathbf{C}^{-1}\,\frac{\partial \mathbf{C}}{\partial \theta_k}\cdot\frac{\partial \mathbf{C}}{\partial \theta_l}\,\mathbf{C}^{-1} + \frac{\partial \ln \Delta}{\partial \theta_k}\,\frac{\partial \ln \Delta}{\partial \theta_l} \tag{67}$$

which is the expression used in equation (12) in this paper.

Appendix III

Modal frequencies and mode shapes are obtained from the eigenvalue solution of the system of equations,

$$\left\{\mathbf{K} - \omega^2\mathbf{M}\right\}\phi = 0 \tag{68}$$

Let K_{ij}, M_{ij} denote elements of the stiffness and mass matrices **K**, **M**, respectively, and ϕ_j denote a component of mode shape vector ϕ. Using indicial notation the *i*th equation in equation (68) can be expressed as

$$K_{ij}\phi_j - \omega^2 M_{ij}\phi_j = 0 \tag{69}$$

Taking partial derivatives in equation (69) one obtains

$$K_{ij}\phi_{j,K} - \omega^2 M_{ij}\phi_{j,K} - \omega_{,K}^2 M_{ij}\phi_j = -K_{ij,K}\phi_j \tag{70}$$

where the subscript, ',K' denotes partial derivative of the variable subscripted with respect to K. Noticing that (1) for a system with concentrated masses $\omega^2{}_{,K}M_{ij}\phi_j = \omega^2{}_{,K}m_j\phi_j$ where m_j is the *j*th element in the diagonal of matrix **M**; and (2) the first mode shape vector component is usually normalized to one as auxiliary condition to solve the eigenvalue problem in equation (68), i.e. $\phi_{1,K} = 0$, the system of equations (70) can be written in matrix form as follows:

$$\begin{bmatrix} -m_1\phi_1 & K_{12} & K_{13} & \cdots & K_{1Q} \\ -m_2\phi_2 & K_{22}-\omega^2 m_2 & K_{23} & \cdots & K_{2Q} \\ -m_3\phi_3 & K_{32} & K_{33}-\omega^2 m_3 & \cdots & K_{3Q} \\ \vdots & \vdots & \vdots & \cdots & \vdots \\ -m_Q\phi_Q & K_{Q2} & K_{Q3} & \cdots & K_{QQ}-\omega^2 m_Q \end{bmatrix}\begin{bmatrix} \omega_{1,K}^2 \\ \omega_{2,K}^2 \\ \omega_{3,K}^2 \\ \vdots \\ \omega_{Q,K}^2 \end{bmatrix} = -\frac{\partial \mathbf{K}}{\partial K}\,\phi \tag{71}$$

Solving the system of linear equations (71) yields the partial derivatives of modal frequencies and mode shape vectors with respect to the first storey lateral stiffness *K*.

Acknowledgements

This research has been funded by the Direccion General de Asuntos del Personal Academico, UNAM, under grant PAPIIT-IN105195. Any opinions, findings, and conclusions are those of the authors and do not necessarily reflect the views of the sponsor.

References

1. P. Shah and F. E. Udwadia, 'A methodology for optimal sensor locations for identification of dynamic systems', *J. Appl. Mech.* **45**, 188-196 (1978).
2. F. E. Udwadia, P. Shah and D. Sharma, 'Uniqueness of damping and stiffness distributions in the study of soil and structural systems', *J. Appl. Mech.* **45**, 181-187 (1978).
3. F. E. Udwadia, 'Some uniqueness results related to soil and building structural identification', *SIAM J. Appl. Math.* **45**, 674-685 (1985).
4. F. E. Udwadia, 'Methodology for optimum sensor locations for parameter identification in dynamic systems', *ASCE J. Engng. Mech.* **120**, 368-390 (1994).
5. S. O. Rice, in N. Wax (ed.), *Mathematical Analysis of Random Noise*, Selected Publications on Noise and Stochastic Processes, Dover, New York, 1954.
6. E. Heredia-Zavoni, 'Structural response to spatially varying earthquake ground motion', *Ph. D. Thesis*, Dept. of Civil Engineering and Operations Research, Princeton University, Princeton, 1993.
7. E. H. Vanmarcke, E. Heredia-Zavoni and G. A. Fenton, 'Conditional simulation of spatially correlated earthquake ground motion', *ASCE J. Engng Mech.* **119**, 2333-2352 (1993).
8. E. Heredia-Zavoni and E. H. Vanmarcke, 'Seismic random vibration analysis of multi-support structural systems', *ASCE J. Engng. Mech.* **120**, 1107-1128 (1994).

SIMULATING EARTHQUAKE GROUND MOTION AT A SITE, FOR GIVEN INTENSITY AND UNCERTAIN SOURCE LOCATION[1]

ABSTRACT

Following a companion article, ground motion acceleration time histories during earthquakes can be described as realizations of non-stationary stochastic processes with evolutionary frequency content and instantaneous intensity. The parameters characterizing those processes can be handled as uncertain variables with probabilistic distributions that depend on the magnitude of each seismic event and the corresponding source-to-site distance. Accordingly, the generation of finite samples of artificial ground motion acceleration time histories for earthquakes of given intensities is formulated as a two-stage Monte Carlo simulation process. The first stage includes the simulation of samples of sets of the parameters of the stochastic process models of earthquake ground motion. The second stage includes the simulation of the time histories themselves, given the parameters of the associated stochastic process model. In order to account for the dependence of the probability distribution of the latter parameters on magnitude and source-to-site distance, the joint conditional probability distribution of these variables must be obtained for a given value of the ground motion intensity. This is achieved by resorting to Bayes Theorem about the probabilities of alternate assumptions. Two options for the conditional simulation of ground motion time histories are presented. The more refined option makes use of all the information about the conditional distribution of magnitude and distance for the purpose of simulating values of the statistical parameters of the ground motion stochastic process models. The second option considers all probabilities concentrated at the most likely combination of magnitude and distance for each of the seismic sources that contribute significantly to the seismic hazard at the site of interest.

Key words: artificial records, conditional simulation, earthquake accelerograms, seismic hazard, stochastic models.

Introduction

For the purpose of structural design it is customary to specify design requirements in terms of a response spectrum of linear response, usually of pseudo-accelerations, together with adequate reduction factors intended to account for system over-strength and for nonlinear response. For the same purpose, intensities are measured in terms of peak values of ground velocity or acceleration or by the ordinates of the response spectrum for the fundamental vibration period of the structure of interest and a specified value of the damping ratio. The value of the intensity specified for design is chosen so as to correspond to a specified hazard level. The latter may be expressed by the value of the return interval of that intensity at the site. Alternatively, it may be made to correspond to a given probability of being exceeded, either during a given time interval or for

---

[1] First published in:
J. Alamilla, L. Esteva, J. García-Pérez & O. Diaz-López, Simulating earthquake ground motion at a site, for a given intensity and uncertain source location, *Journal of Seismology* **5:** 475-485, 2001.

the condition of occurrence of an earthquake of a given magnitude generated at a given distance from the site.

For the cases of some special or very important structures, it may be convenient to base their seismic design on studies of their dynamic response to samples of simulated ground motion time histories representative of those associated with previously established values of the return interval or the probability of occurrence. It is not unusual that the simulated records are determined in such a manner that their response spectra fit as closely as possible the uniform hazard response spectra.

The foregoing approach has some limitations. Usually, the ordinates of a uniform hazard response spectrum reflect the contributions of different seismic sources in the vicinity of the site. The spectral shapes and intensities associated with ground motion time histories of earthquakes generated at those sources vary in accordance with the magnitudes and distances involved. As a consequence, the relative values of the mentioned contributions are not constant with respect to the frequencies of the seismic waves that determine the ground motion. In other words, they are not independent of the natural periods of the systems to be designed. This implies that, for a given earthquake, the relative values of the contributions of the higher modes of vibration to the response, as compared with that of the fundamental mode, differ from those corresponding to the constant-hazard response spectra. To the authors' knowledge, no studies about the practical significance of these discrepancies have been carried out.

A second, more important limitation, arises from not accounting explicitly for the influence of magnitude and distance on the effective duration of the seismic excitation or, more precisely, for the evolution of the instantaneous intensity and frequency content of the ground acceleration. Because of the influence of these variables on the nonlinear response of structural systems, in particular on the strength-and-stiffness degradation of their constitutive force-deformation functions, their values should be chosen in correspondence with those expected to characterize the earthquakes associated with the selected hazard level.

In a companion article (Alamilla et al., 2001), the authors develop a set of parametric functions describing the evolution of the instantaneous intensity and frequency content of ground acceleration. The dependence of the parameters characterizing those functions on magnitude and source-to-site distance is studied for a set of ground acceleration time histories recorded on firm ground sites near the southern coast of Mexico. The results are presented by means of the expected-value functions of those parameters, together with measures of uncertainty and probabilistic correlation associated with them. The article ends with an example that illustrates the process of simulation of a sample of artificial acceleration time histories for a deterministically defined combination of magnitude and source-to-site distance. Previous to the simulation of each record in the sample, a set of values of the parameters of the functions mentioned above is randomly generated, taking into account the expected value functions and the associated covariance matrix for those parameters. Once this set of parameters is available, the simulation of an acceleration time history is carried out in accordance with conventional procedures.

In practical problems, the earthquakes that determine the seismic hazard at a site may be generated at different sources, each characterized by a different spatial location with respect to the site, as well as by a different rate of activity and a different distribution function of the magnitudes. The problem was studied by McGuire (1995), who proposed an approach based on the most likely values of magnitude and distance conditional to a given value of the intensity. Other significant contributions to the problem of 'disaggregating' seismic hazard in terms of the contributions of various intervals of values of magnitude (M) and source-to-site distance (R) are those by Kramer (1996) and Bazzurro and Cornell (1998). The latter authors express seismic hazard at a site as the sum of the contributions of a number of 'bins' associated with different intervals of magnitude, distance and model error. In this manner they obtain probability mass functions of different combinations of M and R conditional on exceeding different values of intensities at the site. Cramer and Petersen (1996) published maps of the most likely combinations of M and R conditional on exceeding different values of peak ground acceleration and of pseudo-acceleration ordinates for several sites in Southern California.

The approach presented in the following pages is more general than those mentioned above. It is based on a bayesian probabilistic formulation that permits to deal explicitly with the joint distribution functions of M and R conditional on the values of alternate measures of intensity. In addition, the simulation of artificial ground motion acceleration time histories follows a procedure that accounts for that probability density function, as well as for that of the parameters of the stochastic process model of the ground motion conditional on M and R.

Joint Distribution of Magnitude and Source-to-Site Distance, Conditional to Given Intensity Values

The joint conditional probability density function of M and R for a given value of the intensity $Y = y$ can be obtained by means of Bayes theorem. According to it,

$$f_{M,R}(m,r \mid y) = k\ f_Y(y \mid m,r)\, f_{M,R}(m,r) \tag{1}$$

In this equation, $f_{M,R}$ (m, r) is the joint marginal probability density function of M and R throughout the potential seismic sources that contribute significantly to the seismic hazard at the site, f_Y $(y|m, r)$ is the conditional probability density function of the intensity Y for $M = m$ and $R = r$, and k is a normalizing constant such that the integral of $f_{M.R}(m,r|y)$ over the domain of possible values of M and R is equal to unity.

Consider now the case when the seismic hazard at the site can be expressed as the superposition of the contributions of several potential seismic sources. Suppose that throughout each source the spatial distribution of the activity is uniform. Suppose, further, that m_{0j} is the lower bound to the earthquake magnitudes generated at the j-th source that will be included in the estimation of earthquake hazard at the site. The value of m_{0j} for any given source is equal to the magnitude that will produce at the site of interest a computed, intensity y_0 equal to the minimum value considered to be significant for the problem at hand. Let $\lambda_j(m)$ be the rate of occurrence of earthquakes with magnitude equal or greater than M at source j per unit time. This quantity can be expressed as $\lambda_{0j}(l–F_{Mj}(m))$, where λ_{0j} is the rate of occurrence of earthquakes with magnitudes greater than m_{0j} at the j-th source, and F_{Mj} (m) is the cumulative probability distribution function of the magnitudes above m_{0j} generated at the same source. Then, if an earthquake is known to have occurred at one of the sources that contribute to seismic hazard at the site, the probability that it originated at the j-th source is equal to $p_j = \lambda_{0j}/\lambda_0$. Here, λ_0 is equal to the sum of the values of λ_{0j} for all the sources. In this case, Eq. l should be replaced by the following:

$$f_{M,R}(m,r \mid y) = kf_Y\,(y \mid m,r) \sum p_j\, f_{(M,R)\,j}(m,r) \tag{2}$$

In this equation, $f_{(M,R)j}(m, r)$ is the joint marginal probability density function of M and R at the j-th source and the other variables were defined above. The summation shown in the second member is extended to all the potential seismic sources.

In order to apply Eqs, 1 or 2, either continuous or discrete expressions for the functions appearing in their second members should be available. The density function $f_Y(y|m, r)$ is easy to derive on the basis of the values of y predicted by an adequate intensity attenuation expression and the probability density function of the statistical error. For each seismic source, $f_{(M,R)j}(m, r)$ is equal to the product of the marginal probability density functions of M and R: f_{Mj} and f_{Rj}. The former can be estimated from the statistical information about magnitudes generated at the source. The latter can be derived from the assumption of uniform spatial distribution of the seismic activity throughout it.

The need to obtain an explicit expression for $f_{M,R}(m, r|y)$ as given by Eqs. l and 2 can be avoided by means of Monte Carlo simulation of values of M and R in accordance with the probability density functions that appear in the second members of Eqs.1 and 2. The first step will be to make a random selection of the source where that earthquake originated. For this purpose, suppose that $v(y)$ is the rate of occurrence of earthquakes with intensities larger than y at the site of interest, and that $v_j(y)$ is the contribution of the j-th source to that rate. Then, if it is known that an earthquake with an intensity equal to y_1 has taken place, the probability that it originated at the j-th source is equal to the ratio q_j of the derivatives of $v_j(y)$ and $v(y)$ with respect to y, both evaluated at $y = y_1$.

Once the source generating the event has been selected, the probability distribution of the statistical error in the applicable intensity attenuation function can be used to generate a value of the ratio y_1/y_c, where y_1 and y_c are respectively the observed and the computed value of the intensity. Because y_1 is known, this will immediately lead to the computed value, y_c. From the distribution of R for the previously selected source, a value r of that variable is randomly generated. Then M is taken equal to m, which is obtained by solving the intensity-attenuation equation, $y_c = y_c(m, r)$.

A hybrid method for the determination of $f_{M,R}(m, r|y)$ is presented in the illustrative examples that follow. It makes use of numerical integration for the determination of $f_M(m|y)$, the probability density function of M, conditioned to $Y = y$ and marginal with respect to R. Then, it uses Monte Carlo simulation in a sequential manner for the generation of pairs of values of M and R. For each pair, the values are generated respectively from the probability density function of M conditional to $Y = y$, and from that of R conditional to $Y = y$ and to the simulated value of M.

Applications

In another paper (Alamilla et al., 2001), the authors of this study present an example that illustrates the conditional simulation of ground acceleration time histories for a given intensity, under the following assumptions:

a) The motion is originated at a point source, whose distance to the site is deterministically known, and
b) The statistical error in the attenuation functions used to predict intensity in terms of magnitude and source-to-site distance is neglected.

In the two examples presented in this article, the foregoing assumptions are replaced by the following:

a) The source of the motion of interest is contained within a finite-size source region, so that the source-to-site distance is not deterministically known, and

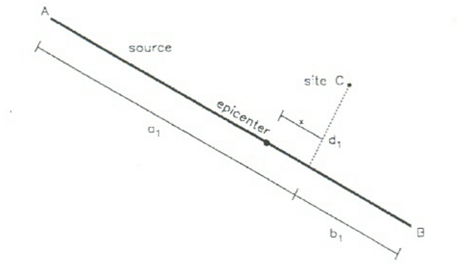

Figure 1. Source location and geometry for Example 1

b) The statistical error in the attenuation functions used to predict intensity in terms of magnitude and distance is explicitly taken into account.

In the general case, the finite-size source region mentioned above may be a linear fault, a two-dimensional fault surface or a diffuse activity volume. For simplicity, the examples presented in the following deal with particular cases of linear faults.

Example 1

Site C in Figure 1 is located in the neighborhood of a vertical strike-slip fault represented in plan by segment AB. All activity is assumed to occur at a depth h_1 = 15 km. Other relevant dimensions are a_1 = 500 km, b_1 = 200 km, d_1 = 50 km. The seismic activity is described by means of the function $\lambda(m)$, the rate of occurrence of earthquakes of magnitude larger than m, per unit time and per unit fault length. The following form is adopted for this function:

$$\lambda(m) = \alpha(e^{-\beta m} - e^{-\beta m_1}), \qquad for \quad m < m_1 \tag{3a}$$

or, alternatively,

$$\lambda(m) = \frac{e^{-\beta m} - e^{-\beta m_1}}{e^{-\beta m_0} - e^{-\beta m_1}} \tag{3b}$$

Here, α and β are parameters that characterize the fault and m_1 is the upper bound to the magnitudes that can be generated at that fault. For engineering purposes, only magnitudes above a threshold value m_0 are relevant. The value that $\lambda(m)$ takes for $m = m_0$ is denoted as λ_0. In this example, α = 0.2057, β = 1.33 and m_1 = 8.2.

From Eqs. 3a and 3b, the probability density function of the magnitudes generated at the fault is given by the following equation:

$$f_M(m) = \frac{\beta e^{-\beta m}}{e^{-\beta m_0} - e^{-\beta m_1}} \tag{4}$$

Suppose that it is necessary to simulate a sample of acceleration time histories to be used in the structural reliability analysis of an engineering system. The intensity of the ground motions to be simulated is specified in terms of the ordinate of the response spectrum for the fundamental natural period of the system. This is equal to 400 cm/s^2, for a natural period of 0.61 s, as in the example presented in the companion article (Alamilla et al, 2001). Starting from Eq. 1, if no information about R is available the probability density function of M conditional to $Y = y$ is equal to

$$f_M(m|\,y) = k\int f_Y(y|\,m,r)\,f_{(M,R)}(m,r)\,\mathrm{d}r \tag{5}$$

On the other hand, the distribution of R conditional to $M = m$, $Y = y$ is equal to

$$f_R(r|\,m,y) = \frac{f_{M,R}(m,r|\,y)}{f_M\,(m|\,y)} \tag{6}$$

This permits obtaining the joint distribution of M and R conditioned to $Y = y$:

$$f_{M,R}(m,r|\,y) = f_M\,(m|\,y)\,f_R(r|\,m,y) \tag{7}$$

Pairs of values of M and R associated with the conditional distribution given by Eq. 1 can be randomly generated in the following manner:

a) $f_M(m|y)$ is represented in discrete form. Its ordinates for a range of values of M are determined from numerical integration of the second member of Eq. 5.
b) $f_R(r|m, y)$ is al so expressed in discrete form. It is calculated by means of Eq. 6.
c) A sample of values of M is generated from the discrete version of the probability density function given by Eq. 5.
d) A value of R is generated for each value of M, in accordance with the discrete version of the probability density function of Eq. 6.

In order to do this, it is necessary to obtain the joint probability density function of M and R, $f_{M,R}(m, r)$, which is simply equal to the product $f_M(m)\cdot f_R(r)$. The first of these factors is the seismic activity of the source, which is known in advance, while the other has to be derived from the spatial distribution of the activity throughout the fault. For the case of uniform spatial distribution of activity, and $a > b$, it is easy to show that

$$f_R(r) = \frac{2Q}{a+b} \qquad \text{for } r < Qb \tag{8a}$$

$$= \frac{Q}{a+b} \quad \mathit{for}\ Qb < r < Qa \tag{8b}$$

$$= 0 \qquad \text{otherwise} \tag{8c}$$

Here, $Q = r/(r^2–d^2–h^2)^{1/2}$.

Using the concepts presented in the preceding paragraphs, several sets of acceleration time histories with specified intensity at site C were randomly generated. Each set included fifty accelerograms, and corresponded to a different assumption regarding the uncertainties associated with earthquake magnitude and focal distance, as well as with the parameters of the amplitude and frequency modulation functions. Those cases are the following:

Case A. The parameters of the amplitude and frequency modulation functions were taken deterministically equal to the values estimated by means of Eqs.16-24 of the companion article by Alamilla et al. (2001).

Case B. Two groups of uncertainties are taken into account in the simulation process, in addition to those concerning the detailed characteristics of the acceleration time histories. Those groups correspond respectively to the values of M and R for a given intensity y, and to the parameters of the amplitude and frequency modulation functions for given values of M and R.

Case C. Uncertainties about the latter parameters are considered, but M and R are taken deterministically equal to their most likely values, conditional to the given intensity, y.

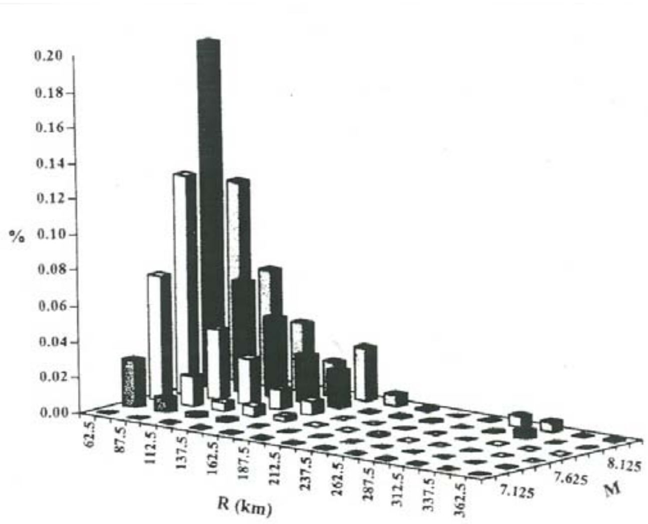

Figure 2. Hystogram of magnitudes and distances conditional to given intensity for Example l

The joint probability distribution of M and R for the specified value of y was generated by Monte Carlo simulation, by sequential application of the discrete versions of Eqs. 5 and 6. The results are presented by the hystogram shown in Figure 2. The most likely combination of those variables corresponds to M = 7.88, R = 62.5 km.

The resulting acceleration time histories have characteristics and variability similar to those found in the example presented by Alamilla et al. (2001) and represented by the sample records shown in Figures 10-13 of that article, with the proper differences associated with the differences in magnitudes and distances. Therefore, it was not considered useful to present samples of them here. Our aim was, instead, to compare the variability measures of the ordinates of the pseudo-acceleration response spectra for the several cases considered in the Monte Carlo simulation process. This is summarized in Table 1, which shows the variation coefficients of the mentioned ordinates for several natural periods. Although some results are in agreement with our expectations, others contradict them strongly. For instance, the smallest variation coefficients correspond to the natural period of 0.50 s, which is closer than any other in the table to the period of 0.61 s, whose spectral ordinate was adopted to define the intensity of the ground motion. Also, the variation coefficients for Case A, for which the parameters of the amplitude and frequency modulation functions were taken as deterministically known, are smaller than those corresponding to Case C, where those parameters were randomly simulated from the most likely values of M and R. However, the variation coefficients for Case B are the smallest of all, with the exception of the values obtained for a natural period of 0.25 s. This was surprising, due to the fact that for this case both the parameters mentioned above and the earthquake magnitudes and distances were taken as uncertain. This may reflect a statistica1 variation, which might perhaps be reduced by using larger samples in the simulation process.

TABLE 1

Variation coefficients of ordinates of response spectra in Example 1

	Natural period		
Case	0.25	0.50	1.00
A	0.30	0.23	0.34
B	0.61	0.19	0.27
C	0.37	0.30	0.57

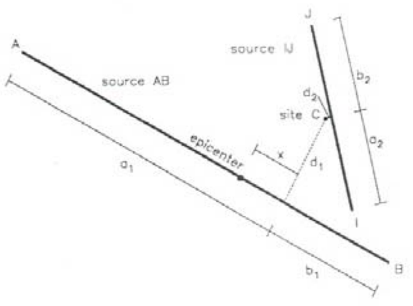

Figure 3. Sources location and geometries for Example 2

Example 2

Seismic hazard at site C in Figure 3 is assumed to be determined by two different potential sources, each corresponding to a vertical plane fault, similar to that considered in Example l. Source AB (segment AB in Figure 3) is identical to that of the mentioned example, but is located at a distance d_1 of 150 km from the site. Source IJ (segment IJ in the figure) has a total length of 300 km, with a minimum distance from the site, d_2, egual to 10 km. Its activity is concentrated at a depth h_2 = 5 km. The seismicity functions of both faults have the form given by Eq. 3b. For fault AB, λ_0 = 0.001, β = 1.33, m_0 = 4.0 and m_1 = 8.2, while for fault IJ these parameters are respectively equal to 0.005, 1.33, 3.0 and 7.0.

As in the previous example, the ground motion intensity is specified by making the ordinate of the linear pseudo-acceleration response spectrum for a vibration period of 0.61 s and a damping ratio of 0.05 equal to 400 cm/s^2.

Within each source, the spatial distribution of seismic activity is taken as uniform. Therefore, under the condition that the source originating a given earthquake is known, the probability density function of R takes the form given by Eqs. 8a-c. The joint conditional density function of (M, R) given $Y = y$ is now that given by Eq. 2, instead of Eq. 1, while the probability density function of M given $Y = Y$ takes the following form:

$$f(m|\, y) = k\sum_j p_j \int f_Y(y|\, m, r)\, f_{(M,R)j}(m, r)\, \mathrm{d}r \tag{9}$$

In this equation, subscript j identifies the source where an earthquake having intensity equal to y at the site is originated, and p_j was defined in the paragraph preceding Eq. 2. After writing an equation similar to Eq. 1, now considering only earthquakes generated at source j, the integrand in Eq. 9 can be shown to be equal to $f_{(M,R)j}(m, r|y)/k_j$, which is the joint probability density function of (*M*, *R*) for earthquakes with intensity equal to *y* generated at source *j*, and k_j is a normalizing constant such that the integral in the second member of Eq. 9 is equal to unity. Thus, Eq. 9 is transformed into the following,

$$f_M(m|\,y) = \sum_j \alpha_j \int f_{(M,R)\,j}(m,r)\,\mathrm{d}r \tag{10}$$

where $\alpha_j = p_j k / k_j$. It is easy to show that $\sum_j \alpha_j = 1$.

This is an immediate consequence of the following relation between the probability density function of the intensity of an earthquake at a given site ($f_Y(y)$) and the probability density functions of the intensities of earthquakes generated at the relevant seismic sources ($f_{Yj}(y)$):

$$f_Y(y) = \sum_j p_j\, f_{Y\,j}(y) \tag{11}$$

The last paragraphs provide criteria for generating pairs of values (*M*, *R*) conditional to $Y = y$ by Monte Carlo simulation. For each pair, the process would be as follows:

a) The source originating the earthquake is randomly selected. This is achieved by simulating the discrete value $J = i$ that identifies the source, from a multinomial distribution with parameters α_j, $j = 1, n_s$, where n_s, is the number of sources, in this case equal to 2.
b) Once the source has been randomly chosen, a value of *M* is generated from the probability function given by the following equation:

$$f_{M\,j}(m|\,y) = \alpha_j \int f_{(M,R)\,j}(m,r|\,y)\,\mathrm{d}r \tag{12}$$

In this equation,

$$f_{(M,R)\,j}(m,r|\,y) = k_j\, f_Y(y|\,m,r)\, f_{(M,R)\,j}(m,r) \tag{13}$$

c) Given the simulated value of $M = m$, a value of *R* is generated from an equation similar to Eq. 6, but specific for the source considered:

$$f_{R\,j}(r|\,m,y) = \frac{f_{(M,R)\,j}(m,r|\,y)}{f_{M\,j}(m|\,y)} \tag{14}$$

The simulated values of *M* and *R* are summarized by the two-dimensional histogram in Figure 4. Each ordinate represents the probability corresponding to the values included in a cell with size $\Delta M \times \Delta R$ of increments of magnitude and distance, respectively. These values are taken here as 0.1 and 5 km. Two clearly defined clusters are evident, each corresponding to one of the sources that determine seismic hazard at the site. The most likely combinations of *M* and *R* for the selected value of the intensity are associated with earthquakes generated at the source farthest from the site (AB). The most likely among all corresponds to $M = 8.1$, $R = 155$ km, with a probability of 0.034. The influence of the other source (IJ) is dominated by the pair of values $M = 6.9$, $R = 15$ km, with a probability of 0.0255.

The probabilities shown in Figure 4 can be used to simulate sets of ground motion time histories, all with intensity equal to that assumed at the outset. The following steps should be followed for each simulation:

a) A combination of M and R is randomly selected in accordance with the probabilities shown in Figure 4.
b) A set of parameters characterizing the reference spectral density, as well as the amplitude and frequency-modulation functions are generated in accordance with the probability density functions described in the companion article by the same authors (Alamilla et al., 2001).
c) Each record is scaled to the specified intensity, in order to account for the uncertainty associated with the ratio of the actual intensity to that of the simulated ground motion time history.

A simplified approach may be followed, according to which all probabilities would be concentrated on two combinations of M and R, one for each of the sources shown in Figure 3. The probability associated with each combination should be that obtained for the corresponding source. The sample giving place to Figure 4 was made of 2000 simulations, out of which 1266 corresponded to source AB, and 734 to source IJ. The resulting probabilities are 0.633 and 0.367, respectively.

For illustration of the simplified approach, two sets of acceleration time histories were simulated for each of the two most likely combinations of M and R mentioned above. Following the procedure described in the companion article by Alamilla et al. (2001), a sample of sets of the statistical parameters of the stochastic models of the ground motion time histories had to be randomly generated prior to the Monte Carlo simulation of the ground motion time histories themselves. In order to study the sensitivity of the statistical properties of the samples of parameters of the stochastic model to the sizes of those samples, two Monte Carlo experiments were carried out, including 1000 and 10000 simulations, respectively. The resulting mean values of some of the most relevant parameters are compared in the following paragraphs with their target values. The parameters selected for this comparison are Δ, Z and ω_g. Briefly, these parameters are respectively the length of the time segment during which the energy contained in the ground motion acceleration time history grows from 25 percent to 75 percent of the total at the end of the earthquake, the standard deviation of the instantaneous acceleration during that segment, and the central frequency of the instantaneous spectral density at the central point of the same segment. A detailed definition of these parameters is presented in the companion article mentioned above (Alamilla et al., 2001).

For M = 8.1 and R = 155 km, the mean values of Δ, Z and ω_g were respectively equal to 8.84 s, 30.5 cm/s^2 and 30.84 radians/s. For M = 6.9 and R = 15 km, the resulting values are 5.19 s, 60.9 s and 44.0 radians/s. These numbers correspond to the samples of size 1000. They are very close to the corresponding target values predicted by generalized attenuation functions presented by Alamilla et al. (2001), and also to those obtained for the samples of size 10000. As expected, the ground motion time histories from the nearest source are characterized by a shorter effective duration and a more pronounced concentration of energy at the higher frequencies than those generated at the farthest source.

Two sets of simulated acceleration time histories, each including six members, are shown in Figures 5 and 6, together with their linear pseudo-acceleration response spectra. A fast look at these sets of record s does not show an agreement with the expectations as evident as that derived from the analysis of the statistical parameters of the

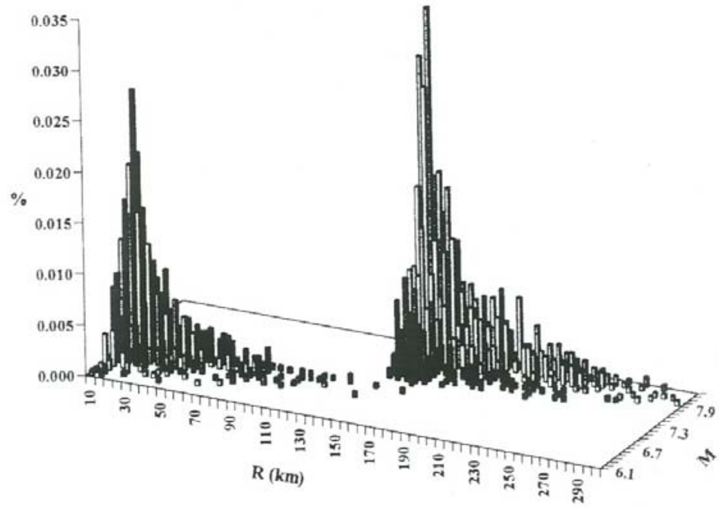

Figure 4. Hystogram of magnitudes and distances conditional to given intensity for Example 2

stochastic process models corresponding to earthquakes generated at each of those sources. A detailed analysis of this apparent contradiction is left for future studies.

In order to integrate a sample of seismic excitations that would reflect the relative values of the contributions of both sources, the simulation would include two steps. First, the source would be randomly selected, in accordance with the probabilities 0.633 and 0.367, mentioned above. Then, a specific ground motion time history would be randomly selected from the set corresponding to the source selected in the previous step.

Concluding remarks

A detailed presentation has been made of the fundamental concepts related to the problem of simulating samples of artificial ground motion time histories for earthquakes of given intensities. For a specific case, the generation of a given sample entails the determination of the joint probability distribution of magnitudes and distances conditional to the specified intensity, the simulation of sets of values of the statistical parameters that describe the stochastic process models of ground motion time histories, to end with the simulation of sets of the time histories themselves. General expressions for the conditional distributions of magnitudes and distances have been presented, and Monte Carlo methods for the sequential generation of pairs of values of M and R complying with those distributions have been proposed, and their application to specific problems has been illustrated.

In the cases studied, ground motion intensity was measured by means of a selected ordinate of the linear pseudo-acceleration response spectrum for damping equal to 0.05 of critical. In the cases presented here, the ordinate selected was assumed to correspond to the fundamental period of vibration of a structure of interest. Alternate definitions of intensity are feasible that may give equal weight to the spectral ordinates for a wide range of natural periods.

As mentioned above, the statistical parameters obtained from the samples of the Monte Carlo simulated values of the parameters characterizing the stochastic process models of ground acceleration time histories coincided with their target values, which were those predicted by the generalized attenuation functions assumed to apply. The fact that the simulated ground motion time histories show a wider variety of statistical properties than expected deserves further study. Probably, some possible explanations of this apparent weakness of the simulation approach proposed may be related to the simplicity of the ground motion model adopted, which does not account for the possible contribution of different wave trains or clearly differentiated multiple events.

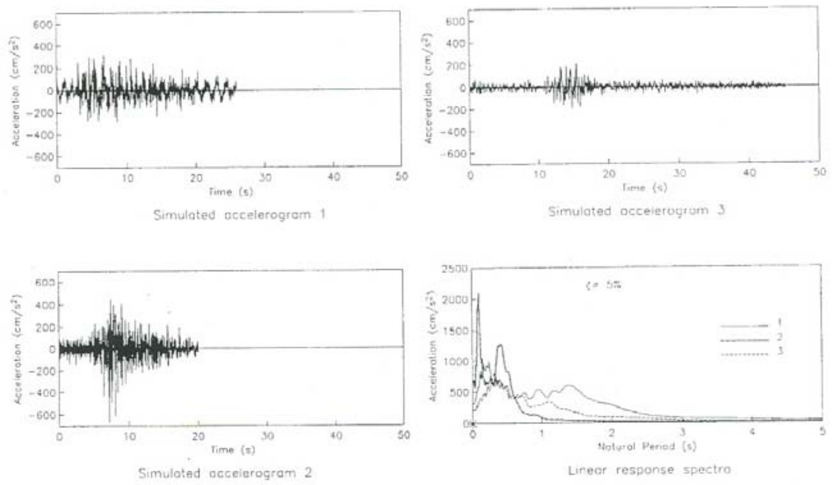

Figure 5a. Simulated accelerograms at the site and linear response spectra. Return interval of 200 years for spectral acceleration at T = 0.610 s, M_s = 8.1, R = 155 km

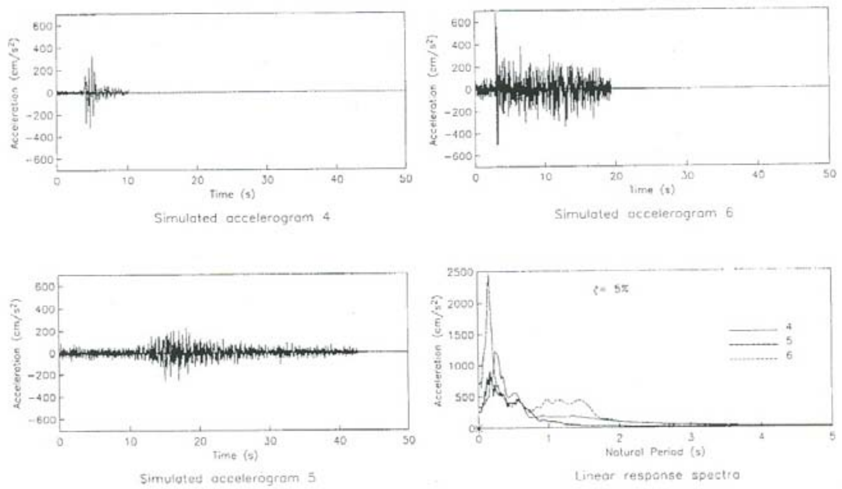

Figure 5b. Simulated accelerograms at the site and linear response spectra. Return interval of 200 years for spectral acceleration at T = 0.610 s, M_s = 8.1, R = 155 km

Another possible contributing factor is the way in which intensities are measured, where all the weight is given to the spectral ordinates associated with a specified vibration period. These concepts should be the object of research efforts in the near future.

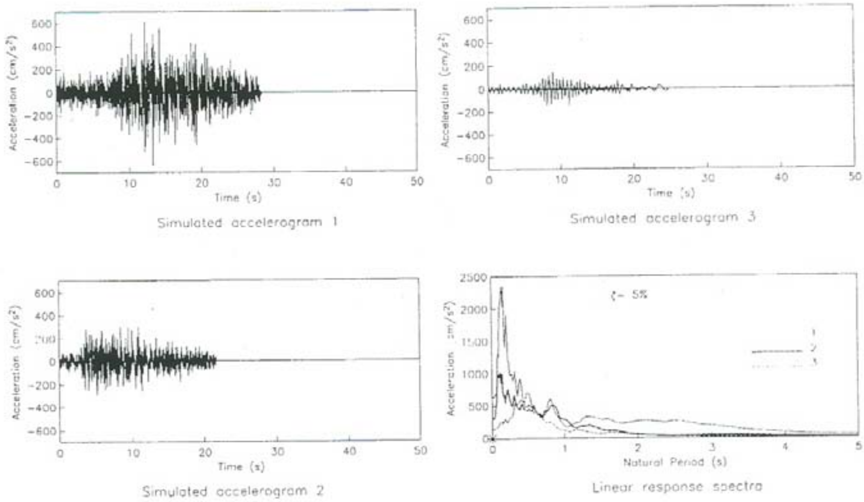

Figure 6a. Simulated accelerograms at the site and linear response spectra. Return interval of 200 years for spectral acceleration at T = 0.610 s. M_s = 6.9, R = 15 km

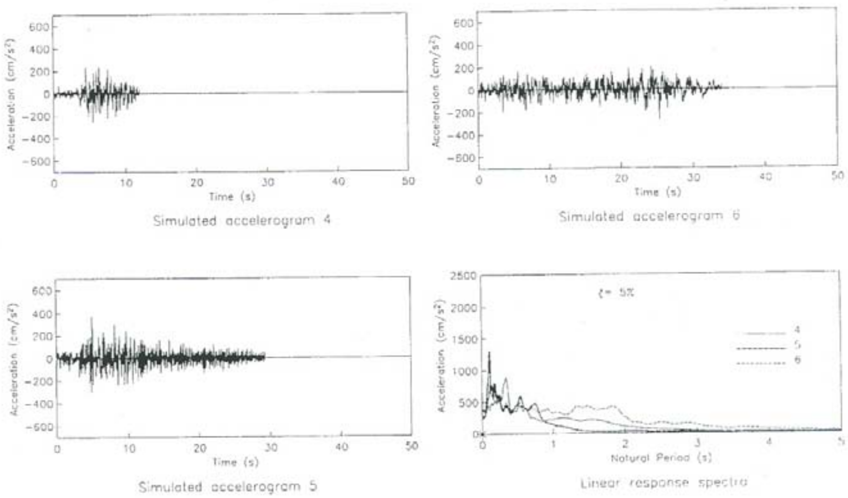

Figure 6b. Simulated accelerograms at the site and linear response spectra. Return interval of 200 years for spectral acceleration at T = 0.610 s, M_s = 6.9, R = 15 km

References

Alamilla,.L, Esteva, L., García-Pérez, J. and Díaz-López, O., 2001, Evolutionary properties of stochastic models of earthquake accelerograms: Their dependence on magnitude and distance, *J*. *Seismol*. 5, 1-21.

Bazzurro, P. and Cornell, C.A., 1998, *Spatial Disaggregation of Seismic Hazard*, Proc. 6th U.S. Nat. Conf. on Earthquake Engineering, Seattle, WA.

Cramer, C.H. and Petersen, M.D., 1996, Predominant seismic source distance and magnitude maps for Los Angeles, Orange and Ventura Counties, California, *Bull. Seism. Soc. Am*. **86**(5), 1645- 1649.

Kramer, S.L., 1996, *Geotechnical Earthquake Engineering*, Prentice Hall, Upper Saddle River, N.J.

McGuire, R.K., 1995, Probabilistic seismic hazard analysis and design earthquakes: Closing the loop, *Bull.*, *Seism. Soc. Am*. **85**(5), 1275-1284.

EVOLUTIONARY PROPERTIES OF STOCHASTIC MODELS OF EARTHQUAKE ACCELEROGRAMS: THEIR DEPENDENCE ON MAGNITUDE AND DISTANCE[1]

ABSTRACT

An approach to generate artificial earthquake accelerograms on hard soil sites is presented. Each time-history of accelerations is considered as a realization of a non-stationary gaussian stochastic process, with statistical parameters depending on magnitude and source-to-site distance. In order to link the values of these parameters for each ground motion record with the corresponding magnitude and source-to-site distance, semi-empirical functional relations called *generalized attenuation functions* are determined. The set of real ground-motion time histories used to obtain these functions correspond to shocks generated at different sources and recorded at different sites in the vicinity of the southern coast of Mexico. The results show significant dispersion in the parameters of the model adopted, which reflect that associated with the real earthquakes included in the sample employed. The problem of conditional simulation of artificial acceleration time histories for prescribed intensities is briefly presented, but its detailed study is left for a companion paper. The criteria and models proposed are applied to generate two families of artificial acceleration records for recurrence intervals of 100 and 200 years at a specific site located in the region under study. The results shown in this article correspond to acceleration time histories recorded on firm ground for earthquakes generated at the subduction zone that runs along the southern coast of Mexico, and cannot be generalized to cases of earthquakes generated at other sources or recorded at other types of local conditions. This means that the methods and functional forms presented here are applicable to these other cases, but the values of the parameters that characterize those functions may differ from those presented here.

Key words: artificial records, attenuation functions, earthquake accelerograms, seismic hazard, stochastic models.

Introduction

When dealing with the problem of establishing reliability-based earthquake-resistant design regulations for ordinary civil engineering structures, seismic excitations are usually specified in terms of *uniform-hazard* response spectra. However, for the study of some earthquake engineering problems, or for the design of special or very important structures, it may be necessary to account for other relevant characteristics of the ground motion time histories. Particularly significant among them is the effective duration or, more precisely, the evolution of the statistical properties (time-dependent variance and frequency content) of a stochastic process model of the ground acceleration during each event. These properties are sensitive to magnitude, source-to-site distance and local conditions.

[1] First Published in:
J. Alamilla, L. Esteva, J. García-Pérez & O. Días-López, Evolutionary Properties of stochastic models of earthquake accelerograms: Their dependance on magnitude and distance, *Journal of Seismology* **5:** 1-21, 2001

Efforts oriented to predicting the properties of strong-ground-motion records in terms of magnitude and distance have focused mainly on the development of attenuation functions of single-parameter (scalar) measures of earthquake intensities. They deal with variables such as peak ground accelerations and velocities (Esteva and Villaverde, 1973; Joyner and Boore, 1981, and many others), ordinates of response spectra (McGuire, 1974) and ordinates of Fourier amplitude spectra (Ordaz and Singh, 1992). The problems of predicting the effective duration (Boore and Joyner, 1984) and the evolution of the instantaneous variance and frequency content of the ground acceleration during each event, as functions of magnitude and distance, have received much less attention.

For the purpose of Monte Carlo simulation of samples of ground acceleration time histories, it is necessary to account for the evolution of the instantaneous statistical properties of ground motion records. One possible way of doing it consists in the use of small-magnitude records as Green's functions of large-magnitude events (Hartzell, 1978; Ordaz, Arboleda and Singh, 1995). According to this approach, a ground motion time history produced at a given site by a large magnitude earthquake may be considered as the superposition of a finite number of time histories resulting from smaller magnitude earthquakes (Green's functions). It is assumed that the large and the small events are all generated at the same source. The time origins of the smaller events are stochastically distributed along a time interval, the duration of which grows with the magnitude of the larger event. The probability distribution of the time origins of the smaller events is obtained after imposing a pre-established scaling condition relating the Fourier amplitude spectra of the elementary event and of the larger one.

One significant asset of the foregoing approach is that it implicity accounts for the specific local conditions at the recording site, as well as for the earth's crust properties along the source-to-site path. However, compared with the approach presented here for the simulation of strong ground motion accelerograms, the method based on the Green's function presents one disadvantage. The method is not directly applicable to cases with source-to-site distances different from those for which Green's functions are available or can be determined from recorded acceleration time histories.

The method for simulation of time histories of earthquake ground motion presented in this study starts with the adoption of a stochastic process model of the ground motion acceleration. The model is defined by a set of functions that describe the evolution of the amplitude and the frequency content of that variable during an earthquake. The forms of those functions and the corresponding parameters are determined on the basis of the information contained in available ground motion records. The mentioned parameters are made to depend on magnitude and source-to-site distance in accordance with empirical equations fitted to represent the statistical properties of samples of recorded acceleration time histories. As in the present study, the samples used for this purpose may inc1ude different combinations of sources and recording sites, but they must constitute homogeneous sets with respect to both the local conditions at those sites and the mechanical properties of the geological formations along the source-to-site paths.

In the following, an earthquake accelerogram is considered as a realization of a nonstationary gaussian stochastic process, with statistical parameters depending on magnitude and source-to-site distance. The model adopted is a gaussian stationary process, modulated in frequency and amplitude, similar to that proposed by Yeh and Wen (1989). The statistical parameters adopted here to describe the process differ from those used by them. These parameters were chosen because their forms of variation with magnitude and distance can be more easily understood than those corresponding to the parameters used by the mentioned authors. In both cases, the parameters serve to determine the amplitude and frequency modulation functions, as well as the spectral density of the basic stationary process before it is affected by those functions.

Our study has several objectives:

a) Developing *generalized attenuation functions* (*GAF*) of the stochastic models of earthquake accelerograms; that is, semi-empirical functional relations linking the statistical parameters of those models with the corresponding magnitudes and source-to-site distances. These parameters are considered as uncertainly defined for given values of the latter variables.
b) Obtaining mean-value vectors and covariance matrices of the joint probability distribution of the parameters mentioned above.
c) Proposing and applying a method for the simulation of earthquake accelerograms associated with given magnitudes and source-to-site distances. The method should account for the uncertainties that characterize the detailed acceleration time histories for given parameters of the ground motion stochastic process models as well as for those associated with the parameters themselves.
d) Evaluating the participation of the two types of uncertainty mentioned above on the global uncertainty associated with the ground motion intensity for given magnitude and focal distance.

Although the formulation presented here is of general applicability, the attenuation functions obtained and the parameters describing the uncertainty attached to their predictions are valid only for the region and type of soil conditions for which they were obtained. The empirical information used includes a collection of firm ground records from a number of large and moderate magnitude earthquakes generated in the vicinity of the southern coast of Mexico.

The method of conditional simulation presented at the end of this article is applicable only to the cases when the earthquake magnitude and source-to-site distance are deterministically known. In more general cases, these variables are described in a probabilistic form, in terms of a prescribed intensity at the site of interest and the probabilistic description of the activity of the relevant seismic sources. These cases are studied in a companion paper (Alamilla et al., 2000).

Ground motion model

Following Yeh and Wen (1989), an earthquake accelerogram is considered as a realization of a gaussian process modulated in amplitude and frequency:

$$\xi(t) = I(t)\,\zeta(\varphi(t)) \tag{1}$$

In this equation, $\xi(t)$ is the ground acceleration as a function of time, t; $I(t)$ is a deterministic amplitude-modulation function; $\varphi(t)$ is a transformation of the scale of time, the function of which is to modulate frequencies, and $\zeta(\varphi(t))$ is a unit variance gaussian filtered white noise, stationary with respect to φ. Therefore, $I^2(t)$ is equal to the instantaneous variance of $\xi^2(t)$. The transformation $\varphi(t)$ serves to represent the variation of the dominant frequency of the acceleration during the earthquake, while the form of the instantaneous spectral density of that variable is assumed to remain constant. In their presentation of the model, Yeh and Wen consider the possibility of adopting a more general formulation, such that the form of the spectral density is also considered to vary during the earthquake. For this purpose, they state that $\xi(t)$ can be expressed as the sum of several products similar to that appearing in the second member of Equation 1; each product corresponds to a given frequency band of the Fourier amplitude spectrum of the accelerogram. However, in their study the mentioned authors work exclusively with the simple form given by Equation l. The same form was adopted here, having in mind the objective of obtaining generalized intensity attenuation expressions to estimate the parameters of the functions in the second member of that equation. Using the more general model envisaged by Yeh and Wen would have been impractical. Another argument in favor of working with Equation l is that it represents an improvement over the stochastic ground motion models more often used for the simulation of ground motion records in practical engineering problems.

On the basis of several available records of strong ground motion acceleration time histories, Yeh and Wen adopted for $I^2(t)$ an expression of the form $At^B\,(D+t^E)^{-1}\,e^{-Ct}$. For the purpose of determining $\varphi\,(t)$, they define a function $\mu_0\,(t)$, equal to the expected value of the total number of zero-crossings of the acceleration time history during time t. From this, it is easy to show that $\varphi\,(t)$ is equal to the ratio $\mu_0\,(1)\,/\,\mu'_0\,(t_0)$, where the prime (') denotes the time derivative and t_0 is the instant at which a reference spectral density is determined for the nonstationary stochastic process that describes the acceleration time history. A polinomial of the form $r_1t\,+r_2t^2+r_3t^3$ was used to represent $\mu_0(t)$.

In the functions defined above, A, B, C, D, E, r_1, r_2 and r_3 are constant parameters, and t is time. The mentioned authors obtained the values of these parameters that lead to the best representations of the recorded time histories. The parameters of the intensity-envelope function $I^2(t)$ were obtained by least-squares fitting to the recorded time histories, while the parameters of the frequency-modulating function were determined from the condition of minimizing the squared differences between the rates of zero-crossings of the actual time histories and those estimated on the basis of function $\mu_0(t)$.

An alternative form for $\mu_0(t)$ is given by the following equation:

$$\mu_0(t) = p\left[2-\exp(-qt)-\exp(-rt^3)\right] \tag{2}$$

Here, p, q and r are positive parameters to be determined for each record in the set of observations. This form offers some advantages over that proposed by Yeh and Wen. According to the former, $\mu_0\,(t)$ tends monotonically to a constant value when t tends to infinity; its time derivative is equal to pq for t = 0, and the two remaining free parameters permit a reasonable fit of the analytical curve to the observations.

In order to apply the model presented in the preceding paragraph to generate simulated records of ground acceleration for prescribed values of magnitude (M) and source-to-site distance (R), it is necessary to obtain functional relations linking these variables with the parameters that determine functions $I\,(t)$ and $\varphi\,(t)$. In the study presented here, it was decided to represent these functions for given values of M and R with forms and sets of parameters that could permit having a better control on the characteristics of the ground motion more directly related to the expected responses of engineering structures. Those parameters should have some physical meaning and, as far as possible, show the smallest probabilistic correlation with each other. This criterion was applied for the adoption of the functional forms and parameters described in the following, instead of those used by Yeh and Wen.

For the purpose of estimating $I(t)$, use is made in the following of a function $W(t)$, which is the expected value of the integral of the square of the earthquake acceleration from the instant the ground motion started until instant t:

$$W(t) = \int_o^t E\left[\xi^2(\tau)\right] \mathrm{d}\tau \tag{3}$$

This function is known as the *cumulative energy function*. Its time derivative is equal to the instantaneous variance of $\xi(t)$, and therefore to $I^2(t)$. This means that $I(t)$ is equal to the square root of the time derivative of $W(t)$.

From the standpoint of their relevance to the estimation of extreme values of structural responses, two significant parameters of the ground motion are its effective duration (when a significant part of $W(t)$ is accumulated) and the average value of $I^2(t)$ during that time interval. Therefore, it was decided to control the function $I(t)$ by expressing it in terms of the variables Δ and Z^2, which are respectively equal to the length of the time interval during which $W(t)$ increases from 25 percent to 75 percent of its value W_1 at the end of the ground motion and the average value of the variance of $\xi(t)$ during that interval. Thus,

$$Z^2 = \frac{W_1}{2\Delta} \tag{4}$$

$W(t)$ was in turn expressed in segmental form in terms of W_1, defined above, and of the times t_a, t_b, t_c and t_d required for $W(t)$ to reach values equal to 0.025, 0.25, 0.75 and 0.975 of W_0, respectively. The meaning of these parameters is illustrated in Figure la where, for clarity, they are designated as $t_{.025}$, $t_{.250}$, $t_{.750}$ and $t_{.975}$, respectively. Once these values are determined, $W(t)$ is represented by five segments:

$$W(t) = b_1 t \qquad \text{for} \quad 0 < t \le t_a \tag{5a}$$

$$= b_1 t + b_2 (t - t_a)^n \qquad t_a < t \le t_b \tag{5b}$$

$$= b_3 t + b_4 t + b_5 t^2 \qquad t_b < t \le t_c \tag{5c}$$

$$= b_6 t + b_7 t + b_8 t^2 \qquad t_c < t \le t_d \tag{5d}$$

$$= W_1 (1 - \mathrm{e}^{-\epsilon t}) \qquad t_d < t \tag{5e}$$

Here, b_1–b_8, n and ϵ are parameters to be estimated on the basis of continuity conditions for $W(t)$ and its time derivative at the instants $t_a - t_d$.

For the purpose of making a statistical description of a ground motion record, its spectral density function $S(\omega, t_0)$ at a reference instant t_0 is required, in addition to the amplitude and frequency modulation functions. The form adopted here for the former is that proposed by Clough and Penzien (1975):

$$S(\omega, t_0) = S_0 \left[\frac{\omega_g^4 + 4\zeta_g^2 \omega_g^2 \omega^2}{(\omega_g^2 - \omega^2)^2 + 4\zeta_g^2 \omega_g^2 \omega^2} \right] \cdot \left[\frac{\omega^4}{(\omega_f^2 - \omega^2)^2 + 4\zeta_f^2 \omega_g^2 \omega^2} \right] \tag{6}$$

In this equation, ζ_g and ω_g are the parameters of Kanai-Tajimi's filler (Kanai, 1957; Tajimi, 1960), representing the energy-content in the intermediate and high frequency ranges, and ζ_f, ω_f the parameters introduced by Clough and Penzien to approximate the energy distribution in the low frequency range. S_0 is a normalizing constant such that the variance of $\zeta(\varphi(t))$ is equal to unity. Its value can be calculated as follows:

$$S_0 = \frac{1}{\pi} \frac{2\zeta_g \zeta_f \left[(\omega_g^2 - \omega_f^2)^2 + \omega_g^2 \omega_f^2 (\zeta_g^2 + \zeta_f^2) + 4\zeta_g \zeta_f \omega_g \omega_f (\omega_g^2 + \omega_f^2)\right]}{\omega_g^4 (\zeta_g \omega_f + \zeta_f \omega_g) + 4\zeta_g^2 \omega_g^2 \left[\zeta_g \omega_f^3 + \zeta_f \omega_g^3 + 4\zeta_g \zeta_f \omega_g \omega_f (\zeta_g \omega_f + \zeta_f \omega_g)\right]} \tag{7}$$

For the purpose of establishing generalized attenuation functions, that is, expressions applicable to the estimation of the parameters of nonstationary stochastic models of ground motion records in terms of magnitude and distance (*M* and *R*), the following global parameters are adopted:

a) To represent the amplitude-modulation function:

$$\Delta = t_c - t_b \tag{8}$$

$$\alpha = (t_b - t_a)/\Delta \tag{9}$$

$$\beta = (t_d - t_c)/\Delta \tag{10}$$

The expressions proposed here are concerned with the ground motion for values of t smaller than t_d. The last value corresponds to the instant when 97.5 percent of the total energy has been liberated, and it is considered that the rest of the ground motion does not have a significant effect on the structural response.

b) For the expected zero-crossing function, the form given by Equation 2 was considered adequate. However, for the purpose of estimating its parameters, it was preferred to use as control variables those given by Equations 11-15. They represent the mean rates of zero crossings of the ground acceleration during successive time intervals (Figure lb). The main reason for going through this intermediate step arises from the previously mentioned convenience of working with parameters that have a clear physical meaning. No attention was paid in this case to the convenience of adopting parameters that show the smallest possible correlation with each other.

$$\eta_a = \mu_a / t_a \tag{11}$$

$$\eta_b = (\mu_b - \mu_a)/(t_b - t_a) \tag{12}$$

$$\eta_0 = (\mu_0 - \mu_b)/(t_0 - t_b) \tag{13}$$

$$\eta_c = (\mu_c - \mu_0)/(t_c - t_0) \tag{14}$$

$$\eta_d = (\mu_d - \mu_c)/(t_d - t_c) \tag{15}$$

In these equations, $t_0 = (t_c + t_b)/2$, μ_i is the expected number of zero-crossings accumulated during the interval $(0, t_i)$, and t_0 corresponds to an accumulated energy approximately equal to 50 percent of the total in the accelerogram. As was done in connection with Figure 1a, subscripts *a*, *b*, *c* and *d* are replaced in Figures 1b and 7 with the fractions of the total energy to which they correspond: .025, .250, .750 and .975, respectively.

The reference spectral density (Equation 6) at instant t_0 is determined by parameters ω_g, ζ_g, ω_f and ζ_f defined above. S_0 is given by Equation 7, which results from the condition of unit variance of $\zeta(\varphi(t))$.

Empirical information

The data-base used for this study consists of 112 accelerograms produced by six earthquakes generated at the subduction zone adjacent to the southern coast of Mexico. The magnitudes ranged between 6.6 and 8.1, the hypocenter longitudes between 98.88° W and 103.06° W, and the source-to-site (hypocentral) distances between 10 and 400 km, approximately (see Table 1 and Figure 2).

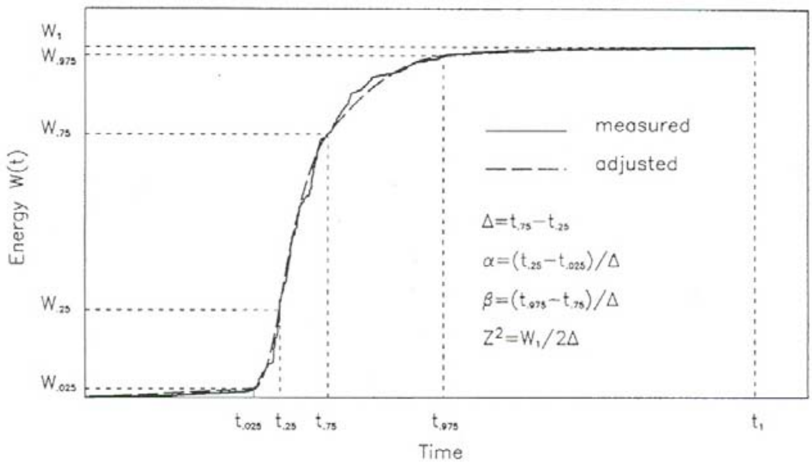

Figure la. Energy function of ground-motion accelerogram

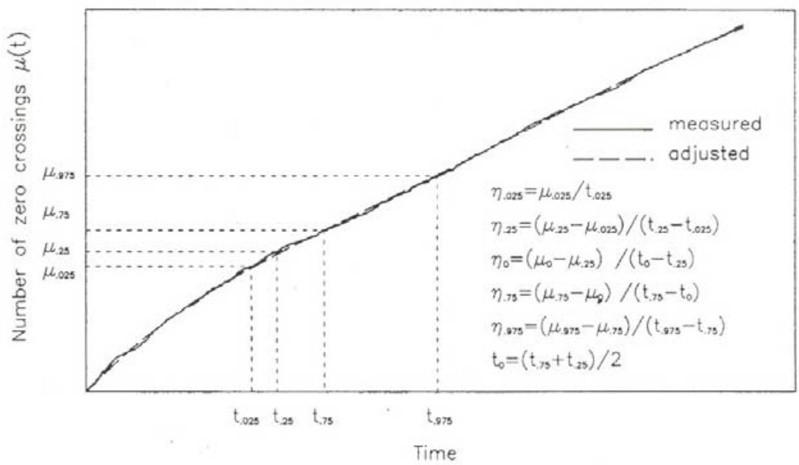

Figure 1b. Number of zero crossings function of ground-motion accelerogram

TABLE 1

Earthquakes included in the analysis

	Magnitude (M)	Latitude (°)	Longitude (°)W
October 25, 1981	7.3	17.880	102.150
September 19, 1985	8.1	18.081	102.942
September 21, 1985	7.6	18.021	101.479
April 30, 1986	7.0	18.024	103.057
October 24, 1993	6.6	16.540	98.980
September 14, 1995	7.2	16.310	98.880

Generalized attenuation functions

Figure 3 shows values of the parameters Δ, α and β, that determine the shape of the amplitude modulation function, plotted in terms of magnitudes for several ranges of values of the source-to-site distance. These parameters are also shown in Figure 4, but now in terms of the source-to-site distances for several ranges of the values of the magnitudes. In the middle part of Figures 3 and 4 it can be observed that α does not vary systematically with either M and R; therefore, it will be taken as a constant, as given in Equation 16, for consistency with the forms adopted to represent the variation of other parameters:[2]

$$\ln \alpha = c \tag{16}$$

Figures 3 and 4 also show that Δ and β vary systematically only with M. The following forms are used to represent them:

$$\ln \Delta = c + bM \tag{17}$$

$$\ln \beta = c + bM \tag{18}$$

Z varies with M and R as shown in Figures 5 and 6. As it should be expected, it grows with M and decreases with R. The curves shown have the following form:

$$\ln Z = \ln k + aM - b\ln(R + R_0) \tag{19}$$

Here, $R_0 = ce^{dM}$; k, a, b, c, and d are constants whose values were estimated in accordance with a nonlinear minimum squares procedure proposed by Bard (1974).

The variation of parameters η_a, η_b, η_0, η_c, and η_d, which characterize the mean numbers of zero crossings, is depicted in Figure 7. In agreement with predictions based on geophysical concepts, these parameters decrease with R. Because no clear systematic variation with M could be identified from the sample, the following relations were adopted:

$$\ln \eta_j = a + bR, \qquad j = a, b, 0, c, d \tag{20}$$

Figures 8 and 9 show the variation of the parameters of the Clough-Penzien spectral density function: ω_g, ζ_g, ω_f and ζ_f. Again as expected, ω_g decreases when either M or R grows. ω_f varies with M in a more pronounced fashion than ω_g, but its variation with R is very slow. ζ_f and ζ_g do not show any variation with either M or R. The forms adopted to estimate these parameters are the following:

$$\ln \omega_g = a + bM + cR \tag{21}$$

$$\ln \zeta_g = c \tag{22}$$

$$\ln \omega_f = a + bM + cR \tag{23}$$

$$\ln \zeta_f = c \tag{24}$$

Best estimates of the coefficients appearing in Equations 16-24 are presented in Table 2. The covariance matrix between the (uncertain) values of those coefficients can

2 For simplicity of notation, symbols *a-c* are used, with different meanings, to represent coefficients in the functional relations between *M*, *R* and different parameters of the stochastic models of ground motion records.

be constructed using the information presented in Tables 3 and 4. The former of these deals with parameters α, Δ, β, ζ of the amplitude modulation function, which appeared to be stochastically independent from the parameters of the reference spectral density (ω_g, ζ_g, ω_f, ζ_f), and those of the frequency modulation function (η_a, η_b, η_0, η_c, η_d), which are considered in Table 4. In each of these tables, the second column shows the values of the variances of the variables listed on the first column, while the other columns show correlation coefficients between pairs of parameters.

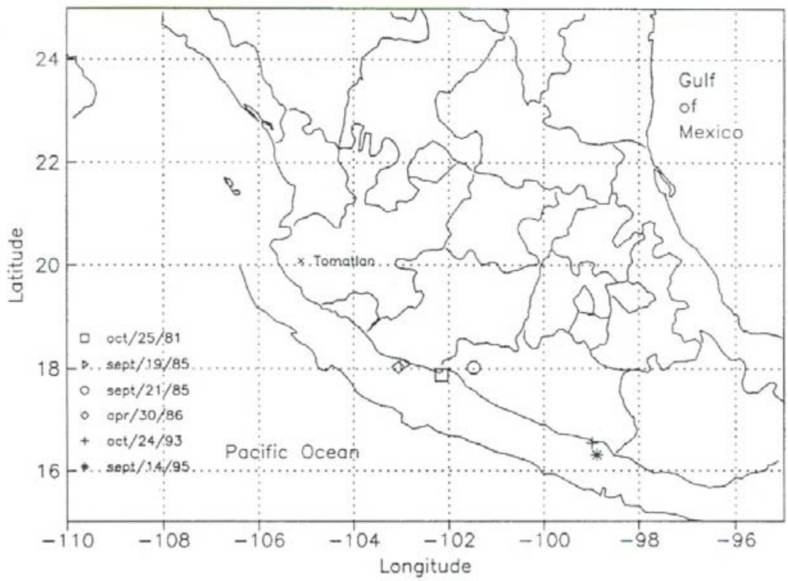

Figure 2. Epicenters of earthquakes included in sample studied

TABLE 2

Best estimates of GAF parameters

Parameter	a	b	c	d	k
In α			$-2.71\cdot10^{-1}$		
In Δ		$3.43\cdot10^{-1}$	$-8.85\cdot10^{-1}$		
In β		$-3.05\cdot10^{-1}$	$2.93\cdot10$		
In Z	$3.43\cdot10^{1}$	$3.15\cdot10^{1}$	$1.08\cdot10$	$1.10\cdot10$	$6.65\cdot10^{3}$
In $\eta_{.025}$	$2.85\cdot10$	$-1.63\cdot10^{-3}$			
In $\eta_{.25}$	$2.54\cdot10$	$-1.43\cdot10^{-3}$			
In η_0	$2.54\cdot10$	$-2.05\cdot10^{-3}$			
In $\eta_{.75}$	$2.48\cdot10$	$-1.92\cdot10^{-3}$			
In $\eta_{.975}$	$2.39\cdot10$	$-1.70\cdot10^{-3}$			
In ω_g	$3.70\cdot10$	$-3.92\cdot10^{-3}$	$-3.21\cdot10^{-3}$		
In ζ_g			$-7.64\cdot10^{-1}$		
In ω_f	$4.65\cdot10$	$-3.99\cdot10^{-1}$	$-8.83\cdot10^{-5}$		
In ζ_f			$-1.45\cdot10$		

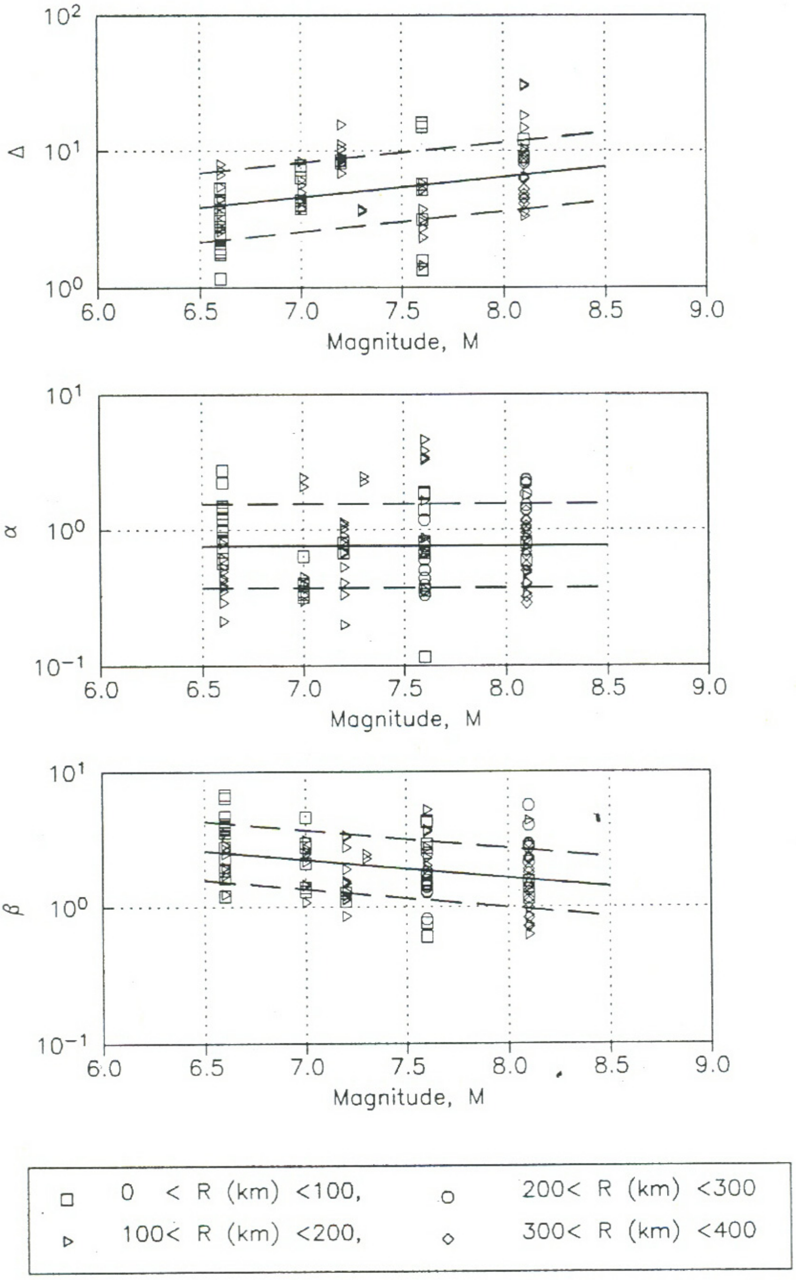

Figure 3. Parameters Δ, α and β vs *magnitude, M. Full and dashed lines represent the mean and the mean $\pm$ one standard deviation, respectively*

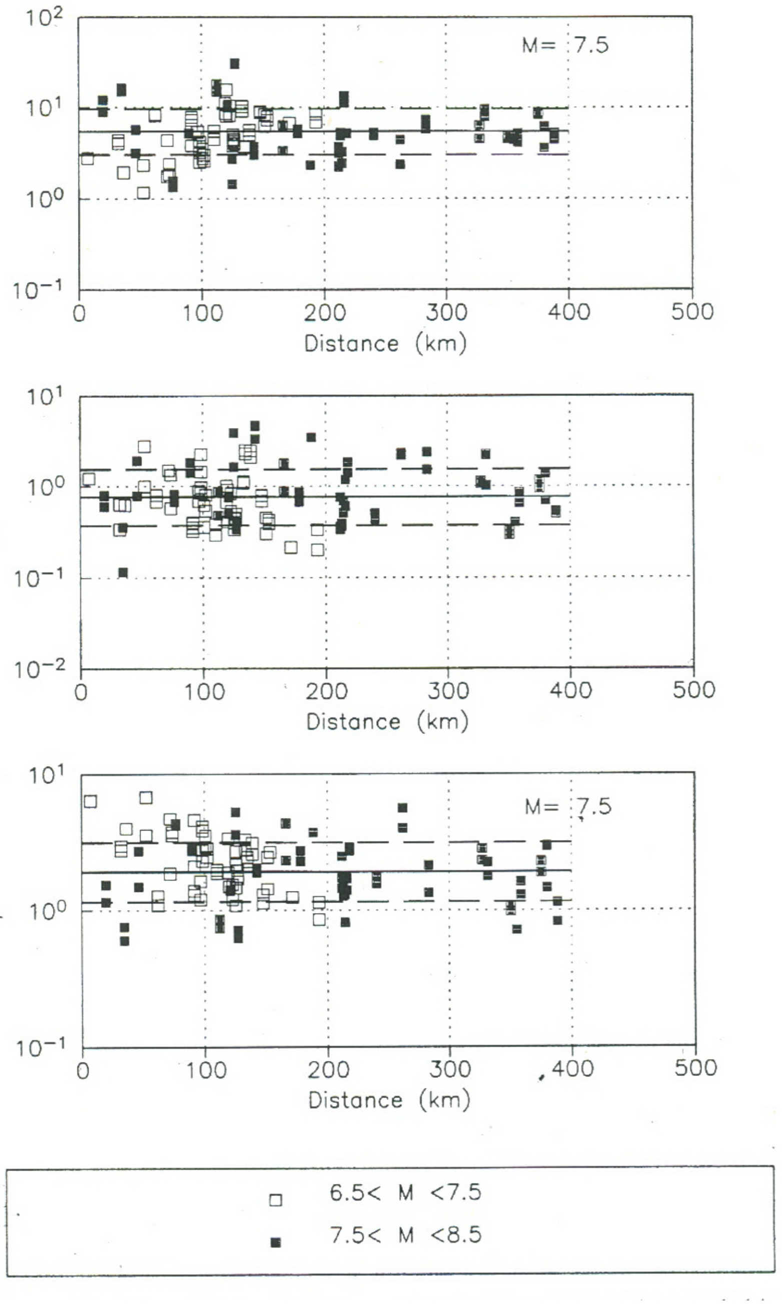

Figure 4. Parameters Δ, α and β vs *distance, R. Full and dashed lines represent the mean and the mean $\pm$ one standard deviation, respectively, for M = 7.5*

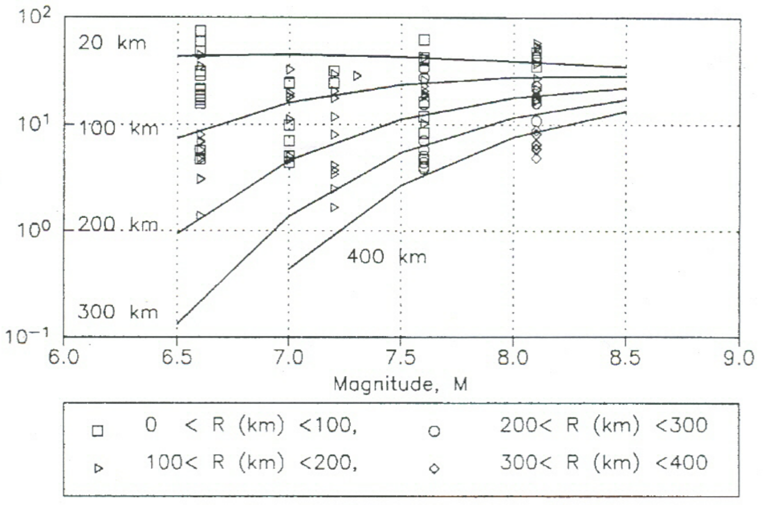

Figure 5. Parameter Z vs *magnitude, M. Full lines show mean values of Z for several distances, R*

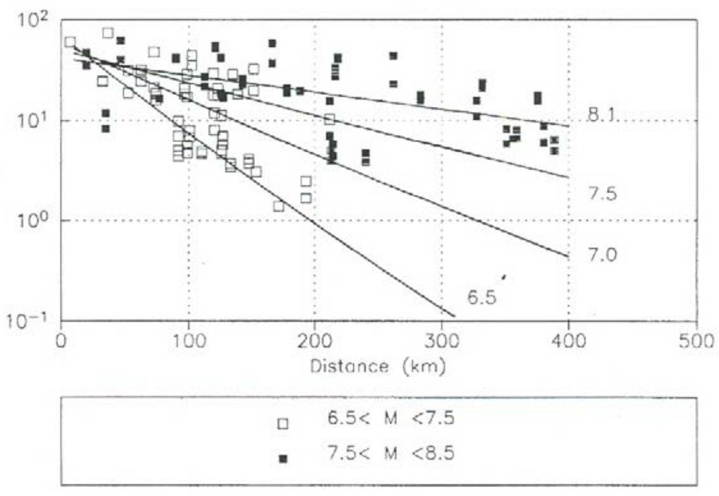

Figure 6. Parameter Z vs *distance, R. Full lines show mean values of Z for several magnitudes, M*

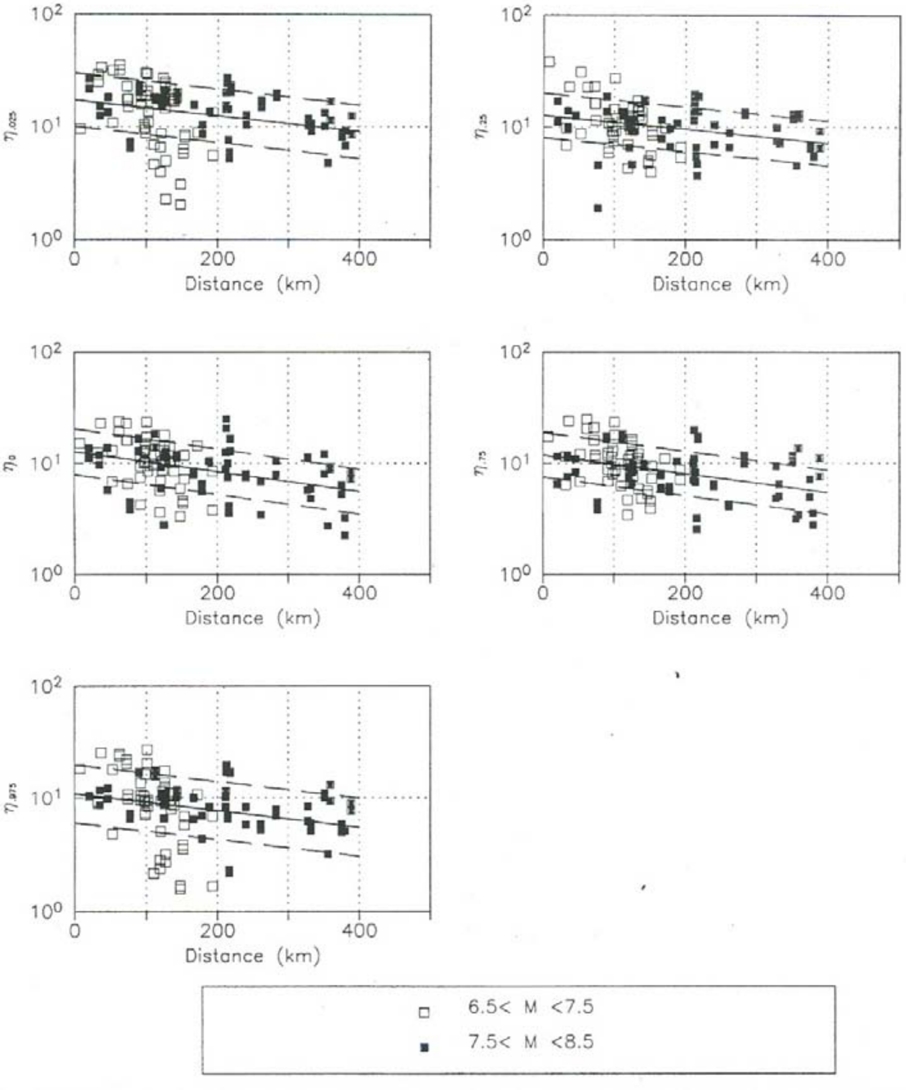

Figure 7. Parameters $\eta_{.025}$, $\eta_{.25}$, η_0, $\eta_{.75}$ and $\eta_{.975}$ vs *distance, R. Full and dashed lines represent the mean and the mean and the mean $\pm$ one standard deviation, respectively*

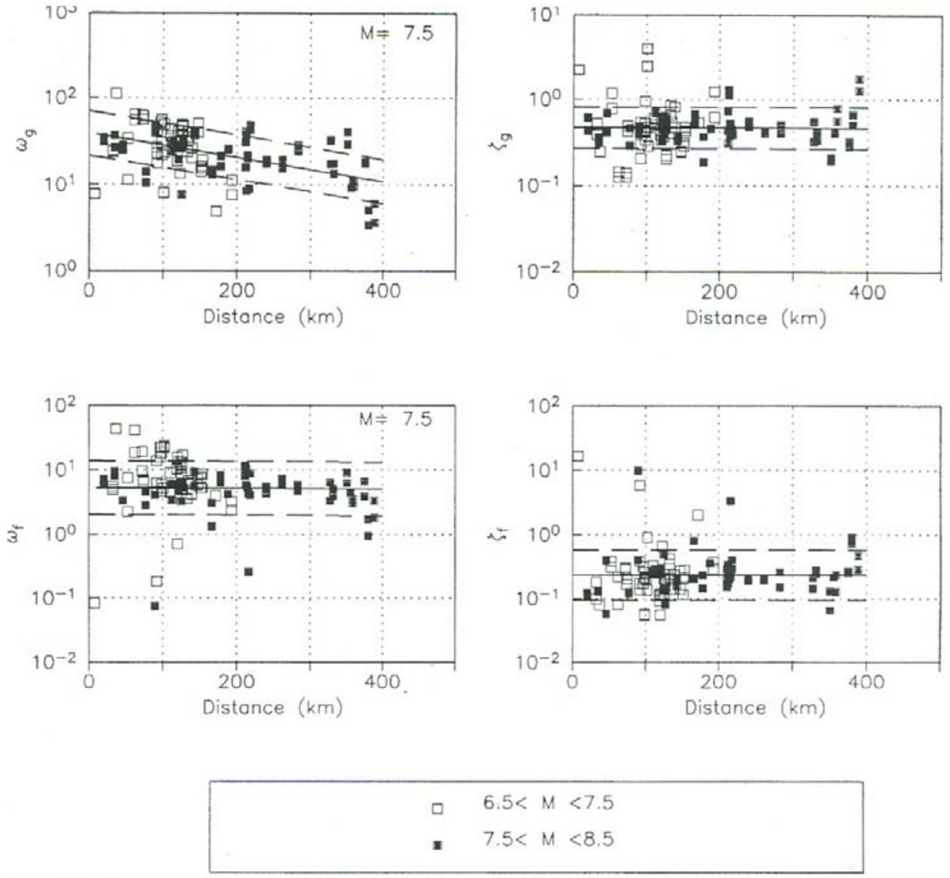

Figure 8. Parameters ω_g, ζ_g, ω_f *and* ζ_f vs *distance, R. Full and dashed lines represent the mean and the mean and the mean* $\pm$ *one standard deviation, respectively, for M = 7.5*

TABLE 3

Covariance properties of parameters of amplitude modulation functions

Parameter	Variance	Correlation coeficients			
		In α	In Δ	In β	1n Z
ln α	0.504	1.000	-0.401	0.624	0.503
ln Δ	0.337		1.000	-0.643	-0.230
ln β	0.251			1.000	0.440
ln Z	0.484				1.000

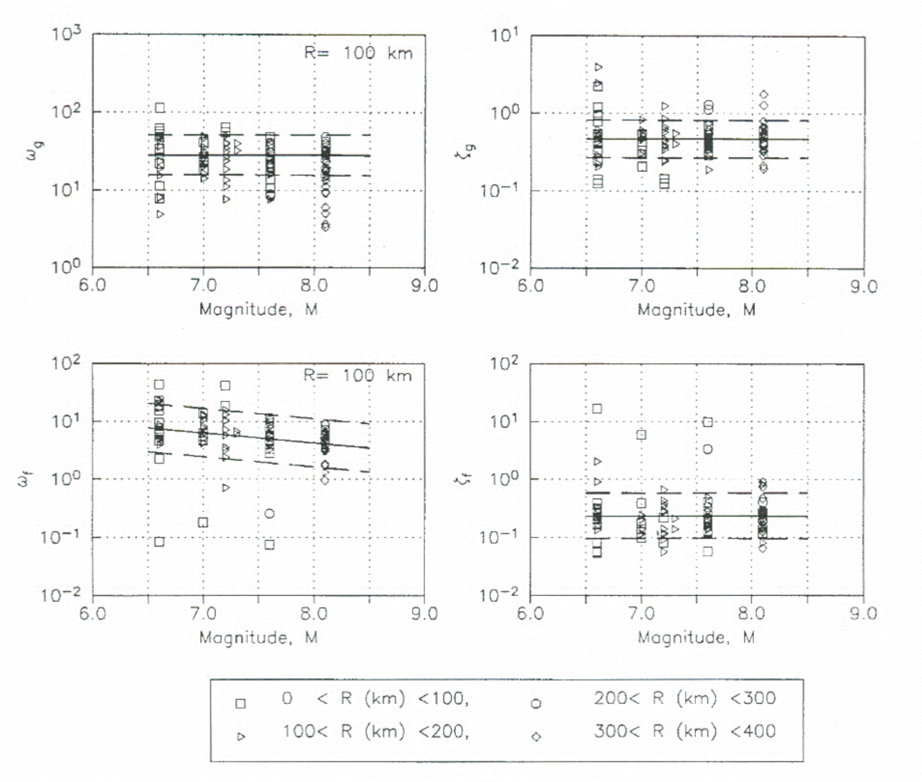

Figure 9. Parameters ω_g, ζ_g, ω_f and ζ_f vs *magnitude, M. Full and dashed lines represent the mean and the mean and the mean $\pm$one standard deviation, respectively, for R = 100 km*

Analysis of the results

The influence of *M* and *R* on the effective duration and, more precisely, on the amplitude modulation function, can be easily appreciated in Figures 3 and 4. According to them, the duration of the time segment Δ, which accounts for the growth of the accumulated energy from 25 to 75 percent of the total, increases with the magnitude but is not sensitive to the distance. It can also be seen that α is insensitive to both variables. This means that the ratios of the average rates of energy growth during intervals (t_a, t_b) and (t_b, t_c) are not influenced by either *M* or *R*. However, the quotient of the lengths of intervals (t_c, t_d) and (t_b, t_c), decreases with the magnitude, but is not sensitive to the distance. This means that the decay time of the ground motion intensity after it reaches its maximum is faster for large magnitude events. However, the mentioned figures and Table 3 show that these results are characterized by significant uncertainties. The negative correlation shown in Table 3 between ln α and ln Δ indicates that larger lengths of the initial intervals in the process of energy accumulation tend to correspond to smaller values of the time necessary for the energy to grow from 25 to 75 percent. The negative correlation coefficient between ln Δ and ln *Z* reflects the fact that for a given value of the energy content in the accelerogram, a longer duration of the record tends to correspond to smaller values of its instantaneous amplitudes.

TABLE 4

Correlation between parameters of frequency modulation and spectral density functions

Parameter	Variance	Correlation coefficients								
		$\ln \eta_{.025}$	$\ln \eta_{.25}$	$\ln \eta_0$	$\ln \eta_{.75}$	$\ln \eta_{.975}$	$\ln \omega_g$	$\ln \zeta_g$	$\ln \omega_f$	$\ln \zeta_f$
$\ln \eta_{.025}$	0.301	1.000	0.589	0.547	0.587	0.828	0.100	0.206	0.112	0.004
$\ln \eta_{.25}$	0.211		1.000	0.780	0.738	0.693	0.355	0.173	0.104	0.054
$\ln \eta_0$	0.219			1.000	0.790	0.720	0.386	0.151	0.164	0.020
$\ln \eta_{.75}$	0.206				1.000	0.734	0.352	0.132	0.131	0.081
$\ln \eta_{.975}$	0.347					1.000	0.139	0.182	0.103	0.061
$\ln \omega_g$	0.347						1.000	-0.583	0.523	-0.418
$\ln \zeta_g$	0.305							1.000	-0.414	0.284
$\ln \omega_f$	0.920								1.000	-0.732
$\ln \zeta_f$	0.815									1.000

Figure 5 shows that the instantaneous amplitudes are not very sensitive to M for small values of R. This can be explained as a consequence of the finite source dimensions, taken into account by means of the term R_0 in Equation 19. The small decreasing trend of Z with respect to M that can be appreciated in the figure for R = 20 km can probably reflect the statistical variability of the observations rather than a phenomenological property, and should not be considered when making seismic hazard estimates for engineering applications. The influence of the finite source dimensions is also evident in the significant differences in the rates of decrease of Z with respect to R that appear in Figure 6.

The parameters η_a, η_b, η_0, η_c and η_d defined by Equations 11-15 represent the rates of zero crossings during successive intervals of the ground motion time history. All of them decrease with R, irrespective of M, as shown in Figure 7. Their rates of decrease are very similar, according to the same figure and with the values of a and b given in Table 2.

Of the parameters of the spectral density function at the reference instant t_0, only the dominant frequency ω_g shows a clear influence of the source-to-site distance. It varies from approximately 6 cycles per second at small values of R to 1.6 for R = 400 km. The other parameters, ω_f, ζ_g and ζ_f, do not show any systematic trend of variation with R, except that their statistical dispersion is in all cases significantly larger for small values of this variable. No systematic influence of M on ω_g could be identified.

Conditional simulation of artificial accelerograms

As mentioned above, design earthquakes are often specified in terms of uniform-hazard response spectra, which are envelopes of the spectral ordinates that correspond to the same return interval, irrespective of the natural vibration periods of the system considered. In other cases, the intensity of each earthquake is measured by the maximum ordinate of the response spectrum for a specified damping ratio, regardless of the value of the period where this maximum occurs. The design earthquake is then defined by the value of the intensity associated with a given return interval. Still, in other cases, seismic excitations are specified as the result of the most unfavorable combinations of magnitude and source-to-site distance that may *probably* or *possibly* affect the sites of interest. In these three groups of cases, it may be necessary to simulate samples of accelerograms with intensities, frequency contents and effective duration (more precisely: evolutionary properties) consistent with the specifications.

When design earthquakes are directly specified in terms of a combination of *M* and *R*, it is customary to state that the intensity adopted for design (in general, the ordinate of the response spectrum for the fundamental period of vibration of the structure of interest) should be taken as that associated with a given probability of being exceeded, conditional to the assumed values of *M* and *R*. Often, this probability is measured in terms of a number of standard deviations of the random intensity above its conditional expected value.

Regardless of the parameter adopted to specify the design intensity, once its value is chosen, *M* and *R* remain as uncertain variables, with their joint probability density function being conditioned to that value. The combination of *M* and *R* to be adopted to simulate accelerograms of the specified intensity can be handled either as uncertain, defined in terms of their conditional distribution, or as deterministic, expressed by the most likely combination of their values, as proposed by McGuire (1995).

In any case, the simulation of accelerograms for given values of *M* and *R* is done in two steps. In the first step, the parameters of the reference spectral density and of the amplitude and frequency modulation functions are generated; in the second, individual records are obtained, starting from those parameters. At the end, the intensity of each simulated record will differ from its target value, thus requiring the introduction of a scaling factor $\in$, which accounts for the random deviations of intensities with respect to the expected values for given parameters of the stochastic model of the ground motion.

In this article, an illustration is presented of the conditional simulation of ground acceleration time histories for the case when *M* and *R* are deterministically known. As mentioned above, the cases when these variables are probabilistically described on the basis of a target ground motion intensity and the probabilistic models of the activity of the relevant seismic sources are treated in detail in a companion paper by the same authors (Alamilla et al., 2000).

Illustrative example

The criteria and models presented above were applied to the Monte Carlo simulation of sets of accelerograms to be used in dynamic response studies oriented to assessing the seismic safety levels of several dams near the southern coast of Mexico (Taboada et al., 1997; Alamilla et al., 1997). The intensities of the artificial records to be generated were taken as the va1ues of the ordinates of the acceleration spectra for the calculated fundamental periods of the dams to be evaluated and a damping ratio equal to 0.05 of critical. In each case, two intensity values were adopted for the simulations, corresponding to return intervals of 100 and 200 years, respectively. The site of Tomatlán (20° N, 105° W, approximately), near the western end of the southern coast of Mexico was selected among the cases studied to illustrate the steps in the conditional simulation procedure and to show the types of results and their variability.

A fundamental period of 0.610 s was estimated for the structure considered. For this period and a damping ratio of 0.05, the spectra1 accelerations corresponding to return intervals of 100 and 200 years reported in previous seismic hazard studies were equal to 400 and 623 cm/s^2, respectively. Due to lack of conditional probability density functions of *M* and *R*, or of their most likely values for these intensities, it was decided to take *R* as the shortest distance from the site to the seismic source represented by the interface between the continental and the subducting plates. For this purpose, use was made of information provided by Pardo (1993) about local seismotectonic features. The value of R obtained in this manner was assumed for the estimation of M, assuming the intensity Y varied in accordance with an attenuation function having the same form as the second member of Equation 19. For this particular case, the intensity Y is the ordinate of the linear pseudo-acceleration response spectrum for 5 percent damping in cm/s^2, a = 1.218, b = 2.069, k = 1499 and R_0 = 221.6 km. The resu1ting value of R was 10 km; M was equal to 8.2 and 8.5 for the 100 and 200 years return intervals, respectively.

Five accelerograms were simulated for each value of the specified intensity Y. For each of the latter, a set of values of the parameters of functions $W(t)$, $\mu(t)$ and $S(\omega, t_0)$ was randomly generated taking the variables listed in Tab1es 3 and 4 as log-normally distributed, and considering the first and second moments of their distributions as given on those tables. The resulting set of parameters served in turn for the generation of an artificial accelerogram. Thus, uncertainties about both the statistical parameters of the underlying stochastic process and the detailed characteristics of each time history, given the former, were accounted for. Finally, for each simulated record a scaling factor, $\in$, was obtained as the ratio of the target intensity to the value generated by Monte Carlo simulation. This factor was applied to the simulated accelerogram before integrating it to the sample of records of a given intensity.

The simulated records, affected by scaling factors ϵ, are shown in Figures 10-13, together with their corresponding response spectra. The differences observed between the general patterns of evolution of the amplitude and frequency of the accelerations for the different time histories are much more pronounced than those usually found in samples of records simulated by methods based on previously established amplitude and frequency functions. These large differences reflect the significant uncertainties associated with the parameters of the non-stationary stochastic process model of the ground acceleration for given values of magnitude and focal distance.

Concluding remarks

Tables 3 and 4, and Figures 3-9, show the significant dispersion that characterizes the statistical parameters of the model adopted to represent strong motion accelerograms as realizations of gaussian stochastic processes with evolutionary spectral density. This dispersion reflects that associated with the characteristics of the real earthquake records included in the sample used in this study. However, due to the restrictions imposed on the amplitude and frequency modulation functions used here, the simulated records are not capable of representing more general possibilities of practical interest. Such are, for instance, the use of different modulation functions for different frequency bands or the occurrence of multiple fault-rupture processes with time delays of the order of tens of seconds.

The collection of real records included in the study are deemed to constitute a homogeneous set of records on firm ground conditions, and seismic sources associated with the subduction zone lying along the southern coast of Mexico. Funds for this study were obtained from a project, mentioned above, oriented to the development of postulated ground motion records for the assessment of the seismic safety of several dams existing near the southern coast of Mexico. Accordingly, all the accelerograms included in the set were recorded on firm ground sites in that region. Thus, records that might be affected by the firm ground amplification characteristics of the trans-Mexican volcanic

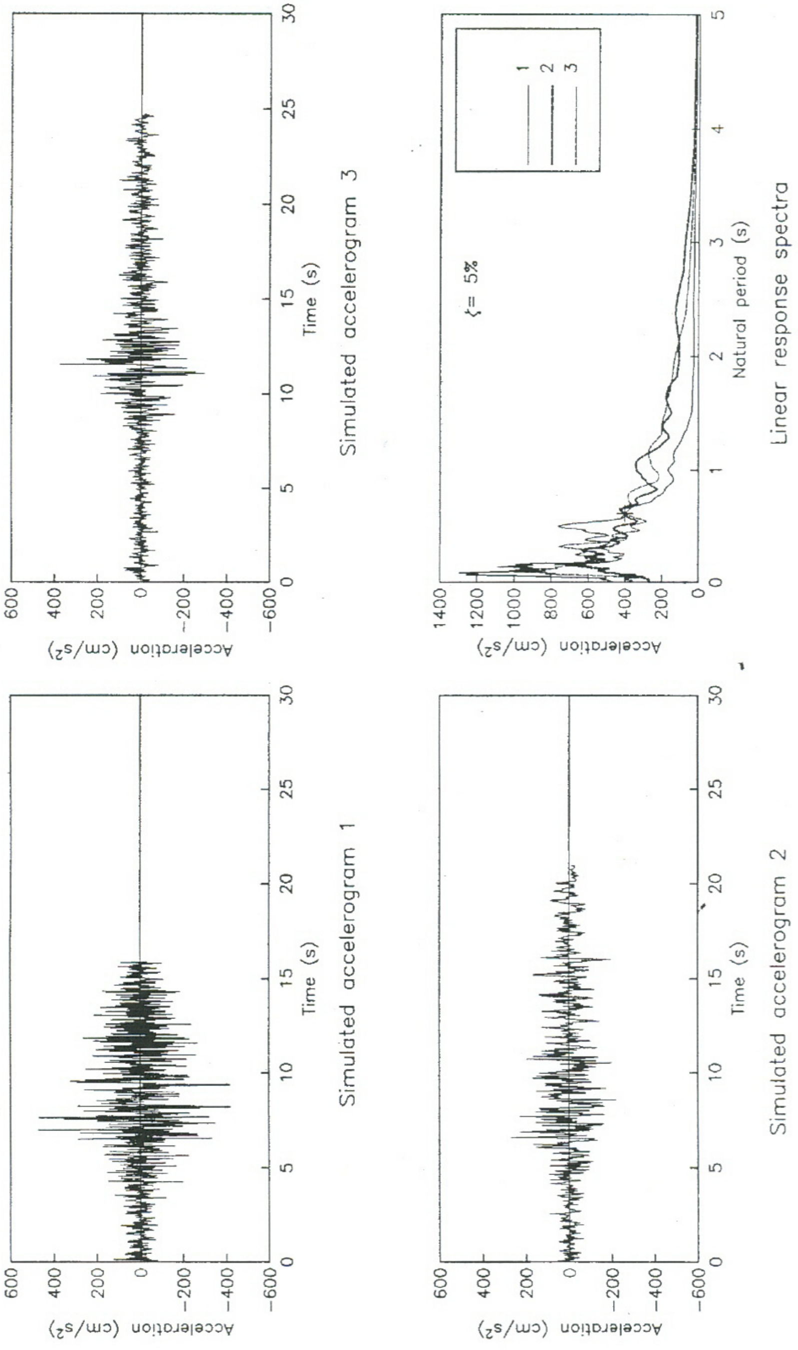

Figure 10. Simulated accelerograms at Tomatlán dam site, and linear response spectra. Return interval of 100 years for spectral acceleration at T = 0.610 s

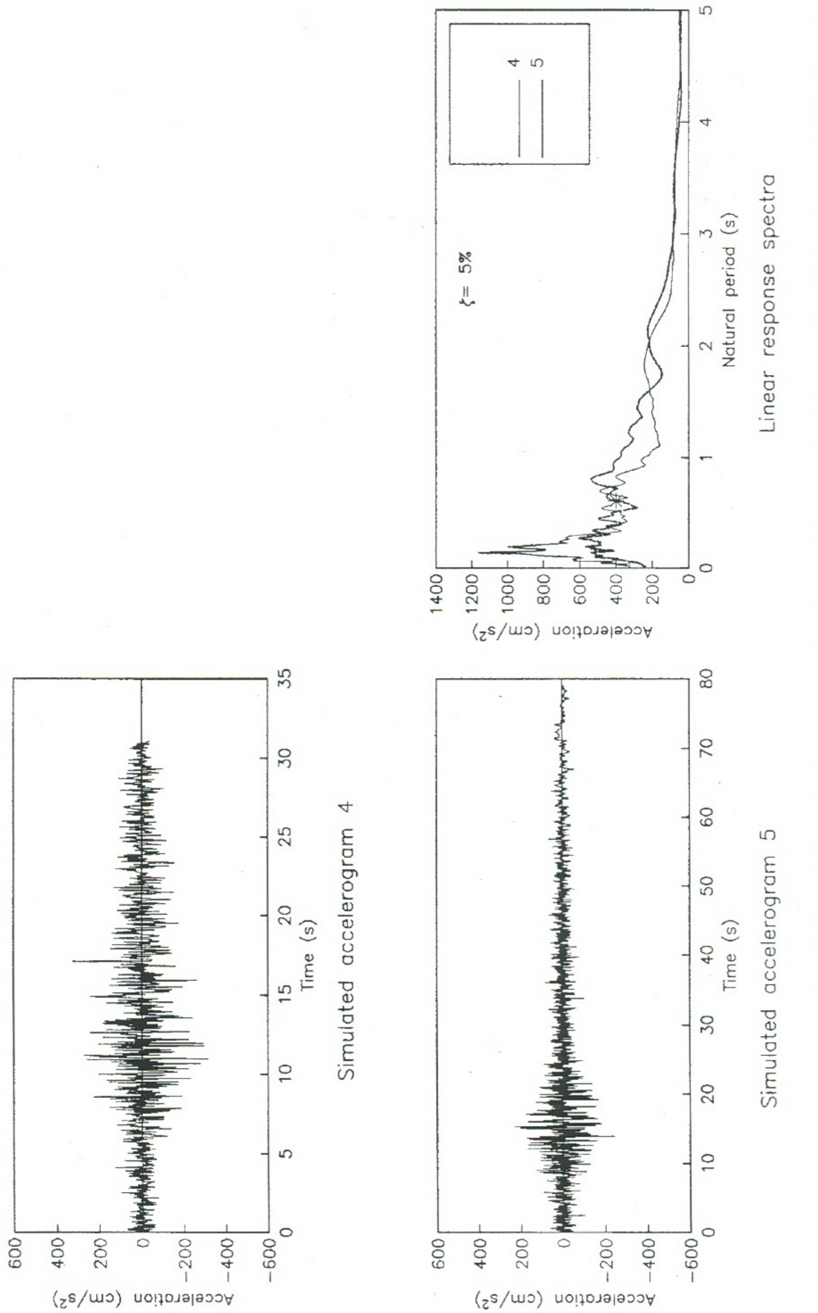

Figure 11. Simulated accelerograms at Tomatlán dam site, and linear response spectra. Return interval of 100 years for spectral acceleration at T = 0.610 s

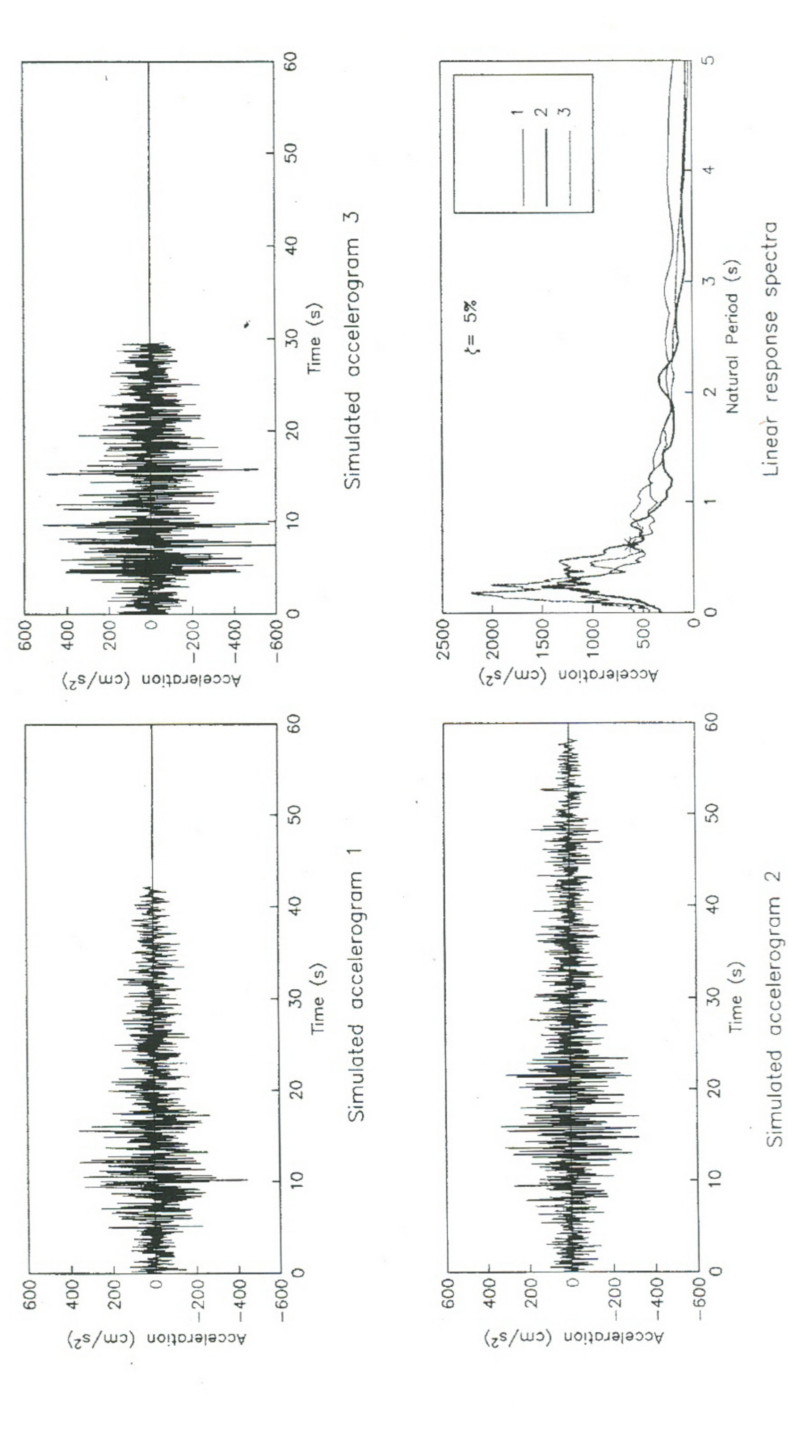

Figure 12. Simulated accelerograms at Tomatlán dam site, and linear response spectra. Return interval of 200 years for spectral acceleration at T = 0.610 s

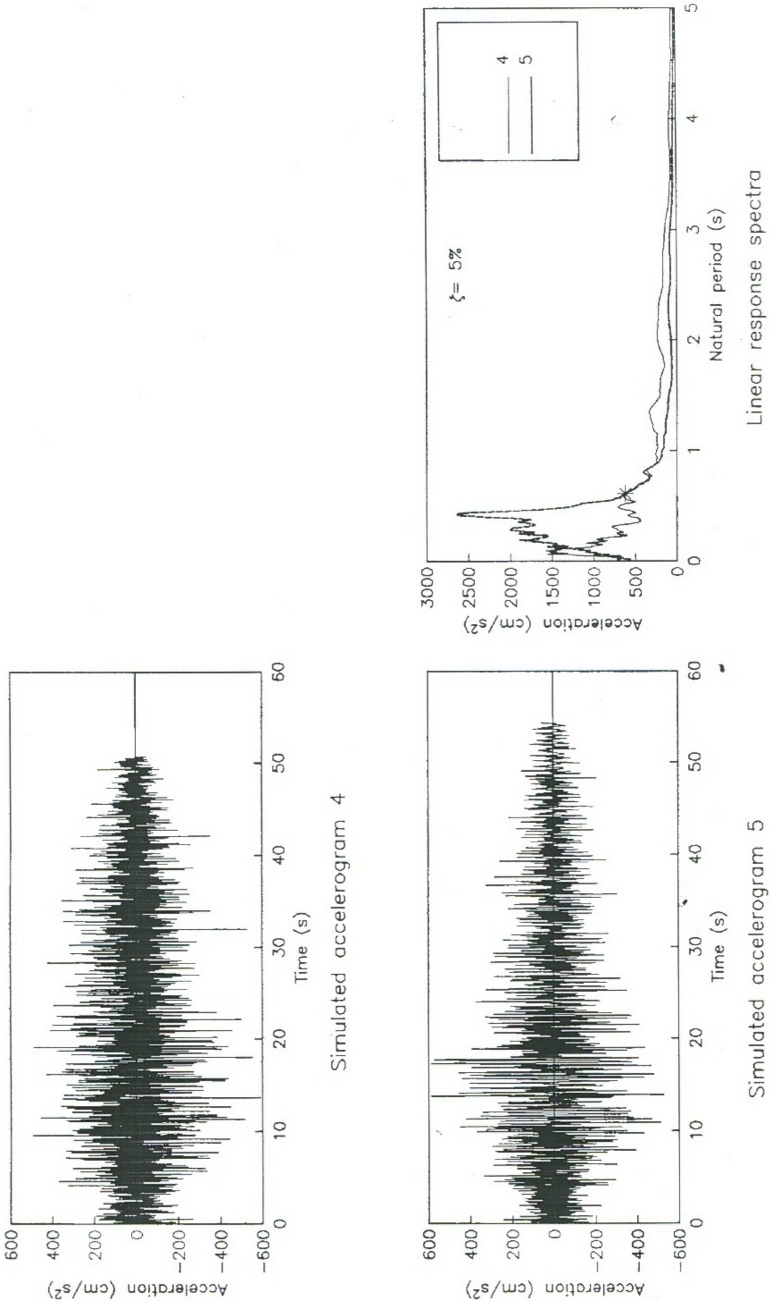

Figure 13. Simulated accelerograms at Tomatlán dam site, and linear response spectra. Return interval of 200 years for spectral acceleration at T = 0.610 s

belt (Ordaz and Singh, 1992) were explicity eliminated. Thus, different generalized attenuation functions should be obtained for the purpose of generating artificial accelerograms on hard soil sites located on that belt; the most obvious case of interest is that of Mexico City.

Finally, it is convenient to note that, in cases where a sufficiently large sample of actual ground motion records is not available, amplitude and frequency modulation functions expressed in terms of magnitude and distance, similar to those presented here, may be established on the basis of simulated records. Thus, the general approach presented here may be advantageously used in combination with records simulated by the Green's function approach for different magnitudes, distances and source-to-site paths.

References

Alamilla, J., Esteva, L., García-Pérez, J. and Díaz-López, O., 1997, *Simulación de movimientos del terreno para sismos con periodos de recurrencia especificados: aplicación a los sitios de algunas presas en México,* Institute of Engineering, National University of Mexico; Report to Comisión Nacional del Agua.

Alamilla, J., Esteva, L., García-Pérez, J. and Díaz-López, O., 2000, Simulating earthguake ground motion a site, for given intensity and uncertain source location, accepted for publication in *Journal of Seismology.*

Bard, Y, 1974, *Nonlinear Parameter Estimation,* Academic Press, New York and London.

Boore, D.M. and .loyner, W.B., 1984, A note on the use of random vibration theory to predict peak amplitudes of transient signals, *BuIl. Seism. Soc. Am.,* **74**, 2035-2039.

Clough, R., Penzien, J., 1975, *Dynamics of Structures,* McGraw Hill, New York.

Esteva, L. and Villaverde, R., 1973, Seismic risk, design spectra and structural reliability, *Proc. Fifih World Conf. Earthq. Eng. Rome*, 2586-2597.

Hartzell, S.H., 1978, Earthquake aftershocks as Green's functions, *Geophys. Res. Lett.* **5**, 1-4.

Joyner, W.B. and Boore, D.M., 1981, Peak horizontal acceleration and velocity from strong-motion records, including records from the 1979 Imperial Valley, California, earthquake, *Bull. Seism. Soc. Am.* 71, 2011-2038.

Kanai, K., 1957, Semi-empirical formula for the seismic characteristics of the ground, *Bull. of the Earthquake Research Institute.* University of Tokyo, **35**, 309-325.

McGuire, R.K., 1974, *Seismic structural response risk analysis incorporating peak response regressions on earthquake magnitude and distance,* Mass Inst. Technol., Dept. Civ. Eng. R 74-51.

McGuire, R.K., 1995, Probabilistic seismic hazard analysis and design earthquakes Closing the loop, *Bull. Seism. Soc. Am.* **85**(5), 1275-1284.

Ordaz, M., Arboleda, J. and Singh, S.K., 1995, A scheme of random summation of an empirical Green's function to estimate ground motions from future large earthquakes, *Bull. Seism. Soc. A.* **85**.

Ordaz, M. and Singh, S.K., 1992, Source spectra and spectral attenuation of seismic waves from Mexican earthquakes, and evidence of amplification in the hill zone of Mexico City. *Bull. Seism. Soc. Am.* **82**, 24-43.

Pardo, M., 1993, *Características sismotectónicas de la subducción de las placas de Rívera y Cocos en el sur de México,* Ph D Thesis, Institute of Geophysics, National University of Mexico.

Taboada, V., Romo, M., Alamilla, J., Esteva, L., García-Pérez, J. and Díaz-López, O., 1997, *Confiabilidad en las presas de Comisión Nacional del Agua*, Institute of Engineering, National University of Mexico, Preliminary Report to Comisión Nacional del Agua.

Tajimi, H., 1960, A statistical method of determining the maximum response of a building during an earthquake, *Proc. Second World Conference on Earthquake Engineering, Tokyo and Kyoto, II.*

Yeh, C.H. and Wen, Y.K., 1989, *Modeling of nonstationary earthquake ground motion and biaxial and torsional response of inelastic structures,* Civil Engineering Studies, Structural Research Series Report No. 546, University of Illinois.

LIFE-CYCLE OPTIMIZATION IN THE ESTABLISHMENT OF PERFORMANCE-ACCEPTANCE PARAMETERS FOR SEISMIC DESIGN[1]

ABSTRACT

A life-cycle formulation is presented for the determination of optimum values of the mechanical properties of a structural system exposed to seismic risk. The resulting values are intended for providing support for the establishment of performance-acceptance criteria and parameters for seismic design A method is developed for the determination of expected damage functions in terms of simplified reference models of the complex nonlinear systems that are typical of engineering practice. The uncertainties associated with the use of the simplified model to estimate peak dynamic responses of the system of interest are accounted for by means of first-order second-moment probabilistic criteria. An illustrative application of the criteria proposed is presented, together with a discussion about the translation of the results of the optimization studies into engineering criteria and methods expressed in conventional design formats.

Keywords: Acceptance criteria; Earthquake resistant design; Optimization; Performance-based design

1. Introduction

Current trends in earthquake resistant design favor the adoption of performance-based criteria. These trends have created the need for efficient and easy-to-apply methods to estimate dynamic displacements and deformation responses of nonlinear systems to moderate and high intensity ground motion. This need is partially satisfied by "push-over" methods, which estimate maximum absolute values of global and local dynamic responses in terms of a single-degree-of-freedom "equivalent system" and a deformation pattern (or lateral response configuration) that approximates that of the system when the relative displacement at its top reaches its maximum. Quantitative measures of the prediction errors of these methods are available for typical seismic excitations on hard ground, for some structural systems formed by members with hysteretic bilinear constitutive functions [1]. For earthquakes on other types of ground, and for structural systems characterized by other types of nonlinear behavior, such measures are not available. Acceptance criteria for performance-based design are formulated in terms of allowable values of maximum relative displacements (such as story distortions) under the occurrence of earthquakes with intensities associated with given return intervals. Very little attention has been given to cost-benefit studies to support the choice of the best combination of return interval and allowable distortions. This paper aims at contributing to fill these gaps, through the development of criteria for establishing acceptance-criteria formats and for determining optimum values of the critical parameters.

[1] First Published in:
L. Esteva, O. Díaz-López, J. García-Pérez, G. Sierra, E. Ismael, Life-cycle optimization in the establishment of the performance-acceptance parameters for seismic design, *Structural Safety*, **24**, (2002) 187-204

Nomenclature

C_0	Initial construction cost of building
C_{0i}	Initial construction cost, ith story
C_{00}	Initial construction cost without earthquake resistance
D_F	Expected value of failure consequences in case of occurrence
D_0	Expected value of cost of damage per unit time
D_S	Expected value of cost of damage per unit time, conditional to survival
$G(\psi_t)$	Damage function for ith story
$p_F(y)$	Failure probability under the action of an earthquake with intensity y
Q	Yield ratio
r_{ci}	C_{0i}/C_0
$S_d(T, Q)$	Nonlinear spectral displacement for period T and yield ratio Q
$S_{dL}(t)$	Linear spectral displacement for period T
U	Objective function
Y, y	Earthquake intensity

Greek symbols

α	Design parameter
α_i	ψ_{0i} / ψ_0
α_s	$S_d(T, Q) / S_{dL}(t)$
γ	Discount (interest) rate per unit time
$\delta(y)$	Expected value of damage for intensity y
λ	Factor that accounts for simultaneous repair actions at several stories
μ	Ductility demand
v_F	Expected failure rate per unit time
$v_Y(y)$	Seismic hazard function
ρ	ψ / ψ_0
ρ_i	ψ_i / ψ
ψ	Global lateral distortion (roof displacement divided by building height)
ψ_F	Global lateral distortion at failure
ψ_i	Lateral distortion at the ith story
ψ_0	Global lateral distortion, estimated as the response of the SRS
ψ_{0i}	Lateral distortion at ith story, estimated in terms of the response of the SRS and the pushover configuration.

The seismic performance of a structural system is determined by the mechanical properties (strength and stiffness: initial values and cyclic degradation properties) of the structural members under the action of alternating deformation cycles with different amplitudes. Under typical practical design conditions, the structural engineer controls the strength and stiffness cyclic degradation properties of the members through the selection of the material and of the types of structural details and connections, as well as through the establishment of the quality control specifications. Then he or she determines the required initial (undamaged) values of the strength and stiffness variables, both for the system as a whole and for each individual member. For practical reasons, performance-based criteria are ordinarily expressed in terms of a number of simultaneous, not equivalent, design conditions. Each condition is referred to an earthquake with a different intensity, associated with a given return interval, and is expressed by means of a set of upper bounds to the global and local (story) distortions resulting from the corresponding dynamic response. The values of the mechanical properties determined in accordance with this multi-level design process should lead to optimum life-cycle performance.

In this paper, the establishment of optimum performance-based seismic design criteria is presented as a two-step process. First, a life-cycle framework is adopted to obtain optimum values of the relevant mechanical properties of typical structural systems, and second, these values are taken as target values of the parameters that should result from application of a conventional multi-level design process. Strictly speaking, the number of independent variables that could be used in the search for the optimum structural system is as large as the number of variables required for specifying the mechanical properties of all its individual members. For practical reasons, the choice should be narrowed down to a significantly smaller number. Two sets of independent parameters are selected here for this purpose. One includes the global system properties, that is, fundamental period and base shear strength. In accordance with present trends in performance-based earthquake resistant design, the base shear strength can be replaced by the lateral deformation capacity, expressed as the displacement at the top of the system, relative to the ground, corresponding to the ultimate capacity limit state associated with the push-over analysis. The other set of parameters determines the patterns of variation of local values of lateral stiffness and strength along the system's height. As shown later, an iterative optimization algorithm is proposed consisting in a sequence of three-step cycles. In the first step of each cycle, the variation patterns of local stiffness- and strength values are assumed. In the second and third steps, optimum values of the fundamental period and the lateral deformation capacity are successively determined with the aid of simplified models derived from conventional push-over analysis of the detailed model of the system established in the first step.

2. Optimum acceptance parameters for multi-level performance-based design

Let α be a vector formed by the values of the parameters that determine the relevant mechanical properties of a system to be designed. Following Rosenblueth [2], the life-cycle optimization analysis is based on the assumption that a repair and reconstruction strategy is adopted a priori, according to which the system is repaired or rebuilt immediately after each damaging earthquake, using the same specifications of the original system. If the uncertainties about the system properties after each restoration action are small as compared to those arising from the intensities and detailed characteristics of the seismic events, the optimum values of the elements of α are those that minimize the following objective function:

$$U = C_0(\alpha) + \frac{D_0(\alpha)}{\gamma} \tag{1}$$

Here, $C_0(\alpha)$ is the initial cost function, D_0 is the expected cost of damage and failure per unit time and γ is an adequate discount (or interest) rate. D_0 depends on the damage function $\delta(y)$, which expresses the expected cost of damage as a fraction of C_0 for an earthquake with intensity equal to y, and on the seismic activity at the site of interest.

$$D_0 = -C_0 \int \frac{\mathrm{d}\nu_Y(y)}{\mathrm{d}y} \delta(y)\,\mathrm{d}\gamma \tag{2}$$

In this equation, $v_Y(y)$ is the yearly rate of occurrence of earthquakes with intensities greater than y at the site, and $\delta(y)$ can be represented in terms of its expected value conditional to survival of the system, $\bar{\delta}(y\,|\,S)$, the probability of failure $p_F\,(y)$ as a function of intensity, and the failure cost ratio, $\delta_F = D_F/C_0$, where D_F is the expected cost of failure, in case it occurs.

$$\delta(y) = \bar{\delta}(y\,|\,S)[1 - p_F(y)] + \delta_F\, p_F(y) \tag{3}$$

For those values of y associated with non-negligible values of $v_Y\,(y)$, $p_F\,(y) << 1$. Under these circumstances, D_0 is equal to $D_S + v_F D_F$, where

$$D_S = -C_0 \int \frac{\mathrm{d}\nu_Y(y)}{\mathrm{d}y} \bar{\delta}(y\,|\,S)\mathrm{d}y \qquad \text{and} \qquad \nu_F = -\int \frac{\mathrm{d}\nu_Y(y)}{\mathrm{d}y} p_F(y)\,\mathrm{d}y \tag{4a, b}$$

In the foregoing equations, $\delta(y)$, $\bar{\delta}(y\,|\,S)$, p_F and v_F are functions of the vector α of system properties, which are independent from the seismic excitations that may affect the system. However, typical structural design recommendations and codified rules may need to be expressed in terms of allowable values of structural responses for seismic excitations associated with specified return intervals. Thus, two alternate approaches will be considered for the selection of the components of vector α; one in terms of system properties and the other in terms of allowable response values for given design earthquakes. Starting with the first approach, the system is defined by its fundamental period of vibration, T, its base-shear coefficient at yield, c_y, and the forms of variation of the local values of strength and stiffness along the building height. These variables, together with the local values of the deformation capacity, determine the value of the lateral distortion at failure, $\psi_F = u_F/H$, where H is the system's height and u_F is the ultimate value of the relative displacement of its top with respect to its base. For convenience in the formulation of an iterative algorithm for the optimization analysis, these parameters will be grouped as follows: $\alpha_1 = T$, $\alpha_2 = c_y$, $\alpha_3 = \psi_F$, and vectors α_K and α_R, which determine respectively the forms of variation of lateral stiffness and strength along the system's height. The values of these parameters will be taken as equal to those that would be calculated by standard models of structural mechanics when the material properties and member cross section dimensions are assumed to adopt their expected values (rather than the nominal values assumed in conventional design practice).

2.1 Damage functions

Given the earthquake intensity, y, the expected cost of damage can be obtained as the sum of the contributions of several segments of the system (Eq.5); in a multistory building, each segment can be made to correspond to one or more stories.

$$\bar{\delta}(y\,|\,S) = \lambda \sum_i r_{ci}\, \bar{g}(\psi_i) \tag{5}$$

In this equation, $r_{\mathrm{ci}} = C_{0i}/C_0$, C_{0i} is the initial cost of the ith segment of the system, $g(\Psi_i)$ a function of the random value Ψ_i of the corresponding local distortion, and $\bar{g}(\Psi_i)$ its expected value for given intensity y. The initial costs C_0 and C_{0i} are functions of the vector α of structural parameters, and so is the joint probability density function of the local distortions Ψ_i. A factor λ, which is a function of the summation that follows it, is introduced to account for the fact that repair costs include the contribution of a fixed amount that reflects the costs of the logistic arrangements that have to be made before the actual repair work starts. As a consequence, λ will in general reach its maximum for infinitely small values of the summation mentioned above, and it will tend asymptotically to a smaller value as that summation grows.

On the basis of empirical information, for a given structural or non structural element or subsystem $g\,(\Psi)$ can be estimated as

$$\bar{g}\,(\psi) = 0, \quad \psi < \psi_{cr}$$
$$\bar{g}\,(\psi) = 1 - \exp(-\kappa(\psi - \psi_{cr})^n), \qquad \psi > \psi_{cr} \tag{6a, b}$$

or, alternatively, as

$$\bar{g}\,(\psi) = 1 - \exp(-a\,\psi^m) \tag{6c}$$

In these equations, ψ_{cr} corresponds to the initiation of cracking. In order to estimate the values of the parameters κ, a, m and n in these equations it is necessary to transform the experimental curves relating physical damage to lateral distortions of structural and nonstructural elements and subsystems into their monetary costs. A collection of such experimental curves has been presented by Reyes [3].

In the foregoing paragraphs only direct repair costs that are determined by the values of lateral distortions are included in the estimation of expected damage costs. In most practical problems, indirect costs such as inconvenience to occupants and business interruption would need to be included. Other types of damage that are determined by the strength and stiffness properties of the system are those related to the amplitudes of local floor velocities and accelerations. These values determine the response of sensitive equipment and the possibility of overturning of equipment, partitions and other types of nonstructural elements. The implications of this type of damage on the optimal solutions are not studied in this article.

2.2 Initial cost functions

In this paper, attention will be focused on those steps of the iterative optimization procedure aimed to determine the stiffness properties that are required to control the response of the system to low and moderate intensity seismic events. Eq. (7) is equivalent to one proposed by Reyes [3] for the total cost of a system, including foundation and nonstructural elements, in terms of its fundamental period of vibration. The influence of the base shear capacity on the initial cost is disregarded, on the grounds that the mentioned capacity shows a significant positive statistical correlation with the lateral stiffness. This supports the adoption of Eq. (7) for the purpose of determining optimum values of stiffness related variables; however, a corresponding expression for initial cost in terms of base-shear capacity must be developed for the purpose of determining optimum values of this design parameter.

$$C_0 / C_{00} = 1 + m_k\,(T_0 - T)^{\beta_k} \tag{7}$$

Here, T_0 is the fundamental period of the system (in seconds) if it were designed only for gravitational loads, C_{00} is the initial cost that would be associated with that design, and m_k, β_k are empirically derived parameters. A limitation hindering the applicability of Eq. (7) is that it depends on T_0, which is ordinarily not available. For fictitious systems with properties similar to those that would be obtained in structures in

Mexico City assuming no design for earthquakes, Reyes [3] derived the relation $T_0 = 0.11N + 0.56$, where N is the number of stories. Alternatively, the reference parameter C_{00} used in Eq. (7) can be made to correspond to the system that would result from application of design rules typical of current practice. This would offer the advantage of starting the optimization process form a system closer to the final solution, thus improving the accuracy of its results and reducing the required computational efforts.

For the purpose of estimating costs of damage, it is convenient to segregate the total cost C_0 into the contributions of the system segments considered in Eq. (5). Then, it is necessary to split each of these contributions into those associated with components of the structural frame, with partitions and similar elements and with floor systems. The latter distinction is necessary because the damage costs for these three types of system components vary differently with the local lateral distortions; in particular, it will be assumed that the components of the floor systems do not suffer any damage as a consequence of those distortions. It must be recalled that the relative contribution of each type of element to the total cost may vary along the building height. Accounting for this poses no major difficulties.

2.3 Control variables for optimization analysis and for practical design criteria

It has been suggested in the foregoing paragraphs to adopt the fundamental period T and the base-shear ratio at yield, c_y, as control parameters for seismic design. T controls the damage levels at low seismic intensities, while c_y and the resulting deformation capacity, ψ_F, control the occurrence of failure. Given the seismic hazard function at the site of interest, these parameters determine the values of C_0 and D_0 of Eq. (1), and must be handled jointly when trying to obtain the combination of their values that minimize U in the same equation. However, in many cases $\nu_F D_F << D_S$ and/or ν_F is not very sensitive to T (that is, to the stiffness parameters, K). Under these circumstances it may be adequate to formulate the optimization analysis for T and K independently of c_y, and ignoring the contribution of $\nu_F D_F$ to the value of D_0. This approach is adopted in the following.

As a consequence of the spatial variability of K, peak values of the local (story) distortion ψ_i will in general be greater than the average value ψ for the whole system. Under practical design conditions, the local values of the lateral stiffness of a system are controlled by imposing upper bounds to the peak values of the local distortions produced by earthquake intensities associated with specified return intervals. In order to develop a design condition consistent with this format that gives place to a system with a fundamental period T equal to that resulting from the optimization analysis, suppose that $S_{dl}(T)$ is the ordinate of the linear displacement response spectrum for the design earthquake, evaluated at the natural period T; suppose also that $\psi = \varepsilon S_{dl}(T)/H$, where ε is a factor that accounts for the contributions of all significant modes of vibration. If the ratio ψ_i/ψ that results from a conventional linear dynamic response analysis is denoted as $r_{\psi i}$, the design condition that would lead to an optimum system can be established as $\psi_i < \psi^*$, where $\psi^* = r_{\psi i}\varepsilon S_{dl}(T)/H$. It may happen that $\psi_i >> \psi$. At first sight, this may lead to conclude that the system resulting from this criterion might be far from the optimum. In order to get a solution that would be closer to the optimum, it would be necessary to handle the local values of the stiffness as independent variables. The practical difficulties that would be associated with the formulation of design criteria that were intended to lead to those values would be insurmountable under practical conditions. The alternative that remains is to obtain the optimum value of ψ^* to be allowed under the action of an earthquake intensity associated with a specified return interval. The problem remains of deciding what return interval to adopt for this purpose. It may be reasonable to take as design intensity the value of y that corresponds to the maximum value of the integrand in the second member of Eq. (2). This problem is left for future studies.

3. Optimization analysis based on simplified reference systems

As shown earlier, the number of variables that affect the peak values of the local distortions (and, therefore, of the expected contributions to overall damage costs) may be extremely large. In order to determine optimum values of the design parameters, large numbers of detailed system models would need to be investigated, which would imply calculating dynamic response and damage functions for a large number of complex systems. This may be avoided by resorting to the use of *simplified reference systems* (SRS's, ordinarily called *"equivalent systems"*). These are single-degree-of-freedom systems with shear-deflection functions similar to those relating the shear at the base of the original system with the displacement at its top ($V - u_N$). For a given system, this function is obtained by means of a push-over analysis, which also provides a set of amplitude-dependent lateral response shapes, which serve to estimate peak values of local distortions on the basis of the peak value of the top displacement. In addition to the uncertainties arising from the stochastic nature of the detailed ground motion time histories, the local distortions estimated with the aid of SRS's are also affected by the uncertainties that result from the simplifications introduced in the structural model. The latter include those associated with the reduction in the number of degrees of freedom, as well as those arising from the inadequate representation of the constitutive functions of the structural members subjected to a number of large-amplitude deformation cycles.

Once a simplified reference system has been adopted, it is easy to obtain the response function $\psi_0(y)$, which represents the expected value of the peak amplitude of the average system distortion. Here and in the following, subscript 0 is used to indicate that the response value of interest is calculated on the basis of the simplified reference system and the lateral distortion configurations produced by the pushover analysis as functions of the amplitude of the roof displacement. Obtaining the expected value of the local distortion $\psi_{0i}(y)$ at location i is then straightforward. The ratio $\rho_i = \psi_i/y_{0i}$ is a random variable; its mean ρ_i and variation coefficient V_{pi} can be estimated on the basis of dynamic response studies of detailed systems to a sample of ground motion time histories representative of the sample used to determine $\psi_0(y)$. For the purpose of determining the optimum design parameters for a specific system, these means and variation coefficients will be estimated for a system with design parameters that are reasonably close to their optimum values, and will be assumed to apply to all other alternatives to be examined.

Counting with the information just described, it will be possible to calculate values of the damage function defined in Eq. (5). The expected value of $g(\psi_i)$ that appears in that equation can be estimated by means of a two-point estimate [4]

$$\bar{g}_i(\psi_i) = \frac{1}{2}\left[g_i\left\{\bar{\psi}_{0i}\,\bar{\rho}_i\left(1+V_{\rho i}\right)\right\} + g_i\left\{\bar{\psi}_{0i}\,\bar{\rho}_i\left(1-V_{\rho i}\right)\right\}\right] \tag{8}$$

More exact expressions can easily be used.

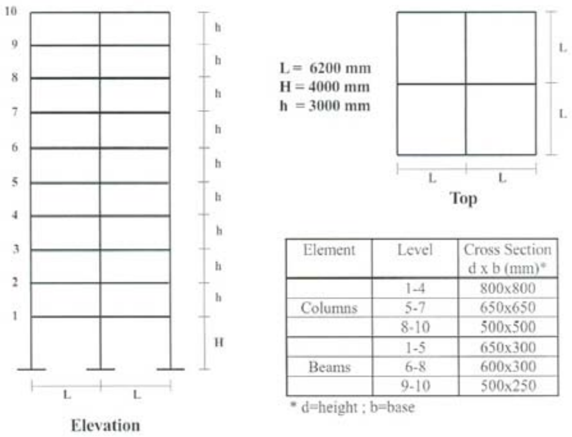

Element	Level	Cross Section d x b (mm)*
	1-4	800x800
Columns	5-7	650x650
	8-10	500x500
	1-5	650x300
Beams	6-8	600x300
	9-10	500x250

Figure l. Basic system

4. Illustrative example

The criteria and models described above are applied in this section to the estimation of expected damage functions for the system whose general configuration and gravitational loads are shown in Fig. l. The cross-sections shown in the figure were taken as the starting point for a successive approximation process aiming to obtain the optimum stiffness properties for the system. The strength properties of all critical sections were determined on the basis of a static analysis for a set of lateral forces giving place to a base-shear coefficient of 0.1 in terms of the nominal values of both the gravitational loads and the mechanical properties of the structural members. This coefficient corresponds to that specified in the current seismic design regulations for reinforced concrete ductile frames in the soft soil area in Mexico City. In order to account for the uncertainties associated with the gravitational loads and with the mechanical properties of this system, these variables were handled as random variables; their probability distributions are summarized in a report by Díaz and Esteva [5]. A push-over analysis was carried out on a detailed model of the system, taking the all uncertainty known variables equal to their expected values. The excitation for this analysis was a base acceleration slowly growing as a linear function of time. This analysis produced the $V - u_N$ function and the set of lateral response curves depicted in Fig. 2. The latter curves represent lateral displacement configurations of the system for different values of the relative displacement of the top with respect to the base. The angle formed by the tangent at a given point in one of these curves with respect to the vertical is equal to the local value of the lateral distortion at that point (ψ_{0i}) when the top displacement and the average distortion are equal respectively to u_N and ψ.

The expected value of the peak relative displacement of the top of the system was estimated for a set of simulated seismic ground motion records with different intensities (measured by the corresponding linear pseudo-acceleration values, $S_a(T)$. For this purpose, use was made of a sdof simplified reference system with a bilinear hysteretic shear-deflection curve that approximated the $V - u_N$ curve shown in Fig. 2. The results are plotted as values of $u_N = \psi_0 H$ in terms of S_a in Fig. 3, which also shows a curve representing the expected values of $\bar{u}_N = \bar{\psi}_0 H$.

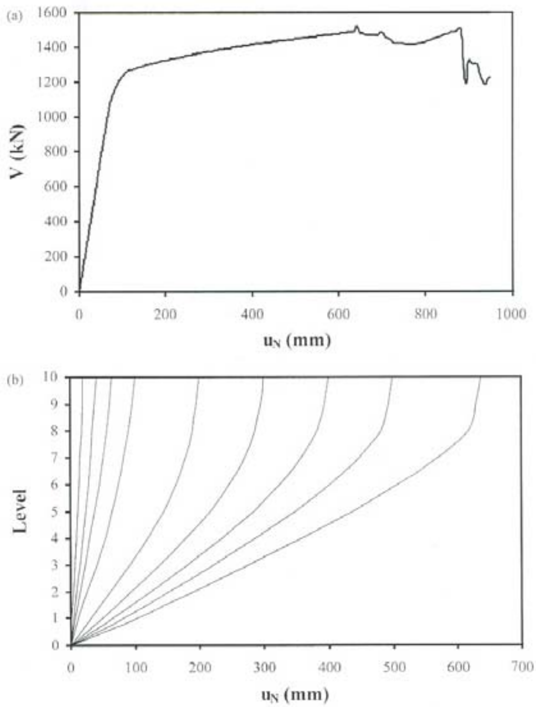

Figure 2. Results of push-over analysis of basic system: (a) V vs *u_N curve; (b) lateral response curves*

In order to estimate the values of the statistical parameters, $\bar{\rho}_i$ and $V_{\rho i}$ used in Eq. (8), a set of detailed models of the system were obtained by Monte Carlo simulation of the values of the gravitational loads and the mechanical properties of the structural members. Each of these systems was then subjected to an artificial ground motion acceleration record randomly selected from a set of simulated records with different intensities. Takeda-type moment-curvature functions were used to represent the behavior of the critical sections of beams and columns under the action of cyclic excitations. The results of these studies were used in combination with the $\bar{\psi}_{0i}$ vs S_a curves described in the preceding paragraph in order to obtain the values of $\bar{\rho}_i$ and $V_{\rho i}$ summarized in Table 1. For each story, the expected value $\bar{g}_i$ (ψ_i) of the local damage ratio was estimated for different intensities by means of Eq. (6c), with a = 2375 and m = 2. The global value of the damage ratio $\bar{\delta}$ (y), as estimated in accordance with Eq. (5), is shown if Fig. 4.

Several systems with the general configuration shown in Fig. 1 were studied, aiming to determine the optimum value of the fundamental period for a ten story system to be built at a soft-soil site in Mexico City, where the seismic hazard is given by an equation of the form $v_Y(y) = Ky^{-r}(1 - (y/y_1)^{\varepsilon})$. Here, y is the earthquake intensity, measured by the ordinate of the linear pseudo-acceleration response spectrum for the fundamental period of the system of interest; r, y_1 and ε are adequate parameters. The fundamental periods of the systems considered ranged between 0.8 and 1.25 times the fundamental period of the original system; the form of variation of the story stiffness along the building height was kept unchanged. As a consequence of this assumption, the forms of the lateral response displacement functions were equal for all the new systems. The $V - u_N$

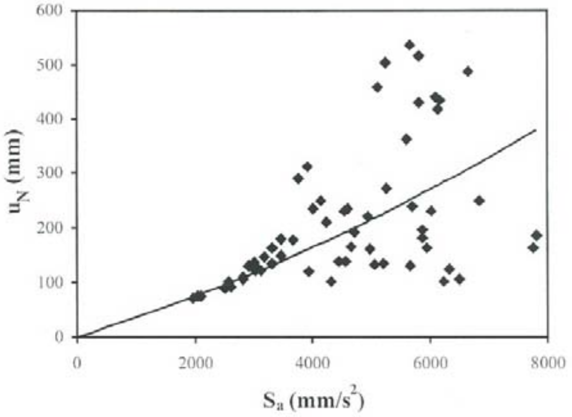

Figure 3. Average-distortion estimates for the reference system

function determined for the original system served to estimate those corresponding to each of the new systems, keeping constant the base shear at yield, while adjusting the values of the initial tangent stiffness in order to make them correspond to the fundamental periods considered.

For the purpose of calculating values of the utility function defined in Eq. (l), it was assumed that contributions of the floor system and the nonstructural members to the initial cost C_0 are equal to 0.1 C_{00} and 0.65 C_{00}, respectively. C_0 was assumed to vary with T in accordance with Eq. (7), with m_k = 0.64 and β_k = 2.48. The minimum value of U was obtained for T= 1.15 s. For this period, the value of S_a that corresponds to a return interval of 10 years (v_Y = 0.1) is equal to 0.140 g. The resulting lateral story distortions are shown in Fig. 5, where the maximum occurs at the fourth story and is equal to 0.0027. This is the value that should be recommended for the serviceability limit design condition for a return interval of 10 years. The wide range of variation of the peak values of the story distortions casts doubts about the validity of an optimization analysis as that presented here, which characterizes the stiffness properties of the system by one single parameter.

TABLE 1

Statistical properties of response ratios $\overline{\rho}_i$

Story	$\overline{\rho}_i$	$\sigma_{\rho i}$
1	0.9061	0.2879
2	0.9097	0.2345
3	0.9751	0.2556
4	1.0381	0.2815
5	1.0557	0.2904
6	1.0596	0.2983
7	1.0406	0.3081
8	0.9536	0.2703
9	0.8937	0.2625
10	0.8842	0.2941

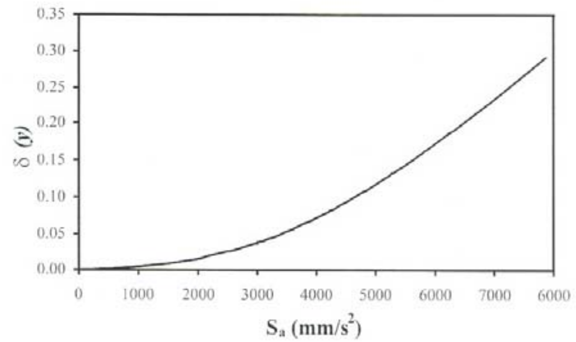

Figure 4. Damage function

An alternative to the approach presented here might take as independent variable the upper bound to the story distortions for a ground motion associated with a given return interval.

5. Accounting for nonlinear dynamic response

Section 4 is based on the simplifying assumptions that $\bar{\delta}\,(y|S) >> \delta_F$ and that the lateral strength remains fixed while the stiffness values of all the structural members vary in a proportional manner. The dependence that exists between strength and stiffness under realistic conditions was ignored. From these assumptions, it was possible to take the fundamental period of the structure of interest as the independent control variable to be used in the optimization process. In the following paragraphs we will examine the problems that appear when both the stiffness and the strength values are permitted to vary under more general conditions. Now we have to face several new problems. One is the incorporation of the parameters, or vectors of parameters, that are needed to describe the stiffness and the strength of each structural system along its height. The dependence between the strength and the stiffness of each structural member must be considered at this step. It is also necessary to develop a sufficiently simple and accurate method to estimate the statistical moments of the significant response variables, which are, in general, the peak values of the global and local (story) distortions.

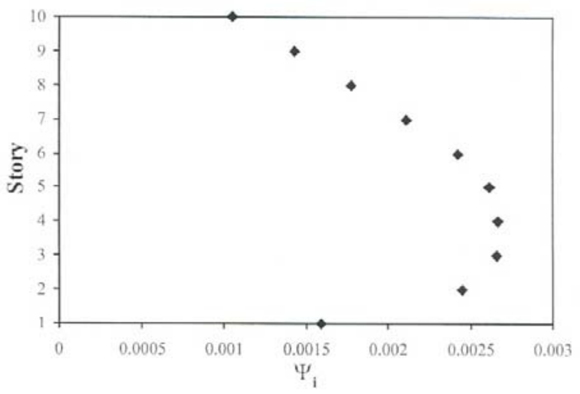

Figure 5. Story distortions for optimum value of natural period

This implies deriving expressions for the calculation of each of those moments as a function of an adequate measure of the ground motion intensity. One way to achieve this consists in fitting analytical expressions to samples of response values obtained by Monte Carlo simulation. This possibility is explored in the following. For this purpose, the uncertainty associated with the response transformation factor (the ratio of the peak value of the structural response variable of interest to the earthquake intensity measure) is disaggregated as explained in the next few lines.

Let ψ now represent the peak value of the global distortion of the building; that is, the ratio of the roof displacement u_N to the building height, H. As above, ψ_i is used to denote the peak value of the local distortion at the ith story. The values of ψ and ψ_i estimated with the aid of the SRS are designated by ψ_0 and ψ_{0i}, respectively. The ratio ψ_{0i}/ψ_0 is denoted by the deterministic variable α_i. The expected value of ψ_0 is estimated by means of the equation $\bar{\psi}_0 = \gamma S_d(T, Q) / H$, where γ is the dynamic participation factor of the response configuration associated with the SRS, and $Sd(T, Q)$ is the expected value of the displacement response spectrum for the natural period T of the SRS and the yield ratio Q. The latter is defined as the ratio of the spectral acceleration for linear response to the yield shear capacity of the same system. The random variables α_S, ρ and ρ_i are now used to represent the ratios $\psi_0/\bar{\psi}_0$, ψ_0, ψ/ψ_0 and $\psi_i/\alpha_i\psi$, respectively.

As an illustration, a ten-story frame with the same general dimensions and gravitational loads as that presented in Section 4 of this article was studied. As in the previous example, it was assumed that this new system would be built at a soft soil site in the valley of Mexico where the dominant ground period is equal to 2 s. The system used as the starting point for the optimization study was designed for a seismic coefficient of 0.10. The cross sections of the members were selected in accordance with the criterion that none of the lateral story distortions estimated for the design earthquake on the basis of gross sections, and including the nonlinear component of the response, exceeded the allowable value of 0.012. The system is supported on friction piles. For the purpose of taking into account dynamic soil-structure interaction in the estimation of dynamic response, its foundation was represented by a set of springs and dampers intended to represent the lateral and the rocking components of the base motion resulting from that interaction. Some results are presented in Figs. 6-12. Fig. 6 presents peak values of the displacement of the SRS of the system under the action of a sample of simulated ground motion acceleration time histories with statistical properties similar to those expected at the intended construction site.

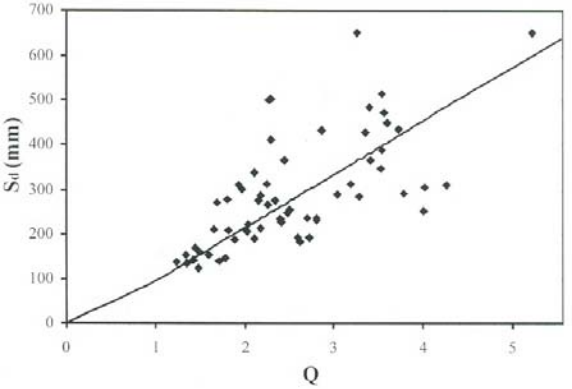

Figure 6. Nonlinear displacement responses in terms of yield-ratio Q

A least-squares fit to the results is also shown in Fig. 6. The ground motion intensities were measured by the ordinates of the displacement spectrum S_d (T, Q), with the yield ratio Q equal to 1. As a consequence, for low values of the intensity the peak displacements are deterministically equal to their expected values given by the fitted curve, which means that in that range α_S is deterministically equal to l. It is also clear from the figure that the dispersion grows with Q. This is a consequence of the random nature of the ratio between the ordinates of the nonlinear and the linear response spectra. It is easy to show that an expression that represents the square of the coefficient of variation of α_S as a function of Q can be obtained by least-squares fitting to the values of $(\alpha_S/\bar{\alpha}_S - 1)^2$. Thus, once the form of the hysteretic response curves used to represent the nonlinear behavior of the SRS is established, the determination of a set of mean-value and variation-coefficient functions for different values of the natural period T at a site offers no significant problems. Figs. 7-9 respectively present values of ρ, ρ_4 and ρ_8 calculated on the basis of the ratios of responses of detailed and simplified models of the system of interest to a number of simulated ground motion time histories with different intensities. The solid lines are the result of least squares fitting to the data. They are intended to represent the expected-value functions of the corresponding variables.

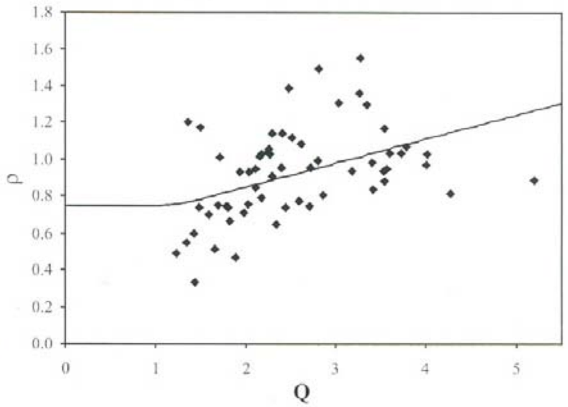

Figure 7. Sample points and fitted curve for ρ

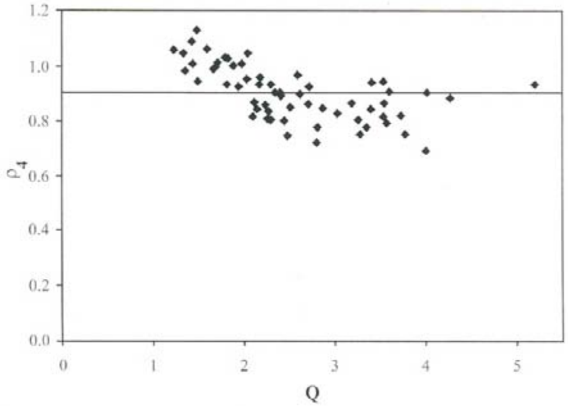

Figure 8. Sample points and fitted curve for ρ_4

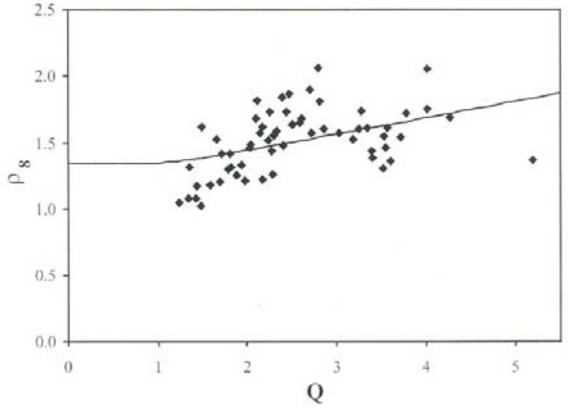

Figure 9. Sample points for fitted curve for ρ_8

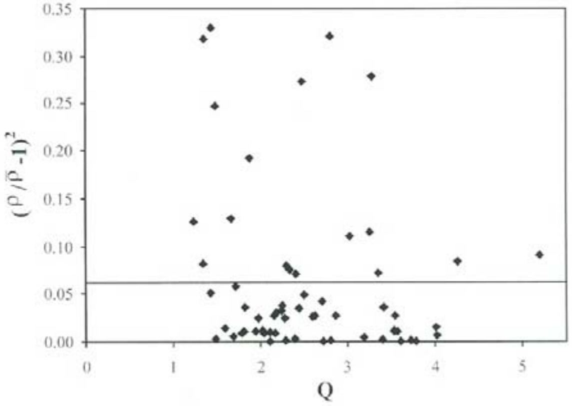

Figure 10. Sample points and fitted curve for the square of the variation coefficient of ρ

The curves depicted in Figs. 7 and 9 are consistent with the trends observed in the values resulting from the dynamic response studies. However, the function fitted to the data in Fig. 8 fails to show the decreasing trend observed in the data. This is a limitation of the form of the family of curves adopted. The values represented in the vertical axis of Figs. 10-12 were chosen in such a manner that their expected values are equal to the squares of the variation coefficients of ρ, ρ_4 and ρ_8, respectively. The diversity of trends and absolute values that characterize both the expected-value and the variation-coefficient functions hinders the possibility of formulating simple and widely applicable recommendations for the estimation of probabilistic seismic response by means of simplified models. This pronounced diversity in trends is determined by the response configurations resulting from the pushover analysis, and is strongly dependent on the characteristics of the excitation applied for this purpose. The study of alternative options for improvement is essential for the advance of easy-to-apply methods for the probabilistic estimation of the seismic response of nonlinear multi-degree-of-freedom systems. These alternatives may include the consideration of lateral load vectors with shapes that evolve in terms of the amplitude of the expected seismic response [6].

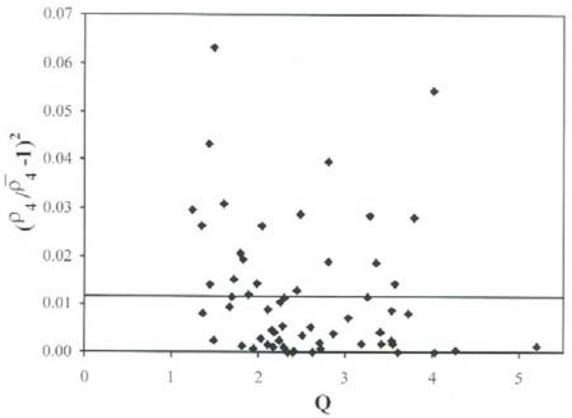

Figure 11. Sample points and fitted curve for square of the variation coefficient of ρ_4

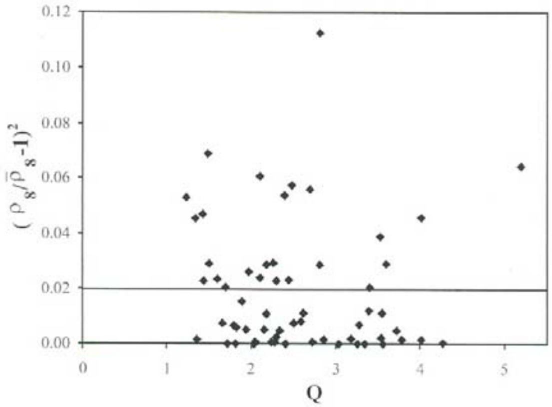

Figure 12. Sample points and fitted curve for square of the variation coefficient of ρ_8

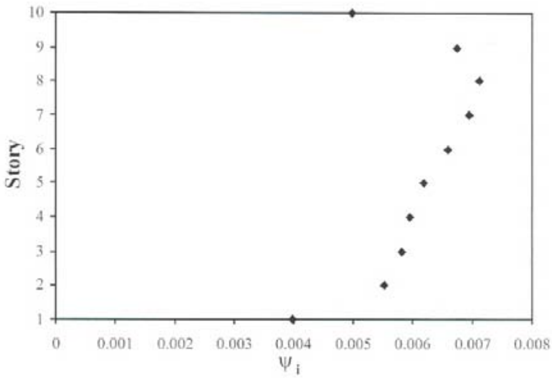

Figure 13. Story distortions for optimum value of natural period

An optimum value of 1.44 s was obtained for the fundamental period of this new system. The resulting values of the story distortions calculated for the ten-year return interval intensity are plotted in Fig. 13. The large variability that was observed in Fig. 5 has been significantly reduced for the present case, as a consequence of the larger uniformity attained for the story distortions produced by the design earthquake.

6. Concluding remarks

Single-degree-of-freedom models of complex nonlinear structural systems can be advantageously used as simplified reference systems for the estimation of expected damage functions associated with different seismic design alternatives in life-cycle optimization studies. An illustrative example of constrained optimization has been presented for the determination of the optimum stiffness parameters when the expected damage function includes only the consequences of non-catastrophic failure modes. In the example presented, the fundamental period of the system was used as a single control variable to determine its stiffness properties. The method presented can be easily extended to the more general case where all significant failure modes and design variables are handled simultaneously. It can be directly applied to the determination of optimum values of system properties for specific cases or for the establishment of codified recommendations for different types or groups of systems. In the latter case, the results of systematic optimization studies made on representative systems may need to be transformed into acceptable values of story distortions for earthquake excitations associated with given return intervals. The wide variability of the peak responses observed in the illustrative example presented above calls the attention to the necessity of studying the possible impact of that variability on both the optimum fundamental period and the resulting utility value.

The considerations in the last paragraph lead to identify the following promising lines for future research:

(a) Improving the methods used to estimate peak values of local and global distortions of nonlinear multi-degree-of-freedom systems with the aid of simplified reference systems, in order to obtain better estimates of the statistical properties of those variables for the practice of engineering design.
(b) Developing efficient methods for the sequential optimization of the strength and stiffness properties that determine the long-term performance of a structural system subjected to high seismic risk conditions.
(c) Developing structural design algorithms intended to lead in a systematic manner to the optimum values of the design parameters for specific cases, making use of the recommendations resulting from studies of general applicability for given types of structural systems.

Acknowledgements

This study was made with the support of CONACYT, the National Council for Science and Technology of Mexico, grant 31181U.

References

[1] Collins KR, Wen YK, Foutch DA. Dual-level seismic design: a reliability-based methodology. Earthquake Engineering and Structural Dynamics 1996; 25(12): 1433-68.

[2] Rosenblueth E. Optimum design for infrequent disturbances. ASCE Journal of the Structural Division 1976; 102(ST9): 1807-25.
[3] Reyes C. The serviceability limit state in the earthquake resistant design of buildings. Doctoral thesis (in Spanish), School of Engineering, National University of Mexico; 1999.
[4] Rosenblueth E. Point estimates for probability moments. Proc Nat Acad Sci USA 975;72(10): 3812-4.
[5] Díaz O, Esteva L. Seismic damage indexes in decisions related to structural safety. Proc. 7th IFIP WG7.5 Working Conference on Reliability and Optimization of Structural Systems, Boulder, CO, 1996.
[6] Chopra AK, Goel RK. A modal pushover analysis procedure to estimate seismic demands for buildings: theory and preliminary evaluation. Pacific Earthquake Engineering Research Center 2001; Report PEER2001/03.

Part 2
Invited contributions

Symposium invitees from left to right and bottom to top

Gustavo Ayala Milián, Sonia E. Ruiz, C. Allin Cornell, Vitelmo Bertero, **Luis Esteva Maraboto**, Anil K Chopra, Sergio M Alcocer, Eduardo Miranda, Rafael Riddell, Roberto Villaverde. Juan M. Espinosa, Enrique Bazán Zurita, Masayoshi Nakashima, Alain Pecker. Craig D Comartin, Polat Gülkan, Palle Thoft-Christensen, Roberto Meli, Jacobo Bielak, Shunsuke Otani, Mohsen Ghafory-Ashtiany, Keh-Chyuan Tsai, Armen Der Kiureghian, Daniel P. Abrams, Juan José Perez-Gavilán E, Mario G. Ordaz S. Niels C. Lind, Miguel P. Romo, Jorge Gutiérrez, Peter Fajfar, Francisco Sánchez Sesma, Ezio Faccioli, Bruce R. Ellingwood, Javier Alonso, Zifa Wang and Juan M.

Daniel P. Abrams
Willett Professor of Engineering
University of Illinois at Urbana-Champaign
2118 Newmark Civil Engineering Laboratory
205 N. Mathews
Urbana, Illinois 61801 USA
d-abrams@uiuc.edu

research interests: earthquake engineering, masonry structures

I have regarded Luis Esteva as a leading earthquake engineer of the world ever since I started in this field some thirty years ago. I am fortunate to have known him as a friend and colleague for most of this time. Being invited to participate in this symposium is indeed a great privilege and honor for me since I highly respect Professor Esteva as a scholar, an engineer, a researcher, a teacher, a very dedicated person to our field and most of all a gentleman. I still feel like a graduate student in his presence. He continues to serve as a role model for me.

Some words, simply spoken, can last a lifetime. I remember a discussion with Luis in Bogota while participating in one of the Colombian national conferences on earthquake engineering about two decades ago when he told me: “The answer is obvious - you just have to think!” In this day and age when computers do much of our thinking, program administration occupies our intellect and the quest for research funding is unending and paramount, I often think back on the wisdom of this statement. I think we, and our practice of earthquake engineering, would be much better off if we spent more time just “thinking” about the pertinent issues and their solutions.

Dan Abrams
September 12, 2005

THE CHALLENGE OF MITIGATING SEISMIC LOSS FOR VULNERABLE BUILDING CONSTRUCTION

ABSTRACT

A general overview is presented in this state-of-the-art paper on the challenge of assessing seismic risk across populations of vulnerable buildings and mitigating associated seismic loss. The premise of the paper is on seismic performance of unreinforced masonry constructed in the United States, but the theme of the discussion is appropriate to any population of building structure worldwide. Past work on this topic is summarized and recommendations for future research, development and implementation are given. Challenges to earthquake engineering researchers are discussed with an aim towards channeling international efforts at mitigating losses in future earthquakes through development of new technologies and implementation of them.

The Challenge

Despite decades of research on the topic, substantial damage, loss, injuries and deaths continue to be seen as a result of each new moderate or strong earthquake worldwide. Vulnerable buildings exist in nearly every urban and rural area across the globe. The potential is high for many of these buildings to incur major damage resulting in significant injuries, deaths and economic loss. Damage and/or collapse of unreinforced masonry buildings, or other non-ductile structures, has been observed since earthquakes have been reported and such damage and loss shall unfortunately continue in the future. This problem is bigger that what can be solved with the collective resources of any one country because vulnerable construction is ubiquitous and highly varied, technologies for response and damage estimation are not necessarily implemented, and motivations to mitigate seismic risk among building owners are secondary to more pressing demands of daily life. In this regard, challenges of reducing earthquake losses based on past research accomplishments and future technological frontiers were outlined by Abrams (1999). A concerted international effort towards seismic risk reduction can and should be done to minimize losses in future earthquakes. This development should include the following elements which are expanded upon in this paper to provide a sample of such a coordinated program.

(i) advanced technologies for defining inventories of vulnerable construction;
(ii) characterization of regional hazards with respect to intensity, occurrence, and spatial variations;
(iii) new methodologies for assessing dynamic response and damage to vulnerable construction;
(iv) new approaches for performance-based seismic rehabilitation; and
(v) outreach programs to educate design professionals and building owners with regarding seismic risk reduction.

Whereas research and development has been done along these lines in Mexico, the United States and other countries, a holistic, international approach to loss mitigation is needed that can only be developed through synergistic collaboration of researchers across political boundaries. This forum of the Esteva Symposium is ideal for putting forth elements of a possible research agenda that would have an impact on mitigating seismic losses to vulnerable construction in many countries worldwide. The challenge is to do this development at a sufficient rate so that losses may be mitigated before the next destructive earthquake occurs somewhere across the globe.

Identifying the Problem

Because the inventory of the built environment is so vast, quantification of the structural properties of every building, or even just the vulnerable ones, is beyond the realm of practicality with current technologies. Though in some sample areas, individual buildings have been surveyed with respect to structural type and number of stories, such reporting for all earthquake-prone areas is beyond budgets of local municipalities or other stakeholders. Methodologies need to be developed that will depict the loss potential across a population of buildings in terms of the most essential features of building systems and their likely distributions across a region of interest. An exploratory study was done in this regard for unreinforced masonry buildings by Omer Erbay (2004) as his doctoral dissertation at the University of Illinois. Elements from this study are presented herein.

An initial step in regional loss estimation is to identify the inventory of vulnerable construction and its location relative to the seismic hazard. As shown in the schematic diagram presented in Fig. 1, clusters of the same structural type are identified on maps (the upper left-hand rectangle in the figure) on which soil variations and earthquake intensities are over laid. Response of each category of building type subjected to the same ground motions is determined to estimate damage and loss for that locality which is then integrated over the entire region to estimate total loss. Methodologies need to be developed to distinguish vulnerable construction by structural type, identify the fragility of each building category on various soil types, and compute regional loss.

Characterizing the Hazard

Knowledge of the seismic hazard is fundamental to assessing the risk across a population of vulnerable buildings. In some areas of the world where earthquakes have

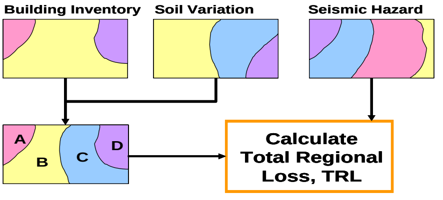

Figure 1. Scheme for grouping of buildings with respect to structure type, soil and ground motion

been recorded, such knowledge is well quantified, but this is the exception and not the rule. Speculation remains great with regard to the intensity, sequnce, frequency content, direction and spatial variation across a region of a future earthquakes. In lieu of a precise depiction of these parameters, loss estimates must be based on approximations. Thus, the accuracy of a loss estimate serving as the basis of a mitigation action plan is limited by the accuracy of representing these ground motion parameters. Such imprecision should be recognized before depicting response or damage of the structural system.

Spatial variation of soil properties across a region or population of buildings must be mapped to discern response and damage of clusters of a particular building type. Studies need to be done to determine if soil-structure interaction effects will be significant for a given type of structural system.

Inventories of Vulnerable Construction

Much of the construction which is vulnerable to seismic excitation has not been engineered, but rather simply built by tradesmen or building owners in accordance with local construction practices. This is particularly true for dwellings but also common for essential facilities such as hospitals, fire stations and emergency response centers. The lateral-force resisting system for these buildings may not be discretely identified (i.e. as a planar frame or shear wall system) since walls or infill panels are placed for architectural reasons, yet act as structural elements. Properties of construction materials are often uncertain and highly variable since their composition is dependent on workmanship, environmental conditions during construction, and availability of indigenous materials. These building systems may lack strength, ductility and/or energy dissipation capability to resist moderate or strong shaking. Moreover, buildings may be vulnerable because their structural systems do not follow conceptual ideals of a light roof, a symmetrical layout in plan of lateral-force resisting elements and floor mass, sufficient lateral strength of vertical elements and adequate connections between structural elements. Buildings with these attributes need to be categorized with respect to their structural type and fragilities.

One challenge is to assess the inventory of vulnerable construction with a minimum amount of rigor yet with an amount of precision consistent with identification of the ground motion parameters. Information gleaned from aerial photographs can identify the type of building from the shape of its footprint with some prior knowledge of the construction types in the region. For example, the rectangular shaped elements digitized

Figure 2. Using aerial photography to identify building populations. (sample from NOVA Digital Systems, Inc.)

in Fig. 2 can be associated with apartment buildings knowing that such buildings are prevalent in a given region. Then the age of construction can be assumed, again on the basis of prior knowledge of typical construction patterns in a specific region. Seismic strength according to codes of that vintage can then be estimated. As well, the number of stories of a group of buildings can be estimated either directly from the aerial photographs, or from inference of what building types should be expected in the region. In this manner, a building inventory data base can be constructed for the purpose of loss assessments. Development of this approach needs to be expanded to include rapid inventory identification techniques for each category of vulnerable building within a region of interest.

In addition, aerial photography can be used to assess damage following earthquakes. Technologies developed by the military have been used for such damage surveys in the past. Results of a correlation study, done after the 2002 Molise earthquake (Fig. 3), demonstrate the correlation between photographed damage and categorization of damage levels observed in the field. Such calibrations should be continued after future damaging earthquakes to refine these procedures.

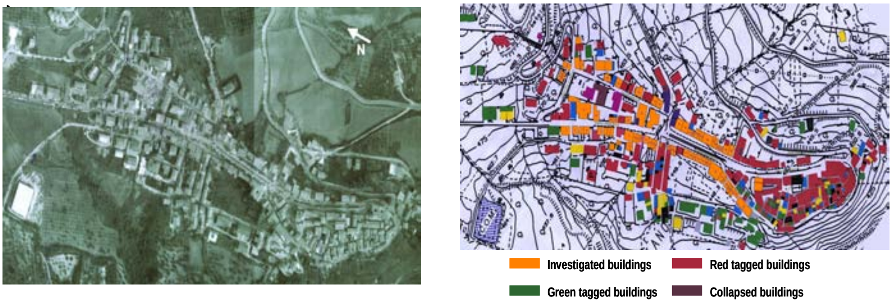

Figure 3. Aerial photograph and damage survey for town of Molise, Italy after November 2002 earthquake (from Erbay, 2004)

Essential Features of Dynamic Response

Computational modeling of dynamic response for each building in a wide population cannot be done. However, computational models can be used to determine response of idealized structures of each building type or category. Such models can be used as the bases for parametric studies from which key features of structural systems are identified. Much of past research on seismic performance of masonry building systems has concentrated on dynamic response of such systems to earthquake motions. In addition to static load reversal tests of masonry pier or wall elements, shaking table experiments of reduced-scale structures have been done to develop and confirm computational models. Results of such research for low-rise buildings constructed of unreinforced masonry have concluded with recommendations for modeling dynamic response as noted below.

Unlike the near-ideal frame or wall structures with rigid floors that are modeled with lumped masses on a vertical stick, and used as examples in many texts on structural dynamics, the majority of vulnerable construction is one or two stories with the floor or roof mass distributed in plan. Thus dynamic response is comprised of essentially two modes of vibration – one as a result of the flexibility of the vertical elements and the other a result of the flexibility of the horizontal elements. Adjustment of diaphragm stiffness and mass, or natural frequency, with that of the vertical elements is thus one method of controlling the amount of inertia force attracted to the system. Walls situated normal to the earthquake excitation may also result in some distress if deflected out-of-plane by flexible diaphragms. Damage models need to be developed that incorporate these dynamic characteristics.

Early research investigating nondestructive evaluation methods by Epperson (1992) explored strength, stiffness and deformation capacity of unreinforced masonry shear walls. This was followed with a study by Tena-Colunga (1995, 1996) of response measurements for an actual, two-story unreinforced masonry building in Gilroy, California, taken during the 1989 Loma Prieta earthquake. This study showed that ground and shear wall accelerations were greatly amplified by floor or roof diaphragms responding at their own frequency within the horizontal plane. Accelerations were high at approximately 1.0g for these diaphragms, yet little damage was observed to masonry walls since base shear forces were much less than lateral strength of the unreinforced masonry shear walls and piers.

A follow-up study of the Gilroy building was done by Costley (1996) where he constructed an idealized two-story unreinforced brick building at half scale for the purpose of testing to near collapse on the University of Illinois shaking table. Unlike the moderate Loma Prieta motions, Costley could excite his test structures with base motions that would incur substantial nonlinear behavior in the masonry structural elements. The predominant mode of response was rocking of the piers between window or door openings at the first story (Fig. 4) which resulted in a non-linear, but elastic response of the structure. Following even the most intense earthquake motions, bed-joint cracks at the top and bottom of these piers closed as a result of gravity stress and thus little damage was observed. Such displacement-controlled behavior is contrary to what is commonly perceived for unreinforced masonry construction. Furthermore, the simultaneous occurrence of rocking piers with vibrating floor diaphragms results in a role reversal for the floor diaphragms acting as a relatively flexible or rigid element. Findings based on measured response of these test structures are given by Abrams (1997). Costley's tests were also replicated with full-scale static tests done at the University of Pavia in Italy which provided correlations between large and reduced-scale tests as well as dynamic versus static testing, both of which have limitations for earthquake engineering research.

Fig 4. Rocking piers of shaking-table structure

Further research studies of seismic behavior of unreinforced masonry building systems at the Georgia Institute of Technology (Moon, 2003) and the US Army Construction Engineering Laboratory (Orton, 2003) in Champaign, Illinois, examined three-dimensional system effects. With financial support from the NSF-sponsored Mid-America Earthquake Center, companion full-scale static tests and half-scale dynamic tests of an idealized two-story, unreinforced brick building system (Fig. 5) were completed. As for the earlier research at the University of Illinois, these tests confirmed the benefits of a displacement-based rocking mode for individual piers and walls as well for the overall structural system. Measured relations between base shear and the roof displacement, as shown in the figure, revealed stable and ductile behavior when subjected to reversals of lateral displacement.

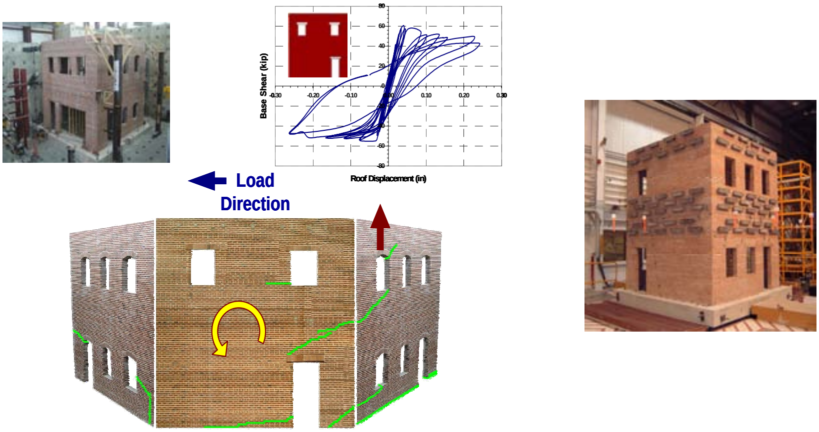

Figure 5. Full-scale static test of URM building system and counterpart half-scale test structure on shaking table

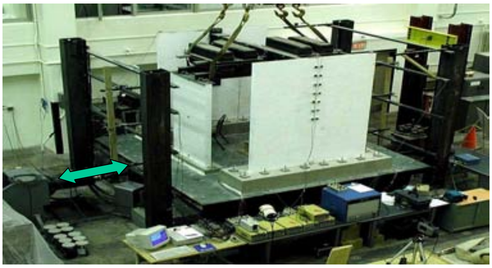

Figure 6. Test of dynamic stability for URM bearing wall structures

Because bearing walls may be excited normal to their plane by inertial loadings as well as being distorted by flexible diaphragms, an experimental study was done to investigate dynamic stability of such walls by Simsir (2004). A symmetrical system consisting of two unreinforced masonry bearing walls, two masonry shear walls and a flexible diaphragm spanning between them (Fig. 6) was constructed at half scale, and subjected to simulated earthquake motions on the University of Illinois shaking table.

Test results showed that because of rocking at the base of the out-of-plane walls, horizontal motions imposed at their top by the flexible diaphragms could be accommodated. Little damage occurred despite the intensity of the ground motion. Dynamic response could be modeled with two degrees of freedom representing translations of the diaphragm mass and wall mass. A conclusion from this study was that even slender walls (with a height-to-thickness ratio exceeding 20) could sustain large transverse accelerations provided that they were well connected to the vibrating diaphragms.

Essential Parameters for Characterizing Performance

Based on the knowledge gained through the research studies mentioned in the preceding section, and using computational models based on experimental results, an extensive parametric study was done by Erbay (2004) to investigate the essential

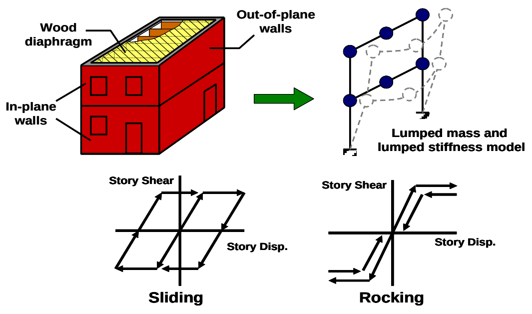

Figure 7. Nonlinear dynamic analysis model for URM buildings

parameters which influence dynamic response and thus damage or performance for vulnerable low-rise buildings constructed of unreinforced masonry.

A computational model capturing the most essential dynamic response characteristics was chosen for the parametric study as shown in Fig. 7. The model lumped both mass and stiffness at a minimal number of degrees of freedom to represent diaphragm vibration as well as in-plane response of shear walls. Nonlinear shear wall properties were varied so that sliding shear mechanisms as well as rocking mechanisms could be examined. Based on thousands of computational runs where the building system, materials and base motions were varied, the following parameters (in rank order with most important first) were identified.

1. number of stories
2. floor area
3. floor aspect ratio in plan
4. story height
5. wall density (wall area divided by floor area)
6. pier height-to-length aspect ratio
7. floor gravity loading
8. elastic and shear moduli of masonry

A methodology to assess loss across a population of low-rise masonry buildings should include collection of inventory information with regard to at least the first four of these parameters. To examine how each of these four parameters can vary across actual populations, data was collected for five case study regions which is summarized in Fig. 8. Data for Memphis and Carbondale were collected by Steve French and Rob Olsansky through a Mid-America Earthquake Center project, while data for San

Francisco was reported on by Bill Holmes and Bret Lizundia in a report published by their firm, Rutherford and Chekene. Data on Urbana was collected by Omer Erbay as part of his doctoral dissertation as was a data collection effort in Molise, Italy. As seen in the figure, the variation of each parameter is similar for each building population. This suggests that a regional loss assessment can use a standard signature trace of these

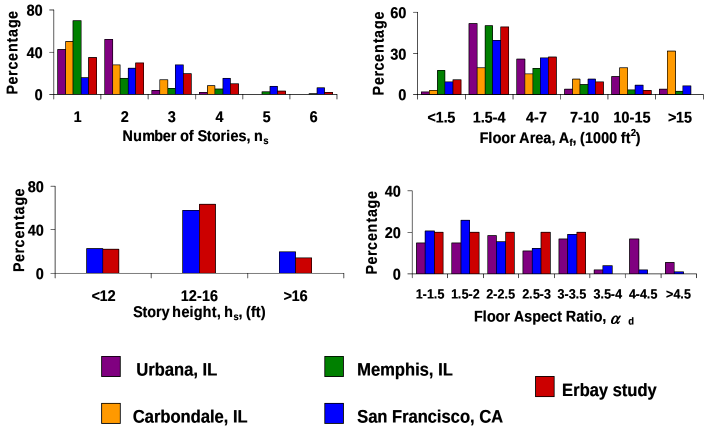

Figure 8. Variation in building attributes for different regions

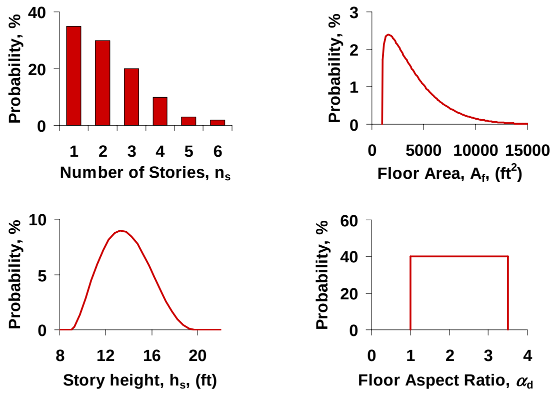

Figure 9. Idealized variation of building attributes

parameter variations in lieu of discrete information collected in the field, provided that the building inventory is somewhat typical. This concept is illustrated in Fig. 9 where idealized variations of these four critical parameters are shown. Using such standard distributions, regional loss can be scaled with respect to the number of buildings in the region, or even more gross parameters such as the number of people living in a community. Again, this is an approximate method for assessing loss with a precision no less than that of characterizing the ground motion. Further development needs to be done to define such parameter distributions for other building populations than unreinforced buildings in typical communities in the United States and other countries. Yet the fundamental basis of the methodology is the same for modeling seismic loss of vulnerable buildings in the world.

Choices for Effective Rehabilitation

Much effort has been done on developing standards for seismic rehabilitation of existing buildings. One document in the United States, developed with support of the US Federal Emergency Management Agency (FEMA, 2000), is the first document of its kind to address performance-based seismic rehabilitation of existing buildings. Known as "FEMA 356" this prestandard includes one chapter on systematic rehabilitation of masonry buildings, including those constructed without reinforcement.

Performance-based engineering concepts for unreinforced masonry buildings in accordance with this chapter are discussed in Abrams (2001). Much of the guidance given in this chapter is on ways to assess likely seismic performance and includes information on modeling URM buildings with static and dynamic, linear and nonlinear computational models. The simplest response analysis is a linear static procedure where seismic demand forces, Q_E, are estimated for individual wall or pier elements based on an elastic analysis. Corresponding element capacity is the product of the element strength, Q_{CE}, times displacement capacity, m, as noted with Equation 1.

$$mQ_{CE} < Q_E \tag{1}$$

For pier or wall elements constructed of unreinforced masonry, the m factor can exceed unity and be as large as ten or more, if the element is prone to rocking or bed-joint sliding which are considered as displacement-controlled actions. If the element is governed by a force-controlled action governed by toe-compressive stress or diagonal tensile stress (cracking through the masonry unit rather than the mortar bed joint) then no displacement capacity is assumed, and the m factor is limited to a value of 1.0. This is the first time that ductility of an element is explicitly considered in a set of rehabilitation requirements, and also the first time that ductility of unreinforced masonry is considered. The implication of this new approach is that masonry buildings may not be as vulnerable as previously thought. Building systems with masonry piers which will rock or slide, accepting displacements imposed upon them, may not necessary need to be rehabilitated. Further research on this topic may likely lead to substantial cost savings for future seismic rehabilitation projects.

Rehabilitation strategies need not be limited to strengthening of individual components. Rather, deformation capacity can be enhanced in critical components. A weaker, but more ductile structure may result in better performance than simply a stronger one. In some cases, strength can be traded for ductility to enhance overall performance.

Undesirable interventions should be avoided at all costs. Structural components that are governed by displacement-controlled mechanisms such as rocking or bed-joint sliding should not be rehabilitated to alter their behavior to a force-controlled mechanism. Contrarily, desirable interventions should be strived for where force-controlled components are rehabilitated to respond in displacement-controlled modes.

Whereas the FEMA pre-standard provides methods for estimating strength and deformation capacity of existing URM walls and piers, they do not provide such information for components rehabilitated via different means. A follow-up document by Lizundia (1993) on a study funded by the National Institute of Standards and Technology provides recommendations for modeling strength and deformation capacity of masonry components rehabilitated in a number of different ways. The Mid-America Earthquake Center has added to this knowledge base where an exploratory investigation (Abrams, 2005) was done to examine the relative merits of various rehabilitation options for modifying behavior of unreinforced masonry piers. This study examined both strength and deformation capacity enhancements using shotcrete overlays, ferrocement surface coatings, reinforced and prestressed cores, and adhered FRP strips. This study contrasted performance with that of plain, unrehabilitated piers with a rocking mechanism. In nearly all cases the benefits of rocking on displacement capacity were superior to that of any of these options. Thus a good evaluation acknowledging nonlinear ductile behavior of piers can be better than making an expensive investment in strengthening. Further research should be done to assess the impact of acknowledging these displacement-controlled actions on mitigating earthquake losses.

Accepting Risk and Taking Action

Damage can be minimized through proper mitigation practice that relies on acknowledgement of the mechanisms and damage patterns addressed above. However, before an engineering assessment is done, the following questions need to be resolved between the building owner and the engineer or architect that will influence the decision-making process regarding whether rehabilitation should be done or not.

- Should an investment be made in rehabilitation? Will the reduction in risk be commensurate or less than the engineering and construction costs, or will rehabilitation costs exceed the anticipated benefits?
- What levels of performance are desired by the owner of the building? Should the building be safe against loss of life or against collapse? Does the building need to be occupied immediately following an earthquake, or do operations within the structure need to be maintained? Are there critical non-structural components (electrical, plumbing, heating, ventilating, partitions, etc.) or vital contents that must be protected against damage?
- Where is the building located with respect to expected seismic intensities, governing building codes, accepted performance levels, or integration within regional economic systems? Rehabilitation techniques which are appropriate near the earthquake source may be impractical far from a fault. Seismic regulations differ depending on location, thus requirements for seismic capacity may vary.
- Once decisions have been made regarding these issues, then an engineering practitioner can prescribe rehabilitation measures that will meet a specified level of performance for seismic demands that will be the most economical for the desired constraints. The remainder of this paper discusses research supporting such performance-based concepts.

A current effort funded by FEMA and coordinated by the Applied Technology Council (project #58) on development of methods for performance-based rehabilitation is examining stakeholder concerns similar to those mentioned above. Future international programs on mitigating seismic loss should include a component examining how specific cultures recognize seismic risk and takes action to reduce it.

Concluding Remarks

Mitigating seismic loss for vulnerable building construction requires an interdisciplinary approach involving seismologists, engineers, constructors, economists, and public policy experts. Methodologies need to be refined to improve on the practicality, ease of use, and accuracy of loss estimates across a region of vulnerable construction so that mitigation action plans can be more easily proposed, assessed and implemented. Loss estimates for sample case study regions need to be done using these refined procedures to assess the likely risk levels and the impact of various rehabilitation measures on reducing such risk. In the event that future earthquakes occur across inventories of vulnerable construction which can be easily depicted, calibration of such methodologies should be pursued. Finally, building owners and other stakeholders need to be educated with respect to such assessment tools and rehabilitation options so that they can reduce their seismic risk accordingly and appropriately.

Such a methodology should be developed independent of the types of construction in any particular country so it will serve as a universal, shared-use procedure for mitigating risk. Thus, research should be done by an international team supported with funds provided by various nations and international agencies. Because earthquakes are not confined by political boundaries, research on mitigating seismic risk should be an international effort.

Acknowledgments

Much of the research referred to in this paper was supported by the Mid-America Earthquake Center headquartered at the University of Illinois at Urbana-Champaign. The MAE Center is supported by the National Science Foundation through the Earthquake Engineering Research Centers Program under award number EEC-9701785. Appreciation is extended to the following graduate research assistants at the University of Illinois for their assistance with much of the research described herein: Shaun Franklin, Omer Erbay, Jaret Lynch, Sarah Orton, Can Simsir and Tracy Smith, as well as their predecessors Tom Paulson, Arturo Tena-Colunga, Gary Epperson and Andrew Costley.

References

Abrams, D.P. (1997). "Response of Unreinforced Masonry Buildings," *Journal of Earthquake Engineering*, Imperial College Press, 1(1), 257-273.

Abrams, D.P. (1999). "Meeting the Challenges of Reducing Earthquake Losses: Engineering Accomplishments and Frontiers," *Earthquake Spectra*, Earthquake Engineering Research Institute, 15(4), 813-823.

Abrams, D.P. (2001). "Performance Based Engineering Concepts for Unreinforced Masonry Building Structures," *Journal of Progress in Structural Engineering and Materials*, Wiley Interscience, 3(1), 48-56.

Abrams, D.P., T. Smith, J. Lynch, and S. Franklin (2005). "Effectiveness of Rehabilitation on Seismic Behavior of Masonry Piers," *Journal of Structural Engineering*, American Society of Civil Engineers.

Costley, A.C., and D.P. Abrams (1996). "Dynamic Response of URM Buildings with Flexible Diaphragms," National Center for Earthquake Engineering Research, *Technical Report NCEER-96-0001*, 298pp.

Epperson, G.S., and D.P. Abrams (1992). "Evaluating Lateral Strength of Existing Unreinforced Brick Masonry Piers in the Laboratory," *Journal of The Masonry Society*, 10 (2), 86-93.

Erbay, O.O., and D.P. Abrams (2004). "A Methodology to Assess Seismic Risk across Populations of Unreinforced Masonry Buildings," *Proceedings of 13th World Conference on Earthquake Engineering*, Vancouver.

FEMA, *Prestandard and Commentary for Seismic Rehabilitation of Buildings* (2000). Federal Emergency Management Agency report 356/357, Washington, D.C.

Lizundia, B., W.T. Holmes, M. Longstreth, A. Kren and D.P. Abrams (1997). "Development of Procedures to Enhance the Performance of Rehabilitated URM Buildings," National Institute of Standards and Technology report prepared by Rutherford and Chekene Engineers, San Francisco.

Moon, F. L. , T. Yi, R. T. Leon, and L. F. Kahn (2003). "Large-Scale Tests of an Unreinforced Masonry Low-Rise Building" *Proceedings of the Ninth North American Masonry Conference*. Clemson, SC.

Orton, S.L., D.P. Abrams, and J. Hayes (2001). "Performance of Rehabilitated Unreinforced Masonry Building Systems," *Proceedings of 9th Canadian Masonry Symposium*, University of New Brunswick.

Simsir, C.C., M.A. Aschheim and D.P. Abrams (2004). "Out-of-Plane Dynamic Response of Unreinforced Masonry Bearing Walls attached to Flexible Diaphragms," *Proceedings of 13th World Conference on Earthquake Engineering*, Vancouver.

Tena-Colunga, A., and D.P. Abrams (1995). "Simplified 3-D Dynamic Analysis of Structures with Flexible Diaphragms," *Journal of Earthquake Engineering and Structural Dynamics*, 24 (2), 221-232.

Tena-Colunga, A., and D.P. Abrams (1996). "Dynamic Response of Building Systems with Flexible Diaphragms," *Journal of Structural Engineering*, 122 (4), American Society of Civil Engineers, 439-445.

Mohsen Ghafory-Ashtiany
Professor and President
International Institute Of earthquake Engineering and Seismology (IIEES)
26 Arghavan st., N. Dibajie, Farmanieh
Tehran, 19537, Islamic Republic of Iran
ashtiany@iiees.ac.ir

Research Interest: Risk Management, Earthquake engineering, Structural dynamics, Random vibration, Seismic hazard assessment.

The worth of an individual and the merits of a scientist and teacher can be assessed through his wisdom, capabilities, leadership and ultimately in his high moral and social fiber. I have known Luis Esteva since the 1970's through his works, from the '80's through conferences, and the '90's by working with him after the Manjil earthquake in Iran. I can testify that Luis will always be recognized as a devoted scientist with the highest human values.

Luis's vision and contributions to seismic hazard analysis, earthquake engineering, building code development and risk reduction implementation—which are well-known—have contributed to the saving of countless lives. What better contribution can a man make in life?

After the June, 1990 Manjil earthquake in Iran, Luis became the technical expert for the World Bank Reconstruction Project in Iran. I have worked closely with him for the development of the Earthquake Hazard Mitigation Program in Iran. When we, for the first time, proposed that 5-10% of the reconstruction loan for WB projects be devoted to research and development, it was through his support that this new initiative was approved. Since then, it has become an integral part of all WB reconstruction projects.

His foresight, contributions to and leadership in the design of the Earthquake Hazard Mitigation Program in Iran made the Manjil earthquake a turning point in risk reduction in Iran, as was his cooperation in the First International Conference Seismology and Earthquake Engineering (SEE-1) in May 1991, attended by more than 1,200 young scientists with strong desires to reduce the earthquake risk in their country. I could mention many more experiences--each one of them contributing to saving lives.

Finally, Luis's calm, humble, sincere, cooperative, helpful and friendly behavior (characteristics of a true teacher) make a him an unforgettable gentleman. I believe that it is his great worth and high moral fiber that prevents Luis from growing old. For as long as I can remember, he hasn't changed.

I wish you a long, healthy and fruitful life, dear Luis.

Ghafory-Ashtiany, M

Mohsen Ghafory-Ashtiany,
6 September 2005

Luis Esteva

First International Conference on Seismology and Earthquake Engineering (SEE1), May 1991. Tehran-Iran



11th World Conference on Earthquake engineering, Acapulco-Mexico, 1996

THE NEW LOOK AT EARTHQUAKE ENGINEERING: SIMPLIFICATION OF THE COMPLEX PHENOMENON

Natural phenomenon act out of our control and most of the time environment and people do not act as how they have been instructed. The existing know-how, research, guidelines, codes, recommendations are not completely being used or being implemented or put on the ground. Quick overview on the past events can verify this claim. After each major earthquake, it has been commonly concluded that: It was a surprising earthquake in sense of ...; The ground motion characteristics was different and it was not expected; Soil behavior and soil-structure interaction was different than it was expected; Failures were due to poor design and construction and due to ignorance of the ABC's of engineering principal, Further code modification, and more code reinforcement is required; and Finally more research and funds are needed. This scenario will be repeated after each earthquake.

To overcome this issue, I believe that "Earthquake Engineering Scientist" should changes their views on the present methodologies and approaches toward simplified, doable, affordable and socially accepted solutions that answers the peoples need in a more directed and to the point approach.

Analysing the success of the medical doctor and their influence on the most of the people and creating an acceptable level of trust between the doctor and the patient, shows that most of the peoples demand are being solved by simple solution and use of almost deterministic solutions which are based on pharmaceutical research going back to Ave-Sina time. Prescription of medicine to a human body with more complexity that earth interior is what engineers should envisage doing for the safety of the built environment using new technologies such as nanotechnology, smart materials, etc. If the simple answers or understandable solutions to become available to the people, they will act different. Definitely majority of the people could not effectively use the existing manuals and guidelines since they do not understand. They have never understood the cause of many diseases, but they have used the prescribed medicines due to the confidence and trust that has built (in most cases) between the doctors and people through history.

We need to classify the engineering issues and provide answers compatible to the level of the knowledge and expertise of the respective implementer and users. Special structures require special class of engineering and should be dealt with highest accuracy and reliability. However, common cases such as housing which carry most of the losses during earthquake should be dealt in prescriptive and simplified and easy-to-do solutions and manners. There is millions of housing units of un-reinforced masonry, wooden, adobe and non-engineered buildings with similar deficiency exist around the world. Can we develop 1-2-3 or A-B-C solutions for their upgrading and improving their safety which can be done by any households? We should not expect these people to ask an engineer to come and make the safety evaluation and after many calculations and drawings bring an unaffordable solution that can never be used or applied. The occupant of these housing units, if they had money they would not live in unsafe buildings. Even for an easier case, affordable housing models that low income people in the rural areas of the world can use without being forced to violate the codes due to the lack of funds. We have not even been fully successful in convincing the decision makers. I know that all of these are not due to our incapability, but it is our duty to provide answers, since we know.

On Risk Communication:

More-over the medical doctors have learned to communicate with general public better (in most cases) than the earthquake engineers in creating concern and sensitiveness on health related issues. I believe that more efforts are required in having an effective earthquake risk communication. This requires simplification on risk mapping and risk communication methodologies and having an innovative educational approach. The trust can be achieved through vulgarization or simplification of earthquake engineering knowledge. This is one of the hardest challenges ahead of us. As an example: Looking at the holy books such as Quran, Bible or any long lasting books such as Shakespeare, Hafez or Moulavi’s poem, we can see that even though they address complex and advance topics, but it can be easily read, understood and used by the people. Since they are multidimensional text, every body understand to its level of knowledge. These texts have been created by experts with highest level of know-how. It is the fact that the simplification of complex phenomenon requires highest level of expertise. Great people always talk simple, while newly taught expert talks complicated. We are talking complex since our knowledge are not enough or we have not diverted our knowledge in that direction. We always try to complicate the methodologies, by adding new factors and new issues, which are absolutely required, justified and correct for complex and special structures; but we have not tried to simplify our approaches for simplified and common cases such as housing units. I strongly believe that for unknown phenomenon such as earthquake, the simplified look at the problem is better.

In conclusion, the effective and innovative program should emphasize on the translation of current know-how into simplified options. In other word the most progressed and developed sciences should be evolved in the most simplified, understandable and doable culturally acceptable instructions. Its implementation requires not only a multi-disciplinary approach, but also a comprehensive educational program for all people that are involved in the implementation of the seismic risk reduction measure. The key factor in the above actions is defiantly innovative approach and changing our views as well as being patient in achieving our goals.

Amado Gustavo Ayala Milián
Research Profesor
Instituto de Ingeniería, UNAM
Mexico D.F 04510, MEXICO
GAyalaM@iingen.unam.mx

Earthquake Engineering and Computational Mechanics

I regard Luis Esteva with high esteem as a great master of the practice of scientific research in engineering. And am honoured to have him as a friend and teacher. As a peer and former student, I am proud to participate in such a memorable event, the celebration of his 70th birthday. What precisely has Luis done to contribute to my education as a researcher? Since the very first moment I met him he has always been a genuine intellectual, inspiring me to be rational in my actions and to maintain the highest of standards in whatsoever I am involved. Luis was one of my teachers at undergraduate level, however, his apparent shyness and coolness did not allow his merit to shine through. Shortly after starting my graduate work, I became one of his research students and it was then that I really began to know him, finding him a delightful person to work with. There was little doubt that with Luis I had a fine and dedicated teacher who was focused on his students and their learning, an outstanding and active researcher, a wonderful role model and mentor for students, and a genuine and honest person. He is reliable and works hard in whatever assignment or task he is involved. To me Luis is one of the shining examples of the members of our Institute responsible for paving the way towards a very bright future as a research institution in engineering. I sincerely hope that we can continue to celebrate with Luis- the person, the teacher and the scientist- through our collective efforts to reach excellence in education and research.

Thank you Luis, for everything up till now and for the years to come.

A Gustavo Ayala
12 September 2005

PERFORMANCE BASED SEISMIC EVALUATION AND DESIGN OF STRUCTURES – A UNIFIED APPROACH

ABSTRACT

This paper presents a new seismic evaluation and design procedure for structures in agreement with the performance-based seismic design philosophy. Throughout the paper, the aims and limitations of current seismic evaluation and design practice and the tendencies of the performance-based seismic design are discussed. The procedure considers the non-linear behaviour of the structural elements, performance indices of current design codes, uniform hazard design spectra and in the case of 3D buildings bi-directional earthquake action. To illustrate the application of the seismic evaluation procedure a typical reinforced concrete plane frame irregular in elevation and designed in accordance with the latest version of Eurocode 8 is used as example. For the illustration of the seismic design procedure an asymmetric building located in Mexico City is designed for a basic design objective with a life safety performance level and a design level corresponding to a design spectrum with a given exceedence rate of the chosen performance index. For validation purposes, results of non-linear step by step analyses of the chosen examples are presented and discussed regarding the potential of the procedure to produce expected global but not necessarily local performances.

Introduction

The occurrence of destructive earthquakes in recent years all around the world, e.g., Mexico City (1985), Loma Prieta (1989), Northridge (1994), Kobe (1995), Turkey (1999) and Taiwan (1999), has made evident that seismic evaluation and design methods proposed and used by current codes do not always provide the safety levels and performance expected when the structures are subjected to design demands.

To overcome this problem, during recent years research efforts have been devoted to develop new seismic evaluation and design methods based on the performance of the structures, aimed to provide better predictions of the performance of structures, closer to the real performance that the structures would undergo when subjected to different seismic demand levels throughout their life span. The actual tendency in the seismic evaluation and design of structures is to use simplified non-linear analysis methods which incorporate in a realistic and explicit way the geometric and behaviour characteristics of the structures to approximately predict their seismic performances for evaluation or design purposes.

This paper presents a new procedure for the seismic evaluation and design of structures in agreement with the current tendencies of the performance-based seismic design philosophy. In the case of design, this procedure offers the possibility of satisfying different performance parameters used to define the design performance level, controlling the damage corresponding to a considered seismic demand given by a design spectrum for a given rate of exceedence of a chosen performance parameter. The proposed procedure is applied to the seismic evaluation of a reinforced concrete frame irregular in elevation and to the performance based seismic design of a reinforced concrete mass asymmetric reinforced concrete building. The results obtained for both buildings are discussed when their found or aimed performances are compared to those obtained using non-linear step by step dynamic analyses.

Performance Based Seismic Evaluation

One of the current challenges of seismic evaluation of structures is to predict, as accurately as possible, the performances that they will exhibit when subjected to design seismic demands, all this considering the non-linear behaviour of the materials, realistic dynamic properties and consistent seismic demands. The answer to this challenge is not an easy task, currently there exist two accepted options for the evaluation of seismic performance, one based on non-linear dynamic step by step analyses (NLDA) with a pre-assigned set of seismic demands, and the other, based on simplified non-linear static analyses (NLSA) methods with the same set of seismic demands or in a more direct way using smooth spectra.

In the first option, the results are obtained using NLDA may be considered as the “exact” results of the response of the structure to one or several earthquake records consistent with the design seismic demand. This option has the advantage of being analytically robust, but the disadvantages of being based on methods of high technological complexity, not commonly known by design engineers, and of giving responses to a limited set of seismic records, presumably obtained from catalogues, generally incomplete, to assure the statistical validity of the obtained results. Although this last disadvantage may be circumvented using a family of synthetic records compatible with the design spectrum, this option is still open to discussion and widely used among researchers. It is important to mention that the main disadvantage of using NLDA is that it involves an expensive process, due to the significant computational and human resources involved in the determination and evaluation of the massive amounts of results derived from the calculations, nevertheless, availability of more efficient computational tools and better education of practicing engineers show the ever increasing weakness of this limitation.

In the second option, justified by the apparent limitations of the first option, simplified NLSA procedures are used as evaluation methods. Evidently, this is an easier option than the NLDA as the methods used are based and developed using simpler concepts. These methods are generally based on the existence of a capacity curve of a structure, generally determined from a pushover analysis using a predetermined distribution of lateral loads, or, depending on the method, from an adaptive distribution of lateral forces. The basis of this type of methods was originally given by Freeman (1975), who proposed a simplistic and partly heuristic evaluation procedure which considered only the contribution of the fundamental mode to the response of the structure. This procedure was later named the Capacity Spectrum Method in documents such as the ATC-40 (ATC 1996). Other examples of NLSA procedures which only consider the contribution of the fundamental mode are that presented in FEMA-273 (FEMA, 1997) and the N2 method (Fajfar and Gaspersic, 1996).

For the same purpose, methods that consider the contribution of higher modes of vibration have also been developed; among which are the evaluation method proposed by Requena and Ayala (2000), the Modal Pushover Analysis (Chopra and Goel, 2000) and the Incremental Response Spectrum Analysis (Aydinogliu 2003, 2004). More recently the results of the ATC-55 Project (FEMA-440) were published by FEMA (2005) containing practical recommendations for improved prediction of the inelastic structural response of buildings to earthquakes.

This paper presents and exemplifies a new integrated method for the seismic performance evaluation and design of structures, which considers the contribution to the performance of higher modes of vibration and uses a smooth response spectrum as design seismic demand. The development of this integrated method was aimed to provide structural engineering practitioners with a simplified seismic evaluation and design methodology, based on readily available knowledge and applicable with commercially available analysis tools, e.g., SAP 2000 (CSI, 2000). The evaluation option of the method as presented may be considered as an evolution of the evaluation method proposed by Requena and Ayala (2000) and formalized by Isaković et al., (2005) for its application to bridges, and for design purposes, an evolution of the method originally proposed by Ayala (2001) for structures with single-mode dominated performances and by Basilio and Ayala (2001) for multi-mode dominated performances.

The most important characteristic of the method is its simplicity as it considers the contribution of higher modes of vibration using existent modal combination rule and constructs the non-linear behaviour curve using evolving modal spectral analyses with modal information corresponding to structures in different damage stages. The method as developed cannot be considered a NLSA method because strictly speaking a pushover analysis is never performed for the construction of the behaviour curve, normally extracted from the capacity curve of the structure which in this case is not required, this characteristic is also present in other methods of evaluation such as that proposed by Aydinogliu (2003) an a number of other authors. The procedure involves four main steps:

Definition of the seismic demand. The seismic demand is defined by a smooth response spectrum corresponding to a chosen seismic demand level. This definition has some advantages as this is the normal way in which it is presented in most current seismic design codes. This spectrum represents the envelope of the response spectra from many seismic records of various intensities, generated at different sources.

Construction of the behaviour curve. The behaviour curve of a reference system is constructed by a series of modal spectral analyses (MSA) each producing an evolving state of damage corresponding to different levels of seismic intensity. The influence of higher modes of vibration in the capacity curve, needed to construct the behaviour curve of the reference system, is taken into account by the modal combination rule (e.g., SRSS or CQC). In this work, a state of damage is updated in the analytical model by adding moment releases at the end sections of the elements which reach their elastic capacity. In principle a new state of damage could be defined every time a plastic hinge is formed, however, for practical applications it is advised to use a reduced number of damage states to avoid the hassle of dealing with an excessively refined behaviour curve. A flowchart for the construction of the behaviour curve is presented in Fig. 1.

Determination of the performance spectral displacement. The inelastic displacement demand of the reference system, here called performance spectral displacement, Sd^*, is calculated using the equal displacement rule, Veletsos and Newmark (1960), with proper consideration of its short periods correction, CEN (2003a).

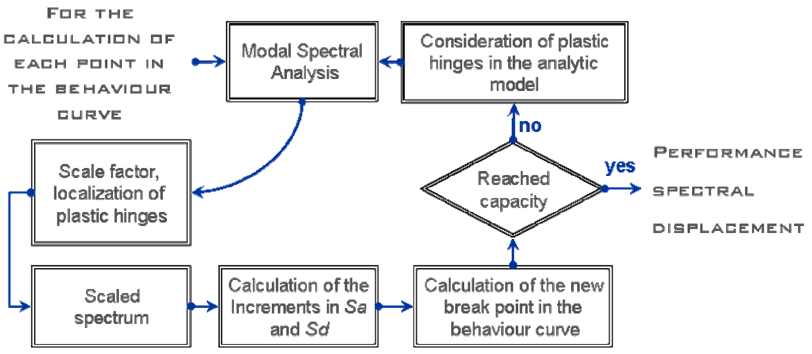

Figure 1. Algorithm for the construction of the behaviour curve

This rule has the drawback of being only valid for firm soil conditions needing more research results for its generalization to soft soil conditions (Ruiz-García and Miranda, 2004). The calculation of the seismic performance of the structure is carried out by summing the scaled responses corresponding to each modal spectral analysis performed.

Performance Based Seismic Design

The PBSD procedure proposed in this work has as basis the method originally developed by Ayala (2001). It involves two main stages: the construction of the behaviour curve associated to a single degree of freedom reference system and the determination of the design forces in the elements by means of ad hoc modal spectral analyses (MSA). The overall design process for a performace level defined by a design ductility is illustrated in Fig 3.

Construction of the behaviour curve. The behaviour curve of a reference system corresponding to the mode of the structure with the highest contribution to the response is constructed by considering two structures with different dynamic properties: one with properties derived from the structure without damage corresponding to a pre-designed structure; the other, the same structure with reduced properties to incorporate a proposed damage distribution expected to occur under design demands.

Determination of the design forces. The distribution of the global lateral strength to the structural elements of the building is carried out by means of modal spectral analyses corresponding to the two performance stages considered with a design elastic spectrum reduced by factors Fe and Fi, defined from the strengths of the elastic system, R_e, as illustrated in Fig. 2.

The overall design process for a performace level defined by a design ductility is illustrated in Fig. 3.

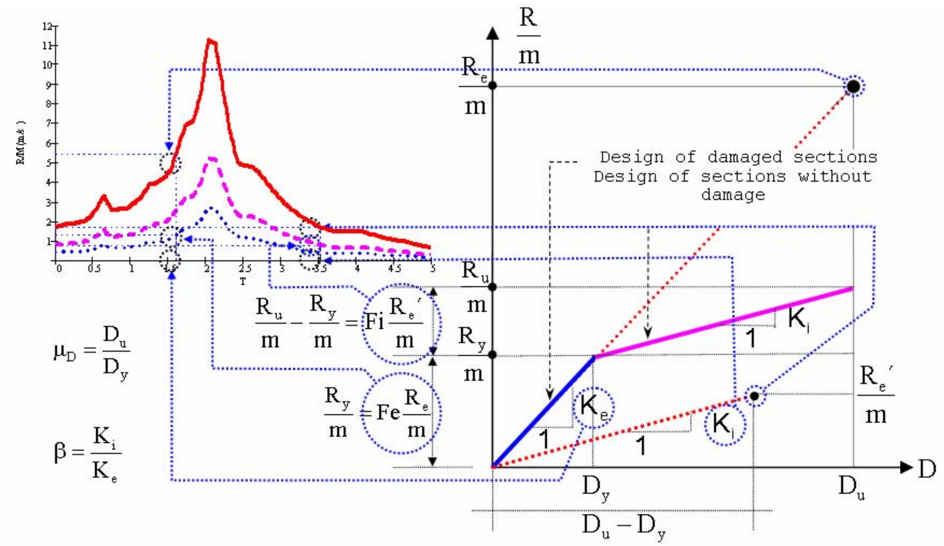

Figure 2. Factors Fe and Fi characterizing the reduction of elastic force

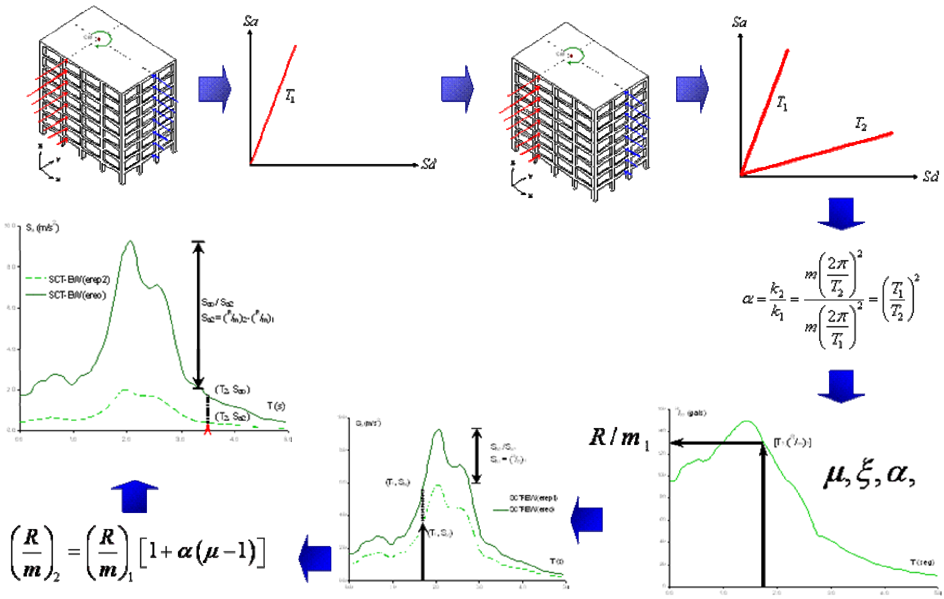

Figure 3. Performance based seismic design process

Superposition of the seismic and gravitational effects. The design forces corresponding to the last design stage in both directions are obtained by summing the element forces of the MSA with the reduced elastic design spectra in their respective directions, differentiating the element forces from the analysis for gravitational loads [GL], for modal spectral analysis in x direction [Sx] and for modal spectral analysis in y direction [Sy], in accordance with a valid code such as the Mexico City code (GDF, 2005).

Application Examples

Seismic Evaluation

The accuracy and potential of the proposed seismic evaluation strategy are validated through its application to a 12 storey reinforced concrete plane frame irregular in elevation, Fig. 4. The structure was analyzed and designed by Alba (2005) in accordance with the current Eurocodes (CEN, 2003a and 2003b). The seismic demand considered was the design spectrum of EC8 (CEN 2003a), corresponding to soils type B, damping ratio ζ=0.05, soil amplification factor S=1.2 and peak ground acceleration a_g=0.30g (where g is the acceleration due to gravity). The details of this spectrum are illustrated in Fig. 5.

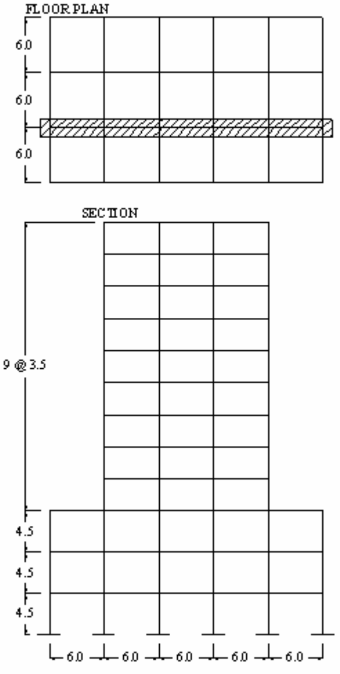

Figure 4. Floor plan and section of the irregular frame used

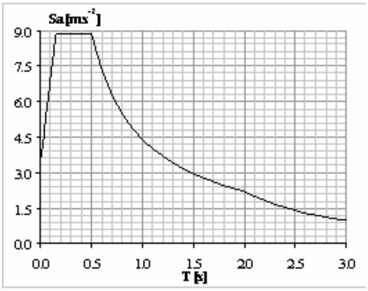

Period 0.0-

$$S_e(T) = a_g \cdot S \cdot \left[1 + \frac{T}{T_b} \cdot (\eta \cdot 2{,}5 - 1)\right]$$

Period -

$$S_e(T) = a_g \cdot S \cdot \eta \cdot 2{,}5$$

Period 0.5-2.0 s

$$S_e(T) = a_g \cdot S \cdot \eta \cdot 2{,}5 \cdot \left[\frac{T_c}{T}\right]$$

Period > 2.0 s

$$S_e(T) = a_g \cdot S \cdot \eta \cdot 2{,}5 \cdot \left[\frac{T_c T_d}{T^2}\right]$$

Figure 5. EC8 Elastic Response Spectrum

Moment-curvature diagrams. Throughout this work, the moment curvature diagrams of the sections were idealized with an elasto-plastic model with the following characteristics: the equal energy rule applies, horizontal second branch, and slope of the first branch defined by the secant at 60% of the yield point on the analytical moment curvature diagram, Fig. 6.

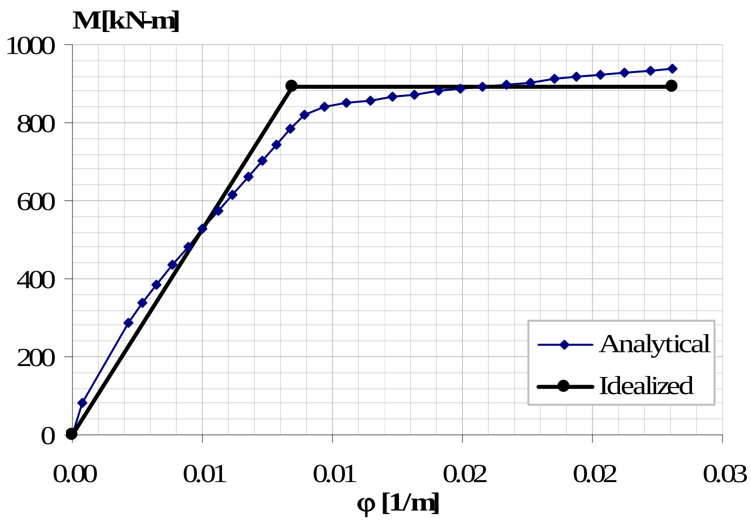

Figure 6. Moment Curvature Diagrams, analytical vs *idealized*

Synthetic accelerograms. To validate the results obtained with this method, a family of 50 synthetic accelerograms, compatible with the target design spectrum, was simulated by Isaković et al.(2005). A sample synthetic accelerogram is presented in Fig. 7(a), where the shape of the accelerogram and the peak ground acceleration may be observed. To establish the validity of the accelerograms simulated, Fig. 7(b) shows the comparison of the target design spectrum and the mean value of the response spectra generated for the family of 50 accelerograms.

Presentation of results The seismic performance obtained with the method here proposed is compared with the mean value of the results of the 50 synthetic accelerograms; the mean of the time history (TH) analysis +/- one standard deviation; and the results obtained with the N2 method, in order to have a comparison with a simpler method. Displacements, interstorey drifts and storey shears are presented, in Figs. 8, 9 and 10 respectively, for the considered example.

Fig. 8 shows a comparison of the distribution of the maximum displacements obtained from the time history analyses of the twelve-storey frame with that of those obtained with the proposed method. It may be observed that they are similar and on the safe region. Whereas, when these displacements are compared with those obtained with the N2 method, they are considerably different and on the unsafe region. This situation makes it evident that the method works for frames with considerable participation of higher modes and that it also works for significant incursions in the non-linear range, as is the case of the considered irregular frame.

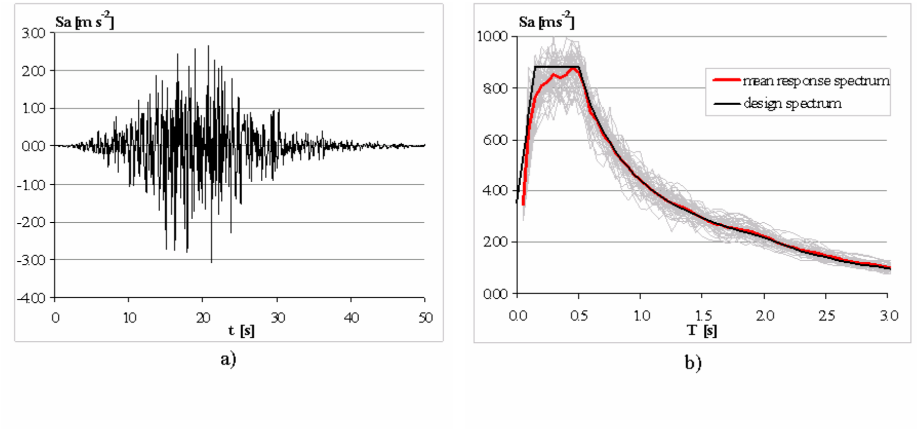

Figure 7. Synthetic accelerogram (a) and comparison of spectra (b)

The interstorey drifts depicted in Fig. 9 show that for the structure evaluated with the proposed method, the results for the lower levels are in good agreement with the statistics of the non-linear TH results and are on the safe side. However, the results for the upper levels are quite different and on the unsafe side. This tendency in the deformed shapes given by the proposed method is due to the use of a modal combination rule to obtain the results. In any case, the results of the proposed method remain within the band generated with the TH response +/- one standard deviation.

Finally, Fig. 10 shows that for the evaluated structure the storey shears calculated with the proposed method and with the N2 method are somewhat smaller than the results of the TH.

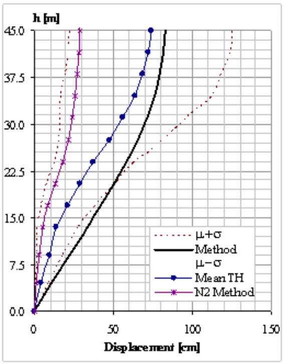

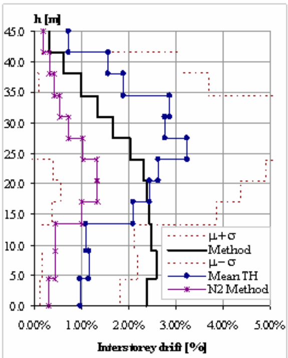

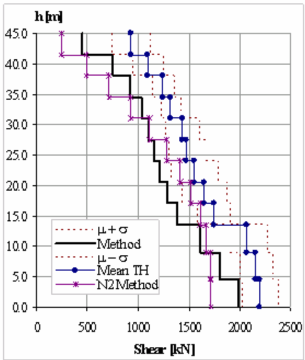

Figure 8. Storey drifts *Figure 9. Interstorey drifts* *Figure 10. Storey shears*

Performance Based Design

The design strategy was applied to a 15-storey RC building with asymmetry given by the distribution of masses at floors. For its design the following assumptions were used: 1) Rigid nodes and cracked inertia moments for the sections, 2) rigid floor diaphragms, 3) masses concentrated at the mass centres of the storeys, 4) P-Δ and soil-structure interaction effects ignored and 5) non-standardized design of the elements.

The model of the undamaged structure is shown in Fig. 11, and the corresponding damaged model in Fig. 12. The fundamental periods corresponding to these models are Te=1.60 s and Ti=3.53 s. The damaged distribution used in the damaged model is consistent with the expected performance level and it is introduced in the analytical model by moment releases at the ends of elements which accept damage. The damage distribution used led to a post-yielding stiffness ratio, β=0.20, proposed as a target parameter and attained through the occurrence of hinges at the beams of the first eight levels.

In this example the design objective of the asymmetric building was for standard occupancy with a life safety performance level and associated seismic design level corresponding to a rare earthquake (SEAOC, 1995). The selected performance level is quantified by a ductility demand of $\mu = 4$, a value which is thought to be associated to acceptable rotation levels of the sections of the structural elements accepting damage in the assumed damage distribution.

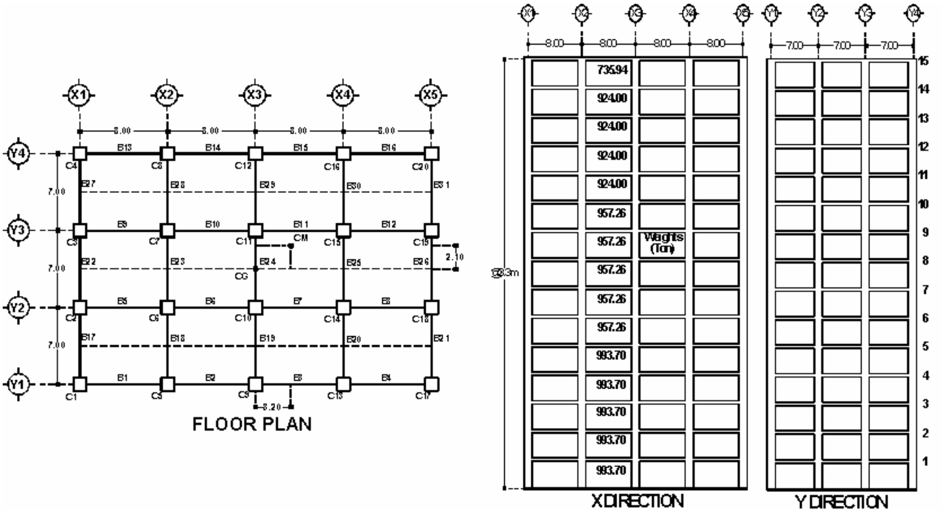

Figure 11. Plan and elevation views of the asymmetric building

The seismic design level is characterized by uniform hazard design spectra associated to a rare earthquake and parameterized by a functional relationship R/m (T, β,μ,Tr), where Tr is the return period of the ductility, $\mu = 4$, of 1000 years and a value of $\beta = 0.20$, Fig. 13, Avelar et al. (2003).

Construction of the behaviour curve. Once a design objective and the corresponding performance and seismic design levels are defined, *i.e.*, standard objective for life protection with μ = 4 and design spectrum R/m (T, β=0.20, μ=4 y Tr=1000 years), the design strength of the reference system is defined by the spectral ordinate corresponding to the fundamental period, T_e, Ry/m=1.28 m/s^2. The yield displacement obtained from the spectrum in the ADRS format is $\Delta y=(1/\omega_e^2)$ Ry/m=0.083 m.

When the performance index is given by a ductility demand, as it is the case of this example the characteristic point of the design stage with damage is obtained from the geometric relationship between the two branches of the behaviour curve and the definition of ductility demand in the ADRS format, Fig.14, Ru/m=Ry/m[1 + β(μ-1)]= 2.067 m/s^2. The strengths [Ry/m] and [Ru/m - Ry/m] are distributed to the structural elements by means of modal spectral analyses using the uniform hazard elastic design spectrum defined as R/m(T, β = 1, μ = 1, Tr = 1000 years), Avelar *et al.* (2003).

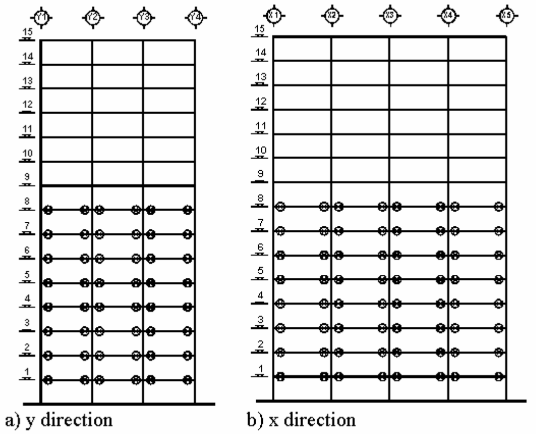

Figure 12. Analytical model with proposed damage distribution

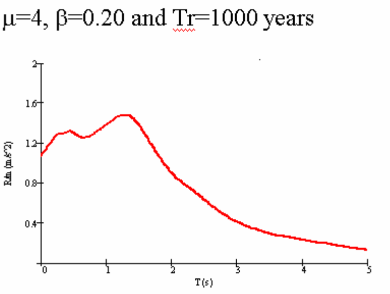

Figure 13. Uniform hazard design spectrum

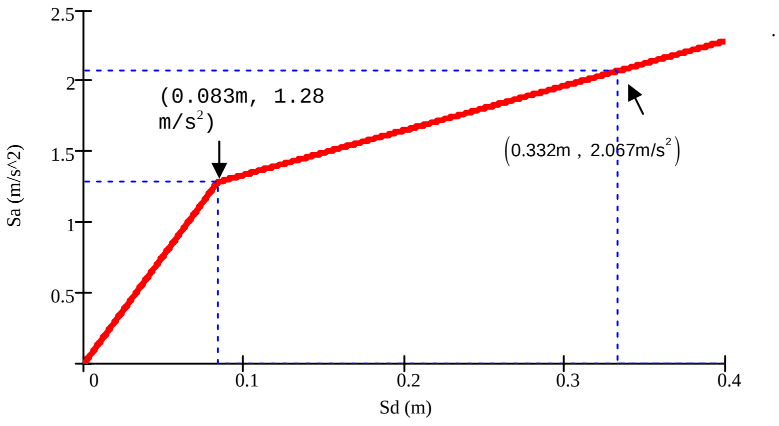

Figure 14. Complete behaviour curve

It is important to mention that it is necessary to check the rotation capacity of the hinged sections to guarantee no local failures, which would stop the structure attaining its design deformation capacity.

The strengths of the elements which admit damage and of those which remain elastic, are defined using an elastic design spectrum reduced by factors Fe = 0.24 and Fi = 0.47 respectively, Fig. 15.

Fig. 16 illustrates the distribution of shears in the columns of the first interstorey. The shown shear values are presented without standardization and are representative of the characteristic strength distribution of the target design objective.

Fig. 17 shows the global behaviour model characterized by bilinear curves in both orthogonal directions to compare the ultimate design of the complete system strengths which are very close to the design behaviour curve and the design base shear obtained.

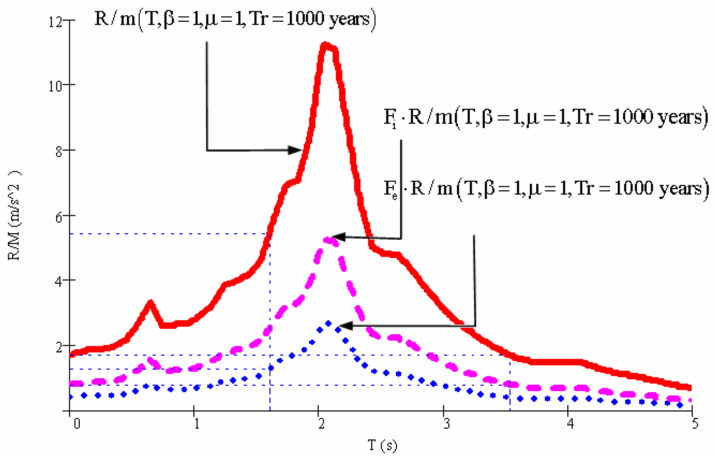

Figure 15. Reduction of the elastic design spectrum

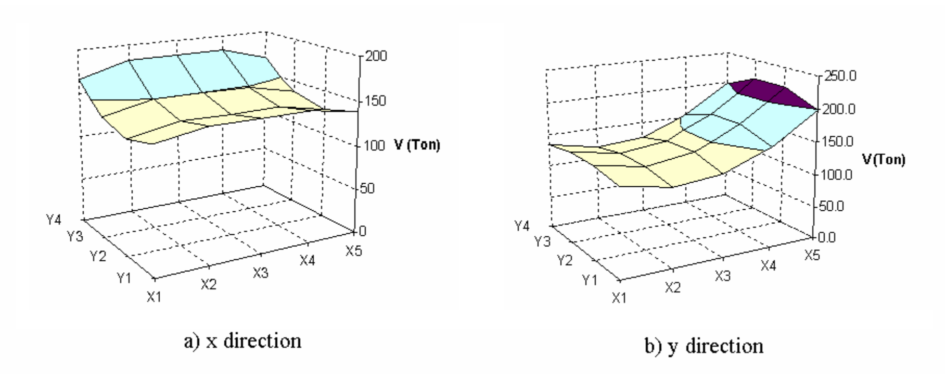

Figure 16. Variation of design shears in the first level columns

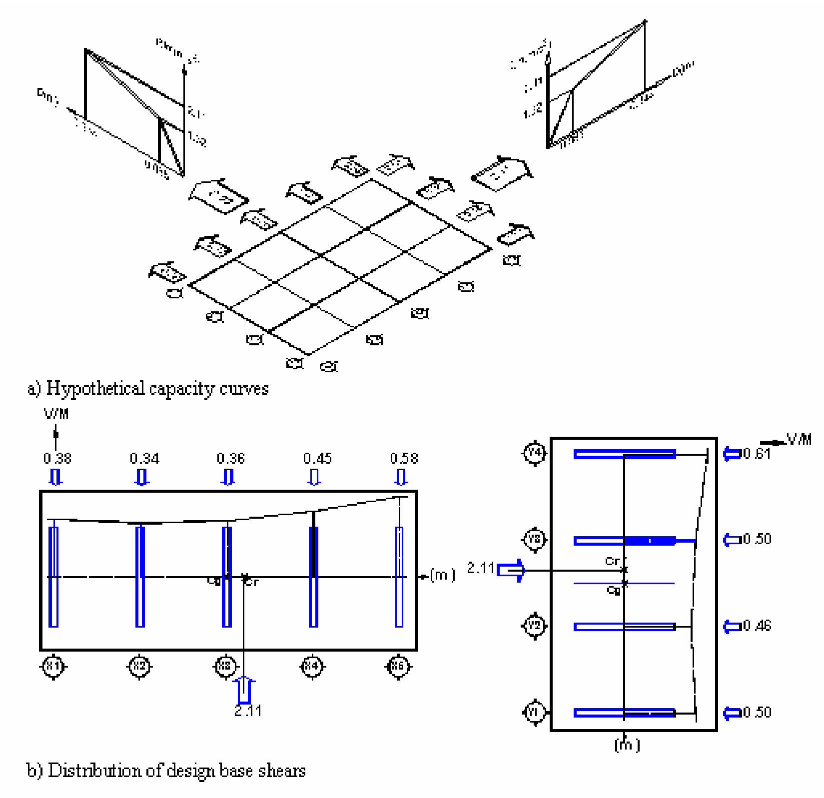

Figure 17. Design base shears

Validation of Results. To validate the seismic performance of the example buildings NLDA were performed for all considered load combinations under the following assumptions:

i). The non-linearities in beams and columns were concentrated at their end sections with a bilinear hysteresis rule without degradation of stiffness or strength and non-standardized designs for the elements.

ii). The damping of the structures was assumed to be of the Rayleigh type.

iii). As seismic demands the NS and EW components recorded at the SCT site during the 1985 México earthquake, records with characteristics compatible with those used to define the design seismic demand for the soil type in which the structure is assumed to be located.

iv). The performance of the building was evaluated for the following combinations of gravitational loading (GL), North-South seismic action (NS) and East–West seismic action (EW): 1) GL+EW+NS, 2) GL+EW-NS, 3) GL+NS+EW and 4) GL+NS-EW.

The design evaluation is carried out revising the parameters that characterize the seismic performance of the structure at global and local levels as calculated wit the non-linear analysis program Canny-E (Li, 1996).

Global ductility of the building. The global ductility of the building, defined as the ratio of the maximum roof displacement, Δu, to the yielding displacement, Δy, was μΔ=5.6.

Maximum roof displacements and interstorey drift. The global displacement of the centre of mass of the roof of the building has a maximum value of Δu=0.45 m and a corresponding interstorey drift of Ψu=0.0091.

Interstorey drifts. Fig. 18, shows the maximum interstorey drifts obtained from the step by step analyses. The largest values were Ψmin=0.017 and Ψmáx=0.021, and from these values the damage in the structural elements may be inferred, since the structural system is formed with seismically detailed RC frames. Existing literature, e.g. Penelis and Kappos (1997), shows that the values of interstorey drifts for the onset of damage are of the order of Ψundamaged=0.005 and for the total damage, of the order of Ψdamaged=0.030.

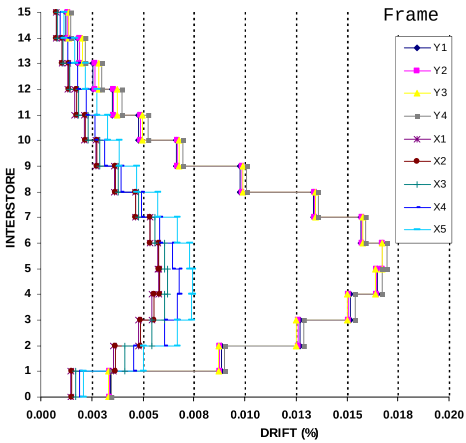

a) Combination 1 GL+EW+NS

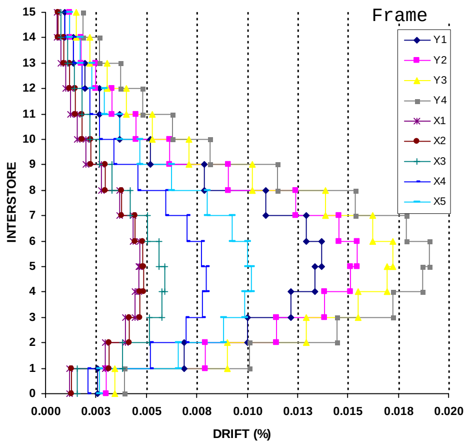

b) Combination 2 GL+EW-NS

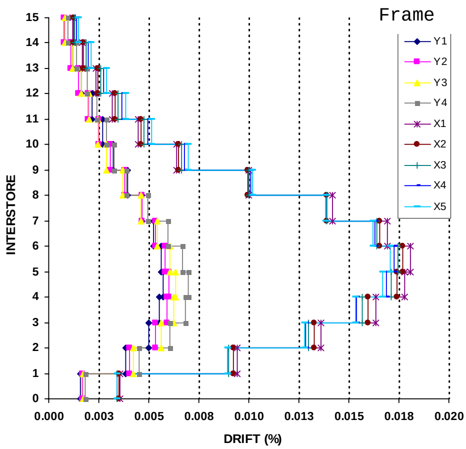

c) Combination 3 GL+NS+EW

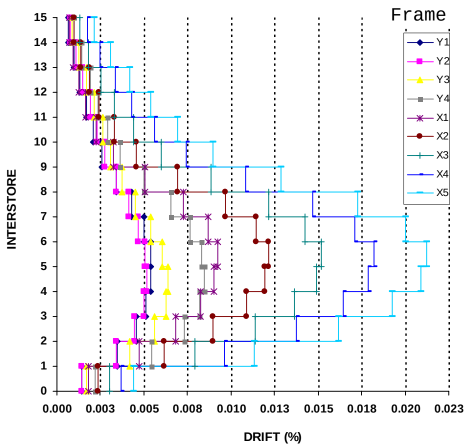

d) Combination 4 GL+NS-EW

Figure 18. Maximum interstorey drifts

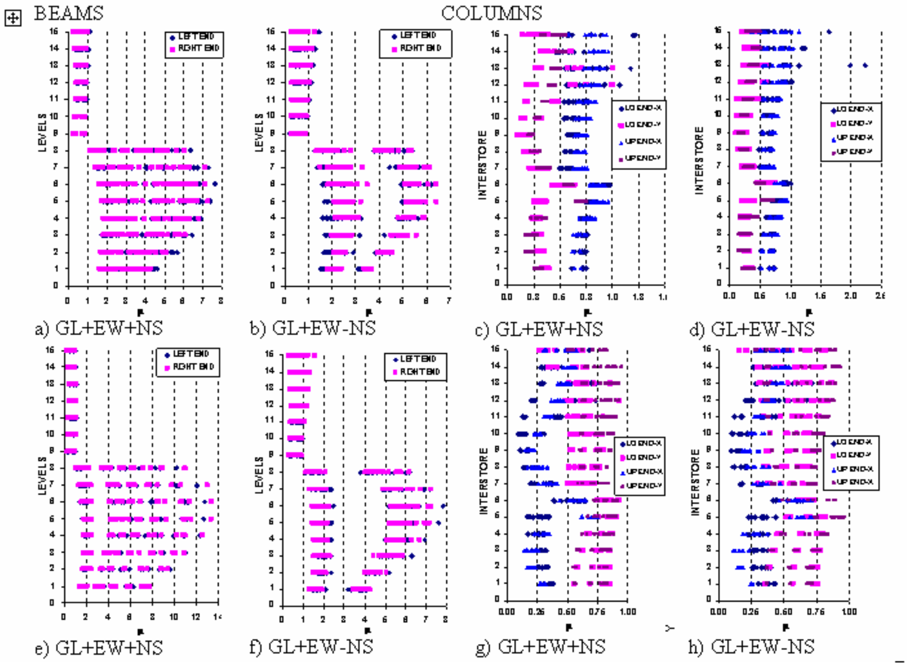

Figure 19. Ductility demands in beam and column elements

Local ductilities in beams and columns. Fig. 19 shows the rotation ductility demands at the end sections of the beams and columns in both directions. It is observed that the largest ductility demands in beams occur at levels 1 to 8 in accordance with the originally proposed damage distribution, with a maximum of μϕbeam with damage = 13.4, and that for the elements in which damage was not accepted, they remained practically elastic with only a few elements with maximum rotation ductilities of μϕbeam without damage= 1.5. For the case of columns it is observed that they remained practically undamaged with limited inelastic incursions i.e., maximum values of rotation ductility demands of μϕcolumn=2.2.

Damage distribution in frames. As illustration, Fig. 20 shows the final distribution of damage in the frames oriented longitudinally and transversally, correspondingly, indicating the maximum ductilities at the end sections obtained from the performed evaluations.

It is important to mention that the damage distribution proposed for design purposes is practically the same as that obtained when the structure is subjected to the design demands, with light ductility demands in other beam and column elements where damage was not supposed to have occurred. It is observed that the ductility demands at all levels maintain certain uniformity. This is not the case in the frames furthest away from the stiffness centre. These demand larger rotation ductilities at end sections, a result of the torsional effect.

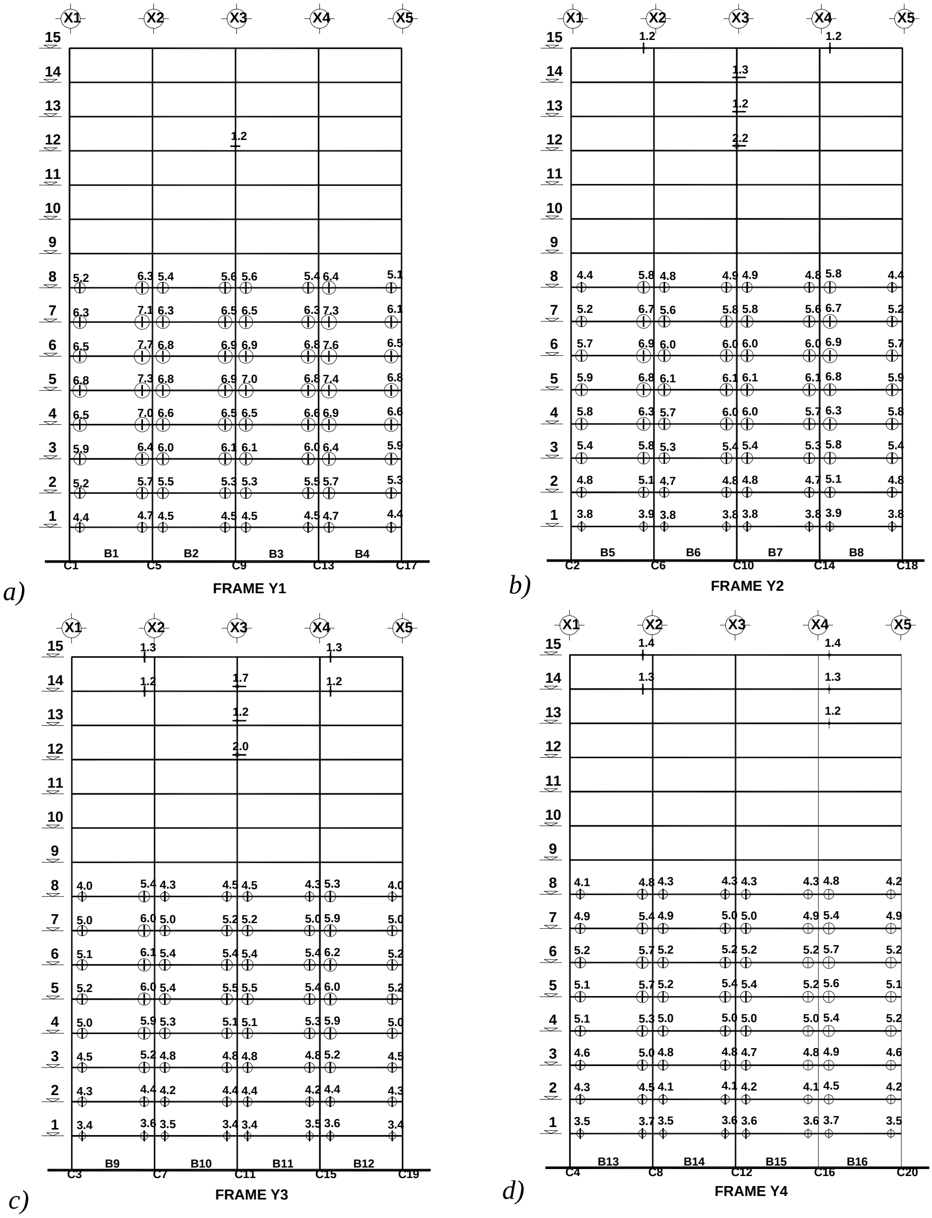

Figure 20. Damage distribution in longitudinally oriented frames (x)

Conclusions

The main conclusions derived from this work are the following:

The method of evaluation/design proposed considers the contribution to the performance of higher modes of vibration, and it is applicable to regular and irregular structures. For structures with a significant contribution of higher modes, the method is more precise than other simplified procedures that do not consider this contribution.

The method takes into account the redistribution of forces in the structure due to non-linear behaviour of the materials.

The seismic demand is defined by means of design spectra given by smoothed spectra.

The behaviour curve is constructed using modal spectral analyses and does not depend on results of pushover analyses with particular lateral force distributions.

The application of the method is simple, as it only requires of the results of a limited number of MSA, an easy and well known procedure which may be applied using commercial analysis software.

The design strategy is consistent with the philosophy of designing a building for a given performance level involving a performance index related to an accepted distribution of damage, proportioning the structure with an adequate lateral strength function of these performance indices.

The deformation capacity of the structure is obtained by means of a proposal of damage distribution, explicitly defined in the design process.

The results obtained in the examples show that the established design objectives are satisfied in an acceptable way and that damage was controlled with the formation of hinges at end element sections without excessive plastic rotations.

The application of modal spectral analysis with accepted mode combination rules gives evaluations and designs corresponding to maximum expected performances, which, although they statistically produced design on the safe side, the validation of performances obtained though TH analyses may have important errors when the performance of the structure is validated only for a limited number of design earthquakes.

Acknowledgements

This research is part of the project “Development of Seismic Design Criteria for Torsion” sponsored by the General Directorate for Affairs of the Academic Personnel of UNAM, (DGAPA). Support for this research came also from the National Council for Science and Technology (CONACYT) the project “Development and Experimental Evaluation of a Performance Based Seismic Design Method”. Partial support by the FCT Fundação para a Ciência e a Tecnologia, under Grant SFRH/BGCT/15126/2004 is also acknowledged. Constructive and fruitful discussions by Mauro Niño and Tatjana Isaković are greatly appreciated.

References

Alba, F. (2005). Seismic performance evaluation method of plane frames (in Spanish), *Master of Engineering Thesis*, UNAM, Mexico.

Antoniou, S., and R. Pinho (2004). Advantages and limitations of adaptative and non-adaptative force based pushover procedures. *Journal of Earthquake Engineering* 8(4), 497-522.

ATC. (1996). ATC-40, Seismic evaluation and retrofit of concrete buildings. Applied Technology Council, Redwood City, Cal.

Avelar, C., A. G. Ayala, and A. Díaz de León (2003). Design spectra determination for performance based seismic design. Applications of Statistics and Probability in Civil Engineering, Der Kiureghian, Madanat & Pestana (eds), Millpress, Rotterdam.

Ayala A. G. (2001). Seismic performance evaluation of structures. A new approach. (in Spanish), Revista Internacional de Métodos Numéricos para Cálculo y Diseño en Ingeniería 17(3), 285-303.

Aydinoglu, M. N. (2003). An incremental response spectrum analysis based on inelastic spectral displacements for multi-mode seismic performance evaluation, Bulletin of Earthquake Engineering 1(1), 3-36.

Aydinoğlu, M. N. (2004). An improved pushover procedure for engineering practice: Incremental Response Spectrum Analysis (IRSA). Proc. of Int. Workshop: Performance-Based Seismic Design Concepts and Implementation, Bled. Slovenia, 345-356.

Basilio I and A. G. Ayala (2001). Performance Based Seismic Design of Frames of Tall Buildings, (in Spanish), Proc. of the XIII National Congress of Earthquake Engineering, Guadalajara, Jal., SMIS, Mexico.

CEN. (2003a). Eurocode 8, Design of structures for earthquake resistance – Part 1: General Rules, seismic actions and rules for buildings. Commission of the European Communities (CEN), Brussels, Belgium.

CEN. (2003b). Eurocode 2, Design of concrete structures, prEN 1992-1-1, Commission of the European Communities (CEN), Brussels, Belgium

Chopra, A., and R. Goel (2002). A modal pushover analysis procedure for estimating seismic demands for buildings, Earthquake Engineering and Structural Dynamics 31(3), 561-582.

CSI. (2003). SAP 2000 Integrated finite element analysis and design of structures, Computers and Structures Inc. Berkeley, Cal.

Fajfar, P., and P. Gaspersic (1996). The N2 method for the seismic damage analysis of RC buildings, Earthquake Engineering and Structural Dynamics 25(1), 31-46.

FEMA. (1997). FEMA 273, NHERP Guidelines for the seismic rehabilitation of buildings, Federal Emergency Management Agency, Washington D.C.

FEMA. (2005). FEMA 440, NHERP Guidelines for the seismic rehabilitation of buildings, Federal Emergency Management Agency, Washington D.C.

Freeman, S. (1978). Prediction of response of concrete buildings to severe earthquake motions, Proc. of Douglas McHenry International Symposium on Concrete and Concrete Structures, Detroit; 589-605.

GDF. (2005). Construction code for the Federal District and Complementary Technical Norms for seismic design (in Spanish), Official Gazette of the Federation, Mexico.

Isaković, T., A.G., Ayala, M.Niño, and F. Alba (2005). Bridge evaluation method using the performance based design philosophy, Proc. of XV National Congress of Earthquake Engineering. Paper V-08, SMIS, Mexico.

Li, K. N. (1996). CANNY-E, Three-dimensional non-linear dynamic structural analysis computer program package, Canny Consultants PTE. LTD, Singapore.

Penelis G. G., and A. J. Kappos. (1997). *Earthquake-resistant concrete structures*, Chapman & Hall. London. UK.

Requena, M. and A. G. Ayala, (2000). Evaluation of a simplified method for the determination of the nonlinear seismic response of RC frames, Proceedings of the Twelfth World Conference on Earthquake Engineering Auckland. New Zealand, paper No. 2109.

Ruiz-Garcia, J. and E. Miranda, (2004). Inelastic displacement ratios for design of structures on soft soil sites, *Journal of Structural Engineering* 130(12), 2051-2061.

SEAOC (1995). Vision 2000. Performance Based Seismic Engineering of Buildings, Structural Engineers Association of California, Sacramento, Cal.

Veletsos, A. and N.Newmark, (1960). Effect of the inelastic behaviour on the response of simple systems to earthquake motions, Proc. of II World Conference on Earthquake Engineering, Japan, Vol. 2, 895-912.

Enrique Bazán Zurita
Senior Staff Engineer
GAI Consultants, Inc.
Pittsburgh Office
385 East Waterfront Drive
Homestead, PA 15120-5005
e.bazan-zurita@gaiconsultants.com

Seismic Engineering

I was certainly most fortunate to work for Luis at the Institute of Engineering of the National University of Mexico. In 1980, Luis graciously allowed me to share with him the José A. Cuevas Award granted by the Colegio de Ingenieros de México. My fortuitous accomplishment was that I had implemented some of Luis' pioneering concepts to estimate seismic risk. To me, the real prize was working with him and having not only an extraordinary learning experience, but also the opportunity to develop a lasting personal relationship with a unique mentor and friend. Luis' applications of Bayesian Statistics to seismicity constitute the basis for current methodologies and display the depth and elegancy that characterizes all his research work. I believe that he has yet to receive the credit he deserves for his original contributions to probabilistic estimations of seismic risk. This note attempts to reciprocate the recognition that Luis generously gives to his colleagues.

Enrique Bazán
Pittsburgh, September 1st, 2005

Jacobo Bielak
Department of Civil and Environmental Engineering
Carnegie Mellon University
Pittsburgh, PA 15213-3890
jbielak@cmu.edu

Computational science and engineering with particular application to earthquake engineering and engineering seismology

Two early events remain vivid in my mind among my many interactions with Luis Esteva. The first experience introduced me to Luis Esteva, the scholar and teacher. The second one, to Luis Esteva, the great companion and fun loving man.

I met Luis for the first time at the beginning of my senior year, as my instructor in a course on Structural Analysis he was teaching at UNAM. Since I liked the way he taught the course very much I thought it would be great if I could write my engineer's thesis under his supervision. Would he agree to serve as my advisor, I asked him? His reply was, 'yes of course, but my research is on earthquake engineering. You will need some background on vibration theory. Have you had vibrations before?" No, I said, as at the time vibrations was not offered at the undergraduate level. Luis turned to his bookcase, pulled out a book and said: here, study it, and come see me when you've learned the material. After recovering from the shock, I saw no alternative, so off I went to study vibrations. His style taught me a great lesson in taking personal responsibility for my own learning. Little did I know that I was now hooked on dynamics. It was all due to Luis. In due course, I finished the thesis, and later learned that Luis had incorporated the results of my research into the Mexico City seismic provisions, in order to address the problem of whip effects in buildings. I was elated.

The second experience occurred upon my return to Mexico after completing my graduate studies in the States. One evening Luis, Ismael Herrera, and I went out together to dinner with our wives. Until then I had known Luis as a great scholar, but quite a serious fellow. We had a great dinner at the Café del Lago, wonderful conversation, laughter and jokes. The last thing I expected is that he would get up and start to dance: not waltzes, but rock-and-roll, mambo and cha-cha-cha. It was quite a sight to see him and Gloria dance the evening away like Fred Astaire and Ginger Rogers. My view of him changed that night. No longer was Luis only the scholar and great engineering practitioner, but also a man full of joy of life.

My experience in working under him during the time I spent at the Institute of Engineering at UNAM also taught me that he is a great humanist and caring human being, a man of great integrity and strong sense of fairness. I learned from him not only technical things which have been with me all my life, but also how to deal with all kinds of expected and unexpected situations.

Thank you, Luis, for your teachings, and most of all for your continuing friendship over the years. It means a lot.

September 1, 2005

SEISMIC DESIGN SPECTRA IN SOFT ZONES OF MEXICO CITY

Sittipong Jarernprasert [(1)], Enrique Bazán [(2)] and Jacobo Bielak[(3)]

ABSTRACT

An approach for deriving inelastic design spectra previously developed by the authors is used in this note to examine seismic design spectra for the soft lakebed region of Mexico City. Based on statistical analyses of *inelastic* response spectra, this approach expresses the yield strength, C_y, required to produce a mean ductility ratio, $\bar{\mu}$, as $C_y(T,\bar{\mu}) = C(T)\bar{\mu}^{-n(T)}$. *C(T)* is interpreted as a mean unreduced inelastic spectrum and the power *n* depends only on the elastic natural period, *T*, of the structure. We use *C(T)* to develop widened spectra for region III b of compressible soil in Mexico City and compare it with the spectra prescribed in the 2003 Mexico City Code. *n(T)* is used to derive reduction factors for considering inelastic behavior. This factor is also compared to the corresponding factors prescribed in the code.

Introduction

Most buildings in Mexico City are designed under the assumption that they will experience significant nonlinear deformations under strong earthquakes. However, in accordance with the City's building code (NTCDS-RCDF, 2003), the seismic analysis is performed with linearly damped *elastic* models. The seismic base shear force is prescribed in terms of unreduced design spectra associated with 5 percent viscous damping, and the inelastic behavior is considered in design by reducing the "elastic" spectrum by a factor which is greater than unity.

The seismic provisions of the current Mexico City Building Code are strongly influenced by the experience and knowledge related to the 1985 Michoacán event. In particular, the design spectra were increased and the inelastic reduction factors were decreased for soft soil zones, in light of the widespread damage that was observed in those zones. Figure 1 presents the elastic spectra for the SCT record of the 1985 earthquake for damping ratios ξ = 0.05 to 0.40. For small values of ξ, these spectra exhibit large distinct peaks close to a period of 2s. These peaks tend to disappear for high-damping spectra. Figure 2 shows the spectra of the same record for elastic-plastic systems for ductility ratios μ = 1, 1.3, 1.6, 2 and 4. The inelastic spectra exhibit significant reductions due to hysteresis, even for a moderate μ = 1.3. The reductions of spectral values due to increasing ductility demands are similar to the reductions of elastic spectra when the percentage of viscous damping is increased. The peaks for higher ductilities tend to shift toward smaller periods, and eventually disappear for μ= 0.4

1. Staff Engineer, Paul C. Rizzo Associates, 105 Mall Blvd, Suite 270-E, Monroeville, PA, 15146. Formerly, Graduate Student, Dept. of Civil and Environmental Engineering, Carnegie Mellon University Pittsburgh, PA 15213, sj2@andrew.cmu.edu
2. Senior Staff Eng., GAI Consultants, Inc., Pittsburgh Office 385 East Waterfront Drive, Homestead, PA, 15146, USA e.bazan-zurita@gaiconsultants.com
3. Professor, Department of Civil and Environmental Engineering, Carnegie Mellon University Pittsburgh, PA 15213. jbielak@cmu.edu

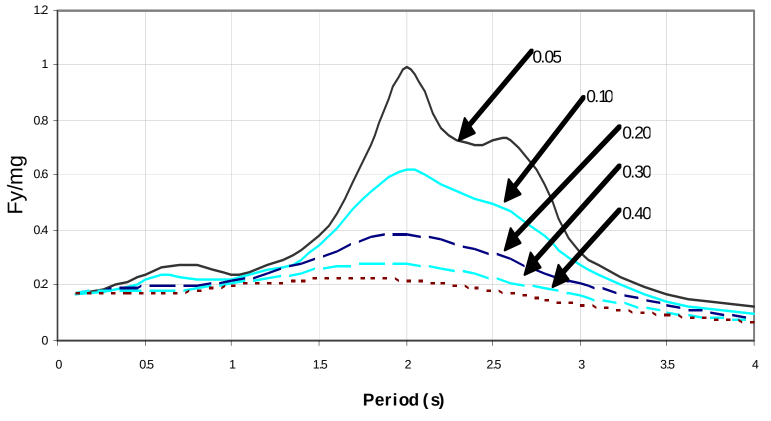

Figure 1. Elastic spectra of the SCT 1985 record for different damping ratios

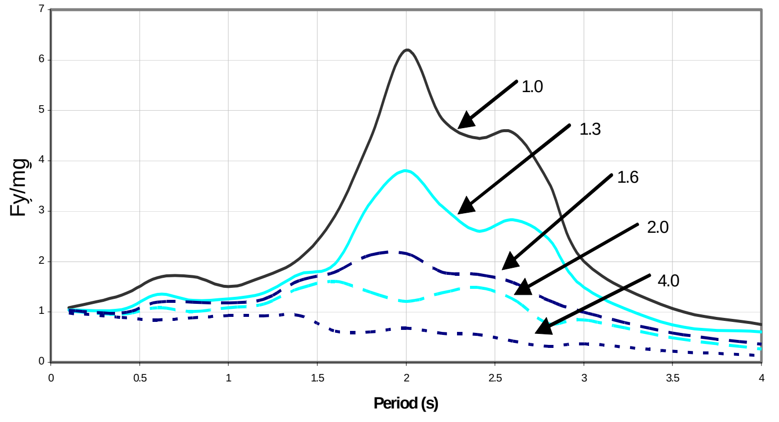

Figure 2. Inelastic spectra of the SCT 1985 record for different ductility ratios

for which the spectrum becomes nearly flat, with slight gradual decrease for increasing period.

The preceding observations prompted a study by Jarenprasert et al (2005) to develop simple rules for establishing inelastic seismic design spectra in the soft lakebed of Mexico City directly from statistical analyses of inelastic response spectra, using a sample of 66 normalized accelerograms, with dominant periods of approximately 2 sec. Five percent viscously damped SDF systems with a bilinear hysteretic force-deformation relationship were used in this study, and the hysteretic behavior was defined by the initial elastic period, T, the yield displacement, u_y, and the slope of the second branch of the force-displacement relationship equal to 2 percent of the initial slope. The seismic coefficient, C_y, is such that the yield force is $V_y = C_yW$, where $W = mg$ is the weight of the structure, m its mass, and g the acceleration of gravity. The dimensionless seismic design coefficient C_y can be expressed as:

$$C_y = \frac{4\pi^2}{T^2} \cdot \frac{u_y}{g} \tag{1}$$

Fig. 3 shows mean elastic spectra of the ensemble of 66 records for damping ratios of 5 to 30 percent and inelastic spectra for mean ductility demands, $\bar{\mu}$, between 1 and 5, all normalized with respect to the dimensionless mean peak ground acceleration $\overline{\text{PGA}}$/g. Even for moderate ductilities, the mean inelastic spectra are much smoother than the 5 percent mean damped elastic spectrum, exhibiting a relatively flat zone for T between 0.6 and 2.0 sec. The peak value for $\bar{\mu}$ = 1.5 is approximately one half that of the elastic spectrum.

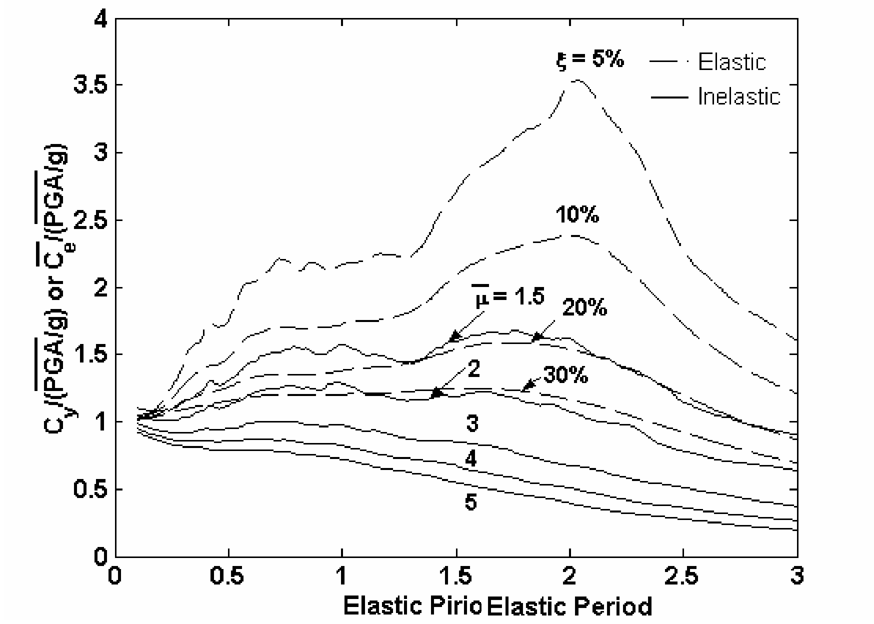

Figure. 3. Normalized spectra $C_y(T, \bar{\mu})$ and $\overline{C_e}\,(T, \xi)$ for different mean ductility ratios, $\bar{\mu}$, and critical damping ratios, ξ

Direct inelastic approach for seismic design spectra

By examining how the inelastic seismic coefficient, C_y, changes with $\bar{\mu}$ within 1.5 and 6.0 Jarernprasert (2005) has shown that C_y can be expressed in terms of the natural period of the structure and the ductility factor, as:

$$C_y(T, \bar{\mu}) = \frac{C(T)}{R_{\bar{\mu}}} \tag{2}$$

where:

$$R_{\bar{\mu}} = \bar{\mu}^{n(T)} \tag{3}$$

C(T) is interpreted as a reference *unreduced* spectrum, which divided by a modifying factor, $R_{\bar{\mu}}$, provides the required inelastic strength C_y that results in a mean target ductility $\bar{\mu}$. Equation (3) has precisely the format adopted in the Mexico City Building Code (DF, 2003), where a reduction factor Q' is similar to $R_{\bar{\mu}}$, and accounts for the hysteretic behavior. $R_{\bar{\mu}}$ varies implicitly with *T* through the power *n*. Notice that taking $n = 1$ is similar to the "equal displacement" rule, except that here C*(T)* is not the elastic 5 percent spectrum. Figure 4 shows the values of *C* and *n* obtained from the regression of the numerical results of C_y on $\bar{\mu}$. A comparison of *C(T)* with the elastic response spectrum for 5 percent damping in Fig. 3 shows that *C(T)* is significantly smaller than the mean elastic spectrum over the entire range of periods. It is also flatter and does not exhibit the strong peak at about the 2 sec dominant period observed in the elastic spectrum. Instead, the peak of the unreduced spectrum is shifted towards the left appearing at T = 1.6 sec.

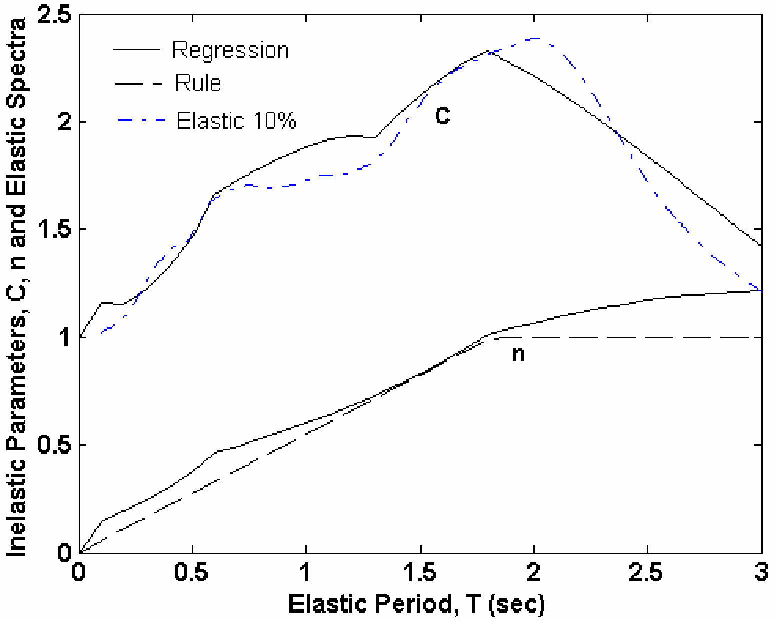

Figure 4. Unreduced spectrum C(*T*) *and power n*(*T*) *in Eqs.* (2) *and* (3), *determined with a regression fit*

For the seismic input used by Jarernprasert et al (2005), very good approximations to *C(T)* are provided by (1) the mean elastic spectrum for 10 percent of critical damping, and (2) the mean inelastic spectrum for a ductility demand of 1.2. Fig. 5 compares *C(T)* with these two approximations and shows that all three spectra have a very similar peak value of approximately 2.4 times the zero period value. Another observation by Jarenprasert *et al* (2005) is that $C_y(T, \bar{\mu})$ for $\bar{\mu} = 2$ can be closely approximated by the elastic mean response spectrum for 30 percent of critical damping. This approach was called SELIS for Surrogate Elastic Inelastic Spectrum and was also found to be applicable to an ensemble of Californian records (Jarernprasert *et al*, 2005a).

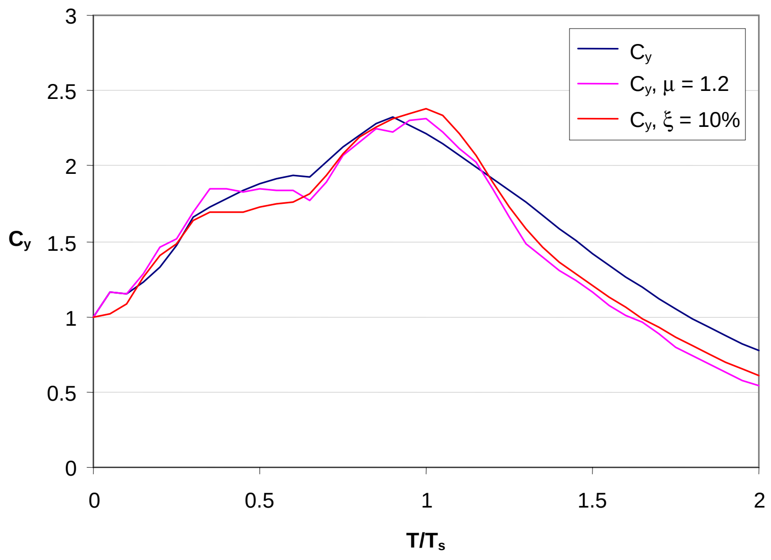

Figure 5. Unreduced spectrum C(*T*) *determined from a regression fit* (*solid lines*), *by 10 % elastic spectrum* (*dashed lines*) *and inelastic spectrum for μ = 1.2* (*dashed-dotted lines*)

Examination of the design spectra in Mexico City

The maximum values of the design spectra for the soft zones of Mexico City differ appreciably from the peaks of 5 percent damped spectra of actual earthquake records. In particular, the maximum prescribed spectral value of 0.45g for the lakebed region is approximately 45 percent of the peak of the 5 percent elastic spectrum of the 1985 SCT record. This seems to indicate that the “elastic” design spectra implicitly incorporate some reductions due to inelastic behavior. Along these lines, Rosenblueth and Gómez (1991) have commented that reductions already included in the unreduced design spectra account partially for the differences between reduction factors specified in Mexico City and California.

In practice, design spectra are widened to account for uncertainties in the structural vibration period, T, and in the seismic input, especially in the dominant periods of the site and Ts, which changes with the amount of soil deformation. In addition, widening can account for period shifts in the peak value in inelastic spectra. Therefore, a meaningful comparison of *C(T)* with design spectra can be conducted by widening *C(T).* For this purpose, we have considered that the normalized shape of *C(T),* which was derived for a site dominant period of 2 seconds, remains the same for any dominant period between 0.85 and 3.0, which are the limits for the flat region of the design spectrum specified in the Mexico City Code (NTCDS-RCDF, 2003) for zone IIIb. The highest spectral value ($c = 0.45$, $a_o = 0.11$) is prescribed for Zone IIIb, where most of the 66 accelerograms used by Jarernprasert et al (2005) were recorded. The peaks of *C(T)* in Fig. 6 are equal to 0.45. It can be noted that the decay of the envelope

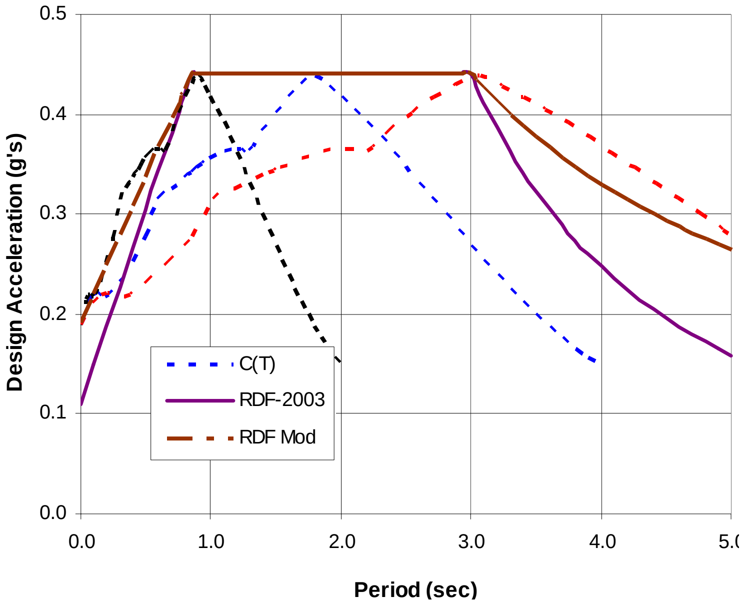

Figure 6. Comparison of widened spectra with the RDF IIb 2003 unreduced design spectrum (Q=1). Widened spectra C(T) (dashed lines) and design unreduced spectrum (solid lines)

after 3 seconds is slower than in the RDF 2003 Code, for which the design spectrum decreases with the period squared. Another noticeable difference occurs at T = 0. Whereas a_o, is equal to 0.11 in the design spectrum code, the corresponding value for *C(T)* is 0.19. It seems that for maintaining the plateau at the same value, a_o should be increased to 0.19 to be more consistent with an “unreduced” spectrum that already reflects some reduction due to inelastic behavior.

Plotted are The reduced spectra corresponding to the widening of *C(T)* presented in Fig. 6, for μ = 2, 3 and 4, are plotted in Figs. 7, 8 and 9 respectively. The reductions for *C(T)* have been calculated using Eq. 3 with the values of *n(T)* shown in Fig. 4. We have also plotted in these three figures the RDF 2003 Code reduced spectra corresponding to Q equal to 2, 3 and 4, respectively. There are no significant differences between reductions calculated with both procedures. In all cases, at short periods, the code reduced spectra are smaller than the one resulting from Eq. 3. The differences are more noticeable when μ = Q = 4, i.e., when the inelastic behavior is more extensive, particularly for periods smaller than 2.0 s.

Figures 7 to 8 include an example of modifications that could be made to the RDF 2003 Code to attain a better match to the spectra obtained by widening *C(T)*. The “modified spectra” are based on increasing a_o from 0.11 to 0.19 and decreasing the spectra for T longer than 3 s, in inverse proportion to T rather than to the square of T.

In addition, the maximum reduction factor has been set as $Q^{0.8}$ rather than Q, and the upper limit for the flat region has been reduced to 2.8, 2.6 and 2.4 s, i.e., [3 – 0.2 (Q-1)] s, for Q = 2, 3 and 4 respectively. These modification lead to a better fit to the widened unreduced spectra based on *C(T)* which constitute the "exact" mean inelastic spectra. We should remark, however, that this was just a matching exercise, aimed to illustrate potential changes. Examination of additional results and consideration of other factors used in design, such as load and strength factors, are required to propose more definitive modifications.

The examination of inelastic spectra of SDF bilinear hysteretic systems with 5 percent critical viscous damping, subjected to a sample of accelerograms recorded in the lakebed region of Mexico City shows that mean inelastic spectra can be defined by dividing an unreduced inelastic spectrum by a reduction factor, in the format used by the current Mexico City code. The unreduced spectrum *C(T)* is appreciably smoother than the 5 percent damped mean elastic spectrum. The peak of *C(T)* can be closely approximated by the peaks of the 10 percent damped elastic spectrum or the inelastic spectrum for a mean ductility demand of 1.2. Associated to *C(T)*, the reduction factor for a given mean ductility demand , μ , is given by μ raised to a power n(T) that depends solely on the natural period of the elastic structure (Eq. 3).

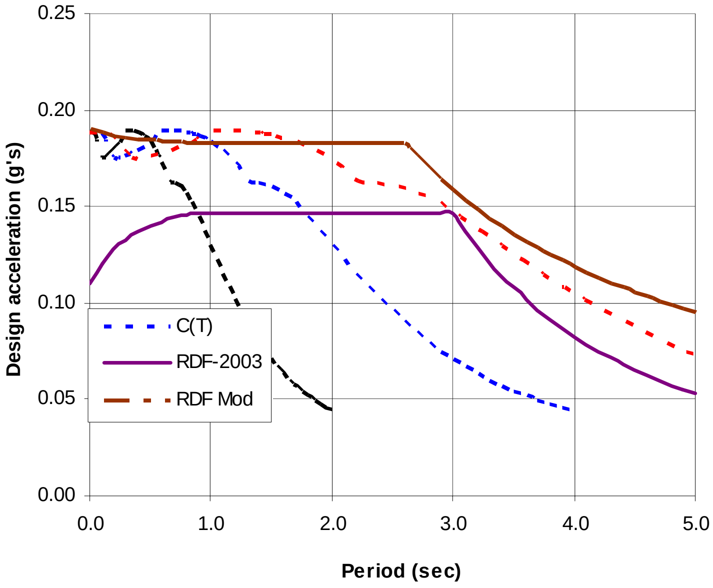

Figure 7. Widened reduced spectra from Eq. 3 (dashed lines), RDF 2003 design spectrum (solid lines) and an example of a modified design spectrum (dash – solid lines), for Q = 2.

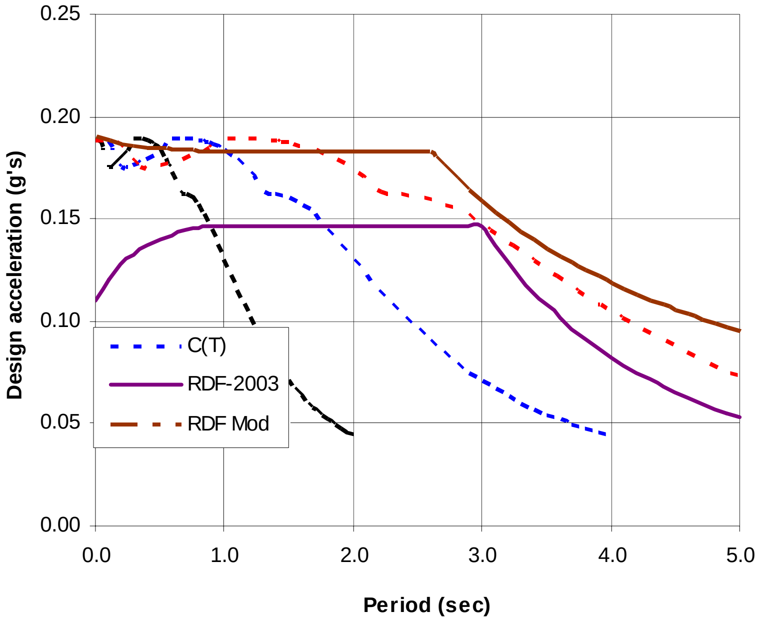

Figure 8. Widened reduced spectra from Eq. 3 (dashed lines), RDF 2003 design spectrum (solid lines) and an example of a modified design spectrum (dash – solid lines), for Q = 3

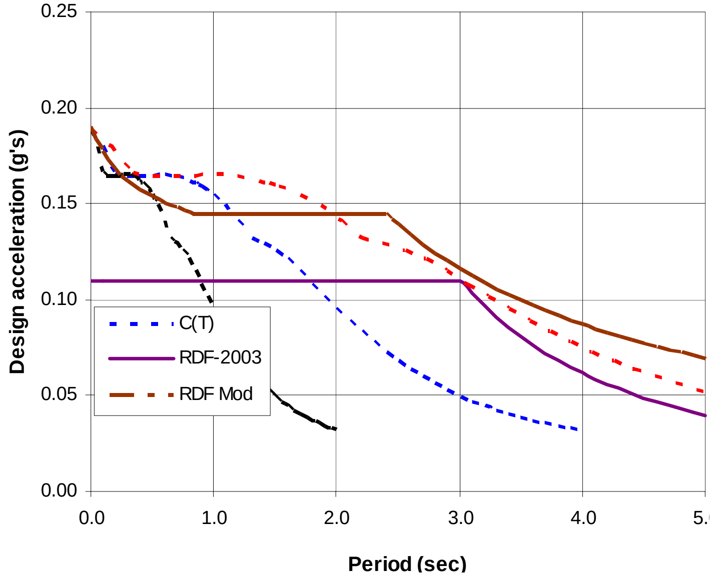

Figure 9. Widened reduced spectra from Eq. 3 (dashed lines), RDF 2003 design spectrum (solid lines) and an example of a modified design spectrum (dash – solid lines), for Q = 4

Concluding remarks

C(T) has been used to develop a widened spectrum for region IIIb of compressible soil of Mexico City. From the comparison of the widened C(T) with a design spectrum prescribed in the 2003 Mexico City Code, it appears that the "elastic spectrum" already incorporates an appreciable reduction due to inelastic behavior. Consistent with this observation, it might be advisable to increase in the code the zero period spectral values.

A comparison of inelastic reduced spectra obtained from statistical analyses of the seismic response and those specified in the 2003 Mexico City Code, indicates that some modifications in the current provisions might be in order to provide a better fit to the results of inelastic analyses.

Acknowldegment

This research was partially supported by the National Science Foundation Division of Engineering Education and Centers under grant 01-21989. The authors are grateful for this support.

References

Jarenprasert, S, (2005). "An inelastic design approach for asymmetric structure-foundation systems," Ph.D. Thesis, Carnegie Mellon University, Pittsburgh, PA, 2005.

Jarernprasert, S, E Bazán and J Bielak (2005). "Inelastic Seismic Design Spectra in Mexico City," XIII National Conference on Seismic Engineering, Mexico, D.F., Mexico

NTCDS-RCDF (2003). "Normas técnicas complementarias para diseño por sismo," *Reglamento de Construcciones para el Distrito Federal*, Gaceta Oficial del Departamento del Distrito Federal, Mexico.

Rosenblueth, E and R Gómez, 1991, "Comentarios a las Normas Técnicas Complementarias para Diseño por Sismo," Series Instituto de Ingeniería No. ES-7, México D.F., México

Professor Anil K Chopra
Johnson Chair in Engineering
University of California
Department of Civil and Environmental Engineering
Berkeley, CA 94720-1710 USA
chopra@berkeley.edu

Dynamics of structures, earthquake engineering

Although I had known Luis Esteva for many years, the opportunity to work closely with him came only a few years ago when he become President of the International Association for Earthquake Engineering (IAEE). I interacted with Luis in my role as Editor of *Earthquake Engineering and Structural Dynamics*, the official journal of IAEE. During the period 2002-2004, the journal underwent major changes, which involved difficult negotiations with other organizations. I went to him several times asking for advice; in fact, so many times that I am sure that he grew to dread my emails. Every time I asked for his help, I admired his ability to identify immediately the essence of the problem, how he was able present his views calmly and effectively in the midst of disagreement, and was steadfast in searching for solutions that were fair to all parties.

Anil K. Chopra
August 12, 2005

ESTIMATING SEISMIC DEMANDS FOR STRUCTURES IN ENGINEERING PRACTICE: CONSTRAINED BY COMPUTER SOFTWARE, BUILDING CODES, AND BUILDING EVALUATION GUIDELINES

ABSTRACT

The main thesis of this paper is that adoption of improved analytical procedures for estimating seismic demands for structures in engineering practice is constrained by the lack of computer software that implement these techniques and by prevailing codes of practice. Two classes of structures, concrete dams and buildings, are chosen to illustrate different aspects of this contention.

Part A: Arch Dams

Analysis Procedures

The dynamic analysis of arch dams is especially complicated because they must be treated as three-dimensional systems that recognize the semi-unbounded size of the reservoir and foundation rock domains, and the following factors should be considered: dam-water interaction, wave absorption at the reservoir boundary, water compressibility, and dam-foundation rock interaction.

A series of Ph.D. theses [Chakrabarti and Chopra 1973; Hall and Chopra 1980; Fenves and Chopra 1984 (a); Fok and Chopra 1985; Zhang and Chopra 1990; Tan and Chopra, 1995] at the University of California, Berkeley, during 1970 to 1995, culminated in the substructure method formulated in the frequency domain, and its implementation in computer programs EAGD-84 for two-dimensional analysis of concrete gravity dams [Fenves and Chopra 1984 (b)] and EACD-3D-96 for three-dimensional analysis of arch dams [Tan and Chopra 1996] both of which were distributed *pro bono* by the National Information Service for Earthquake Engineering. Extensive parametric studies of the earthquake response of actual dams led to an understanding of how each of the preceding factors influences the response, and the practical range of conditions where each factor is significant.

Commonly used finite element analysis techniques for dams, however, ignore most of these factors. Typically, hydrodynamic effects are represented by an added water mass moving with the dam, implying water compressibility is neglected. Also ignored in these analyses is the partial absorption of hydrodynamic pressure waves by the sediments invariably deposited at the reservoir bottom and sides, or even by rock underlying the reservoir. The foundation rock is usually assumed to be massless and a portion is included in a finite-element idealization of the system. This extremely simple idealization of the foundation rock, in which only its flexibility is considered but inertial and damping effects are ignored, is popular because the foundation impedance matrix (or frequency-dependent stiffness matrix) is very difficult to determine for unbounded domains.

Although all of these factors known to be significant in the response of concrete dams were included in computer software developed before desktop computer became standard by graduate students at the University of California, Berkeley, they made no effort to develop input and output interfaces that were user friendly. Thus, they remained primarily as research programs with limited application to actual projects. Easier to use, the EAGD-84 program was chosen as the analytical tool for the seismic safety evaluation of several concrete gravity dams, but the less convenient EACD-3D-96 program was used only for a few arch dam projects.

However, starting in 1996, the U.S. Bureau of Reclamation (USBR) embarked upon a major program to evaluate the seismic safety of dams and found it necessary to consider water compressibility, reservoir boundary absorption, and dam-foundation rock interaction effects. Among the 12 dams investigated were: (1) Deadwood Dam, a 50-m high single curvature dam; (2) Monticello Dam, a 100-m high single curvature dam; (3) Morrow Point Dam, a 150-m high double curvature dam; and (4) Hoover Dam, a 221-m high thick arch dam. The results of EACD-3D analyses of these dams, conducted by L. Nuss and R. Munoz (USBR staff) are presented next.

Implications of Neglecting Water Compressibility

We compare the earthquake-induced stresses in two of the four dams computed under two conditions: water compressibility considered or neglected (Figs. 1 and 2). These figures permit the following observations: the effects of water compressibility, which are generally significant, vary with the location on the dam surface. By neglecting water compressibility, the stresses may be significantly underestimated, as in the case of Monticello Dam (Fig. 1), or significantly overestimated as in the case of Morrow Point Dam (Fig. 2). Thus, water compressibility should be included in the analysis of arch dams; however, most standard finite element analysis software neglects water compressibility.

Implications of Neglecting Foundation Rock Inertia and Damping

We compare the earthquake-induced stresses in each of the four dams, computed under two conditions considering: (1) dam-foundation rock interaction; and (2) foundation rock flexibility only (Figs. 3 through 6). For these two conditions, the largest arch stress on the upstream or downstream face of the dam is 476 psi versus 844 psi for Deadwood Dam; 730 psi versus 1410 psi for Monticello Dam; 665 psi versus 1336 psi for Morrow Point Dam; and 758 psi versus 2204 psi for Hoover Dam. If only foundation rock flexibility is considered (i.e., foundation rock is assumed to be massless), the stresses are overestimated by a factor of 2 (approximately) for the first three dams and by a factor of 3 (approximately) for Hoover Dam.

As demonstrated in the above examples, stresses are overestimated as a result of ignoring the foundation rock material and radiation damping. Because such overestimation of stresses may lead to overconservative designs of new dams and to the erroneous conclusion that an existing dam is unsafe, and, hence, requires remediation, it is imperative that dam-foundation rock interaction effects should be included in earthquake analysis of concrete dams. However, dynamic analyses for most seismic safety evaluation projects assume massless foundation rock, thus ignoring dam-foundation rock interaction effects, because most commercial and proprietary computer software is based, erroneously, on these simplifying assumptions.

Advancement of Engineering Practice

Most of the research developments to include the effects of dam-water interaction, water compressibility, reservoir boundary absorption, and dam-foundation rock interaction in analysis of dams were reported over twenty years ago for gravity dams and over ten years ago for arch dams. However, the profession has resisted using these analytical advances, in part because they have not been incorporated in widely used commercial software.

The state of earthquake engineering practice for dams is not likely to advance unless user-friendly software is developed for desktop computers that includes these interaction effects in linear and nonlinear analysis of dams considering spatial variations in ground motion.

Part B: Buildings

Building Code Development

Most buildings are designed according to procedures specified in building codes, which define the state of practice. In the United States, for example, the most recent code is the International Building Code, first developed in 2000 and subsequently revised in 2003. The structural analysis procedures in this code are based on the *NEHRP Recommended Provisions for Seismic Regulations for New Buildings and Other Structures* (1997), which, in turn, are based on the ATC-3-06 document (1978).

ATC-3-06 represented a major departure from traditional U.S. seismic codes. The new features relevant to structural analysis included:

- Response modification factors (R factors) to reduce elastic response of the structure due to realistic ground motions to obtain design forces; the R factors were dependent on ductility, damping, and past performance of a given structural system.
- Strength-based design instead of allowable stress design.
- Provisions for dynamic (modal) analysis.
- Provisions to consider soil-structure interaction effects.

The ATC-3-06 document was the result of a massive effort during 1974 through 1976 by a team of nearly 70 experts from around the country, and it was reviewed by various overview panels and committees. Although all prominent engineers and academics were involved, its acceptance into formal code documents was a slow process. Evolution of ATC-3-06 to the 1997 NEHRP provisions took twenty years. Until the analysis procedures in the latter were adopted into the IBC (2000), they did not become a part of structural engineering practice in the United States. In contrast, many of the ideas in ATC-3-06 were incorporated very quickly into the 1976 Mexico Federal District Code by Emilio Rosenblueth, who participated in the ATC-3-06 project.

Building Evaluation Guidelines

In contrast to the slow progress in building codes, the guidelines for seismic evaluation of buildings evolved rapidly after the Loma Prieta (1989) and Northridge (1994) earthquakes in California. Two major guideline documents appeared: ATC-40 (1996) and FEMA 273 (1997) [and its successor FEMA 356 (2000)]. According to these guidelines, seismic demands are computed by nonlinear static analysis of the structure subjected to monotonically increasing lateral forces with an invariant heightwise distribution until reaching a roof displacement determined from the deformation of an inelastic SDF system derived from the pushover curve.

According to the ATC-40 guidelines, the deformation of the inelastic SDF system is estimated by the capacity-spectrum method, an iterative method requiring analysis of a sequence of equivalent linear system; the method is typically implemented graphically. Unfortunately, the ATC-40 iterative procedure does not always converge; when it does converge it does not lead to the exact deformation (Chopra and Goel, 2000). Because convergence traditionally implies accuracy, the user could be left with the impression that the calculated deformation is accurate, but the ATC-40 estimate errs considerably. This is demonstrated in Fig. 7a, where the deformation estimated by the ATC-40 method is compared with the value determined from inelastic design spectrum theory and three different $R_y - \mu - T_n$ equations. Both the approximate and theoretical results are presented for systems covering a wide range of period values and ductility factors subjected to ground motions characterized by an elastic design spectrum. The discrepancy in the approximate result presented in Fig. 7b shows that the ATC-40 method underestimates by 40-50% the deformation over a wide range of periods (Chopra and Goel, 2000).

Prompted by research results, such as those reported above, the ATC-55 (or FEMA-440) project was launched in 2002 to develop improved procedures to estimate seismic demands. The two flaws in the ATC-40 capacity spectrum method—lack of convergence in some cases and large errors in many cases—appear to have been rectified in the FEMA-440 report (Comartin et al., 2004). The optimal vibration period and damping ratio parameters for the equivalent linear system are now derived by minimizing the differences between its response and that of the actual inelastic system. Such an equivalent linear method would obviously give essentially the correct deformation. However, the benefit in making the equivalent linearization detour is unclear when the deformation of an inelastic system can be readily determined using available equations for the inelastic deformation ratio [e.g., Ruiz-Garcia and Miranda, 2003; Chopra and Chintanapakdee, 2004) or from the inelastic design spectrum (e.g., Chopra, 2001).

The nonlinear static procedure (NSP) in FEMA-356 requires development of a pushover curve, a plot of base shear versus roof displacement, by nonlinear static analysis of the structure subjected first to gravity loads, followed by monotonically increasing lateral forces with a specified invariant height-wise distribution. At least two force distributions must be considered. The first is to be selected from among the following: first mode distribution, equivalent lateral force (ELF) distribution, and response spectrum analysis (RSA) distribution. The second distribution is either the “uniform” distribution or an adaptive distribution; several options are mentioned for the latter, which varies with change in deflected shape of the structure as it yields. The other four force distributions mentioned above are defined as follows:

1. First-mode distribution: $s_j^* = m_j \phi_{j1}$, where m_j is the mass and ϕ_{j1} is the mode shape value at the *j*th floor.
2. ELF distribution: $s_j^* = m_j h_j^k$, where h_j is the height of the *j*th floor above the base, and *k* varies between 1 and 2, depending on the fundamental vibration period.
3. RSA distribution: $\mathbf{s}^*$ is defined by the lateral forces back-calculated from the story shears determined by response spectrum analysis of the structure, assumed to be linearly elastic.
4. “Uniform” distribution: $s_j^* = m_j$.

Each of these force distributions pushes the building in the same direction over the height of the building (Fig. 8).

The limitations of the FEMA-356 force distributions are demonstrated in Figs. 9 and 10, where the resulting estimates of the median story drift and plastic hinge rotation demands imposed on the SAC–Los Angeles buildings by the ensemble of 20 SAC ground motions are compared with the "exact" median value determined by nonlinear response history analysis (RHA). The FEMA-356 lateral force distributions provide a good estimate of story drifts for the 3-story building. However, the first-mode force distribution grossly underestimates the story drifts in the upper stories of the 9- and 20-story buildings, showing that higher-mode contributions are especially significant in the seismic demands for upper stories. Although the ELF and RSA force distributions are intended to account for higher-mode responses, they do not provide satisfactory estimates of seismic demands for buildings that remain essentially elastic (SAC Boston buildings) or buildings that are deformed far into the inelastic range (SAC Los Angeles buildings) (Goel and Chopra, 2004). The "uniform" force distribution seems unnecessary because it grossly underestimates drifts in upper stories and grossly overestimates them in lower stories. Because FEMA-356 requires that seismic demands be estimated as the larger of results from at least two lateral force distributions, it is useful to examine the upper bound of results from the four force distributions considered. This upper bound also significantly underestimates drifts in upper stories of taller buildings but overestimates them in lower stories (Fig. 9). The FEMA-356 lateral force distributions provide a good estimate of plastic hinge rotations for the 3-story building, but either fail to identify, or significantly underestimate, plastic hinge rotations in beams at the upper floors of 9- and 20-story buildings (Fig. 10). Many discussions of the potential and limitations pushover analysis are available in the literature (e.g., Naeim and Lobo, 1998; Krawinkler and Seneviratna, 1998; Elnashai, 2001; Fafar, 2002).

Despite the limitations of the ATC-40 procedure for estimating the target roof displacement and the FEMA 273/356 nonlinear static procedure for estimating seismic demands, these procedures have had profound influence on engineering practice not only in the United States, where these procedures were developed, but in several other countries, and they continue to be used. Eventually, they will be replaced by improved procedures that are emerging, but their acceptance into codes and guidelines is likely to be a slow process. Because it is so difficult to make major modifications to such documents, it is imperative that in the future any analytical procedure should be thoroughly researched and tested before it is included.

Improved Nonlinear Static Procedures

It is clear from the preceding discussion that the seismic demand estimated by NSP using the first-mode force distribution (or others in FEMA-356) should be improved. One approach to reducing the discrepancy in this approximate procedure relative to nonlinear RHA is to include the contributions of higher modes of vibration to seismic demands. It is well known that when higher-mode responses are included in the RSA procedure, improved results are obtained for linearly elastic systems.

Although modal analysis theory is strictly not valid for inelastic systems, the fact that elastic modes are coupled only weakly in the response of inelastic systems (Chopra and Goel 2002, 2004) permitted development of the *modal pushover analysis procedure* (MPA). In this MPA procedure, the peak "modal" demand r_n (n denotes mode number) is determined by a nonlinear static or pushover analysis using the modal force distribution $\mathbf{s}_n^* = \mathbf{m}\boldsymbol{\phi}_n$ (m is the mass matrix and $\boldsymbol{\phi}_n$ is the nth vibration mode) up to a target displacement determined from the deformation of the *n*th-"mode" inelastic SDF system;

and the peak modal demands r_n are then combined by an appropriate modal combination rule.

Figures 11 and 12 show the median values of story drift and beam plastic rotation demands, respectively, for SAC—Boston, Seattle, and Los Angeles buildings—including a variable number of "modes" in MPA superimposed with the "exact" result from nonlinear RHA. The first "mode" alone is inadequate in estimating story drifts, but with a few "modes" included, story drifts estimated by MPA are generally similar to the upper floors of all buildings and also in the lower floors of the Seattle 20-story building. Including higher-"mode" contributions also improves significantly the estimate of plastic hinge rotations. In particular, plastic hinging in upper stories is now identified, and the MPA estimate of plastic rotation is much closer—compared to the first-"mode" result—to the "exact" results of nonlinear RHA.

Based on structural dynamics theory, the MPA procedure retains the conceptual simplicity and computational attractiveness of the standard pushover procedures with invariant lateral force distribution. Because higher-mode pushover analyses are similar to the first-mode analysis, MPA is conceptually no more difficult than procedures now standard in structural engineering practice. Because pushover analyses for the first two or three modal force distributions are typically sufficient in MPA, it requires computational effort that is comparable to the FEMA-356 procedure, which requires pushover analysis for at least two force distributions. Without additional conceptual complexity or computational effort, MPA estimates seismic demands much more accurately than FEMA-356 procedures (Goel and Chopra 2004).

Advancement of Engineering Practice

Building codes should explicitly state the underlying basis for each provision, so that it can be improved as we develop a better understanding of structural dynamics and earthquake performance of structures. Such a transparent format should be combined with a mechanism to incorporate improvements more quickly than has been feasible in the past.

Design codes and evaluation guidelines for buildings should be consistent with research results and actual performance of structures during earthquakes. They should be tested extensively before promulgation. The ATC-40 and FEMA-273 documents do not seem to have satisfied this requirement.

Presently, developers of commercial software are followers, in the sense that they implement analysis procedures specified in building design codes and evaluation guidelines. To advance the state of engineering practice, they should become leaders in incorporating research results—for example, improved nonlinear static procedures—into their software so that the profession can use these procedures during the many years they are being considered by committees for possible adoption in building evaluation guidelines.

Closing Comments

This paper has attempted to demonstrate that adoption of improved analytical techniques for estimating seismic demands for structures in engineering practice is constrained by the lack of computer software that implement these techniques and by prevailing codes of practice. The structural types and analytical procedures chosen to illustrate this contention were obviously based on my research experience. However, the overall issue is of broader concern and other researchers may be able to identify supporting examples from their own experience.

References

Applied Technology Council (1978). Tentative provisions for the development of seismic regulations for buildings, *Report ATC-3-06, NBS Special Publication 510, NSF Special Publication 78-08*.

Applied Technology Council (1996). Seismic evaluation and retrofit of concrete buildings, *Report ATC-40*, ATC, Redwood City, Calif.

Building Seismic Safety Council (1997). NEHRP guidelines for the seismic rehabilitation of buildings, *FEMA-273*, Federal Emergency Management Agency, Washington, D.C.

Chakrabarti, P., and A. K. Chopra (1972). Earthquake Response of Gravity Dams Including Reservoir Interaction Effects, *Report No. EERC 72-6*, Earthquake Engineering Research Center, University of California, Berkeley, 161 pp.

Chopra, A. K. (2001). *Dynamics of Structures: Theory and Applications to Earthquake Engineering*, 2nd ed., Prentice Hall, Upper Saddle River, N.J., 844 pp.

Chopra, A. K., and C. Chintanapakdee (2004). Inelastic deformation ratios for design and evaluation of structures: single-degree-of-freedom bilinear systems, ASCE, *J. Struct. Engrg*., 130 (9), 1309–1319.

Chopra, A. K, and R. K. Goel (2000). Evaluation of NSP to estimate seismic deformation: SDF systems, ASCE, *J. Struc. Engrg.*, 26, 482–490.

Chopra, A. K., and R. K. Goel (2002). A modal pushover analysis procedure for estimating seismic demands for buildings, *Earthq. Engrg. Struc. Dyn*., 31, 561–582.

Chopra, A. K., and R. K. Goel (2004). A modal pushover analysis procedure to estimate seismic demands for unsymmetric-plan buildings, *Earthq. Engrg. Struc. Dyn*., 33 (8), 903–927.

Comartin, C. D., et al. (2004). A summary of FEMA-440: improvement of nonlinear static seismic analysis procedures, *Proceedings*, 13th World Conf. Earthq. Engrg., Paper 1476, Vancouver, British Columbia, Canada.

Fenves, G., and A. K. Chopra (a) (1984). Earthquake analysis and response of concrete gravity dams, *Report No. UCB/EERC-84/10*, Earthquake Engineering Research Center, University of California, Berkeley, 213 pp.

Fenves, G., and A. K. Chopra (b) (1984). EAGD-84: A computer program for earthquake analysis of concrete gravity dams, *Report No. UCB/EERC-84/11*, Earthquake Engineering Research Center, University of California, Berkeley, 78 pp.

Elnashai, A. S. (2001). Advanced inelastic static (pushover) analysis for earthquake applications, *Struc. Engrg. Mech*., 12 (1), 51–69.

Fajfar, P. (2002). Structural analysis in earthquake engineering—a breakthrough of simplified nonlinear methods, *Proceedings,* 12th Eur. Conf. Earthq. Engrg., London, Paper Ref. 843.

Fok, K.-L., and A. K. Chopra (1985). Earthquake analysis and response of concrete arch dams, *Report No. UCB/EERC-85/07*, Earthquake Engineering Research Center, University of California, Berkeley, 207 pp.

Goel, R. K., and A. K. Chopra (2004). Evaluation of modal and FEMA pushover analyses: SAC buildings, *Earthq. Spectra*, 20, (1), 225–254.

Hall, J. F., and A. K. Chopra (1980). Dynamic response of embankment, concrete-gravity and arch dams including hydrodynamic interaction, *Report*

No. UCB/EERC-80/39, Earthquake Engineering Research Center, University of California, Berkeley, 220 pp.

Krawinkler, H., and G. D. P. K. Seneviratna (1998). Pros and cons of a pushover analysis of seismic performance evaluation, *Engrg. Struc.*, 20 (4-6), 452–464.

Naeim, F., and R. M. Lobo (1998). Common pitfalls in pushover analysis, *Proceedings*, SEAOC Annu. Conv., Reno, Nev.

Ruiz-Garcia, J., and E. Miranda (2003). Inelastic displacement ratios for evaluation of existing structures, *Earthq. Engrg, Struc. Dyn*., 32 (8),1237–1250.

Tan, H. C., and A. K. Chopra (1995). Earthquake analysis and response of concrete arch dams, *Report No. UCB/EERC-95/07*, Earthquake Engineering Research Center, University of California, Berkeley,168 pp.

Tan, H. C., and A. K. Chopra (1996). EACD-3D-96: A computer program for three-dimensional earthquake analysis of concrete dams, *Report No. UCB/SEMM-96/06*, University of California, Berkeley, 131 pp

Zhang, L., and A. K. Chopra (1991). Computation of spatially-varying ground motion and foundation-rock impedance matrices for seismic analysis of arch dams, *Report No. UCB/EERC-91/06*, Earthquake Engineering Research Center, University of California, 121 pp.

(a)

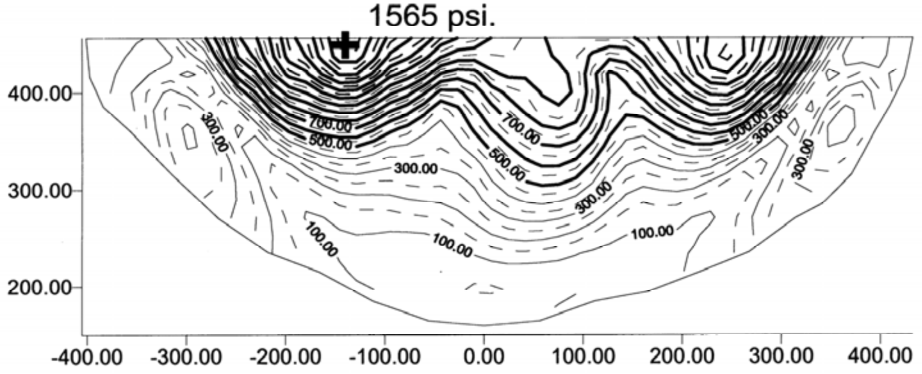

(b)

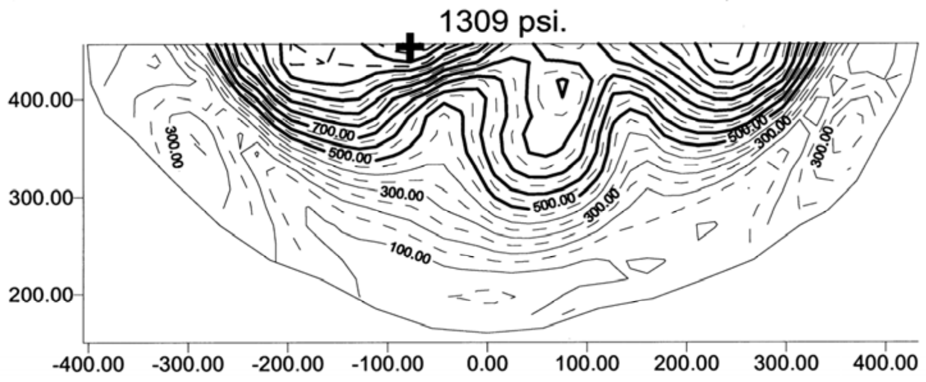

Figure 1. Peak values of earthquake-induced stresses in Monticello Dam computed under two conditions: (a) water compressibility considered, and (b) water compressibility neglected

(a)

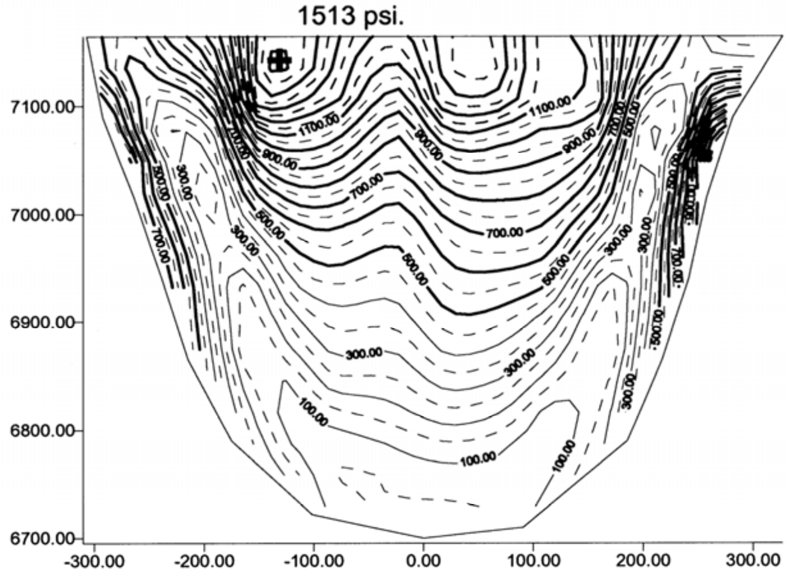

(b)

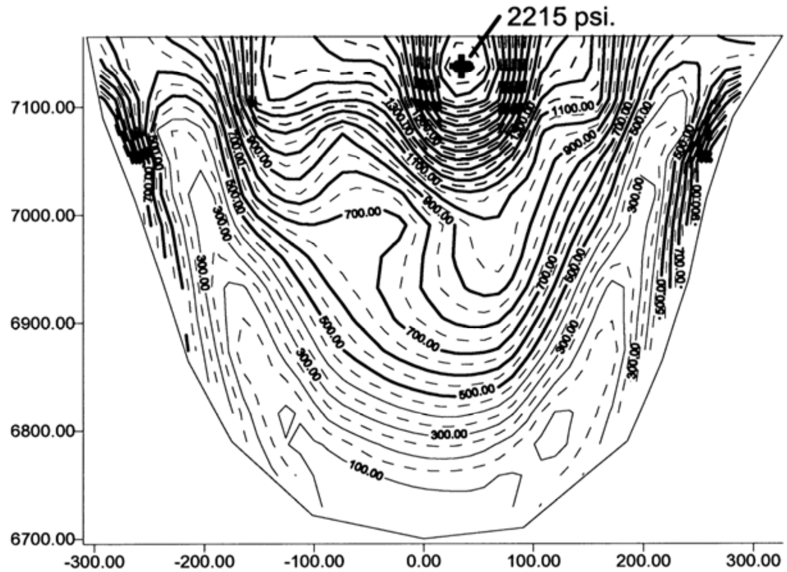

Figure 2. Peak values of earthquake-induced stresses in Morrow Point Dam computed under two conditions: (a) water compressibility considered, and (b) water compressibility neglected

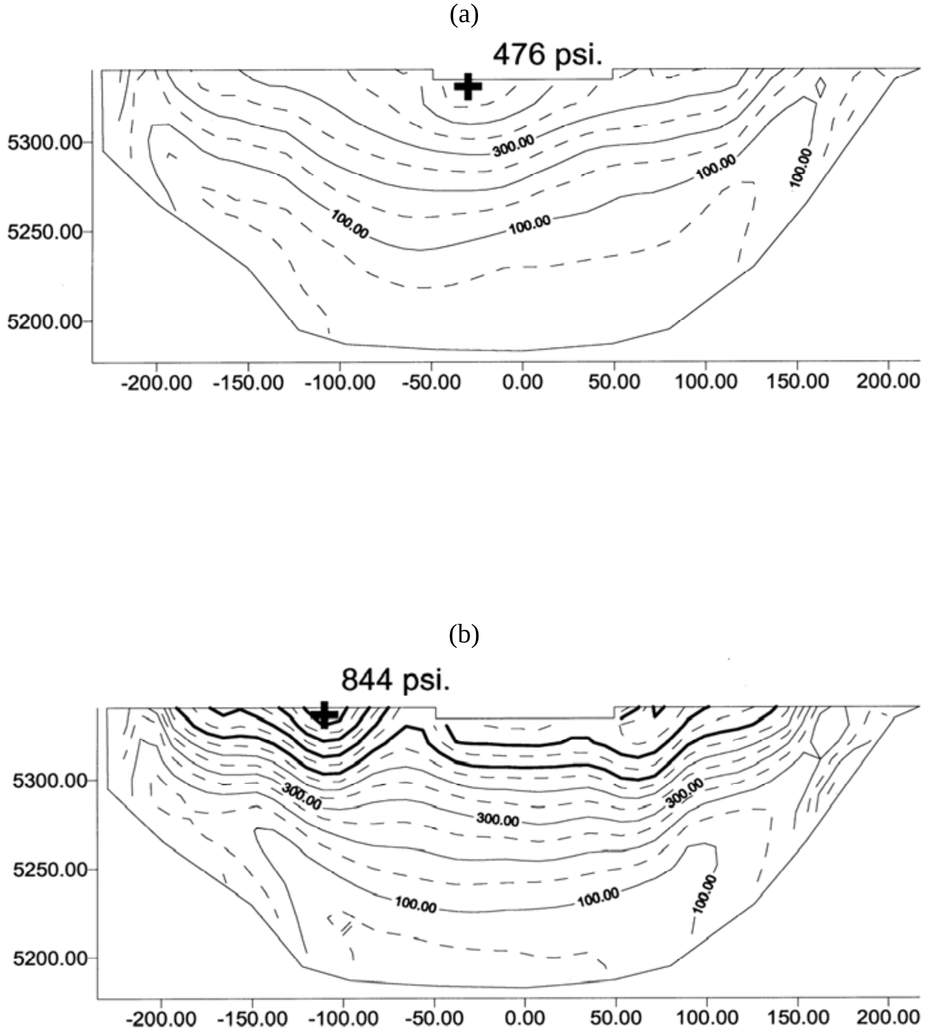

Figure 3. Peak values of earthquake-induced stresses in Deadwood Dam, considering (a) dam-foundation interaction, and (b) foundation rock flexibility only

(a)

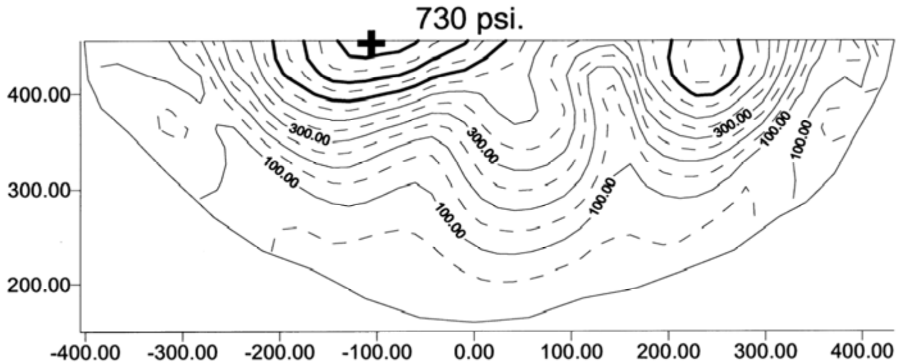

(b)

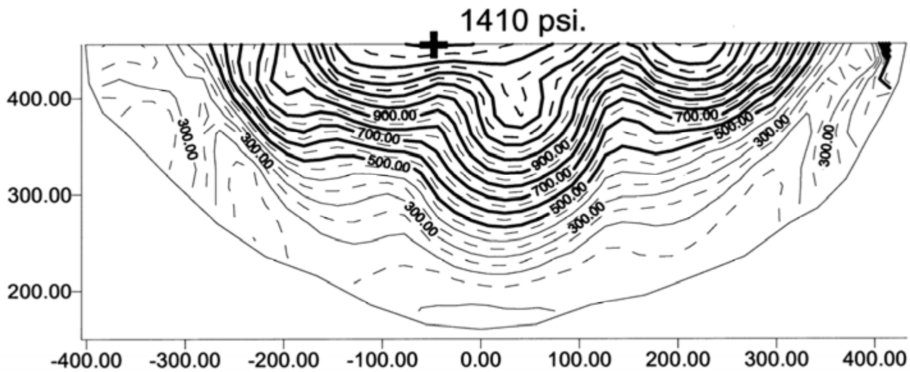

Figure 4. Peak values of earthquake-induced stresses in Monticello Dam, considering (a) dam-foundation interaction, and (b) foundation rock flexibility only

(a)

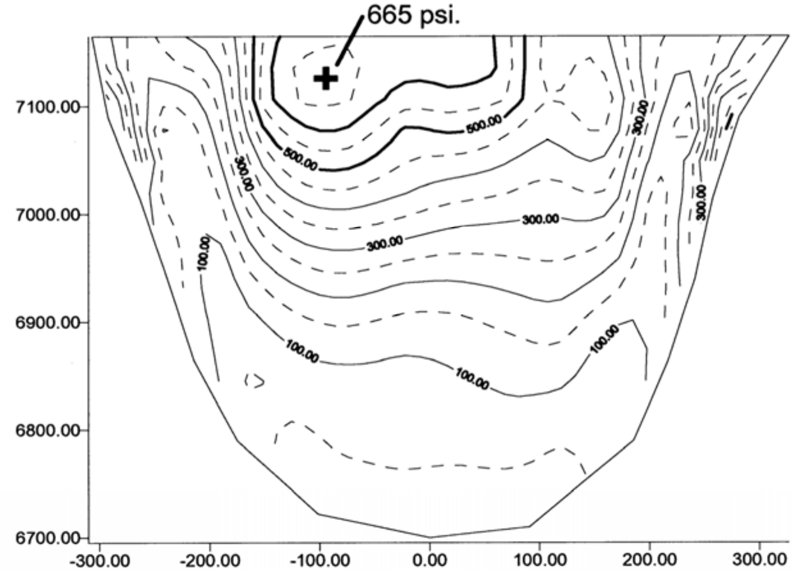

(b)

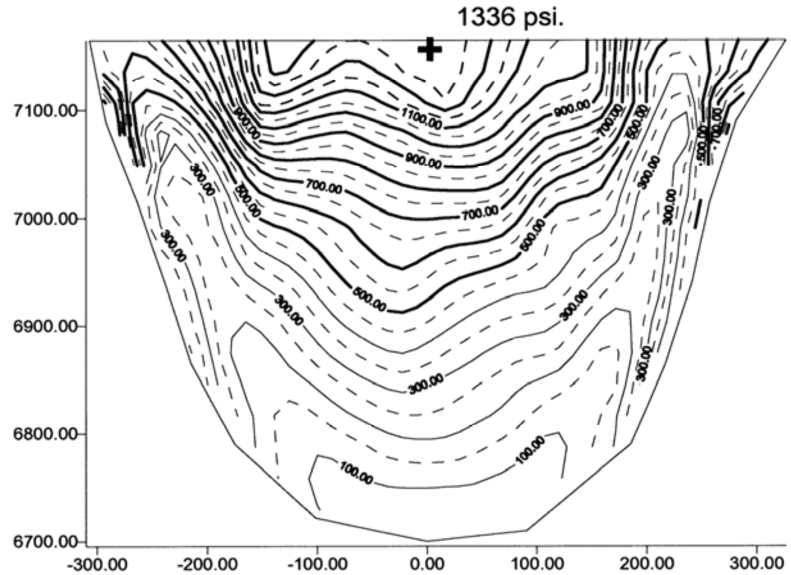

Figure 5. Peak values of earthquake-induced stresses in Morrow Point Dam, considering (a) dam-foundation interaction, and (b) foundation rock flexibility only

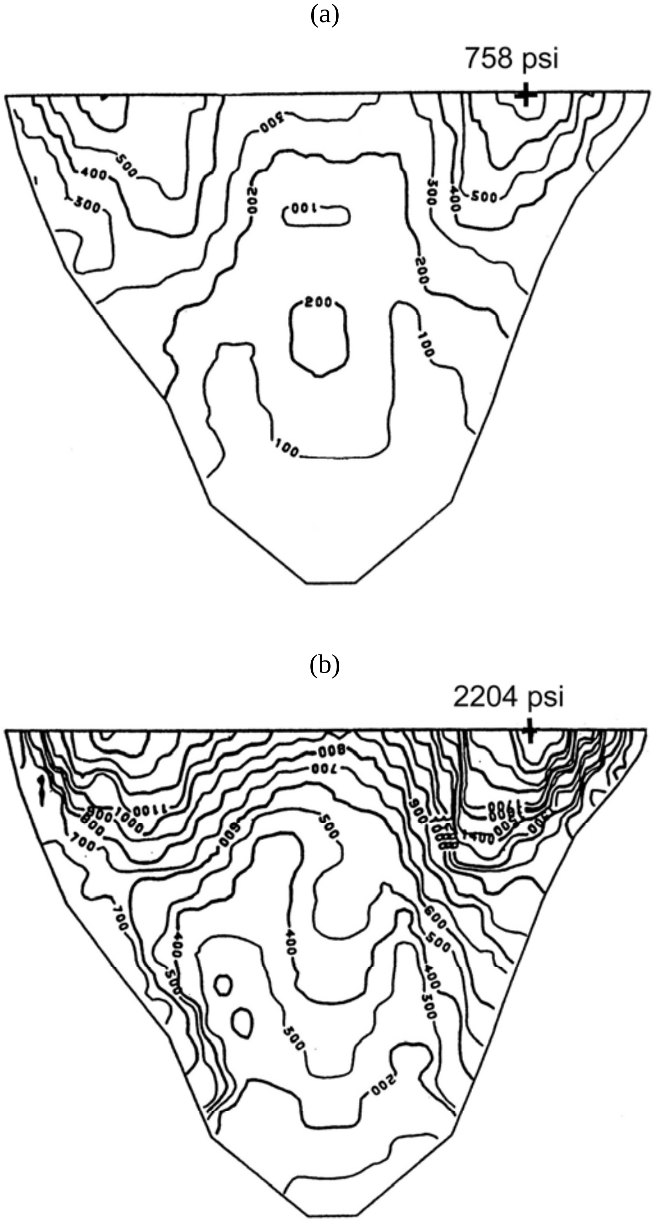

Figure 6. Peak values of earthquake-induced stresses in Hoover Dam, considering (a) dam-foundation interaction, and (b) foundation rock flexibility only

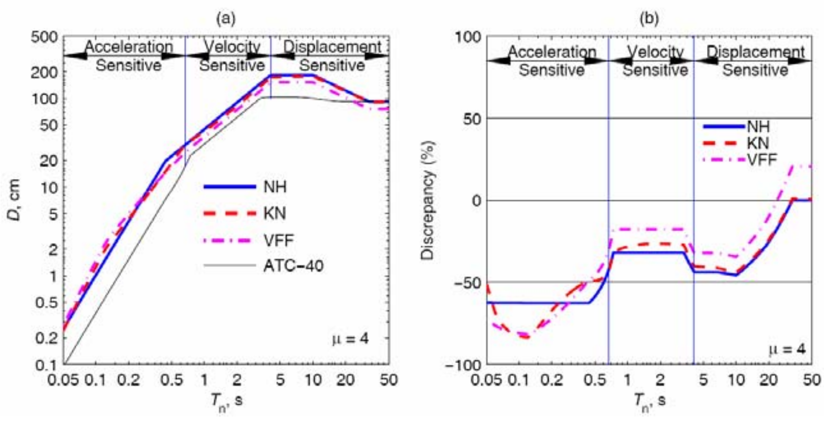

Figure 7. Deformations computed by ATC-40 and from inelastic design spectrum using three different $R_y - \mu - T_n$ equations (identified by NH, KN, and VFF; part (a) compares deformations and part (b) shows discrepancy in ATC-40 method. [Adapted from Chopra and Goel, 2000]

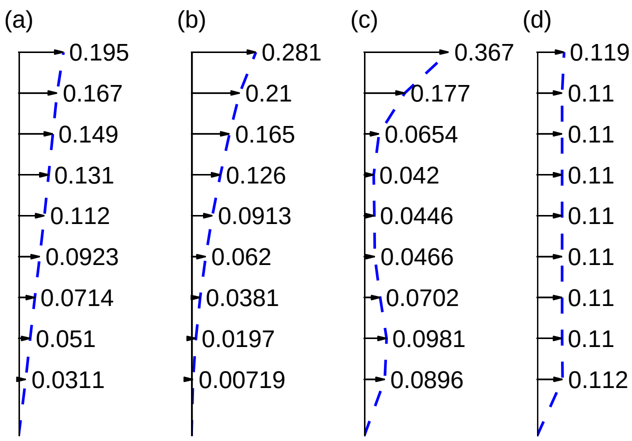

Figure 8. FEMA-356 force distributions for SAC-Los Angeles 9-story building: (a) first mode, (b) ELF, (c) RSA, and (d) “uniform”

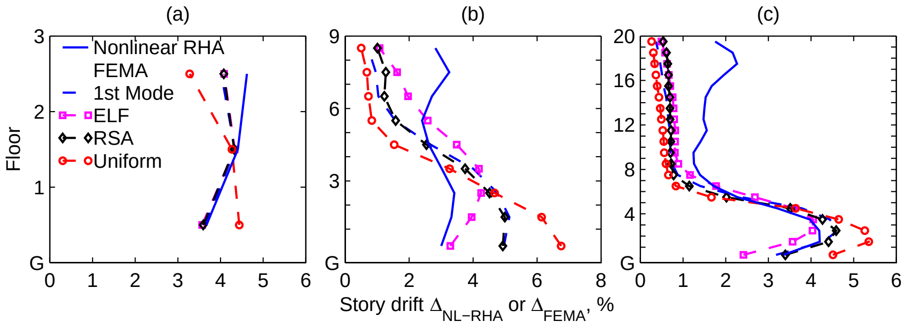

Figure 9. Median story drifts for SAC-Los Angeles buildings: (a) 3-story; (b) 9-story; (c) 20-story. Determined by nonlinear RHA and four FEMA-356 force distributions: first Mode, ELF, RSA, and "uniform" (Goel and Chopra 2004)

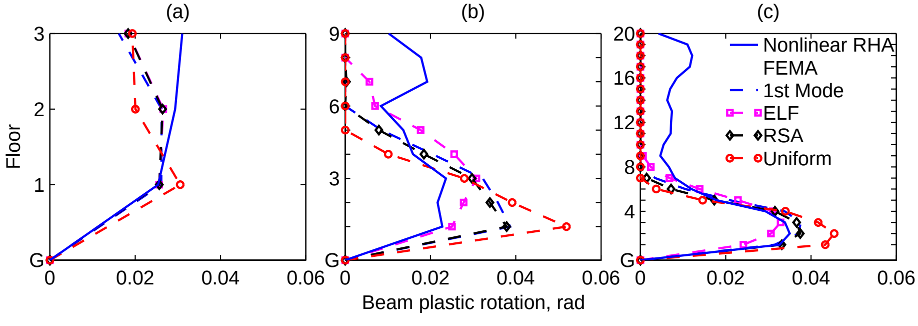

Figure 10. Median plastic rotations in interior beams of SAC–Los Angeles buildings: (a) 3-story; (b) 9-story; (c) 20-story. Determined by nonlinear RHA and four FEMA-356 force distributions: first Mode, ELF, RSA, and "uniform" (Goel and Chopra 2004)

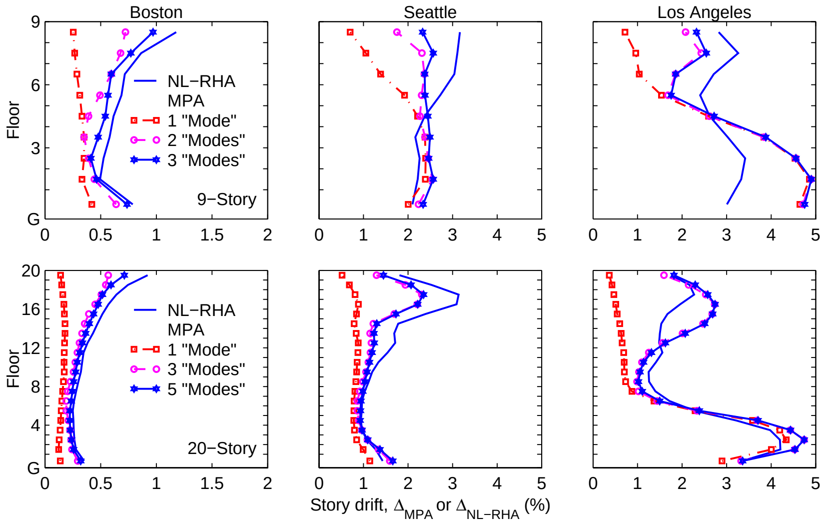

Figure 11. Median story drifts determined by nonlinear RHA and MPA with variable number of "modes"; P-Δ effects due to gravity loads are included (Goel and Chopra 2004)

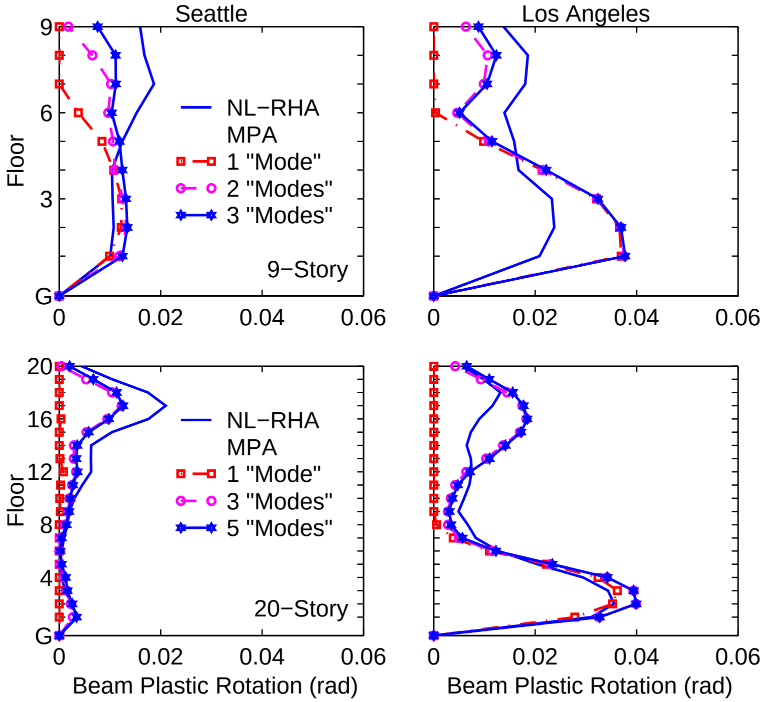

Figure 12. Median plastic rotations in interior beams determined by nonlinear RHA and MPA with variable number of "modes"; P-Δ effects due to gravity loads are included (Goel and Chopra 2004

Palle Thoft-Christensen
Professor Emeritus
Aalborg University
Sohngaardsholmsvej 57, DK-9000 Aalborg, Denmark
ptc@bt.aau.dk

Main research interests: Structural reliability, structural optimization, life-cycle cost analysis, deterioration of materials, bridge engineering, stochastic dynamics.

On this occasion I would like to appreciate the scientific contributions Professor Luis Esteva has made to the IFIP working group WG7 on "Reliability and Optimization of Structural Systems". This working group has organized 12 conferences since its start in 1985, and Professor Esteva has presented papers at 6 of these conferences, namely at the 3rd conference in Berkeley, USA, 1990, at the 5th conference in Takamatsu, Japan, 1993, at the 6th conference in Assisi, Italy, 1994, at the 7th conference in Boulder, USA, 1996, at the 9th conference in Ann Arbor, USA, 2000, and at the 11th conference in Banff, Canada; 2004. The titles of the papers were:

- Calibration of Seismic Reliability Models,
- Influence of Cumulative Damage on the Seismic Reliability of Multi-Storey Frames (with O. Diaz),
- Towards Consistent-Reliability Structural Design for Earthquakes,
- Seismic Damage Indexes in Decisions related to Structural Safety (with O. Diaz),
- Seismic Reliability of Structural Systems: A Model Based on the reduction of Stiffness and Deformation Capacity (with O. Díaz-López, J. García-Pérez, and D. Pérez-Gómez),
- A Maximum Likelihood Approach to System Reliability with Respect to Seismic Collapse (with E. Ismael).

These papers contain excellent contributions where a number of issues in structural reliability are related to earthquake theory and applications. The working group has really taken advantage of his outstanding research on earthquake engineering. Professor Esteva has been a member of the Working Group since 1993. Also, Professor Esteva has participated in several other IFIP working groups and conferences with an impressive, broad spectrum of advanced papers related to application of theoretical topics on earthquake engineering. He is now retiring from the National University of Mexico, but his research work in the above-mentioned organizations and several other organizations and institutions will be remembered for many years ahead.

Finally, I would like to thank Professor Esteva for the joyful hours we have spent together in many countries all over the world. His very kind and positive attitude to new ideas has been a great inspiration to all of us.

Palle Thoft-Christensen

RECENT PROGRESS IN MODELLING DETERIORATION OF REINFORCED CONCRETE STRUCTURES

ABSTRACT

The main purpose of this paper is to give an overview of some recent progress made in modelling of deterioration of reinforced concrete structures. The review is not claimed to be complete. It is based on some of the author's contributions in this research area especially the papers (Thoft-Christensen 2001) and (Thoft-Christensen, Svensson and Frandsen 2005).

In the paper, corrosion of reinforced concrete structures is discussed from the point of view of corrosion products. The different types of corrosion products are presented and the important diffusion coefficient is discussed. Modelling of corrosion initiation, corrosion propagation, corrosion cracking and corrosion crack opening is presented.

Introduction

The classical modelling of deterioration of reinforced concrete structures is based on observations of the deterioration of existing structures and on comprehensive experiments in laboratories all over world. By such observations the so-called deterioration profile (deterioration, reliability, or capacity as a function of time) may be estimated. A large number of such observation profiles have been estimated by curve fitting. The advantage of this approach is that the deterioration profile is described by simple curves which are easy to use in analysis and design of reinforced concrete structures, see e.g. (Ellingwood 2005). The disadvantage is that it is not easy to estimate the deterioration profiles for new structures and new materials, since the deterioration curves are not directly related to physical, mechanical, or chemical parameters.

In a recent more modern approach on the estimation of the deterioration is based on a detailed understanding of the chemical and physical processes that take place during deterioration. This approach is used in this paper. In the paper, only deterioration related to corrosion of the reinforcement is considered, since corrosion of the reinforcement is one of the major reasons for deterioration of reinforced concrete structures. Initially, the main effect of corrosion is reduced strength of the structural element in question due to a reduced cross-section of the reinforcement, and therefore, also a reduction of the structural reliability. However, there is a close interaction between corrosion and the bond between the concrete and the reinforcement. A reduced bond will also influence the structural reliability of the structure and must therefore be included in a complete estimation of the deterioration process. Important research on bonding is taking place in several research institutions, see e.g. (Lundgren 2002) and (Maurel, Dekoster and Buyle-Bodin 2005).

The corrosion is a serious problem due to the reduction of the reinforcement and since the volume of the rust products is higher than the volume of the corroded steel. The porous zone around the steel/concrete surface can to some extent absorb the higher volume of the rust products. However, at a certain time the total amount of corrosion products exceeds the amount of corrosion products needed to fill the porous zone around the reinforcement. The rust products will then create expansive pressure on the surrounding concrete. The expansion of the concrete near the reinforcement will initiate tensile stresses in the concrete. After some time with increasing corrosion the tensile stresses will reach a critical value and corrosion cracks may develop. With further production of rust, the crack opening will increase and eventually result in spalling. This last part of the corrosion process is still not well understood. More research is certainly needed to clarify these important problems for a corroded reinforced concrete structure.

Chloride-Induced Corrosion

Chloride-induced corrosion has been investigated by e.g. (Neville 2000). Reinforced concrete is an excellent type of structure from a corrosion point of view, since the alkaline environment in the concrete maintains a passive film on the surface of the reinforcement, and this film protects the reinforcement against corrosion. However, if the concrete is penetrated by e.g. water or carbon dioxide, then this passive film breaks down and the reinforcement is open to corrosion. An anodic region is established, where the passive film is broken down, whereby an electrochemical cell is formed. The passive surface is the cathode, and the electrolyte is the pore water in the concrete. At the anode the following reactions take place:

$$\begin{aligned} &Fe \rightarrow Fe^{++} + 2e^{-} \\ &Fe^{++} + 2(OH)^{-} \rightarrow \mathbf{Fe(OH)_2} \\ &4Fe(OH)_2 + 2H_2O + O_2 \rightarrow 4\,\mathbf{Fe(OH)_3} \end{aligned} \tag{1}$$

Chloride ions Cl^{-} activate the unprotected surface and form an anode. The chemical reactions are

$$\begin{aligned} &Fe^{++} + 2Cl^{-} \rightarrow FeCl_2 \\ &FeCl_2 + 2H_2O \rightarrow \mathbf{Fe(OH)_2} + 2HCL \end{aligned} \tag{2}$$

It follows from Eqs. (1) and (2) that two rust products $Fe(OH)_2$ and $Fe(OH)_3$ are produced in this case.

TABLE 1. Volume of corrosion products corresponding to corrosion of 1 cm^3 Fe

Corrosion product	**Colour**	**Volume, cm^3**
Fe_3O_4	Black	2.1
$Fe(OH)_2$	White	3.8
$Fe(OH)_3$	Brown	4.2
$Fe(OH)_3,3H_2$	Yellow	6.4

The different types of rust products are interesting to study because they have great influence on corrosion cracking, since the volume of the rust products corresponding to a given volume of the steel varies a lot. This problem has been studied for several corrosion products by (Nielsen 1976). He has obtained the rust volumes corresponding to corrosion of 1 cm^3 Fe, see Table 1.

The Chloride Diffusion Process

The penetration of chloride ions into the concrete is difficult to model. Some simplifying assumptions are needed. There seems to be a general agreement that a model based on diffusion theory is a reasonably good approximation. If the chloride concentration C_0 on the surface of the concrete and the diffusion coefficient D for concrete are independent of space (location) and time, then Fick's law of diffusion can represent the rate of chloride penetration into concrete, as a function of depth from the concrete surface and as a function of time

$$\frac{dC(x,t)}{dt} = D \ \frac{d^2C(x,t)}{dx^2} \tag{3}$$

where $C(x,t)$ is the chloride ion concentration, as % by weight of cement, at a distance of x cm from the concrete surface after t seconds of exposure to the chloride source. D is the chloride diffusion coefficient expressed in cm^2/sec. The solution of the differential Eq. 3 is

$$C(x,t) = C_0 \left\{ 1 - \mathrm{erf}\left(\frac{x}{2\sqrt{D \ \cdot t}} \right) \right\} \tag{4}$$

where C_0 is the equilibrium chloride concentration on the concrete surface, as % by weight of cement, erf is the error function.

The chloride ingress with a time-dependent chloride concentration at the concrete surface has been investigated by (Frederiksen, Mejlbro and Poulsen 2000) and by (Mejlbro 1996) on the basis of a solution of the diffusion law with time-dependent diffusion coefficient and time-dependent surface concentration. (Mejlbro and Poulsen 2000) have considered the special case where the time dependent chloride concentration on the surface is approximated by a piecewise set of linear functions versus time. Such an approach is relevant for e.g. bridges where de-icing salt containing chloride is used during the winter period.

It is further assumed that a corrosion process is initiated when the chloride concentration at the site of the reinforcement reaches a certain critical chloride corrosion threshold value C_{cr}. The critical chloride threshold depends on the type of concrete and several other factors, see e.g. (Frederiksen 2000). If C_{cr} is assumed to be the chloride corrosion threshold and d is the thickness of the concrete cover, then the corrosion initiation period T_{corr} can be calculated. The time T_{corr} to initiation of reinforcement corrosion is

$$T_{corr} = \frac{d^2}{4D} (erf^{-1}(\frac{C_{cr} - C_0}{C_i - C_0}))^{-2} \tag{5}$$

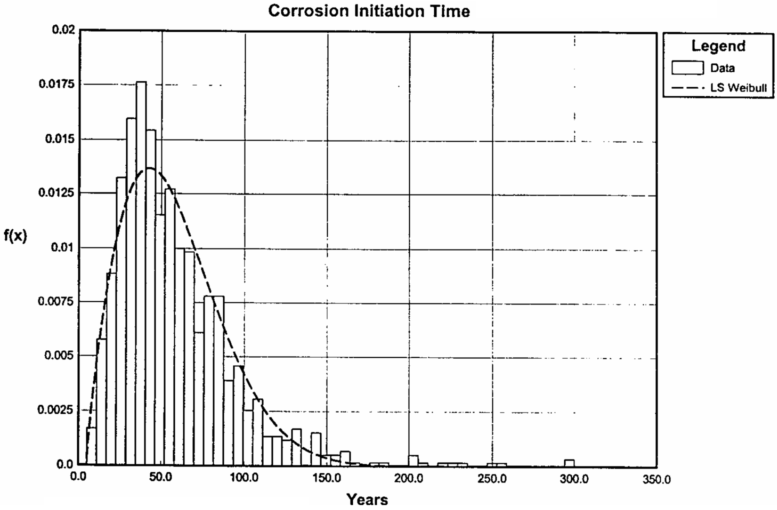

Figure 1. Density function of the corrosion initiation time T_{corr} (Thoft-Christensen 2000)

On the basis of Eq. 5 outcomes of the corrosion initiation time T_{corr} have been performed on the basis of the following data by simple Monte Carlo simulation (Thoft-Christensen 2000)

Initial chloride concentration:	0 %,
Surface chloride concentration:	Normal (0.650 ; 0.038),
Diffusion coefficient:	Normal (30 ; 5),
Critical concentration:	Normal (0.3 ; 0.05),
Cover:	Normal (40 ; 8).

A Weibull distribution can be used to approximate the distribution of the simulated data. The Weibull distribution is $W(x; \mu, k, \varepsilon)$, where μ = 63.67, k = 1.81 and ε = 4.79 . The corresponding histogram and the density function are shown in Fig. 1.

The Diffusion Coefficient *D*

It follows from Eq. 5 that the time to corrosion imitation T_{corr} is inversely proportional to the diffusion coefficient D. It is therefore of great interest to get a good estimate of D. The diffusion coefficient D is not a real physical constant for a given concrete structure, since it depends on a number of physical factors. The most important factors are the water/cement ratio w/c, the temperature Φ, and the amount of e.g. silica fume (s.f.), see (Jensen 1998) and (Jensen, Hansen, Coats and Glasser 1999). The data presented in this section are all based on (Jensen 1998) and (Jensen, Hansen, Coats and Glasser 1999).

Fig. 2 shows the diffusion coefficient D as a function of the water-cement ratio w/c and the temperature Φ °C for cement pastes with 0 % silica fume. It is clear from Fig. 2 that the diffusion coefficient D increases significantly with w/c as well as the temperature Φ. It is clearly of great importance to get good estimates of w/c and Φ. The w/c value to be used is the original w/c value when the concrete was produced. If the original value of *w/c* is not available, then it can be estimated by testing of the concrete. The temperature Φ is more complicated to estimate, since the temperature usually varies a lot. As a first estimate, it is suggested to use an equivalent value based on information of the variation of the temperature during the year at the site of the structure. The addition of silica fume is of great importance for the chloride ingress. Silica fume additions reduce the chloride ingress because of changes in the pore structure (Jensen 1998).

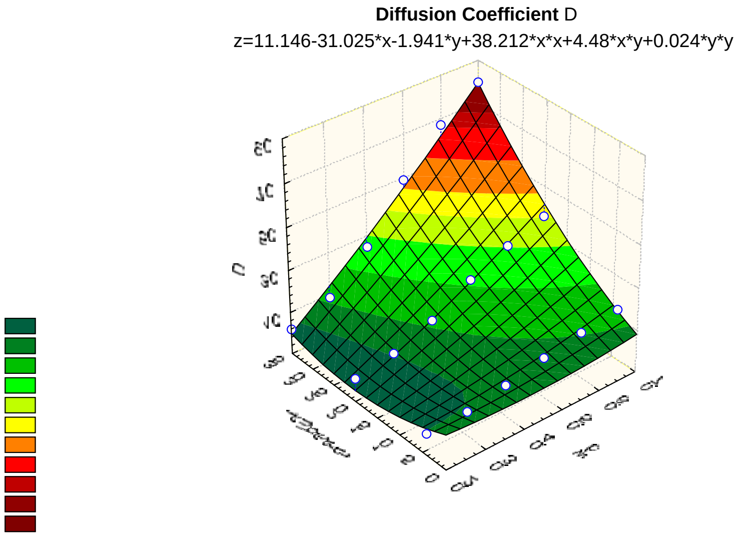

Figure 2. The diffusion coefficient D $(10^{-12}\ m^2/s)$ *as a function of w/c and of the temperature* Φ (Thoft-Christensen 2002)

Initiation of Corrosion Cracks

The corrosion process after corrosion initiation is very difficult to model, since a large number of changes in the rebars as funtions of the time have been observed and reported in the literature. The simplest model is to assume that the diameter $d(t)$ of the reinforcement bars at the time $t > T_{corr}$ is modelled by

$$d(t) = d_0 - c_{corr} i_{corr} (t - T_{corr}) \tag{6}$$

where d_0 is the initial diameter, c_{corr} is a corrosion coefficient, and i_{corr} is the rate of corrosion. Based on a survey, three models for chloride penetration have been proposed (the initial chloride concentration in the concrete is assumed to be zero): low, medium, and high deterioration, (Thoft-Christensen & Jensen 1996). There is a porous zone around the steel/concrete surface caused by the transition from paste to steel, entrapped/entrained air voids, and corrosion products diffusing into the capillary voids in the cement paste. When the total amount of corrosion products exceeds the amount of corrosion products needed to fill the porous zone around the steel, the corrosion products create expansive pressure on the surrounding concrete. Close to reinforcement bars the concrete has some porosity. Very close to the bars the porosity is close to 1, but the porosity decreases with the distances from the bars. The porosity is typically of the order of 0.5 about 10-20 μ m from the bars. Let t_{por} be the thickness of an equivalent zone with porosity 1 around a steel bar, and let t_{por} be modelled by a lognormal distribution with the mean 12.5 μ m and a standard deviation of 2.54 μ m. Further, let the density ρ_{rust} of the rust product and the initial diameter d_0 be modelled by normal distributions N (3600,360) kg/m^3 and N (16,1.6) mm, respectively. Then it can be shown by Monte Carlo simulation that the volume of the porous zone W_{porous} with a fairly good approximation can be modelled by a shifted lognormal distribution with a mean 2.14e$-$03 kg/m, a standard deviation 0.60e$-$03 kg/m and a shift of 0.82e$-$03 kg/m, see (Thoft-Christensen 2000).

After a certain time the rust products will fill the porous zone completely and then result in an expansion of the concrete near the reinforcement. As a result of this, tensile stresses are initiated in the concrete. With increasing corrosion the tensile stresses will reach a critical value and cracks will be developed. During this process the corrosion products at initial cracking of the concrete will occupy three volumes, namely the porous zone W_{porous}, the expansion of the concrete due to rust pressure W_{expan}, and the space of the corroded steel W_{steel}. The corresponding total amount of critical rust products W_{crit} needed to fill these volumes is

$$W_{crit} = W_{porous} + W_{expan} + W_{steel} \tag{7}$$

Using Monte Carlo simulation it can be shown that W_{expan} with a good approximation can be modelled by a normal distribution N(0.0047 , 0.0011) kg/m when the data shown above are used, see (Thoft-Christensen 2000). Finally, W_{steel} can be written

$$W_{steel} = \frac{r_{rust}}{r_{steel}} M_{steel} \tag{8}$$

where ρ_{steel} is the density of steel and M_{steel} is the mass of the corroded steel. Clearly, M_{steel} is proportional to W_{crit}. Liu & Weyers (1998) have calculated the factor of proportionality for two kinds of corrosion products as 0.523 and 0.622. For simplicity, it will be assumed that $M_{steel} = 0.57 W_{crit}$. Therefore, Eq. 7 can be rewritten

$$W_{crit} = \frac{\rho_{steel}}{\rho_{steel} - 0.57\rho_{rust}} (W_{porous} + W_{expan}) \tag{9}$$

Let ρ_{steel} be modelled by a normal distribution N(8000 ; 800) kg/m^3. Then by Monte Carlo simulation it can be shown that W_{crit} with a good approximation can be modelled by a normal distribution N(0.010 ; 0.0027) kg/m, see (Thoft-Christensen 2000). The rate of rust production as a function of time t (years) from corrosion initiation (Liu & Weyers 1998) can be written

$$\frac{dW_{rust}(t)}{dt} = k_{rust}(t) \frac{1}{W_{rust}(t)} \tag{10}$$

i.e. the rate of corrosion is inversely proportional to the amount of rust products W_{rust} (kg/m). The factor $k_{rust}(t)$ (kg^2/m^{2}year) is assumed to be proportional to the annual

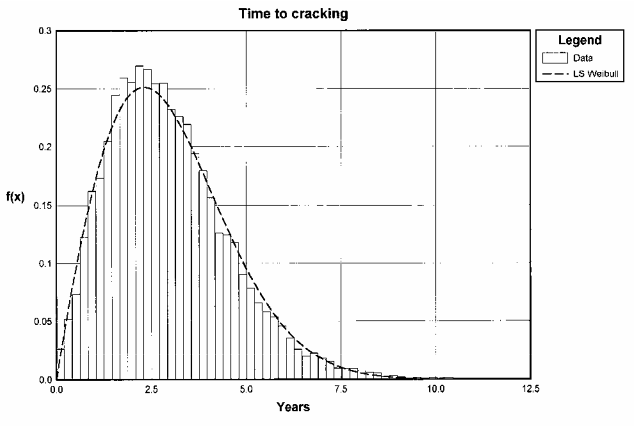

Figure 3. Density function of Δt_{crack} (Thoft-Christensen 2000).

mean corrosion rate $i_{cor}(t)$ (μ A/cm^2) and the diameter *d* (m) of the reinforcement. The proportionality factor depends on the types of rust products, but is here taken as 0.383e − 3.

$$k_{rust}(t) = 0{,}383 \times 10^{-3}\, d i_{corr}(t) \tag{11}$$

By integration

$$W_{rust}^2(t) = 2\int_0^t k_{rust}(t)dt \tag{12}$$

Let $i_{cor}(t)$ be modelled by a time-independent normally distributed stochastic variable N(3 ; 0.3) (μ A/cm^2) then the time from corrosion initiation to cracking Δt_{crack} can be estimated by (16) by setting $W_{rust}(\Delta t_{crack}) = W_{crit}$.

$$\Delta t_{crack} = \frac{W_{crit}^2}{2k_{rust}} = \frac{W_{crit}^2}{2 \times 0.383 \times 10^{-3}\, d i_{corr}} \tag{13}$$

Then it can be shown by Monte Carlo simulation that Δt_{crack} with a good approximation can be modelled by a Weibull distribution W (3.350 ; 1.944 ; 0) years, see Fig. 3. The mean is 2.95 years and the standard deviation is 1.58 years. The mean value of T_{crack} is of the same order as the experimental values (and the deterministic values) obtained by (Liu & Weyers 1998).

The Crack - Corrosion Index

After formation of the initial crack the rebar cross-section is further reduced due to the continued corrosion, and the opening of the crack is increased. Experiments by (Andrade, Alonso & Molina 1993) show that the function between the reduction of the rebar diameter Δd and the corresponding increase in crack opening $\Delta crack$ measured on the surface of the concrete specimen can be approximated by a linear function $\Delta crack = \gamma\Delta d$, where the crack-corrosion factor γ is of the order 1.5 to 5, see Fig. 4.

An approximate relation between the decrease in the steel bar diameter Δd_r and the increase in the hole Δd_{hole} can easily be obtained by considering the volume of the produced rust products $\pi\Delta dd\alpha$ ($\alpha = \rho_{steel}/\rho_{rust}$ is the relation between the densities of the steel and the rust product; see Table 1) and the volume due to the expansion of the hole $\pi\Delta dd+\pi\Delta d_{hole}d_{hole} + c\Delta crack$; see Fig. 5. By equalizing these two volumes and assuming that $d \approx d_{hole}$ one gets

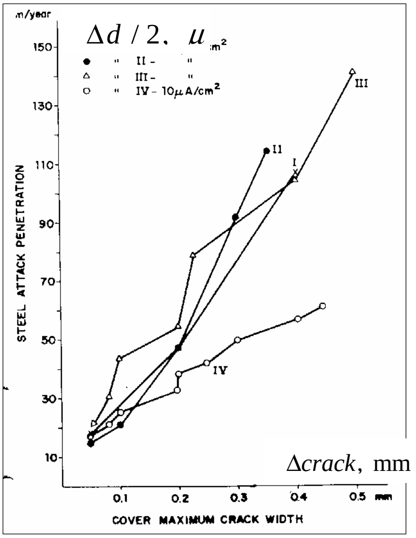

Figure 4. Loss in rebar diameter Δd versus the increase in crack opening $\Delta crack$ (Andrade, Alonso & Molina 1993)

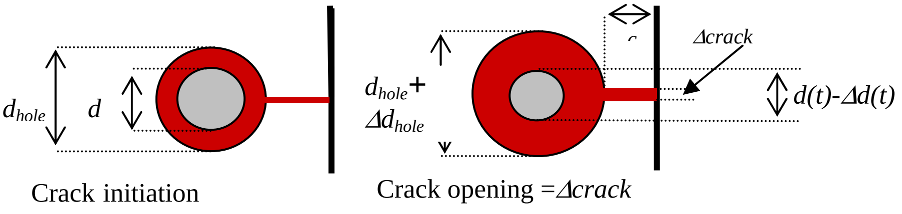

Figure 5. Crack opening increase from crack initiation (opening ~ 0 mm) to $\Delta crack$

$$(\alpha\text{-}1)\ \Delta dd \approx \pi\Delta d_{hole}d_{hole} + \text{crack volume} = \pi\Delta d_{hole}d_{hole} + c\Delta crack \qquad (14)$$

where c is the cover. Therefore,

$$\Delta d \approx (\Delta d_{hole} + c\Delta crack/\pi d)/(\alpha\text{-}1) \qquad (15)$$

FEM-Modelling of Corrosion Cracking in a Beam Cross Section

The first FEM estimation of the crack-corrosion index $\gamma = \Delta w_{crack} / \Delta D_{bar}$ was presented at the IFIP TC7 Conference on "System Modelling and Optimization" in Sophia Antipolis, France, July 2003, see Thoft-Christensen (2004), using FEMLAB/MATLAB. A rectangular beam cross-section with only one reinforcement bar was considered, see figure 6. The diameter of the hole around the rebar at the time of crack initiation is d_{hole} = 20 mm and that the cover is c = 10 mm.

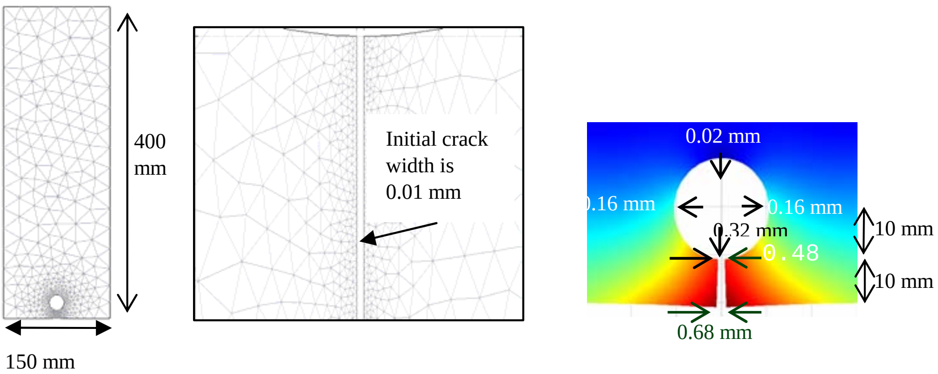

Figure 6. FEM net. The total net to the left, and the local net near the crack in the middle, and the displacement at the right, Thoft-Christensen (2004)

In the FEM modelling the rectangular cross-section in a long beam (plain strain) is assumed to have a hole at the location of the reinforcement and a crack (0.01 mm) from the hole to the boundary. The material is assumed to be linear elastic with the modulus of elasticity $E = 25\times10^9$ Pa. It is assumed that the pressure on the boundary of the hole from the increasing corrosion products can be modelled as a uniform loading (pressure) $p = 1\times10^8$ N/m at the boundary of the hole. The increase in the crack opening is Δw_{crack} = 0.67 mm and the average increase in the hole diameter is ΔD_{hole} = 0.31 mm.

For the example shown in Fig. 6 one gets by Eq. 15

$$\Delta d \approx (0.31+0.67\times10/(20\times\pi))/(\alpha-1) = 0.42\times(\alpha-1)-1 \qquad (16)$$

and

$$\gamma \approx \Delta crack/\Delta d = 1.60\times(\alpha-1) \qquad (17)$$

or γ equal to 1.8 and 5.1 for black and brown rust, respectively, in good agreement with the values obtained by the experiments in Fig. 5.

The results of a similar FEM analysis of a cross-section like the one illustrated in figure 6 are presented for 10 different combinations of the cover c and the diameter d in (Thoft-Christensen 2003). The conclusion is that γ increases with the cover c for a fixed rebar diameter d, and that γ also increases with the diameter d for a fixed cover c. A similar analysis with 30 combinations of d and c, but with a different cross-section partly confirms this conclusion, see (Thoft-Christensen 2005). In the same paper it is also investigated whether the distance b from the crack to the nearest uncracked vertical side of the beam is important for the estimate of crack-corrosion index γ. The same cross-section is used, but the hole and the crack are placed at different distances from the vertical side of the beam. The conclusion is that the distance b to the vertical side of the beam is only significant if b is smaller than twice the rebar diameter. Otherwise, with a fairly good approximation, γ seems to be independent of b.

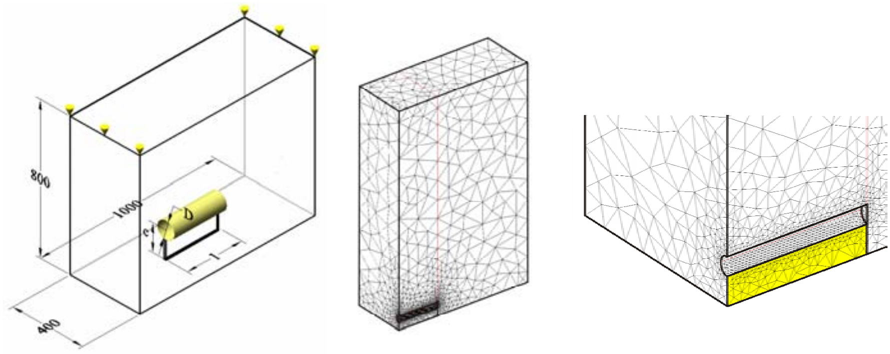

Figure 7. Beam element with corroded part of the reinforcement and the initial crack from the rebar to the surface of the beam is shown to the left. In the middle the FEM-net is shown for one quarter of the beam, and to the right the FEM-net near the reinforcement and the crack is shown.

FEM Modelling of Corrosion Cracking in a Beam

In this section the procedure used in 2D-modelling of corrosion crack propagation is extended to a 3D-modelling of a reinforced concrete beam, see (Thoft-Christensen, Svensson and Frandsen 2005). The 2D-moddeling in section 2 is based on several assumptions and simplifications, e.g. that the movement of corrosion products is restricted to the considered cross-section. In a 3D-modelling the corrosion products may also move in the direction of the reinforcement. Further, it is possible in a 3-D modelling to consider situations where only parts of the reinforcement are corroded. Eventually, this modelling should be able also to handle pit corrosion.

A beam element with the dimensions 400×800×1000 mm is considered. It contains only one rebar with the diameter d = 20 mm, and the cover c, see Fig. 7. Corrosion is supposed to take place in the central part with the length l ($0 < l < 1000$ mm) of the reinforcement. An initial thin crack (crack width ≈ 0 mm) connects the corroded part of the reinforcement with the surface of the beam as shown in Fig. 7.

The FEM model of the beam element is assumed to have a cylindrical hole at the location of the reinforcement and a crack (≈ 0 mm thick) from the hole to the lower boundary of the beam element. The beam element material is assumed to be linear elastic with the modulus of elasticity module $E = 25\times10^9$ Pa. It is assumed that the pressure on the boundary of the hole due to increasing corrosion products can be modelled as a uniform loading (pressure) $p = 1\times10^8$ N/m^2 normal to the boundary of the hole. Due to symmetries, the FEM analysis is based on only one quarter of the considered beam element. The FEM analysis is performed with 5 covers *c* = 20, 30, 40, 50, and 60 for the corrosion length *l* = 10, 20, 30, 40, 50, 100, 200, 300, 400, 500, 600, 700, 800 900, and 1000 mm. The crack-corrosion index $\gamma = \Delta crack / \Delta d$ is calculated for each combination of the above-mentioned values of the cover *c* and the corrosion (crack) length l . It follows from Fig. 8 that the crack-corrosion index γ decreases with decreased length *l* especially for small lengths of *l*. $\gamma \rightarrow 0$ in the case of pit corrosion ($l \rightarrow 0$).

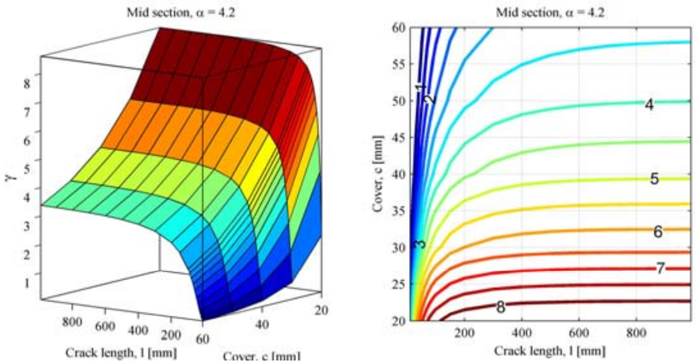

Figure 8. The crack-corrosion index γ(l, c) estimated on basis of the mid section of the corroded part of the rebar

Conclusions

During the last 20-30 years, the interest in improving the modelling of deterioration of structural materials has been growing in all countries. Hundreds of papers have been published in material science journals and in all kind of engineering journals. A great number of conferences and meetings have been organized. New materials with interesting properties have been developed and new types of exciting structures have been designed. Very tall buildings, offshore structures, long bridges etc. are new challenges for architects and engineers. All this combined with a need to maintain the infrastructures everywhere have shown a need for a more precise and reliable description of strength and deterioration of structural materials.

In this paper the deterioration of reinforced concrete structures is presented with special emphasis on the corrosion crack opening during corrosion of the reinforcement. The first sign that something is wrong with a reinforced structure is often corrosion cracks leading to spalling and eventually to failure of the structure. However, corrosion-based failure is only one of several failure modes, but in many countries it is one of the most important types of failure.

It is therefore of great interest to design a reinforced concrete structure so that corrosion is not likely to take place in the planned lifetime of the structure, say 100 years. Especially structures near or in the sea and bridges, where de-icing is used, have a high risk of failure. It is therefore of great importance to understand the chemical, physical, and mechanical properties of reinforced materials. To this purpose a great number of deterministic and stochastic models for deterioration of reinforced structures have been developed. Some models are very complicated, others are simpler.

In this paper a framework for a complete model of the total deterioration process of reinforced concrete structures resulting from corrosion of the reinforcement is presented. The model includes chloride ingress, corrosion initiation, corrosion propagation, crack initiation, and crack opening models. The model is made as simple as possible, but may easily be extended to include space dependence, time dependence, and inhomogeneous and anisotropic materials.

It is necessary to make all models presented in this paper stochastic, since a number of uncertain parameters are included in the models. This includes the diffusion coefficient, the corrosion parameters, the rebar diameter, and the concrete cover etc., but also model uncertainties. The deterministic models presented are easily made stochastic by assuming that the involved parameters are stochastic variables or stochastic processes.

References

Andrade, C., Alonso, C. and Molina, F.J. (1993). Cover Cracking as a Function of Bar Corrosion: Part 1-Experimental Test. *Materials and Structures*, 26, pp. 453-464.

Ellingwood, B.R. (2005). Challenges to Condition Assessment of Aging Civil Infrastructure: Research and Implementation. Proceedings of *ICOSSAR 2005*, Rome, June 2005, cd-rom, Millpress, Rotterdam, 2005.

Frederiksen, J.M., Mejlbro, L. and Poulsen, E. (2000). The HETEK model of Chloride Ingress into Concrete made simpler by Approximations. *Testing and Modelling the Chloride Ingress into Concrete* (eds. C. Andrade and J. Kropp), RILEM Proceedings, PRO 19, 317-336.

Frederiksen, J.M. (2000). Chloride Threshold Values for Service Life Design. *Testing and Modelling the Chloride Ingress into Concrete* (eds. C. Andrade and J. Kropp), RILEM Proceedings, PRO 19, 397-414.

Jensen, O. M. (1998). Chloride Ingress in Cement Paste and Mortar Measured by Electron Micro Analysis. *Technical Report Series R No.51*. Department of Structural Engineering and Materials, The Technical University of Denmark.

Jensen, O. M., Hansen P.F. , Coats A.M. and Glasser, F.P. 819999. Chloride Ingress in Cement and Mortar. *Cement and Concrete Research*, 29, pp.1497-1504.

Liu, Y. and Weyers, R.E.. (1998). Modelling of the Time to Corrosion Cracking in Chloride Contaminated Reinforced Concrete Structures. *ACI Materials Journal*, 95, pp. 675-681

Lundgren, K. (2002). Modelling the Effect of Corrosion on bond in Reinforced Concrete. *Magazine of Concrete Research* 54 (3), 165-173.

Maurel, O., Dekoster, M. and F. Buyle-Bodin (2005). Relation between Total Degradation of Steel Concrete Band and the Degree of Corrosion of RC Beams Experimental and Computational Studies. *Computers and Concrete* 2, 1-18.

Mejlbro, L. (1996). The Complete Solution of Fick´s Second Law of Diffusion with time-dependent Diffusion Coefficient and Surface Concentration. *Durability of Concrete in Saline Environment*. CEMENTA, Danderyd, Sweden.

Mejlbro, L. and Poulsen, E. (2000). On a model of Chloride Ingress into Concrete exposed to De-Icing Salt containing Chloride. *Testing and Modelling the Chloride*

Ingress into Concrete (eds. C. Andrade and J. Kropp), RILEM Proceedings, PRO 19, 337-354.

Neville, A.M. (2000). *Properties of Concrete.* Fourth and Final Version, Prentice Hall.

Nielsen, A. (1976). Hvid, grøn og sort rust (in Danish). *Nordisk Beton*, Nr. 2.

Thoft-Christensen, P. and Jensen, F.M. (1996). Revision of the Bridge Assessment Rules Based on Whole Life Performance: Concrete, Final Report, *Highways Agency Contract DPU 9/3/44.* CSRconsult ApS, December 1996.

Thoft-Christensen, P. (2000). Modelling of the Deterioration of Reinforced Concrete Structures. *Proceedings of IFIP Conference on Reliability and Optimization of Structural Systems*, Ann Arbor, Michigan, pp.15-26.

Thoft-Christensen, P (2001). What Happens with Reinforced Concrete Structures when the Reinforcement Corrodes? Proceedings 2nd International Workshop on "life-cycle Cost Analysis and Design of Civil Infrastructure Systems", Ube, Yamaguchi, Japan. *Maintaining the Safety of Deteriorating Civil Infrastructures*, 35-46.

Thoft-Christensen, P. (2002). Stochastic Modelling of the Diffusion Coefficient for Concrete. *Proceedings of IFIP Conference on Reliability and Optimization of Structural Systems*, Osaka, Japan, pp.151-159.

Thoft-Christensen, P. (2003). FEM Modelling of the Evolution of Corrosion Cracks in Reinforced Concrete Structures. Proc. *IFIP WG7.5* Conference on "Optimization and Reliability of Structural Systems", Banff, Canada, pp. 221-228.

Thoft-Christensen, P. (2004). Modelling Corrosion Cracks. Proc. IFIP TC7 Conference, Sophia Antipolis, France, 2003. In J. Cagnol & J-P. Zolesio (editors), *Information Processing: Recent Mathematical Advances in Optimization and Control*. Mathematical Computational Sciences, Presses de l'Ecole des Mines de Paris, pp. 25-33.

Thoft-Christensen, P. (2005). Service Life Definitions Based on Corrosion Crack Width. Proceedings of *ICOSSAR 2005*, Rome, June 2005, cd-rom, Millpress, Rotterdam, 2005.

Thoft-Christensen, P., Svensson, S. and Frandsen, H.L. (2005). 3D-Modelling of Corrosion Crack Opening. Proc. *IFIP WG7.5* Conference, Aalborg Denmark.

Prof. C. Allin Cornell
Professor Emeritus
Stanford University
110 Coquito Way
Portola Valley, Ca, US, 94028
cornell@stanford.edu

Probabilistic methods in structural engineering

Luis Esteva has been one of my two most knowledgeable and influential tutors in earthquake engineering and probability. In the summer of 1966 Luis and I were both working at UNAM beside my second such tutor, Emilio Rosenblueth. But Luis was the one who was then also deeply interested in the questions of earthquake occurrence and ground motion prediction, and their representation for engineering hazard assessment purposes. My own work in that field owes a great deal to the openness and patience with which Luis discussed his ongoing studies. His example has also set a standard for me with respect to the importance of keeping our sometimes seemingly esoteric work in probabilistic methods grounded in the needs of engineering practice. The two of us have since shared many concentrated technical and pleasant social hours not only at UNAM and at MIT and Stanford, where I sought his multi-month visits, but also in the many cities around the world that this profession takes you. For all that, Luis Esteva, I thank you and salute you on this special day in your career.

Allin Cornell,
August 10, 2005

ON EARTHQUAKE RECORD SELECTION FOR NONLINEAR DYNAMIC ANALYSIS

ABSTRACT

The apparently simple act of selecting accelerograms for use in conducting nonlinear dynamic analysis has been the subject recent study (e.g., Baker 2005c) and conclusions are emerging. This paper attempts to elucidate those conclusions by starting from very ideal and simplified cases to deduce observations that are supported by more through numerical studies of nonlinear MDOF structural models. A direct and an indirect approach are discussed. To insure both lack of bias and adequate confidence limits in the estimation of response and response likelihoods, the selection of the spectral shape and number of the records is found to be dependent on the site, the structure and ground motion level. With proper choice of the spectral shape scaling of the records should not cause significant bias.

Introduction

It might be said that both Luis Esteva's career and my own have been highly focused on a single problem: estimating the annual frequency, λ, that an earthquake induces in a particular structure some specified behavior state. We have worked separately, together and with many colleagues and students on pieces of and the whole of this issue. There is a half century of literature on this subject with many approaches, simplifications, and results. Yet many of us are still working hard on the subject. Modern computational resources have accelerated the progress, opening opportunities, for example, for large statistical samples of nonlinear dynamic analyses of multi-degree-of-freedom models of structures both for research and for applications. But the increased computational power is also being used by the structural modelers to improve the detail and accuracy of their FEM models. This verisimilitude is especially important as we attempt to push our studies to the extreme damage and collapse domains of behavior important to life safety assessment. Therefore there will always be a demand to limit the number of dynamic analyses used to estimate λ. Even when, as in research contexts, computational limits may be less restrictive than in practice, there remain open many questions about which accelerograms to run in any particular situation. These questions arise both in practice and research.

Current best record-selection practice even in research (e.g., ASCE 2005, Stewart 2002) has the seismologist providing of the order of 10 or fewer records that represent magnitudes and distances identified by probabilistic seismic hazard analysis (PSHA) disaggregation (e.g., Bazzurro 1999) to be the most likely to have caused the event that a particular response spectral ordinate equals the level associated with a particular mean annual rate of exceedance. These records are then scaled as necessary to match the level of the uniform hazard spectrum in one manner or another. An important implication of this practice is that the result is dependent on the character of the seismicity that surrounds the site and the mean return period of interest. It is implicit too that it believed that the magnitude and distance of a record do or may affect the structural response. It is also clear that nothing beyond single-degree-of-freedom (SDOF) linear structural behavior is used in the selection. While many questions surround various elements of this practice (e.g., the number of records, the impact of the scaling, etc.), especially for application to rare, severe response of nonlinear multi-degree-of-freedom (MDOF) structures, it has only recently begun to be investigated for accuracy and effectiveness.

The objective of this paper is to back up briefly to look at the problem from a simple but perhaps fundamental perspective that may give us insights into what to look for and what to avoid in selecting accelerograms for nonlinear time history analysis. This may also suggest some of the compromises we are making in current practice and research.

With these objectives I shall be making, for the purpose of clarity of exposition, various specializations and restrictions and simplifications, most of which could be expanded or generalized without significant effort. For example I take it as a given that the fundamental objective is the estimation of λ. Note that special cases include, for example, the annual frequency (or, approximately, probability) of collapse, of roof drift angle greater than 3%, of maximum interstory drift in the first floor greater than its (random) capacity, etc. Such limit state frequencies are at the basis modern approaches to earthquake codes, guidelines, advanced practice, and performance-based earthquake engineering. They are the first step toward estimation of more direct decision variables involving consequences such as lives lost, economic damage to structure or non-structural elements, and lost occupancy time. Other limitations in the paper will be simple site hazard and structural representations.

Direct Approaches

In the best of circumstances λ would be estimated by monitoring the response of the building itself for a sufficient number of years to estimate λ with the desired accuracy. Suppose for simplicity that single response variable, θ, is of concern (say the maximum interstory drift ratio - MIDR - in a frame). Then, just as with empirical flood frequency analysis, we would need only order and plot these values versus i/n (where n is the number of years of observation) as an empirical complementary cumulative mean annual rate of exceedance function (CCDF), $\lambda_\theta(x)$. The value of x at $\lambda_\theta(x) = 0.001$ would be the estimated 1000 year mean return period MIDR. Even, however, if the structure had been built and monitored, for safety level λ_θ's of the order of 10^{-3} or less, this would require 10,000 or more years of data[1].

Somewhat more realistically the response will be estimated from linear/nonlinear dynamic analysis of a numerical model of the structure, be it an existing building or a proposed design. (We assume here that such numerical models are precise.) Then we would need "only" to have had an accelerometer in place at the site for these 10,000 years. All the records (above some practical threshold, say 1000 in total) would need to be run and their resulting values of θ plotted as above. While this case remains completely unrealistic it is an excellent hypothetical model to repeatedly return to as we

[1] The basis for this statement is that simple binomial trials statistics suggests it requires a sample size of about 10/p to estimate small probability p with a standard error of about +/- 30% of p. To reduce this number to 15% would require 4 times as many years.

consider how to address practical record selection. This record set of some 1000 records would implicitly contain records generated by a multitude of magnitudes from different sources at various distances and azimuths over various travel paths, and this set would fully and properly represent all the characteristics of ground motion that might possibly affect the structure's response. What is more, all these characteristics, including site effects, all appear in this large hypothetical set of *in situ* recordings in exactly the correct relative frequency of occurrence, both marginally and jointly. Our objective in practical record selection is to reproduce this condition or, rather, to approximate it as best we can.

Lacking this ideal set of records at our site we turn either to the catalogue of recordings or to simulation. Not wishing in this short note to take on the questioning of just how realistic various current modes of simulating accelerograms are, I limit myself to the catalogue[2]. I further presume that all these recordings are free from instrumentation limitations. Many good catalogues (or virtual catalogues) are readily available today with thousands of records (e.g., PEER 2005). Going to the catalogue of accelerograms recorded elsewhere to represent what has happened at my single site over years is an example of "trading space for time". It carries with it the need to try to understand what is important to the problem at hand to gain confidence that the trade has been fair and the conclusions accurate. So we must ask which records in the catalogue with which characteristics are "right" for my site and in what proportion should select them.

Suppose first, again for simplicity of exposition, that the threat at our site is a single fault segment, located R kilometers from the site[3], which produces only "characteristic" events, i.e., full segment ruptures with very similar magnitudes[4], M, and which does so in a Poisson way with known[5] mean rate λ_o. Then, hoping/assuming (again for simplicity, but close to current practice) that M and R are sufficient representations of the source and path and that, say, "firm soil" (or some like category among the current catalogue representations) is a sufficient characterization of our site, we might logically sort the catalog for all such records and run them through the numerical analysis to obtain values of θ. Ordering and plotting them versus i/m (where m is the number of records found) would produce what we would hope to be a reasonable and accurate estimate of $G_{\theta}(x)$, the complementary cumulative distribution function (CCDF) of θ given an event on the fault. With this result it follows that $\lambda_{\theta}(x) = \lambda' \ P[\theta>x|\ \text{event}] = \lambda' \ G_{\theta}(x)$. How much data does this require? Suppose, as in coastal California, λ' is 1/ (several hundred years), then for $\lambda_{\theta}(x)$ of the order of 10^{-3} to 10^{-4} we need $G_{\theta}(x)$ to be of the order of 0.1. Reasonably confident estimation requires m to be about[6] 100. Apart from the computational cost, there, of course, are not nearly enough such specific (M, R, firm soil) records in current or foreseeable catalogues

2 For approaches using simulated records see, for example, Han 1997, Luco 2002 or Jalayer 2005.

3 Measured in some relevant way, e.g., as closest distance to the rupture surface.

4 A more fundamental approach might be to use rupture length rather than the more heavily processed M to characterize events and select records.

5 Again we assume that this is known accurately. Indeed we shall assume throughout this and all such seismicity information to follow is perfectly known.

6 Making "a distribution assumption", i.e., fitting this data to a named probability law such as one with an exponential or power form, and estimating its parameter values can reduce this number by a factor of 2 to 3 at the risk of inducing errors in the upper tail by having made the wrong parametric modeling assumption.

(especially as one would like them to be from 100 independent events). Therefore we must relax the constraints and accept events within an interval[7] M+/-Δ_M and R+/- Δ_R. Immediate questions are: how wide need these bins be to gather an adequate sample size? How much accuracy in θ is given up by using the "wrong" M and R, and how does that increase as say Δ_M gets larger? And are there ways to modify the records to make them "more nearly right"? The simplest, common illustration of this is, say, scaling up by some amount the accelerograms that are from "too small" M's or "too large" R's. And does such scaling induce biases of it own? Before addressing such questions, let us release at least one of the previous unrealistic limitations.

We need to recognize that the assumption of a simple single {M, R} scenario is not only unrealistic but impacts our record selection discussion. Even with a single dominant neighboring fault there may be lesser magnitudes at various locations (and distances) that contribute to the likelihood of exceeding any θ level, x. Further there are inevitably other seismic sources that also contribute to the hazard. These additional scenarios complicate record selection to the degree that they needed to be represented in the analysis. For such cases we need write:

$$\lambda_\theta(x) = \sum_i G_{\theta|M,R}(x \mid m_i, r_i)\, \lambda(m_i, r_i) \tag{1}$$

in which the individual mean rates of occurrence, λ, and conditional CCDF's, G, are identified for each of the interesting (here discretized) set of {M,R} scenarios. Records would have to be selected as above for each such scenario. Even if there are only 5 to 10 such scenarios the number of records and analyses needed may mount once again into the 1000 range.

Intensity Measure-based Approaches: In Principle

To address these challenges the seismic community has used for decades the notion of what some of us now call an "intensity measure" (IM); examples include PGA and first-mode-period spectral acceleration, $S_a(T_1)$, to serve as an intermediate variable in such assessments. The estimation of the mean rate of exceedance of the IM is the subject of PSHA and the responsibility of earth scientists not structural analysts. The equation for $\lambda_{IM}(y)$ looks just like Eq. 1 with $G_{\theta|M,R}$ replaced by $G_{IM|M,R}$. The last function is obtained from standard strong ground motion attenuation "laws". This PSHA problem is again outside the scope of this discussion; we assume that $\lambda_{IM}(y)$ is available for almost any IM we might chose. It is important to recognize that this a site-specific product reflecting all the {M,R} scenarios. Therefore it has captured a major portion of the specific nature of our site. In particular it has released us from the need to have 10,000 years of recordings at the site in order to measure how frequently important magnitudes occur at critical distances from the site, and how certain measures (IM'S) of the amplitudes of their motions depend on magnitude and attenuate with distance. How completely and adequately this job has been completed for the objective of structure-specific $\lambda_\theta(x)$ estimation remains to be discussed.

[7] Let us drop further explicit discussion of soil conditions. This is not to say that this is not a very important issue. Some portion of the variability in records from similar but different sites would presumably not be found from event to event at the same site. This question is related to the current discussion ergodicity (Anderson 1999)

Returning to the estimation of $\lambda_{\theta}(x)$, it is clear that IM's can likely play a key role. Let us see how. The total probability theorem (e.g., Benjamin 1970) always permits an expansion of $\lambda_{\theta}(x)$ into (e.g., Bazzurro 1998).

$$\lambda_{\theta}(x) = \int G_{\theta|IM}(x \mid y) \left| d\lambda_{IM}(y) \right| \qquad (2)$$

in which the last factor is the absolute value of the derivative of $\lambda_{IM}(y)$, or, loosely, the mean rate of occurrence of a value of the IM equal to y. Having, as we do, $\lambda_{IM}(y)$, our problem is transformed into estimating $G_{\theta|IM}$, the conditional probability that $\theta > x$ given IM = y. Consider first our original ideal case where we have some 10,000 years of recordings directly from our site. For a given level of y, we would select a random sample from those records that have this (or approximately) this IM level, analyze the structure under them, and process as usual to estimate $G_{\theta|IM}$ versus x for this y level.

How many records would this require? Suppose we are interested again in about 10^{-3} to 10^{-4}. Then we should look at levels of y such that $\lambda_{IM}(y)$ is in this range as well, since it is well known that $\lambda_{IM}(y)$ not $G_{\theta|IM}$ dominates the integral in Eq. 2. Indeed this is so true that generally[8] the estimation of $G_{\theta|IM}$ can be reduced to estimating well the *mean* of θ and only roughly its standard deviation and distribution shape. Accepting this statement as at least a rough approximation we can estimate the required sample size to be of order[9] only 10. This enormous reduction in the necessary sample size is possible because the variability in θ given IM is small relative that in θ marginally. This reduction is the consequence of the PSHA analysis of the IM "absorbing" most of the total variability in θ, leaving only the conditional variability of θ given IM to be estimated from the structural dynamic analyses. Under some practical circumstances only one such level (or "stripe") may be adequate, in particular if there is interest in only a single level of x (e.g., 3% drift) or of mean frequency (e.g., 2% in 50 years); in this case this an extremely attractive approach to the record selector and structural analyst. Unlike the previous approach this number is independent of the number of sources contributing to the hazard. However more than one level of y may be necessary; 3 to 5 or more levels may be required if $\lambda_{\theta}(x)$ is needed for a broad range of x values[10] (Jalayer 2003), raising the required sample size to order 100. In any case this IM-based approach is in principle very efficient[11] and accurate, at least in the ideal case when the large site-specific sample is available. Even with this nominal perfect sample there remain interesting questions as to what variable is best to use as the IM. For MIDR prediction, PGA for example leads to larger required sample sizes than $S_a(T_1)$ simply because it is less well correlated with MIDR for moderate to long period structures. We shall not pursue this question of which IM to use here except (later) to the degree it impacts our focus: record selection.

---

8 Exceptions include case where the IM hazard curve is very steep and the dispersion of θ given IM is large in the region of interest.

9 The basis for this is that the log of $\lambda_{\theta}(x)$ is roughly proportional 2 to 3 times the mean of the log of x. Therefore the +/-30% standard error in λ_{θ} mentioned above requires about a 10% standard error in the mean of x. This in turn requires a sample size equal to the square of the coefficient of variation (COV) of x divided by this 0.1. The COV of say MIDR of an MDOF frame structure given a reasonable choice of IM (such as Sa(T1)) is less than 0.3 to 0.5 plus for very severe degrees of nonlinearity.

10 Especially near global collapse when the dependence on y may be very nonlinear and the dispersion broad.

11 It can be interpreted as an application of conditional Monte Carlo analysis.

Intensity Measure-based Approaches: In Practice

Now we must return to the real world and ask how records are to be selected in the IM-base approach when we must depend not on a ideal site-specific catalog but on the existing catalog of recordings. This question is commonly asked and answered in practice but rarely in a very formal way. Given the discussion above it should not be a surprise that this is not a trivial formal question. There is no error in the application in the formulation of Eq. 2 and we have assumed that we have an accurate site-specific assessment of $\lambda_{IM}(y)$. Therefore the problem reduces to how one should select records to estimate $G_{\theta|IM}$. The simple answer is we chose them so that we get the right answer. This is more complex than simply what is an adequate sample size because there is now the question of suitability of records recorded elsewhere to this site. The contention is that this question can be addressed only if one considers carefully the structure of concern (and the IM at hand). Let us consider two simple structures to get a sense of what is involved.

Single DOF Linear Structure

Suppose to begin that our structure is simply a linear oscillator, and that we have selected the IM to be the common one: $S_a(T_1)$ where T1 is the natural period of the structure. Our objective is to select records from an available catalog to estimate $G_{\theta|IM}(x|y)$ accurately. In this case record selection for dynamic analysis purposes is clearly trivial. One can select *any* record (no matter, for example, what its M, R, or relative strength), scale it such that its IM = y, run the dynamic analysis and get, of course[12], $\theta = y$ because in this case IM and θ are the same. Further as all records will produce the same value, only a single record is necessary for perfect accuracy. In addition the same record can be used perfectly accurately for all levels, y, of the IM, only scaling is required. This absolute robustness with respect to record selection and scaling and this low dispersion (with its implied computational efficiency) are all a direct result of the selection of the IM, and the simple structure. Had the IM been another popular choice, PGA, none of these conclusions would hold. Because many structures are known to be "first-mode-dominant" it follows further that these desirable properties of $S_a(T_1)$ as an IM are likely to hold to some degree for many real structures, at least in the linear range. Therefore, it can be anticipated that many concerns about record selection for such cases are unwarranted. Dynamic analysis of linear first-mode-dominated structures is seldom needed, however. Nonetheless it suggests that this IM is a natural starting point from which to look for improvements for more complex structures. Certainly those candidates for IM, such as PGA, that create record selection sensitivity for this simplest structural problem are not strong initial choices for the more realistic structural problems.

[12] Provided, as I assume here for argument's sake, our structure has 5% damping as is standard for the attenuation laws used in PSHA. If our structure has a different damping level there will be an offset dependent on average on the degree to which the two damping levels differ and there will be some comparatively mild dispersion from record to record. There is no evidence that this effect is dependent on M or R or other such record properties.

Two DOF Linear Structure

Suppose next that our structure is, say, a two-story frame that can be represented accurately by a 2-DOF linear model. Further continue to assume that the IM is still $S_a(T_1)$, where T_1 is the first-mode period. How now should the catalog be searched for records for dynamic analyses to be used? For the purposes of illustrating the principles, let us further assume that in fact the simple square-root-of-sums-of-squares (SRSS) approximation is exact[13]. In this case given that IM = $S_a(T_1)$ = y, the response of interest can be written:

$$\theta = \sqrt{c_1^2\, y^2 + c_2^2\, S_a^2(T_2)} \tag{3}$$

in which c_1 and c_2 are coefficients depending on the dynamic properties of the structure. This form makes it clear that (given $S_a(T_1)$) θ is simply a function of the random variable $S_a(T_2)$, where the probability distribution of $S_a(T_2)$ is the *conditional* distribution of $S_a(T_2)$ given $S_a(T_1)$. We shall take advantage of this below. One can also re-write Eq. 3 as

$$\theta = c_1 y \sqrt{1 + \frac{c_2^2\, S_a^2(T_2)}{c_1^2 y^2}} \tag{4}$$

In this form it is clear, first, that our concern is only with cases in which the second mode makes a comparatively strong contribution to θ, as indicated by the ratio under the radical, and, second, that θ is simply a function of the (random) spectral ratio $R_{2/1} = S_a(T_2)/\ S_a(T_1)$ - still conditioned, of course, on $S_a(T_1)$ = y. The former observation implies that the record selection is trivial and robust in the first-mode dominated case, as discussed above. The latter observation emphasizes that once the IM level is given it is the only relative value, $S_a(T_2)/y$, (or *spectral shape*) that matters. This notion carries over to other structures as well. Knowledge of this fact supports the practice of selecting records from {M, R} bins that dominate the site hazard, because M is known to have some effect (in the mean at least) on spectral shape. The fact is even more evident in the common practice of first selecting records whose spectral shapes closely match that of the UHS or of the median spectrum given the dominant M and R, and then scaling them to match the level of the target spectrum. Neither of these practices, however, reflects the *conditional* nature of this dependence. We address this issue this next.

To estimate well $G_{\theta|IM}(x|y)$ when the second mode is important we clearly need to select records from the catalog that capture accurately the conditional distribution of $S_a(T_2)$ given $S_a(T_1)$ = y (or equivalently of $R_{2/1}$ given $S_a(T_1)$ = y). This distribution is not readily available today[14]. But we can get guidance as follows.

In order to understand better how in principle record selection should proceed in this case, we shall once again simplify by assuming, for the moment, that a single M = m and R = r scenario dominates our site's hazard. Conventional attenuation laws are based on the fact any Sa(T) value has a lognormal distribution with the mean of the

[13] Again one might ask: then why is dynamic analysis necessary? It is not, of course, but I again appeal to the sake of the argument.

[14] It happens that they can be found from disaggregation of vector-valued PSHA (Bazzurro 2002), public tools for which are under development (Somerville 2005).

natural log, call it $\mu_{\ln S}$, equal to specified function of m and r and with standard deviation of the log, $\sigma_{\ln S}$, equal to another such function. It is reasonable to assume further that the spectral accelerations at two different periods are jointly lognormal with correlation coefficient[15] of the logs ρ. In this case the conditional mean of log $S_a(T_2)$ given $S_a(T_1)$ = y is:

$$E[\ln(S_a(T_2)|\, S_1 = y] = \mu_{\ln S_a(T_2)} + \rho \frac{\sigma_{\ln S_a(T_2)}}{\sigma_{\ln S_a(T_1)}}(\ln y - \mu_{\ln S_a(T_1)}) \tag{5}$$

The median, η, of $S_a(T_2)$ given $S_a(T_1)$ = y is *e* raised to this power or:

$$\eta_{S_a(T_2)|S_1(T_1)=y} = \eta_{S_a(T_2)} \exp[\rho\sigma_{\ln S_a(T_2)}\, \varepsilon_{S_a(T_1)}\,] \tag{6}$$

in which $\varepsilon_{S_a(T_1)} = (\ln y - \mu_{\ln S_a(T_1)})/\sigma_{\ln S_a(T_1)}$ is the deviation (in log terms) of $S_a(T_1)$ away from its expected value (given M =m and R=r). The *conditional* median spectral ratio or shape is Eq. 6 divided by y or

$$\eta_{R2/1} = \frac{\eta_{S_a(T_2)}}{\eta_{S_a(T_1)}} \exp[-\varepsilon_{S_a(T_1)}\sigma_{\ln S_a(T_1)}(1-\rho\frac{\sigma_{\ln S_a(T_2)}}{\sigma_{\ln S_a(T_1)}})] \tag{7}$$

Note that this conditional shape is the marginal median shape times an exponential that is negative and proportional to ε and (1-ρ) under the reasonable assumption that the two σ's are about equal. For the larger values of y of most engineering interest ε is positive and the conditional median shape at other periods is *below* the one we expected "on average". The degree to which it is below depends on how far the selected level y of $S_a(T_1)$ is above its median and how weakly correlated the two spectral ordinates are. This correlation decays with separation between the two periods[16]. The implication is that the conditional median spectral shapes of interest are somewhat peaked around T_1 relative to the median shape. This in turn means that if the response of the first mode is higher than expected the response of the second mode will be relatively less than one would expect otherwise. These conclusions have been verified empirically (Baker 2005c). Fig. 1 shows plots of predicted spectra, including one median spectrum and two that are conditional on Sa(0.8s) being at the 1.5 ε level. It also shows these three spectra scaled to a common value of Sa(0.8s). Note that the two positive ε spectra are more peaked than the median spectrum and have very similar shapes despite the half-unit magnitude difference in their causative earthquake.

If the structure has an important second-mode contribution to θ, a first-order requirement towards estimating well $G_{\theta|IM}(x|y)$ would be to select records that have approximately this median shape value. Note that for higher values of y that this shape is not the median shape. Therefore the practices of using the UHS shape or the median shape of the dominant M and R scenario[17] are not as accurate as they might be for the rare events of common engineering interest.

---

[15] A recent study of this correlation coefficient is to be found in (Baker 2005b). It depends primarily on the ratio T_1/T_2 and is effectively independent of magnitude and distance.

[16] For separation of modal periods by a factor of 3 the value of ρ might be about 0.6 and $\sigma_{\ln Sa}$ about 0.7 implying for ε equal 1 the shape is about 25% lower and for ε equal 2 the shape is 40% lower. The effect on θ will depend on the importance of the second mode to the response quantity in question.

[17] For our special case here that the seismic threat is limited to single {M,R} scenario, the UHS shape and the median shape (given these M and R values) are virtually identical (differing only to the degree that the

A direct way to select the records in this simple linear 2-DOF case is to calculate the spectral *ratio* at T_1 and T_2 for all the records and select records such that their median is about that given in Eq. 7. Then they may be scaled such that $S_a(T_1)$ equals level y and the dynamic analyses run to find $G_{\theta|IM}(x|y)$. Note in particular that for this linear 2-DOF case the records selected will need to change as y changes, that the M and R of the records are immaterial per se (only their spectral ratio matters), and that the selected records may be scaled to any degree without loss of accuracy.

Even in the linear 2-DOF case we have made simplifications. In the record selection we have tried only to match the conditional central value not the variability of the spectral ratio. This is also quite feasible but will not be pursued further here. Further if we do not have a single {M,R} pair the determination of this conditional median shape is not trivial. In principle there must be a weighting over all $\{m_i,r_i\}$ pairs[18]. It may be sufficiently accurate in some cases to use disaggregation to determine a single dominant {M,R}and then apply the reasoning above as if it were the only threat. This would already be a step beyond current practice.

A second more indirect way to select the records for this case is to chose records (from the general magnitude range; R is less critical as it has little mean effect on strong motion spectral shape) that have the required level of ε (consistent with the level y), and then scale them to the correct level of $S_a(T_1)$. This too should on average at least capture the more peaked spectral shape associated with the higher levels of y and ε of primary interest.

More General Structures

While the conclusions from the simple 1 and 2-DOF linear structure are in principle limited to these simple cases, they suggest several generalizations that can be made, which have been verified in recent studies with nonlinear SDOF and MDOF frame models (e.g., Iervolino 2005, Baker 2005c, Tothong 2005). The objectives in record selection and scaling for accurate estimation of $G_{\theta|IM}(x|y)$ are to capture primarily the proper general amplitude (via the IM level) and secondarily the spectral shape given that IM level. For the common IM $S_a(T_1)$ once the first objective is met the estimation of $G_{\theta|IM}(x|y)$ is fairly robust with respect to the records selected as long as the structure is first-mode dominated and only moderately nonlinear.

For other structures it can be important to select the records to capture the appropriate spectral shape. This was demonstrated for higher modes ($T_2/T_1 < 1$), but it is clear from our understanding of nonlinear dynamic behavior that it is equally important to reflect properly the longer periods when the structure experiences substantial "softening". While there are no direct ways (similar to that used above for the 2-DOF case) to identify one or a few unique longer periods to focus upon and analyze, it should be clear that an objective of matching the conditional median spectral ratio would apply to each period of interest. Hence it follows that the entire *conditional* median spectral shape is logical first-order target for record selection for all structures. It should be re-emphasized that this shape is not the same as the median or UHS shape unless the level of y is near the median value of the IM $S_a(T_1)$, and that this shape will change as y changes, being most different from the median shape for large, rare values of the IM,

log standard deviations are different at different periods).

[18] As mentioned in footnote 14 such information will become available in time.

which is when strong degrees of nonlinearity may occur. It is the author's belief, while not proven here, that for more general structures (as was shown here for the 1 and 2-DOF linear structures) it is not critical to capture the "causative" magnitude[19] if the spectral shape itself has been selected well. Magnitude is primarily just a proxy for the median shape.

We saw above that arbitrary levels of scaling of the records was not a cause of response bias in the 1 and 2-DOF linear structures, provided (in the 2-DOF case) that the spectral shape was correct. It is the author's experience that, with this same proviso, this conclusion is more generally true (e.g., Shome 1998, Baker 2005c).

It should be noted that the schemes discussed above are based on the common use of linear first-mode period spectral acceleration as the IM. It has been found that other choices of the IM may provide even more robustness with respect to record selection (Luco 2002, Luco 2005, and Tothong 2005), just as $S_a(T_1)$ provides more such robustness than PGA. These new IM's are based on inelastic spectral acceleration. Another major objective of seeking improved IM's is the reduction of the number of records and analyses needed to achieve a specified level of confidence in the estimate (recall it was set here as a standard error of estimation of $\lambda_\theta(x)$ of about +/- 30%, or of the conditional mean of θ of about +/- 10%). This is achieved by finding "better response predictors", i.e., IM's that reduce the variance of θ given IM = y for various levels of y (i.e., degrees of structural nonlinearity). This so-called IM efficiency (Luco 2005) issue has not been addressed here.

Further this study of the record selection problem presumes that the model of the structure is available at least to the level of knowing the general range of its first-mode period. (Because of the high correlation between two comparatively nearby periods there is little loss of accuracy or efficiency if the period T of the Sa(T) used as the IM is some distance from that of the final first- natural period of the structural model. (Of course whether that model estimates well the first-natural period of the real structure is another problem, which does not influence how we should best analyze the model we have.) While the general principles above hold for all cases the judgments stated as to accuracy and effectiveness depend on the author's experience with building-like structures, which at least in the linear range tend to have no more than two or three most-important elastic modes. Other cases, including those in which the record selection is done (for good or bad reasons) without knowledge of the structure or those where there are many very important response measures sensitive individually to different portions of the input spectrum, have not as yet been studied in this way. Short of using different IM's, records, and analyses for the different subsets of these cases (a strategy which is permitted in the nuclear arena, e.g, NRC 1997), it is clear that some compromise well have to be made with respect both to efficiency (implying larger sample sizes or larger standard errors) and perhaps to the accuracy (or record selection robustness).

Conclusions

We conclude that the selection of records for use in nonlinear seismic time history

[19] Exceptions may be when the response is duration sensitive and magnitude serves as a proxy for duration. The peak displacements of nonlinear framed structures do not seem to be duration sensitive even when strength degradation is involved.

analysis of MDOF models of structures can benefit from starting from a defined structural objective, here estimation of the mean annual frequency of some structural response measure, θ, exceeding level x, i.e., $\lambda_\theta(x)$, and then asking how that might be directly and/or indirectly estimated in various ideal and simplified cases. Discussion of the ideal case in which 10,000+ years of recordings have been made at the site reveals that numerous (order 1000) records and time history analyses will be required (save, perhaps, special techniques to reduce this number). Recognizing that the recorded accelerograms must come from catalogs of data recorded at many sites and caused by many sources, it becomes clear that record selection must allow in some way for the failure of such data to reflect the relative frequency with which various events at various distances will affect the site. In short in this form the record selection problem is very site-seismicity dependent. This complicates the selection problem and increases the number of analyses necessary for accurate estimation of $\lambda_\theta(x)$.

Turning to an intensity-measure-based formulation of the analysis and estimation problem, one finds that the PSHA analysis leading to the IM hazard curve, $\lambda_{IM}(y)$, captures much of the site-specific seismicity issue and of the variability in θ. Now one needs to select records to estimate $G_{\theta|IM}(x|y)$, the CCDF of the θ conditional on IM = y. Even though this CCDF may have to be evaluated at several levels of y, this approach leads to significantly reduced record selection and sample size needs. But again the ideal problem is compromised by the need to select records from the available record set rather than a site-specific catalogue. Two, simplest structural dynamic models, namely linear 1- and 2-DOF systems, are discussed with the objective of understanding the benefits and challenges of the record selection and scaling problem for "real" (nonlinear MDOF) structural models. The conclusions are that, while the sample sizes may be smaller with the IM-based procedure, to the degree that the structure is not first-mode dominated or not nearly linear, care may be needed in selection of the records (and particularly with respect to their spectral shape), to insure that a bias is not introduced in the estimation of $G_{\theta|IM}(x|y)$ and hence in $\lambda_\theta(x)$. In particular it appears that the spectral shape needs to reflect properly the level of ε, which is a measure of the $S_a(T_1)$ IM level *relative to* its expected value (given the M and R scenarios of primary interest at the site). This shape is, for the positive ε's of engineering interest, more peaked than the UHS or median spectral shape (given a dominant scenario {M,R} pair). *Provided this shape is captured* it appears that the M and R selection criteria may be significantly relaxed and that scaling records to match the level y of the IM will not induce significant bias. These conclusions are supported by current research on nonlinear MDOF frames (e.g., Baker 2005a, Baker 2005c, Iervolino 2005).

It is noted that, while the focus here has been on estimating $\lambda_\theta(x)$, the conclusions here apply to "more deterministic" current-code-practice objectives, such as estimating the mean of θ "given the 2% in 50 ground motion". Since this concept in quotes exists only for a scalar ground motion measure (and not, for example, for an entire spectrum), it can be taken here to mean the 2% in 50 $S_a(T_1)$ IM level. Setting y equal to that level y* for which $\lambda_{IM}(y^*) = 0.0004$, this problem can be stated as estimating the mean of the distribution $G_{\theta|IM}(x|y)$, i. e., the conditional mean of θ given $S_a(T_1) = y^*$. It will be recalled that concerns about the required sample sizes and about biasing that distribution were cast above in terms of that mean. More modern codes are based on a target value of $\lambda_\theta(x)$ (rather than $\lambda_{IM}(y)$). Therefore the discussion above applies directly to them.

Acknowledgements

This simple paper depends strongly on the far more elegant and complete PhD thesis work of Dr. Jack Baker (Baker 2005c). I want to acknowledge his primary contributions, and the many good discussions with him, Polsak Tothong, and Iunio Iervolino on this subject. This work was supported by the Earthquake Engineering Research Centers Program of the National Science Foundation, under Award Number EEC-9701568 through the Pacific Earthquake Engineering Research Center (PEER). Any opinions, findings and conclusions or recommendations expressed in this material are those of the authors and do not necessarily reflect those of the National Science Foundation.

References

American Society of Civil Engineers (2005). *Seismic design criteria for structures, systems, and components in nuclear facilities*, Structural Engineering Institute, Working Group for Seismic Design Criteria for Nuclear Facilities, *ASCE/SEI 43-05*, Reston, Va., 81 pp.

Anderson, J. and J. N. Brune (1999). "Probabilistic seismic hazard analysis without the ergodic assumption", *Seismological Research Letters*, 10 (1) 19-28.

Baker, J. W. and C. A. Cornell (2005a). "A vector-valued ground motion intensity measure consisting of spectral acceleration and epsilon", *Earthquake Engineering & Structural Dynamics*, 34, 1193-1217.

Baker, J. W. and C. A. Cornell (2005b) "Correlation of response spectral values for multi-component ground motions", Accepted for publication, *Bulletin of the Seismological Society of America.*

Baker J.W. and C. A. Cornell (2005c). Vector-valued ground motion intensity measures for probabilistic seismic demand analysis, *John A. Blume Earthquake Engineering Center Report No. 150*, Stanford University, Stanford, http://blume.stanford.edu/Blume/Publications.htm.

Bazzurro, P., C. A. Cornell, N. Shome, and J. E. Carballo (1998). "Three Proposals for Characterizing MDOF Nonlinear Seismic Response", *Journal of Structural Engineering, ASCE* 124 (11), 1281-1289.

Bazzurro, P., and C. A. Cornell (1999). "On Disaggregation of Seismic Hazard," *Bulletin of Seismological Society of America,* 89 (2), 501-520.

Bazzurro, P. and C. A. Cornell (2002). "Vector-Valued Probabilistic Seismic Hazard Analysis (VPSHA)," *Proceedings 7th U.S. National Conference on Earthquake Engineering*, Boston, MA.

Benjamin J.R. and C. A. Cornell (1970). *Probability, Statistics, and Decision for Civil Engineers*, McGraw-Hill, New York, 684 pp.

Han S.W. and Y. K. Wen (1997). Method of reliability-based seismic design: Equivalent nonlinear systems, *Journal of Structural Engineering* 123 (3), 256-263.

Iervolino, I., and C. A. Cornell (2005). "Record selection for nonlinear seismic analysis of structures", *Earthquake Spectra* 21 (3), 685-713.

Jalayer F., (2003). Direct probabilistic seismic analysis: Implementing non-linear dynamic assessments, *Ph.D. Thesis*, Stanford University, Stanford, CA, 244 pp.

http://www.stanford.edu/group/rms/

Jalayer F. and C. A. Cornell (2003). A technical framework for probability-based demand and capacity factor design (DCFD) seismic formats, *Pacific Earthquake Engineering Research Center Report PEER 2003-08*, University of California at Berkeley, Berkeley, CA, 106 pp.

Jalayer F., J. L. Beck, and K. A. Porter (2004). Effects of ground motion uncertainty on predicting the response of an existing RC frame structure, *Proceedings 13th World Conference on Earthquake Engineering*, Vancouver, Canada.

Luco, N. and C. A.Cornell (2005). "Structure-specific scalar intensity measures for near-source and ordinary earthquake ground motions," *Earthquake Spectra*, Submitted.

Luco, N., M. Mai, C.A. Cornell, and G. Beroza (2002). "Probabilistic seismic demand analysis at a near-fault site using ground motion simulations based on a kinematic source model," *Proceedings 7th U.S. National Conference on Earthquake Engineering*, Boston, MA.

Nuclear Regulatory Commision (1997). "Identification and characterization of seismic sources and determination of safe shutdown earthquake ground motion", *Regulatory Guide 1.165*. www.nrc.gov/reading-rm/doc-collections/reg-guides/power-reactors/active/01-165/ (accessed 8/17/2005)

PEER strong motion database (2005). http://peer.berkeley.edu/smcat/ (accessed 6/29/2005).

Shome, N., C. A. Cornell, P. Bazzurro, and J. E. Carballo (1998). "Earthquakes, records and nonlinear responses," *Earthquake Spectra* 14 (3), 469-500.

Somerville P.G. and H. K. Thio (2005). Probabilistic vector-valued seismic hazard analysis for near-fault ground motions, *Southern California Earthquake Center Project Report* (in preparation).

Stewart J.P., S. J. Chiou, J. D. Bray, R. W. Graves, P. G. Somerville, and N. A. Abrahamson (2002). Ground motion evaluation procedures for performance-based design, *Soil Dynamics and Earthquake Engineering*, 22 (9-12), 765-772.

Tothong P. and C. A. Cornell (2005). Near-fault ground motions for seismic demand analysis (manuscript in preparation).

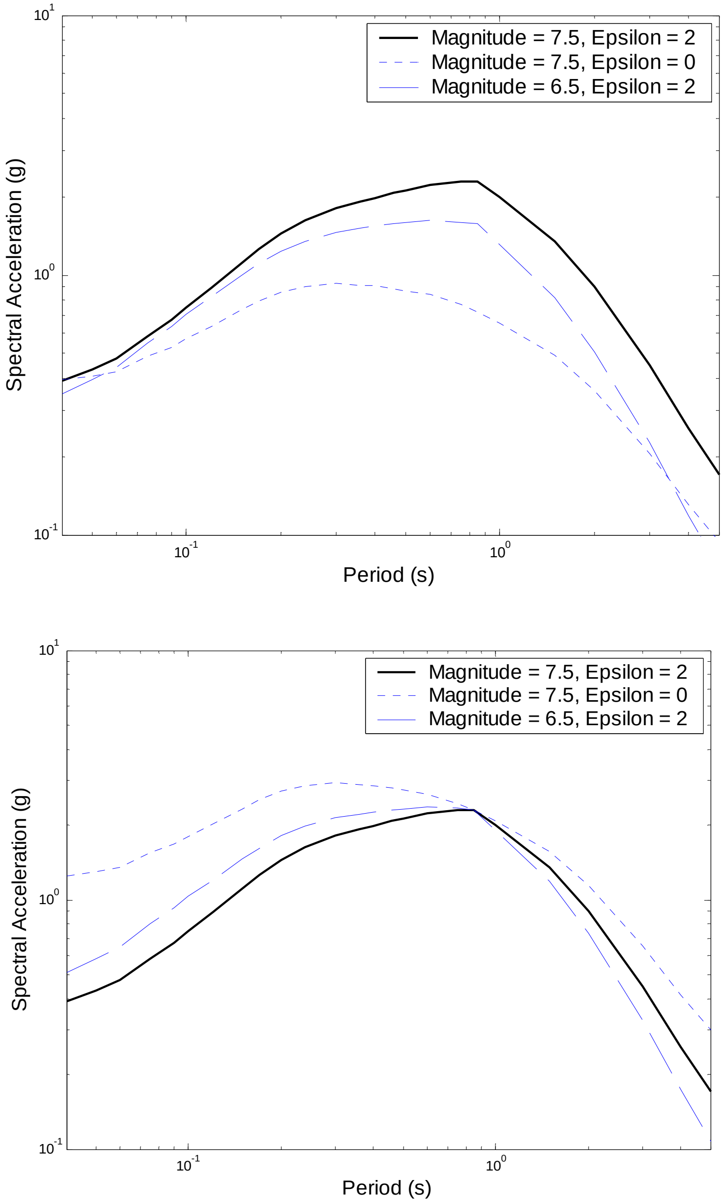

Figure 1. (upper) *Expected response spectra for three scenario events;* (lower) *Expected response spectra for three scenario events, scaled to have the same S_a(0.8s) value. Source: Baker 2005a*

Bruce R. Ellingwood
School of Civil and Environmental Engineering
Georgia Institute of Technology
790 Atlantic Drive
Atlanta, GA 30332-0355 USA

Applications of methods of probability and statistics to structural engineering; structural reliability analysis; load modeling and analysis of combinations of loads; safety and serviceability criteria for structural design; abnormal loads and progressive collapse; response of structures exposed to fires; probabilistic risk assessment of engineered facilities.

I first became familiar with Luis' research as a graduate student at the University of Illinois in the early 1970's, where I studied his seminal paper, co-authored with Dr. Rosenblueth, that was presented at the 1971 ACI Convention in Denver on probabilistic bases for codes. I consider this paper to be one of the classics in the development of reliability-based codified structural design, and it is one of a handful of papers that I require all my graduate students to read, regardless of their individual research interests. We became personally acquainted during the ICOSSAR Conference in Trondheim, Norway, in 1981, on which occasion we spent a delightful (if cold and rainy) weekend together touring Oslo before returning home. Since then, it has been my pleasure to work with Luis for many years on the Editorial Board of the *Journal of Structural Safety*. As a long-time Board member, Luis' insightful reviews of manuscripts have contributed significantly to the journal's scholarly reputation.

Luis' contributions to structural reliability and to earthquake engineering are internationally recognized, of course. But beyond that, he has encouraged and stimulated others of us in our own endeavors, with comments, positive suggestions and critiques that are always made in a kindly fashion.   Luis is one of the true gentlemen in my field of structural reliability, and I consider his friendship a privilege. I am delighted to be included in this symposium in his honor.

Bruce R. Ellingwood

SEISMIC FRAGILITY ASSESSMENT OF LIGHT-FRAME WOOD RESIDENTIAL CONSTRUCTION

ABSTRACT

Approximately 90 percent of the housing in the United States is light-frame wood construction. Residential building construction practices have evolved over the years, and most light-frame wood structures have not been structurally engineered. This state of affairs is changing, however, as a result of the tremendous losses suffered in the residential building inventory in recent hurricane and earthquake disasters. New concepts and methodologies are evolving to better predict and evaluate the performance of wood frame residential structures exposed to natural hazards and to support improved building practices. This paper summarizes a portion of a recent study in which the behavior of light-frame wood structures under earthquake and hurricane hazards was examined using stochastic methods, leading to fragilities for typical lateral force-resisting shear wall systems subjected to various levels of ground motion.

Introduction

The vulnerability of wood residential construction to earthquake ground motion was apparent following the 1994 Northridge earthquake, where the property losses to residences ($US 20 billion) were greater than the losses for any other type of building construction. New concepts and methodologies are required to improve current residential building practices and to enhance the performance of light-frame wood frame construction during earthquakes. In this study, the behavior of wood frame lateral force-resisting system subjected to earthquakes is examined in a simulation-based reliability assessment. Performance levels (continued occupancy, life safety, etc.) for wood frame buildings are defined in terms of lateral drift limits in FEMA 273/356 (1997).

Model of Lateral Force-Resisting System

Shear walls are the primary lateral earthquake force-resisting systems in wood residential construction. Under severe earthquake ground motion, such systems exhibit highly nonlinear hysteretic behavior, characterized by significant stiffness degradation, pinching of the hysteresis loops and energy dissipation. The hysteretic behavior is strongly dependent on the shear wall aspect ratio, presence of openings or doors, and the sheathing and nailing patterns used in construction. Numerical models were developed as part of the CUREE-Caltech Woodframe Project to predict the force-displacement response of wood shear walls with or without openings under quasi-static cyclic loading (CUREE, 2001; Folz and Filiatrault, 2001). These models are used in this study to define the hysteretic behavior under strong ground motion in a planar structural model of typical one and two-story residential buildings developed in OpenSees, a finite element platform developed at the Pacific Earthquake Engineering

Research (PEER) to perform nonlinear dynamic time history analysis of structural systems subjected to earthquake ground motion.

Verification that the building performance objectives are met requires a mapping between each objective stated qualitatively (e.g., continuation of building occupancy following a 50%/50-yr event) and a response quantity and limit state (force or deformation) that can be checked using principles of structural analysis and mechanics. This mapping invariably requires that the behavior of the building structural system be considered as a whole, and presents one of the major challenges for performance-based engineering (Rosowsky and Ellingwood, 2002). According to FEMA 273 (1997), the immediate occupancy, life safety and collapse prevention performance levels for lateral force-resisting structural elements in light-frame wood construction subjected to seismic effects are related to transient maximum lateral drifts of 0.01, 0.02 and 0.03, respectively. These limits are adopted herein.

Shear wall performance during earthquake is impacted by uncertainties in both seismic loading and structural resistance. The uncertainty in seismic demand is reflected in the suites of ground motions chosen for the simulation. In the results presented in the following section, the shear walls are assumed to be seismically anchored, and the SAC Project ground motions for Los Angeles were used in the analysis. The uncertainty in seismic demand is very large in comparison to the variability in the shear wall capacity (Li and Ellingwood, 2004). Thus, this latter source of uncertainty is not included in the evaluation.

Structural Response to Earthquake Ground Motions

The maximum drifts for three ground motion ensembles determined by nonlinear dynamic analysis are rank-ordered in terms of the probability that the drift is exceeded and are plotted in Figure 1. The deformation limit for life safety is 2% drift, or 1.92 in (49 mm) displacement in a wall 8 ft (2.4 m) in height. The probability of exceeding this limit is virtually 0 for the 50%/50yr ground motions, while it is about 15% and 40% for the 10%/50yr and 2%/50yr ground motions, respectively. Assuming that the seismic demand can be described by a lognormal distribution, the fragility, or conditional probability that drift demand on the shear wall exceeds a specified drift limit, can be expressed as a function of spectral acceleration at the fundamental building period (Li and Ellingwood, 2004). Figure 2 presents these fragilities for the immediate occupancy, life safety and collapse prevention performance levels in FEMA 273 (1997).

Conclusions

The fragility of light-frame wood shear walls is a starting point for assessing the performance of wood frame residential construction subjected to earthquakes. The fragility depicts the uncertainty in shear wall performance in a format that is uncoupled from the basic seismic hazard. In this form, the role of uncertainty may be easier for a non-specialist decision-maker to grasp than a point or interval estimate of risk obtained from a fully coupled risk assessment that typically would involve very small probabilities (Ellingwood, 2001). The seismic fragilities can be used to assess the performance of wood frame residential construction under various levels of seismic hazards, and to evaluate proposed changes to construction practices that are aimed at improving building performance.

Acknowledgement

The research described in this paper draws upon a doctoral dissertation by Dr. Yue Li, supervised by the author and was supported, in part, by the National Science Foundation under Grant No. CMS-0049038. This support is gratefully acknowledged.

References

CUREE Publication No. W-04 (2001), “Woodframe project case studies”, CUREE-Caltech Woodframe Project, Consortium of Universities for Research in Earthquake Engineering.

Ellingwood, B.R. (2001), “Acceptable risk bases for design of structures,” Progress in Structural Engineering and Materials, 3:170-179.

FEMA-273, “NEHRP guidelines for the seismic rehabilitation of buildings.” Report FEMB-273, Federal Emergency Management Agency, Washington, DC, 1997.

Folz, B. and Filiatrault, A. (2001), “Cyclic analysis of wood shear walls,” Journal of Structural Engineering, ASCE, 127(4):433-441.

Li, Y. and Ellingwood, B. (2004), “Assessment of wood residential construction subjected to earthquakes,” Proc. 13th World Conf. on Eqk.Engrg. Vancouver, B.C., Canada (Paper 2537 on CD-ROM).

Rosowsky, D.V and Ellingwood, B.R. (2002), “Performance-based engineering of wood frame housing: a fragility analysis methodology,” Journal of Structural Engineering, ASCE, 128(1):32-38.

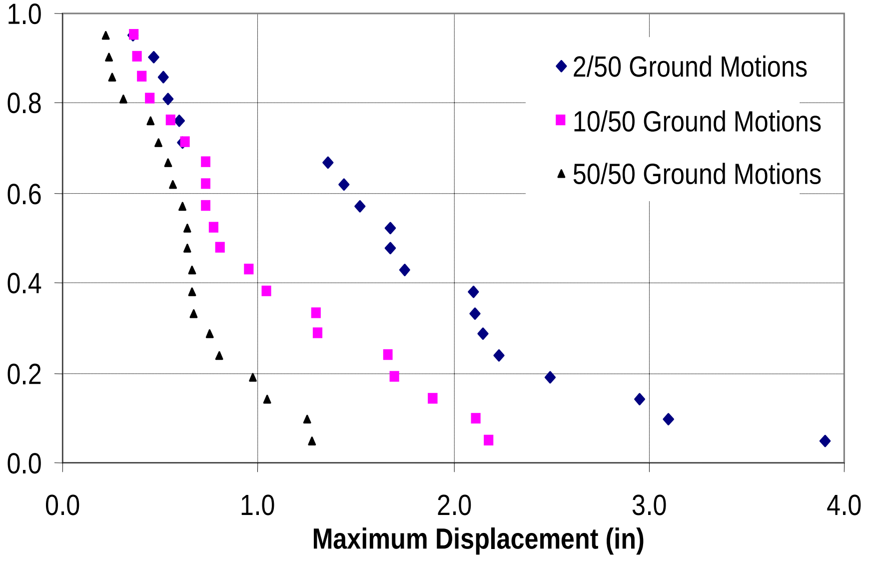

Figure 1. Probability vs *dsplacement*

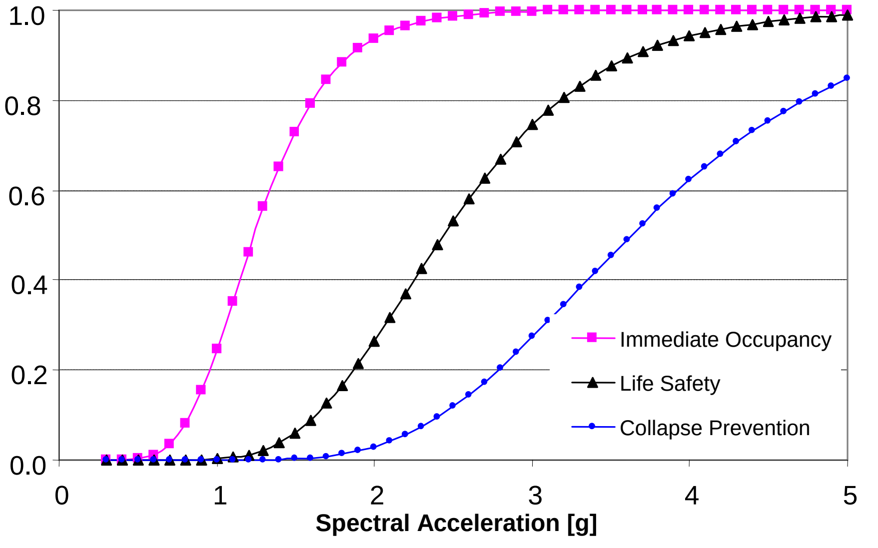

Figure 2. Conditional Probability of Failure (Fragility) of Shear Wall

Ezio Faccioli
Professor of Earthquake Engineering
Politecnico (Technical University)
Piazza L. da Vinci, 32
20133 Milano, Italy
faccioli@stru.polimi.it

Engineering seismology, seismic risk, seismic wave propagation.

Because I have spent there some of the best years in my life, in the 1970es, Mexico remains my "second country", after my own; decades have elapsed since, but I keep with Mexico a deep relationship of affection and cultural attraction. Inevitably, though, people have changed; some of my closest Mexican friends, like Emilio Rosenblueth, alas, are no longer with us. Luis is one remarkable exception: since we first met in the spring of 1971, and worked together at a joint paper for the 1972 Rome WCEE, he has always been there, human and "institutional" point of reference at the Instituto de Ingenieria (even when he had other roles at UNAM), unchanged in his quiet modesty and preserving his peculiar wit and humour intact. Recently, when, as a newly elected member of the IAEE Board of Directors, I resumed a technical interchange with Luis as President , it was no surprise to find in him the same openness and willingness to understand the reasons of others, and the patience and intelligence of mediating among different positions in order to make some progress. Rare virtues, in these days!

Ezio Faccioli,
July 28th, 2005

AN ATTEMPT AT IMPROVING FELT INTENSITY ASSESSMENTS OF HISTORICAL EARTHQUAKES BY MEANS OF INSTRUMENTALLY BASED CORRELATIONS

Ezio Faccioli and *Carlo Cauzzi*[1]

ABSTRACT

This contribution deals with the task of realistically assessing macroseismic intensities of historical earthquakes that have caused heavy damage to cities, and it is motivated by the critical relevance that "historical" intensities may acquire when constructing earthquake damage scenarios. Using for calibration a carefully selected set of earthquake data from the Mediterranean region (mostly Italy), two different empirical correlations for estimating intensity are proposed: one using magnitude and distance as independent parameters, and the other a ground motion parameter (maximum velocity or acceleration). The application of the two correlations is illustrated for the case history of Catania city (Italy), suffering destruction by a late 17th century earthquake for which extensive historical documentation of damage exist.

Introduction

In many regions of the world it is becoming increasingly frequent to perform earthquake damage scenarios studies for cities at risk. The aim is to improve seismic emergency planning, to evaluate social and economic costs, and to identify priorities in retrofitting and risk mitigation programs. In a scenario study for a city, earthquakes at least as severe as those occurring in the historical record represent a natural reference. Scenario earthquakes and the ensuing ground motions can in principle be described in either a deterministic or a probabilistic way, but repetitions of events that have caused severe damage or destruction to a city in the past are priority candidates for deterministic simulations. These have been performed for such diverse urban contexts as those of Tokyo, San Francisco, Lisbon, Izmir, to quote only a few.

For most cities in Europe, the severity of the damage inflicted by past earthquakes is condensed into a single felt intensity value (in the EMS98, MSK, or MCS scales), often rather uncertain. This may be due, among other causes, to lack/incompleteness of contemporary written records (e. g., only the damage to few important buildings such as churches, palaces etc. was reported), or interaction of the earthquake with a built environment vastly different from the present one, or occurrence of more that one strong shock (causing cumulated damage) in a short lapse of time. In seismic scenario studies, uncertainty in the intensity of "reference" earthquakes will in turn strongly affect that of the damage estimations, such as may be obtained from the Damage Probability Matrix approach, or from equivalent formulations using a statistical score assignment for vulnerability assessment (so-called "macroseismic" approaches). More sophisticated damage evaluation tools are available, i. e. mechanical modeling

[1] Ph. D. student, Department of Structural Engineering, Politecnico di Milano, Italy.

approaches. These use response spectra to describe ground motions, and capacity curves for different classes of structures to identify damage limit states. Recent European research work on the subject [notably in the Risk-UE research project, see Mouroux et al. 2004] indicates that the mechanical approaches may suffer from insufficient field validation, and that they should preferably be used in conjunction with a macroseismic approach. Hence, making reference to the latter, it is hereinafter assumed that the severity of a scenario earthquake is to be specified in terms of macroseismic intensity.

The problem to be tackled here is: for a city where a seismic scenario is needed, how can one independently validate intensities (I) of past earthquakes based on the historical record, especially when strong ground shaking is involved? From a deterministic perspective, one could: 1. Use a relationship attenuating the epicentral intensity I_0 of the earthquake (if known) as a function of distance d to the city, that is $I = f(I_0, d)$; 2. Estimate I as a function of magnitude and distance, i. e. use a relation of the form $I = f(M, d)$, if available; 3. Use an empirical correlation of intensity (dependent variable) with a strong motion parameter y (independent variable) like maximum horizontal ground velocity, v_{max}, or acceleration, a_{max}, i. e. $I = f(y)$.

We discard here Option 1 because I_0 is typically estimated from epicentral area intensities and, hence, will be affected by the same uncertainties. Option 2 seems better because magnitude can be constrained by tectonic considerations (e.g. length of active faults) and by instrumental seismicity data. In this case, a relationship of the desired form $I = f(M, d)$ needs to be expressly derived from reliable recent data in the Mediterranean region, of main interest here. Option 3 would clearly be good if strong motion data are available from strong recent earthquakes, but can also be considered as a second step in a process where ground motion maps would be simulated first, e. g. to conduct damage evaluations by a mechanical modeling approach. Clearly, in such option one increases the overall uncertainty of the estimates by compounding those of the two steps, e. g. an attenuation relation $y = f(M, d)$ and the correlation $I = f(y)$.

In the next section, Option 2 is considered first, i. e. deriving an attenuation relation of the form $I = f(M, d)$ based on a carefully selected set of data. Subsequently, the derivation of a correlation $I = f(y)$ will be carried out, using the same set of calibration data; note that – with the significant exception of those developed by Wald et al. (1999) currently used to produce SHAKEMAPS in Western US - most existing correlations are of the inverse form $y = f(I)$ but, obviously, these cannot be simply inverted for the use intended here. Finally, the application that originated the whole study, concerning the city of Catania, Italy, will be presented.

Estimating intensities from diverse parameters

The calibration data set

To assemble a suitable calibration data set, we started from an Italian earthquake data set selected for estimating peak acceleration from intensity (Margottini et al. 1992). These data (see the Appendix) consist of 2 instrumental parameters, i. e. maximum horizontal ground acceleration (a_{max}, the largest of two horizontal components) and Arias intensity, and of 4 intensity values, namely general and local MCS , and general and local MSK–64 intensities. The intensities in question had been directly assessed by

Margottini et al. (cit.) in the field during the strongest Italian earthquakes since 1980; "local" intensities describe the damage to buildings located within few hundreds of m from the accelerograph station, while "general" intensities refer to the damage in the entire town or village closest to the station. We retained here only the general intensities by Margottini et al. (cit.), since we could not assess local values for the additional earthquakes included in our data set.

The MCS intensity scale, introduced in Italy around 1937, is still used in this country to assess the severity of historical earthquakes because it takes into account only the total damage, without distinguishing the different types of buildings, and does not consider reinforced concrete structures. Based on a detailed comparison between their MSK-64 and MCS intensity ratings for all earthquakes considered, Margottini et al. found no statistically significant difference between the two scales in the range from IV to VIII degrees (see the Appendix), in partial contrast to previous (possibly less accurate) suggestions to raise by about one degree the MCS intensity with respect to the MSK value in the range > VI (Levret and Mohammadioun 1984). Herein, we have extended the assumption $I_{MCS} = I_{MSK}$ also to some non-Italian earthquakes (see the Appendix).

Following Margottini et al., who found no significant statistical dependence of their correlations upon local ground conditions, we neglected the influence of such conditions in our derivations.

Concerning Italian earthquakes, we expanded the Margottini et al. subset of observations by adding data from the strongest events recorded between 1970 and 1980, beginning with the destructive 1976 Friuli sequence. We also included the most significant events occurring in the 1990s and early 2000s, mostly with $5.0 < M < 6.0$, for which strong motion records were available. However, since the felt intensities of "useful" Italian data do not exceed VIII, we deemed it necessary to complete the data set with a few additional strong earthquakes (intensities ≥ VIII) from the Mediterranean region, having regard to some similarities in terms of tectonic features and of built environment. These include the Izmit, Turkey event of August 1999, and the Boumerdes, Algeria earthquake of May 2003. Additional data from moderate recent Greek earthquakes were also included, such as Aigion 1995 and Athens 1999. Papadopoulos et al. (2004), from their macroseismic observations of the Athens earthquake, give an indication analogous to that by Margottini et al. (cit.) on the basic equivalence of the EMS-98 (assumed similar to MSK-64) and MCS scales in the aforementioned range. As to the MM intensity ratings in the VI to VIII range used for the destructive 2003 Algeria earthquake and for some Greek earthquakes (the National Observatory of Athens uses a scale similar to MM), they were assumed equivalent to MCS (see Levret and Mohammadioun 1984).

As a final remark on felt intensities (Appendix), half-degree ratings such as V-VI or VI-VII, denoting in most cases an uncertain attribution, were effectively treated as 5.5 and 6.5 to simplify the treatment (but we are aware that some interpretative problems are involved because - at least in European practice - intensity scales are regarded as an "ordinal" classification of effects).

The maximum velocities and accelerations to be correlated with intensity were mostly drawn in the form of corrected data from the European Strong Motion Database (Ambraseys et al. 2002), to ensure a reasonable degree of uniformity in the sample; we did, however, independently perform the baseline correction of the acceleration time series and their integration to velocities for several records, finding in most cases good agreement. For some Italian earthquake records, not available in the European database, we directly processed the uncorrected data.

The complete data set used is described in the Appendix, including the sources of the event magnitudes and locations, and of the source-to-station distances.

Estimating intensity from magnitude and distance

An attenuation relation of the form

$$I = c_1 \ln d + c_2 M_W + c_3 , \tag{1}$$

has been adopted for estimating intensity I, where c_1, c_2 and c_3 are numerical coefficients, and M_w = moment magnitude; this expression had been used in early studies (Esteva and Rosenblueth 1964, Cornell 1968) with d = focal distance. Herein, we have taken

$$d = \sqrt{r^2 + 2^2} \qquad (d, r \text{ in km}) \tag{2}$$

with r = epicentral distance for earthquakes with $M_w < 5.5$, and r = shortest distance from site to the surface projection of the ruptured fault for $M_w \geq 5.5$, in analogy to current attenuation expressions for strong motion parameters (e. g. Ambraseys *et al.* 1996). Eq. 2 contains a fictitious depth value of 2 km, attributed to each earthquake, in order to avoid singularities in attenuation at vanishing distances. The choice of the fictitious depth being to a good extent arbitrary, we verified that among the values 2, 5, 10, 15, 18, and 20 km, the first one yielded a slightly lower standard error in the estimate of I and a slightly higher coefficient of determination of the regression. However, the main reason for keeping a low value of the fictitious depth is that it fits better the intensity observations at small source distances.

Least square regression in the independent variables ln d and M_w , using the set of 76 data entries listed in the Appendix, yielded for Eq. 1 the values

$$c_1 = -\,0.65 \qquad c_2 = 1.087 \qquad c_3 = 1.91 \qquad \sigma_I = 0.57 \qquad R^2 = 0.72. \tag{3}$$

The standard error of the estimate is seen to be about one intensity degree, and the coefficient of determination R^2, albeit low, seems acceptable for the type of correlation at hand. The relation thus obtained is constrained by observations in the interval 1.5 km $\leq r \leq$ 120 km, and $3.8 \leq M_w \leq 7.4$. Fig. 1 illustrates the relation for different magnitudes, together with the intensity data, as a function of the distance d. One practical indication of interest is that the epicentral intensities ($d \leq$ about 5 km) predicted for M_w 5.0, 6.0 and 7.0 are roughly VII, VIII, and IX, respectively. Being obtained from a limited data set, the indication should not be overemphasised; it may be noted, however, that the relationship $M_w = 0.43\, I_0 + 2.18$ used in the most recent compilation of the catalogue of Italian earthquakes (Gruppo di Lavoro CPTI 2004), yields the much higher intensities IX and XI for M = 6 and 7, respectively.

The residuals of the regression were checked both as a function of magnitude and of distance; only a negligible negative trend for increasing distance has been detected.

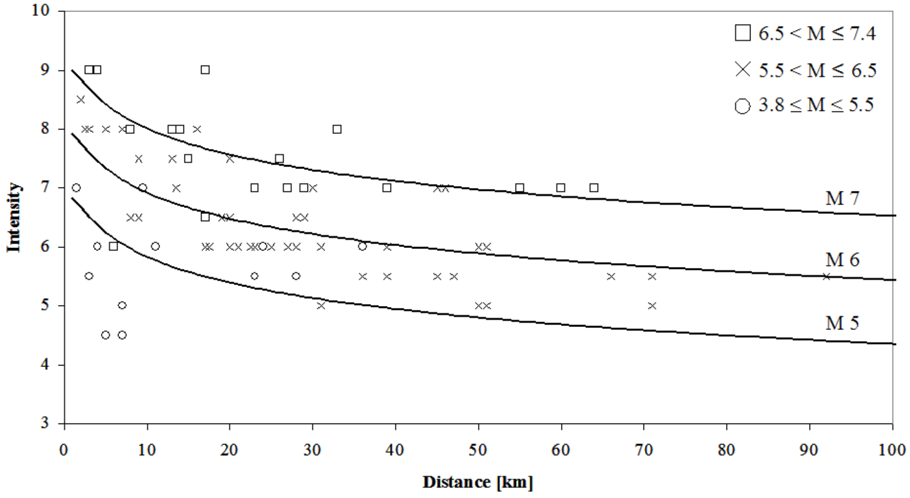

Figure 1. The felt intensity data as a function of distance and magnitude, with the regression curves obtained for 3 representative magnitudes

Estimating intensity from a strong ground motion parameter *y*

A correlation of the form

$$I = a \log y + b \tag{4}$$

has been chosen, where y stands either for maximum horizontal ground velocity (v_{max} = largest of two observed peak values, v_a = average of the two), or acceleration. Least square fitting of the data in the Appendix provided the values of *a* and *b*, and of other statistical measures, listed in Table 1.

TABLE 1. Coefficients of the linear regression *I* vs. log *y* of Eq. 4

Independent variable	***a***	***b***	R^2	**Standard error**
v_{max} [m/s]	1.65±0.16	8.52±0.21	0.59	0.69
v_a [m/s]	1.66±0.16	8.62±0.21	0.59	0.69
a_{max} [m/s^2]	1.83±0.25	6.57±0.10	0.40	0.83

The intensity estimates provided by Eq. 4 are evidently less accurate than those obtained from Eq. 1, 2, and 3, even neglecting uncertainty in the ground motion parameters; also, maximum ground velocities appear to be a better predictor of intensity that the maximum accelerations.

The 1693 Catania case history

The motivation for developing the previous empirical relationships arose in the course of the earthquake scenario studies for the Italian city of Catania, conducted in the cited Risk–UE project (Mouroux et al. 2004). Catania, which is located at the foot of Mt. Etna, the highest active volcano in Europe, has a particularly severe record of earthquake damage: two destructive events took place close to the city in the last 1000 years, plus a number of damaging events. The first of the two severest earthquakes struck in 1169, with estimated epicentral intensity I_0 = X and M_w = 6.6; the second in 1693, with I_0 estimated at XI (Boschi and Guidoboni 2001, Gruppo di Lavoro CPTI04 2004). The 1693 felt intensity in Catania is reported as X (Boschi and Guidoboni cit.) or X-XI (Monachesi and Stucchi 1997), while magnitude estimates range from 7.1 ("equivalent" macroseismic magnitude, Boschi and Guidoboni cit.) to 7.4 (M_w, Gruppo di Lavoro CPTI04 cit.). In the most complete and recent reference on earthquakes and volcanic eruptions hitting Catania, i. e. the book by Boschi and Guidoboni (cit.), an extended discussion is devoted to contemporary written sources relating of fairly substantial tsunami phenomena apparently caused by both the previous earthquakes, although much better described for the second event. While this evidence, for both the previous earthquakes, lends support to a fault rupturing offshore as seismic source, identified as the Malta Escarpment fault (see Fig. 2a), the assumption is not universally accepted.

The 1693 earthquake, in addition to being closer to us in time, had a catastrophic impact over much of Eastern Sicily which sparkled in the following years a major reconstruction process in Catania and other important population centers of the region. For these reasons, this event is a compulsory reference for earthquake scenario studies in the city, and we focus here our attention on it. To properly frame the task of evaluating the actual severity of the ground shaking, it is useful to note that:

- the 1693 earthquake was in reality a sequence of two destructive shocks: the first occurring on Jan. 9, with M>6 and I = VIII in Catania (Boschi and Guidoboni, cit.), the second and strongest on Jan. 11, producing obvious cumulative damage effects;
- the felt intensity rating of X most recently assigned to Catania for January 11 relies on damage descriptions of 104 monumental buildings (97 of which were damaged, 7 undamaged, Boschi and Guidoboni cit.); these were mostly churches, known to be more vulnerable than other masonry constructions (Lagomarsino and Podestà 2004).

The question then arises: is a local intensity X a credible engineering option for a seismic scenario of Catania today ? The two previous remarks make us believe that an intensity X in Catania for the January 11 shock is likely to be overestimated. To substantiate this evaluation, the empirical relations of the previous section were applied.

In the first case, to derive intensity as a function of magnitude and distance, we adopted the prevailing assumption of a seismic rupture along the Malta Escarpment (see Faccioli and Pessina 1999), a major normal fault of regional significance, schematically represented as a red line in the inset of Fig. 2a. Shown in the same inset is also the Catania municipal area and its location in Eastern Sicily: the city area proper occupies roughly the northern portion of the municipality, and its distances from the previous fault are typically between 10 and 15 km. Taking a 7.2 magnitude, and using Eq. 1, 2 and 3 through a GIS yields the intensity distribution over the municipal area given in

Fig. 2b. In the city area the prevailing intensity is VIII, and does not exceed VIII-IX in its portion closest to the source. If one standard error is added to the estimates, the maximum intensity in the area of interest does not exceed IX.

As a second option, we apply the empirical correlation of Eq. 4 to a map of v_{max} values generated – for the same reference earthquake on the Malta Escarpment fault - by means of the attenuation relation for peak ground velocity calibrated on Italian strong motion data (Sabetta and Pugliese 1987), assuming average soil conditions. This is a conservative assumption, because in most of the city massive, exposed lava flows are the prevailing (rock-like) ground condition. The peak velocity ranges between about 40 and 60 cm/s in the city area. Transforming v_{max} into intensity values through Eq. 4 leads to the intensity map in Fig. 2c. The prevailing intensity in the city area is still around VIII, but somewhat smaller than in the previous case.

The two alternative intensity evaluations exhibit remarkable mutual consistency and, as one would have expected, they point to less catastrophic picture than the "historical" scenario. Hence, we conclude that a felt intensity VIII - IX represents a realistic assessment of the severity of the January 11, 1693 mainshock (alone) in the city.

Conclusions

Felt intensity ratings of historical earthquakes hitting important urban centers provide invaluable data especially when the historical record spans over many centuries, a not uncommon circumstance in Europe. The importance of such ratings should not only be viewed in the context of regional seismicity studies or earthquake catalogues, but also in that of earthquake damage scenarios. Uncertainties that inevitably affect the intensity assessments based on the interpretation of written and other historical records, often result in an overestimation of the severity of ground shaking (e.g. a high intensity may be attributed to an old earthquake in a city where a few masonry churches were heavily damaged, although it is now well known that these structures are quite vulnerable). To cope at least in part with this shortcoming, we have developed two empirical correlations based on instrumental data, using a very carefully selected and documented set of observations, mostly from Italian earthquakes. While the size and quality of this calibration data set can certainly be improved, the application of the correlations to a well documented case history indicates that significant reductions in the earthquake ground shaking severity may result from it, pointing to significant implications for the revision of earthquake catalogues and felt intensity databases.

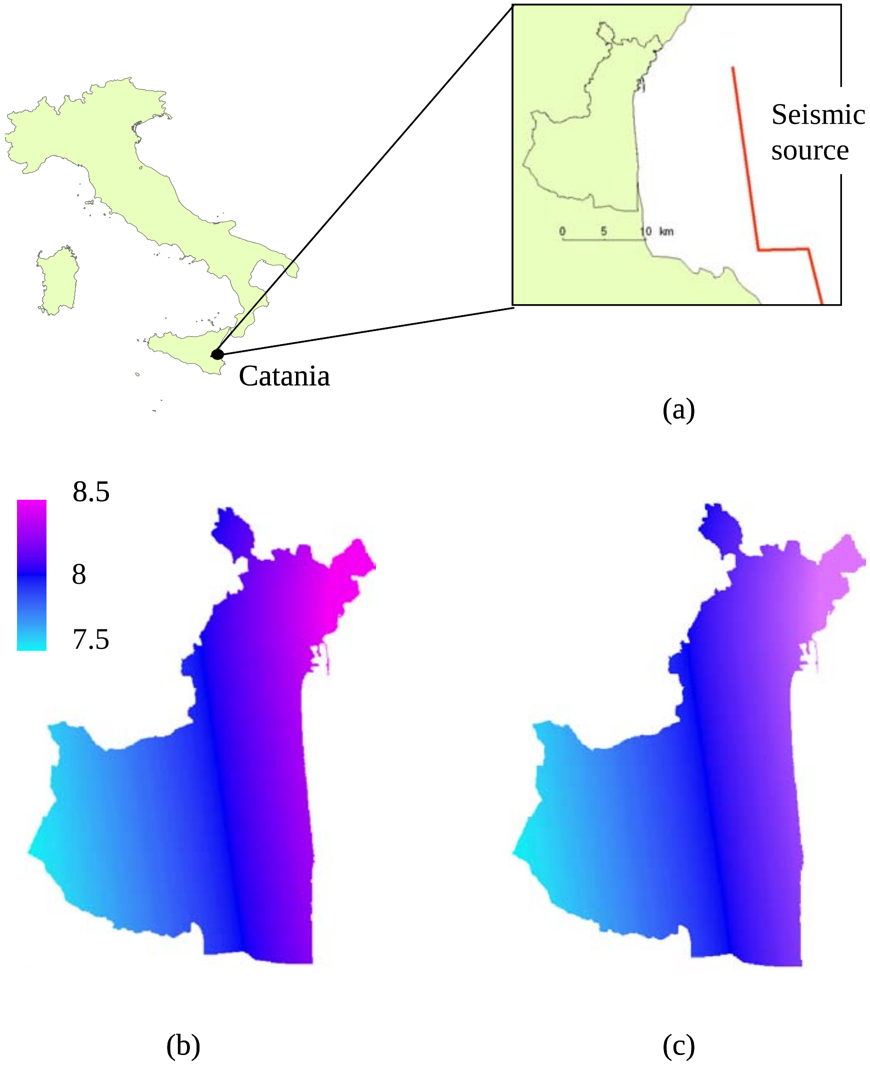

Figure 2. (a) *Location of Catania city in Italy, in the inset the municipal boundaries and the trace of the offshore Malta Escarpment fault.*
(b) *Intensity distribution generated over the municipality through Eq. 1, 2, and 3 for an M_w 7.2 event rupturing the fault in (a).*
(c) *Intensity distribution generated through Eq. 4 from a peak velocity map, as described in the text.*

Appendix

TABLE A1. Intensity and instrumental data (sources given in footnotes at end of Table; v_{max}, a_{max} is the largest of two horizontal peak values, v_a the average of the two).

Date Time (Magnit M_w[(1)])	**Epicentral area**	**Recording Station** (distance[(2)] km)	**I** MCS	**I** MSK (or MM)	v_{max} (m/s)	v_a (m/s)	a_{max} (m/s^2)
06/05/1976 20.00 (6.4)	Friuli, NE Italy	Tolmezzo (16)	8[(3)]		0.32[(4)]	0.26	3.35
		Castelfranco Veneto (120)	5[(3)]		0.03	0.03	0.30
		Barcis (46)	7[(3)]		0.02	0.02	0.32
15/09/1976 9.21 (5.9)	Friuli	Buia (7)	8[(3)]		0.07	0.06	0.85
15/09/1976 3.15 (6.0)	Friuli	Gemona (3[(5)])	8[(3)]		0.59[(5)]	0.50[(5)]	6.00[(5)]
15/04/1978 23.33 (6.1)	NE Sicily	Patti (9)	7-8[(3)]		0.15	0.10	1.56
		Naso (13)	7-8[(3)]		0.08	0.07	1.47
		Milazzo (20)	7-8[(3)]		0.03	0.03	0.73
19/09/1979 21.35 (5.9)	Valnerina, Central Italy	Cascia (2.5)	8[(3)]		0.11	0.09	1.99
		Nocera U. (39)	6[(3)]		0.04	0.03	0.81
		Bevagna (31)	5[(3)]		0.01	0.01	0.35
23/11/1980 18.34 (6.9)	Irpinia, S Italy	Arienzo (60)	7[(6)]	7[(6)]	0.03	0.03	0.34
		Bagnoli I. (6)	6[(6)]	6[(6)]	0.32	0.27	1.83
		Brienza (23)	7[(6)]	7[(6)]	0.11	0.10	2.15
		Mercato S. S. (33)	8[(6)]	7[(6)]	0.12	0.09	1.35
		Sturno (14)	8[(6)]	6[(6)]	0.63	0.50	3.04
		Calitri (13)	8[(6)]	8-9[(6)]	0.27	0.27	1.70
		Rionero in V. (29)	7[(6)]	7[(6)]	0.10	0.08	1.00
		Bisaccia (27)	7[(6)]	7[(6)]	0.17	0.16	0.91
		Torre del Greco (64)	7[(6)]	7[(6)]	0.05	0.04	0.61
		Tricarico (55)	7[(6)]	7[(6)]	0.05	0.04	0.45
		Bovino (39)	7[(6)]	7[(6)]	0.03	0.03	0.46
29/04/1984 5.03 (5.6)	Gubbio, Centr. Italy	Pietralunga (20)	6[(6)]	6[(6)]	0.08	0.07	1.80
		Umbertide(17)	6[(6)]	6[(6)]	0.01	0.01	0.34
		Peglio (50)	5[(6)]	5[(6)]	0.02[(8)]	0.02[(8)]	0.44[(8)]

07/05/1984 17.50 (5.9)	Abruzzo, Centr. Italy	Atina (13.5)	7(6)	7(6)	0.04	0.04	1.08
		Isernia (30)	7(6)	7(6)	0.04(8)	0.03(8)	0.69(8)
		Ortucchio (27)	6(6)	5-6(6)	0.04	0.03	0.85
		Pontecorvo (28)	6(6)	6(6)	0.06	0.05	0.67
		Roccamon.(45)	7(6)	7(6)	0.04	0.04	0.42
11/05/1984 10.41 (5.5)	Abruzzo	V.Barrea (1.5)	7(6)	7(6)	0.09	0.08	2.23
15/03/1988 12.03 (4.5)	Reggio E., N Italy	Novellara (3)	5-6(4)		0.02	0.01	0.27
05/05/1990 7.21 (5.4)	Potenza, S Italy	Rionero in V. (36)	6(4)		0.05	0.05	0.85
		Tricarico (24)	6(4)		0.02	0.02	0.35
		Brienza (28)	5-6(4)		0.07	0.05	0.94
13/12/1990 0.24 (5.6)	E. Sicily	Sortino (29)	6-7(3)		0.07	0.05	1.03
		Giarre (45)	5-6(3)		0.02	0.02	0.38
		Vizzini (50)	6(3)		0.04	0.04	0.71
		Noto (51)	6(3)		0.05	0.04	0.88
15/03/1993 23.43(4.0 M_L)	Cuneo, NW Italy	Demonte (5)	4-5(7)		0.01	0.01	0.81
15/10/1996 9.56 (5.4)	Correggio, N Italy	Novellara (9.5)	7(7)		0.09(8)	0.08(8)	1.98(8)
		Sorbolo - Pezzani (23)	5-6(7)		0.05(8)	0.05(8)	1.37(8)
03/09/1997 22.07 (4.5)	Umbria, Centr. Italy	Colfiorito (4)	6(7)		0.06	0.05	1.13
07/09/1997 23.28 (4.2M_L)	Umbria	Colfiorito (7)	5(7)		0.01	0.01	0.73
10/09/1997 6.46 (3.8 M_L)	Umbria	Colfiorito (7)	4-5(7)		0.01	0.01	0.44
26/09/1997 9.40 (6.0)	Umbria-Marche	Colfiorito (2(9))	8-9(7)		0.19(8)	0.17(8)	3.11(8)
		Castelnuovo - Assisi (19)	6-7(7)		0.13	0.10	1.6
		Bevagna (21)	6(7)		0.08	0.08	0.78
		Borgo Cerreto - Torre (23)	6(7)		0.04	0.04	1.08
		Matelica (20)	6-7(7)		0.09(8)	0.08(8)	1.13(8)
		M. Fiegni (25)	6(7)		0.01	0.01	0.32
		Norcia - Altavilla (31)	6(7)		0.04	0.03	0.60
		Cascia (36)	5-6(7)		0.01	0.01	0.22
		Forca Canapine (39)	5-6(7)		0.01	0.01	0.32
		Gubbio (28)	6-7(7)		0.03	0.03	0.85
		Leonessa (51)	5(7)		0.01	0.01	0.34

		Pietralunga (47)	5-6[7]		0.02	0.02[1]	0.65
		Cagli (50)	6[7]		0.01	0.01	0.20
		Rieti (66)	5-6[7]		0.02	0.02	0.18
		Senigallia (71)	5-6[7]		0.04	0.04	0.46
		Peglio (71)	5[7]		0.03	0.03	0.70
		Pennabilli (92)	5-6[7]		0.01	0.01	0.15
09/09/1998 11.28 (5.6)	Basilicata, S Italy	Lauria-Galdo (17.5)	6[7]		0.13[8]	0.12[8]	2.45[8]
		Lauria S. Giovanni (22.5)	6[7]		0.14[8]	0.13[8]	1.70[8]
11/04/2003 9.26 (4.6M_d)	NW Italy	Tortona (11)	6[10]		0.03[8]	0.03[8]	0.89[8]
15/06/1995 0.15 (6.5)	Aigion, Greece	Aigion (5[11])		8	0.48[12]	0.46[12]	5.30[12]
17/08/1999 0.01 (7.4)	Izmit, Turkey	Gebze (8[13])		8[13]	0.46[13]	0.40[13]	2.64[13]
		Izmit-Met. Ist. (4)		9[13]	0.54[13]	0.43[13]	2.22[13]
		Yarimca-Petkim (3)		9[13]	0.85[13]	0.82[13]	3.15[13]
		Düzce (17)		9[13]	0.61[13]	0.55[13]	3.76[13]
07/09/1999 11.57 (6.0)	Athens, Greece	Athens 2 (Chalandri) (9)		6-7[14]	0.06	0.05	1.57
		Athens 3 (Kallithea) (8)		6-7[14]	0.15	0.14	2.96
		Athens 4 (Kipseli) (8)		6-7[14]	0.09	0.08	1.17
21/05/2003 18.44 (6.8)	Boumerdes, Algeria	Dar El Beida (15) [15]		7-8[16] (MM)	0.41[16]	0.34[16]	5.40[16]
		Hussein Dey (26)[15]		7-8[16] (MM)	0.19[16]	0.18[16]	2.69[16]
		Keddara Dam 1 (17)[15]		6-7[16] (MM)	0.18[16]	0.15[16]	3.33[16]

[1] Moment magnitudes from Gruppo di Lavoro CPTI (2004) for Italian earthquakes, the Harvard CMT Catalog for events with M_w >5.5 and the USGS National Earthquake Information Center.

[2] Epicentral distance for M_w <5.5, otherwise shortest distance to surface projection of rupture area; unless otherwise indicated, sources of distance data are Sabetta and Pugliese (1987) and Ambraseys *et al*. (2002). For some low magnitude Italian events, epicentral distances were directly calculated from available epicentral and station coordinates.

[3] Database DOM4.1 (Monachesi and Stucchi 1997).

[4] Ambraseys et al. (2002), corrected data; unless otherwise indicated, this is the source of all entries in the v_{max}, v_a, and a_{max} columns.

[5] Distance from Aoudia et al. (2000); corrected ground motion data provided by Italy's National Institute of Geophysics and Volcanology (INGV), see also Rovelli et al. (1991).

[6] Margottini et al (1992).

[7] Bollettino Macrosismico (Gasparini and Vecchi 1988 to 1999), describing also the procedure followed to assign the intensity ratings.

[8] From our own baseline correction and integration of raw acceleration data provided by Italy's Department of Civil Defence (Dipartimento Protezione Civile - Ufficio del Servizio Sismico Nazionale).

(9) Distances of accelerograph stations for this event obtained from rupture areas given in Hernandez *et al.* (2004).
(10) Intensity from INGV (2003).
(11) Obtained from map in Bernard et al. (1997).
(12) From corrected data kindly provided by Prof. G. Gazetas.
(13) Fault distances to accelerograph stations and v_{max}, v_a, and a_{max} values from Akkar and Gülkan (2002); intensities from same source, confirmed by Prof. P. Gülkan (2004).
(14) Papadopoulos et al. (2004); also Papaioannou (2004).
(15) Distances to accelerograph stations computed from the Zemmouri fault trace in Hamdache et al. (2004).
(16) Site intensities (and intensity map) from Belazougui (2004); v_{max}, v_a, and a_{max} values from corrected data kindly provided by M. Belazougui.

References

Ambraseys, N., Simpson, K. and J. Bommer (1996). Prediction of horizontal response spectra in Europe, *Earthquake Engineering Struct. Dynamics* 25, 371–400.

Ambraseys, N., Smit, P., Sigbjornsson, R., Suhadolc, P. and Margaris, B. (2002), Internet -Site for European Strong-Motion Data, European Commission, Research-Directorate General, Environment and Climate Programme, http://www.isesd.cv.ic.ac.uk/ESD/.

Akkar, S., and P. Gülkan (2002). A critical examination of near-field accelrograms from the Sea of Marmara region earthquakes, *Bull. Seism. Soc. Am*. 92 (1), 428 – 447 (Dedicated Issue Izmit, Turkey, Earthquake of 17 August 1999).

Aoudia, A., Sarao', A., Bukchin, B., and P. Suhadolc (2000). The Friuli 1976 event: a reappraisal 23 years later, *Geophys. Res. Letters* 27, 573 – 576.

Belazougui M. (Director of National Center of Appled Research in Earthquake Engineering, Algiers) (2004). Written communication to P. Mouroux.

Bernard, P., Briole, P., B. Meyer et al. (1997). The Ms = 6.2, June 15, 1995 Aigion earthquake (Greece) : evidence for low angle normal faulting in the Corinth rift, *J. of Seismology* 1, 131-150.

Boschi, E., Guidoboni, E., Ferrari, G., Mariotti, D., Valensise, G., and P. Gasperini (2000). Catalogue of Strong Italian Earthquakes from 461 b. C. to 1997, Introductory Texts and CD Rom, *Annali di Geofisica* 43(4).

Boschi, E., and E. Guidoboni (2001). *Catania terremoti e lave*, INGV and SGA, Editrice Compositori, Bologna, Italy.

Cornell C. A. (1968). Engineering seismic risk analysis, *Bull. Seism. Soc. Am*. 58 (5), 1583 – 1606.

Esteva, E., and E. Rosenblueth (1964). Spectra of earthquakes at moderate and large distances, *Sociedad Mexicana de Ingenieria Sísmica* II, 1-18.

Faccioli, E., and V. Pessina, Editors (1999). *The Catania Project. Earthquake damage scenarios for a high risk area in the Mediterranean*, CNR – Gruppo Nazionale per la Difesa dai Terremoti, Rome, Italy.

Gasparini, C., and M. Vecchi, Eds., (1988 to 1999). *Bollettino Macrosismico*, Istituto Nazionale di Geofisica, Rome, Italy.

Gruppo di lavoro CPTI (2004). *Catalogo Parametrico dei Terremoti Italiani, versione 2004 (CPTI04) (Parametric Catalogne of Italian Earthquakes, 2004 version)*, Istituto Nazionale di Geofisica e Vulcanologia (INGV), Bologna. http://emidius.mi.ingv.it/CPTI/.

Gülkan, P. (2004). Written personal communication to E. Faccioli.

Hamdache M., Peláez, J., and A. Yelles-Chauche (2004). The Algiers, Algeria earthquake (M_W 6.8) of 21 May 2003 : preliminary report, *Seism. Res. Letters* 75(3), 360-367.

Hernandez, B., Cocco, M., Cotton, F., Stramondo, S., Scotti, O., Courbouleux, F., and M. Campillo (2004). Rupture history of the 1997 Umbria-Marche (Central Italy) main shocks from the inversion of GPS, DInSAR and near field strong motion data, *Annals of Geophysics* 47(4), 1355-1376.

INGV (2003). Istituto Nazionale di Geofisica e Vulcanologia – Campi Macrosismici, www.ingv.it/~roma/attivita/pererischio/macrosismica/macros/campi/effettirecenti/lista.html

Lagomarsino, S., and S. Podestà (2004). Seismic vulnerability of ancient churches: II. Statistical analysis of surveyed data and methods of risk analysis, *Earthquake Spectra 20(2)*, 395-412.

Levret, A., and B. Mohammadioun (1984). Determination of seismic reference motion for nuclear sites in France, *Engineering Geology* 20, 25-38.

Margottini, C., Molin, D., and L. Serva (1992). Intensity versus ground motion: a new approach using Italian data, *Engineering Geology* 33, 45-58.

Monachesi, G., and M. Stucchi (1997). *DOM4.1 An intensity database of damaging earthquakes in the Italian area*, http://emidius.mi.ingv.it/DOM/.

Mouroux, P., Bertrand, B., Bour, M., Le Brun, B., Depinois, S., Masure, P., and the Risk – UE Team (2004). The European Risk-UE Project : and advanced approach to earthquake risk scenarios, *Proc. 13th World Conference on Earthquake Engineering, Vancouver, B. C., Canada*, Paper No. 3329.

Papadopoulos G., Matsumoto, H., Ganas, A., Karastathis, V., and S. Pavlides (2004). Deformation patterns associated with the M 5.9 Athens (Greece) earthquake of 7 September 1999, *J. of Seismology* 8(3), 381-394.

Papaioannou, C. (2004). Written personal communication to Prof. K. Pitilakis.

Rovelli, A., Cocco, M., Console, R., Alessandrini, B., and S. Mazza (1991). Ground motion waveforms and source spectral scaling from close-distance accelerograms in a compressional regime area (Friuli, Northeastern Italy), *Bull. Seism. Soc. Am*. 81 (1), 57 – 80.

Sabetta , F., and A. Pugliese (1987). Attenuation of peak horizontal acceleration and velocity from Italian strong-motion earthquakes, *Bull. Seism. Soc. Am*. 77(5), 1491-1513

Wald, D., Quitoriano, V., Heaton, T., and H. Kanamori (1999). Relationships between peak ground acceleration, peak ground velocity, and Modified Mercalli Intensity in California, Earthquake Spectra 15(3), 557-564.

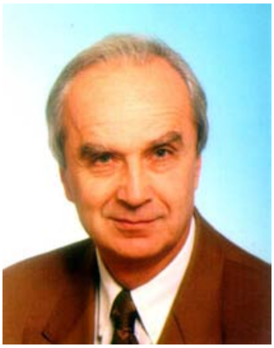

Professor Peter Fajfar
University of Ljubljana
Jamova 2, SI-1000 Ljubljana, Slovenia
Peter.Fajfar@ikpir.fgg.uni-lj.si

Main research interests:
Linear and nonlinear analysis of structures, Performance-based seismic design

It is an immense pleasure for me to be able to participate at the symposium to honor the person and achievements of Professor Luis Esteva. He is truly a remarkable person. His contributions to the general understanding of earthquake engineering are enormous. He has won the respect and admiration of all for his excellent research work and wonderful personality.

I do not remember when exactly I met Luis for the first time. It was at one of the early conferences on earthquake engineering. Since then, I have had not only the pleasure of listening to many of his inspiring presentations, but also the privilege of having valuable personal discussions. He has always impressed me with his energy and enthusiasm. Although my narrow research field was different from his, I have benefited a lot from his important ideas and original concepts. More recently, I was fortunate to have an opportunity to work under skillful Luis's leadership in the International Association for Earthquake Engineering and to cooperate with him on the topics related to the international journal Earthquake Engineering and Structural Dynamics. Here I noticed Luis's diplomatic skills and ability to find smooth solutions of the problems.

Luis, thank you for your friendship and your continuous support and best wishes for future achievements in Earthquake Engineering and for many continued years of happiness.

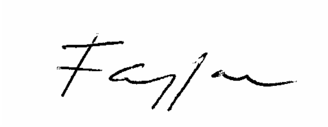

Peter Fajfar
2. August 2005

THE EXTENSION OF THE N2 METHOD TO ASYMMETRIC BUILDINGS

ABSTRACT

The paper deals with the extension of the N2 method to asymmetric building structures, represented by a 3D structural model. The results of recent parametric studies suggest that in the majority of cases an upper limit for torsional effects can be estimated by a linear dynamic (spectral) analysis. Based on this observation, it is proposed that the results obtained by pushover analysis of a 3D structural model be combined with the results of a linear dynamic (spectral) analysis. The former results control the target displacements and the distribution of deformations along the height of the building, whereas the latter results define the torsional amplifications. In the paper, first the theoretical background of the transformation of a 3D MDOF model to an equivalent SDOF model is given. Then, the proposed extended N2 method is summarized and applied to a test example of an asymmetric three-storey reinforced concrete frame ("SPEAR") building. The results are compared with results of nonlinear dynamic time-history analyses.

Introduction

Simplified methods for seismic analysis based on nonlinear static (pushover) analysis represent a relatively simple and efficient tool for seismic assessment of structures. They have become very popular in research and also in application. Originally, all methods were limited to planar structural models. Recently, attempts have been made to extend the applicability of simplified methods to asymmetric structures, which require a 3D analysis, *e.g.* (Ayala and Tavera 2002), (Aydinoglu 2003), (Chopra and Goel 2004), (Fujii et al. 2004), (Yu et al. 2004) and (Zárate and Ayala 2004).

One of simplified nonlinear methods is the N2 method (Fajfar and Fischinger 1988, Fajfar and Gašperšič 1996, Fajfar 2000), which has been implemented in Eurocode 8 (Annex B of Part 1). In the N2 method, seismic demand is determined from inelastic spectra and depends on the period of the idealized equivalent SDOF system. The transformation from the MDOF to an equivalent SDOF system is based on the assumption of a time-invariant displacement shape. This assumption represents the major limitation of the applicability of the method. It works well in the case of planar structural models with small influence of higher modes. In the case of asymmetric building structures, represented by a 3D structural model, several modes may substantially contribute to the response and the torsional effects may not be properly taken into account by a straightforward extension of the N2 method to 3D models, used in some earlier publication by the authors (Fajfar 2002, Fajfar, Kilar et al. 2002, Fajfar, Magliulo et al. 2002, Kilar and Fajfar 2002). The results of recent parametric studies suggest that in the majority of cases an upper limit for torsional effects can be estimated by a linear dynamic (spectral) analysis (Peruš and Fajfar 2005, Marušić and Fajfar 2005). Based on this observation, it has been proposed that the results obtained by pushover analysis of a 3D structural model be combined with the results of a linear dynamic (spectral) analysis (Fajfar et al. 2005). The former results control the target displacements and the distribution of deformations along the height of the building, whereas the latter results define the torsional amplifications. The same or a similar approach for the estimation of torsional effects can be applied to other pushover-based methods.

A combination of linear dynamic and pushover analyses has also been used by Tso and Moghadam (1997) and Moghadam and Tso (2000). However, in their method the target displacements for different substructures (*e.g.* planar frames or walls) are determined by the 3D elastic dynamic analysis of the model representing the whole structure. 2D pushover analyses of most critical substructures are then performed.

In the paper, the proposed extended N2 method is summarized and applied to a test example of an asymmetric three-storey reinforced concrete frame building (»SPEAR« building, pseudo-dynamically tested in full-scale in ELSA). The results are compared with results of nonlinear dynamic time-history analyses.

Description of the N2 method

In this chapter, the steps of the simple version of the N2 method, extended to asymmetric structures, are described. A simple version of the spectrum for the reduction factor is applied. It should be noted, however, that the suggested procedures used in particular steps of the method can be easily replaced by other available procedures. Additional information on the N2 method can be found in (Fajfar 2000, planar version) and (Fajfar 2002, extended version).

Step 1: Data

A 3-D model of the building structure is used. The floor diaphragms are assumed to be rigid in the horizontal plane. The number of degrees of freedom is three times the number of storeys N. The degrees of freedom are grouped in three sub-vectors, representing displacements at the storey levels in the horizontal directions x and y, and torsional rotations $\mathbf{U}^T = [\mathbf{U}_x{}^T, \mathbf{U}_y{}^T, \mathbf{U}_z{}^T]$.

In addition to the data needed for the usual elastic analysis, the non-linear force - deformation relationships for structural elements under monotonic loading are also required. The most common element model is the beam element with concentrated plasticity at both ends. A bilinear or trilinear moment - rotation relationship is usually used.

Seismic demand is traditionally defined in the form of an elastic (pseudo)-acceleration spectrum S_{ae} ("pseudo" will be omitted in the following text), in which spectral accelerations are given as a function of the natural period of the structure T. In principle, any spectrum can be used. However, the most convenient is a spectrum of the Newmark-Hall type. The specified damping coefficient is taken into account in the spectrum.

Step 2: Seismic Demand in AD Format

Starting from the usual acceleration spectrum (acceleration versus period), inelastic spectra in acceleration – displacement (AD) format can be determined. For an elastic SDOF system, the following relation applies

$$S_{de} = \frac{T^2}{4\pi^2} S_{ae} \tag{1}$$

where S_{ae} and S_{de} are the values in the elastic acceleration and displacement spectrum, respectively, corresponding to the period T and a fixed viscous damping ratio.

For an inelastic SDOF system with a bilinear force - deformation relationship, the acceleration spectrum (S_a) and the displacement spectrum (S_d) can be determined as

$$S_a = \frac{S_{ae}}{R_\mu} \tag{2}$$

$$S_d = \frac{\mu}{R_\mu} S_{de} = \frac{\mu}{R_\mu} \frac{T^2}{4\pi^2} S_{ae} = \mu \frac{T^2}{4\pi^2} S_a \tag{3}$$

where μ is the ductility factor defined as the ratio between the maximum displacement and the yield displacement, and R_μ is the reduction factor due to ductility, i.e., due to the hysteretic energy dissipation of ductile structures. Note that R_μ is not equivalent to the reduction factor R used in seismic codes. The code reduction factor R, which is in Eurocode 8 called behaviour factor q, takes into account both energy dissipation and the so-called overstrength R_s. It can be defined as $R = R_\mu R_s$.

Several proposals have been made for the reduction factor R_μ. In the simple version of the N2 method, we will make use of a bilinear spectrum for the reduction factor R_μ

$$R_\mu = (\mu - 1)\frac{T}{T_C} + 1 \qquad T < T_C \tag{4}$$

$$R_\mu = \mu \qquad T \geq T_C \tag{5}$$

where T_C is the characteristic period of the ground motion. It is typically (e.g. in Eurocode 8) defined as the transition period where the constant acceleration segment of the response spectrum (the short-period range) passes to the constant velocity segment of the spectrum (the medium-period range). Eqs. 3 and 5 suggest that, in the medium- and long-period ranges, the equal displacement rule apply, i.e., the displacement of the inelastic system is equal to the displacement of the corresponding elastic system with the same period.

Starting from the elastic design spectrum, and using Eqs. 3 to 5, the demand spectra for the constant ductility factors μ in AD format can be obtained. They represent inelastic demand spectra. It should be noted that the construction of these spectra is in fact not needed in the computational procedure. They just help for the visualisation of the procedure.

Step 3: Pushover Analysis

Using a pushover analysis, a characteristic non-linear force - displacement relationship of the MDOF system can be determined. In principle, any force and displacement can be chosen. Usually, base shear and roof (top) displacement are used as representative of force and displacement, respectively. The selection of an appropriate lateral load distribution is an important step within the pushover analysis. A unique solution does not exist. Fortunately, the range of reasonable assumptions is usually relatively narrow and, within this range, different assumptions produce similar results. One practical possibility is to use two different displacement shapes (load patterns) and to envelope the results.

Lateral loads are applied in mass centres of different storeys. The vector of the lateral loads **P**, which generally consists of components in three directions (forces in the x and y direction and torsional moments) is determined as

$$\mathbf{P} = p\,\mathbf{\Psi} = p\,\mathbf{M}\,\mathbf{\Phi} \tag{6}$$

where **M** is the mass matrix. The magnitude of the lateral loads is controlled by *p*. The distribution of lateral loads $\mathbf{\Psi}$ is related to the assumed displacement shape $\mathbf{\Phi}$. (Note that the displacement shape $\mathbf{\Phi}$ is needed only for the transformation from the MDOF to the equivalent SDOF system in Step 4). Consequently, the assumed load and displacement shapes are not mutually independent as in the majority of other pushover analysis approaches. The procedure can start either by assuming displacement shape $\mathbf{\Phi}$ and determining lateral load distribution $\mathbf{\Psi}$ according to Eq. 6, or by assuming lateral load distribution $\mathbf{\Psi}$ and determining displacement shape $\mathbf{\Phi}$ from Eq. 6. Note that Eq. 6 does not present any restriction regarding the distribution of lateral loads.

Generally, $\mathbf{\Phi}$ can consist of non-zero components in three directions (two horizontal directions and of torsional rotation). In such a case (coupled displacement shape) lateral loads also consist of components in three directions. The procedure can be substantially simplified if lateral loads are applied in one direction only. This is a special case that requires that also the assumed displacement shape has non-zero components in one direction only, e.g.

$$\mathbf{\Phi}^{\mathrm{T}} = [\mathbf{\Phi}_{\mathrm{x}}^{\mathrm{T}}, \mathbf{0}^{\mathrm{T}}, \mathbf{0}^{\mathrm{T}}] \tag{7}$$

This special case is used in the proposed extended version of the N2 method. It should be noted, however, that even in this special case of uncoupled assumed displacement shape, the resulting displacements, determined by a pushover analysis of an asymmetric structure, will be coupled, i.e. they will have components in three directions.

From Eqs. 6 and 7 it follows that the lateral force in the x-direction at the *i*-th level is proportional to the component $\mathbf{\Phi}_{\mathrm{x,i}}$ of the assumed displacement shape $\mathbf{\Phi}_{\mathrm{x}}$, weighted by the storey mass m_i

$$P_{x,i} = p\,m_i\,\mathbf{\Phi}_{\mathrm{x,i}} \tag{8}$$

Such a relation has a physical background: if the assumed displacement shape was equal to the mode shape and constant during ground shaking, i.e. if the structural behaviour was elastic, then the distribution of lateral forces would be equal to the distribution of effective earthquake forces and Eq. 6 was “exact”. In inelastic range, the displacement shape changes with time and Eq. 6 represents an approximation. Nevertheless, by assuming related lateral forces and displacements according to Eq. 6, the transformation from the MDOF to the equivalent SDOF system and vice-versa (Steps 4 and 6) follows from simple mathematics not only in elastic but also in inelastic range. No additional approximations are required, as in the case of some other simplified procedures.

In the proposed method, lateral loading, determined according to Eqs. 6 and 7, is applied independently in two horizontal directions, in each direction with + and - sign.

Step 4: Equivalent SDOF Model and Capacity Curve

In the N2 method, seismic demand is determined by using response spectra. Inelastic behaviour is taken into account explicitly. Consequently, the structure should, in principle, be modelled as a SDOF system. Different procedures have been used to determine the characteristics of an equivalent SDOF system. One of them, used in the current version of the N2 method, is summarized below.

The starting point is the equation of motion of a 3D structural model (with 3N degrees of freedom) representing a multi-storey building (damping is not taken into account because it will be included in the spectrum)

$$\mathbf{M}\,\ddot{\mathbf{U}} + \mathbf{R} = -\mathbf{M}\,\mathbf{s}\;a \tag{9}$$

R is a vector representing internal forces, a is the ground acceleration as a function of time, and **s** is a vector defining the direction of ground motion. In the case of uni-directional ground motion, e.g. in the direction x, the vector **s** consists of one unit sub-vector and of two sub-vectors equal to 0.

$$\mathbf{s}^{\mathrm{T}} = [\mathbf{1}^{\mathrm{T}}, \mathbf{0}^{\mathrm{T}}, \mathbf{0}^{\mathrm{T}}\,] \tag{10}$$

In the N2 method, ground motion is applied independently in two horizontal directions. Consequently, two separate analyses have to be performed with two different **s** vectors (vector (10) and a similar vector that corresponds to the ground excitation in the y-direction). A derivation, presented in (Fajfar 2002) yields the following formulas.

The displacement and force of the equivalent SDOF system D^* and F^* are defined as

$$D^* = \frac{D_t}{\Gamma}\,, \qquad F^* = \frac{V}{\Gamma} \tag{11), (12}$$

where D_t is the top displacement of the MDOF system and

$$V = p\,\mathbf{\Phi}^T \mathbf{M}\,\mathbf{s} = pm^* \tag{13}$$

is the base shear of the MDOF model in the direction of ground motion. m^* is the equivalent mass of the SDOF system

$$m^* = \mathbf{\Phi}^T\,\mathbf{M}\,\mathbf{s} \tag{14}$$

The constant Γ controls the transformation from the MDOF to the SDOF model and vice- versa. It is defined as

$$\Gamma = \frac{\mathbf{\Phi}^T \mathbf{M}\, \mathbf{s}}{\mathbf{\Phi}^T \mathbf{M} \mathbf{\Phi}} = \frac{m^*}{L^*} \tag{15}$$

Note that m^* depends on the direction of ground motion. Consequently, Γ, D^*, and F^* also depend on the direction of ground motion. In the case of ground motion in one (x) direction (Eq. 10) and assuming a simple uncoupled displacement shape (Eq. 7), the following equations apply

$$m_x^* = \sum m_i \Phi_{x,i} \tag{16}$$

$$V_x = \sum p m_i \Phi_{x,i} = \sum P_{x,i} \tag{17}$$

$$\Gamma = \frac{\sum m_i \cdot \Phi_{x,i}}{\sum m_i \cdot \Phi_{x,i}^2} \tag{18}$$

Eq. 18 is the same equation as in the case of planar structures. Consequently, the transformation from the MDOF to the SDOF system and vice versa is exactly the same as in the case of a planar structure.

Γ is usually called the modal participation factor. Note that the assumed displacement shape **Φ** is normalized – the value at the top is equal to 1. Note also that any reasonable shape can be used for **Φ**. As a special case, the elastic first mode shape can be assumed.

The same constant Γ applies for the transformation of both displacements and forces (Eqs. 11 and 12). As a consequence, the force - displacement relationship determined for the MDOF system (the V - D_t diagram) applies also to the equivalent SDOF system (the F^* - D^* diagram), provided that both force and displacement are divided by Γ.

In order to determine a simplified (elastic - perfectly plastic) force – displacement relationship for the equivalent SDOF system, engineering judgement has to be used. In regulatory documents some guidelines may be given. In Annex B of Eurocode 8 (CEN 2004) the bilinear idealization is based on the equal energy principle. Note that the displacement demand depends on the equivalent stiffness which, in the case of the equal energy approach, depends on the target displacement. In principle, an iterative approach is needed, in which a target displacement is assumed, the bilinear idealization is made and the target displacement is determined. This value is then used then as the new approximation for target displacement. According to Eurocode 8, the displacement at the formation of plastic mechanism can be used as the initial approximation for target displacement. Iteration is allowed but not required.

The graphical procedure (visualization), used in the simple N2 method, requires that the post-yield stiffness is equal to zero. This is because the reduction factor R_μ is defined as the ratio of the required elastic strength to the yield strength. The influence of a moderate strain hardening is incorporated in the demand spectra. It should be emphasized that moderate strain hardening does not have a significant influence on displacement demand, and that the proposed spectra approximately apply for systems with zero or small strain-hardening.

The elastic period of the idealized bilinear system T^* can be determined as

$$T^* = 2\pi \sqrt{\frac{m^* D_y^*}{F_y^*}} \tag{19}$$

where F_y^* and D_y^* are the yield strength and displacement, respectively.

Note that, alternatively, first the bilinear idealization of the pushover curve can be made and then the transformation to the equivalent SDOF system can be made. The same equations apply.

Finally, the capacity diagram in AD format is obtained by dividing the forces in the force - deformation (F^* - D^*) diagram by the equivalent mass m^*

$$S_a = \frac{F^*}{m^*} \tag{20}$$

The procedure is applied for both horizontal directions, in each direction with + and - sign.

Step 5: Seismic Demand for the Equivalent SDOF System

The determination of the seismic demand for the equivalent SDOF system is illustrated in Fig. 1 (for medium- and long-period structures, for which the "equal displacement rule" applies; for short-period structures see e.g. (Fajfar 200)). Both the demand spectra and the capacity diagram have been plotted in the same graph. The intersection of the radial line corresponding to the elastic period T^* of the idealized bilinear system with the elastic demand spectrum defines the acceleration demand (strength), required for elastic behaviour S_{ae}, and the corresponding elastic displacement demand S_{de}. The yield acceleration S_{ay} represents both the acceleration demand and the capacity of the inelastic system. The reduction factor R_μ can be determined as the ratio between the accelerations corresponding to the elastic and inelastic systems

$$R_\mu = \frac{S_{ae}(T^*)}{S_{ay}} \tag{21}$$

Note that R_μ is not the same as the reduction (behaviour, response modification) factor R used in seismic codes. The code reduction factor R takes into account both energy dissipation and the so-called overstrength. The design acceleration S_{ad} is typically smaller than the yield acceleration S_{ay}.

If the elastic period T^* is larger than or equal to T_C, the inelastic displacement demand S_d is equal to the elastic displacement demand S_{de} (see Eqs. 3 and 5, and Fig. 1). From triangles in Fig. 1 it follows that the ductility demand, defined as $\mu = S_d / D_y^*$, is equal to R_μ

$$S_d = S_{de}(T^*) \qquad T^* \geq T_C \tag{22}$$

$$\mu = R_\mu \tag{23}$$

If the elastic period of the system is smaller than T_C, the ductility demand can be calculated from the rearranged Eq. 4

$$\mu = (R_\mu - 1)\frac{T_C}{T^*} + 1 \qquad\qquad T^* < T_C \tag{24}$$

The displacement demand can be determined either from the definition of ductility or from Eqs. 3 and 24 as

$$S_d = \mu D_y^* = \frac{S_{de}}{R_\mu}\left(1+\left(R_\mu - 1\right)\frac{T_C}{T^*}\right) \tag{25}$$

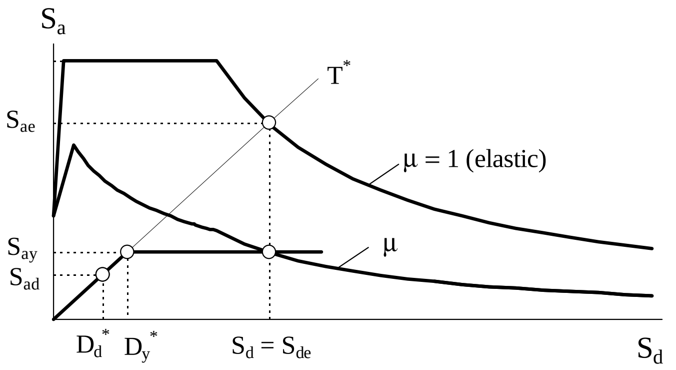

Figure 1. Elastic and inelastic demand spectra versus capacity curve

In both cases ($T^* < T_C$ and $T^* \geq T_C$) the inelastic demand in terms of accelerations and displacements corresponds to the intersection point of the capacity diagram with the demand spectrum corresponding to the ductility demand μ. At this point, the ductility factor determined from the capacity diagram and the ductility factor associated with the intersecting demand spectrum are equal.

All steps in the procedure can be performed numerically without using the graph. However, visualization of the procedure may help in better understanding the relations between the basic quantities. Two additional quantities are shown in Fig. 1. S_{ad} represents a typical design strength, i.e. strength required by codes for ductile structures, and D_d^* is the corresponding displacement obtained by linear analysis.

The procedure is applied in two horizontal directions, in each direction with + and - sign. Usually, the results obtained for both signs are similar. In such a case, the larger value of two values, obtained for + and – sign, can used as the target displacement (displacement demand at CM) in each horizontal direction. Alternatively, the complete analysis can be performed for both signs and the envelopes of all relevant quantities can be taken as the end result.

Step 6: Global Seismic Demand for the MDOF Model

The displacement demand for the SDOF model S_d is transformed into the maximum top displacement D_t of the MDOF system (target displacement) by using Eq. 11.

Step 7: Determination of Torsional Effects

Torsional effects are determined by a linear modal analysis of the 3D mathematical model, independently for excitation in two horizontal directions and combining the results according to the SRSS rule.

Step 8: Local Seismic Demand for the MDOF Model

Under monotonically increasing lateral loads with a fixed pattern (as in Step 3), the structure is pushed to D_t. It is assumed that the distribution of deformations throughout the height of the structure in the static (pushover) analysis approximately corresponds to that which would be obtained in the dynamic analyses. Separate 3D pushover analyses are performed in two horizontal directions.

The correction factors to be applied to the relevant results of pushover analyses are determined. The correction factor is defined as the ratio between the normalized roof displacements obtained by elastic modal analysis and by pushover analysis. The normalized roof displacement is the roof displacement at an arbitrary location divided by the roof displacement at the CM. If the normalized roof displacement obtained by elastic modal analysis is smaller than 1.0, the value 1.0 is used, i.e. no de-amplification due to torsion is taken into account. Correction factors are defined for each horizontal direction separately. Note that the correction factor depends on the location in the plan. All relevant quantities obtained by pushover analyses are multiplied with appropriate correction factors. For example, in a perimeter frame parallel to the X-axis, all quantities are multiplied with the correction factor determined with pushover results obtained for loading in the X-direction and for the location of this frame. The relevant quantities are, for example, deformations for the ductile elements, which are expected to yield, and the stresses for brittle elements, which are expected to remain in the elastic range.

Step 9: Performance Evaluation (Damage Analysis)

Expected performance can be assessed by comparing the seismic demands, determined in Step 8, with the capacities for the relevant performance level. The determination of seismic capacity is not discussed in this paper. Global performance can be visualized by comparing displacement capacity and demand.

Test example - SPEAR building

The test structure represents a typical older three-storey reinforced concrete frame building (Fig. 2a). The storey heights amount to 3.0 meters. The structure was experimentally and numerically investigated in the SPEAR project (www.strulab.civil.upatras.gr/spear/). In the analyses, presented in this paper, a model developed before the tests (the "final pre-test model", the details of the model will be presented elsewhere) was used. The CANNY program (Li 2002) was employed. The mathematical model consists of beam elements. Flexural behaviour of beams was modelled by one-component lumped plasticity elements, composed of elastic beam and two inelastic rotational hinges. Rotational hinges were defined with the tri-linear moment-rotation envelope, which includes pre-crack, post-crack and post-yield parts, and Takeda's hysteretic rules (Cross-peak trilinear model CP3) in time-history analysis. The plastic hinge was used for the major-axis bending only. For flexural behaviour of columns also a one-component lumped plasticity model was used, with two independent plastic hinges for bending about the two principal axes. The eccentricities between the mass centres and approximate stiffness centres amount to about 10 % and 14 % in the X- and Y-directions, respectively. The total mass of the structure amounts to 195 tons. The three fundamental periods of vibration of the building (considering some inelastic deformations - cracks due to gravity load), amount to 0.63 s, 0.58 s, and 0.45 s. The first mode is predominantly in the X-direction, the second predominantly in the Y-direction, whereas the third mode is predominantly torsional.

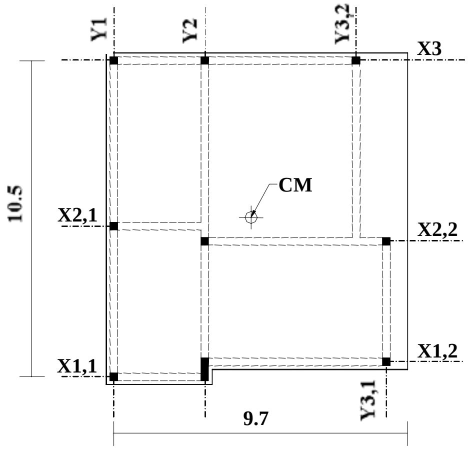

Figure 2a. Schematic plan of the SPEAR building.

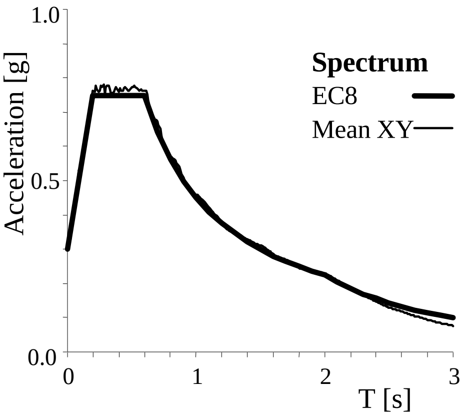

Figure 2b. Mean of the elastic spectra for 5% damping and the elastic spectrum according to EC8 Type 1 Soil C; a_g = 0.3 g.

In dynamic analyses, bi-directional semi-artificial ground motion records were used. The horizontal components of seven recorded ground motions were fitted to the EC8 elastic design spectrum (Type 1, soil C, Fig. 2b). The ground motions were scaled to peak ground acceleration $a_g = 0.3$. For each record 8 different combinations of directions and signs of components were applied. In modal analysis, which provides results needed for the determination of the torsional influences in the N2 method, the same EC8 spectra were applied in both horizontal directions. Five percent damping was used in all analyses. In time-history analysis Reyleigh damping (with instantaneous stiffness matrix) was applied. The P-Δ effect was not taken into account.

Analysis by the extended N2 Method

Pushover analyses were performed in two horizontal directions with lateral loads based on the fundamental mode shapes in the relevant direction, i.e. x-components of the first mode shape were used in X-direction, and y-components of the second mode shape were used in Y-direction. Loading was applied with + and – sign.

The results of pushover analyses are shown in Fig. 3. Iteration was used for determination of the bilinear idealization of pushover curves, as described in Step 4 of the procedure. (Note that in the test example the alternative with the idealization of the pushover curve for the MDOF system was used.) The idealized force – displacement relationships are plotted in Fig. 3.

The capacity curves and the elastic and inelastic demand spectra are shown in Fig. 4. In both horizontal directions, larger displacement demands apply to the loading with the + sign. For the equivalent SDOF system they amount to 12.8 and 11.1 cm in X- and Y- direction, respectively, whereas the corresponding top displacements of the MDOF system in CM amount to 15.8 and 14.2 cm. The displacement ductility demands (regarding the yield point of the idealized bilinear systems) amount to about 2.5 in both directions.

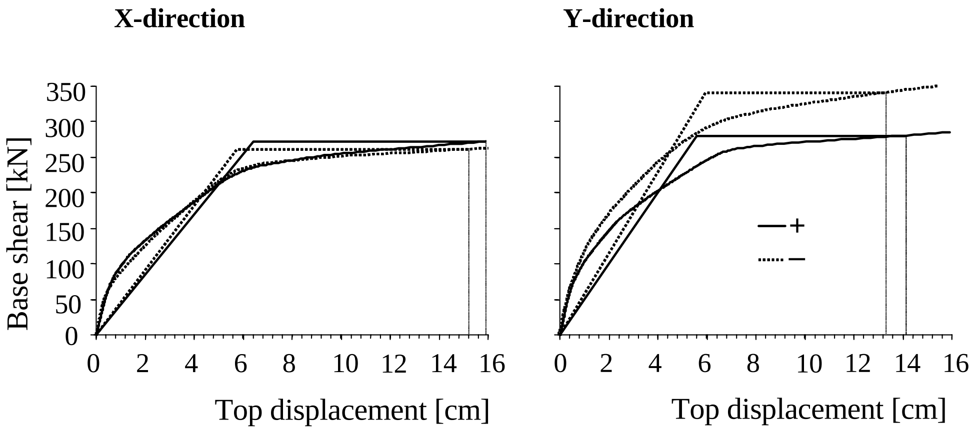

Figure 3. Pushover curves and bilinear idealizations for loading with + and - sign

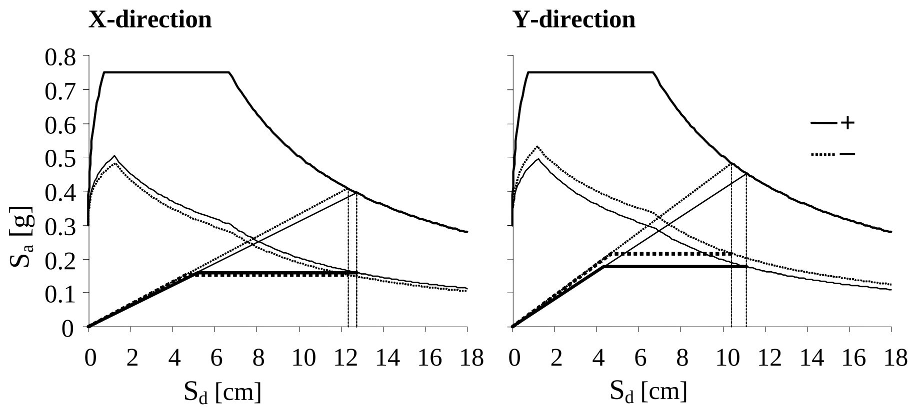

Figure 4. Elastic and inelastic demand spectra and capacity curves (for loading with + and – sign)

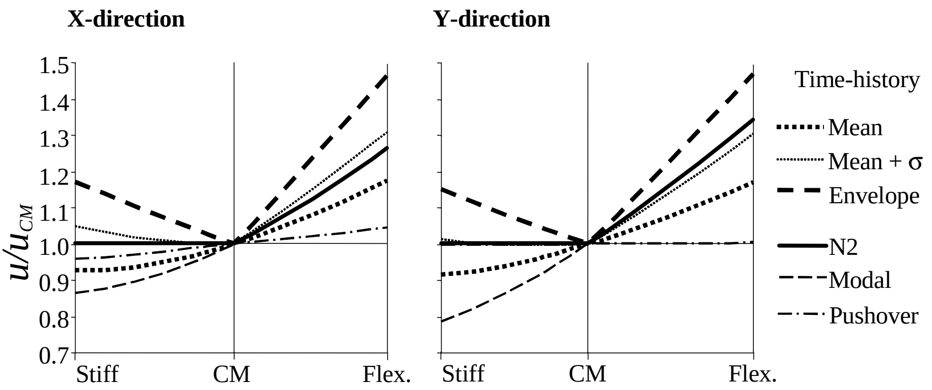

Figure 5. Torsional effects in terms of normalized top displacements obtained by the N2 method, by modal analysis, by time-history analysis (mean, mean + sigma values and envelope) and by pushover analysis

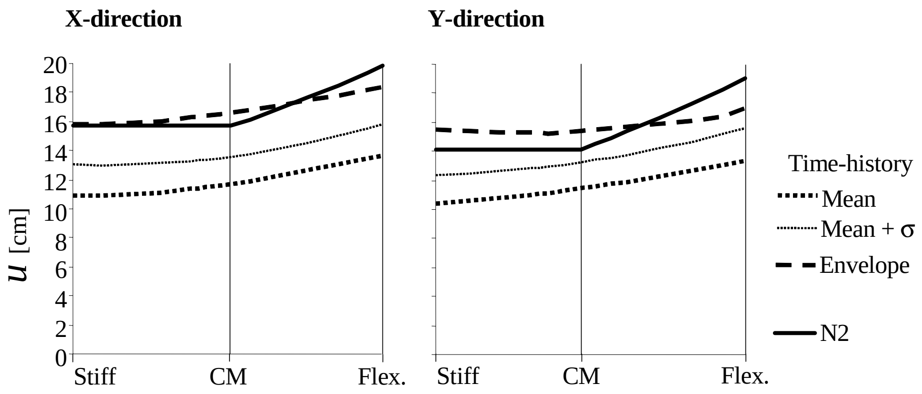

Figure 6. Displacement (in plane) at the top of the building obtained by N2 and time-history analyses

Torsional effects in terms of normalized roof displacements determined by the proposed extension of the N2 method are presented in Fig. 5. The N2 results are compared with the results of elastic modal (spectral) analysis, non-linear time-history analysis for a_g = 0.30 g, and pushover analysis.

The static analysis suggested that some cracks (non-linear deformations) occurred already due to gravity loads. This state was assumed as the initial ("elastic") state of the building, and the modes of vibration of the building in such a condition were taken into account for the modal analysis. Modal analysis was performed independently for the loading in both horizontal directions, using the CQC rule for the combination of different modes, which is considered appropriate for structures with closely spaced modes. The results of analyses for both directions were combined by the SRSS rule.

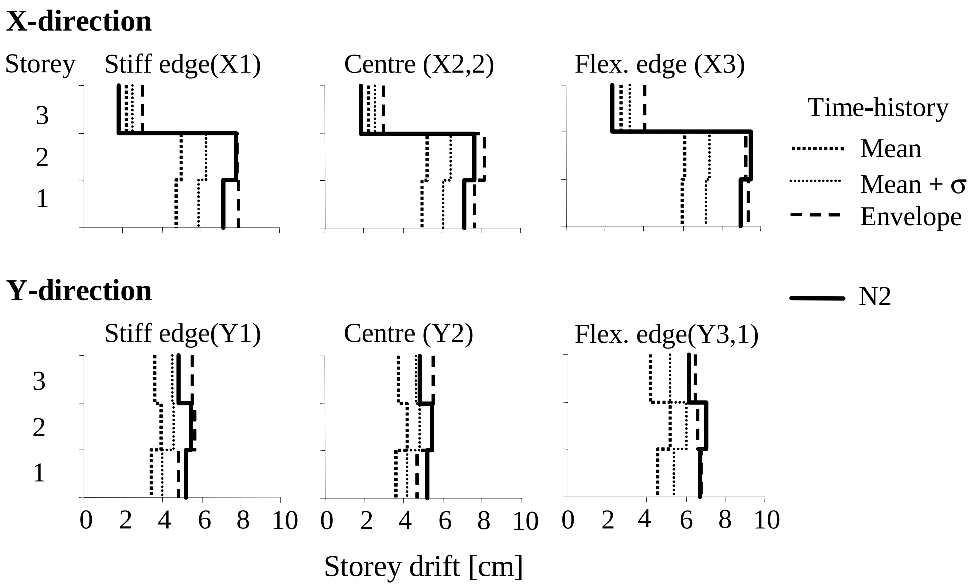

Figure 7. Storey drifts obtained by the N2 method and time-history analysis.

According to the proposed extension of the N2 method, the results of elastic modal analysis are used to determine the torsional effect, provided that amplification due to torsion occurs. Consequently, the N2 results coincide with the line obtained by elastic modal analysis on the stiff side. No de-amplification due to torsion is allowed in the N2 method. So a constant value of 1.0 applies on the stiff side of the building. If compared with the mean results of nonlinear time-history analyses, the proposed N2 approach is conservative. The N2 results are close to mean+σ values. However, it should be noted that the torsional effects are in general higher if the ground motion intensity is lower (see Fajfar et al 2005). Moreover, some particular ground motions can produce very high torsional influences, as demonstrated by the envelope of results.

A pushover analysis with forces applied in the centre of masses at each floor at the same target displacement yields very small torsional rotations. According to the proposed extension of the N2 method, the results of pushover analysis are corrected by multiplying them by the ratio between the N2 normalized displacements and normalized displacements obtained by pushover analyses. The correction factors amount to 1.29, 1.22, 1.21 for columns and beams in the frames Y3,1, Y3,2, and X3, respectively. For other frames the factors are small (from 1.00 to 1.05).

Absolute values of roof displacements are plotted in Fig. 6. The N2 displacements in CM are 34 % and 23 % larger than the mean values obtained by time-history analysis and are larger than the mean +σ. Note, however, that the standard deviation of the sample of accelerograms is very small because all accelerograms are fitted to the same spectrum. In the case of recorded accelerograms, the coefficient of variation for displacements usually amounts to about 0.3. On the other hand, the idealization of the pushover curve according to EC8 is conservative, i.e. leading to a low effective stiffness and high effective period.

Storey drifts in different frames are shown in Fig. 7. The distribution of drifts along the height of the building obtained by the N2 method is comparable with the distribution obtained by nonlinear dynamic analysis. The N2 drift estimates are conservative with the exception of the top storey in X-direction.

The seismic assessment of the structure, which is made by comparing demand with capacity, is not discussed in this paper.

Conclusions

Structural response to strong earthquake ground motion cannot be accurately predicted due to large uncertainties and the randomness of structural properties and ground motion parameters. Consequently, excessive sophistication in structural analysis is not warranted. The N2 method, like some other simplified non-linear methods, provides a tool for a rational yet practical evaluation procedure for building structures for multiple performance objectives. The formulation of the method in the acceleration – displacement format enables the visual interpretation of the procedure and of the relations between the basic quantities controlling the seismic response. This feature is attractive to designers. Of course, the N2 method is, like any approximate method, subject to several limitations (see, e.g. Fajfar 2000).

In this paper, the extended N2 method, which can be used for analysis of plan-asymmetric building structures, has been summarized and applied to a test example. The transformation of the MDOF to the equivalent SDOF system can be performed by the same equation as in the case of planar systems. The consideration of the torsional effects is based on two observations:

The torsional amplification of displacements determined by elastic dynamic analysis can be used as a rough, mostly conservative estimate also in the inelastic range. Any favourable torsional effect on the stiff side, *i.e.* any reduction of displacements compared to the counterpart symmetric building, which may arise from elastic analysis, will probably decrease or may even disappear in the inelastic range.

The results obtained by the proposed procedure are influenced both by nonlinear static (pushover) and elastic dynamic analysis. Displacement demand (amplitude and the distribution along the height) at the mass centres is determined by the usual N2 method, which is based on pushover analysis. The amplification of demand due to torsion is determined by elastic dynamic analysis, while reduction of demand due to torsion is not taken into account. Such an approach yields in most cases a conservative estimate of torsional influences. Note, however, that inelastic torsion is characterized by large inherent randomness and uncertainty.

In the case of the test structure analyzed in this paper, a comparison with results of dynamic analyses suggests that the N2 results are conservative. The conservatism originates both from the determination of the target displacement at the mass centre and from the determination of torsional effects. Note that the accuracy of the estimated target displacement depends considerably on the bilinear idealization of the pushover curve, which controls the initial period of the idealized equivalent SDOF system.

References

Ayala, A. G., and E. A. Tavera (2002). A new approach for the evaluation of the seismic performance of asymmetric buildings, *Proc., 7th Nat. Conf. on Earthquake Engineering*, EERI, Boston.

Aydinoglu, M. N. (2003). An incremental response spectrum analysis procedure based on inelastic spectral displacements for multi-mode seismic performance evaluation, *Bulletin of Earthquake Engineering*, 1(1), 3-36.

CEN (2004). Eurocode 8 – Design of structures for earthquake resistance, Part 1, European standard EN 1998-1, Brussels: European Committee for Standardization, December 2004.

Chopra, A. K., and R. K. Goel (2004). A modal pushover analysis procedure to estimate seismic demands for unsymmetric-plan buildings, *Earthquake Engineering and Structural Dynamics*, 33(8), 903-927.

Fajfar, P., and M. Fischinger (1988). N2 – A method for non-linear seismic analysis of regular buildings, *Proc., 9th World Conference on Earthquake Engineering*, Tokyo, Kyoto, Vol.5, 111-116.

Fajfar, P., and P. Gašperšič (1996). The N2 method for the seismic damage analysis of RC buildings, *Earthquake Engineering and Structural Dynamics*, 25, 23-67.

Fajfar, P. (2000). A nonlinear analysis method for performance-based seismic design, *Earthquake Spectra*, 16(3), 573-592.

Fajfar, P. (2002). Structural analysis in earthquake engineering - a breakthrough of simplified non-linear methods, *Proc., 12th European Conference on Earthquake Engineering*, London, UK, Keynote lecture.

Fajfar, P., V. Kilar, D. Marušić, I. Peruš, and G. Magliulo (2002). The extension of the N2 method to asymmetric buildings, *Proc., 4th forum on Implications of recent earthquakes on seismic risk*. Technical report TIT/EERG, 02/1, Tokyo Institute of Technology, Tokyo, 291-308.

Fajfar, P., G. Magliulo, D. Marušić, and I. Peruš (2002). Simplified non-linear analysis of asymmetric buildings, *Proc., 3rd European workshop on the seismic behaviour of irregular and complex structures*, De Stefano, M. and Rutenberg, A. (eds.), Florence, Italy.

Fajfar, P., D. Marušić, and I. Peruš (2005). Torsional effects in the pushover-based seismic analysis of buildings, *J. Earthquake Engr.*, in print.

Fujii, K., Y. Nakano, and Y. Sanada (2004). Simplified nonlinear analysis procedure for asymmetric buildings, *Proc., 13th World Conference on Earthquake Engineering*, Vancouver, Canada, Paper No. 149.

Kilar, V., and P. Fajfar (2002), Seismic analysis of eccentric R/C buildings by the N2 method, *Proc., 3rd European workshop on the seismic behaviour of irregular and complex structures*, De Stefano, M. and Rutenberg, A. (eds.), Florence, Italy.

Li, K. N. (2002). *3-dimensional nonlinear static and dynamic structural analysis computer program CANNY 99*, CANNY Consultants Pte Ltd., Singapore.

Marušić, D., and P. Fajfar (2005). On the inelastic seismic response of asymmetric buildings under bi-axial excitation, *Earthquake Engineering and Structural Dynamics*, 34(8), 943-963.

Moghadam, A. S., and W. K. Tso (2000). 3-D pushover analysis for damage assessment of buildings, *Journal of Seismology and Earthquake Engineering* (Tehran), 2(3), 23-31.

Peruš, I., and P. Fajfar (2005). On the inelastic torsional response of single-storey structures under bi-axial excitation, *Earthquake Engineering and Structural Dynamics*, 34(8), 931-941.

Tso, W. K., and A. S. Moghadam (1997). Seismic response of asymmetrical buildings using pushover analysis, *Proc., International Workshop on Seismic Design Methodologies for the Next Generation of Codes*, Fajfar, P. and Krawinkler, H. (eds.), Bled, Slovenia, A.A. Balkema, Roterdam, Brookfield, 311-321.

Yu, Q. S. K., R. Pugliesi, M. Allen, and C. Bischoff (2004). Assessment of modal pushover analysis procedure and its application to seismic evaluation of existing building, *Proc., 13th World Conference on Earthquake Engineering*, Vancouver, Canada, Paper No. 1104.

Zárate, A., and A. G. Ayala (2004). Validation of single storey models for the evaluation of seismic performance of multi-storey asymmetric buildings, *Proc.,13th World Conference on Earthquake Engineering*, Vancouver, Canada, Paper No. 2213.

Professor Jorge Gutiérrez

Director, National Laboratory for Materials and Structural Models *LANAMME*, School of Civil Engineering, University of Costa Rica, San José, Costa Rica.
Chairman, Costa Rican Seismic Code Committee
P.O.Box 321-2010, San José, Costa Rica
jorgeg@lanamme.ucr.ac.cr
Earthquake resistant design of buildings, structural dynamics, structural adequacy of historical and vernacular buildings

The name of Luis Esteva has been a personal referent since the time when, as a student, I learned about the Esteva and Rosenblueth equation for estimating EQ's peak ground accelerations. Later on, as a young professor, I had the privilege of meeting him in several of the Latin American Seminars on EQ Engineering that a group of colleagues, with more enthusiasm than financial resources, organized in different countries since the late 70's. From our very first meeting he impressed me with his warm and friendly personality. Very soon I came to appreciate his vast culture and enormous wealth of knowledge, permanently available for everyone. When it was the time to organize the Seminar in Costa Rica, we invited him to deliver the inaugural lecture. He delighted us with a profound dissertation on the intricacies of seismic design that is still remembered as a masterpiece by all the privileged attendants.

In 1997, Luis and Haresh Shah were in Costa Rica, offering their advice on a seismic hazard study for the earthquake prone Nicoya Peninsula. At that time, the Costa Rican Seismic Code Committee was facing the challenge of drafting a new Code. We wanted it to belong to "the next generation of codes", including Performance Based Engineering *PBE* considerations. We invited them to a meeting and, for several hours, we interchanged ideas and received their generous advice. Our efforts culminated with the publication of the Costa Rican Seismic Code-2002, where *PBE* considerations were included in a rational and practical way. For that reason, I selected the subject for this important occasion, when Luis's friends and colleagues offer a well deserved tribute to a life full of generous contributions and meaningful achievements.

We all recognize Luis Esteva as a multitalented human being. What I personally admire the most is his remarkable talent to conceal his huge talent.

Jorge Gutiérrez
August 28, 2005

PERFORMANCE-BASED ENGINEERING IN THE COSTA RICAN SEISMIC CODE

ABSTRACT

In earthquake prone regions of the world, Performance-Based Engineering *PBE* aims at the important and rational goal of managing seismic risk to minimize social disruption and economic loss. As a result, there is a very strong commitment among the academic and professional engineering communities to develop a new generation of Seismic Codes where *PBE* will be explicitly accounted for. However, this ambitious task will not be easily achieved as most traditional Codes have evolved from empirical formulations where the nonlinear inelastic response of the structure is accounted for by simple but conceptually weak Reduction Factors *R* applied to an elastic design spectrum.

In contrast, the Costa Rican Seismic Code *CRSC* has implicitly considered constant ductilitiy inelastic design spectra since it was first published in 1974. The latest version, *CRSC-2002* (CFIA 2003), introduces a conceptual framework for *PBE* and explicitly considers the structural ductility in the inelastic design spectra, allowing for a Capacity Spectrum Method *CSM* that has clear conceptual and practical advantages over the methods being considered in the USA (ATC 1996; SEAOC 1999; ASCE 2000). This paper discusses the *PBE* philosophy of the *CRSC-2002* and describes the Capacity Spectrum Method *CSM*, a non linear alternative for the structural analysis that allows the evaluation of the response parameters required for the assessment of the building performance. The Displacement-Based Plastic Design *DBPD* method, an effective and rational procedure for EQ resistant design of buildings in complete agreement with the *PBE* conceptual framework of the *CRSC-2002*, is also presented.

Introduction

Performance-Based Engineering, *PBE,* may be defined as *the integrated effort to design, construction and maintenance needed to produce engineered facilities of predictable performance for multiple performance objectives* (Fajfar and Krawinkler 1997). In earthquake prone regions and countries, it aims at the ambitious and rational goal of managing seismic risk to minimize social disruption and economic loss by allowing well informed decisions for the selection of Performance Objectives *PO* comprehensively defined for different classes of built structures according to their social and economic importance. For *PBE* to be implemented (SEAOC 1995), the national and regional Seismic Codes and engineering standards of most countries and regions must undergo radical changes, as most of them are essentially concerned with the prevention of the catastrophic collapse of buildings and the subsequent large death toll due to severe earthquakes. Furthermore, due to historic reasons, Seismic Codes were not initially concerned with the inelastic response of the structures, limiting their considerations to the definition of lateral forces accounting for the seismic effects, to be combined with gravity loads in an structural design based on allowable stresses. As earthquake ground motions were measured and dynamic methods developed to evaluate the structural response, Reduction Factors *R* had to be introduced to match the empirically defined lateral forces representing the earthquake effects upon the structure with the much larger theoretical values resulting from elastic analyses. Eventually, codes explicitly recognized structural ductility and overstrength as the main reasons for the *R* factors. However, as design seismic coefficients, obtained from elastic spectra and reduced by *R* factors, do not correspond to actual constant ductility inelastic spectra, the capacity to estimate the inelastic deformations of the structural elements and components, which is essential to *PBE,* is severely limited. These limitations are readily apparent when trying to implement conceptually sound procedures for *PBE* considerations, as evidenced in a vast majority of seismic codes.

In contrast, since the first Costa Rican Seismic Code *CRSC* was drafted in 1973, it included explicit considerations for ductility, inelastic deformations and displacements, ultimate strength and capacity design concepts. Therefore, the *CRSC-2002*, the latest version of the Code (CFIA 2003) incorporates *PBE* concepts and considerations in a rational, practical and conceptually simple way. This paper comments those considerations and presents them in the following sections: a) Performance Objectives; b) Definition of earthquake ground motion demands; c) Procedures for estimation of parameters for structural response and related damage limits and d) The Displacement-Based Plastic Design method as a design alternative for *PBE*.

Performance Objectives

The *CRSC-2002* classifies buildings according to their importance and hazard level in five categories: A.- Essential; B.- Hazardous: C.- Special: D.- Normal and E.- Miscellaneous. A single Performance Objective is assigned to each category, defined in terms of a ground intensity level and its corresponding building performance. Three ground shaking intensity levels are defined: moderate, severe and extreme. Severe ground shaking corresponds to a Return Period *RP* of 500 years, whereas moderate and extreme ground shaking are respectively defined as having 0.75 and 1.5 times the intensity levels corresponding to severe ground shaking. These three levels are accounted by means of an importance factor *I*, with values of 0.75, 1.0 and 1.5, that directly affects the Seismic Coefficient *C*, as it will be commented in the next section. Regarding building performance, two levels are defined: Immediate Occupancy *IO* and Life Safety *LS*. When the simpler methods of linear elastic analysis are used, the basic parameter related with these building performances is the inter-story drift; for the alternative non-linear methods of analysis, more refined procedures for the verification of building performance, like the inelastic internal deformations of the structural elements or components, may be used. The Code Performance Objectives are summarized in Table 1.

The decision to consider only one Performance Objective for each Category of Importance and Hazard Level may be considered as rather limited. Nevertheless, it recognizes the present lack of experimental data required for reliable evaluations of building performances. For the time being, the main objective was to introduce the *concept* of building performance in the Code; the shift to multiple Performance

Objectives, as well as the development of more refined methods to evaluate building responses in terms of precise engineering parameters and their related building performance, should be accomplished in a future revision of the Code.

TABLE 1. Building Performance Objectives according to Categories of Importance and Hazard Level in the *CRSC-2002*

		Immediate Occupancy *(IO)*	**Life Safety *(LS)***
Ground Intensity Levels	Extreme (I = 1.5)	A (Essential)	B (Hazardous)
	Severe (I = 1.0)	C (Special)	D (Normal)
	Moderate (I = .75)		E (Miscellaneous)

Earthquake Ground Motion Demand

As mentioned, one of the main advantages of the *CRSC* for *PBE* considerations is the use of Seismic Coefficients C obtained from design spectra that explicitly consider the structural ductility instead of using the Reduction Factors R common in USA codes. Indeed, the Seismic Coefficient is defined as:

$$C = a_{ef}\ I\ FED\ /\ SR \tag{1}$$

where a_{ef} is the design effective peak acceleration; I is the already commented Importance Factor. *FED* (for Spectral Dynamic Factor is Spanish) is an envelope function that depends on the seismic zone, the ground site, the global structural ductility and the structural period. *SR* (for Overstrength in Spanish) represents the ratio of actual to nominal structural strengths. Each term requires further specific comments.

The design effective peak acceleration corresponds to a 500 year *RP*; that is, to severe ground shaking, as commented in the previous section. Values for specific ground sites and seismic zones are as follows:

TABLE 2. Design effective peak accelerations a_{ef} for severe ground shaking (*RP*= 500 years)

Ground site (*)	**Seismic Zone II**	**Seismic Zone III**	**Seismic Zone IV**
S_1	0.20	0.30	0.40
S_2	0.24	0.33	0.40
S_3	0.28	0.36	0.44
S_4	0.34	0.36	0.36

* S_1 = Rock; S_2 = Firm soil; S_3 = Medium dense soil; S_4 = Soft soil.

Table 2 was adopted from SEAOC's Blue Book (SEAOC 1999) with minor modifications. The three seismic zones for the country (zones II, III and IV, corresponding to a_{ef} rock values of 0.20, 0.30 and 0.40 of g respectively) are presented in the seismic zoning map of Fig. 1 and were derived from the country's most recent seismic hazard study (Laporte et al. 1994). As mentioned in the previous section, the Importance Factor *I* is used to scale up or down those peak accelerations for extreme and moderate ground shaking intensity levels, respectively.

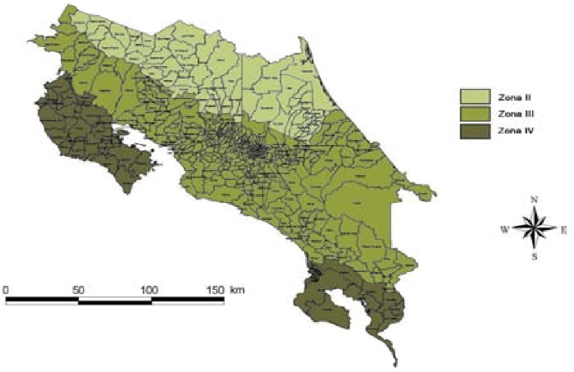

Figure 1. Seismic zones in the Costa Rican Seismic Code – 2002 (After CFIA 2003)

The *FED* envelope functions are normalized constant ductility design spectra. As seismic zones and ground sites affect the ratios between maximum ground accelerations, velocities and displacements, the resulting elastic design spectra (evaluated in all cases for a 5% of critical damping) will be different for each one of the twelve combinations of Table 2, leading to twelve different figures. In addition to the elastic spectrum, each figure contains constant ductility spectra for five different structural ductility values (1.5, 2, 3, 4 and 6) obtained with well known procedures (Newmark and Hall 1987; Newmark and Riddell 1980). For illustrative purposes, two of these figures are presented next; note that for short periods both converge to 1.0 as they are normalized spectra.

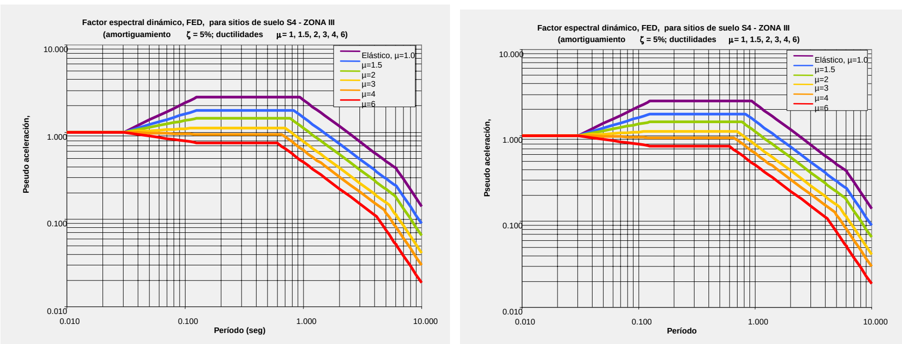

Figure 2. CRSC-2002 constant ductility FED functions for Seismic Zone III and Ground Sites S_1- Rock (left) and S_4- Soft Soil (right) (After CFIA 2003)

The ductility in the *FED* figures is called assigned global (i.e. structural, not local) ductility and it represents a value likely to be developed by a particular structure. Its numerical value is assigned from several considerations: the structural type (i.e. moment resisting frames, dual, wall or cantilevered-column structural systems), the vertical and plan structural regularity conditions and the local ductility of the structural elements and components, as defined from their structural materials and detailing. Values range from 6.0 for regular (vertical and plan) steel or concrete moment resisting frames with their elements and components detailed for optimum local ductility to 1.0 for cantilevered column systems with moderate local ductility or structural irregularities.

The last factor affecting the Seismic Coefficient *C* is the Overstrength *SR* which, following Paulay (Fajfar and Paulay 1997), the code defines as "*the ratio of the maximum probable strength developed within a structure to an adopted reference* (i.e. nominal) *strength*". It is obvious that, in order to compare actual ground shaking demands with maximum probable strengths, this factor should not divide the Seismic Coefficient but multiply the nominal structural strength; however, as both alternatives lead to identical results, *SR* was left in the demand side of the equation. The main reason was "political" as the design effective peak accelerations a_{ef} had been significantly increased from the values of the previous Code, which did not consider Overstrength explicitly. The *CRSC-2002* defines only two values of *SR*. A value of 2.0 is defined for moment resisting frames, dual and wall systems whose seismic ground shaking effects are defined in terms of lateral forces and linear elastic analysis; on the other hand, a value of 1.2 is defined for cantilevered-column systems or for any structural system analyzed with non linear methods of analyses, where the ultimate inelastic strengths of the structure are calculated.

The use of Seismic Coefficients *C* that are derived from the actual inelastic response spectra of a particular structural model, allows for the design of other particular structural models as long as proper response spectra are derived for them. For instance, in frame or shear wall buildings built with prefabricated concrete elements joined with debonded prestressed tendons, it is possible to reach considerable interstory drifts with practically no structural damage (Priestley and Tao 1993). However, the behavior of these structural systems is closer to a non linear-elastic model rather than the usual elasto-plastic model. Non linear-elastic models do not have hysteretic energy dissipation and therefore tend to produce larger displacements and deformations than elasto-plastic models. To apply the *CRSC-2002* in the design of this promising type of prefabricated buildings, response spectra have been derived for non linear-elastic models (Hernández 2003, Hernández and Gutiérrez 2005). The results, presented in the form of incremental functions for the Seismic Coefficients *C* of the *CRSC-2002*, have already been used in Costa Rica for the design of this promising type of prefabricated concrete buildings.

Most important, Seismic Coefficients *C* that are indeed constant ductility design spectra derived from response spectra of specific structural models, give a tremendous advantage to the *CRSC-2002* for *PBE* as they avoid the need for the conceptually weak methodology of using an elastic spectrum with an increased viscous damping to account for the nonlinear behavior, that have been the trademark of most USA proposals (ATC 1996, ASCE 2000). Besides being conceptually weak, this methodology leads to wrong results (Chopra and Goel 2000 and 2001b). This important advantage will become apparent in the following section.

Structural Response and Related Performance

Once the earthquake ground motion demand has been defined, *PBE* requires the evaluation of the structural response, which should be able to describe the building performance in terms of such parameters as absolute and relative structural displacements, internal deformations and cumulative damage of the structural members and components, absolute accelerations, as well as its effects on architectonic and other non structural systems and components. These parameters must be calculated by means of reliable analytical models of the building and the input ground motions. They should be complete enough to allow for a quantification of damage, providing the design engineer with a reliable estimation of the building performance, which in turn should lead to well informed risk managing decisions by engineer officials or decision makers.

The problem with the above procedure is that, as mentioned, most current seismic codes (IAEE 1996 and 2000; ICC 2003) use force-based design procedures with linear elastic analyses for lateral forces derived from an elastic design spectrum reduced by a force reduction factor to account for inelastic behavior. Even if in the definition of the seismic lateral forces these codes accept that buildings will deform beyond their linear elastic limits -inelastic response- the linear elastic model is quite limited and the calculated parameters, basically internal forces and a crude estimation of inelastic displacements and interstory drifts, do not allow for a precise estimation of the building performance. The next subsections will discuss the four analytical methods contained in the *CRSC-2002*, classified into the general categories of linear and non-linear methods.

Linear Methods of Analysis

The *CRSC-2002* maintains the so called Static and Dynamic Methods of analysis included in previous *CRSC* as well as in most codes around the world. Essentially the Dynamic Method corresponds to a linear elastic modal superposition method, whereas the Static Method considers only a linear first mode approximation with the fundamental period obtained from Rayleigh's Method once the elastic displacements have been obtained. Due to these rather crude approximations, this method is limited to regular buildings having heights of five stories or less.

The linear elastic Dynamic Method uses mode superposition with as many modes as necessary to capture the most relevant features of the elastic response but its main conceptual weakness is the use of inelastic design spectra, reduced by ductility considerations, either implicit or explicit. In addition, for these elastic methods, the overstrength factor *SR*, that reduces the Seismic Coefficient *C* and the corresponding lateral forces representing the earthquake ground motions, is taken as 2.0 recognizing the presence of an important reserve strength, mostly due to the plastic hinge formation process and the resulting inelastic redistribution of forces characteristic of ductile structures.

It is clear that, due to ductility and overstrength considerations, the structural displacements obtained from the elastic analysis should be much smaller than the inelastic displacements likely to develop in the structure, which are the real indicators of the building performance. To correct this situation the *CRSC-2002* estimates the inelastic interstory drifts multiplying the values obtained from the elastic analysis by the assumed structural ductility and the overstrength:

$$\Delta^{(i)} = \mu \, SR \, \Delta^{(e)} \tag{2}$$

where $\Delta^{(i)}$ and $\Delta^{(e)}$ are respectively the inelastic and elastic interstory drifts; μ is the assigned structural ductility used for the calculation of the Seismic Coefficient C and SR is the structural overstrength. Obviously, the maximum probable base shear strength is the elastic design base shear –nominal strength– multiplied by the overstrength SR. These results are represented in the following figure, which also contains a curve representing the actual maximum probable strength and inelastic interstory drifts that these approximations are trying to match:

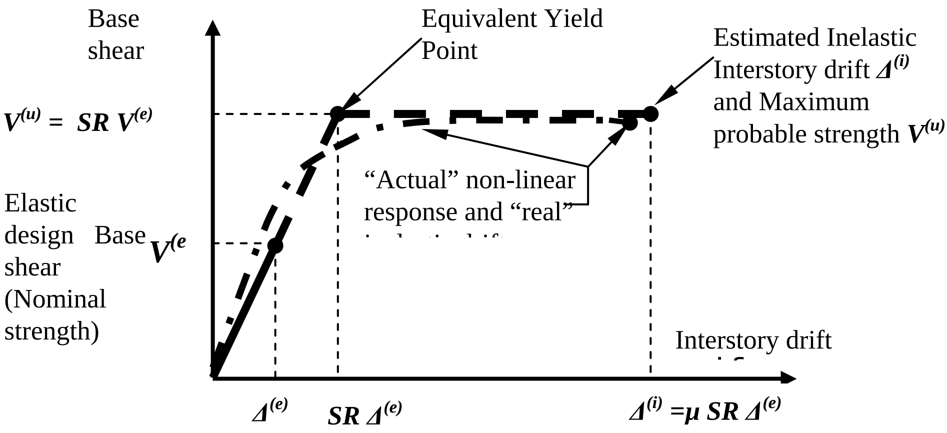

Figure 3. Estimation of inelastic interstory drifts and maximum probable structural base shear strength from the linear elastic Static or Dynamic Methods of CRSC-2002

Surprisingly, at least for regular buildings, these rather crude approximations do produce reasonably good results for inelastic interstory drifts when compared with the more refined non-linear Capacity Spectrum Method *CSM* that will be presented in the next subsection (Bravo 2002; Ramirez 2002). However, the Static and Dynamic Methods of the *CRSC-2002*, or any of the similar linear elastic methods presented in Seismic Codes, provide only an approximated estimation of the structure inelastic interstory drifts, but do not provide the designer with any information about the most important parameters that are essential for a proper evaluation of the building performance, particularly internal deformations and cumulative damage of the structural members. To evaluate these parameters, non-linear methods of analysis turn out to be essential.

Non-linear Methods of Analysis

For a non-linear analysis capable to provide all the significant structural parameters required for *PBE*, the first obvious option is a Response History Analysis *RHA*, involving a time step solution of the multi-degree-of-freedom equations of motion that represent the multistory building (Chopra 2001). Although very sophisticated, this analysis is cumbersome and time consuming. Furthermore, as the direct use of the design spectra is not possible, multiple analyses for a family of accelerograms statistically related to the design spectra are required, followed by a statistical analysis of all their responses. Nevertheless, the *CRSC-2002* includes *RHA* as an optional method of analysis.

As an intermediate alternative between the simple but incomplete linear elastic Static and Dynamic Methods and the cumbersome *RHA*, the Capacity Spectrum Method *CSM* has been proposed (Freeman 1998; ATC 1996; ASCE 2000). This is a non-linear static method that performs a pushover analysis to determine the capacity curve, representing the lateral base force versus a representative lateral displacement, usually at the roof. For each significant point in the capacity curve, the state of absolute and relative displacements and internal deformations, as well as their corresponding external and internal forces, are determined for the entire structure. The earthquake ground motion demand is expressed in terms of the design spectra, represented on a S_a-S_d plot with pseudo-acceleration S_a on the vertical axis, and inelastic displacement S_d on the horizontal. The capacity curve is then expressed in the same S_a-S_d plot by simple scale factors determined from well known principles of structural dynamics (Chopra 2001) and the Performance Point *PP* is calculated. This point allows the evaluation of the peak lateral displacements of the building relative to the ground, and the corresponding base shear, associated with the design earthquake. For these values, the corresponding interstory drifts and the corresponding inelastic deformations of all elements and components, necessary for the evaluation of the Performance Objectives, can be evaluated.

As mentioned, the use of Seismic Coefficients *C* that are indeed constant ductility inelastic design spectra, provide to the users of the *CRSC-2002* a Capacity Spectrum Method that has considerable conceptual and practical advantages (Chopra and Goel 1999) over the methods currently proposed in USA (ATC 1996; FEMA 2000). The method is presented in the Code in a very systematic way and will be described next:

a) For the particular Seismic Zone and Ground Site, a S_a-S_d plot is obtained with pseudo-acceleration S_a on the vertical axis, and inelastic displacement S_d on the horizontal, through the following equations:

$$S_a = C\, g \tag{3}$$

$$S_d = \mu\, (S_a / \omega^2) = \mu\, (T/2\pi)^2\, S_a \tag{4}$$

where the Seismic Coefficient *C* is calculated from Eq. 1 with *SR* = 1.2 instead of 2.0 as the Capacity Spectrum Method is a non-linear method of analysis; μ is the specific global ductility; ω the fundamental natural frequency and *T* the corresponding fundamental period. A family of S_a-S_d spectra for different ductility is illustrated by the colour curves of Fig. 5.

b) Next, a non-linear pushover analysis is performed to the structure. For this analysis, the *CRSC-2002* recommends a distribution of lateral forces proportional to the fundamental mode of vibration. From the resulting Capacity Curve, the intrinsic structural limit displacement, corresponding to the point where the structure reaches its intrinsic or inherent capacity, is determined. This value is defined as the displacement associated with those internal deformations of the structural members or components that have been previously defined as limiting values for a particular building performance, for instance immediate occupation or life safety. From the Capacity Curve, an idealized bilinear response and its corresponding Equivalent Yield Point are defined. Next, the structural global intrinsic ductility, defined as the ratio of the intrinsic structural displacement to the Equivalent Yield Point displacement, can be estimated. These concepts are illustrated in Fig. 4.

c) As the values of the structural Base shear and the Roof displacement are respectively proportional to the spectral values S_a and S_d, the Capacity Curve of the previous step can be converted to an Capacity Spectrum Curve, represented in a S_a-S_d plot; this is easily achieved through well known relations from structural dynamics (Chopra 2001). This transformation allows the Structural Response, now represented by the Capacity Spectrum Curve, and the earthquake ground motion demand,

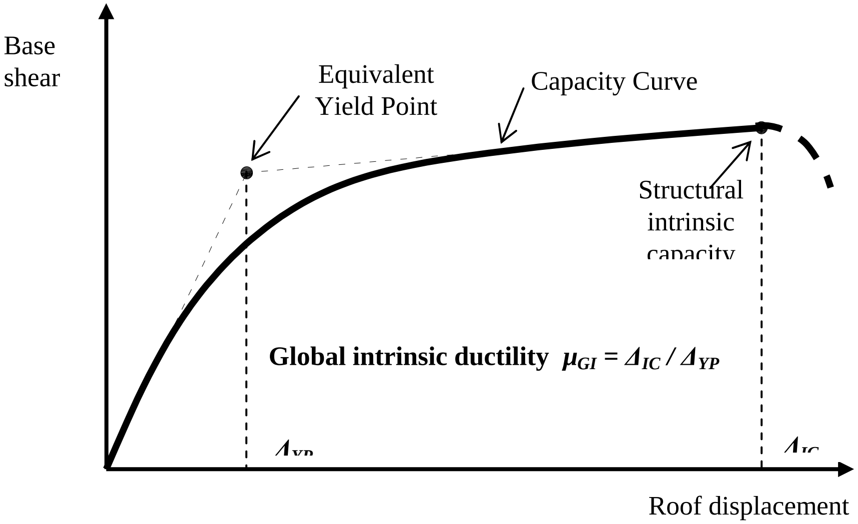

Figure 4. Pushover Capacity Curve, Equivalent Yield Point and global intrinsic ductility in the Capacity Spectrum Method of the CRSC-2002.

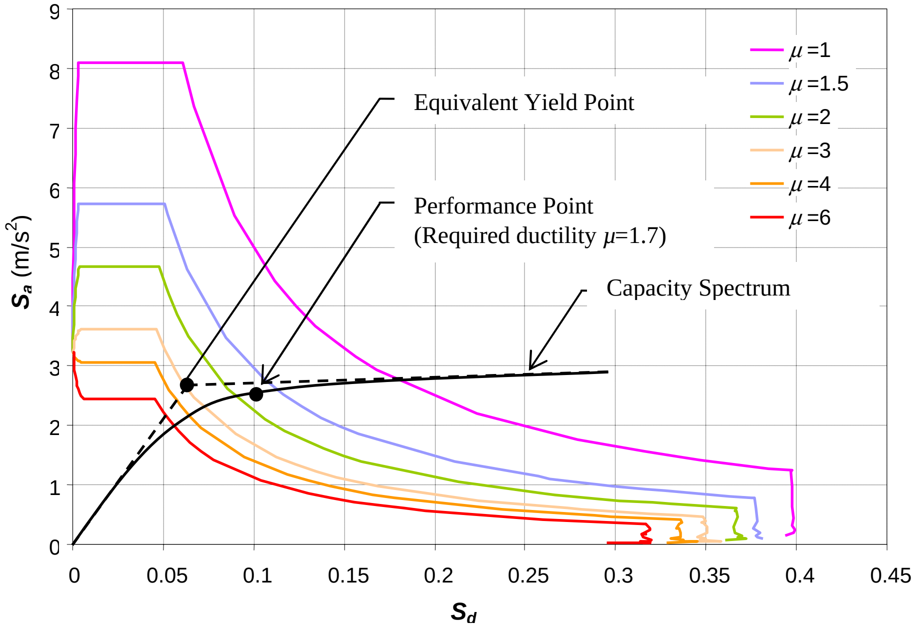

Figure 5. Graphic calculation of the Performance Point and its corresponding required ductility according to the Capacity Spectrum Method CSM of the CRSC-2002.

also expressed in a in a S_a-S_d plot, to share a common graph, as illustrated in Fig. 5. From this figure the structural Performance Point is readily obtained as the point in the Capacity Spectrum Curve whose global ductility –ratio of S_d at Performance Point to S_d corresponding to Equivalent Yield Point- approximates the ductility interpolated from the Earthquake ground motion constant ductility demand curves. This ductility is called required ductility and represents the structural ductility demanded by the Earthquake ground motion to the particular structure; obviously the required ductility should never exceed the intrinsic ductility, as this condition implies a transgression to the Performance Objectives. In the example of Fig. 5, the Performance Point corresponds to a required ductility of 1.7, obtained simultaneously as the ratio of this point to the Equivalent Yield Point and as the interpolated value between the μ = 1.5 and 2.0 constant ductility curves.

d) From the S_a and S_d values corresponding to the Performance Point, the corresponding structure Base shear and Roof displacement are easily obtained. The associated absolute inelastic displacements and interstory drifts, as well as the internal deformations for all elements and components, can also be obtained by interpolating the results from the two steps of the pushover analyses flanking the Performance Point; this information allows the evaluation of the building performance. If desired, the Maximum Probable Strength can be obtained from the Base shear at the Performance Point multiplied by the overstrength factor *SR*=1.2; however, this parameter is not as important for *PBE* as the inelastic displacements, the interstory drifts or the internal deformations.

The Displacement-Based Plastic Design method

The Capacity Spectrum Method *CSM* presented in the previous section is a conceptually simple and easy to apply methodology for the non-linear analysis of structures subjected to seismic ground shaking. However, as a method of analysis, it is indeed a verification process, as the structure needs to be already designed, with its structural layout and all its structural elements well defined, as a step previous to the analysis. This is not a limitation for the evaluation of existing structures, which was the initial motivation for *PBE* (ATC 1996; ATC 1997), but it is certainly a problem for new buildings that do require a previous design of the structure, including a definition of the strengths and stiffness of all structural elements as well as the force-deformation relationships of the potential plastic hinge sections as input data for the analysis with the *CSM.* Surprisingly, the strengths and stiffness of the structural elements are usually obtained through elastic methods of analysis (Priestley 2000), representing a severe limitation for *PBE* as the structure is initially defined without any considerations to important features as the inelastic redistribution of forces due to plastic hinge formation or the resulting failure mechanism, which are totally absent from the analysis. In consequence, under severe ground shaking, the structure may undergo uncontrolled severe inelastic deformations resulting in an unexpected and undesirable performance.

For the sake of conceptual consistency and in order to be able to design and build a structure that, when subjected to a non-linear analysis or, most important, to a real earthquake ground shaking, will behave in a rather predictable way according to the desired Performance Objectives, the definition of all element strengths and stiffness should be obtained trough plastic design methods (Hodge 1981; Moy 1996). The author still remembers the passionate words of Professor V. V. Bertero in his memorable lectures on plastic design: "*with plastic design you tell the structure what to do whereas with elastic design the structure is telling you what she wants to do*"; a crucial difference indeed.

For plastic design, a precise definition of the earthquake ground motion demand becomes of paramount importance as it should consider the inelastic response characteristics of the structure which, as already commented, is poorly represented by the elastic design spectra with Reduction Factors *R* of most USA codes. To overcome this limitation, the Displacement-Based Plastic Design *DBPD* method has been developed by the author; this conceptually simple method is consistent with the Capacity Spectrum Method *CSM* of the *CSCR-2002* described in the previous section and can be summarized in the following six steps, also represented in Fig. 6. A more detailed description as well as numerical examples can be found elsewhere (Gutiérrez and Alpízar 2004):

Step 1. Initial dimensions and displacement shape

Following Simple Plastic Theory *SPT* principles (Hodge 1981; Moy 1996) the preliminary element strengths and their corresponding dimensions are initially defined as the values required to resist the gravitational loads. Accordingly, the minimum strength of each beam is selected to withstand the critical gravity load combination. In addition, at each structural joint, the capacity design principle of *strong columns-weak* *beams* defines the minimum column strength. Minimum code requirements must also be considered.

Next, a displacement shape is selected in agreement with the target interstory drift corresponding to the building Performance Objective. This target drift may be defined from limit internal deformations of critical structural elements or components or from specific considerations for non-structural systems. A displacement shape proportional to the first mode of the initially dimensioned structure, but scaled by a factor Y_{tar} to satisfy the target design interstory drift, is recommended (Fig. 6.1).

Step 2: Target design displacement for an equivalent SDOF system

Once the displacement shape is defined, the target displacement $S_{d\,tar}$ for the corresponding single degree of freedom *SDOF* system is calculated from principles of dynamics (Chopra 2001):

$$S_{d\,tar} = \frac{u_N}{\Gamma \phi_N} = \frac{Y_{tar}}{\Gamma}; \qquad \Gamma = \frac{L}{M^*} \tag{5}$$

For a system with lumped-masses m_i at each level:

$$M^* = \sum_{i=1}^{N} m_i \phi_i^2 \text{ ; Generalized Mass} \tag{6}$$

$$L = \sum_{i=1}^{N} m_i \phi_i \text{ ; Participation factor} \tag{7}$$

where N is the number of stories.

Step 3: Earthquake ground motion demand.

The earthquake ground motion demand is obtained from the constant-ductility inelastic design spectrum corresponding to the structure target ductility $\mu_{G\,tar}$. This value is defined from the selected Performance Objective as well as from the building structural classification, its plan and vertical regularity conditions and the local ductility of its structural elements and components.

As commented in the previous section, the constant-ductility spectrum for an elasto-plastic system must be represented in a S_a-S_d plot with S_d corresponding to the inelastic peak displacement. From this plot, the corresponding pseudo-acceleration S_a is obtained for the target displacement $S_{d\,tar}$ previously defined (Fig. 6.3). Furthermore, the expected elastic period of the structure T_{el} can also be calculated with the following expression:

$$T_{el} = 2\pi \sqrt{\frac{S_{d\,tar}}{S_a \mu_{G\,tar}}} \tag{8}$$

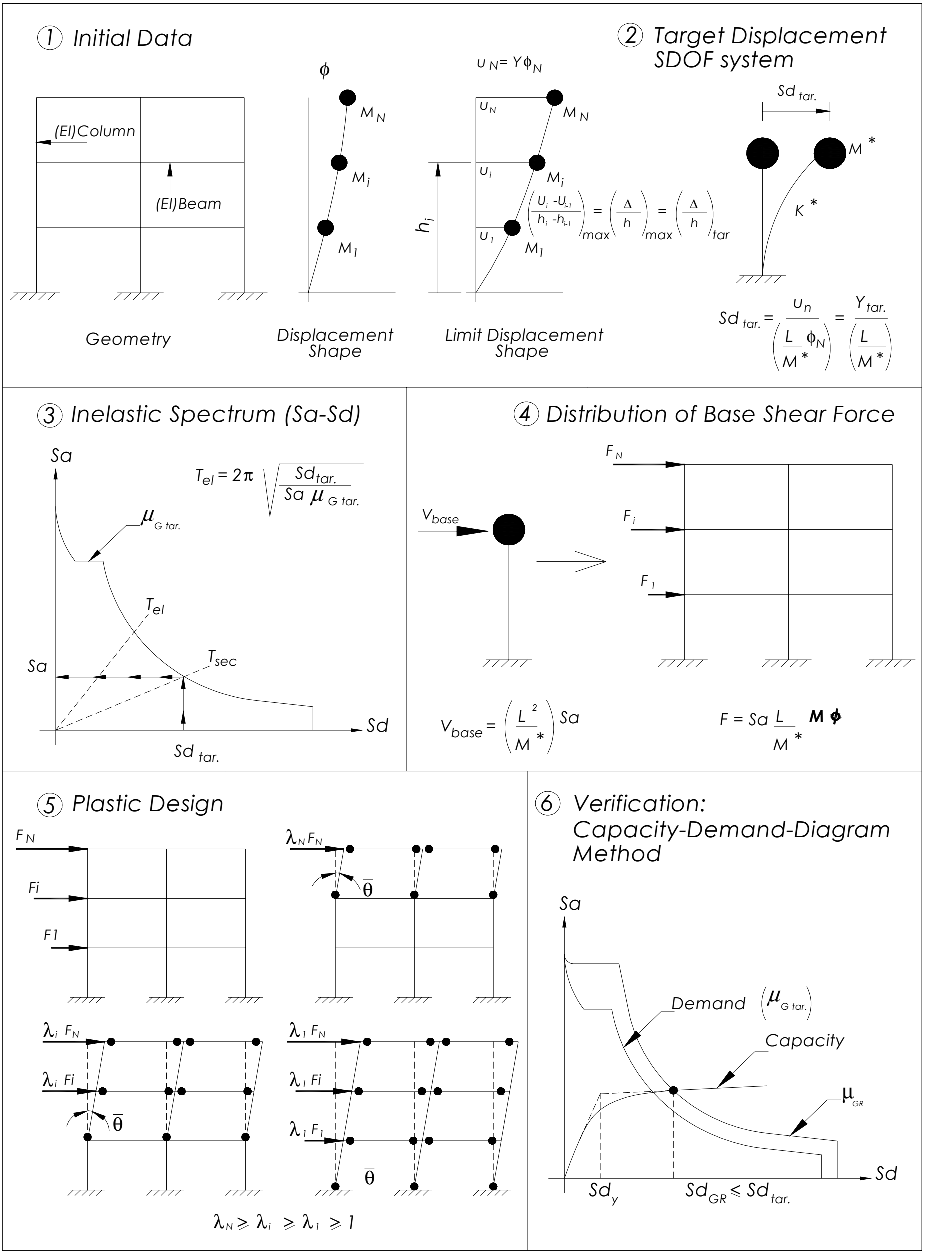

Figure 6. The six steps of the Displacement-Based Plastic Design DBPD method. (After Gutiérrez and Alpízar 2004).

If the calculated elastic period T_n , corresponding to the stiffness of the structure defined in Step 1, is greater than the value calculated by Eq. 8, it would not be possible to fully reach the global target ductility $\mu_{G\ tar}$ without exceeding its target displacements

$S_{d\ tar}$. In this case, to be able to satisfy both targets at the Performance Point, the stiffness of the structure should be suitably increased.

Step 4: Distribution of base shear force

Once S_a is obtained, the Base shear force can be calculated from simple principles of dynamics (Chopra 2001):

$$V_b = \frac{L^2}{M^*} S_a \tag{9}$$

This force is then vertically distributed in proportion to the masses and the selected displacement shape, to obtain the forces at each level (Fig. 6.4):

$$\mathbf{F} = S_a \frac{L}{M^*} \mathbf{M} \boldsymbol{\phi} \tag{10}$$

where, in addition to the previously defined terms, **F** is the vector representing the forces at each level, **M** is the Mass Matrix of the structure and $\boldsymbol{\varphi}$ its fundamental mode.

Step 5: Plastic design

To define the strength of all the structural elements, a plastic design is performed considering a series of partial collapse mechanisms, starting from the top story and descending to the lower levels. To prevent these undesirable partial lateral collapse mechanisms, all of them should have a safety factor greater than 1.0, say ≥1.05. In contrast, the desired complete collapse mechanism, with plastic hinges forming at the base columns, should be equal to 1.0 to guarantee that it will precede all undesired partial collapse mechanisms (Fig. 6.5). Once all the lateral collapse mechanisms have been considered and the required strengths of the structural elements have been defined, it is convenient to check for other possible mechanisms, such as soft-story. Indeed, according to the Upper Bound Theorem of Plastic Theory, the calculated safety factor may be on the unsafe side if an unforeseen mechanism, with a lower than unity safety factor, precedes the desired collapse mechanism. This design method may also consider *P-Δ* effects, overstrength of structural elements and rigid-finite-joint dimensions (Alpízar 2002).

Step 6: Verification procedure: Capacity Spectrum Method

Finally, to validate the design procedure, the Capacity Spectrum Method CSM of the CRSC-2002, described in the previous section, is applied (Fig. 6.6). As already explained, with this procedure the Performance Point is readily determined as the point where the ductility, determined from the Spectrum Capacity Curve and from the design spectra coincide (Fig. 5). For this point, the required ductility, the structure inelastic absolute displacements and interstory drifts, the internal inelastic deformations of the structural members and all other required parameters necessary to determine the building performance, can be determined, as well as any unforeseen undesirable collapse mechanism identified. In general terms, as the structural design and the verification process using the *CSM* are actually based in the same concepts and procedures, the latter usually becomes a self-fulfilling prophesy, with results very close to the selected target values.

Obviously, the previously commented Response History Analysis *RHA* considered in the *CRSC-2002* can also be used for the verification procedure and, for particular ground motion accelerograms, should produce more precise results than the *CSM*. In order to compare these two alternative verification methods, analytical results have been obtained for a series of shear building models having 5 and 10 stories in height, two different stiffness distributions and six target ductility values. Each building model was designed for 4 actual ground motion accelerograms, resulting in a total of 96 study cases. The results (Salas 2005; Salas and Gutiérrez 2005) show reasonable agreement between the *CSM* and *RHA* methods for the 5 story buildings. For the 10 story buildings, as the higher mode effects ignored in the *CSM* tend to become significant, more refined verification procedures that consider these effects, like the Modal Pushover Analysis *MPA* (Chopra and Goel 2001a) are recommended over the *CSM*. Studies involving *RHA* of more realistic building models, designed with the *DBPD* method, are being carried out.

Concluding Remarks

By defining earthquake ground motion demands by means of Seismic Coefficients derived from constant ductility inelastic design spectra and introducing non linear analysis procedures such as the Capacity Spectrum Method *CSM* or the Response History Analysis *RHA* method, the Costa Rican Seismic Code-2002 has been able to incorporate Performance Based Engineering *PBE* concepts and considerations in a rational, practical and conceptually simple way. Important practical limitations still remain, basically the lack of reliable data for building performance determination. However, this can be easily accounted for in new revisions of the Code without major modifications in the text and within the basic conceptual framework that has been presented here.

The Displacement-Based Plastic Design *DBPD* method is a very effective tool for *PBE* as it allows for the selection of the target global ductility and drift limits associated with the desired performance of the building. In this method Plastic Theory is used to determine the required strength of each structural element, necessary to produce a desired collapse mechanism and to reach a selected Performance Point under the earthquake ground motion demand represented by the constant ductility design spectra of the *CRSC-2002*. Hence, the *DBPD* method is an explicit design procedure that uses the *CSM* of the *CRSC-2002* as the analytical tool to verify the design. For low rise buildings, where higher mode effects are unimportant, the *DBPD* method leads to precise designs, able to control the inelastic response of buildings within the established parameters corresponding to the selected Performance Objectives.

Acknowledgements

The author wishes to thank the Organizing Committee of the Luis Esteva Symposium “Earthquake Engineering Challenges and Tendencies” for the opportunity to express his respect and high esteem to Professor Luis Esteva in such a rich academic environment. He also acknowledges and thanks his colleagues in the Costa Rican Seismic Code Committee and the National Laboratory for Materials and Structural

Models *LANAMME*, as well as his graduate students at the University of Costa Rica, for all the fruitful discussions, support and feedback that made this work possible.

References

Alpízar M. (2002). Idoneidad Sísmica de Edificios Prefabricados con Juntas Secas Tipo Híbrida (JSTH), *M.Sc. Thesis*, University of Costa Rica. (In Spanish)

ASCE (2000). *FEMA 356: Prestandard and Commentary for the Seismic Rehabilitation of Buildings, American Society of Civil Engineers*, prepared for the SAC Joint Venture, published by the Federal Emergency Management Agency, Washington D.C.

ATC (1996). *ATC-40: The Seismic Evaluation and Retrofit of Concrete Buildings*, 2 volumes, Applied Technology Council, Redwood City, CA.

ATC (1997). *NEHRP Guidelines for the Seismic Rehabilitation of Buildings, FEMA 273*, prepared by ATC for the Buildings Seismic Safety Council, funded by the Federal Emergency Management Agency FEMA, Washington, D.C.

Bravo, A. (2002). Relación entre Ductilidad Local y Ductilidad Global Asignada en Edificios de Concreto Reforzado tipo Dual diseñados según la propuesta del Código Sísmico de Costa Rica 2002, *M.Sc. Thesis*, University of Costa Rica. (In Spanish)

Chopra, A.K. (2001). *Dynamics of Structures: Theory and Applications to Earthquake Engineering*, 2nd Edition, New Jersey: Prentice Hall.

Chopra A.K. and R.K. Goel (1999). Capacity-Demand-Diagram Methods Based on Inelastic Design Spectrum, *Earthquake Spectra*; 15(4): 637-56.

Chopra A.K. and R.K. Goel (2000). Evaluation of NSP to Estimate Seismic Deformation: SDF Systems, *Journal of Structural Engineering, ASCE*; 126(4): 482-90.

Chopra, A.K. and R.K. Goel (2001a). A Modal Pushover Procedure to Estimate Seismic Demands for Buildings: Theory and Preliminary Evaluation., *Report No. PEER-2001/03*. Pacific Earthquake Engineering Research Center, University of California, Berkeley.

Chopra A.K. and R.K. Goel (2001b). Direct Displacement-Based Design: Use of Inelastic vs. Elastic Design Spectra, *Earthquake Spectra*; 17(1): 47-64.

CFIA (2003). *Código Sísmico de Costa Rica – 2002*, Colegio Federado de Ingenieros y de Arquitectos de Costa Rica, Editorial Tecnológica de Costa Rica. (In Spanish)

Fajfar, P. and H. Krawinkler , Editors (1997). *Seismic Design Methodologies for the Next Generation of Codes*, Balkema, The Netherlands, pg. XVIII.

Fajfar, P. and T. Paulay (1997). Notes on definitions of overstrength factors, in Fajfar, P. and H. Krawinkler, Editors. *Seismic Design Methodologies for the Next Generation of Codes*, Balkema, The Netherlands, 407-409.

Freeman, S.A. (1998). Development and Use of Capacity Spectrum Method, Paper 269, *Proceedings 6th U.S. National Conference on Earthquake Engineering*, May 31-June 4, Seattle, Washington.

Gutiérrez, J. and M. Alpízar (2004). An Effective Method for Displacement-Based Earthquake Design of Buildings. Paper 1512, *Proceedings 13th WCEE*, Vancouver, B.C., Canada, August 1-6, 2004.

Hernández, D. (2003). Respuesta Sísmica de Osciladores Simples con Comportamiento Elástico No-Lineal. *M.Sc. Thesis*, University of Costa Rica. (In Spanish)

Hernández, D. and J. Gutiérrez (2005). Respuesta Dinámica de Osciladores Simples con comportamiento Elástico No-Lineal: implicaciones para el Diseño Sismo-

Resistente de Edificios Prefabricados de Concreto. Accepted for publication, *Proceedings VIII Seminario de Ingeniería Estructural y Sísmica*, San José, Costa Rica, September 21-23, 2005. (In Spanish)

Hodge, P.G. (1981). *Plastic Analysis of Structures,* McGraw-Hill.

IAEE (1996 and 2000). *Regulations for Seismic Design - A World List – 1996* and *Supplement – 2000*, International Association for Earthquake Engineering, Japan.

ICC (2003). *International Building Code 2003*, International Code Council Inc.

Laporte, M. et al. (1994). Seismic Hazard for Costa Rica, *NORSAR Technical Report No. 2-14*, Kjeller, Norway.

Moy, .S.S.J. (1996). *Plastic Methods for Steel and Concrete Structures,* 2nd Edition, Great Britain: Macmillan Press Ltd.

Newmark N.M. and W.J. Hall (1987). *Earthquake Spectra and Design*, Earthquake Engineering Research Institute, California, USA.

Newmark N.M. and R. Riddell (1980). Inelastic Spectra for Seismic Design, *Proceedings 7th WCEE,* Istanbul, Turkey; (4): 129-36.

Priestley, M.J.N. (2000). Performance Based Seismic Design. *Proceedings 12thWCEE*, New Zealand.

Priestley M.J.N and J.R. Tao (1993). Seismic Response of Precast Prestressed Concrete Frames with Partially Debonded Tendons, *PCI Journal,* 38(1): 58-69.

Ramírez, H. (2002). Ductilidad Local y Ductilidad Global Asignada en Marcos Regulares de Concreto Reforzado Diseñados según Propuesta del Código Sísmico de Costa Rica 2002, *M.Sc. Thesis*, University of Costa Rica. (In Spanish)

Salas, L.D. (2005) Validación del Método de Diseño Plástico Basado en Desplazamientos (DPBD) mediante Análisis No-Lineal de Respuesta en el Tiempo, *M.Sc. Thesis*, University of Costa Rica. (In Spanish)

Salas, L.D. and J. Gutiérrez (2005). Validación del Método de Diseño Plástico Basado en Desplazamientos mediante Análisis No-Lineal de Respuesta en el Tiempo, Accepted for publication, *Proceedings VIII Seminario de Ingeniería Estructural y Sísmica*, San José, Costa Rica, September 21-23, 2005. (In Spanish)

SEAOC (1995). *VISION 2000: Performance Based Seismic Engineering of Buildings*, Structural Engineers Association of California, Sacramento, CA.

SEAOC (1999). *Recommended Lateral Force Requirements and Commentary,* 7th Edition, Seismology Committee, Structural Engineers Association of California, Sacramento, CA.

Polat Gülkan

MIDDLE EAST TECHNICAL UNIVERSITY
Disaster Management Research and Implementation Center, DMC
06531 Ankara
TURKEY,
a03516@metu.edu.tr

Main interests: Site-Dependent Spectra, Empirical Attenuation, Performance of Buildings

As for a remembrance involving Luis Esteva, may I offer one where I noted his strict punctuality? After the EERI meeting in February 2005 in Ixtapa, he and I agreed to share a cab to the airport that was some 40 km away from the hotel. We figured it would require a certain span of time to drive there (sometimes through towns along the way), and arranged to meet at the lobby area some 2 hours prior to flight time. I happened to bring my bag to the meeting point some 15-20 minutes ahead of time, and then by chance met an acquaintance whom I hadn't seen for many years. We were deep in mutual reminiscences with this friend when I noticed Luis circling us expectantly. My first thought was that my conversation had carried me past the agreed time, and began to apologize for it, but Luis cut me short, saying: "no, we still have time. I just came up from my room to see if you were ready, I still must go to my room, and fetch my wife and our bags! I like checking ahead to make sure that time is kept."

CAVEATS FOR NONLINEAR RESPONSE ASSESSMENT OF SHORT-PERIOD STRUCTURES

ABSTRACT

Seismic response of a lightly reinforced stiff shear wall structure subjected to ground motions classified as near- or far-field according to their distance to causative faults is investigated. A model structure that has previously been studied both experimentally and analytically in the context of a coordinated research project is re-examined. The structural model is a five-story lightly reinforced shear wall, subjected analytically to 55 different ground motion records on firm soil sites. Several response parameters are obtained by linear and nonlinear analyses. Additional analyses are performed to investigate the validity and range of applicability of the most widely used approximate displacement based analysis procedures. The approximate procedures considered in the study are found to be deficient in representing the actual response of the structure employed here regardless of the type of excitation, so modifications are suggested for improved results.

Keywords: near-field, far-field, approximate procedure, reinforced concrete shear wall, pushover analysis

Introduction

Recent focus on the use of simplified procedures in performance-based earthquake engineering has led to comprehensive research resulting in improved techniques applicable for buildings with generally regular geometrical and structural features. These methods are intended to provide basically an adequate level of equivalent linearization applicable to these types of systems so that the calculated nonlinear deformations match results calculated for linear systems of varying complexity. It should be recalled that all linearization techniques are designed to minimize the error in this calculation. In the final analysis the performance of performance based methods has not been tested by nature, so the goodness of a given method is assessed against results calculated for another method or technique. In this article we examine the accuracy of a number of commonly used methods in calculating the response of a short-period structural mockup that had been previously tested on a shake table. Our blind predictions of its response were successful, so this has encouraged us to use many more naturally recorded ground motions to calculate its response with use of a number of currently used methods and compare this with a fully nonlinear analysis.

Antecedents

The International Atomic Energy Agency (IAEA), in cooperation with the EU Joint Research Center (JRC), has initiated research to investigate the safety implications of near-field earthquakes on nuclear facilities. This calls for a critical assessment of the validity of displacement-based procedures for stiff structures that are typical for nuclear sites. These investigations stem from the need to develop reliable guidelines for safety re-evaluation of existing nuclear structures. A coordinated research project (CRP) on safety significance of near fault earthquakes was launched by IAEA in 2002. The objective of this CRP has been to propose the most appropriate earthquake engineering practice to assess the seismic vulnerability of typical structures in nuclear facilities subjected to the effects of near-fault earthquakes. The research was crafted to use experimental data available from earlier investigations. A series of benchmark shaking table experiments had been carried out in the Saclay Nuclear Center in France in 1997. One particular specimen from that program, CAMUS1, has been re-studied in the CRP organized by IAEA. This specimen is a 1/3-scale model of a representative 5- story reinforced concrete building detailed according to current French practice (Combescure *et al* (2002)). It is considered a typical example for a stiff structure, but its reinforcement details are more typical of residential construction.

In the first phase of the investigations, a reliable and representative analytical model of the tested specimen was developed, based on the accurate duplication of physical conditions and loadings imposed during the laboratory tests. The experimentally measured results have been predicted analytically with convincing accuracy as presented in (Kazaz *et al* (2005)). This article is complementary to the first phase. It deals with the analytical assessment of the seismic response of the CAMUS1 structure under a suite of 55 ground motion records. The ground motion set selected for the study contains far- (FFE) and near-field (NFE) earthquake records on firm soil sites where nuclear power facilities are typically built. The near-fault records used in this study do not necessarily exhibit the forward directivity characteristic, i.e. a long-duration pulse of high velocity dominating the event. Only a few records we use contain such dominant velocity pulses.

The response of the structure calculated using nonlinear response history analyses is considered to be “exact,” because the analytical model we have constructed has successfully predicted the observed response (including local strains, curvatures and shear forces or moments) of the specimen on the shaking table in the preceding stage. The structure is then re-analyzed using approximate static procedures. The results are examined to evaluate accuracy and validity of the approximate nonlinear static analysis procedures for similar types of structures. Most nonlinear response procedures are based on the dynamics of SDOF systems, so this exercise also provides an understanding of the degree of extrapolation that is acceptable in arriving at estimates of the response of MDOF systems.

Analytical and Experimental Model

The analytical model used in the nonlinear dynamic analyses is a realistic duplication of the CAMUS1 specimen used in the experimental program. In all of the following discussion, these results will be considered as “exact” for comparison with analytical results.

The experimental program consisted of testing a 1/3-scale representative component of a 5-story reinforced concrete shear wall building on shaking table at Commissariat a l’Energie Atomique (CEA) in the Saclay Nuclear Center. The specimen, named CAMUS1, had a total mass of 36 tons with additional masses attached to it. The walls had no openings, and were linked by square slabs (1.7m x 1.7m). A heavily reinforced concrete footing allowed anchorage to the shaking table. The total height of the model was 5.10 m. They had a width of 1.7 m and thickness of 6 cm. The specimen had a measured fundamental natural frequency of 7.24 Hz. The dimensions and the mass distribution of the specimen are shown in Fig. 1. The experimental study provided the measured response quantities of the model shear walls subjected to different input seismic motions. The walls were loaded in their own plane. The input motions were representative of near fault as well as of far fault ground motions selected for the purpose of comparing any effects such different ground motions may produce on the structure.

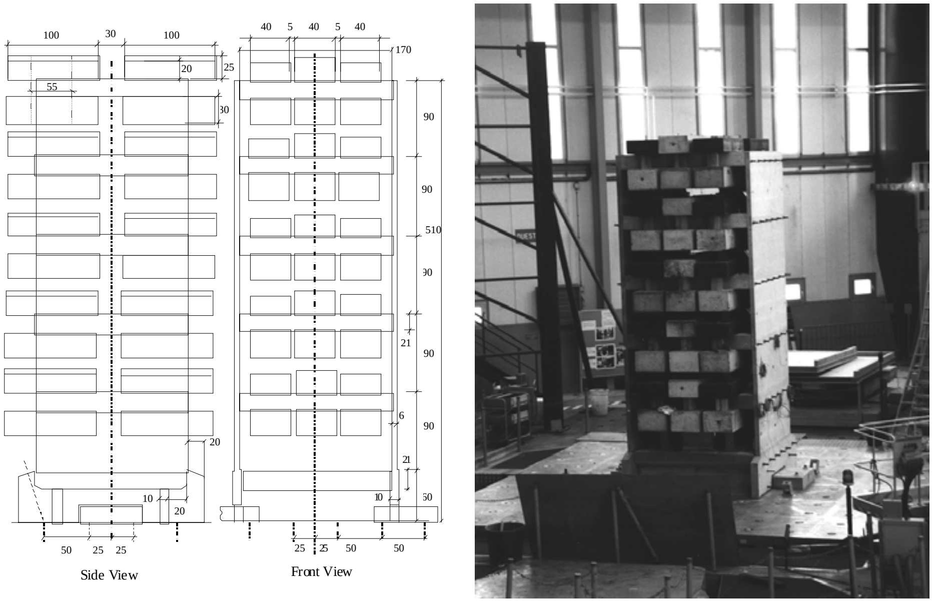

Figure 1. CAMUS specimen

A finite element model of the tested shear walls as shown in Fig. 2 was created (ANSYS 2002). The actual material properties and boundary conditions in the experiment were implemented in the model to reflect the required aspects of the test specimen. The finite element model of the test specimen has a computed fundamental frequency of 7.28 Hz.

The experimentally measured and numerically computed response quantities including top story displacement, base shear, bending moment at the base, top story horizontal accelerations and the local results such as strains were found to be in very good agreement. In Fig. 3, the comparison of base shear, base moment, top displacement and top story horizontal acceleration are given for the fourth sequentially applied ground motion. The results, given in detail elsewhere (Kazaz *et al.* (2005)), clearly indicate that the analytical model developed here is able to display the inelastic response of the tested specimen quite satisfactorily. The same model has been employed in this study to perform further analyses for a suite of 55 ground motions that are described next.

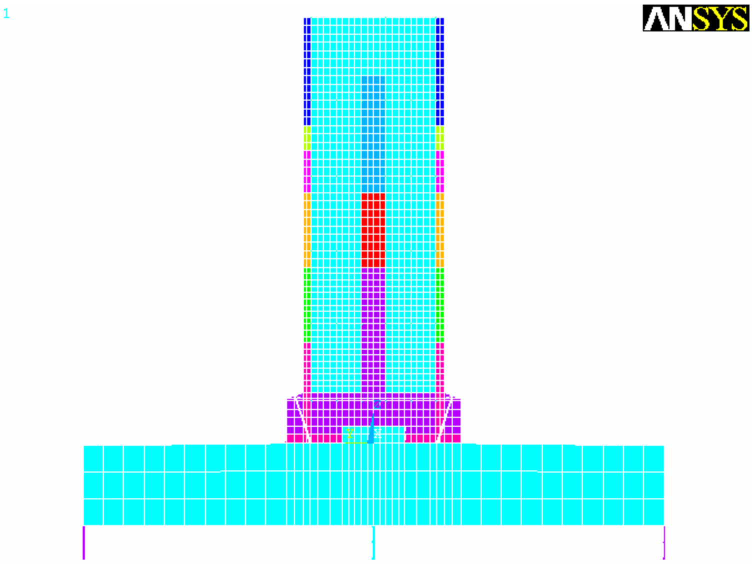

Figure 2. Analytical model

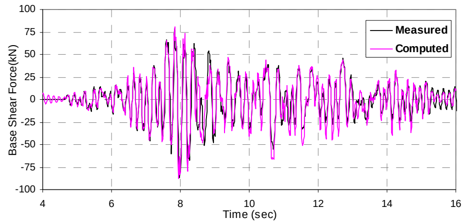

(a) Comparison of base shear

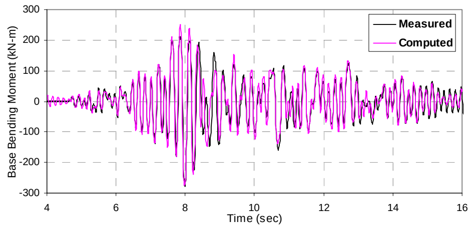

(b) Comparison of bending moment at base level 1

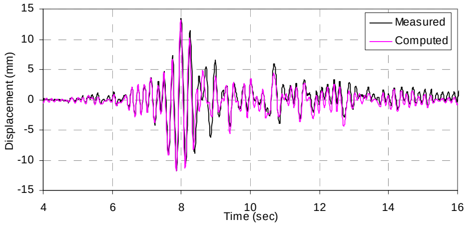

(c) Top floor acceleration time history comparison

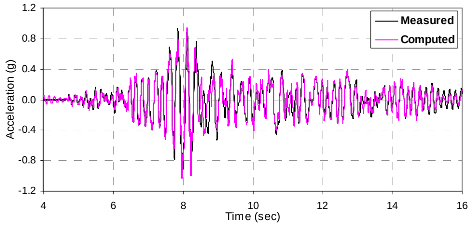

(d) Top floor acceleration time history comparison

Figure 3. Comparison of experimental and computed global response parameters for Run4

Ground Motion Database

The selected ground motion set consists of 55 records obtained from 20 earthquakes of which 31 are near-field seismograms. The database was intended to cover both NFE and FFE records. These ground motion records were classified according to their site-to-source distance based on the recommendations given by Martinez-Pereira *et al.* (1998). Since the model is a 1/3 scale of a real structure, the ground motions used in the analyses were also scaled in the time axis by a factor of 1/3. Analytical Results

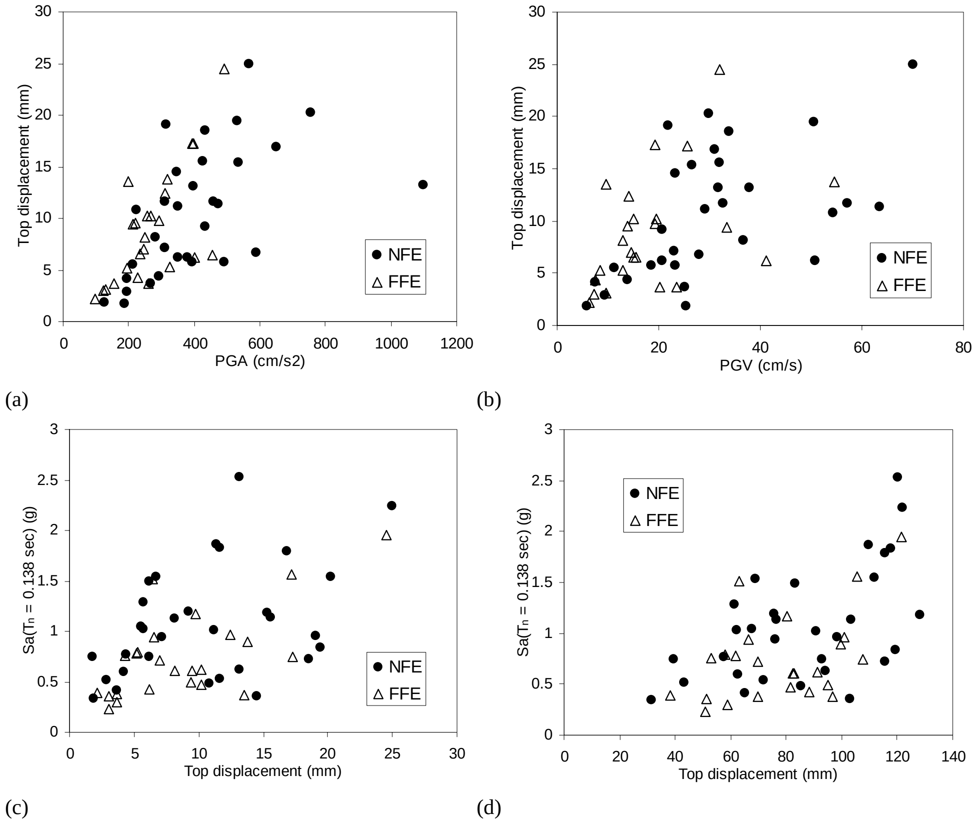

Figure 4. Correlation of top-level displacement with (a) *PGA, and* (b) *PGV, and Correlation of response parameters with Sa (Tn),* (c) *Max. Roof Displacement,* (d) *Max. Base Shear*

Nonlinear Time History Analyses

The selected ground motions were applied to the model and various nonlinear response parameters from time history analyses were determined. Correlation of typical strong motion parameters with the calculated response quantities of the structure was investigated first. For the selected ground motion database, as evidenced from Fig. 4.a and 4.b, no clear trend was observed between the structural deformations and the strong ground motion parameters such as PGA and PGV for either type of ground motion. Nevertheless, since the largest induced force is related to PGA for stiff structures, it correlates better than PGV with top displacement. Another commonly used ground motion intensity measure is the spectral acceleration at the fundamental period of the structure, S_a (T_1). The spectral acceleration reveals a loose correlation for the top floor displacement and the base shear as shown in Fig. 4.c and 4.d, the dispersion being smaller for base shear. In Fig. 4.c and 4.d the yield displacement and base shear of the structure are shown in the respective square. The dispersion is more significant as the structure responds in the inelastic range due to the effect of strength and stiffness degradation.

Pushover Analysis

Full nonlinear time history analysis for a multistory building is the principal tool that provides the most intimate insight about its response to earthquake excitations. A complete time history analysis is quite demanding and computationally expensive as compared to static analysis. As an alternative, nonlinear static pushover analyses are carried out by applying lateral forces at the mass locations of the structural system, assuming that they will account for the distribution of inertia forces acting at the story levels during the dynamic excitation of the structure. This procedure can provide considerable insight for the nonlinear behavior of the structure although it conceals unresolved uncertainties and approximations. The load patterns that are typically used in the pushover analyses are calculated by utilizing modal analyses of the structure. The first mode shape or a combination of modes is used as the representation of the dynamic loading. In the elastic range of the dynamic excitation, results obtained with these prescribed load patterns agree with the exact solution in many cases.

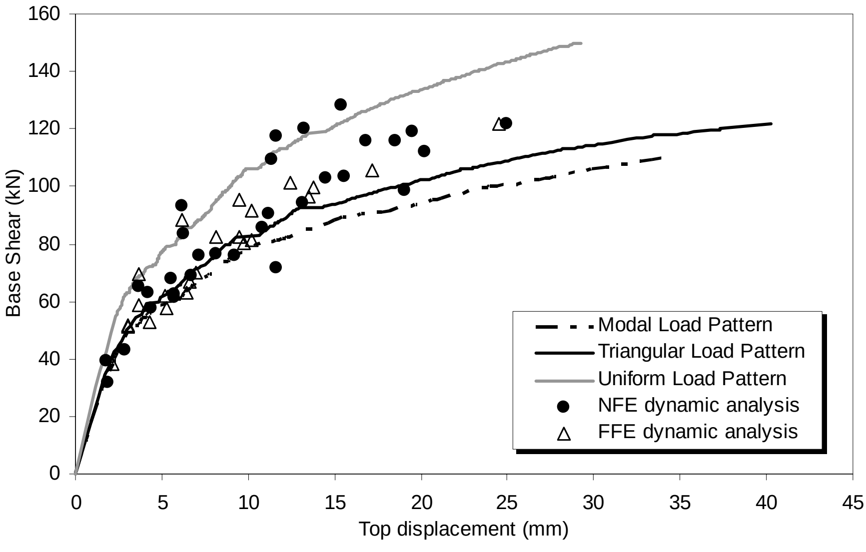

Figure 5. Pushover curves compared with dynamic analysis results

The CAMUS structure was analyzed next using the pushover analysis procedure to compare with the “exact” results. Three distinct vertical distributions of lateral loads were applied. In the first loading shape called modal push pattern, a vertical distribution of lateral forces proportional to the shape of the fundamental mode in the plane of the shear wall was used. Next, a triangular lateral load pattern representing the contribution of each story mass to the inertia force relative to the sum of inertia forces was utilized. Lastly, a uniform distribution consisting of lateral forces at each level proportional to the total mass at these levels was used. The pushover curves of these three different loadings are plotted in Fig. 5 which also displays the results of nonlinear dynamic analyses from the ground motions contained in the dataset.

As seen in Fig. 5 for structures dominantly responding in the fundamental mode, the modal load pattern seems to serve as the lower bound for the seismically induced base shear, and the uniform load pattern acts as an upper bound for the same parameter. As stated in Anderson *et al.* (1987), it was observed that for the ground motion records that exhibit long acceleration pulses where the duration of the pulse is larger than the natural period of the structure, a higher inelastic displacement demand is induced on the structure. Furthermore we observed that acceleration spikes of high amplitude and short duration induce high base shear demand on the structure. The points that are above the upper enveloping curve in Fig. 5 belong to ground motions supporting our observation: Run2, Bingöl (2003) NS component, Ito-Oki EW component, Tabas and Friuli NS component.

Linear Time History Analyses

Linear time history analyses were carried out to investigate their accuracy in estimating the inelastic deformation demands. Time history results for roof displacement of the linear model are plotted against the nonlinear time history results in Fig. 6.

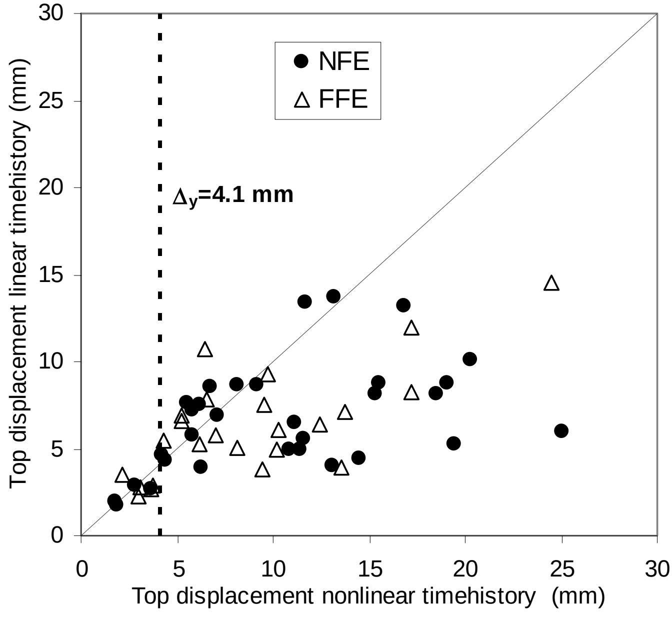

Figure 6. Linear vs nonlinear top displacement time history analysis

The results presented in Fig. 6 confirm that as the nonlinearity and ductility demand increases in the system the ability of linear analysis in predicting the inelastic top displacement diminishes. For stiff and short period systems, such as considered here, if the period of the structure is much shorter than the predominant period of the input record, then the equal displacement rule does not hold. In fact, the nonlinear analyses of the test structure showed that, the inelastic model produced greater deformations than did the corresponding elastic model except in a few cases, which is consistent with the generally accepted wisdom that derives from single degree of freedom analyses. This follows from the fact that when a system with a short initial period yields, its period elongates and shifts closer toward the predominant period of the ground motion. The exceptions are those cases where the spectral acceleration ordinates corresponding to undamaged (elastic) state are much higher than the values corresponding to softened state, leading to higher deformations even if the structure behaves elastically. This observation is valid for moderate degree nonlinearity and is strongly dependent on the base shear yield strength of the structure. The response spectra of ground motions supporting this comment are named in Figure 7.

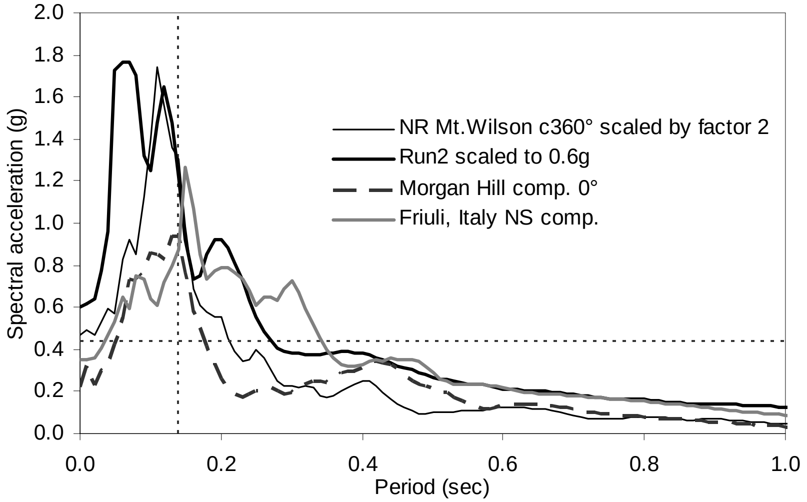

Figure 7. The ground motions with period smaller than that of the structure

Displacement Based Procedures

The motivation for research dealing with the development of simplified procedures that are used to estimate the inelastic displacement demand of structures has essentially been to find an alternative approach as substitute to nonlinear response history analyses that involve analytical complexity and computational expense. These simplified procedures generally rely on the reduction of MDOF systems to equivalent SDOF representations. The two most commonly used procedures of this nature are the Capacity Spectrum Method of ATC-40 (ATC 40 (1996)), and the Displacement Coefficient Method contained in FEMA 356 (2000). These procedures have been evaluated by many researchers, highlighting their weaknesses as well as their adequacy. Sometimes conflicting findings have led to uncertain and incompatible conclusions on their range of validity. Unlike many previous investigations that either deal with SDOF systems (Miranda (2001, 2002), and Chopra 2003) or generic MDOF systems (Chintanapakdee 2003), this study evaluates the accuracy of these procedures for the CAMUS1 model that has been studied experimentally and analytically. It is based on nonlinear response history analyses under a comprehensive suite of ground motions. In addition, the nonlinear analyses of the equivalent SDOF systems and a proposed modification to the CSM have been carried out to test their success in matching the exact results.

SDOF analyses

The inelastic response (generally the roof displacement with which damage may be associated) of a MDOF system can be estimated from the corresponding equivalent SDOF system in varying degrees of accuracy depending on the particular ground motion used in the analysis and the structural properties of the MDOF system. There is a divergence between the ductility demands imposed on multistory buildings and SDOF systems. Two particular parameters give rise to the differences between the ”input” and ”output” ductility demands (deformations) of SDOF and MDOF systems. These are higher mode contributions and inter-story drift demands (local response behavior of MDOF system) (Chopra (2000)). These two characteristics cannot be incorporated directly into the structural characteristic of a SDOF system, where they are subsumed in a single bilinear force-deformation relation. So in cases where the contribution of these two parameters to the structural response is limited or negligible a good estimation of global deformation demand of a MDOF system can be obtained, otherwise the contribution of these effects must be taken into account with certain correction coefficients.

A nonlinear SDOF system with bilinear force-deformation relation with some post elastic-stiffness can be described completely with the following parameters; T (elastic period), ξ (damping), either of m (mass) or k (stiffness of the system in the elastic range), $\eta = f_y/W$ (yield base shear coefficient), and α (post elastic stiffness coefficient). Yield base shear coefficient (η), or base yield strength (f_y), given in Eq. (1) is determined in the design stage for a desired ductility level under a postulated ground motion effect that defines the constant ductility response spectrum.

$$f_y = \frac{A_y}{g} W \tag{1}$$

In the above equation, A_y is the pseudo acceleration corresponding to yielding of the SDOF system with pre-defined ductility level and W is the weight of the structure.

To determine the response of the CAMUS structure by employing equivalent SDOF systems, a representative SDOF model of the MDOF structure was obtained. The accuracy of this approximate procedure depends strongly on how well various structural aspects of the MDOF are represented by the corresponding SDOF system. Examination of the pushover curves obtained for the three aforementioned lateral load patterns revealed that the triangular load pattern provides the best representation of the dynamic behavior for all ground motions except those with high amplitude acceleration spikes, so it has been used for further analyses. It is also important to note that the change in the initial slope of pushover curve due to bilinearization also requires a change in the natural period of the system that is modified with $T_e = T_n.(K_i/K_e)^{0.5}$. The following steps were implemented to convert bilinear MDOF system's capacity curve to that of SDOF counterpart.

1) In constructing a relation between the MDOF system and its equivalent SDOF system, a widely accepted procedure that is based on the fundamental mode properties of the MDOF system was used. The horizontal axis of the load deformation curve describing the global roof displacement was divided by the factor PF_1 which is the modal participation factor for the first mode obtained by assuming that the mode shape is normalized to unity at the top of the structure, Eq. (2).

$$PF_1 = \frac{\Phi_1^T.M.1}{\Phi_1^T.M.\Phi_1} \tag{2}$$

2) We note that, to keep the effective period (T_e) and damping ratio (ξ) of the corresponding SDOF system the same as the fundamental mode properties of the multistory structure, we can either use the total weight of the MDOF structure (W), and derive a new elastic stiffness (K_e^*) by using Eq. (3), or by keeping the elastic stiffness (K_e) of the bilinear curve constant we can calculate a modified weight for structure (W^*). Regardless of which weight and elastic stiffness pair is used, they must give the same elastic period calculated by Eq. (3).

$$T = 2\pi\sqrt{\frac{W/g}{K}} \tag{3}$$

3) By using the initial stiffness (K_e^*) of the pushover curve, the yield base shear value [$f_y=(\Delta_y/PF_1).K_e^*$] for SDOF system is calculated.
4) Lastly, $\alpha. K_e^*$ will define the post elastic strain hardening stiffness of the SDOF system. In Table 1, the force-deformation parameters used for SDOF analysis are given for both cases.

TABLE 1. Bilinear structural characteristics of MDOF system and SDOF counterpart

Properties	***MDOF system***	***SDOF system (Stiffness unchanged)***	***SDOF system (Mass unchanged)***
T (secs)	0.145	0.145	0.145
ξ	0.02	0.02	0.02
$k_{initial}$ (kN/m)	18090	18090	31920
k_{post} (kN/m)	1312	1312	2314
α	0.0725	0.0725	0.0725
$(\Delta_{roof})_y$	4.10	3.0	3.0
V_{by} (kN)	74.2	54.4	95.76
W (tons)	17	9.634	17
V_{by}/W	0.436	0.576	0.574

The effective period of multi story structure was calculated as 0.145 sec due to bilinearization (the calculated natural period of the MDOF system was 0.138 sec). Modal participation factor, PF_1 was calculated as 1.364 assuming the deflected shape as triangular. The effective mass coefficient resulting from the triangular load assumption was calculated as 0.818, leading to the amount of mass mobilized in dynamic action as 0.818W.

The roof displacements calculated using the equivalent SDOF models having bilinear hysteretic behavior is plotted against the exact roof displacements obtained from nonlinear time history analysis of MDOF structure as shown in Fig. 8. For motions that impose large inelastic displacements the equivalent SDOF model underestimates the displacements regardless of the type of ground motion. The response of elastic SDOF system gave better results than the inelastic one in many of the cases.

Although the multistory structure was assumed to respond predominantly in the first mode, in the later stages of nonlinearity the results of SDOF model deviated from the exact displacements, causing significant underestimates of global displacement demand. This can be attributed to the influence of local response as opposed to the global response. Upon yielding at any level, significant ductility demands were imposed on particular sections due to inelastic excursions. It should be noted that this observation contravenes the behavior of frame structures that have reduced roof displacement due to local concentration of inelasticity, such as at a soft story. The inelastic displacement demands computed using the equivalent SDOF systems tend to underestimate the global roof displacement of the structure (Fig. 8.b). A similar trend was observed in linear response history analysis of the MDOF structure (Fig. 6).

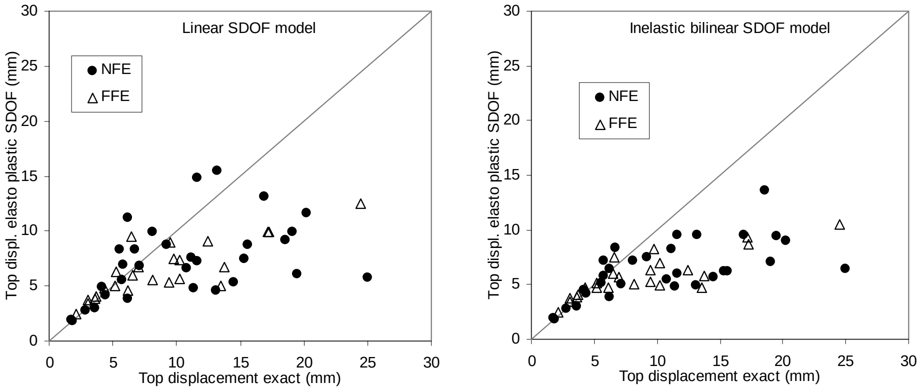

(a) (b)

Figure 8. Comparison of "exact" non-linear and SDOF model results, (a) Linear model (b) Inelastic bilinear model

Capacity Spectrum Method (CSM)

The capacity spectrum method initially characterizes seismic demand using a reduced elastic response spectrum. This spectrum is plotted in ADRS format which allows the demand spectrum to be "overlaid" on the capacity spectrum for the building. The intersection of the demand and capacity, if located in the linear range of the capacity, would define the actual displacement for the structure; however this is not normally the case as most of analyses include some inelastic nonlinear behavior (ATC 40 (1996)).

The Nonlinear Static Procedures in ATC-40 is based on the Capacity Spectrum Method originally developed by Freeman et al. (1975) that uses equivalent linearization. In equivalent linear methods, the inelastic deformation demand of a nonlinear system is approximated by the elastic response of an equivalent elastic SDOF system that has a smaller stiffness and larger damping than the inelastic system.

To locate the point where demand and the capacity are equal, a point on the capacity curve close to the elastic displacement is selected as an initial estimate. Using the spectral acceleration and displacement defined by this point, reduction factors to apply to the 5 percent elastic response spectra to account for the hysteretic energy dissipation, or effective damping, associated with the specific point are calculated. The relationship between effective damping (β_{eff}) and the displacement ductility ratio (μ) adopted by ATC-40 procedure is given in Eq. (4) based on the post elastic stiffness ratio (α) and the hysteretic behavior type factor (κ). If the reduced demand spectrum intersects the capacity spectrum at or near the initial assumed point that point is considered as the solution. If the intersection is not reasonably close to the initial point, then a new point is assumed and the process repeated until a solution is reached. This is the performance point where the capacity of the structure matches the demand for the specific earthquake.

$$\beta_{eff} = 0.05 + \kappa \frac{2(\mu - 1)(1 - \alpha)}{\pi\mu(1 + \alpha\mu - \alpha)} \tag{4}$$

The procedure outlined above was applied to the model structure employed in order to compute its inelastic displacement demands for the set of ground motions considered in this study. The results were distinctively investigated for NFE and FFE records and are compared with the exact values in Fig. 9.a. Although no clear evidence of superiority of one set of results on the other was observed, a relatively better correlation for NFE earthquakes is notable.

A clear outcome is that the Capacity Spectrum Method significantly underestimates the inelastic displacements for both NFE and FFE records when the ductility demand is high. The principal reason for this outcome is the unrealistic reduction in the demand, i.e. reduced elastic response spectrum, owing to exaggerated damping values. The estimated damping value to take into account the inelastic behavior in the system is well above twenty percent in many of the cases. The equal energy principle used in effective damping calculation for CSM can be faulted on two points:

- Derivation of equivalent damping that accounts only for the hysteretic cycle of maximum deformation, neglecting other, smaller amplitude yield excursions leads to high damping ratios as it does not include the reduction in stiffness and strength. The level of maximum deformation cannot alone account for the state of damage occurring in the structure, because the number of excursions and reversals would be parameters for the increased effective damping.
- Nonlinear time history analysis results revealed that the maximum displacement occurs after a few reversals of motion. We cannot attribute the same damage state for the structure prior to maximum excursion and following it, especially for near fault earthquakes where commonly a single pulse causes the one-sided maximum displacement excursion. Reduction of the force on the basis of maximum defor-

mation will in turn reduce the driving forces that cause the maximum deformation.

A possible remedy to overcome this problem would be to use other methods that are based on more realistic assumptions for computing the equivalent viscous damping. The substitute damping (β_S) given in Eq. (5) was proposed by Gülkan and Sözen (1974) to determine the equivalent viscous damping that considers approximately the influence of inelastic excursions. Here, μ is the ductility factor that describes the ratio of maximum displacement excursion to the displacement at the yield.

$$\beta_S = (1 + 10(1 - 1/\sqrt{\mu}))/50 \tag{5}$$

The underlying principle in Eq. (5) is based on the idea that the response of reinforced concrete structures to strong earthquake motions is controlled by two basic phenomena: reduction in stiffness and increase in energy dissipation capacity. Furthermore, the maximum dynamic response of reinforced concrete structures, represented by SDOF systems, can be approximated by linear response analysis using a reduced stiffness and a substitute damping. Substitute damping represents the increase in energy dissipation capacity through the use of Eq. (6).

$$\beta_S \left[2m\omega_o \int_0^t (\dot{u})^2 \, dt \right] = -\int_0^t m \ddot{u}_g \, \dot{u} \, dt \tag{6}$$

Eq. (6) is based on the assumption that the energy input from a ground motion is entirely dissipated by an imaginary viscous damper which has a damping ratio equal to substitute damping. In this equation, β_S is the substitute damping ratio, m is the mass, t is the total duration of response, u_g is the ground acceleration, and $\dot{u}$ is the velocity of the mass. ω_o is equal to the natural frequency of the system with reduced stiffness (Gülkan and Sözen calculated ω_o as the square root of the ratio of maximum absolute acceleration to maximum absolute displacement). We note that Eq. (6) takes into account all inelastic excursions, not only that with the largest amplitude in calculating the equivalent damping coefficient. Equation (5) was incorporated into the algorithm of CSM procedure as described in ATC-40 instead of the equivalent viscous damping to compute the inelastic displacements demands.

The results obtained by substitute damping were superior to those obtained by equivalent damping as shown in Fig. 9.b. This finding emphasizes the significance of the accuracy in calculating the damping used in the CSM. It has been observed that the approximate nonlinear static procedures give better results with near field records of small-to-moderate magnitude earthquakes than the far field ones when the strong motion duration is short and the excitation imposes a few yield excursions on the structure due to pulse like motion. This is so because, if we assume the nonlinear time history of a particular structure to be the combination of responses of different equivalent linear systems that characterize the change of structural stiffness upon yielding and increase in damping because of sustained damage, a structure responding to a pulse-like near-field record of a moderate magnitude earthquake will be more likely to be represented with a *unique* equivalent linear system. A more realistic representation of the equivalent damping would then improve the results further.

A recent document, FEMA 440 (2004), devoted to evaluating existing approximate displacement-based procedures to address their drawbacks proposes a procedure that uses the effective period (T_{eff}) and equivalent viscous damping (β_{eff}) expressions given in Eqs. (7) and (8), respectively, to obtain improved results when applying the CSM procedure. In these equations, the constants A, B, C, D, G, H, I and J depend on the hysteretic model and the post elastic slope of the capacity curve. For the shear wall structure employed here the coefficients are: A=4.61, B=-0.95, C=10.9, D=1.6, G=0.12, H=-0,02, I=0.17 and J=0.12, respectively.

For $\mu < 4.0$:

$$\beta_{eff} = A(\mu - 1)^2 + B(\mu - 1)^3 + \beta_0 \tag{7a}$$

$$T_{eff} = \left[G(\mu - 1)^2 + H(\mu - 1)^3 + 1\right]T_0 \tag{7b}$$

For $4.0 \leq \mu \leq 6.5$:

$$\beta_{eff} = C + D(\mu - 1) + \beta_0 \tag{8a}$$

$$T_{eff} = \left[I + J(\mu - 1) + 1\right]T_0 \tag{8b}$$

The results of the improved procedure are compared with the exact inelastic displacement demands in Fig. 9.c. An immediate observation is that the tendency to underestimate the displacements as the inelasticity increases in the system observed for the conventional CSM procedure is also true for the new procedure.

The findings of our analyses presented here are in conflict with the observations made by other researchers as presented in FEMA 440. Our results are valid for the structure employed here, a stiff multi-story structure with a fundamental period of 0.145 sec, and seems to suggest that CSM in ATC-40, a widely used approximate nonlinear analysis procedure, underestimates the displacement demands. The evaluation of results presented in FEMA 440 and elsewhere (Akkar *et al.* (2000)), however, indicates the opposite trend that for structures with fundamental periods smaller than 0.5 sec the CSM of ATC-40 overestimates the results by a large margin. There might be two main reasons for this inconsistency. The first is that we use an actual stiff structure whereas the FEMA-440 evaluations are based on the SDOF analyses. This, however, seems not to be the case because our SDOF analyses show quite good agreement with the CSM estimates as shown in Fig 10.a. Thus the main reason appears to stem from the solutions of SDOF systems that represent unrealistically stiff structures. The SDOF systems employed in other research programs display unrealistic ductility ratios, as can be observed in Fig. 10.b that presents commonly used relationships for strength reduction factor (R), ductility demand (μ) for a given period (T). At small periods representing stiff structures, the ductility demand of the system increases drastically reaching values in the order of tens which could not be attained by real structures. because of the very small displacements involved. This indicates that for stiff structures SDOF-based evaluations of approximate procedures can be misleading Its simplicity in application notwithstanding, CSM as defined in ATC 40 or FEMA 440 has other drawbacks.

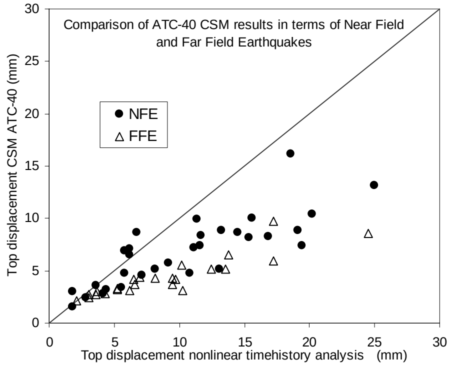

(a) Comparison of top displacement obtained by ATC-40 CSM with the "exact" ones

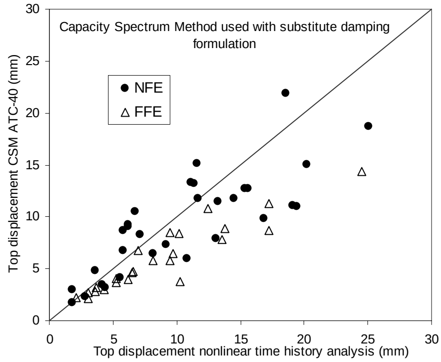

(b) Capacity Spectrum Method with substitute damping

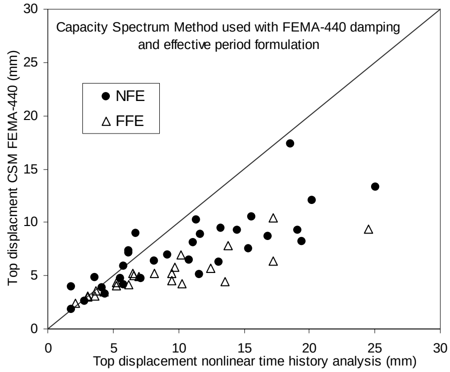

(c) Capacity Spectrum Method with FEMA-440 damping and period formulation

Figure 9. Comparison of CSM results with different effective period and damping

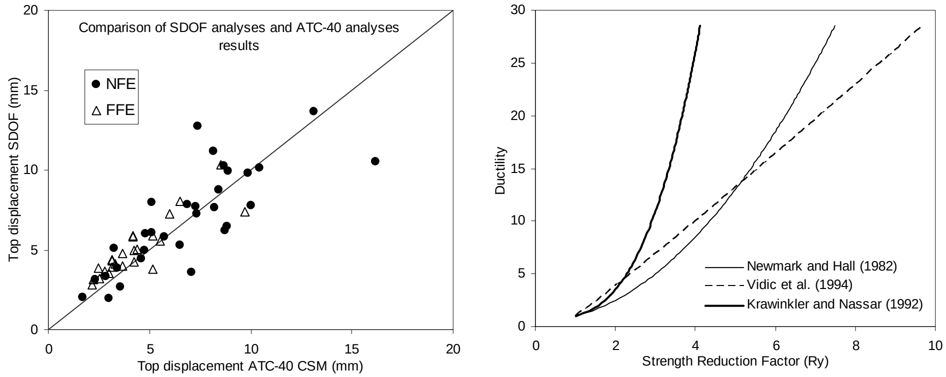

(a) (b)

Figure 10. (a) *Comparison of SDOF model analyses and ATC-40 Capacity Spectrum Method*, (b) *Relationship for strength reduction factor (R) and ductility ratio (μ) for T=0.14 sec*

The most significant of these shortcomings that our analyses have identified are listed as follows:

In the conversion of force-displacement curve to the acceleration-displacement response spectra (ADRS format) the same modal participation factor (PF_1) and modal mass coefficient (α_1), calculated with elastic properties, are used even in the nonlinear range. Both PF_1 and α_1 decrease as the system digresses into the inelastic range.

Excessive damping values different from the customary value of 5 percent cause significant modifications in the shape of the response spectrum. This may change the definition of the spectral regions, masking other features of the ground motion (Akkar *et al.* (2000)). Exaggerated damping values cause great underestimation in the earthquake response spectra demand and this finally results in grossly underestimated target displacements. Upon yielding, for the target displacements very close to yield point unrealistically high effective damping values may be calculated. This represents a great shift in the viscous damping with only a small increment in the inelastic displacement of the structure.

Displacement Coefficient Method (DCM) in FEMA 356

A simpler procedure, the Displacement Coefficient Method, is proposed in FEMA 273/356 (2000) to predict the inelastic displacement demand using the building's capacity curve and the elastic site-specific response spectrum. The displacement demand is calculated using Eq. (9) that takes into account various characteristics of the structure and the ground motion through different adjustment coefficients.

$$\delta_t = C_0\, C_1\, C_2\, C_3\, Sa\, \frac{T_e^2}{4\pi^2}\, g \tag{9}$$

The coefficient C_0 relates the top floor displacement of the structure to the displacement of an equivalent single degree of freedom system (SDOF). C_1 modifies the elastic displacement to obtain the corresponding inelastic displacement. The coefficient C_2 depends on the structural system and varies with the hysteretic behavior. The increase in the displacement demand due to P-Δ effect is taken into account through the coefficient C_3. This approximate procedure is applied to a system that has bilinear capacity curve so the original curves are needed to be idealized which would have an effective fundamental period (T_e).

The DCM was applied to the model structure here to determine its approximate inelastic displacement demand under the ground motion set considered. The "exact" roof displacements compared with results from the DCM are given in Fig. 11. It is observed from the figure that the estimates of roof displacement are improved in comparison to the results of the CSM. The better prediction capacity can be attributed to the coefficients (C_1, C_2 and C_3), that all amplify the response and take into account effects arising from nonlinearity utilized in DCM. However, the dispersion is quite significant, especially for NFE records. The equivalent SDOF solutions presented in Fig. 8.b reveal that the exact inelastic displacement demands are underestimated which is inconsistent with the findings of other research, such as Miranda and Ruiz-Garcia (2002), and FEMA 440. The main reason for the discrepancy arises from the differences in results between the elastic perfectly plastic hysteretic models and bilinear models. The structure we have used has significant post elastic yield stiffness that reduces the inelastic displacement significantly, especially at large displacement ductility demand as compared to elastic perfectly plastic models that are mostly employed by earlier research.

The characteristics of the ground motion set employed as well as the structure considered here exercise significant influence on the observed discrepancies. The wall type structures are too stiff to display large inelastic deformations leading to small ductility ratios and insignificant strength reduction values. Therefore, the inelastic displacement ratios (C_1) based on SDOF solutions appear not to be applicable to the structures with high yield strength capacity similar to that employed here.

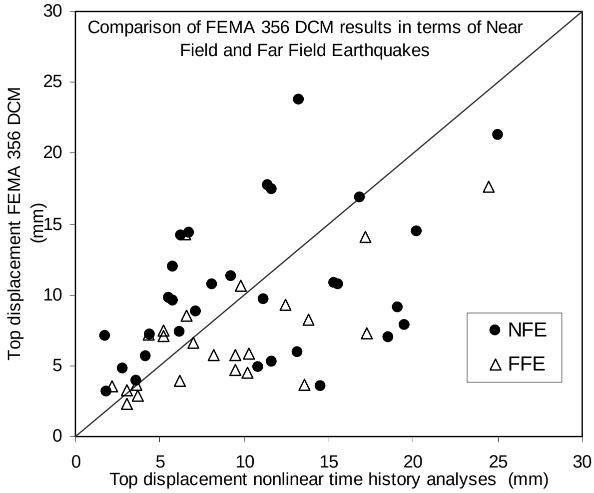

Figure 11. Top displacements obtained from DCM for NF and FF earthquakes.

The accuracy of DCM depends strongly on the system and the ground motion because the coefficients in Eq. (9) are derived from the analyses of SDOF systems that themselves are not uniformly capable of representing adequately the behavior of the MDOF system considered in this investigation as discussed in the preceding sections.

Discussion

The results derived for this particular short-period structural assembly must be carefully interpreted to judge their general applicability. There exists a complex interaction between the types of ground motions used and the response these would generate in the analytical model of a particular test specimen. Our analytical model did not respond exclusively in the inelastic range for all input records, although for most trials it did, so the ductility demand varied from less than 1 to 6. The base motions fell into two groups defined as near- and far-field. It is still instructive to take stock of the performance of all the currently developed approximate approaches toward estimating the top-level translation of the model by comparing them with what would be considered to be "exact" displacement that follows from a general nonlinear analysis. We have been preoccupied with the global displacement because this is the quantity that best correlates with damage potential and performance evaluation. Force quantities such as base shear or overturning moment are supportive of conclusions that are drawn from global displacements, but their interpretation is less straightforward.

Table 2 is the numerical expression of visual information contained in Figs. 6, 8.b, 9 and 11 that consistently have been arranged to differentiate between near- and far-field records.

In a number of trials the elastic yield displacement limit of 4.1 mm was not transcended, so, not surprisingly, linear analysis results match experiments best. The vision provided by the other approaches is reflected better by the deviation than with the mean alone. Entries into this table are the top displacement calculated according to the corresponding approximate method divided by the exact number. We note that refinements in the CSM have indeed improved its accuracy, but for this set of records it is still on the unsafe side.

TABLE 2. Comparison of Displacements

		Elastic range			Inelastic range			Overall		
		FFE	*NFE*	*All*	*FFE*	*NFE*	*All*	*FFE*	*NFE*	*All*
Linear MDOF (Fig. 6)	*Mean*	0.97	0.98	0.98	0.81	0.74	0.77	0.84	0.78	0.81
	St. Deviation	0.39	0.15	0.28	0.38	0.58	0.50	0.37	0.53	0.46
SDOF (Fig. 8.b)	*Mean*	1.09	0.97	1.03	0.59	0.72	0.66	0.69	0.76	0.73
	St. Deviation	0.22	0.19	0.19	0.18	0.47	0.38	0.18	0.44	0.35
CSM ATC40 (Fig. 9.a)	*Mean*	0.85	1.01	0.93	0.50	0.70	0.61	0.57	0.75	0.67
	St. Deviation	0.09	0.39	0.27	0.11	0.44	0.34	0.11	0.43	0.33
CSM subsitute damp. (Fig. 9.b)	*Mean*	0.86	1.12	0.99	0.69	0.96	0.85	0.72	0.99	0.87
	St. Deviation	0.12	0.39	0.27	0.14	0.54	0.42	0.13	0.51	0.39
CSM FEMA 440 (Fig. 9.c)	*Mean*	0.99	1.27	1.13	0.60	0.73	0.68	0.68	0.82	0.76
	St. Deviation	0.10	0.54	0.37	0.16	0.43	0.34	0.15	0.44	0.34
FEMA 273/356 (Fig. 11)	*Mean*	1.05	1.97	1.51	0.90	1.12	1.02	0.93	1.26	1.11
	St. Deviation	0.37	1.16	0.81	0.50	0.74	0.64	0.46	0.80	0.67
Number of ground motions		5	5	10	19	26	45	24	31	55

The scatter in DCM is greatest among all of the methods examined here, and it is the only approach for which the average estimate ratio is greater than unity. The substitute damping ratio used in conjunction with the CSM is the next best performing method. Its prediction falls some 13 percent too low, but has a smaller standard deviation. Surprisingly, a linear approximation shows better average estimation capacity than both of the CSM formulations, but its scatter is large.

Table 3 is similarly arranged for base shear estimates. From here we note that FEMA 440 represents a significant improvement over ATC 40, and the displacement overestimates in FEMA273/356 translate into even larger base shear force overestimates. Interestingly, for the MDOF system considered here, the ratio of the elastic to “exact” inelastic forces is relatively stable at an average value of 1.6. This may be interpreted as the R value for T = 0.14 sec.

TABLE 3. Comparison of Base Shear Forces

		Elastic range			Inelastic range			Overall		
		FFE	*NFE*	*All*	*FFE*	*NFE*	*All*	*FFE*	*NFE*	*All*
Linear MDOF	*Mean*	1.62	1.33	1.48	1.61	1.58	1.59	1.61	1.54	1.57
	St. Deviation	0.56	0.45	0.48	0.65	0.64	0.63	0.62	0.60	0.61
SDOF	*Mean*	1.28	1.13	1.21	0.93	0.86	0.89	1.01	0.90	0.95
	St. Deviation	0.10	0.17	0.13	0.18	0.40	0.32	0.17	0.37	0.30
CSM ATC40	*Mean*	0.95	1.08	1.01	0.74	0.79	0.77	0.78	0.84	0.81
	St. Deviation	0.07	0.15	0.11	0.18	0.30	0.25	0.16	0.28	0.23
CSM subsitute damp.	*Mean*	0.99	1.14	1.07	0.82	0.90	0.87	0.86	0.94	0.90
	St. Deviation	0.10	0.18	0.14	0.11	0.34	0.26	0.10	0.31	0.24
CSM FEMA 440	*Mean*	1.15	1.29	1.22	0.93	0.92	0.92	0.97	0.98	0.98
	St. Deviation	0.07	0.26	0.18	0.17	0.39	0.31	0.15	0.36	0.29
FEMA 273/356	*Mean*	1.66	2.44	2.05	1.58	2.09	1.87	1.59	2.14	1.90
	St. Deviation	0.64	0.74	0.65	0.74	0.83	0.78	0.70	0.81	0.76
Number of ground motions		5	5	10	19	26	45	24	31	55

Conclusions

We believe that the investigation described in this article has displayed the analytical power of computational structural mechanics as applied to the detailed assessment of the dynamic response of a test mockup to strong base motions. It has also served as a reminder that approximate simplified methods that have been developed and refined over the last few decades enable the analyst with some ability to predict the likely limits of displacement response, and by its extrapolation, levels of damage that structural assemblies are likely to experience under a prescribed earthquake. Unlike previous research focusing on SDOF analyses, a comprehensive ground motion data set was used to evaluate the response of an analytical model that is a highly reliable representation of a particular experimental structure. The results obtained from nonlinear time history analyses indicated that short-period structures that are typically used for nuclear facilities respond to both near and far field records in firm soils in similar manner. The top floor displacement that is very commonly used in displacement based performance engineering as a design as well as performance parameter was similar for the same level of far-field and near-field earthquakes.

The equivalent SDOF systems are not adequate in representing the actual performance especially in the region of significant nonlinearity even for systems where elastic response is dominated by the first mode. The procedures such as DCM in FEMA 273 that use coefficients derived from the SDOF analyses must be re-examined before extrapolating their applicability in general.

Among the available approximate procedures implemented here DCM of FEMA-273 yielded the most satisfactory results. The worst predictions were obtained from the CSM in ATC-40, the major reason being the over estimation of the viscous damping leading to severely underestimated displacements. A significant improvement leading to more accurate predictions of the response was achieved when the substitute damping was incorporated into the CSM, although it appears that even smaller damping should be invoked for better prediction.

The results based on SDOF analyses might be misleading for stiff structures that are incapable of exhibiting large inelastic deformations. As other research has also confirmed the SDOF results imply unrealistically large ductility ratios for these structures, but large ductility demand does not translate into large damping ratios.

It has been observed that for stiff structures used for nuclear facilities none of the available approximate displacement based procedures is in its current form appropriate for an assessment of performance. For design purposes where the ground motion is represented by a design spectrum, the DCM of FEMA 273 and CSM in ATC-40 in conjunction with the substitute damping may be used if only the mean response is desired.

Acknowledgements

The investigation presented here has been in part jointly sponsored by the International Atomic Energy Agency and the Joint Research Center of European Commission under grant No. 20788-2003-05 F1ED ISP TR. We owe a debt of gratitude to Vito Renda, Deputy Head of Unit, ELSA-JRC for his continued support. The constructive comments of Dr. Sinan Akkar are gratefully acknowledged. The findings, opinions and conclusions presented in this article are those of the authors, and do not necessarily reflect views of either of the sponsors.

References

Combescure, (2002) D. IAEA CRP-NFE Camus Benchmark: Experimental Results and Specifications to the Participants. *Rapport DM2S, SEMT/EMSI/RT/02-047/A*,.

Kazaz, I., Yakut, A. and Gülkan, P. (2005), Numerical Simulation of Dynamic Shear Wall Tests: A Benchmark Study. Submitted to *Computers and Structures*.

ANSYS Engineering Analysis System (2002), User and Theoretical Manual. ANSYS, Inc. South Pointe, Canonsburg, Pennsylvania, Release 7.0 UP20021010.

Martinez-Pereira, A. and Bommer, J. J. (1998), What is the Near-field?. *In Seismic Design Practice into the Next Century*, 245-252, eds. Booth, E., Balkema.

Anderson, J.C. and Bertero, V.V. (1987), Uncertainties in Establishing Design Earthquakes. *Journal of Structural Engineering*, ASCE 113(8), 1709-1724.

ATC 40 (1996), Seismic Evaluation and Retrofit of Concrete Buildings, Volume 1; *Applied Technology Council*, California Seismic Safety Commission.

FEMA 356 (2000), Pre-standard and Commentary for the Seismic Rehabilitation of Buildings; *Federal Emergency Management Agency*, Washington, D.C.

Miranda, E. (2001), Estimation of Inelastic Deformation Demands of SDOF Systems. *Journal of Structural Engineering*, ASCE 127(9), 1005-1012.

Miranda, E., Akkar, D. S. and Ruiz-Garcia, (2002), J. ATC-55: Summary of Evaluation of Current Nonlinear Static Procedures-SDOF Studies; *Applied Technology Council*, California Seismic Safety Commission.

Chopra, A. K., Goel, R. K. and Chintanapakdee, C. (2003), Statistics of Single-Degree-of-Freedom Estimate of Displacement for Pushover Analysis of Buildings. *Journal of Structural Engineering*, ASCE 129(4), 459-469.

Chintanapakdee, C. and Chopra, A. K. (2003), Evaluation of Modal Pushover Analysis Using Generic Frames. *Earthquake Engineering & Structural Dynamics*, 32, 417–442.

Chopra, A. K. (2000), Dynamics of Structures: Theory and Application to Earthquake Engineering; 2nd edn., Prentice-Hall, New York.

Freeman, S. A., Nicoletti, J. P., and Tyrell, J.V. (1975), Evaluations of Existing Buildings for Seismic Risk: A case study of Puget Sound Naval Shipyard, Bremerton. Proceedings of First U.S. NCEE, EERI, Berkeley, Washington, 113-122.

Gülkan, P. and Sözen, M., A. (1974), Inelastic Response of Reinforced Concrete Structures to Earthquake Motions. *ACI Journal*, December, 604-610.

FEMA 440 (2004), Improvement of nonlinear static seismic analysis procedures, Draft Camera-Ready. *Applied Technology Council*, California Seismic Safety Commission.

Akkar , S. D. and Miranda, E. (2005), Statistical Evaluation of Approximate Methods for Estimating Maximum Deformation Demands on Existing Structures. *Journal of Structural Engineering*, ASCE 131(1), 160-172.

Akkar, S. D. and Gülkan, P. (2000), Comparative Performance Evaluation of Displacement Based Design Procedures for Near Field Earthquakes, *12th World Conference on Earthquake Engineering*, Auckland, New Zealand, Paper No. 0444.

Miranda, E. and Ruiz-Garcia, J. (2002), Evaluation of Approximate Methods to Estimate Maximum Inelastic Displacement Demands. *Earthquake Engineering and Structural Dynamics*, 31(3): 539-560

Newmark, N. M. and Hall, W. J. (1982), Earthquake Spectra and Design. EERI, Berkeley, CA.

Vidic, T., Fajfar, P. and Fischinger, M. (1994), Consistent Inelastic Design Spectra: Strength and Displacement. *Earthquake Engineering and Structural Dynamics*, 23(5) 507-521.

Nassar A.A. and Krawinkler H. (1991), Seismic Demands for SDOF and MDOF Systems. *Report No.95*, John A. Blume Earthquake Engineering Center, Stanford University.

Ernesto Heredia Zavoni

Investigador
Instituto Mexicano del Petróleo
Eje Central 152, México DF 07730
eheredia@imp.mx

Risk analysis, structural reliability, random vibrations, offshore engineering, earthquake engineering

I feel a lot fortunate to have met and worked with Prof. Luis Esteva. About a year after I had graduated from Princeton, I initiated a series of collaborations with him at the Instituto de Ingenieria at UNAM, where I had started working under an invitation by the late Prof. Emilio Rosenblueth. From the first time I had an interview with Prof. Esteva in his office, to start discussing a joint project, he struck me with his sound academic knowledge and clear thoughts. However it was the feeling that I had met an extraordinarily humble and witty man, with a refined sense of humor, what impressed me the most at that time. Over the years that followed since our first meeting, I got to know Luis closely and became a friend of his. We developed research projects together focusing on life cycle risk analysis of structures in seismic environments, with emphasis on probabilistic modeling of deterioration and maintenance strategies. I remember the flavor of being enriched by someone who could propose ingenious ideas for facing research challenges and solve technical problems, and who could at the same time welcome one with warmth and transfer into one a great deal of enthusiasm about ones own work. He has certainly been a source of inspiration and motivation. Some of the seminal ideas we had a chance to discuss helped set the framework for developing my career later on at the Mexican Petroleum Institute. My family has had the honor to enjoy his company as well and he is included in our memories of some important family events. When it comes to Luis, I can only think of friendship, honesty, sharing and ethics. If, on top of that, we consider his knowledge, experience, smartness, humbleness, and his love and passion for music, we are before someone who can certainly be reckoned in history as a great human fellow. I can only thank having been around him and for sure having had the opportunity to express my gratitude to him.

Ernesto Heredia Zavoni,
August 25, 2005

James O. Jirsa
Professor
Department of Civil Engineering
University of Texas at Austin
Austin, Texas 78712
Jirsa@uts.cc.utexas.edu

Design and behavior of reinforced concrete structure, earthquake engineering, rehabilitation of structures

Luis, I am pleased to have the opportunity to participate in this symposium honoring your achievements. You have devoted your career to improving our understanding of the hazards that we face in seismic zones. I have always appreciated your calm demeanor, infectious smile, and good humor; just as I have the intensity of your desire to make the world a safer place for people who must live with natural disasters.

Your leadership in the earthquake engineering community in Mexico City, in the Americas, and worldwide have brought great distinction to you and your Mexican colleagues and you have been a steady voice during times of stress and distress. I have always been grateful for the assistance you provided following the 1985 earthquake when I and others from the University of Texas came to study the aftermath of that earthquake. For us it was a wonderful learning experience—and probably the closest to Texas that we will ever see. I know it was a time when you were totally occupied with duties related to recovery following the earthquake but you and your colleagues took the time to greet and brief us and to make the visit productive.

Earthquake engineering is a field where there are no boundaries or limits to the exchange of information and knowledge. We learn together or we fail together. You have been a great proponent for the exchange of ideas to reach our goals. You are a role mode *par excellence*, a good friend, and a valued colleague. Congratulations on this occasion and on all that you have achieved.

Jim Jirsa
26 August 2005

CHALLENGES IN SEISMIC REHABILITATION OF STRUCTURES

ABSTRACT

There are few problems in earthquake engineering that are more complex than those associated with understanding the performance of existing buildings and determining how that performance can be improved to mitigate damage and loss of life in future earthquakes. The objective of this presentation is to describe some of the lessons learned from the Mexico City experience, to review some of the research that has been done, and to discuss the challenges that lie ahead.

Introduction

The 1985 Mexico City earthquake provided the impetus for studies of rehabilitation techniques that would reduce the risk posed by existing buildings. The development of design guidelines and updating of such documents is usually accomplished through a combination of laboratory studies and field experience. Furthermore, the issues are not easily studied in parts or in small scale because of the complexity of the interactions between different elements of the existing structure and between the existing structure and new elements added during rehabilitation. The variety of different situations is immense. As a result, one of the best sources of information for understanding the behavior of existing structures before or after rehabilitation is reconnaissance studies after an earthquake occurs. The lessons learned in Mexico City have been repeated in other mega-cities located in regions of high seismicity.

In rehabilitation design, the structural engineer is faced with selecting an option that will correct the deficiencies in the building and satisfy the owner of the structure and the local building officials. In some cases, the existing lateral force-resisting elements may be so difficult and expensive to modify that new alternate lateral load-carrying elements are introduced into the structure. To accomplish the task facing the designer, knowledge of building performance both from field reconnaissance and from laboratory studies is needed. Much can be learned from an understanding of the rehabilitation techniques implemented by others. In this regard, Mexico City after 1985 is a rich source of information.

Overview of Building Damage from 1985 Earthquake

Most of the buildings damaged during the 1985 earthquake were located in the lake bed zone. Another important characteristic was the almost harmonic motion registered in the lake zone and the high energy content at periods greater than one second. The duration of strong motion between about 40 and 70 seconds and the harmonic characteristics of the ground motion created significant ductility demands on buildings and increased both the extent and level of damage (Fundacion ICA, 1988). Many engineered buildings that were seriously damaged during the 1985 earthquake were medium height, reinforced concrete buildings (6 to 15 floors) that had natural periods close to period of the dominant ground motion. The dynamic response of these moment-resisting frame structures was greatly amplified. Buildings with masonry bearing walls performed quite well during the earthquake. Bearing wall buildings were generally less than 5 stories high and were much stiffer than framed buildings of comparable height.

In Table1, information on 379 buildings that partially or completely collapsed or were severely damaged during the 1985 earthquake is summarized (Iglesias and Aguilar 1988). The buildings are listed according to structural type and number of stories. Concrete buildings represent 86% of the total, 47% were built between 1957 and 1976, and 21% were built after 1976. Damage was concentrated in buildings with 6 to 15 stories and most of these mid-rise buildings were concrete structures.

TABLE 1. Summary of Damage

TYPE OF STRUCTURE	EXTENT OF DAMAGE	NUMBER OF STORIES				TOTAL
		<5	6-10	11-15	>15	
R/C Frames	Collapse Severe	37 23	47 62	9 14	0 0	93 99
R/C Frames & Shear Walls	Collapse Severe	0 2	1 1	0 2	0 1	1 6
Waffle Slab	Collapse Severe	20 6	31 33	6 19	0 1	57 59
Waffle Slab & Shear Walls	Collapse Severe	0 0	0 2	0 3	0 0	0 5
R/C Frames & Beam-Block Slab	Collapse Severe	3 0	0 1	0 2	0 2	3 5
Steel Frames	Collapse Severe	6 0	1 2	3 1	1 3	10 6
Masonry Bearing Walls	Collapse Severe	8 19	0 1	1 1	0 0	9 21
Masonry B. Walls with R/C Frames in Lower Stories	Collapse Severe	1 3	0 1	0 0	0 0	1 4
TOTAL	Collapse and Severe	128	183	61	7	379

The main modes of failure that were observed in the 1985 earthquake are listed in Table 2. The results were obtained from a survey of 331 buildings in the most affected zone in Mexico City that represented the majority of severely damaged or collapsed buildings (Meli 1987).

Structural configuration problems were a major cause of failure. Most configuration problems were associated with the contribution of non-structural elements to the building response. Of the buildings that suffered collapse or severe damage, 42 percent were corner buildings (Rosenblueth and Meli, 1986). Changes in stiffness or mass over the height of the building also were a contributing factor. Changes in stiffness were due to drastic changes in the structural configuration or changes in the size or the longitudinal and transverse reinforcement in columns, or to the location and number of infill walls. Abrupt mass changes resulted from floor dead loadings which were

TABLE 2 Type of Damage (Meli, 1987)

MODE OF FAILURE OBSERVED	% OF CASES
Shear in columns	16
Eccentric compression in columns	11
Unidentified type of failure in columns	16
Shear in beams	9
Shear in waffle slab	9
Bending in beams	2
Beam-column joint	8
Shear and bending in shear walls	1.5
Other sources	7
Not possible to identify	25

considerably greater than that for which the building had been designed originally. Building pounding was quite common during the 1985 earthquake because of the proximity of adjacent buildings. Much of the column damage can be attributed to pounding especially when the slab levels of two adjacent buildings did not coincide.

It should be noted that these lessons had been learned in previous earthquakes elsewhere in the world and they have been relearned since 1985. Why we continue to see the same problems may be the result of paying insufficient attention to observations from previous earthquakes, political and financial constraints that limit the implementation of new techniques and new codes, or a lack of data on which to base decisions that would lead to a reduction in losses.

Features of Rehabilitation Techniques Used in Mexico City

A report on the rehabilitation work in Mexico City and details of 12 case studies in which different techniques were used was prepared by a team of US and Mexican engineers (Aguilar, et al, 1996; Brena 1990; Iglesias, et al, 1988; Teran, 1988).

Modification of Existing Elements

In Mexico City, concrete jacketing was the most common technique used to increase stiffness and ductility as well as the axial, flexural, and shear strength of existing elements. To develop yield in the longitudinal bars, continuity had to be provided at the ends of the element. For columns this was done by extending bars through the slabs as shown in Figure 1. For beams, the reinforcement was extended through the column core or was bent around the original column. In most cases, the jackets consisted of angles at the corners with straps welded to provide a continuous hoop around the column as shown in the Figure 1.

In many structures, material was added to increase the size of frame elements that were damaged or that had inadequate strength for design lateral loads. To obtain

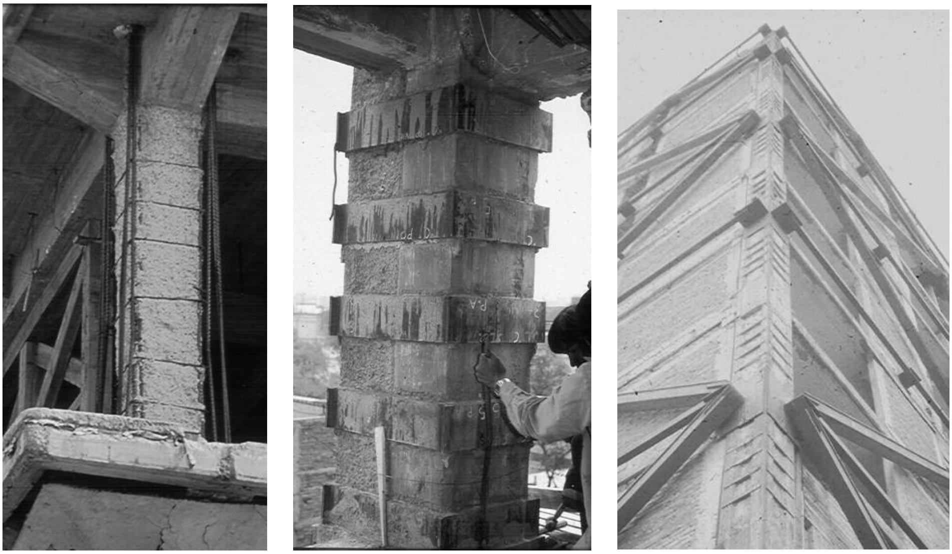

Figure 1. Examples of column jacketing

Figure 2. Jacketing of moment-resisting frame

monolithic behavior, the existing material surface was prepared by roughening the old concrete surface and using epoxy grouted dowels embedded in the concrete interface.

Because the lake zone has such difficult soil conditions, many structures were rehabilitated with beam and column jackets to strengthen the existing moment-resisting frame (Figure 2) and avoiding costly modifications to the foundation.

Addition of new walls

Concrete shear walls were used to eliminate stiffness eccentricities in a building or to increase lateral load carrying capacity. The new walls were located in the perimeter of the structure thereby reducing interior interference. Wall reinforcement was made

Figure 3. Addition of wall.

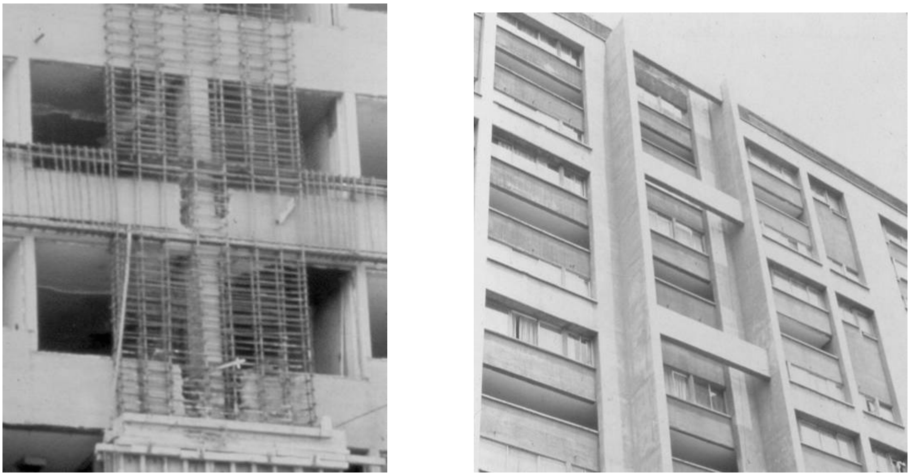

Figure 4. Addition of distributed wall elements.

continuous over the height of the building. Holes were bored into the slab to allow continuity of longitudinal reinforcement, improve the force transfer between the wall and the slab, and allow better concrete compaction near the wall-slab interface. If there were beams in the perimeter frames, the walls had to be offset to pass the longitudinal reinforcement. Structural wall were attached to existing columns whenever possible so that gravity forces would reduce the uplift generated at the ends of the wall due to overturning moments as lateral loads increased. Distributed wall elements provided increased lateral capacity but did not result in large forces applied to the foundation as would the long walls shown in at the left of Figure 3. The addition of new “wing wall” elements to a moment resisting frame can be seen in Figure 4. .

Addition of steel braces

The key feature of this technique was anchorage of steel elements to the existing concrete structure. In some cases, braces were welded to collars or steel jackets that

Figure 5. Steel bracing systems

surrounded the columns. Steel column jackets provided also provide additional column capacity to resist the vertical forces generated by the steel braces. In other cases, steel elements located in the perimeter frames were fixed using anchors into the concrete or through bolts clamp the brace against the exterior face of columns floor beams. Infill braces were used when the existing beams and columns had adequate shear capacity to resist the lateral forces induced by the braces. In Figure 5, several steel bracing systems are shown.

Addition of Cable Bracing

Tension braces or cables were used to eliminate the problems associated with inelastic buckling of bracing systems and to take advantage of the original structure with minimal modifications. In many cases the axial loads generated by the cables required that columns be strengthened by one of the techniques described previously.

Research on Rehabilitation Techniques

The most common deficiencies in existing reinforced concrete structures tend to be related to detailing of transverse reinforcement, continuity of primary reinforcement, and cross-sectional area of lateral force-compression resisting elements. In some cases, the deficiency is the result of changes in design codes that require larger lateral force resistance and more ductility at critical locations where hinges are expected to form, and in other cases the deficiency may be due to errors in construction, changes made by owners or tenants that have reduced the lateral capacity or ductility of the structure, or by changes in the occupancy of the structure that result in higher loads on the system. To provide data for use in developing design guidelines for rehabilitation, an extensive research effort was carried out in the US. Although, work was underway prior to the 1985 earthquake, the Mexico City experience resulted in an acceleration of the research activity. A brief outline of that research follows.


Figure 6. Cable bracing systems


Figure 7. Test frame with strong beams and weak columns and strengthening with wing walls

Column Jacketing for Weak Column-Strong Beam Frames

Wing walls

One of the most common types of existing systems in the US are those that have weak column-strong beam frames. The columns have inadequate shear capacity to develop column hinges and brittle shear failures occur. The weak column system has been a key feature in much of the research conducted in the past 25 years at the University of Texas in collaboration with Degenkolb Engineers in San Francisco. A 3 story-2 bay frame was strengthened using "wing walls" as shown in Fig. 7 (Bush, *et al.*1990).

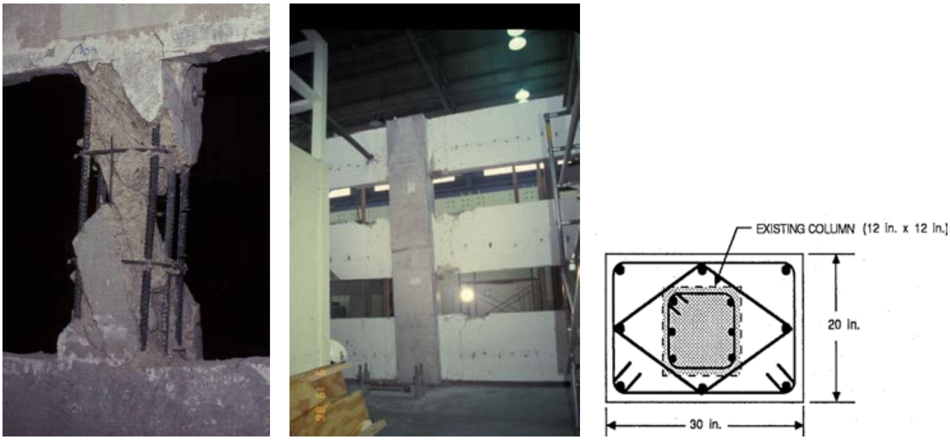

Figure 8a. Damaged existing column encased in new section

Jacketing of Damaged Column

In Figure 8a, the cross section of a severely damaged column in the frame structure is shown. The damaged columns were jacketed and the frame was retested. The damaged concrete in the existing column had little effect on the calculated strength of the column assuming that the section was monolithic (Stoppenhagen, et al, 1995).

Shotcrete or Cast-in-Place Jackets to Improve Shear of Ductility

Another technique that was studied was retrofitting weak columns with concrete jackets. Figure 8b shows a column jacketed with shotcrete over a new cage of reinforcement to provide added confinement and shear capacity (Bett, *et al.* 1988). A series of beam-column joints (shown on the right in Figure 8b) was tested at the University of Texas as part of a joint CONACYT/NSF research effort (Alcocer and Jirsa, 1993).

Steel Jackets for Improving Splice or Anchorage Capacities

In some existing structures, a major deficiency is the lack of sufficient anchorage or splice length at critical locations, such as the bottom of a column where a splice is located for facilitating construction. In many older structures, the splice was designed for compression only. However, when the structure is subjected to ground motions, the splices may be at a location where flexural hinging develops. The compression splice can not develop tension and a premature failure occurs at that location. Such details are not easily corrected using concrete jackets. A series of tests was conducted using steel jackets to improve the confinement in the hinging region and the splice strength (Aboutaha, *et al.* 1996, 1999-1). These splices also become critical if the column in which they are located is part of the boundary element for new infill or structural walls. Confinement is excellent near the corners where the steel plates are connected but the efficiency of the steel plates reduces as the distance from the corner increases. To improve the confinement away from the corners, some plates were anchored as shown in Figure 9.

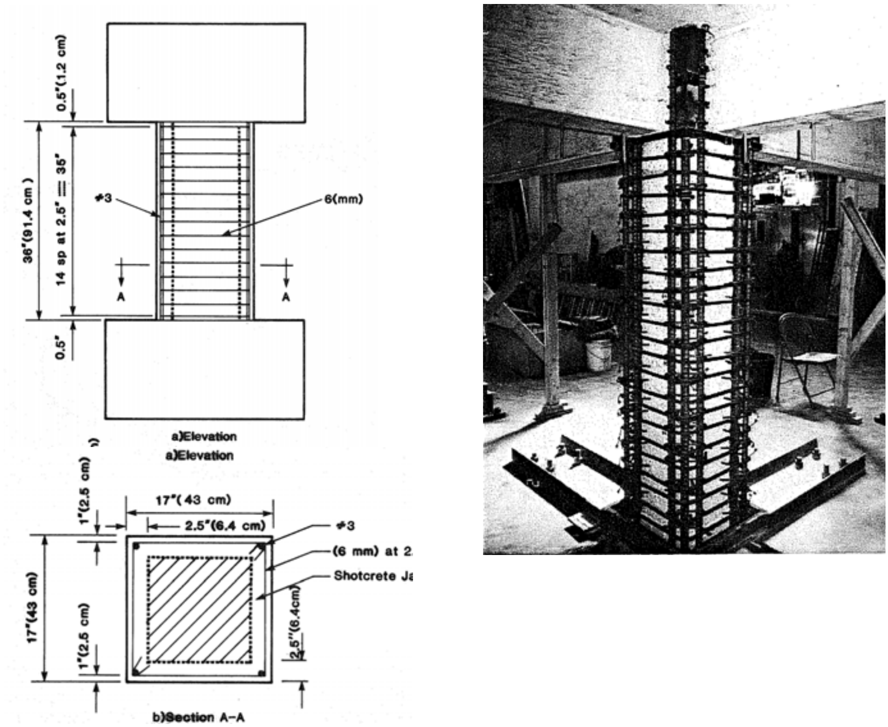

Figure 8b. Column jackets

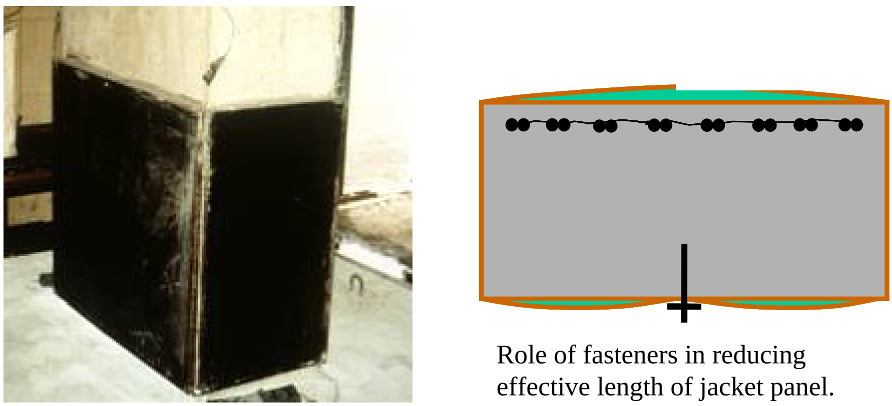

Figure 9. Steel jacket to improve splice capacity

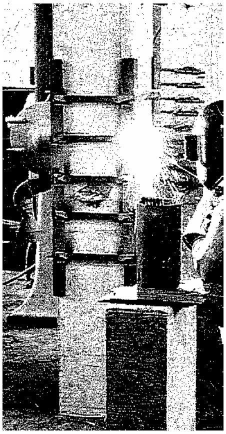

a) Welded straps and angles

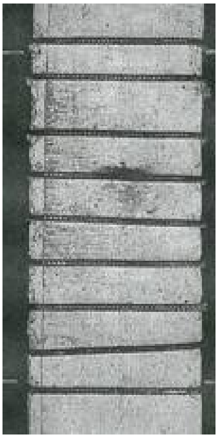

b) External ties

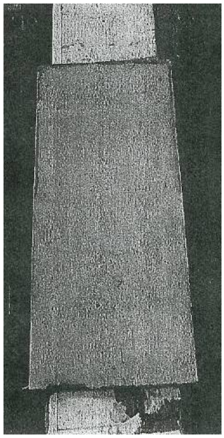

c) Grouted external ties

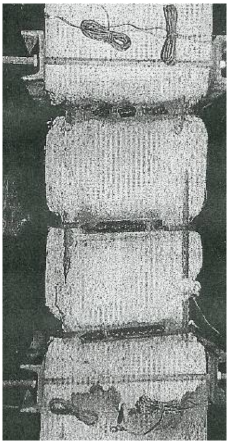

d) Cover removed for new ties

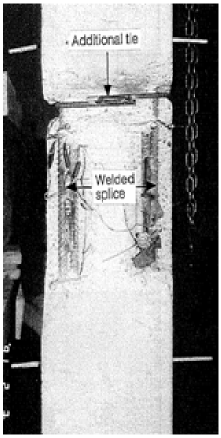

e) Welded splices

Figure 10. Confinement added along splice length

Confinement of Splices Using Plates or Reinforcing Bars

Another series of specimens with inadequate splice lengths was tested to determine the effectiveness of several other details shown in Figure 10 for providing confinement (Valluvan, *et al.* 1993). The section contained four longitudinal bars, one in each corner.

Steel jackets for improving shear capacity of columns

A series of tests was conducted to study the effectiveness of steel jackets for strengthening shear deficient columns (Aboutaha *et al.* 1999-2).

Addition Of Structural Walls

Shotcrete or cast-in-place infill walls

One of the simplest schemes for strengthening a structure is to remove existing non-structural infill walls and replace them with reinforced concrete walls that are well connected to the existing frame. The use of shotcrete provides a way of placing the material without the need for concrete formwork and also eliminates the problem with consolidating concrete against the bottom of the beams or floor (Jirsa 1996). Three shotcrete infill walls were tested—one solid wall, one with a window, and one with a door opening (left side in Figure 11). In addition two cast in place walls were tested—one with a door and one with a new wall cast against the existing frame rather than as an infill (right side of Figure 11). By facing the wall on the columns the wall bypasses the frame and makes the process somewhat easier to realize in field applications.

Figure 11. Frames prior to application of shotcrete or cast-in-place infill wall

Studies were carried out to determine the factors that influence shear transfer between new concrete cast against an existing concrete surface. The variables at the interface included the number and spacing of bars crossing the interface, the roughness of the interface, interface material (fresh concrete cast against existing concrete, gap filled with dry pack material, epoxy), and position of casting (horizontal, vertical, or overhead). The results of these tests are reported in Bass *et al.* 1989.

Precast Panel Infill Walls

In order to minimize the amount of concrete that must be cast-in-place when new walls or infills are added to an existing structure, a scheme using precast panels was designed and tested (Frosch *et al.* 1996). The concept was investigated with a two-story test specimen shown in Fig. 12. The arrangement of the precast panels is shown. The panels had keyed edges to improve shear transfer and the grouted joints between panels contained continuous vertical and horizontal wall reinforcement. Vertical post-tensioning tendons were installed at the ends of the walls near the columns to provide tensile capacity for the columns that had inadequate splice lengths.

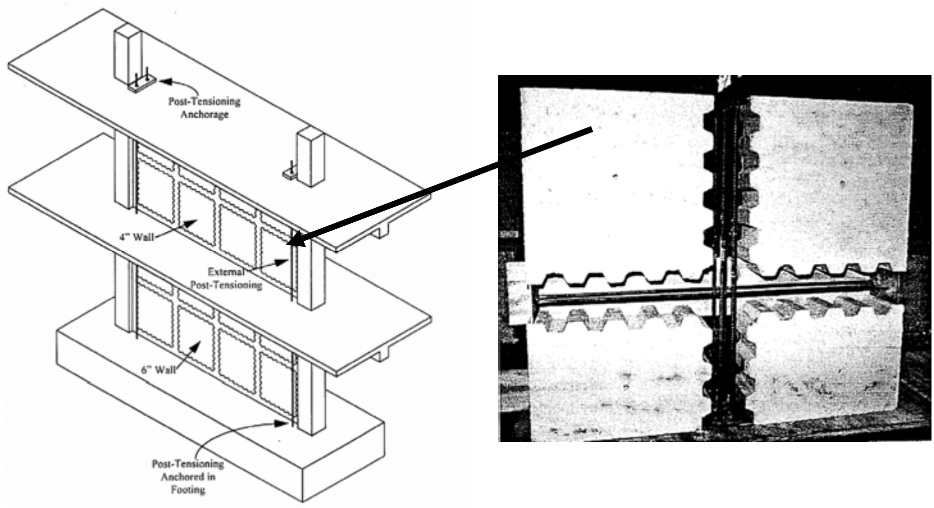

Figure 12. Precast,post-tensioned infill wall system

Observations

The purpose of the tests discussed above was to provide details that would allow desirable mechanisms of failure to develop in existing buildings—flexural hinging if possible. In order to accomplish this objective, the tests indicated that it is essential to provide the following conditions:

- Members must be adequately confined to prevent concrete crushing failures at regions of high moment or compression.
- Primary flexural reinforcement must be continuous or spliced adequately to allow the reinforcement to yield.
- Transverse reinforcement or external jackets must be provided to prevent shear failure before flexural hinging develops.
- The transfer of forces between new and existing concrete surfaces must be sufficient to prevent excessive slip from developing along the interface and to permit the elements that are made up of both new and old concrete to be designed as monolithic sections.

Future Challenges

For a twenty-year period, a great deal of experimental research was conducted that led to the development of guidelines that are now used for the evaluation of existing buildings. However, the limitations of that research are apparent as designers attempt to implement those guidelines. More research is needed and the cost of that research will be much higher than before because large-scale test assemblies or portions of structures will need to be tested. There is a need for tests of structures in-situ because we need to understand better structure-foundation-soil interactions and using existing materials. As a profession we must define research programs that will capture the imagination of political leaders in an era of major research expenditures for biomedical studies, nanotechnology, space exploration, and environmental concerns. Unlike many fields, the civil engineering and infrastructure field has no dominant industries. It is a very diverse industry with many competing elements and no strategic plan.

One of the problems we face is that overall spending for research in the US is not increasing in real dollars. Research budgets have stagnated in the face of increasing needs and higher costs. The problem is illustrated in Figure 13. In view of the trends shown, it will be necessary for our profession to articulate a vision of the future as influenced by civil engineers that is so compelling that the public will call on our leaders in government and industry to do something. In fact, this is what happens after major disasters or crises when funding flows to address problems whose solution is seen as essential to society. The increase in earthquake engineering research following major events (generally defined by the number of lives lost) is an example of such a reaction. If we want to compete with our colleagues in the sciences and medicine for the shrinking funding pool, we must become as proactive and creative as they have been.

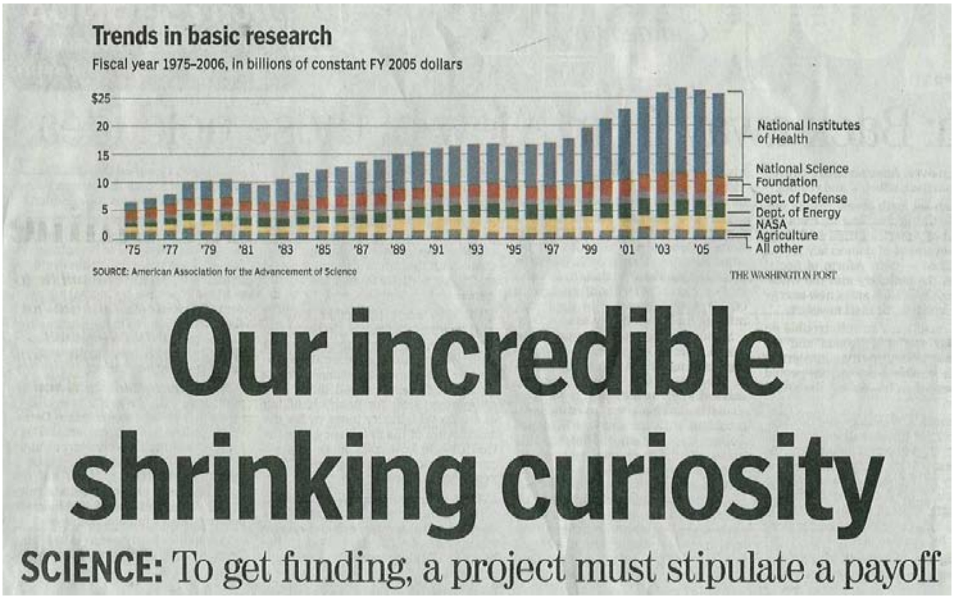

Figure 13. Research Expenditures in the US from 1975 to 2006[*]

However, in many of our universities and engineering programs, declining civil engineering

Enrollments are an indication that civil engineering is a mature field and that little new is happening. As a result, funding is diverted from civil engineering to rapidly growing fields such as communication or information technology and biomedical engineering. But as the world's population expands, the demand for more extensive

[*] From an article in the Austin American Statesman, May 1, 2005 written by Rick Weiss of the Washington Post

and complex civil infrastructure, clean environment, and mitigation of the effects of natural hazards in the world's mega-cities will not diminish and civil engineering must play an essential role in addressing those issues.

Concluding Remarks

I hope that our celebration of the accomplishments of Prof. Luis Esteva will stimulate us to get involved to determine our future rather than to sit by and let others determine it. I believe that society values our contributions and holds civil engineers in fairly high esteem. As earthquake specialists, we have an opportunity to build on the exchanges of knowledge that are routine in our field and make the world more livable and safer.

Acknolwedgements

Without the help and friendship of many colleagues from Mexico, it would not have been possible to compile information on buildings that were damaged and/or rehabilitated in Mexico City. Special thanks to Jesus Iglesias, Roberto Meli, and Enrique del Valle for their assistance in the research that followed the 1985 earthquake. Finally, I would like to express my appreciation to the many graduate students whose efforts made the research described in the paper a reality.

References

Aboutaha, R., Engelhardt, M.D., Jirsa, J.O., and Kreger, M.E. (1996). Seismic Retrofit of R/C Columns Using Steel Jackets, *ACI* SP-160, Seismic Rehabilitation of Concrete Structures, pp. 59-72.

Aboutaha, R.S., Engelhardt, M.D., Jirsa, J.O., and Kreger, M.E (1999-1). Rehabilitation of Shear Critical Concrete Columns by Use of Rectangular Steel Jackets, *ACI Structural Journal* 96 (1), American Concrete, pp. 68-78.

Aboutaha, R.S., Engelhardt, M.D., Jirsa, J.O., and Kreger, M.E. (1999-2). Rehabilitation of Shear Critical Concrete Columns by Use of Rectangular Steel Jackets, *ACI Structural Journal* 96 (1), pp. 68-78.

Aguilar, J., Brena, S. F., del Valle, E., Iglesias, J., Picado, M., Jara, M., Jirsa, J. O., (1996). Rehabilitation of existing reinforced concrete buildings in Mexico City: Case studies, PMFSEL Report 96-3, University of Texas at Austin.

Alcocer, S.M., and Jirsa, J.O. (1993). Strength of Reinforced Concrete Frame Connections Rehabilitated by Jacketing, *ACI Structural Journal* 90 (3).

Bass, R.A., Carrasquillo, R.L., and Jirsa, J.O. (1989). Shear Transfer Across Concrete Interfaces, *ACI Structures Journal* 86 (4), pp. 383-393.

Bett, B.J., Klingner, R.E., and Jirsa, J.O. (1988). Lateral Load Response of Strengthened and Repaired RC Columns, *ACI Structural Journal* 85 (5), pp. 499-508.

Breña, S. F. (1990), An overview of rehabilitation techniques used in reinforced concrete buildings in Mexico City, Thesis, Master of Science in Engineering, The University of Texas at Austin, December.

Bush, T., Talton, C. Roach, and Jirsa, J.O. (1990). Behavior of a Structure Strengthened Using Reinforced Concrete Piers, *ACI Structural Journal* 87 (5), pp. 557-563.

Frosch, R.J., Li, W., Jirsa, J.O., and Kreger, M.E. (1996). Retrofit of Non-Ductile Moment-Resisting Frames Using Precast Infill Wall Panels, *Earthquake Spectra* 12 (4).

Fundacion ICA, A.C., (1988). Experiencias derivadas de los sismos de septiembre de 1985, Limusa, Mexico, D.F.

Iglesias, J. and Aguilar, J., (1988). Identificación de daños ocasionados por los sismos de 1985, 1979 y 1957 en la Zona Metropolitana, Estudios de Sismicidad en el Valle de Mexico, *3a Parte, Capitulo III, Anexos I and II, Departamento del Distrito Federal and Centro de las Naciones Unidas para los Asentamientos Humanos* (HABITAT), Mexico, D.F.

Iglesias, J., Robles, F., De La Cera, J. and Gonzalez, O., (1988). Reparación de estructuras de concreto y mamposteria, Universidad Autónoma Metropolitana, Mexico, D.F.

Jirsa, J.O. (1992). Response of Frame-Infill Wall Structures, Transactions of Workshop on Non-Linear Seismic Analysis of Reinforced Concrete Buildings, Bled Slovenia, July.

Meli, R., (1987). Evaluation of performance of concrete buildings damaged by the September 19, 1985 Mexico Earthquake; *The Mexico Earthquakes-1985: Factors Involved and Lessons Learned*, ASCE, pp. 308-327.

Rosenblueth, E. and Meli, R., (1986). The 1985 Earthquake: Causes and effects in Mexico City, *Concrete International*, May, pp. 23-34.

Rosenblueth, E., Emergency regulations and the new building code, *The Mexico Earthquakes-1985: Factors Involved and Lessons Learned*, *ASCE Special Publication*.

Stoppenhagen, D. R., Jirsa, J. O., and Wyllie, Jr., L. A. (1995). Seismic Repair and Strengthening of a Severely Damaged Concrete Frame," *ACI Structural Journal* 92 (3), pp 177-197.

Teran, A., (1988), Review of repair techniques for earthquake damaged reinforced concrete buildings, Thesis, Master of Science in Engineering, The University of Texas at Austin, December.

Valluvan, R., Kreger, M.E., Jirsa, J.O. (1993), "Strengthening of Column Splices for Seismic Retrofit of Non-ductile RC Frames," *ACI Structural Journal* 90 (4), American Concrete Institute.

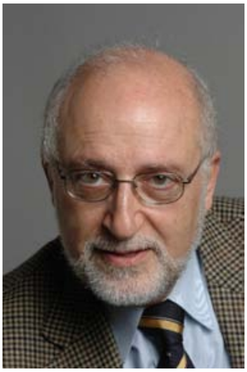

Armen Der Kiureghian
Taisei Professor of Civil Engineering
University of California
723 Davis Hall, Berkeley, CA 94720
adk@ce.Berkeley.edu

Structural reliability, risk analysis, stochastic dynamics, earthquake engineering.

I first came to know of Luis Esteva in 1974, while a doctoral student at the University of Illinois at Urbana-Champaign. My interest in probabilistic methods had led me to the seminal paper by Rosenblueth and Esteva in 1972, which was the first to propose a code format based on the lognormal distribution – a format that is now omnipresent in many established or proposed probabilistic design procedures. At the time, Luis Esteva was a towering figure in my imagination, distant and unapproachable. It was not until 1980 that I met him personally at the 7th World Conference in Earthquake Engineering in Istanbul, Turkey. The meeting was an eye opener: not only Professor Esteva was not a "towering" figure, he was undeniably friendly, approachable and kind. I do not remember when it was that I dared to drop the "Professor" title when addressing him, but his gentle and friendly attitude had a lot to do with it. Over the years I have enjoyed the pleasure of his company on many occasions, and have learned a lot from his papers and comments. The magnitude of his research accomplishments and service to the profession, the depth of his knowledge in probabilistic methods and earthquake engineering, and the breadth of his general knowledge are truly amazing. But what is even more significant is his humility, his ability to encourage young researchers, and, above all, his gentleness. In my imagination now, Luis Esteva is the quintessential Mexican gentleman and scholar.

Armen Der Kiureghian
August 10, 2005

PROBABILITY CONCEPTS FOR PERFORMANCE-BASED EARTHQUAKE ENGINEERING

ABSTRACT

A framework formula for performance-based earthquake engineering has been proposed by the Pacific Earthquake Engineering Research Center (PEER). This paper addresses two aspects of that formula. One deals with the probabilistic information that one can obtain from the result of this formula, which is expressed in terms of the mean annual frequency of an earthquake effect exceeding a specified threshold. The other critically examines the predominant method for computing the probability distribution of a demand parameter for a given intensity of ground motion and suggests an alternative.

Introduction

Earthquake engineering, perhaps more than any other field of engineering, must confront and deal with uncertainties. The randomness in the occurrence of earthquakes in time and space, the vast uncertainty in predicting the intensities and other characteristics of the resulting ground motions, and large imperfections in the predictive models used to assess structural demands and capacities under cyclic loads, all compel us to make use of probabilistic methods in order to consistently account for the underlying uncertainties and make quantitative assessments of safety and reliability. Such analysis is also required for informed decision making for design, retrofit or maintenance of structures.

Luis Esteva has prominently contributed to the development and use of probabilistic methods to advance earthquake engineering. Indeed, he has contributed to many aspects of the field, including the development of probabilistic code formats (Rosenblueth and Esteva 1972), modeling and estimation of seismicity (Hasofer and Esteva 1985), seismic reliability assessment of structures (Esteva and Ruiz 1989, Esteva *et al*. 2001), development of optimal solutions for seismic instrumentation (Heredia-Zavoni and Esteva 1998, Heredia-Zavoni *et al*. 1999), performance-based seismic design criteria (Esteva *et al*. 2002) and maintenance (Montes-Iturrizaga *et al*. 2003), and selection of ground motion intensity measures for performance-based earthquake engineering (Giovenale *et al*. 2004). He has developed methods motivated by real-world needs, which are scientifically sound, yet simple and practical. His work has influenced the practice of earthquake engineering not only in Mexico, but also throughout the world. This is evidenced by the numerous citations to his papers, which one finds by searching the international earthquake engineering literature. One hopes and anticipates that his contribution and influence will continue for many years to come.

After many years of early development, the earthquake engineering community is finally moving towards incorporating probabilistic methods in a systematic way in the design and decision-making for earthquake effects on structures and other constructed facilities. One important manifestation of this is the effort in the Pacific Earthquake

Engineering Research Center (PEER) for developing a performance-based earthquake engineering (PBEE) methodology. According to Moehle and Deierlein (2004), "performance-based earthquake engineering seeks to improve seismic risk decision-making through assessment and design methods that have a strong scientific basis and that express options in terms that enable stakeholders to make informed decisions. A key feature is the definition of performance metrics that are relevant to decision making for seismic risk mitigation." Implicit in this definition is the understanding that all relevant uncertainties in the design or decision-making are properly and consistently accounted for in computing the performance metrics.

As a contribution to this symposium honoring Luis Esteva, I have decided to discuss some probabilistic concepts related to the PEER PBEE methodology. Judging from Esteva's recent work, I believe this topic is of interest to him. After a brief introduction of the framework formula on which the methodology is based, I discuss the various types of probabilistic information that one can obtain from the mean annual frequency of occurrence, which is the main output of the formula. I then offer a critical discussion of the predominant method for computing the distribution of structural demand measures for a given intensity, which uses recorded ground motions. Potential shortcomings of the method are described and an alternative approach is suggested. It is hoped that these discussions enhance and refine the usefulness of the PEER PBEE methodology and framework formula.

The PEER PBEE Methodology

The PEER PBEE methodology is based on a framework formula that estimates the mean annual frequency of events where a specified variable exceeds a given threshold. Originally proposed by Cornell and Krawinkler (2000)[1], the formula has the form

$$\lambda(dv) = \int_{dm}\int_{edp}\int_{im} G\big(dv \mid dm\big)\left|\mathrm{d}G(dm \mid edp)\right|\left|\mathrm{d}G(edp \mid im)\right|\left|\mathrm{d}\lambda(im)\right| \tag{1}$$

in which *im* denotes an intensity measure (e.g., the peak ground acceleration or the spectral acceleration at a selected frequency), *edp* denotes an engineering demand parameter (e.g., an interstory drift), *dm* denotes a damage measure (e.g., the accumulated plastic rotation at a joint), *dv* denotes a decision variable (e.g., dollar loss, duration of downtime), $G(x \mid y) = \Pr(x < X \mid Y = y)$ denotes the conditional complementary cumulative distribution function of random variable X given $Y = y$, $dG(x \mid y)$ is the differential of $G(x \mid y)$ with respect to x, and $\lambda(x)$ denotes the mean frequency of $\{x < X\}$ events per year. Absolute values are used on the three differential quantities since they are negative. The resulting quantity, $\lambda(dv)$, denoting the annual frequency of events where the decision variable *DV* exceeds the threshold *dv*, is the principal decision metric advocated by PEER for seismic risk mitigation. Similar formulas can be written for the annual frequencies $\lambda(dm)$ and $\lambda(edp)$ involving 2 and 1-dimensional integrals, respectively.

An important advantage of the framework formula (1) is that it decomposes the task of assessing the decision metric into the subtasks of seismic hazard analysis,

---

[1] The original version by Cornell and Krawinkler did not include the intermediate variable *EDP*. This variable and the corresponding integral were added in later publications of PEER.

$\lambda(im)$, structural response analysis, $G(edp|im)$, damage analysis, $G(dm|edp)$, and loss analysis $G(dv|dm)$, each of which may be handled by a different group of experts (Porter 2003, Moehle and Deierlein 2004). This decomposition is made possible through the fundamental assumption that, conditioned on *EDP*, *DM* is independent of *IM*, and, conditioned on *DM*, *DV* is independent of *EDP* and *IM*. Another fundamental assumption is that the structure is restored to its initial condition after each damaging earthquake event.

A number of investigators have suggested the use of formulas similar to (1) to compute the probability distribution of extreme *EDP*, *DM* or *DV* values for all earthquakes occurring during a specified period of time, typically one year or the lifetime of the structure. It has been shown in Der Kiureghian (2005) that, if there are non-ergodic uncertainties (i.e., uncertainties which do not renew at each earthquake occurrence, such as epistemic model uncertainties), then such use of the formula entails an error, which can be significant if the probability of interest is greater than around 0.01. Therefore, caution must be exercised in the use of (1) for computing probabilities. More on this is described below.

In the following two sections, two aspects of the PEER framework formula are discussed. The first deals with the types of information that one can gain from the mean annual frequency $\lambda(x)$, where x may denote a *DV*, *DM* or *EDP* threshold. The second deals with the methods available for computing the conditional distribution of an *EDP* for a given *IM*, i.e., the complementary CDF $G(edp\,|\,im)$.

What Can We Learn from $\lambda(x)$?

As mentioned earlier, $\lambda(x)$ denotes the mean annual frequency of occurrences of an earthquake effect X (e.g., a *DV*, *DM* or *EDP*) exceeding the threshold x. Assuming X is non-negative, a plot of $\lambda(x)$ versus x may appear as in Figure 1. Three distinct characteristics of this curve are noted:

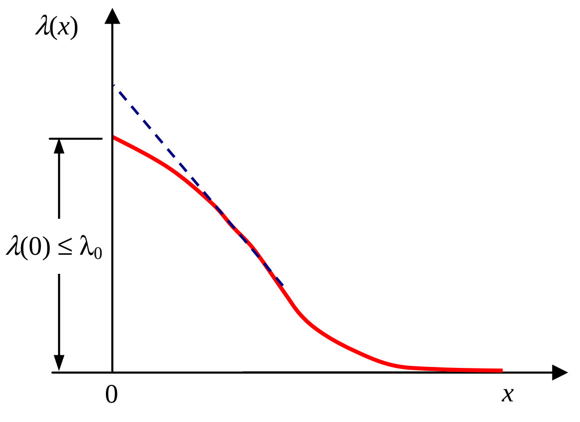

Figure 1. Typical plot of the annual frequency of occurrence of events $\{x < X\}$

1. For X denoting a *DV*, *DM* or *EDP* quantity, $\lambda(x)$ is a non-increasing function of x.
2. As x approaches zero, $\lambda(x)$ approaches a finite value $\lambda(0)$. When X denotes an *EDP* quantity, $\lambda(0)$ is the mean annual frequency of all earthquakes considered in the hazard analysis of the site. We denote this value as λ_0. When X denotes a *DV* or *DM* quantity, $\lambda(0)$ is the annual frequency of earthquakes that cause finite damage and loss. Note that in this case $\lambda(0)$ can be smaller than λ_0, since some low-intensity earthquakes may not cause any damage or loss. In practice, one often computes $\lambda(x)$ for a few selected thresholds and uses extrapolation to construct the curve for small thresholds. For example, the tangent approximation shown in Figure 1 as a dashed line (usually in a semi-logarithmic plot) is often used. Obviously, the above interpretations of $\lambda(0)$ can be helpful in constructing a better approximation of $\lambda(x)$ for small thresholds.
3. The far tail of the curve normally drops off to zero for high thresholds, though for *DV* and *DM* quantities it is possible to imagine a sharp drop at a threshold $x_{\max}$ corresponding to the total damage or loss that can be sustained by the structure.

In addition to providing the mean annual frequency of events, the function $\lambda(x)$ provides the information described below.

Observe that $\lambda(x)$ denotes the mean number of earthquakes in a year that cause $\{x < X\}$, whereas λ_0 represents the mean number of all earthquakes in the same time period. It follows that the ratio $\lambda(x)/\lambda_0$ denotes the long-term fraction of earthquakes that produce an X exceeding the given threshold x. Thus, the function

$$F(x) = 1 - \frac{\lambda(x)}{\lambda_0} \tag{2}$$

represents the CDF of X for a randomly selected earthquake, and its derivative

$$f(x) = -\frac{1}{\lambda}\frac{d\lambda(x)}{dx} \tag{3}$$

represents the corresponding probability density function (PDF). Since $\lambda(0) \le \lambda_0$ (the inequality applying when X represents a *DV* or *DM* quantity), a plot of $F(x)$ may appear as in Figure 2. The discontinuity at $x = 0$ occurs when $\lambda(0) < \lambda_0$. As a result, the PDF of X, which is also depicted in Figure 2, includes a probability mass at $x = 0$, which is equal to the fraction of earthquakes that cause no damage or loss.

The probability distribution shown in Figure 2 is that of X for a randomly selected earthquake. Since a randomly selected earthquake is a lot more likely to have a low than a high intensity, this distribution is not the appropriate one for decision-making or for safety assessment. A quantity of interest for this purpose is the probability distribution of the largest X that can occur in a given period of time, T, say the life of the structure. We denote this by X_T. This distribution is of special interest when X denotes an *EDP* or *DM* quantity.

If the occurrences of $\{x < X\}$ events in successive earthquakes can be considered to be statistically independent, then an approximation of the CDF of X_T is given by

$$\Pr(X_T \le x) \cong [F(x)]^{\lambda_0 T} \tag{4}$$

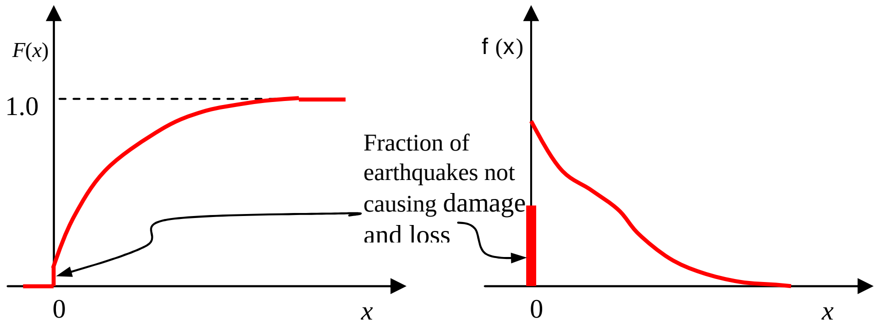

Figure 2. Conceptual plots of the CDF and PDF of X

where $\lambda_0 T$ represents the mean number of events during T. The approximation lies in the fact that the mean number of events is used. Alternatively, again under the assumption of statistical independence, the occurrences of $\{x < X\}$ may be assumed to constitute Poisson events in time. In that case, the distribution of X_T is given by

$$\Pr(X_T \le x) = \exp\{-\lambda_0 T[1 - F(x)]\} \tag{5}$$

In general, the distributions in (4) and (5) are nearly the same in the tail region of x.

Dependence between successive occurrences of events $\{x < X\}$, however, may occur when uncertainties are present, which do not renew at each earthquake event. These uncertainties, denoted "non-ergodic" in Der Kiureghian (2005), may arise from the unknown characteristics of the structure, or from epistemic uncertainties present in the assessment of seismic hazard or in the modeling of the structural response. A correct formulation of the distribution of X_T for that case is presented in Der Kiureghian (2005) and will not be described here. It is noted, however, that, in the presence of non-ergodic uncertainties, the approximations in (4) and (5) generally produce conservative results, i.e., underestimate the probability of the event $\{X_T \le x\}$. This is because the statistical dependence between the successive $\{x < X\}$ events is usually characterized by a positive correlation. (If the capacity of the structure is on the low side, then it is so for all earthquakes.) One quick way to account for this effect is to replace $\lambda_0 T$ in (4) and (5) with a reduced value representing the mean number of *equivalent statistically independent events*. This kind of an approximation was used in Der Kiureghian (1980) in developing approximate expressions for the mean and standard deviation of the extreme of a random process. Numerical studies can be performed to determine the reduction factor for various levels of non-ergodic uncertainties, possibly as a function of x.

Now observe that for a variable X, the differential quantity $\lambda(x) - \lambda(x + \mathrm{d}x) = -\mathrm{d}\lambda(x)$ describes the mean number of events $\{x < X \le x + \mathrm{d}x\}$ per year. Thus, the product $-x\,\mathrm{d}\lambda(x)$ describes the expected cumulative value of the outcomes of X in this differential range in one year. Integrating over the entire range, one obtains the expected cumulative value of all X values in one year

$$\begin{aligned}
\mathrm{E}\left[\Sigma X\right] &= -\int_0^\infty x\,\mathrm{d}\lambda(x) \\
&= -x\lambda(x)\Big|_0^\infty + \int_0^\infty \lambda(x)\,\mathrm{d}x \\
&= \int_0^\infty \lambda(x)\,\mathrm{d}x
\end{aligned} \tag{6}$$

where, in the second line, we have used integration by parts. Thus, the area underneath the $\lambda(x)$ versus x curve gives the mean cumulative value of the X values for all earthquakes occurring in one year. Obviously, the quantity $\mathrm{E}[\Sigma X]$ is of great value when X denotes a *DV* quantity, such as a dollar loss or down time, in which case it represents the mean total annual dollar loss or the mean total annual down time, respectively. These estimates clearly would be valuable in performance-based design or retrofit decisions. The quantity $\mathrm{E}[\Sigma X]$ may also be useful for certain *DM* quantities, such as the dissipated energy or accumulated plastic strain or rotation in a member or joint. However, for an *EDP* quantity, the above measure may not be of much value. For example, if X denotes an interstory drift, then $\mathrm{E}[\Sigma X]$ is the mean of the sum of all interstory drift values occurring in one year. This measure has little relevance to reliability or safety of the structure.

In summary, we have shown that the function $\lambda(x)$, where x may denote a *DV*, *DM* or *EDP* threshold, offers a wealth of information beyond the mean frequency of {x < X} events, which can be useful in performance-based earthquake engineering. Specifically, this function can be used to compute the distribution of X for a random earthquake, as well as an approximation of the distribution of the extreme value of X for all earthquakes occurring during a given period of time. Furthermore, this function can be used to compute the expected cumulative value of X values for all earthquakes in a given period of time. It is noted that, while the lower limit of $\lambda(x)$ may not be important for computing the distribution of the extreme value X_T, it is clearly important for computing the expected cumulative value $\mathrm{E}[\Sigma X]$ in (6). In fact, as Figure 1 suggests, the left end of $\lambda(x)$ dominates the area underneath the curve. The use of λ_0 as a benchmark for determining $\lambda(0)$, as described in the beginning of this section, is useful for accurately determining $\lambda(x)$ for small x values.

Computation of $G(edp \mid im)$

The predominant method for computing the distribution of an *EDP* for a given intensity threshold $IM = im$ is based on nonlinear time history analysis using recorded ground motions, commonly known as Incremental Dynamic Analysis or IDA (Vamvatsikos and Cornell 2002). For the given *im*, a disaggregation of the hazard leads to a pair of predominant magnitude and distance. Recorded ground motions are then selected that have similar magnitude and distance characteristics. The recorded motions are scaled to have the same *im* level. For example, if *im* represents the spectral acceleration at the fundamental period of the structure, then the recorded ground motions are all scaled to produce the same spectral acceleration at that frequency. Nonlinear structural dynamic analysis is then performed for the ensemble of selected recorded ground motions and the *edp* value for each record is determined. The median and coefficient of variation (c.o.v.) of the sample of *edp* values are estimated and a lognormal distribution is fitted to these statistics. Usually the same set of records is used for a range of *im* levels with varying scaling factors. The IDA has proven to be an effective method of approximate probabilistic analysis and has gained considerable popularity among researchers and practitioners interested in PBEE. The discussion in this section deals not with the method of analysis in IDA, but with the choice of recorded ground motions for the analysis.

In a parametric study such as IDA, it would be convenient to use simulated ground motions, or a stochastic representation of the ground motion. The choice for recorded ground motions is made, primarily because the design profession views simulated ground motions with suspicion and as not representing real earthquakes. In the author's opinion, one could equally question whether scaled versions of recorded ground motions are realistic representations of earthquakes. However, there are other problems with the choice of recorded motions, as described below, which make the option of using simulated ground motions, or a stochastic representation of the ground motion, worthy of consideration.

The site of a given structure has its unique characteristics. These include the local soil conditions, the geologic setting of the site, the position of the site relative to seismic sources, and the characteristics of the surrounding ground, which forms the medium through which seismic waves propagate. It would be ideal if one would have a large set of recorded ground motions at the site of interest, from which one could select the desired sample of ground motions for each *im* level for IDA. Such a sample would be inherently consistent with the specific characteristics of the site. However, this is not the case, as no individual building site has a sufficient number of recorded ground motions to provide a workable sample. As a result, when the choice is limited to recorded ground motions, one is forced to use accelerograms that are recorded at many different sites. The problem is that such a sample of ground motions includes the variation inherent in the characteristics of the recording sites, which is irrelevant to the site of interest. In other words, the sample of multiple-site recorded ground motions potentially has more variability than one would expect from the sample ground motions at a given site. The result is a potential overestimation of the variability in the distribution of *EDP* for a given *im*. In contrast, a stochastic model of the ground motion can be constructed that is specific to the site of interest. Either simulation or nonlinear stochastic dynamics can then be used to compute the conditional distribution of the *EDP*.

To test the above hypothesis, the six-story building model in Figure 3 is considered. The building has nonlinear story stiffnesses, which are modeled by the Bouc-Wen hysteresis law. The hysteresis loops for the 1st and 6th story columns are also shown in Figure 3. Following the conventional approach, 10 recorded ground motions are selected (same as those used by Moehle *et al*. 2005) and are scaled to have the same spectral accelerations at the fundamental period of the structure based on its initial stiffness, which is 0.6 s. The scaled pseudo-acceleration spectra of the selected ground motions can be seen in Figure 4 (left), where the average of the 10 spectra is also shown. The selected *im* is the spectral acceleration of 1g at 0.6s period. As the second alternative, the ground motion at the site is modeled as a stochastic process having 10s stationary strong-motion duration with a power spectral density characterizing the site of interest. Three models are considered: (a) a white noise excitation characterizing a rock site with a very broad spectrum of frequencies, (b) a wide-band Kanai-Tajimi power spectrum

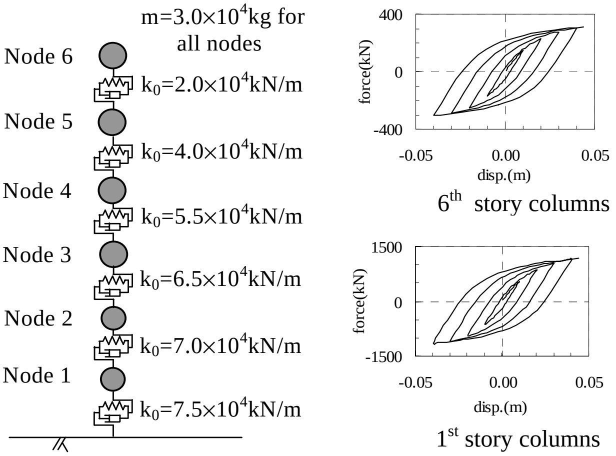

Figure 3 Model of 6-story building with hysteresis loops of 1st and 6th story columns

characterizing a firm ground with a predominant frequency of 2.5 Hz and a bandwidth parameter of 0.6, and (c) a narrow-band Kanai-Tajimi power spectrum characterizing a soft ground with a predominant frequency of 1.5 Hz and a bandwidth parameter of 0.3. The average pseudo-acceleration spectra of these motions, scaled at the fundamental period of the structure, are shown in Figure 4 (right) together with the average spectrum of the recorded motions.

Table 1 shows the estimated mean and c.o.v. of two selected *EDP*s, i.e., the peak values of the 1st and 6th interstory drifts, based on the two approaches. The statistics based the recorded motions are estimated from the sample of 10 nonlinear dynamic analysis using the selected recorded ground motions. The statistics for each of the stochastic inputs are computed by a nonlinear random vibration analysis method, the details of which will not be described here, except to stress that the accuracy of these estimates have been verified by Monte Carlo simulations.

Two observations in Table 1 are noteworthy. First, we observe a variation in the mean *EDP* values depending on the stochastic model selected for the site. This is, of course, expected, since the characteristics of the site must surely influence the *EDP* value. For example, the mean value of the 6th interstory drift is much smaller for the soft site, because the motion for this site is deficient in higher frequencies that significantly contribute to this response.

This kind of differentiation obviously is not possible with the recorded ground motions, unless one is able to select recorded motions that accurately reflect the conditions at the site of interest. The second important observation is that, regardless of the stochastic model used for the site, the c.o.v. of the *EDP* estimates based on the recorded ground motions is about twice the estimated c.o.v. based on the stochastic models. It is argued here that this large variability in the *EDP* estimate is partly due to the mixing of recorded ground motions from different sites. Such an overestimation of the variability could have a significant influence on the computed metrics for PBEE.

Another shortcoming of using recorded ground motions has to do with the robustness of the results. Specifically, independent analysts are likely to arrive at different estimates of the distribution of the *EDP*, depending on their selected recorded motions. With the stochastic model, once the model is selected, any independent analyst should arrive at the same result.

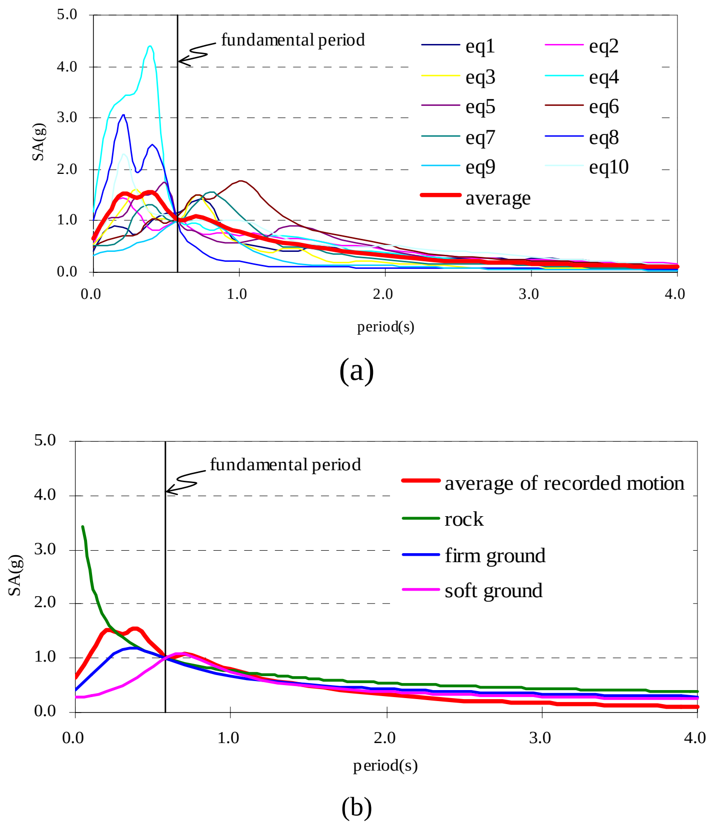

Figure 4 Scaled pseudo-acceleration spectra of recorded (a) *and stochastic* (b) *ground motions*

TABLE 1. *EDP* statistics based on recorded and stochastic ground motions

EDP	Input motion		Mean, m	C.o.v.
1^{st} inter-story drift	Recorded motions		0.0263	0.390
	Stochastic:	rock site	0.0252	0.206
		firm site	0.0215	0.203
		soft site	0.0210	0.226
6^{th} inter-story drift	Recorded motions		0.0238	0.334
	Stochastic:	rock site	0.0385	0.164
		firm site	0.0307	0.179
		soft site	0.0199	0.176

In summary, the conventional method of using recorded ground motions for the estimation of the conditional distribution of an *EDP* for a given *im* may grossly overestimate the variability in the *EDP* due to the mixing of ground motions from different sites. Furthermore, with this approach, it is not easy to account for the specific characteristics of the site, as recorded ground motions consistent with those characteristics may not be available. As an alternative, it is argued that a stochastic characterization of the ground motion specific for the site of interest may lead to a more realistic estimate of the distribution of *EDP*. This approach will also produce a more robust estimate of the distribution of an *EDP*.

Acknowledgment

The author is grateful to Kazuya Fujimura for carrying out the numerical analysis reported in Figures 3 and 4 and Table 1.

References

Cornell, C. A., and H. Krawinkler (2000). Progress and challenges in seismic performance assessment. *PEER Center News*, Spring 2000. http://peer.berkeley.edu/news/2000spring/index.html

Der Kiureghian, A. (1980). Structural response to stationary excitation. *Journal of Engineering Mechanics Division*, ASCE, 106(6), 1195-1213.

Der Kiureghian, A. (2005). Non-ergodicity and PEER's framework formula. *Earthquake Engineering & Structural Dynamics,* to appear.

Esteva, L., O. Díaz-López and J. García-Pérez (2001). Reliability functions for earthquake resistant design. *Reliability Engineering & System Safety* 73, 239-262.

Esteva, L., O. Díaz-López, J. García-Pérez, G. Sierra and E. Ismael (2002). Life-cycle optimization in the establishment of performance-acceptance parameters for seismic design. *Structural Safety* 24, 187-204.

Esteva, L., and S. E. Ruiz (1989). Seismic failure rates of multistory frames. *Journal of Structural Engineering*, ASCE 115, 268-284.

Giovenale, P., C. A. Cornell and L. Esteva (2004). Comparing the adequacy of alternative ground motion intensity measures for the estimation of structural responses. *Earthquake Engineering & Structural Dynamics* 33, 951-979.

Hasofer, A. M., and L. Esteva (1985). Empirical Bayes estimation of seismicity parameters. *Structural Safety* 2, 199-205.

Heredia-Zavoni, E., and L. Esteva (1998). Optimal instrumentation of uncertain structural systems subject to earthquake ground motions. *Earthquake Engineering & Structural Dynamics* 27, 343-362.

Heredia-Zavoni, E., Montes-Iturrizaga and L. Esteva (1999). Optimal instrumentation of structures on flexible base for system identification. *Earthquake Engineering & Structural Dynamics* 28, 1471-1482.

Moehle, J., and G. G. Deierlein (2004). A framework methodology for performance-based earthquake engineering. *Proceedings, 13th World Conference on Earthquake Engineering*, Vancouver, Canada, August 1-6, 2004. (CD-ROM).

Moehle, J., B. Stojadinovic, A. Der Kiureghian and T.Y. Yang (2005). An application of PEER performance-based earthquake engineering methodology. *PEER Digest*. To appear.

Montes-Iturrizaga, R., E. Heredia-Zavoni and L. Esteva (2003). Optimal maintenance strategies for structures in seismic zones. *Earthquake Engineering & Structural Dynamics* 32, 245-264.

Porter, K. A. (2003). An overview of PEER's performance-based earthquake engineering methodology. *Proc. 9th Int. Conf. On Applications of Statistics and Probability (ICASP9) in Civil Engineering*, San Francisco, CA, July 2003, A. Der Kiureghian *et al*., Eds., 2, 973-980.

Rosenblueth, E. and L. Esteva (1972). Reliability basis for some Mexico codes. *Special Pub. SP-31*, American Concrete Institute, 141-155.

Vamvatsikos, D., and C. A. Cornell (2002). Incremental dynamic analysis. *Earthquake Engineering & Structural Dynamics* 31, 492-514.

Niels C. Lind
Distinguished Professor Emeritus
Institute for Risk Research
University of Waterloo
404-1033 Belmont Avenue
Victoria, BC, Canada
nlind@telus.net

Structural Safety, Rational Design

What I remember best from the 40 years or so that I have had the privilege to know Luis Esteva, is not any specific incident but two special qualities he has in good measure. They are his personal modesty and his sense of humour. Together they make him an especially congenial person. Both these qualities must have served him well in his daily relations with people whether as a colleague, teacher, scholar, researcher, supervisor, or family member. Most endearing is the warmth that goes with his great sense of humour – paradoxically reflected not so much in his own wit, but his ability to enjoy and share even the little pleasures of my not-very-good jokes.

Niels Lind
July 20, 2005

THE WELFARE ECONOMICS OF STRUCTURAL SAFETY

ABSTRACT

Structural safety is an important component of what a nation needs to serve the welfare of its people -- but just one component among many. The Life Quality Index of human development indicates human welfare in general but, in particular, also the level of structural safety that best serves the public interest. Practical application is illustrated by the optimal design of a multi-storey office building in three locations of high earthquake risk.

Introduction

Structural safety is but a part of the safety we require to live well and free of fear. Structural safety is thus an integral part of human welfare in modern society. As such, structural safety should conform to an overall societal strategy that aims to enable people to enjoy long lives to their full potential. The strategy is to maximize human development given society's capacity to commit available resources to competing demands. To a fair degree human development can be quantified by dedicated compound social indicators. One such indicator is the Life Quality Index (LQI) developed by Nathwani et al. (1997), calibrated to recent extensive data from North America and the EU (Rackwitz 2003, Nathwani et al. 2005). The LQI is used in the following to derive the optimal safety margin for a structure. The objective of this paper is to show how one can derive the optimal level of safety for a particular structure, the level that is in harmony with a specific measure of the human welfare in a jurisdiction.

It is widely understood and accepted that structures should be designed to minimize lifecycle cost. Great progress has been made in the twentieth century to represent the stochastic aspects of the variables that enter the lifecycle costs. These variables are often predominantly economic, and then the lifecycle costs are not controversial. However, the designer must sometimes reckon with the possibility of substantial injury and loss of life, of cultural treasures or environmental damage; and must then choose how to valuate all expected costs on some broadly acceptable common scale. Whereas structural optimization conventionally addresses weight, initial cost or lifetime cost subject to various constraints, LQI-optimization is suggested here as more appropriate, because it models achievement of public welfare consistent with the ability to commit scarce resources wisely.

Once the variables have been quantified it is of course possible just to pick some reasonable valuation in a common currency. For example, there have been many attempts to find a "value of a human life" by observing court awards, revealed preferences or willingness-to-pay. These approaches are unsatisfactory because the choice is wide and simply delegates the arbitrary valuation to others. As a matter of professional obligation and ethics, it is important to derive the valuation of wealth, life and health from broadly acceptable principles by a transparent rationale, consistent with the societal capacity to commit resources, which is limited. The Life Quality Index with its corresponding Time Principle (Nathwani et al. 1992, Nathwani et al. 2005, Pandey et al. 2005), outlined below, provides clear direction to decision-makers.

Experience has shown that reason produces better and more justifiable decisions than emotion or unsubstantiated judgment. The engineering profession is expected and morally obliged to apply rationality in design, construction and operation. Except as constrained by law, the engineer must exclusively serve the interests of his client. For the individual civil structural engineer this means satisfying all applicable codes and standards as a minimum. However, the onus is on the civil and structural engineering profession as a whole to see that the systems and structures can be produced and maintained as rationally as possible. Cost and safety must be “balanced” – but balancing requires that they are commensurate.

A structure behaves in two complementary modes: Normal performance and malfunction. In the former all costs are material: The intrinsic cost of the structure as designed, the cost of its production, and the cost of its maintenance and decommissioning. Each is to be taken at net present value, raising the question of interest rates and design life. The expected cost of malfunction involves, in addition to the costs of repair, substitution and loss of service, the loss of life and injury.

The Life Quality Index

The Life Quality Index (LQI) expresses the utility of social income over the expected work-free life time of a person. It is derived from a Cobb-Douglas production function (Samuelson 1970) of capital, labour and technology level, together with the assumption of optimal life-time trade-off between work and leisure (Pandey et al. 2005).

The Life Quality Index is a general tool that can be used to support programs and practices for managing risk. It allows a transparent and consistent basis for determining the net benefit arising from projects, programs, standards and policies undertaken at some cost to improve safety or enhance the quality of life. The LQI can help authorities promote the goal of maximizing net benefit to a group (nation, state, province or subpopulation) in terms of the length of healthful, resourceful life for all members at all ages. A subsidiary but practical use of the LQI is in the evaluation of risks and setting standards for risks, such as the application to structural design described in this paper.

A long life in good health and the wealth available to choose among many options are two primary factors that reflect the human development of a group. Human development has been characterized as a “process of enlarging people’s choices” (UNDP 1990). The Life-Quality Index of a group is a function of two social indicators, the statistics *E* and *G*, that indicate its development in comparison with other groups. Except for an arbitrary constant factor the LQI has the form

$$L = L(E,G) = E^K G \tag{1}$$

where *G* is the Gross Domestic Product per person [per year] and *E* is the expectancy at birth of life in good health, i.e. adjusted for state of health. This life expectancy has been validated as a universal indicator of social development, public health and some aspects of environmental quality. E and G have been in use for over half a century to express the longevity and wealth of a nation in numbers. Both are reliably measured. The LQI is precise, but can only provide accurate comparison between groups and over time if the variables *E* and *G* are similarly comparable. For this purpose *G* must be corrected for purchasing power and inflation: *G* is the purchasing power parity of the Real Gross Domestic Product per person per year. When it is to be used in risk management, life expectancy must be corrected for health state as mentioned, because many risks involve not just loss of life but also injury and sickness. The parameter K is a measure of the trade-off we place on consumption and the value we attach to time free of work. If K is chosen equal to the ratio of time not spent in economic activity to its complement, then the LQI will reflect the value (in terms of time expended) that people apparently attach to the production of wealth (Nathwani et al. 1992). The calibrated value of K is 5.0 based on economic productivity data for Canada, France, Germany, U.K. and U.S.A. over 33 years since 1970. Formal derivation, interpretation and calibration of the LQI have been presented elsewhere (Pandey et al. 2005).

Assessing a Risk Intervention

The LQI can be used to determine an acceptable level of expenditure that can be justifiably incurred on behalf of the public in exchange for more safety or an appropriate reduction in the risk. A risk reduction intervention, for example the increase of a safety factor, can be expected to have an infinitesimal impact on mortality and thus life expectancy E.

Any undertaking that would affect the public by modifying risk through expenditure will have an impact, dL, on the Life Quality Index. The *LQI criterion* is the requirement that the net benefit dL be positive; by Eq. (1)

$$dL/L = dG/G + K\, dE/E > 0 \tag{2}$$

Further, among several options, one that maximizes the dL is indicated as preferable. In Eq. (2) dG may represent the monetary cost of implementing a regulation ($dG<0$) or the monetary benefits that arise from a project ($dG>0$). The term dE is the change in life expectancy due to a change in the level of risk to the population associated with the undertaking. The LQI criterion is invariant under a monotonically increasing transformation of L.

The LQI criterion, Eq.(2) is consistent with the concept of "societal willingness to pay" that originates from the definition of compensating variation by Hicks (1939). A person's "willingness to pay," has been defined as the sum received by or from the individual which, following a change in the social well-being of the individual, leaves her at her original level of well-being. Such a sum should not be confused with the individual's actual psychological willingness to pay. Moreover, the actual societal willingness to pay is a political issue. A less controversial concept is the capacity to commit resources. Per person capacity to commit resources is obtained from Equation (2) by setting $dL/L = 0$ and rearranging the terms to yield

$$-dG = G\, K\, dE/E \quad (\$/\text{person/year}) \tag{3}$$

When the benefits accrue to a population of size N, then the aggregated value of justified expense, i.e., the amount that will not alter the population life-quality is equivalent to the *societal capacity to commit resources (SCCR)*

$$\text{SCCR} = (-dG)\, N = NGK\, dE/E \ (\$/\text{year}) \tag{4}$$

It is a principle of welfare economics that the benefits of a safety program in the public interest are most appropriately measured by the aggregate capacity to commit resources on behalf of those paying for and those benefiting from the program. The LQI measure is consistent with this principle. The rationale for using LQI in support of public policy decisions rests on the acceptance of the potential Pareto improvement criterion, which requires that the gainers gain enough to compensate the losers fully. For the societal benefit test, this requirement indicates that the net benefit should be positive, whether actual compensation occurs or not.

Concepts of life-time utility, discounting, and age-related variation of preferences for consumption and survival have been discussed in scattered forms in the literature. The main value of the LQI approach is to integrate all these concepts consistently and comprehensively into a welfare model that also satisfies the principles of utility theory and rational decision making (Pandey et al. 2005).

The Time Principle

The LQI approach to risk assessment presents another advantage that should appeal to the mind of an engineer. It has been shown by Pandey et al. (2005) to be equivalent to the commonsense Time Principle that: *A prospect to save life or produce wealth is optimal if no alternative presents a greater life expectancy net of work-time cost* (Lind 2002). In other words, if you must work to gain some life expectancy, the amount of work time should not exceed the expected gain.

Application

To use the LQI in a risk assessment, consider a population of 1 million. If a risk intervention that would permanently reduce the probability of death by 10^{-6} per person/year for all age groups in the population, then a total of one life would be "saved" every year. The Canadian male life table (1995-1997) shows that this reduction in risk would extend the life expectancy (LE) at birth of 75.42 years by 26 hours. The life expectancy of a person of age 35 is 42.11 year. The risk reduction would increase life expectancy by 8.5 hours. The real GDP/person in 2003 is C$ 34,675 (in 1997 constant Canadian dollars) and K is taken as 5. By Eq.(4), the SCCR for the 35-39 year age group equals 3.99 $/person/year. An age-averaged value of SCCR as 3.78 C$/person/year is obtained by the procedure given by Pandey and Nathwani (2003). Thus, an amount up to SCCR = C$3.78 million (about US$3.07 million) should be invested if thereby one fatality will be prevented. This value is used in the following example.

An Application in Civil Structural Engineering

No project can be acceptable unless life safety is assured, so protection of life is a primary duty in engineering. Yet, life safety does not necessarily govern design; considerations of material and economic losses may be sufficient to dictate the level of safety. This is borne out in the study by Wen (2001), who considered the optimal design of a nine-storey steel frame office building in downtown Los Angeles CA, Seattle WA, and Charleston SC (Figure 1). The design life was 50 years. The discount rate was taken as 5%.

Twelve buildings were designed according to the NEHRP 97 provisions to a wide range of lateral force. The building was classified as commercial for professional, technical and business services and had a Special Moment Resisting Frame structure. In a sensitivity study Wen (2001) first set the "value of life" to US$1.74 million, and found the optimal values of the yield force coefficient for earthquake plus wind at the three locations to be 0.198, 0.115 and 0.146 respectively (see Table 1). Setting next the “value of life” to zero reduced the optimal yield force coefficient by approximately 0.006, 0.022 and 0.014, i.e.3%, 19% and 9% respectively. Accordingly, within the set of twelve candidate structures (Wen 2001), ignoring the “value of life” made no difference to the optimal structures at Los Angeles and only little difference at Charleston. When instead the SCCR-value of $3.07 million is used (Table 1) the weight of the required frame is unchanged in Los Angeles and Charleston, but is increased in Seattle.

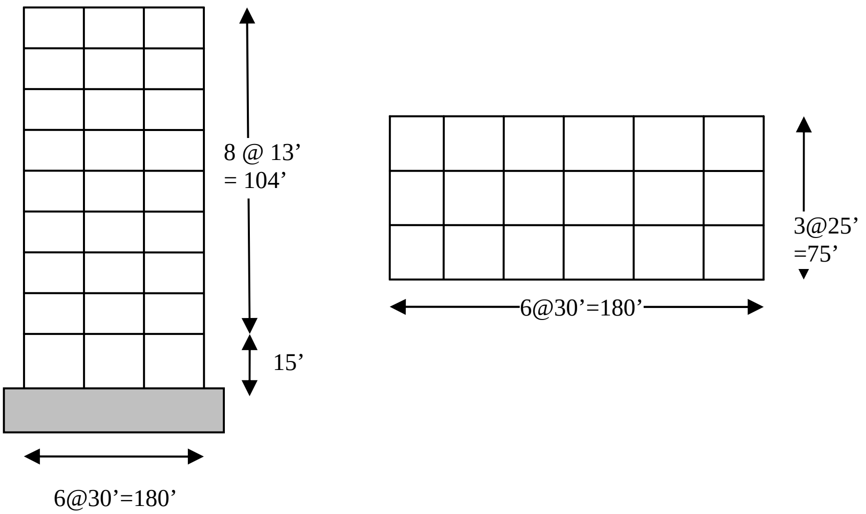

Figure 1. Elevation and plan of a nine-storey steel frame office building (after Wen (2001))

TABLE 1. Comparison of optimal designs of three buildings for wind and earthquake loadings

	Los Angeles			Seattle			Charleston		
SCCR, US$M	0	1.74	3.07	0	1.74	3.07	0	1.74	3.07
Yield coefficient	0.192	0.198	0.198	0.093	0.115	0.132	0.132	0.146	0.157
Structure No.	S8	S8	S8	S3	S4	S5	S5	S6	S6
Weight, kips	5356	5356	5356	5138	5183	5224	5224	5267	5267
Weight diff.	0	--	0	-0.9%	--	0.8%	-0.8%	--	0

Discussion and Conclusion

Some tentative conclusions can be drawn and much can be learned from Table 1. First, the societal capacity to commit scarce resources (SCCR) to life safety does make a difference for some structures. It is a design variable that should not be ignored or assigned arbitrarily. It is also noted that for some other structures, even quite similar to the aforementioned ones, the SCCR makes no difference. Further, it is not obvious (except perhaps in hindsight) precisely *when* the SCCR can be responsibly ignored. Admittedly its influence in the cases studied by Wen (2001) on the overall cost of a building is minuscule. For example, if the discount rate is raised from 5% to 7% for the Seattle structure, the optimal yield coefficient drops more than when the risk to life is completely ignored.

It is noted that some densely populated areas, such as part of the American West Coast, have a high risk of “megathrust” subduction-zone earthquakes. The potential loss of life is very high and data are scarce and anecdotal (Onur and Seemann 2004). Further quantification of the earthquake risk to buildings (particularly low-period ones) is advisable for such areas.

The wide range of life-saving interventions adopted in transportation, health care, environmental protection, occupational health and other sectors show that societies are in fact willing to pay enormous sums to reduce the risk of death. Conversely, many cost-effective life-saving interventions remain unimplemented. The risk has often not even been quantified, so that the amount paid per life was known neither to the decision-maker, nor to those who paid, nor to the beneficiaries. There are generally good political reasons whether to implement or not, but not scientific ones. For professionals in engineering and health management, however, the use of arbitrary SCCR values is not justified. For structures with high human exposure, such as some large public facilities (schools, theatres, dams, vehicles, aircraft structures etc.), a defendable and transparent SCCR value should be put forth by professional organizations and openly agreed between government and the profession for application in codes and standards.

The Life Quality Index expresses the average social income utility over the expected work-free life time of a person. It derives from the economics of human welfare, expressing optimal management of available capital and technology under a life-time trade-off between work and leisure. The Life Quality Index establishes structural safety as an instrument of the overall social strategy for well-being.

Acknowledgments

Over many years the author has been privileged by and received much benefit from continuing discussion with Luis Esteva and other pioneers in the areas of structural safety and rational design in the face of uncertainty. It is especially appropriate of this time to thank Luis Esteva for many years of stimulus and support. Thanks are due to Ove Ditlevsen, Jatin Nathwani, Mahesh Pandey and Ruediger Rackwitz for discussions about the LQI and the economics of human welfare.

References

Hicks, J.R. (1939). The foundation of welfare economics. *The Economic Journal*, 49(196), 696-712.

Lind, N. (2002). “Social and economic criteria of acceptable risk,” *Reliability Engineering and System Safety*, 78, Issue 1, October, 21-26.

Lind, N.C., Nathwani, J.S. and Siddall, E. (1992). *Managing Risks in the Public Interest*. Institute of Risk Research, University of Waterloo Press, Waterloo, Canada.

Nathwani, J.S., Lind, N.C., Pandey, M.D. (1997). *Affordable Safety by Choice: The Life Quality Method.* Institute for Risk Research, University of Waterloo, Canada, pp 230.

Nathwani, J.S., Pandey, M.D.,. Lind, N.C. (2005). A Standard for Determination of Optimal Safety in Engineering Practice, *Proc. IFIP Conf. Aalborg, Denmark, May* (in print).

Onur, T. and Seemann, M. R. (2004). Probabilities of significant earthquake shaking in communities across British Columbia: Implications for emergency management. Paper No. 1065, *13th World Conference on Earthquake Engineering, Vancouver, BC, Canada*, August 1-6.

Pandey, M.D. and Nathwani, J.S. (2003). Life-Quality Index for the estimation of societal willingness-to-pay for safety. *J. Structural Safety*, 26(2), 181-199.

Pandey, M.D., Lind N.C. and Nathwani, J.S. (2005). The LQI derivation and calibration consistent with fundamental principles of economic theory, (submitted).

Rackwitz, R. (2003). Optimal and acceptable technical facilities involving risks. *J. Risk Analysis*, 24, 297-331.

Samuelson, P.A. (1970). *Economics*. 8th Edition. McGraw Hill Inc., New York, NY.

United Nations Development Program (1990). *The Human Development Report*. Oxford University Press, UK.

Wen, Y. K. (2001). Minimum lifetime cost design under multiple hazards, *Reliability Engineering and System Safety* 73, 223-231.

Eduardo Miranda
Dept. of Civil and Environmental Engineering
Stanford University
Terman Engineering Center, Rm 293
Stanford, CA 94301-4020
emiranda@stanford.edu

Main research interests:
Performance-based design, Displacement-based design, Seismic design and performance of nonstructural components

Luis Esteva has made remarkable contributions to the field of Earthquake Engineering. His work in Probabilistic Seismic Hazard Analysis and in particular his pioneer 1967 paper are well known internationally. Here however, I would like to highlight some of his contributions in other areas of Earthquake Engineering. Of his many (hundreds) publications, I reproduce here two excerpts of a chapter Luis wrote in 1980 for a book edited by Emilio Rosenblueth. I first read this chapter when I was an undergraduate student at UNAM and over the years it has become one of my favorite papers.

While referring to seismic codes at the beginning of his chapter Luis wrote [*]:

> "Base shear coefficients and design response spectra are taken as measures of response parameters, as the latter are usually expressed in terms of accelerations and equivalent lateral forces acting on linear systems. But these variables are no more than indirect measures of system performance during earthquakes: they serve to control the values of more significant variables, such as lateral deflections of actual nonlinear systems, global and local ductilities, and safety margins with respect to instability failure (second-order effects). Because the relations of control variables to actual response are affected by the type and features of the structural system, better designs will be obtained if these relations are understood and accounted for, in contrast with blindly applying codified recommendations."

In the same chapter Luis also wrote the following:

> "Engineering design is rooted in society's need to optimize. The general goal of optimization can be expressed in terms of direct, particular objectives: seismic design aims at providing adequate safety levels with respect to collapse in the face of exceptionally intense earthquakes, as well as with respect to damage to adjacent constructions; it also seeks to protect structures against excessive material damage under the action of moderate intensity earthquakes, to ensure simplicity of the required repair, reconstruction or strengthening works in

---

[*] Esteva, L. (1980), "Design: General", chapter 3 in *Design of Earthquake Resistant Structures*, Ed. E. Rosenblueth, John Wiley & Sons, Inc., New York, pp. 54-99. Also available in Spanish through IMCYC.

case damage takes place, and to provide protection against the accumulation of structural damage during series of earthquakes."

"Achievement of the foregoing objectives requires much more than dimensioning structural members for given internal forces. It implies explicit consideration of those objectives and of the problems related with nonlinear structural response and with the behavior of materials, members, and connections when subjected to several cycles of high-load reversals. It implies as well identifying serviceability conditions and formulating acceptance criteria with respect to them."

"Establishment of design conditions follows cost-benefit studies, where the initial costs required to provide given safety levels and degrees of protection with respect to material losses are compared with the present value of the expected consequences of structural behavior. This is obtained by adding up the costs of failure and damage that may occur during given time intervals, multiplied by their corresponding probabilities and by actualization factors that convert monetary values at arbitrary instants in the future into equivalent values at the moment of making the initial investment."

"Let D be the cost of damage caused by an earthquake on a structure, which includes damage to the structure, its contents as well as all other consequences (such as loss of human lives and indirect effects) expressed in monetary terms, then the probability density function of D every time a significant event takes place is

$$f_D(d) = \int \frac{\mathrm{d}Q(y)}{\mathrm{d}y} f_{D|Y}(d \mid y)\ \mathrm{d}y$$

where $Q(y)$ is the conditional cumulative probability distribution of the earthquake intensity given that a significant event has occurred, and $f_{D|Y}(d|y)$ the probability density function of D conditional to every possible value of earthquake intensity."

The first excerpt describes what many years later would become known as "displacement-based design" while the second excerpt published 25 years ago describes, of course, what we now know as "performance-based design".

From these paragraphs it is clear that Luis was back then, but continues to be today, at the forefront of Earthquake Engineering. For those who have not read this chapter, especially for those in the newer generations of earthquake engineering students, I strongly recommend reading it and learning more about the extraordinary humble man who wrote it.

I feel extremely honored to have been invited to participate in this symposium on his honor and more so to be counted as one of his friends. Hats off to you Luis!

Eduardo Miranda
September 2005

Eduardo Miranda

SIMPLIFIED ANALYSIS TOOLS FOR RAPID SEISMIC EVALUATION OF EXISTING BUILDINGS IN URBAN AREAS

ABSTRACT

Simplified analysis tools that make feasible rapid assessment of large inventories buildings in urban areas with a minimum amount of information about the buildings are presented. The simplified seismic analysis tools use a continuum model consisting of a flexural beam coupled with a shear beam. The model permits to obtain estimates of the seismic response of multi-story buildings with only three parameters, that is, only one parameter in addition to the two that are required to define a linear elastic single degree of freedom system. The simplified method is computationally very efficient and permits to obtain estimates of the response of a multi-story building in fractions of a second, hence providing an excellent tool to incorporate record-to-record variability and modeling uncertainty in probabilistic performance assessments of existing buildings. Results of lateral deformation time histories, floor acceleration time histories and floor response spectra computed with the simplified method have been compared to those measured during earthquakes in more than 80 instrumented buildings in California. Evaluation of the results indicates that the proposed analysis tool provides relatively good results of not only peak values of response parameters but in most cases also of time history results. Based on the simplified model two new type of spectra are presented. These spectra, referred to as generalized interstory drift spectrum and generalized building peak acceleration, have ordinates that provide the intensity of parameters closely correlated with structural and nonstructural damage.

Introduction

Seismic performance assessment of large inventories of buildings has traditionally been done by estimating performance through the use of empirical correlations between peak ground motions parameters such as peak ground acceleration (PGA) and peak ground velocity (PGV) with modified Mercalli intensity. In the United States the best known example of this approach is the “ShakeMap” (Wald, et al. 1999a). The Instrumental Intensity map used in ShakeMap is based on a combined regression of recorded peak acceleration and velocity amplitudes (Wald, et al. 1999c). The empirical relationships between PGA and PGV with MMI used in ShakeMap are based on a much larger data set than that used by Trifunac and Brady (1975) who developed one of the first relationships between peak ground motion parameters and MMI. Unfortunately, empirical correlations of peak ground acceleration and peak ground velocity with the Modified Mercalli Intensity are characterized by a very large scatter of data points. For example, Trifunac and Brady (1975) reported that, for a given intensity, the scatter was equal to about one order of magnitude in PGA or PGV. Despite using a significant larger data set, the empirical relationships obtained by Wald et al. (1999c) show approximately the same scatter. For example, peak ground acceleration ranging from 5 cm/s^2 to 450 cm/s^2 produced a MMI of V. Similarly, according to the data collected by Wald et al. (1999c), areas subjected to peak ground accelerations of 300 cm/s^2 (31%g) could be associated with Modified Mercalli Intensities of V, VI, VII or VIII. This range of MMI's corresponds to distinctly damage descriptions ranging from "very light damage" to "moderate to heavy damage", making performance predictions not very reliable. Although correlation is improved when using peak ground velocity, the correlation remains relatively low.

Several studies have shown that rather than estimating seismic performance directly from peak ground motion parameters, a better estimation of earthquake damage can be obtained by first obtaining an estimate of the building seismic response and then obtaining an estimate of damage from peak structural response parameters. An improved performance assessment can be obtained if single-degree-of-freedom (SDOF) systems are used as analytical models to estimate building response. This approach, which was pioneered by Luis Esteva and Emilio Rosenblueth in the late 60's, are now widely used all over the world. Tools for seismic risks of urban areas in the U.S. (e.g. HAZUS) and in Europe (e.g., EU-Risk) used this approach in which building damage is estimated from response spectral ordinates (peak responses of SDOF systems).

Although SDOF systems provide a much better a much better basis for estimating possible damage in buildings than peak ground acceleration or peak ground velocity, they still have a number of important disadvantages. Among others, SDOF systems cannot account for the contribution of higher modes, which are particularly important for predicting acceleration demands in buildings. Furthermore, even if displacements response spectrum ordinates are used, they only provide a measure of the overall lateral deformation in the building and do not take into account concentrations in lateral deformations in certain stories that usually occur in buildings.

It is well know that structural damage and many kinds of nonstructural damage in buildings are the result of lateral deformations. In particular, several studies have concluded that the structural response parameter that is best correlated with seismic damage is the peak interstory drift ratio, which is defined as the difference in lateral displacements in between two consecutive floors normalized by the interstory height. Similarly, other studies have shown that damage to contents and many types of nonstructural components is primarily related to peak floor accelerations and to floor spectral ordinates. Hence, much better performance estimates can be achieved by first computing peak interstory drift demands and peak floor acceleration demands. However, conventional analysis techniques (e.g., finite element models) require a great deal of time to generate building models and to run the analyses which makes the process extremely time consuming. Furthermore, the information that is required to build these improved building models is usually not available to the engineers who are interested in assessing the seismic performance of large inventories of buildings.

The objective of this paper is to present new analysis tools for rapid assessment of building response. The new analysis tools are based on a continuous model that consists of a combination of a flexural beam and a shear beam. By modifying a single parameter this model can consider lateral deformations varying from those of a flexural beam all the way to those of shear beam. Hence, it permits to account for a wide range of modes of lateral deformation that represent more closely those occurring in multistory buildings. Mode shapes, modal participation factors and period ratios required to compute the response of the model are all computed with closed-form solutions and are a function of only one parameter. This provides a highly efficient computational tool which at the same time only requires a minimum amount of information about the building whose seismic response is being assessed, making it then particularly valuable when evaluating large inventories of buildings. New types of spectra and response maps based on this building model are also presented.

Simplified Building Model

The simplified model consists of a linear elastic continuum model. Continuum models have been proposed before for approximating the response of buildings to wind or seismic forces. For a review of previously-proposed models the reader is referred to Miranda and Taghavi (2005) and Miranda and Akkar (2005). The proposed continuum model consists of a combination of a flexural cantilever beam and a shear cantilever beam deforming in bending and shear configurations, respectively (Figure 1). It is assumed that along the entire length of the model, both beams undergo identical lateral deformations. Furthermore, mass and lateral stiffness are assumed to remain constant along the height of the building.

As shown by Miranda and Akkar (2005), the response of uniform shear-flexural model shown in Figure 1 when subjected to an horizontal acceleration at the base $\ddot{u}_g(t)$ is given by the following partial differential equation:

$$\frac{\rho}{EI}\frac{\partial^2 u(x,t)}{\partial t^2}+\frac{c}{EI}\frac{\partial u(x,t)}{\partial t}+\frac{1}{H^4}\frac{\partial^4 u(x,t)}{\partial x^4}-\frac{\alpha^2}{H^4}\frac{\partial^2 u(x,t)}{\partial x^2}=-\frac{\rho}{EI}\frac{\partial^2 u_g(t)}{\partial t^2} \tag{1}$$

where ρ is the mass per unit length in the model, H is the total height of the building, $u(x,t)$ is the lateral displacement at non-dimensional height $x=z/H$ (varying between zero at the base of the building and one at roof level) at time t, c is the damping coefficient per unit length, EI is the flexural rigidity of the flexural beam and α is the lateral stiffness ratio defined as

$$\alpha = H\sqrt{\frac{GA}{EI}} \tag{2}$$

where GA is the shear rigidity of the shear beam. The lateral stiffness ratio, α is a dimensionless parameter that controls the degree of participation of overall flexural and overall shear deformations in the continuous model and thus, it controls the lateral deflected shape of the model. A value of α equal to zero represents a pure flexural model (Euler-Bernoulli beam) and a value of $\alpha \rightarrow \infty$ corresponds to a pure shear model. Intermediate values of α correspond to multistory buildings that combine overall shear and flexural lateral deformations.

The mode shapes of the simplified model are given by (Miranda and Taghavi, 2005):

$$\phi_i(x)=\sin(\gamma_i x)-\gamma_i\beta_i^{-1}\sinh(x\beta_i)-\eta_i\cos(\gamma_i x)+\eta_i\cosh(\beta_i x) \tag{3}$$

where β_i and η_i are nondimensional parameters for the *i*th mode of vibration which are given by

$$\beta_i=\sqrt{\alpha^2+\gamma_i^2} \tag{4}$$

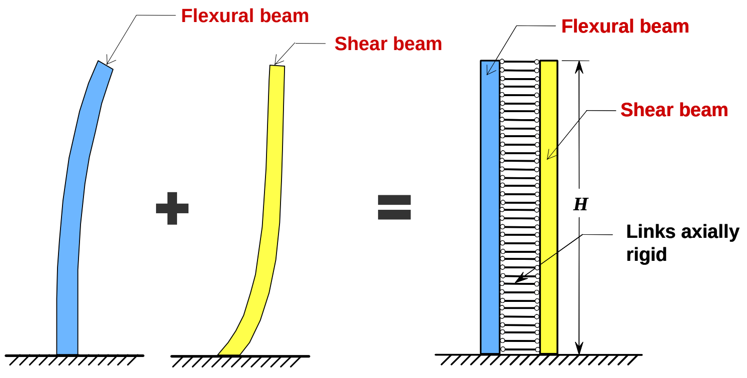

Figure 1. Simplified continuum model to estimate the seismic response of buildings

$$\eta_i = \frac{\gamma_i^2 \sin(\gamma_i) + \gamma_i \beta_i \sinh(\beta_i)}{\gamma_i^2 \cos(\gamma_i) + \beta_i^2 \cosh(\beta_i)} \tag{5}$$

and γ_i is the eigenvalue of the *i*th mode of vibration corresponding to the *i*th root of the following characteristic equation:

$$2 + \left[2 + \frac{\alpha^4}{\gamma_i^2 \beta_i^2}\right] \cos(\gamma_i)\cosh(\beta_i) + \left[\frac{\alpha^2}{\gamma_i \beta_i}\right] \sin(\gamma_i)\sinh(\beta_i) = 0 \tag{6}$$

Periods of vibration corresponding to higher modes can be computed as a function of the fundamental period of vibration of the building T_1 by using period ratios computed as

$$\frac{T_i}{T_1} = \frac{\beta_1 \gamma_1}{\beta_i \gamma_i} \tag{7}$$

Since the masses are assumed to remain constant, the modal participation factors Γ_i can be computed with the following equation:

$$\Gamma_i = \frac{\int_0^1 \phi_i(x)dx}{\int_0^1 \phi_i^2(x)dx} \tag{8}$$

Integrals shown in equation (8) can be solved in closed-form solution. Readers interested in these closed-form solutions are referred to Miranda and Akkar (2005). As shown by these equations, mode shapes and modal participation factors, which control the spatial distribution of seismic demands, are fully defined only on a single parameter, the lateral stiffness ratio α.

While assuming the mass to remain constant along the height of buildings is reasonable in most cases, assuming that the lateral stiffness remains constant along the height of the building is perhaps only a reasonable assumption for one to three-story buildings. However, Miranda and Taghavi (2004) have shown that the product of modal shapes and modal participation factors as well as period ratios are relatively robust and are not significantly affected by reductions in lateral stiffness. In the same study, it was similarly shown that reduction in masses along the height of the building also do not affect significantly the dynamic characteristics of the model. Although Miranda and Taghavi (2005) provided expressions to compute the dynamic characteristic of non-uniform buildings, they concluded that in many cases, using the dynamic characteristics of uniform models could provide reasonable approximations to the dynamic characteristics of non-uniform models.

Relative Displacements

The contribution of the *i*th mode of vibration to the lateral displacement (relative to the ground) at non-dimensional height $x=z/H$ at time t is given by

$$u_i(x,t) = \Gamma_i \phi_i(x) D_i(t) \tag{9}$$

where Γ_i is the modal participation factor of the *i*th mode of vibration, $\phi_i(x)$ is the amplitude of *i*th mode at nondimensional height x, and $D_i(t)$ is the relative displacement response of a SDOF system, with period T_i and modal damping ratio ξ_i corresponding to those of the *i*th mode of vibration, subjected to ground acceleration $\ddot{u}_g(t)$. The product $\Gamma_i\phi_i(x)$ controls the spatial variation of the contribution of the *i*th mode to the total response, while $D_i(t)$ controls its time variation. Assuming that the structure remains elastic and that it has classical damping, the displacement at non-dimensional height $x=z/H$ at time t is given by

$$u_i(x,t) = \sum_{i=1}^{m} \Gamma_i \phi_i(x) D_i(t) \tag{10}$$

where m is the number of modes contributing significantly to the response. Taghavi and Miranda (2005) have shown that for most buildings with 30 or less stories only three modes are necessary for each direction. More recently, Reinoso and Miranda (2005) have shown that for high rise buildings and response parameters strongly influenced by higher modes (such as floor accelerations) including five or six modes may be necessary.

Taghavi and Miranda (2005) compared the response computed with the simplified model to that computed with detailed finite-element models of a ten-story steel moment resisting frame building and a twelve-story reinforced concrete building whose properties were available in the literature. Additionally, they compared the response computed with the model to that recorded in four instrumented buildings in California that have been subjected to earthquakes. In all cases, it was shown that the simplified model provided very good results. More recently, Reinoso and Miranda (2005) validated the model by comparing the response computed with the simplified continuous model to that recorded in five high rise buildings in California in various earthquakes.

The simplified method of analysis is currently being evaluated by comparing the seismic response recorded in a large number of instrumented buildings in California to that computed with the model. Figures 2 to 5 show examples comparing relative displacement (relative to the base of the building) time histories of five instrumented buildings in California. All of these analyses have been conducted assuming that the lateral stiffness and mass of the continuous system remains constant along the height of the building, and models were fully defined only using three parameters, namely the fundamental period of vibration of the building, a damping ratio that characterizes the damping in the model and the lateral stiffness ratio. In equations 9 and 10 one could use different damping ratios for computing $D_i(t)$ for each mode. However, for simplicity and in order to keep the number of parameters to a minimum, here it has been assumed the same damping ratio for all modes. Furthermore, the base of the model has been assumed as fixed and torsional deformations have been neglected. As shown in these figures, despite the important simplifications, the model is capable of capturing relatively well the peak and the most important features of the response of the buildings.

Interstory Drift Ratios

The interstory drift ratio at the *j*th story can be computed as

$$IDR(j,t) = \frac{1}{h_j}\sum_{i=1}^{m} \Gamma_i\left[\phi_i\left(x_{j+1}\right) - \phi_i(x_j)\right]D_i(t) \tag{11}$$

where h_j is the floor to floor height of the jth story, and $\phi(x_{j+1})$ and $\phi(x_j)$ are the mode shape values corresponding to the *j*th+1 and *j*th floor computed with equation (3), respectively. If the interstory height is assumed to remain constant along the height of the building, it can be shown that for buildings with 6 or more stories a relatively good estimation of the interstory drift at non-dimensional height $x=z/H$ at time t can be computed with

$$IDR(j,t) \approx \theta(x,t) = \frac{1}{H}\sum_{i=1}^{\infty} \Gamma_i \phi_i^{'}(x) D_i(t) \tag{12}$$

where H is the total building height above ground, $\theta(x,t)$ is the rotation in the simplified model at height x at time t, and $\phi_i^{'}(x)$ is the first derivative of the *i*th mode shape $\phi_i(x)$ with respect to non-dimensional height x. The derivative of the mode shapes with respect to non-dimensional height x is obtained by taking the derivative of Eq. (3) with respect to x as follows:

$$\phi_i^{'}(x) = \gamma_i \cos(\gamma_i x) - \gamma_i \cosh(\beta_i x) + \eta_i \gamma_i \sin(\gamma_i x) + \eta_i \beta_i \sinh(\beta_i x) \tag{13}$$

Generalized Interstory Drift Spectrum

Motivated by the relatively good results produced by the model, Miranda and Akkar (2005) developed a new type of spectra that, unlike conventional response spectrum, the ordinates provide a direct estimation of peak interstory drifts that are likely to occur in buildings.

The new spectrum, referred to as the *generalized interstory drift spectrum* (GIDS) can be considered as an extension of Iwan's drift spectrum (Iwan, 1997). However, unlike Iwan's drift spectrum which is only applicable to buildings that can be modeled as shear beams, the GIDS is capable of considering a wide range of buildings ranging from those that can be modeled as flexural beams all the way to those that can be

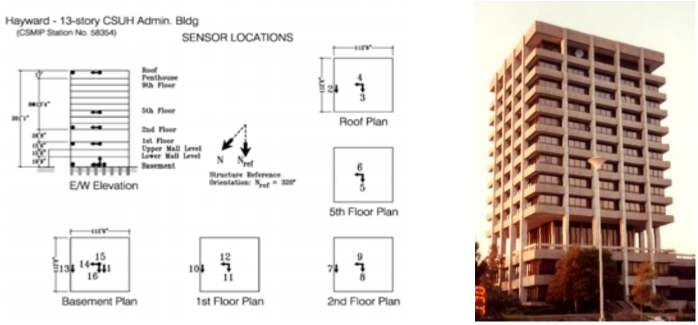

Figure 2. Sensor location and photograph of a 13-story RC building in Hayward California

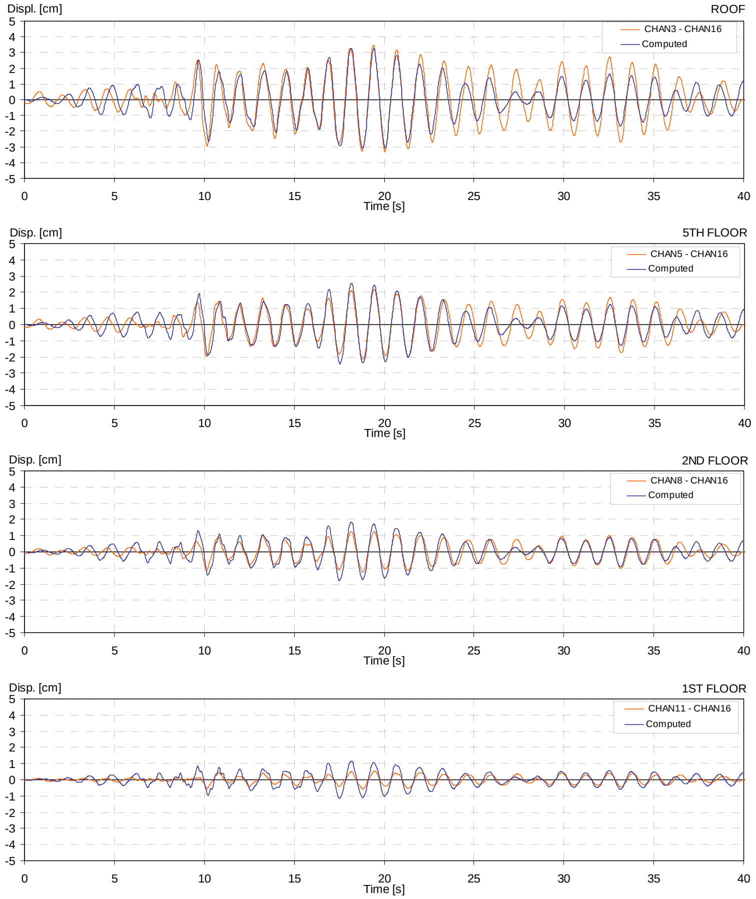

Figure 3. Comparison of computed and recorded relative displacements in the NS components of the 13-story building in Hayward California during the 1989 Loma Prieta earthquake

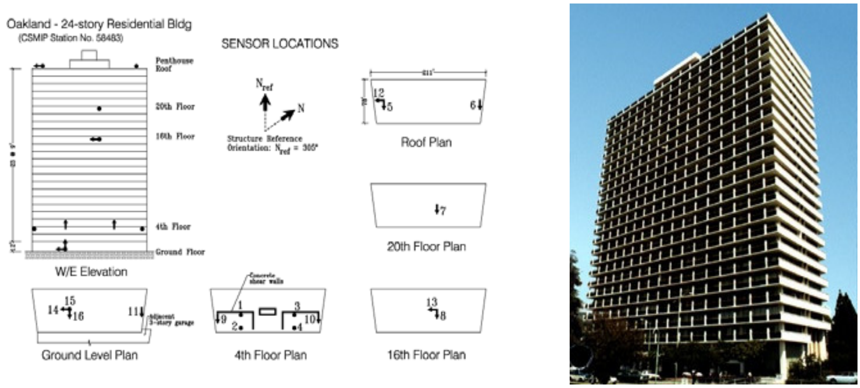

Figure 4. Sensor location and photograph of a 24-story RC building in Oakland California

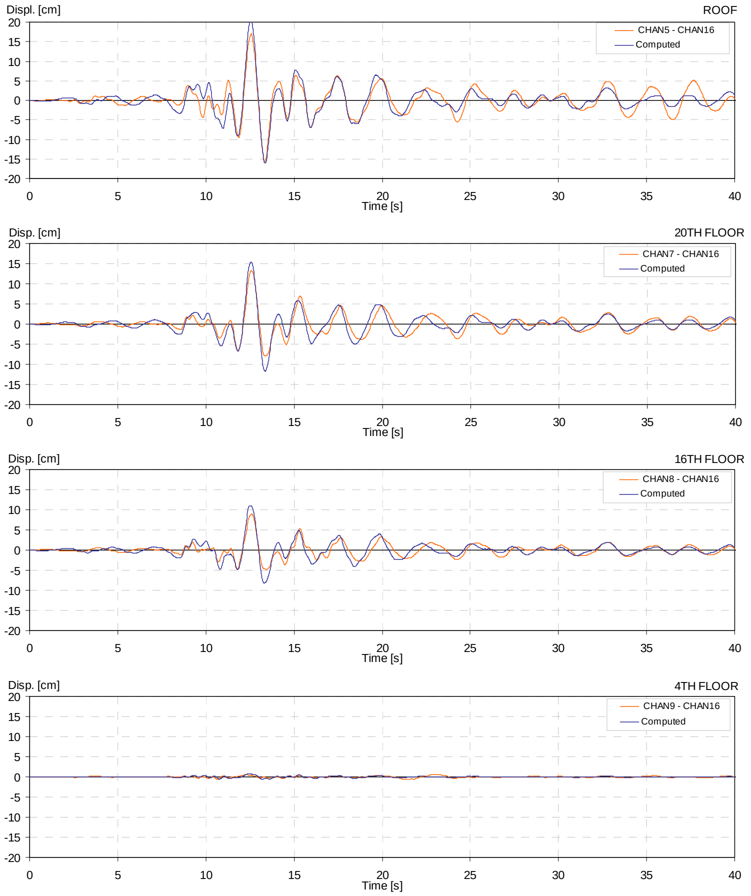

Figure 5. Comparison of computed and recorded relative displacements in the NS components of the 24-story building in Oakland California during the 1989 Loma Prieta earthquake

modeled as shear beams. Besides being able to consider a wide range of types of deformation the GISD has other advantages. For example, the GISD is based on modal analysis techniques that are familiar to structural engineers while Iwan's spectrum is based on wave propagation techniques that are typically not known to structural engineers. Furthermore, the GIDS uses a classical damping which as shown in figures 3 and 5 is capable of reproducing the recorded response of buildings and avoids the problems that are encountered when using the damping model used in the conventional drift spectrum (the reader is referred to Kim and Collins, 2002 or Miranda and Akkar, 2005 for a description of these problems).

The ordinates of the *generalized interstory drift spectrum* (GIDS) are defined as the maximum peak interstory drift demand over the height of the building and are computed as

$$IDR_{\max} \equiv \max_{\forall t,x} \left| \theta(x,t) \right| \tag{14}$$

The generalized interstory drift spectrum is a plot of the fundamental period of the building in the abscissas versus $IDR_{\max}$ in the ordinates. Similarly to the response spectrum, the GIDS provides seismic demands for a family of systems with different periods of vibration. However, instead of having ordinates of maximum relative displacement, maximum relative velocity or maximum acceleration of SDOF systems, the GIDS provides a measure of peak interstory drift demands, which is a demand parameter that is better correlated with damage. In particular, the GIDS provides a rapid estimation of peak interstory drift demand in buildings with different periods of vibration.

If the same damping ratio is used for the *m* contributing modes, then the model is fully defined by using only four parameters: (1) the fundamental period of vibration of the building, T_1; (2) a modal damping ratio that represents the damping ratio in the building, ξ; (3) the lateral stiffness ratio α; and (4) the building height, H. Since the derivative of the modes, modal participation factors and period ratios can be computed in closed-form solution, the GIDS is computationally very efficient, requiring just a few seconds in most personal computers. If empirical relations between building height and fundamental period are used, the number of parameters is then reduced from four to three.

Figure 6 presents generalized interstory drift spectra for four different values of α values computed for the NS component of the Rinaldi Receiving Station from the 1994 Northridge earthquake and the N49W component of the Takatori Station from the 1995 Hyogo-ken-Nambu (Kobe) earthquake. Results presented in this figure were computed using Eqs. (13) and (14) considering the first six modes of vibration (i.e., m=6). For a given fundamental period of vibration, the total height of the model needed in Eq. (13) was computed using the relationship used for steel moment-resisting frames in the 1997 UBC code (ICBO, 1997), namely, T_1=0.0853$H^{0.75}$, where H is in meters. It can be seen that the influence of α is relatively small for fundamental periods of vibration smaller than 1.5s. However, for longer fundamental periods of vibration the differences become larger. In particular, it can be seen that interstory drift demands can be larger or smaller than those computed with a model corresponding approximately to a shear beam (α=650) indicating that Iwan's drift spectrum may underestimate or overestimate drift demands for buildings that cannot be modeled as shear beams.

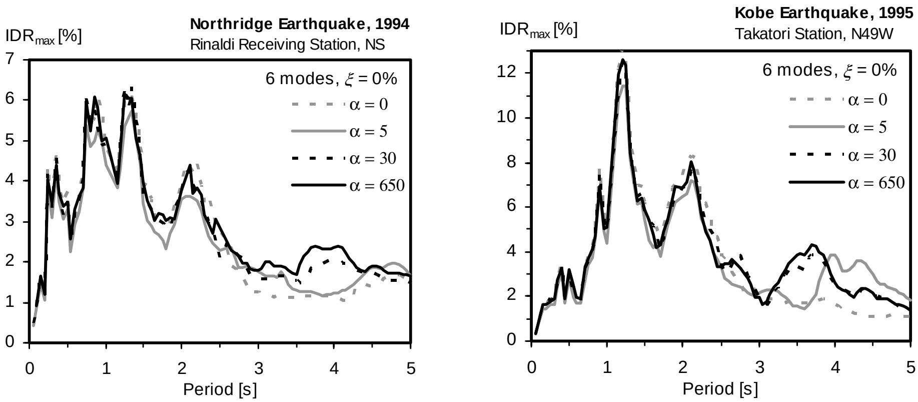

Figure 6. Influence of α on generalized interstory drift spectra (after Miranda and Akkar, 2005)

Floor Accelerations Demands

While structural damage and many kinds of nonstructural damage are primarily caused by interstory drift demands, Miranda and Taghavi (2005) have shown that damage to building contents, ceilings, light fixtures, piping and many other types of nonstructural components is primarily related to peak floor accelerations and to floor spectral ordinates. The simplified model shown in figure 1 can also be used to estimate floor acceleration demands in buildings. Unlike lateral displacements or interstory drifts that are often dominated by the fundamental mode of vibration, floor accelerations are typically strongly influenced by higher mode response even more building of moderate height.

The total floor acceleration at non-dimensional height *x=z/H* can be computed as

$$\ddot{u}^t(x,t) \cong \ddot{u}_g(t) + \sum_{i=1}^{m} \Gamma_i \, \phi_i(x) \ddot{D}_i(t) \tag{15}$$

where $\ddot{D}_i(t)$ is the relative acceleration of a SDOF system with a period of vibration equal to that of the *i*th-mode of vibration of the structure. In the proposed method, the damping ratio in all modes is assumed to be the same and equal to a damping ratio that approximately characterizes the damping in the structure. It should be noted that Eq. (15) would be exact for the building shown in figure 1 only if the actual modes shapes, frequencies of vibration and modal participation factors of the building are used, and only if the summation included an infinite number of modes. Therefore, the main sources of error in the proposed method when applied to real buildings responding elastically are: (a) truncation error (e.g., only considering the first three modes of vibration); (b) use of approximate mode shapes and approximate modal participation factors; and (c) simplified representation of the damping in the structure.

Equation (15) can be also be written in terms of, more familiar, absolute modal acceleration times histories as follows:

$$\ddot{u}^t(x,t) \cong \left[1-\sum_{i=1}^{m}\Gamma_i\ \phi_i(x)\right]\ \ddot{u}_g(t)+\sum_{i=1}^{m}\Gamma_i\ \phi_i(x)\ddot{D}_i^t(t) \tag{16}$$

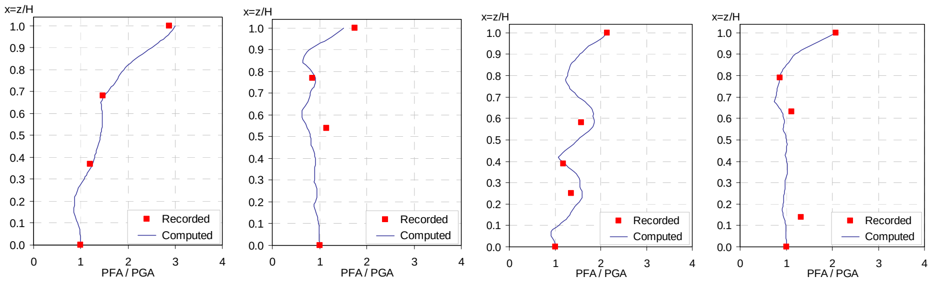

9-story Bldg. Hayward 14-story Bldg. Hollywood 13-story Bldg. Hayward 24-story Bldg. Oakland

Figure 7. Comparison of computed and recorded variation of peak floor acceleration demands in four reinforced-concrete buildings located in California

where $\ddot{D}_i^t(t)$ is the absolute acceleration time history of a SDOF system with a period of vibration equal to that of the *i*th-mode of vibration of the structure.

Peak floor accelerations computed with equation (15) for four buildings are shown in figure 7. In this figure peak floor accelerations at instrumented floors have been normalized by the peak acceleration recorded at the base of the building and are indicated in the figure by red squares. Also shown in the figure are the normalized peak floor acceleration demands computed with the proposed simplified method. It can be seen that again, the proposed method is capable reproducing relatively well the variation of acceleration demands along the height of the buildings. Furthermore, it can be seen that the distribution of acceleration demands may differ considerably from the linear variation that is commonly assumed in many building codes. Taghavi and Miranda (2003) have shown that, unlike present U.S. recommendations which for the design of nonstructural components assume that the variation of floor acceleration demands is period-independent, this variation is strongly influenced by the fundamental period of vibration of the structure and also, but to a lesser degree, by the lateral stiffness ratio.

While capturing peak floor accelerations with simplified models and a limited number of parameters in building is challenging, the estimation of floor acceleration time histories and ordinates of floor spectra are even more challenging as they depend on an accurate estimation of frequencies of vibration of higher modes. In the proposed method the same parameter is used to control the spatial variation of the motion within the building and period ratios, therefore it is interesting to explore the level of accuracy that can be obtained with the proposed simplified analysis method when estimating these response parameters that are strongly influenced by higher modes. Figures 17 to 20 show comparison of recorded floor acceleration time histories with those computed with the approximate method and comparison of 5% damped floor spectra computed with recorded and approximate acceleration time histories. As shown in these figures the model is able to capture quite well these response parameters as well.

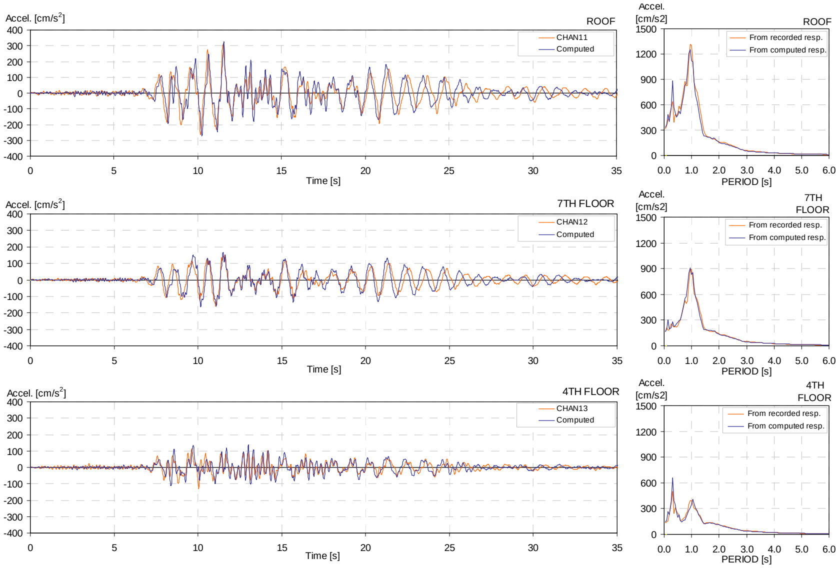

Figure 8. Comparison of computed and recorded acceleration demands in the EW components of a 9-story building in San Bruno California

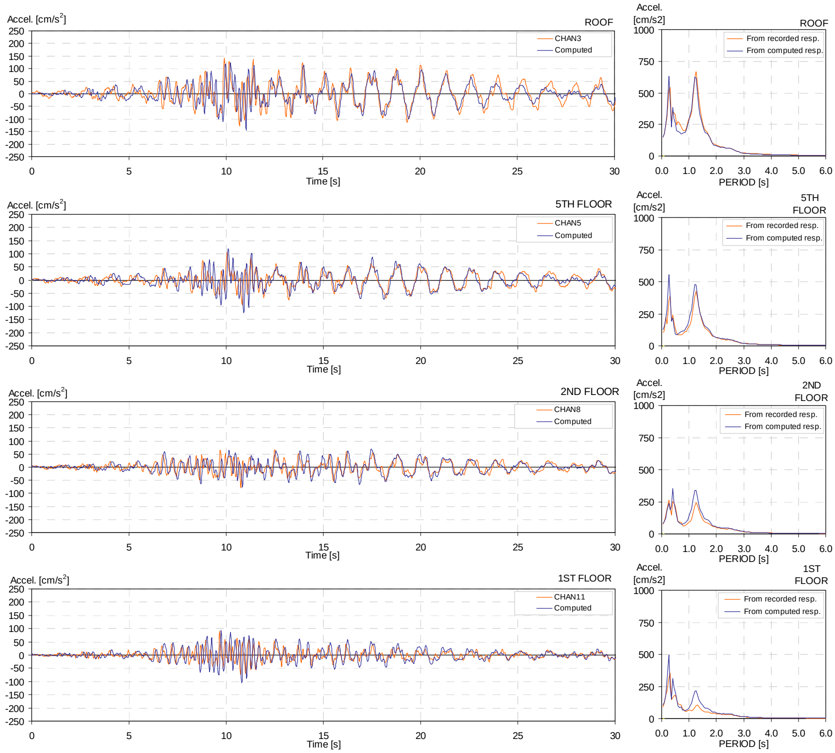

Figure 9. Comparison of computed and recorded acceleration demands in the NS components of a 13-story building in Hayward California

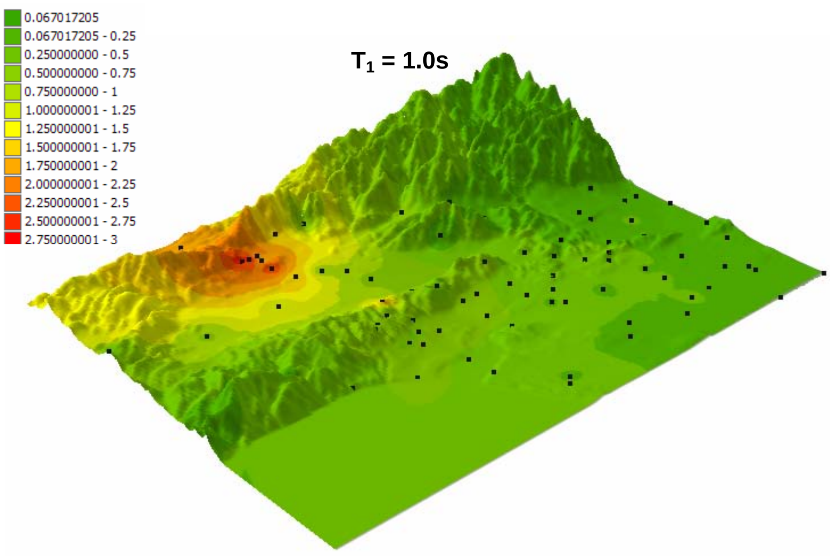

Figure 10. Maximum IDR_{max} contour map for moment-resisting buildings with fundamental periods of vibration of 1.0s computed using 91 recording stations deployed in the Los Angeles metropolitan area and triggered during the 1994 Northridge earthquake.

Rapid Damage Assessment

Many studies have indicated that interstory drift ratios are correlated very well with structural damage in buildings. Because of its many computational advantages, the generalized interstory drift spectrum described in the previous sections, can be used in rapid damage assessment at urban areas with wide range of structural systems for a major earthquake event. This can be accomplished by analyzing continuous models corresponding to different structural systems at instrumented locations. A typical example is presented for the Los Angeles Metropolitan area in Figure 10. This three dimensional contour map was prepared by using the ground motions recorded at 91 strong motion stations that were triggered during the 1994 Northridge earthquake in the city of Los Angeles and San Fernando Valley.

Ground motions were downloaded from the website of COSMOS Virtual Data Center (http://db.cosmos-eq.org) and all of them are either free-field records or ground motions recorded at the ground floor of one-story buildings. Figure 10 shows interstory drift demands for buildings with fundamental periods T_1=1.0s corresponding to mid-rise moment-resisting reinforced concrete frame buildings in this region. The value of α was taken as 12.5 and the mean fundamental period empirical relationship by Chopra and Goel (2000) was used to compute the building height as a function of the fundamental period of vibration. Mean interstory drift ratios of both horizontal components are computed at each recording station using 5 percent damping ratio.

Summary and Conclusions

The map presented in Figure 10 indicates that for the given distribution of strong motion stations, frame buildings with fundamental periods of approximately 1.0s located in the northern portion of the San Fernando Valley were subjected to large interstory drift demands and therefore more susceptible to serious structural/nonstructural damage compared to those of stiffer or more flexible buildings in the same region. Another important observation from this map is the consistency of computed interstory drift demands with the reported rupture direction.

It should be noted that even though the elaboration of the map shown in figure 10 involves the computation of the seismic response of both directions of building models located at more than 90 recording stations, they can be computed in personal computers within a few minutes after an earthquake provided that ground motions are sent to a central location using telemetry. These maps can provide a valuable tool in rapid damage assessment as well as for planning purposes using various ground motion scenarios.

Instead of placing an identical structure at each location where a ground motion recording instrument is located, it is possible to use the ground motions recorded in the city to conduct an analysis of large number of existing structures within the city, hence extending the concept of structural building analysis to structural “city” analysis.

New analytical tools for rapid building seismic response estimation aimed at rapid seismic performance assessment of large inventories buildings in urban areas have been presented. The simplified seismic analysis tools make use of continuum models consisting of a flexural beam coupled with a shear beam.

Unlike sophisticated analysis models that require a significant amount of information and are computationally very demanding, the proposed analytical tool is fully defined by only three or four parameters. That is, only one or two parameters in addition to those required to define a linear elastic single degree of freedom system. Seismic response computation using the proposed analytical tool takes only fractions of a second in most personal computers, hence allows for the rapid assessment of hundreds of buildings, within few minutes after an earthquake. A typical case study from the 1994 Northridge earthquake was presented to demonstrate how the proposed procedure can be used as an efficient tool to serve for such a purpose.

It should be noted that the proposed analytical tools have not been developed as replacement of more refined and accurate models. The simplified models can be particularly helpful for the following applications:

1. Screening tool to identify buildings that are likely candidates for more detailed analyses.
2. Screening tool to identify buildings and urban regions that are more likely to be damaged in future earthquakes
3. As a tool to conduct parametric studies to identify structural parameters or ground motion parameters that increase seismic demands on buildings
4. Planning tool for emergency managers and city officials by using motions from previous ground motions or synthetic ground motions from possible future events.
5. For loss estimation of large inventories of building by insurance or reinsurance companies.

6. To provide early performance estimates within minutes of a seismic event.

Acknowledgements

Portions of the work presented in this paper have been conducted by the author in collaboration with Shahram Taghavi, and Profs. Sinan Akkar and Eduardo Reinoso. Their assistance is greatly acknowledged. Special thanks are also given to Dr. Masayuki Kohiyama for providing assistance to the author in the use of GIS software.

References

Applied Technology Council (1982), "An investigation of the correlation between earthquake ground motion and building performance", ATC-10, Palo Alto, California, Nov.

Chopra, A.K., and Goel, R.K. (2000). "Building period formulas for estimating seismic displacements," *Earthquake Spectra*, 16(2), 533-536.

Gülkan P and Akkar S. (2002). "A simple replacement for the drift spectrum," *Engineering Structures*, 24(11), 1477-1484.

International Conference of Building Officials (ICBO). (1997). "Uniform Building Code," International Conference of Building Officials, Whittier, California.

Iwan, W.D. (1997). "The drift spectrum: a measure of demand for earthquake ground motions," *J. Struct. Engrg.,* ASCE, 123(4), 397-404.

Kim, J., and Collins, K.R. (2002). "Closer look at the drift demand spectrum," *J. Struct. Engrg.,* ASCE, 128(7), 942-945.

Kircher, A. et al. (1997), "Development of Building Damage Functions for Earthquake Loss Estimation", Earthquake Spectra, 13,4, pp. 663-682

Miranda, E., and Akkar, S. (2005). "Generalized Interstory Drift Spectrum." Submitted for publication to *J. of Structural Engineering*, ASCE.

Miranda, E., and Taghavi, S. (2005). "Approximate floor acceleration demands in multistory buildings I: formulation." *J. of Structural Engineering*, ASCE, 131(2), pp., 203–211.

Murphy, J. R.; O'Brien, L. J. (1977), "The correlation of peak ground acceleration amplitude with seismic intensity and other physical parameters", Bulletin of the Seismological Society of America, 67, 3, June, pp. 877-915

Reinoso, E. and Miranda, E. (2005), "Estimation of floor acceleration demands in high-rise buildings during earthquakes," to appear in the June issue of *J. of Tall Buildings*, Wiley.

Rihal, S. (1991), "Correlation Between Recorded Building Data and Nonstructural Damage During the Loma Prieta Earthquake", *SMIP91 Seminar on Seismological and Engineering Implications of Recent Strong-Motion Data.*

Taghavi, S. and Miranda, E. (2005). "Approximate floor acceleration demands in multistory buildings II: applications." *J. of Structural Engineering*, ASCE, 131(2), pp., 212–220.

Trifunac, M. D.; Brady, A. G. (1975), "On the correlation of seismic intensity scales with the peaks of recorded strong ground motion", *Bulletin of the Seismological Society of America*, 65, 1, Feb, pp. 139-162

Wald, David J.; et al. (1999b), "TriNet ShakeMaps: rapid generation of peak ground motion and intensity maps for earthquakes in Southern California," *Earthquake Spectra*, 15,3, pp. 537-555.

Wald, David J.; et al. (1999c), "Relationships between peak ground acceleration, peak ground velocity, and modified Mercalli intensity in California," *Earthquake Spectra*, 15,3, pp. 557-564.

Masayoshi Nakashima
Professor
Disaster Prevention Research Institute, Kyoto University
Gokasho, Uji, Kyoto 611-0011 JAPAN
Director
Director, Hyogo Earthquake Engineering Research Center (E-Defense), National Research Institute for Earth Science and Disaster Mitigation (NIED)
1501-21, Nishikameya, Mitsuta, Shinjimicho,
Miki, Hyogo, 673-0515 JAPAN
Steel structures, Experimental techniques, Base-isolation

My personal acquaintance with Luis began in 1987, when I visited Mexico City for the first time. I was a member of a Japan International Cooperation Agency (JICA) team, in Mexico to examine the possibilities of Mexican-Japanese collaboration on earthquake engineering research. One day, the team visited Luis' office, and I shook hands with him. I am sure that he does not remember that occasion, but I recall vividly the striking modesty and kindness of this highly respected researcher in the earthquake engineering community. More than fifteen years later we met again, this time in Kobe, Japan. He was there as a distinguished guest at the inauguration ceremony of E-Defense, the world largest shaking table, on the outskirts of Kobe. It was a two-day ceremony, featuring an inauguration party held on January 15, 2005 and the inauguration's international symposium held on January 16, 2005. He was a keynote speaker at the symposium, delivering a very solid message about the past accomplishments, present problems, and future challenges of earthquake engineering and expressed great expectations for the contribution of E-Defense to earthquake disaster mitigation worldwide. We are very thankful to Luis for his strong support of E-Defense. On behalf of Luis's many Japanese friends, I express my sincere appreciation of his long-time leadership in the advancement of earthquake engineering, and wish him continuing health and leadership.

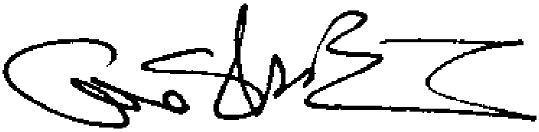

Masayoshi Nakashima
August 10, 2005

TEST ON COLLAPSE BEHAVIOR OF STRUCTURAL SYSTEMS

ABSTRACT

Damage observed in the 1995 Hyogoken-Nanbu (Kobe) earthquake highlighted the importance of accumulating real data by experimentation regarding the earthquake response, damage, and collapse of structures. Full-scale tests to complete collapse in real time are indispensable. Four series of such tests conducted by the writer are presented, including complete failure tests applied to steel beams, columns, and connections, and full-scale tests applied to a steel moment frame. A newly built large shaking table owned by E-Defense is introduced, and its mission, strength, and status are outlined. Ongoing research projects including the NEES/E-Defense program are described.

Lessons Learned from 1995 Hyogoken-Nanbu (Kobe) Earthquake

The 1995 Hyogoken-Nanbu (Kobe) earthquake caused devastating damage to buildings and infrastructure in Kobe and its vicinity [Architectural 1995, Kinki 1995, Nakashima et al 1998a, Nakashima 2001]. The earthquake taught us lessons about structural, economical, societal, cultural, and human factors. Since the earthquake, much research and development has been implemented for the mitigation of earthquake disasters. The 1995 Kobe earthquake, however, was not the sole motivation. Japan is destined to suffer from large earthquakes on a regular basis. Figure 1 shows a map of Japan, and the bold line indicates an ocean ridge called the Nankai trough, running deep along the Pacific Coast of Japan. The trough is divided into three regions, Tokai, Tonankai, and Nankai, reading from east to west. Slips and ruptures have occurred periodically in these regions.

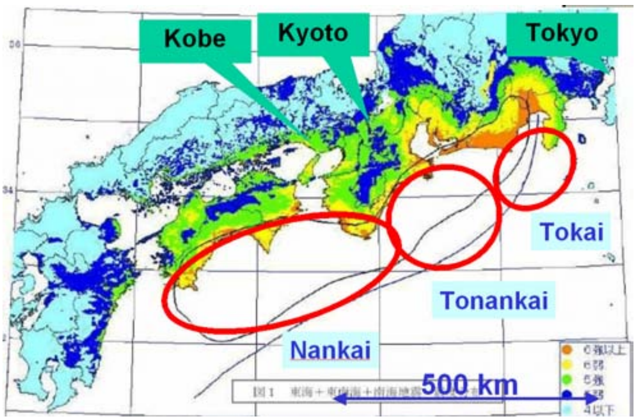

Figure 1. Nankai Trough and periodical large earthquake

Table 1 shows the historical earthquakes related to the slips and ruptures of the three regions [Council 2004]. In some earthquakes, one or two of the regions ruptured; all three regions ruptured simultaneously in other cases. The frequency of occurrence was between one hundred and one hundred and fifty years. Observing the pattern of these previous earthquakes, Japan is to be hit by large earthquakes in the middle of the twenty-first century. Contemporary science is not able to predict the date and time of the next rupture precisely, but the public throughout Japan is fully aware that within several decades Japan will be hit by a very large earthquake.

TABLE 1. Historical records of Nankai, Tonankai, and Nankai ruptures

Year	Earthquake	Toka	Tonankai	Nankai
1605	Keicho	□ ›	□ ›	
1701	Hoei	□ ›	□ ›	□ ›
1854	Ansei	□ ›	□ ›	□ ›
1944	Tonankai		□ ›	
1946	Nankai			□ ›
20xx	**NEXT**	?	?	?

In 2005, the Council of National Disaster Mitigation, chaired by the Prime Minister of Japan, disclosed an estimate of the damage that Japan will sustain if the Nankai trough were ruptured again [Council 2004]. Table 2 shows the damage statistics in terms of the number of houses and buildings collapsed, the death toll, and direct capital loss for various combinations of ruptures. Should the three regions rupture all together, about forty million people, equivalent to one-third of the entire population of Japan, would be affected, about one million houses and buildings would collapse, about twenty-five thousand people might lose their lives, and the economic loss might amount to close to one trillion US dollars. As Tables 1 and 2 clearly indicate, the earthquake disaster was, is, and will remain the most critical national problem in Japan.

TABLE 2. Damage estimates for possible Nankai, Tonankai, and Nankai ruptures

	Tokai	Tonankai & Nankai	Tokai & Tonanka & Nankai	1995 Kobe
Collapse (x 1000)	460	629	940	105
Death	9,200	17,800	24,700	6,400
Loss (billion $)	260 - 370	380 - 570	530 - 810	100

Needs of Structural Test

Regarding the 1995 Kobe earthquake, the writer is convinced that the following two lessons are most notable in the structural aspect.

(1) Cities and towns throughout Japan have large stocks of old buildings and infrastructural systems whose seismic capacity is insufficient. To prepare for future large earthquakes, it is crucial to accurately evaluate their existing seismic capacities and then to retrofit and rehabilitate them accordingly.

(2) Much larger shaking than that contemplated in current seismic design is known to be possible. Evaluation of the reserve seismic capacity of existing buildings and infrastructural systems, development of design and construction technologies to enhance the seismic capacity, and implementation of these technologies for real design and construction are critical.

As evidence of (1), Fig. 2 shows a photo taken in downtown Kobe immediately after the 1995 Kobe earthquake. Two RC buildings, standing side by side, disclosed a clear contrast in damage; the one on the right side lost the third story completely, while the one on the left side looked nearly intact from the exterior. The ages of the structures were significantly different. The severely damaged building was nearly forty years old and had been constructed according to obsolete design and construction practices, whereas the undamaged building was relatively new. This distinctive contrast demonstrates that earthquake-resisting capacity can differ significantly among structures.

Figure 2. A contrast of damage observed in 1995 Kobe earthquake.

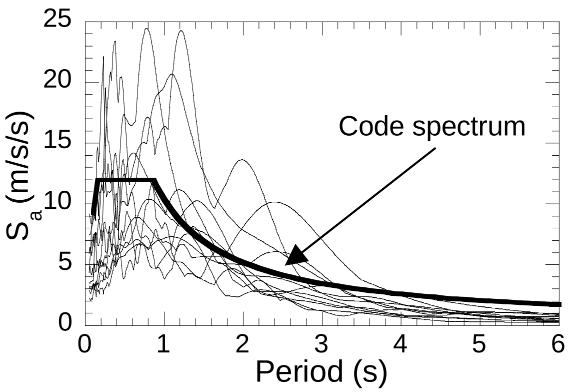

Figure 3. Pseudo accelerations of strong motions recorded in 1995 Kobe earthquake.

As evidence of (2), Fig. 3 shows the pseudo-acceleration spectra of eleven strong motions recorded in the 1995 Kobe earthquake [6], together with the design spectrum stipulated for large earthquakes in the current Japanese seismic design code. It is evident that quite a few records possess significantly larger pseudo-accelerations than the code acceleration. Ground motions that would exceed those considered in the seismic code were also obtained in other recent earthquakes, e.g. the 1999 Tottoriken-Seibu, 2000 Geiyo, and 2004 Chuetsu earthquakes.

In light of lessons (1) and (2) cited above, it is crucial to identify the state of *complete collapse* in which the structure no longer can sustain gravity and as a result will kill people in the structure. This need is relevant to the characterization of the *collapse margin*, defined as the reserve capacity that the structure possesses for loads greater than that specified in seismic code up to the collapse. The collapse margin is difficult to characterize because of the scarcity of real data. Severe earthquake ground motions that would cause structure collapses occur very rarely, which makes it difficult to monitor or measure the real behavior of structures subjected to such events. The interactions between members and system behavior are known to be complex; hence tests on a structural system that involve force redistribution due to member yielding and plastification are indispensable. Building structures, however, are massive, and it is difficult to fabricate and load them in the laboratory, while miniature models are known to fail to duplicate real building behavior because of lack of similitude. Advances in numerical analysis methods, particularly those using the finite element method, are notable, but the analyses insufficiently duplicate the behavior of structures to collapse, which involves significant material nonlinearity, strength and stiffness degradations, and topology changes such as fracture, separation, and detachment.

For the past ten years, much research has been conducted in the name of "performance-based seismic design" on the development of innovative systems by which to enhance the functionality, operability, and safety of structures. Base-isolation and passive dampers are typical examples; indeed, numerous inventions have been proposed toward this end. All such research and development must, however, be checked for expected actual performance before being transferred with confidence to real design and construction practices. Here, experimentation again plays a very important role to provide *real data* for performance checking. The accumulation of such data is not sufficient, because tests in the full-scale are rare due to limitations of loading devices. Furthermore, not a few materials used for new inventions are affected significantly by the rate of loading, which aggravates the situation because of the scarcity of facilities that are capable of conducting large dynamic loading tests on a realistic scale.

The need for *real data* obtained by experimentation is deemed extremely urgent for the advancement of earthquake engineering, particularly for issues pertinent to collapse (relative to mildly inelastic, rather stable action), rate-of-loading (dynamic loading relative to quasi-static loading), realistic-scale (relative to miniature models), and structural systems (relative to components)

Example Tests Conducted to Reproduce Complete Failure and Collapse

Over the past few years, the writer and his group have conducted tests that focused directly on the issues of collapse in realistically scales structural systems. They are summarized below.

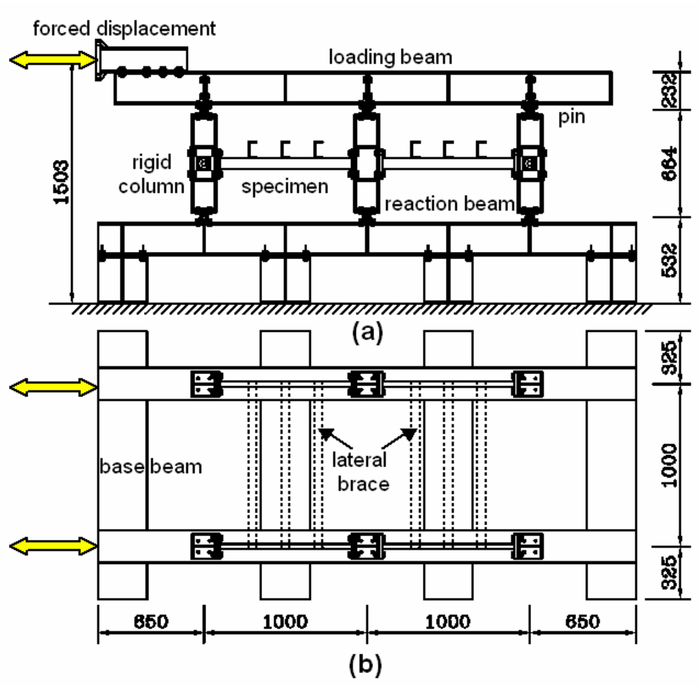

Figure 4. Test setup for reproduction of complete failure of steel beams

Behavior to Complete Failure of Steel Beams Subjected to Cyclic Loading [Liu et al 2003]

An experimental study was conducted on steel beams subjected to cyclic loading to extremely large deformations (Fig. 4).

The study aimed to collect information on beam hysteretic behavior up to complete failure, in the belief that such information is needed for the establishment of performance-based design. Test beams were about 1/10-scale models, and the effects of RBS details and lateral braces arranged at beam top flanges were examined. Behavior up to the cyclic loading amplitude of 0.06 rad was commensurate with behavior observed in many previous studies [Fig. 5(a)]. Behavior in extremely large deformations from 0.1 to 0.5 rad amplitudes was significantly different from the behavior in large deformations (to 0.06 rad amplitude) (Fig. 6). The RBS beam failed earlier in the reduced cross-section, primarily due to strain concentrations at the section [Fig. 5(b)]. Lateral braces also caused strain concentrations, leading to earlier fractures. Significant increase in the maximum resistance was observed in extremely large deformations for beams not braced laterally. Tensile axial forces induced in the beam according to the geometry change were responsible for the increase.

Instability and Complete Failure of Steel Columns Subjected to Cyclic Loading [Nakashima and Liu 2005]

In a testing system designed for large deformations, structural columns were loaded to complete failure, defined as either complete separation of the column or inability to sustain the prescribed axial load. The test system consisted of very large stroke quasi-static jacks, digital displacement transducers that can ensure accurate measurement of large deformations, hydraulic pump units capable of controlling oil flow, controllers that control the jack motion, and separate personal computers for operating the jack controllers and for supervising and measuring data (Fig. 7). These components were connected on-line for data and signal operations, which enables automatic and accurate load control for tests that lead specimens to complete failure. Six columns having a square tube cross-section were tested in cyclic loading conditions, with axial load and column length as major parameters. The load-deformation relationships obtained from the tests were presented in detail, and relationships among the deformation capacity, failure mode, slenderness, and axial load were discussed (Fig. 8). An intermediate axial load of 30% of the yield axial load was effective in retarding the occurrence and growth of cracks, resulting in larger deformation capacity to complete failure. Finite element analysis accurately duplicated the experimental behavior up to a large inelastic range including material yielding, strain hardening, and local buckling. It failed to simulate the experimental behavior in a very large deformation range where the column surfaces crashed and contacted each other (Fig. 19). More experimental data is strongly needed on the behavior of structural systems and elements at and near complete failure.

(a) (b)

Figure 5. Behavior of beams in large deformations: (a) *Lateral torsional buckling;* (b) *fracture*

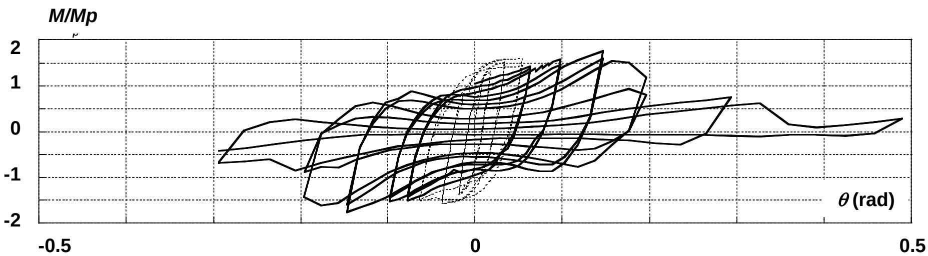

Figure 6. End moment – end rotation relationships to complete failure

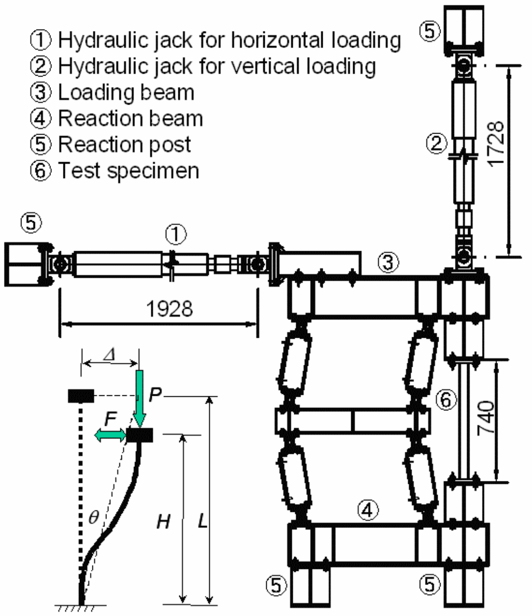

Figure 7. Test setup for reproduction of complete failure of steel columns

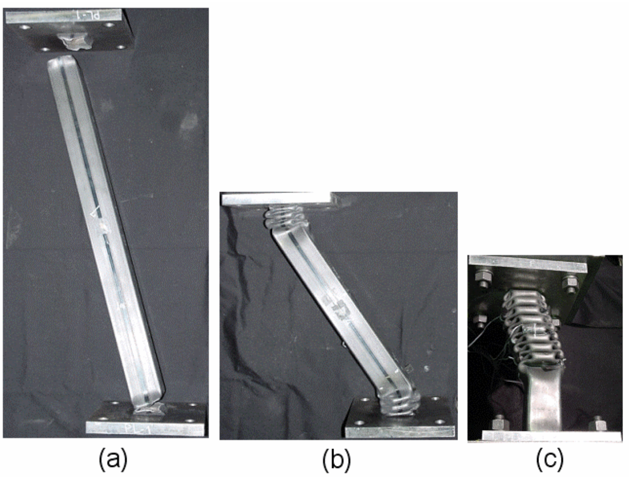

Figure 8. Test specimens at end of loading: (a) No axial load; (b) medium axial load; (c) large axial load

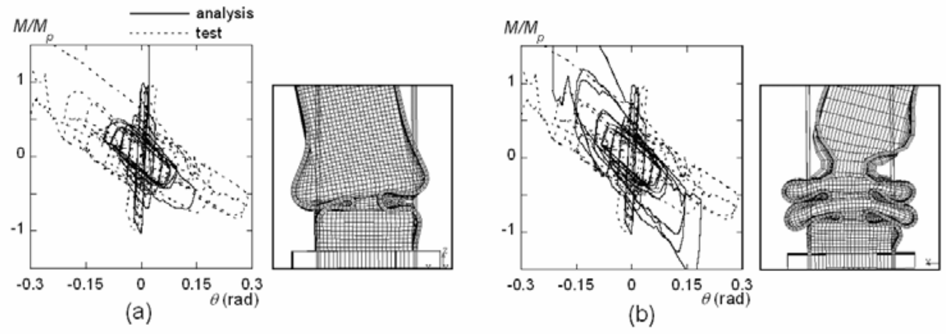

Figure 9. Comparison with test and finite element analyses: (a) *Slip option;* (b) *glue option*

Tests of Welded Beam-Column Subassemblies I: Global Behavior and II: Detailed Behavior [Nakashima et al 1998b, Suita et al 1998]

Cyclic loading tests were applied to fourteen full-scale beam-column subassemblages (Fig. 10). Efforts undertaken in the Japanese steel community in response to damage observed at welded beam-to-column connections in the 1995 Hyogoken-Nanbu (Kobe) Earthquake were introduced. The major test parameters chosen in this study were: type of steel, type of connection, type of weld access holes, type of weld tabs, and type of loading. The test results were presented in terms of the ductility capacity of the test specimens. Major findings were as follows. All specimens developed plastic rotations and cumulative plastic rotations of 0.03 rad and 0.3 rad. respec tively, suggesting that the ductility capacity of the specimens was sufficient in light of present Japanese seismic design. Dynamic loading had no detrimental effect on ductility capacity (Fig. 11). A significant rise in temperature observed in the dynamic loading tests was the likely cause of the larger ductility capacity and more ductile fracture. Fracture surfaces were examined from fractography analysis. Changes in material hardness before and after the test are also investigated, and the correlation between the hardness increase and cumulative plastic strain was quantified (Fig. 12). Modified details for the weld access hole had the effect of preventing cracks initiating from the toe of the weld access hole.

Figure 10. Test setup for fracture of steel beam-to-column connections

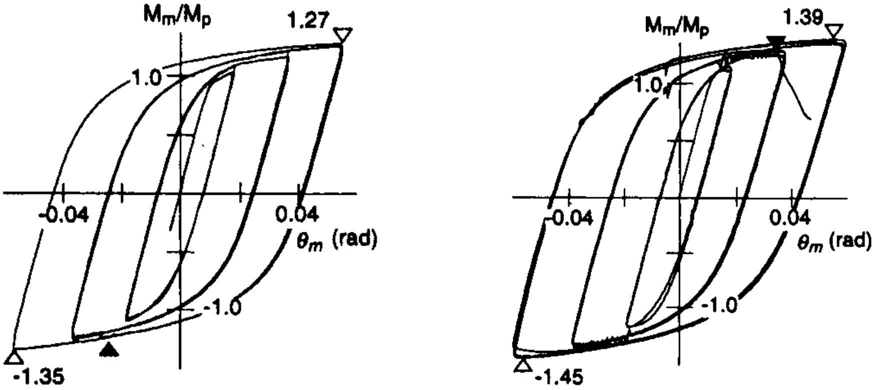

(a) (b)

Figure 11. End moment – end rotation relationships: (a) *Quasi-static loading;* (b) *dynamic loading*

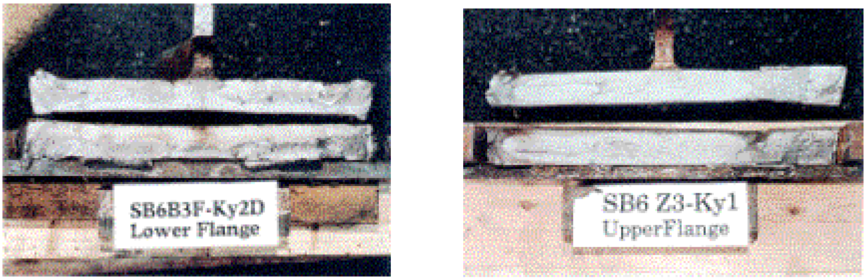

(a) (b)

Figure 12. Fracture surfaces: (a) *Brittle fracture in quasi-static loading;* (b) *ductile fracture in dynamic loading*

Test on Full-Scale Three-Story Steel Moment Frames and Assessment of Numerical Analysis to Trace Inelastic Cyclic Behavior [Nakashima et al 2006]

A test on a full-scale model of a three-story steel moment frame (Fig. 13) was conducted, with the objectives of acquiring real information about the damage and serious strength deterioration of a steel moment frame under cyclic loading, studying the interaction between the structural frame and nonstructural elements, and examining the capacity of numerical analyses commonly used in seismic design to trace the real cyclic behavior. The outline of the test structure and test program was presented, results on the overall behavior were given, and correlation between the experimental results and the results of pre-test and post-test numerical analyses was discussed. Pushover analyses conducted prior to the test predicted the elastic stiffness and yield strength very reasonably. With proper adjustment of strain hardening after yielding and composite action, numerical analyses were able to duplicate the cyclic behavior of the test structure with great accuracy up to a drift angle of 1/25 (Fig. 14). The analyses could not trace the cyclic behavior for larger drifts, in which serious strength deterioration occurred due to the fractures of beams and anchor bolts and the progress of column local buckling (Fig. 15).

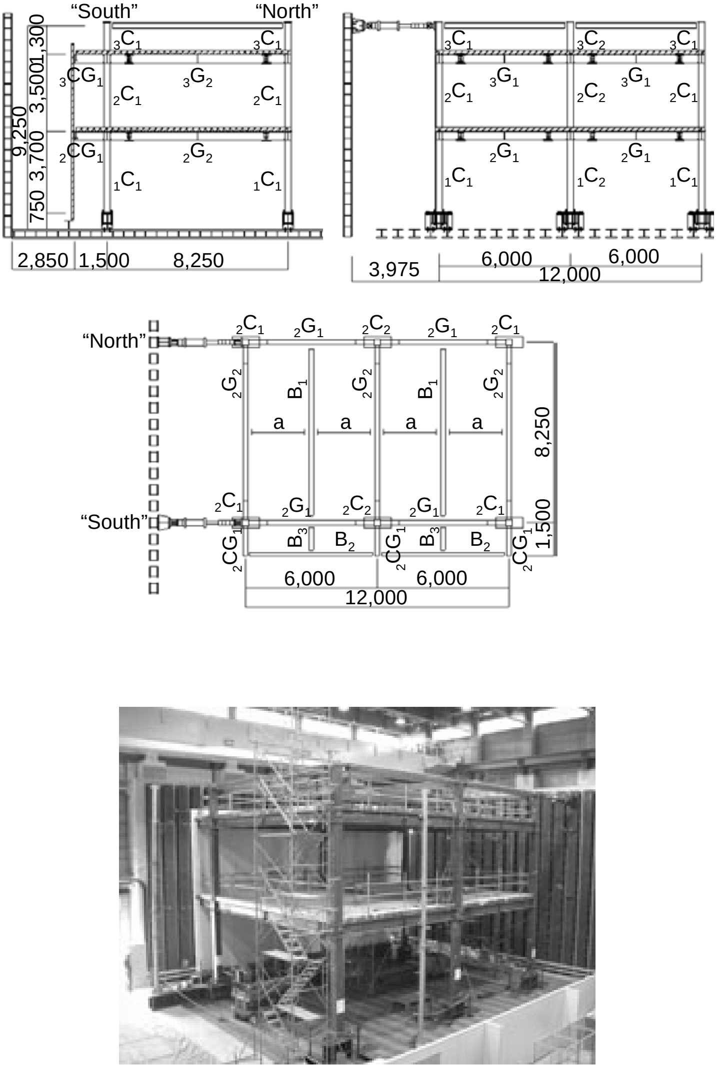

Figure 13. A three-story full-scale steel moment frame

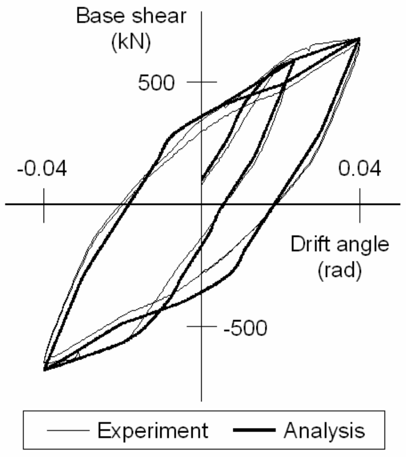

Figure 14. Comparison of test and analysis for behavior with mild plasticity.

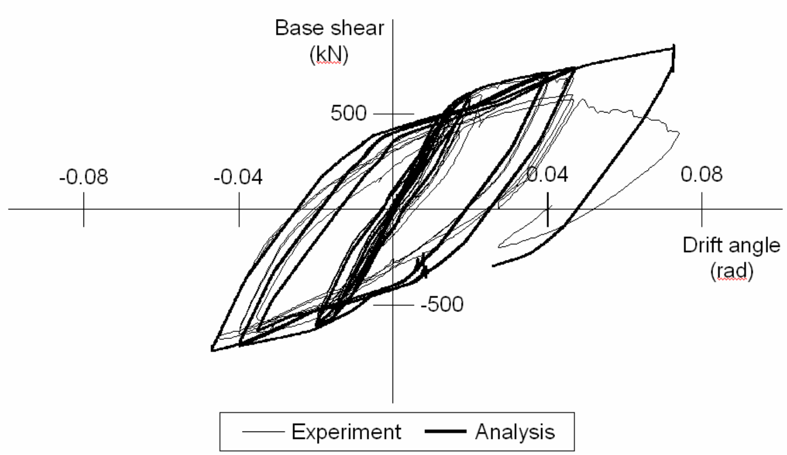

Figure 15. Comparison of test and analysis for behavior with serious strength deterioration.

Development and Completion of E-Defense

Over the last ten years, the National Research Institute for Earth Science and Disaster prevention (NIED) had been constructing a shaking table facility, known as E-Defense [Hyogo 2005]. E-Defense was completed in March 2005, and its operation started in April 2005. The Hyogo Earthquake Engineering Research Center was established on October 1, 2004, to manage research projects using E-Defense and to operate and maintain the facility. E-Defense has the unique capacity to experiment with life-size buildings and infrastructural systems in real earthquake conditions, and stands as a tool of ultimate verification. With this feature, E-Defense should help expedite the transfer of various research outputs into the practice of earthquake disaster mitigation.

Figure 16 is a bird's eye view of E-Defense, located in a city called Miki on the north of Kobe City. The heart of the facility is a jumbo shaking table in the center of the site. The table is attached to five actuators in each horizontal direction and supported by fourteen actuators installed vertically underneath the table (Fig.17). Table 3 shows the major specifications of the table. The table is 20 meters by 15 meters in the plan dimension. It can accommodate a specimen up to a weight of 12 MN (1,200 metric ton). The unique feature of the table is that can produce shaking of a velocity of two meters per second and a displacement of one meter in the two horizontal directions simultaneously. As far as the capacity is concerned, the table owned by E-Defense appears to be the largest shaking table in the world.

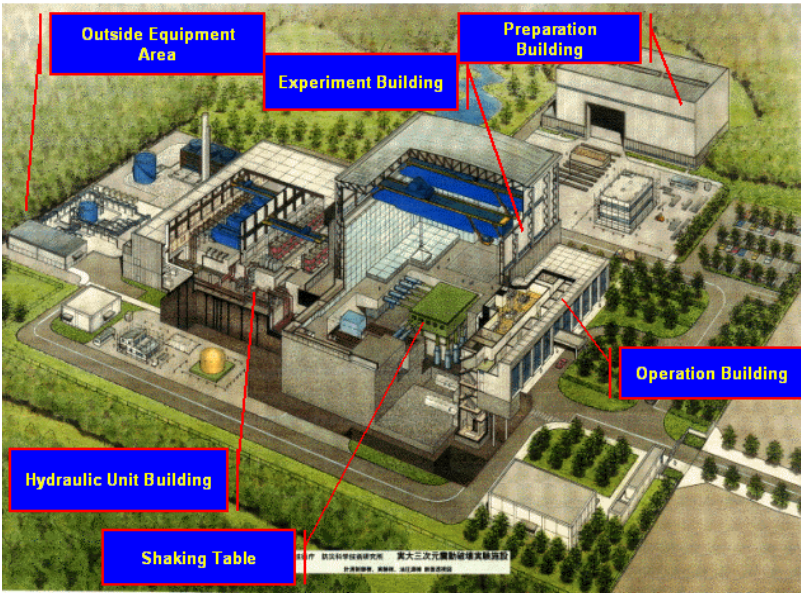

Figure 16. A bird eye view of E-Defense

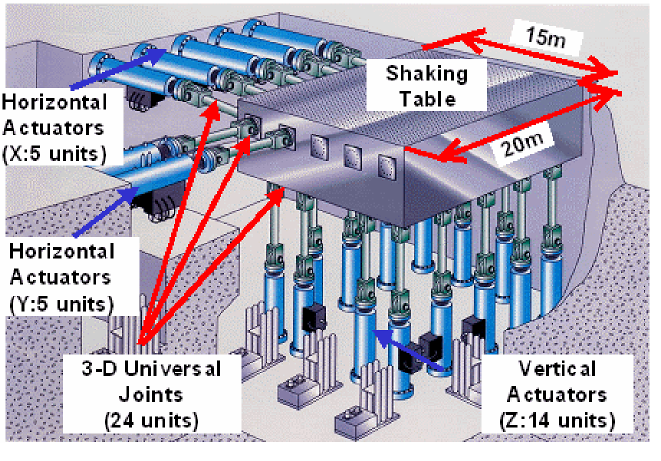

Figure 17. Shaking table of E-Defense

TABLE 3. Major specifications of shaking table

3D Full-Scale Earthquake Testing Facility		
Payload Size Driving Type	12 MN (1,200 tonf) 20 m x 15 m Accumulator Charge Electro-Hydraulic Servo Control	
Shaking Direction	X & Y Horizontal	Z Vertical
Max. Acceleration (at Max. Loading)	>9 m/s/s	>1.5 m/s/s
Max. Velocity	2 m/s	0.7 m/s
Max. Displacement	1 m	0.5 m
Max. Allowable Moment	Overturning Moment 150 MN x m	Yawing Moment 40 MN x m

Construction of E-Defense was in near completion in the fall of 2004, and since that time a series of tests on performance calibration have been conducted, without specimens in the first phase and with real-size specimens in the second phase. Figures 18 shows examples for the table performance check. One shows how the table motion was duplicated with the "basic control," while the other shows how it was improved by the application of a specially designed "advanced control." In both cases, the JMA Kobe record (6.17 m/s/s, 8.18 m/s/s, and 3.32 m/s/s in the maximum acceleration of the EW, NE, and vertical components), a strong motion recorded at the 1995 Kobe earthquake, was applied to the table. The basic control was found to be satisfactory, and the advanced control augumented the accuracy.

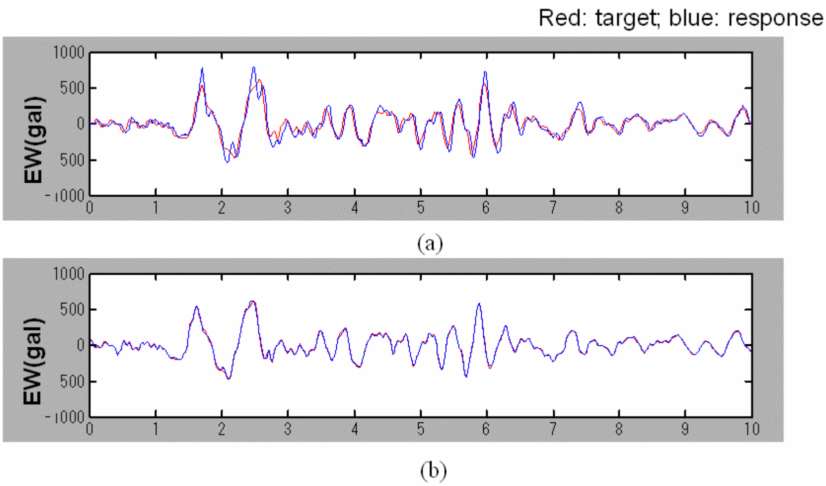

Figure 18. Reproduction of ground motion record (JMA Kobe record)

Regarding the performance test with specimens, the very first application was made for a two-story wood house tested on January 15 and 16, 2005 at the inauguration ceremony of E-Defense. The house had two stories, with ten meters by eight meters in plan and ten meters in height (Fig.19). The JMA Kobe record shook the house in all three dimensions. The total weight of the specimen was about 800 kN, far lighter than the maximum weight accommodated by the table; hence the control was easy, and the test ran successfully. The test was carried out for demonstration to the public, and the specimen was designed to be very earthquake-resistant (to avoid any inconvenience). Accordingly, the specimen revealed only minor damage even for the unscaled JMA Kobe record.

Figure 19. A two-story wood house tested at E-Defense

The ongoing test featured a five-story steel braced frame (Fig. 20) on the table. The frame is twenty meters tall, fifteen meters by ten meters in plan, 6MN in weight, and built very strongly so that the frame would remain elastic even under the strongest shaking. The natural frequency of the frame is 5.0 Hz when all braces are installed, and 3.0 Hz when they are removed. According to the performance test of the table without any specimen, the resonant frequency of the table system (reflecting the table dynamics) is about 4.4 Hz. The two natural periods assigned to the specimen sandwich the table

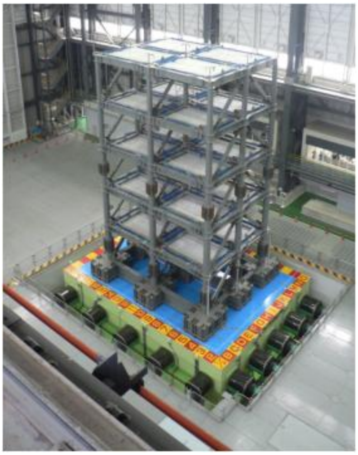

Figure 20. A five-story steel frame for tests of table performance checking

resonance period; hence the overall performance can be checked even in the most difficult circumstances of control. Furthermore, an overturning moment approximately equal to 150 MN x meter is to be imposed onto the table, which is another challenge for the table control. The test is ongoing at the time of this writing, and more details will be published soon.

Ongoing Projects at E-Defense

E-Defense participates in a comprehensive research project named “Special Project for Mitigation of Earthquake Disaster in Urban Areas” sponsored by the Japanese Ministry of Education, Culture, Sports, Science, and Technology, nicknamed MEXT. The project started in 2002 and will extend for a period of five years. Four major thrust areas have been established; first is the evaluation of earthquakes and strong motions; second is the evaluation and enhancement of the earthquake resistance of structures; third is the simulation for disaster responses; and fourth is the integration of the first three projects for the enhancement of better countermeasures to be taken by our society. Among the four areas, E-Defense deals primarily with the second category.

In the project, three targets were chosen. One is wood houses, another is reinforced concrete buildings, and the third comprises soils and foundations. There are sensible reasons for the choice of the three targets. Wood is by far the most popular material for Japanese houses. People are always very keen about the safety of their shelters against earthquakes. Reinforced concrete is used most commonly for apartment buildings and schools. This building type is also very involved in the daily life of the Japanese public. Soils in particular liquefaction and lateral spreading are of serious concern throughout Japan.

At the time of writing, the project has completed its first three years. E-Defense was not available until 2005; hence a variety of tests in this project were conducted using other facilities. Full-scale tests are scheduled in 2005 and 2007 for the three types of structures (Fig. 21).

Figure 22(a) shows a 1/3-scale wall-frame, fabricated as a replica of the first full-scale RC test to be tested in the winter of 2005 to 2006 at E-Defense. The 1/3 scale frame was six storeys tall, with two by three spans in plan and a total weight of 1.5 MN. The test was conducted last winter on the shaking table owned by NIED at Tsukuba, Japan. The frame was shaken to a complete first-story collapse, as shown in Fig. 22(b).

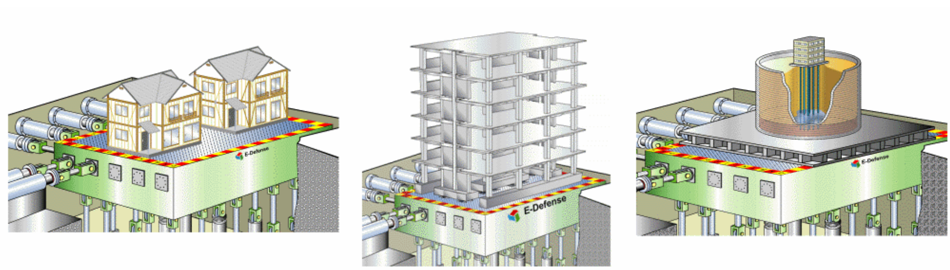

(a) (b) (c)

Figure 21. Three tests scheduled at E-Defense for 2005 to 2007: (a) *Wood houses;* (b) *RC frame;* (c) *soil-structure interaction*

(a) (b)

Figure 22. One-third scale six-story RC frame: (a) *Before test;* (b) *after test exhibiting first-story collapse.*

Collaboration Between E-Defense and NEES

Stimulated in 1995 by the Kobe earthquake, discussions and plans for the construction of E-Defense bore fruit after ten years, and the facility was completed in March 2005. The United States of America also implemented a national project on the upgrade of experimental facilities used for earthquake engineering, named the George E. Brown, Jr. Network for Earthquake Engineering Simulation (NEES), completed in the i fall of 2004 [George 2005]. Earthquake disaster and its mitigation is a very critical problem in both countries; NEES and E-Defense facilities have similar missions and functions in research on the mitigation of earthquake disasters, and the two countries have a very long history of collaboration on earthquake engineering research and practices. In consideration of this, a very natural outcome is research collaboration through complementary usage of the two facilities.

Since the spring of 2004, the research communities in the United States and Japan have conducted an extensive discussion regarding visible and close research collaboration.

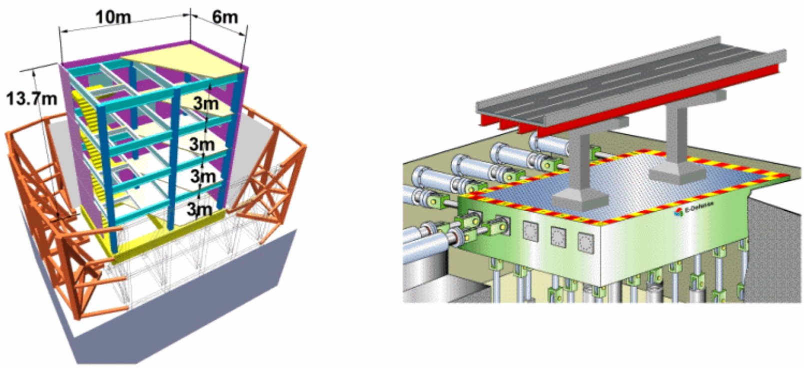

(a) (b)

Figure 23. Structures considered in NEES/E-Defense joint project: (a) *steel frame;* (b) *bridge*

The two communities met a few times including three planning meetings held in April 2004 in Kobe, July 2004 in Washington DC, and January 2005 in E-Defense, respectively. To strengthen and formalize the collaboration, a memorandum of understanding (MOU) between NSF and Japanese Ministry of Education (MEXT), and another MOU between NEES and NIED are being prepared. As a result of the series of meetings, the parties reached an agreement that “steel buildings” and “bridges” would be the immediate targets of research collaboration between the two countries (Fig. 23). In addition, NEES and E-Defense have formalized collaboration on the advancement of cyber-infrastructure in both countries. Details of the collaboration can be found in [13].

E-Defense and International Collaboration

As indicated in the previous sections, E-Defense is a very large shaking table, probably the largest in the world, but NIED is in no manner boasting about the size of E-defense. NIED fully understands that “large” is not synonymous with “good.” After all, good and useful research is achieved only through intellect and enthusiasm of the participants in the test. To this end, E-Defense tries its best to recruit as many experts available in Japan as possible for research projects conducted at E-Defense, and wishes to implement community-based research that involves all layers of researchers and professionals engaged in earthquake engineering. E-Defense also has a goal of positive and effective collaboration within the international community of earthquake engineering to collect and make the best use of the intellect and enthusiasm throughout the world and to collaborate on the mitigation of earthquake disasters in all the regions that are prone to earthquake disasters.

References

Architectural Institute of Japan (1995). *Preliminary Reconnaissance Report of the 1995 Hyogoken-Nanbu Earthquake*, 216pp.

Council of National Disaster Migitation (2004). *http://www.bousai.go.jp/jishin/chubou/*

George E. Brown, Jr. Network for Earthquake Engineering Simulation (NEES) (2005). *http://www.nees.org/index.php*

Hyogo Earthquake Engineering Research Center, National Research Institute for Earth Science and Disaster Prevention (NIED) (2005). *http://www.bosai.go.jp/hyogo/ehyogo/index.html*

Kinki Branch of the Architectural Institute of Japan (1995). *Reconnaissance report on damage to steel building structures observed from the 1995 Hyogoken-Nanbu Earthquake*, Steel Committee, Osaka (in Japanese with attached abridged English version).

Liu, D., Nakashima, M., and Kanao, I. (2003). Behavior to complete failure of steel beams subjected to cyclic loading,” *Journal of Engineering Structures*, 25(3), 525-535.

Nakashima, M., Inoue, K., and Tada, M. (1998a). Classification of Damage to Steel Buildings Observed in the 1995 Hyogoken-Nanbu Earthquake. Engineering Structures, 20,(4-6), 271-281.

Nakashima, M., et al. (1998b). Tests of welded beam-column subassemblies I: Global behavior," *Journal of Structural Engineering*, 124(11), 1236-1244.

Nakashima, M., Matsumiya, T., and Asano, K. (2000). Comparison in earthquake responses of steel moment frames subjected to near-fault strong motions recorded in

Japan, Taiwan, and the U.S., *International Workshop on Annual Commemoration of Chi-Chi Earthquake*, Taiepi, Taiwan, 112-123.

Nakashima, M. (2001). *APPENDIX C. Overview of Damage to Steel Building Structures Observed in the 1995 Kobe Earthquake*, Past Performance of Steel Moment-Frame Buildings in Earthquakes, Federal Emergency Management Agency, Report FEMA-355E, C-1-C24.

Nakashima, M. and Liu, D. (2005). Instability and complete failure of steel columns subjected to cyclic loading, *Journal of Engineering Mechanics*, ASCE, 131(6), 559-567.

Nakashima, M., Matsumiya, T., Suita, K., and Liu. D. (2006). Test on full-scale three-story steel moment frames and assessment of numerical analysis to trace inelastic cyclic behavior," *Journal of Earthquake Engineering and Structural Dynamics* (accepted for publication).

Suita, K., Nakashima, M, and Morisako, K. (1998). Tests of welded beam-column sub-assemblies II: Detailed behavior, *Journal of Structural Engineering*, ASCE, 124(11), 1245-1252.

Shunsuke Otani
Professor
Faculty of Engineering, Chiba University
1-33 Yayoi-cho, Inage-ku, Chiba 263-8522, JAPAN
shunsuke.otani@faculty.chiba-u.jp

Earthquake engineering, design of reinforced concrete structures, structural dynamics

Emilio Rosenblueth was the big name in earthquake engineering from the Institute of Engineering, UNAM since the early 1950s. A new research field using stochastic processes attracted the attention of young researchers from the middle of the 1960s. Luis Esteva worked on his doctoral thesis in this pioneering field under the direction of Rosenblueth and published the essence of the thesis as “Seismicity Prediction: A Bayesian Approach” in the proceedings of the Fourth World Conference on Earthquake Engineering, held in Santiago, Chile, in 1969. As a graduate student, I saw his name in many literatures as an established young researcher in this field. Fortunately or unfortunately, I was more interested in deterministic approaches of earthquake engineering. However, I made copy of his papers, whenever possible, dreaming that someday I would study his approach. The first time I met Luis, the short witty quiet giant, was, when I discussed the use of an earthquake simulator in earthquake engineering research in a small meeting room of the Institute of Engineering shortly after my dissertation. Since then, we often met in international conferences and symposia, never in technical sessions of our mutual interest, but mostly in the reception.

After the 1985 Mexico Earthquake, he was the leader in Mexico to study the consequence of the earthquake disaster and to revise the building code requirements. The Architectural Institute of Japan dispatched an earthquake damage investigation team consisting of 26 researchers and engineers, headed by Professor Y. Kanoh. Upon my request as the secretary of the team, Luis, representing the Institute of Engineering, agreed to host the Japanese team. We held a meeting to present our knowledge of earthquake engineering to Mexican engineers during the investigation. We owe the success of our investigation to sincere and generous hospitality of Luis and Institute of Engineering.

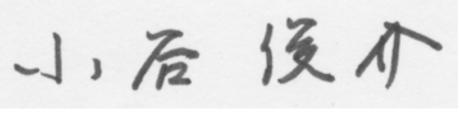

Shunsuke Otani,
September 2005

FUTURE OF EARTHQUAKE ENGINEERING
- APPLICATION OF SMART MATERIALS AND SYSTEMS -

ABSTRACT

The smart structural system is defined as a structural system, provided with the functions of sensors, actuators and/or processors, which can automatically adjust structural characteristics in response to the external disturbances and environment toward structural safety and serviceability as well as the elongation of structural service life. The need for smart systems increased with the development of performance-based engineering. Some examples of smart materials and smart systems are introduced in the paper.

Introduction

The conventional structural design has been developed to achieve a set of intended performances of a structure under pre-selected static loads. Uncertainties in loads and structural responses are dealt by the use of safety factors such as load factors and strength reduction factors. The dynamic disturbances such as earthquake inertia forces and wind pressure forces were represented by simplifying equivalent static forces in design. Such treatment of dynamic disturbances was a significant advancement in engineering in the early twentieth century.

With the development of computer technology and understanding of nonlinear behavior of structural members, it became possible to calculate realistic dynamic response of a structure under a given set of time-varying disturbance. A building structure as designed can be analyzed under design excitation, and the response of the structure as well as members can be examined with respect to the performance criteria. Damping is recognized as a major source of energy dissipation to reduce the response amplitudes under dynamic excitation. Various passive and semi-active damping devices as part of structural control are currently installed in buildings to control their response amplitudes; e.g., viscous dampers and hysteretic dampers. At the same time, the ductility of structural members after yielding was recognized to be important for the safety of a structure under earthquake excitation.

The 1995 Kobe earthquake disaster indicated that the state of the art in earthquake resistant design and construction can achieve the protection of human lives even under severe earthquake motions. Despite the high casualty from the earthquake disaster, the damage rate of reinforced concrete buildings was shown to be extremely small if designed and constructed in accordance with the current building code requirements in Japan. Architectural Institute of Japan studied the damage level of all reinforced concrete buildings in the most severely shaken area. Figure 1 shows the damage rate of reinforced concrete buildings designed and constructed using the 1981 building code requirements; buildings suffering major damage needed the repair work before reuse, and buildings suffering minor damage could be used without repair work. The damage rate of buildings constructed in accordance with the then governing requirements was extremely low. Although most of buildings suffered light structural damage, some of buildings lost their function due to the damage in architectural elements.

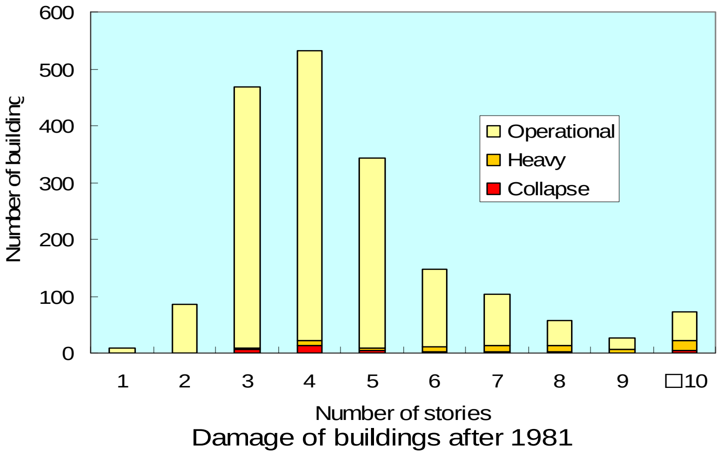

Figure 1. Damage rate of reinforced concrete buildings designed and constructed using building coded requirements at the time of the 1995 Kobe Earthquake Disaster

The protection of human lives is certainly the minimum earthquake engineering objective, but it is not sufficient in the advanced society. The continued functioning of some specific types of buildings such as disaster management centers, medical centers and information technology centers was found to be essential even from the maximum feasible earthquake for the immediate recovery from the disaster. Conventional earthquake resistant design methodology cannot meet the new performance requirement; i.e., new technology such as vibration control needs to be introduced to limit the response of such important buildings.

Deterioration of structural performance with age is another issue. Mechanical properties of some materials decay with age. Some materials need maintenance work for the enhanced durability. The deterioration of a structural system needs to be sensed and the health state should be continuously monitored. The damage should be repaired.

A smart structural system is defined as a structural system that can sense the state of the structure and detect damage, restrain damage propagation, adjust structural characteristics in response to external disturbance and environment to control the response, adapt its configuration to optimum state for the environment, and minimize the system life-cycle cost by maximizing its performance through its adaptive capabilities. Monitoring of structural health state is also important to detect the damage under extraordinary loading as well as the deterioration under normal use. The repair and maintenance work of such damage can extend the life of a structure.

The concept of a smart structural system was initially developed in the field of aerospace engineering where the sole objective is to provide the safe and comfortable transportation. For this objective, (a) the airplane is equipped with the most advanced mechanical system, (b) the airplane is operated by trained pilots manually or automatically to adjust its speed, height and direction suitable for flight objectives and environments, and (c) the mechanical system of an airplane is carefully and extensively maintained between flights. Higher costs can be tolerated for the safety and improved performance.

The nature of a building structure is obviously quite opposite to that of an airplane; (a) a building structure is not maneuvered after construction (although the lighting and air conditioning may be operated with occupancy), (b) the performance objectives of a building vary with loading environments; i.e., serviceable under normal loading and safe under extraordinary loading, (c) a building may not be regularly maintained after construction, (d) the value of a building cannot be evaluated by the structural point of view alone, but should consider "beauty", "economy", and "function." Therefore, the smart structural system for building structures is defined as a structural system provided with functions of sensors, actuators and/or processors, which can automatically adjust structural characteristics, in response to external disturbances and environment, toward structural safety and serviceability as well as the elongation of structural service life.

The Building Research Institute (BRI), Ministry of Construction, Japan and the U.S. National Science Foundation (NSF) carried out the U.S.-Japan Cooperative Research Program on Autoadaptive Media (Smart Structural Systems) from April 1998 to March 2003. Research items and plans are executed in three research thrusts: (a) smart materials, (b) sensing and monitoring for damage detection, and (c) smart structural systems. Research targets were

- Development of concept and methods to evaluate the performance of smart structural systems,
- Development of sensing and monitoring methods of structural performance, and
- Development and evaluation of structural elements using smart materials.

This paper introduces some of findings of the cooperative program. Additional references on smart materials can be found in ASCE Journal of Engineering Mechanics (Ansari and Leung 1997, Journal of Engineering Mechanics 1997).

Smart Materials

Various new materials with high performance capability have been developed and their characteristics were investigated in the field of aeronautical engineering. Some of the materials were expensive at the time of development, but the cost has been reduced with popular use in practice. The following smart materials and devices have been considered for structural application in the U.S.-Japan cooperative research; (a) Shape memory alloys, (b) Controllable fluids, (c) Electro/magneto-strictive elements, and (d) High-performance cementitious composites

Shape Memory Alloy

There are families of shape memory alloys (SMA), such as Nitinol family (Ni-Ti alloy), Cupper family (Cu-Zn, Cu-Al-Ni, and Cu-Sn alloys), Iron family (Fe-Pt, Fe-Pd, Fe-Ni-Co-Ti, Fe-Ni-C, and Fe-Mn-Si Alloys) and others (Au-Cd, Fe-Pt, In-Cd, and Ni-

Al alloys) that exhibit two distinct characteristics depending on the temperature and stress levels; (a) shape memory effect, and (b) super-elasticity.

The shape memory effect is an ability to deform at a low temperature and then return to their original shape after heating to a higher temperature with or without the effect of external mechanical stresses (Figure 2 (a)); the shape memory effect is caused by the transformation between the martensite and the austenite phases. The transformation from the austenite to the martensite phase takes place without shape change. In the martensite phase, strains can be stored through a mechanical twinning process of molecule configuration. On heating the material returns to the austenite phase of regular configuration releasing the strain. The material can generate high actuation forces in response to this temperature changes. The super-elasticity is a characteristic of the material to exhibit nonlinear quasi-elastic stress-strain relation with small residual deformation after the removal of stresses (Figure 2 (b)).

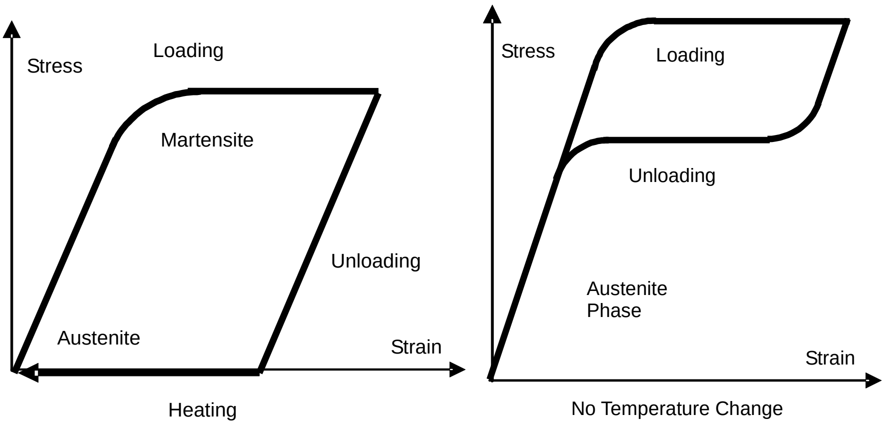

(a) Shape memory effect (b) Super elasticity effect

Figure 2. Shape memory effect and super elasticity effect of shape memory alloys

The SMA materials were normally provided as wires or rods. Therefore, the material is normally used as tension resisting elements. The high cost of the material and poor availability of large size SMA rods make it difficult to use the material in structures; currently 16.5-mm diameter rods are the largest available for practical application. The work on the SMA rods such as welding and cutting is difficult; the bits for normal carbon steel were found unsuitable for cutting threads on the SMA rods.

The SMA material has been used in the form of tensile braces for seismic reinforcement in buildings to dissipate small hysteretic energy but dominantly to cause small residual displacement after loading by the super-elastic property of the alloy. For example, the SMA rods may be used as anchor bolts at column bases and at beam-column joints to control the residual deformation (Figure 3); small residual deformation can be observed in SMA anchor bolts while slippage behavior can be observed upon reloading in steel anchor bolts. Wires were used as longitudinal reinforcement for concrete members and tendons for prestressing members making use of their superelastic property; single crack opens at the critical section, but the crack closes upon unloading.

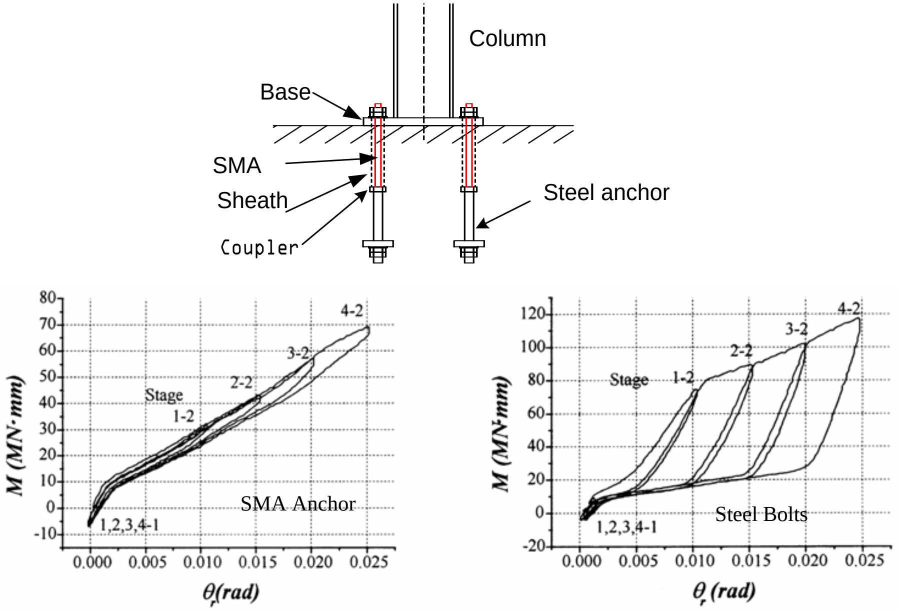

Figure 3. Use of SMA at column base

A series of material tests indicated that (a) the SMA rods dissipated less energy under superelastic condition than the wire, (b) the SMA material did not exhibit noticeable superelastic properties in compression, (c) the stress-strain relations are different in tension and compression, (d) Poisson's ratio in tension and compression is similar at the initial stage, but that in compression becomes larger than that in tension, (e) hysteretic energy dissipation decreases with velocity (Fig 4), and (f) the rods in some cases fractured in a brittle manner under cyclic loading. The production of the large-size SMA rods and the material properties for energy dissipation and ductility should be improved for practical application of the SMA materials.

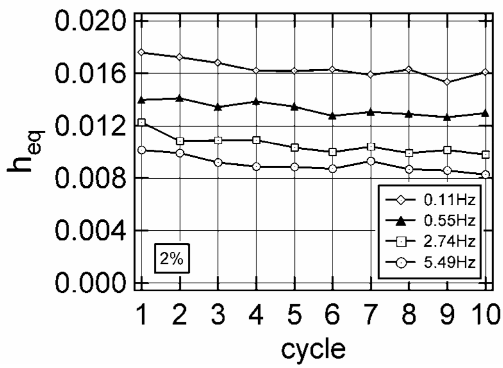

Figure 4.Decay of equivalent hysteretic damping factor with driving frequency (2% Strain)

Controllable Fluids

Controllable fluids, such as electro-rheological (ER) and magneto-rheological (MR) fluids, contain fine metallic particles which line up when exposed to an electric or magnetic field (Figure 5). With small power of the electric current or magnetic flux, the free-flowing linear viscous fluid changes to semi-solid in milliseconds. The yield resistance of the semi-solid against flow is proportional to electric current or magnetic flux.

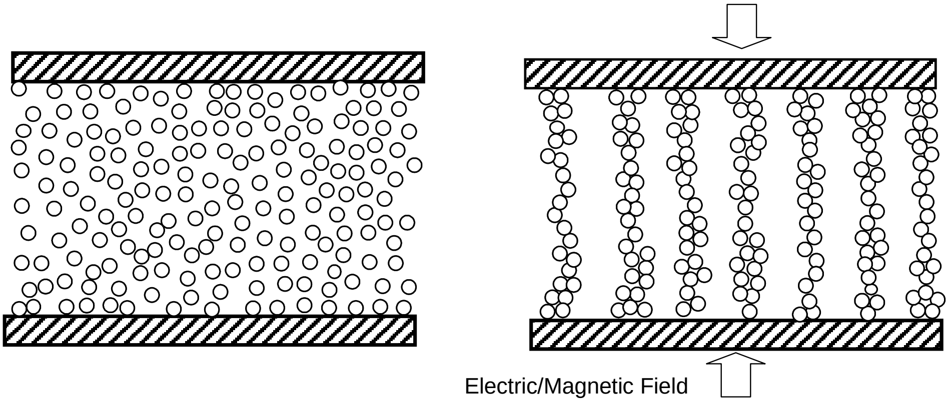

(a) Without electric/magnetic field. (b) With electric/magnetic field.

Figure 5. Properties of controllable fluid

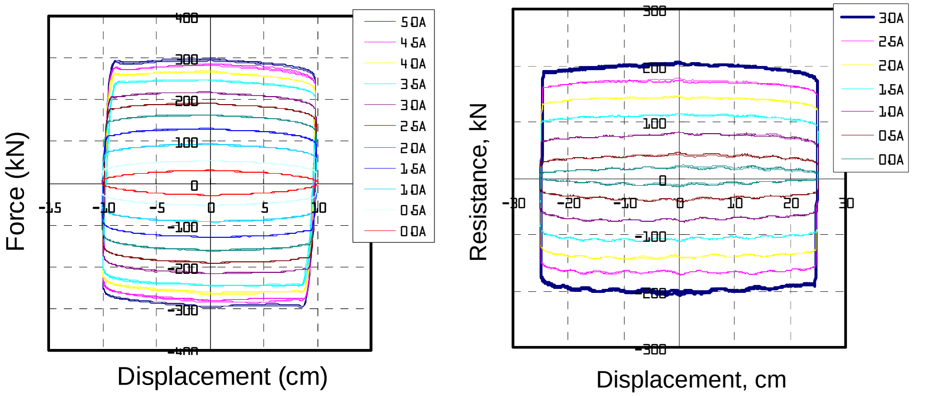

Figure 6. Force-deformation relation of 400-kN MR damper under different control magnetic flux

The controllable fluids can be used to control the flow of liquid in a hydraulic device. The MR-damping device develops yielding resistance proportional to the level of magnetic field after the velocity reaches a limiting value (Figure 6). The stiffness of bracing members or the viscosity of damping devices can be adjusted with small power to optimize the response of a structure during an earthquake or high wind to achieve desired performance (semi-active or active damper). The MR fluid was found superior to the ER fluid in the application for semi-active vibration control.

The yield resistance of the MR fluid slightly increases with loading rate, and decreases with increasing temperature. The delay in the response of an MR damper to the controlling signal was around 0.01 sec, but the delay increased to 0.2 sec when the level of control signal was low. The response of an MR damper can be modeled by the Bingham plastic model, which consists of parallel dashpot and friction slider.

A 400 kN-capacity ±475 mm-stroke MR-damping device was developed for the verification of performances in a realistic scale; e.g., force-deformation and force-velocity relationship under different temperatures and under different loading rates. The stability and durability of the MR fluid with age and the control strategy for the effective use of MR dampers need to be further studied.

Induced Strain Actuator (ISA)

Electro-strictive (piezoelectric ceramics) and magneto-strictive elements, called induced strain actuators (ISA), change their own shape in response to external electric/magnetic fields (Figure 7), or produce electric current in response to the change in shape; hence ISA devices can be used as actuators as well as sensors. The actuating force amplitude is large for small controlling deformation, but the force amplitude decreases with increasing deformation demand. The ISA actuators can be connected in series to increase the deformation amplitude. These materials have been widely used for the small precision machine because of their advantage in size, fast reaction, high power and high accuracy.

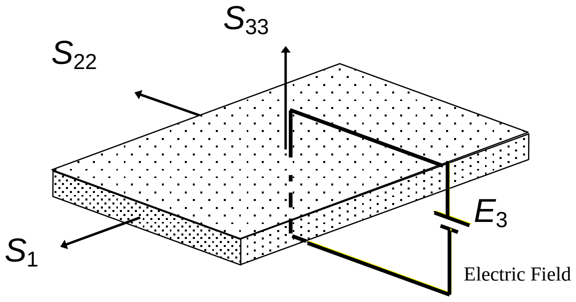

Figure 7. Deformation of electric-strictive element in response to electric field

For a level of control signal, the amplitude of actuating forces decreases with increasing displacement stroke. For the same level of actuating force demand, a magneto-strictive actuator has longer stroke than an electro-strictive actuator.

The delay between the input signal and actuator response was 0.010 sec when the friction force was reduced and 0.005 sec when the friction force was increased. The friction resistance is not influenced by the velocity. Therefore, the ISA actuator is often used in an active vibration control of the platform supporting a precision machine under ambient vibration.

An example of the ISA (piezoelectric actuator) use is a semi-active friction damper; the friction force is controlled by the electric voltage. Two types of friction dampers were developed (Figure 8); i.e., (a) friction force was controlled by increasing contact pressure with controlling electric current, (b) initial prestressing force was reduced with controlling electric current. The latter mechanism can work as a passive damper even in case when the control of the piezoelectric (PZT) actuator is lost by an accident.

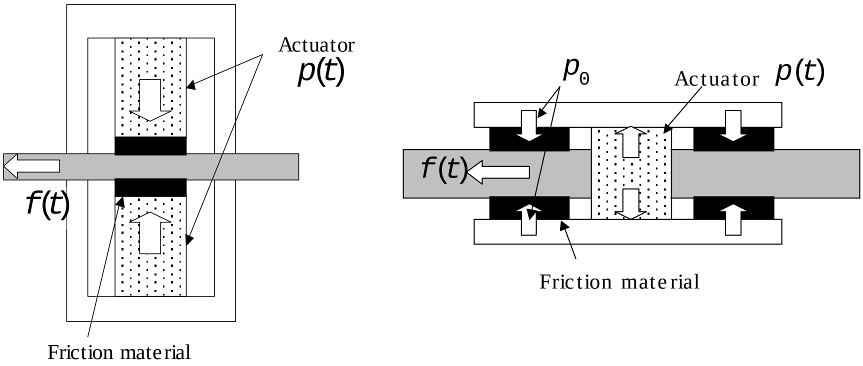

Figure 8. Concept of piezoelectric friction dampers

If the PZT actuators, such as polymers based ISA films or distributed ISA devices, are placed on both sides of a plate subjected to electric voltage signals of opposite sign, the bending motion of the plate may be excited. For example, piezoceramic actuators were used to control noise transmission of partitions in a building. This system, placed to counteract the vibration of the partition, was shown effective to supplement the conventional noise reduction method, which often is not effective in a low frequency range.

The stress-state of membrane structure is difficult to measure because the membrane is very light and flexible. The placement of foil strain gages may change the mass and stiffness of the membrane. PVDF (Polyvinylidene Fluoride resin) was successfully used to measure strains on flexible membrane (Figure 9) or control the tension in the membrane.

High-performance Fiber Reinforced Cementitious Composite (HPFRCC)

High-performance cementitious fiber reinforced composite (HPFRCC) is normal mortar or concrete containing chopped fibers (typically less than 2% depending on fiber types, interface and matrix characteristics). The diameter of the polymer fiber is 12 to 40 μm and the length is around 10 to 15 mm while the diameter of steel fiber commonly used in the past is typically about 400 μm. The tensile strength of polymer fibers is comparable to that of the steel fiber.

The material was developed using micro-mechanical principles in the early 1990s (Li 1992). HPFRCC exhibits strain-hardening characteristics with superior strain capacity; additional fine cracks are formed in the uncracked region. In this fashion, widening of limited and concentrated cracks will not occur. Figure 10 shows the force-deformation relations of 100x200x400 mm normal reinforced concrete column and reinforced HPFRCC column.

Wide cracks concentrated at the top and bottom of the columns. Normal reinforced concrete column failed in shear with wide diagonal cracks. HPFRCC column developed flexural yielding after formation of fine diagonal cracks and developed large

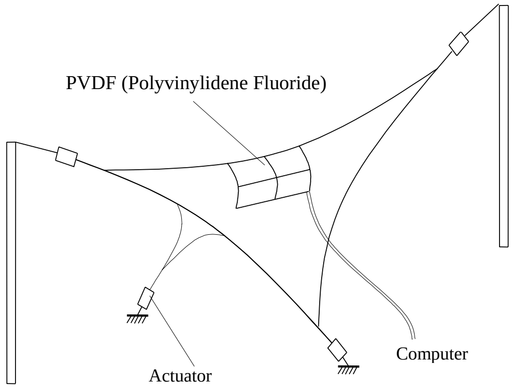

Figure 9. PVDF sensors for membrane structure

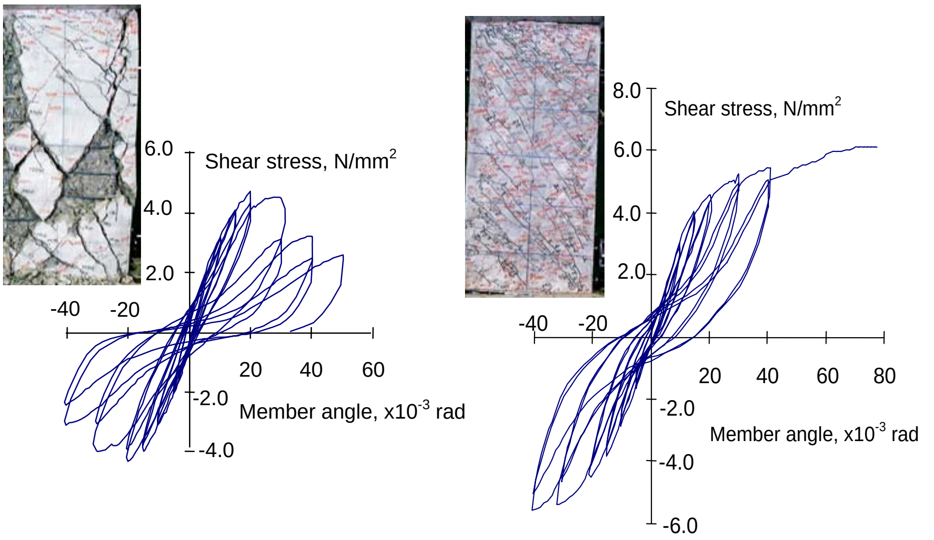

(a) Reinforced Concrete Member

b) HPFRCC Member

Figure 10. Force-deformation relation of reinforced concrete and HPFRCC members

ductility after flexural yielding. The high ductile behavior of HPFRCC is especially suitable for critical elements in seismic applications where large energy absorption, reparability, serviceability, durability and spalling resistance are required.

The application of HPFRCC can be found to replace steel reinforced concrete composite members, in which the construction becomes difficult due to the placement of reinforcing bars outside the steel element. It was suggested to remove the reinforcement cage in the member and use HPFRCC direct with steel element (Figure 11). The test result showed a good performance developing good bond between the steel element and HPFRCC (Figure 12). The force-deformation relation is similar to that of a steel reinforced concrete member. The easiness of construction without reinforcing

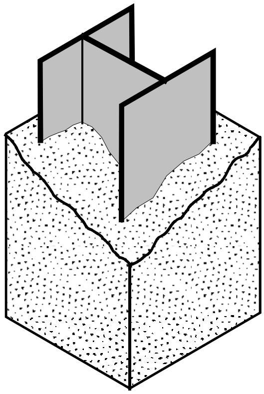

Figure 11. HPFRCC concrete encased steel member

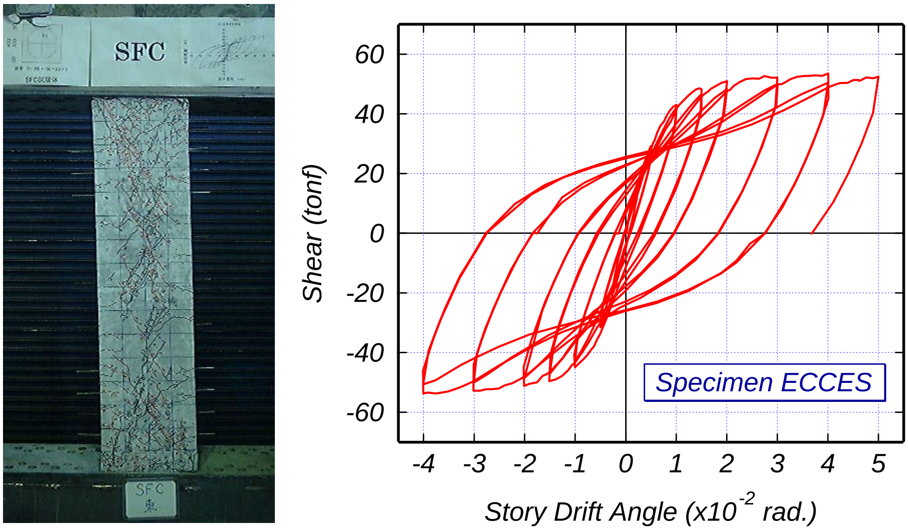

Figure 12. Crack patterns and hysteretic characteristics of HPFRCC encased steel member

bars appears to be attractive in construction.

The higher level of performance is required for some types of buildings for the disaster recovery management, for the treatment of the injured, and for the use of information technology. Smart structural systems are one of solutions to realize high performance of building structures. The smart structural system for building structures is defined as "a structural system with a certain level of autonomy relying on the embedded functions of sensors, actuators and/or processors that can automatically adjust structural characteristics, in response to external disturbances and environment, toward structural safety and serviceability as well as the elongation of structural service life."

Smart Structural Systems for Buildings

Auto-adaptive structural system changes structural characteristics in response to the external disturbances and environment by embedded functions of sensors, actuators or processors using smart materials. Typical examples are found in the application of vibration control technology in buildings. Various types of dampers may be used such as visco-elastic damper, tuned-mass damper, hysteretic damper, magneto-rheological fluid damper, electro-rheological fluid damper (Figure 13). Some dampers can be used in passive, semi-active or active mode. The system reduces response amplitudes of a structure during an earthquake.

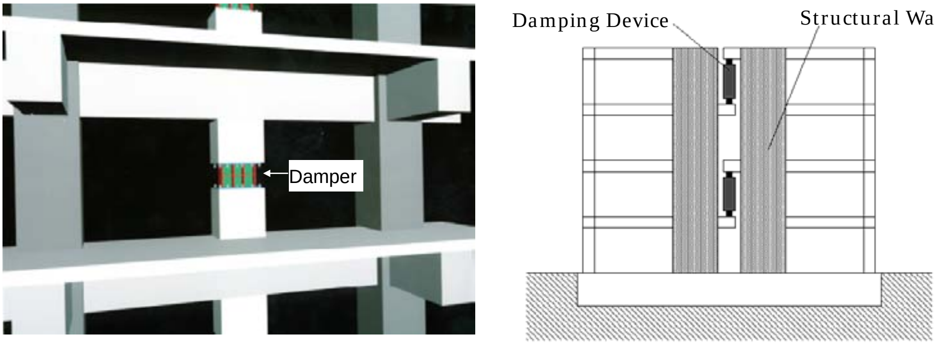

Figure 13. Dampers in building

The base isolation system of a building normally consists of isolator devices, restoring force device and damping device placed in a layer. A normal base-isolated system can reduce the acceleration response, but the deformation of the isolation layer sometimes becomes excessive. The MR-damping device or the ISA damping device in semi-active control mode in a base isolated specimen could reduce both response displacement and acceleration amplitudes.

The out-of-plane vibration of slabs may be controlled by placing the ISA film elements at the top and bottom faces of the slab (Figure 14). The vibration of the slab may be monitored and the counter-acting control signal may be fed to the actuators to cancel the motion.

Final Remarks

Performance-based engineering requires the close observation and strict control of the response of a structure during the life-time and extraordinary events. The performance objectives vary from a building to another depending on the performance specification outlined by the building owner. Advanced materials and engineering, especially vibration control technology, need to be applied to meet the requirements.

The damage should be detected by monitoring in the extreme loading cases. Health monitoring under normal loading is essential for the prolonged use of a structure. The deterioration of structural performance with age should be repaired. Limited natural resources will not permit the scrap-and-build approach of construction.

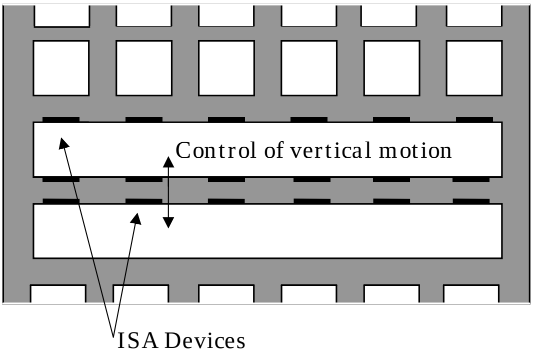

Figure 14. Vibration control of slabs

Acknowledgements

The paper introduces the research findings of the U.S.-Japan Cooperative Research Program on Development of Smart Materials and Systems, sponsored by Building Research Institute, Japan, and U.S. National Science Foundation. Professor Mete A. Sozen of Purdue University and the author acted as co-chairmen of the Joint Technical Coordination Committee in the United States and Japan. The author expresses his sincere appreciation to the chairmen of Japanese Working Groups for their leadership carrying out the research; Professor Akira Wada of Tokyo Institute of Technology, Professor Takafumi Fujita of University of Tokyo, and Professor Yoshikazu Kitagawa of Keio University. Dr. Mitsumasa Midorikawa was in charge of the program at Building Research Institute.

References

Ansari, F., A. Maji and C. Leung, Ed., (1997). Intelligent Civil Engineering Materials and Structures, A Collection of State-of-the-art Papers in the Applications of Emerging Technologies to Civil Structures and Materials, Journal of Engineering Mechanics, American Society of Civil Engineers, Vol. 123, No. 3, 299 pp.

Journal of Engineering Mechanics (1997). Special Issue on Structural Control: Past, Present, and Future, American Society of Civil Engineers, Vol. 123, No. 9, pp. 897-958.

Li, V. C. (1992). Performance Driven Design of Fiber Reinforced Cementitious Composites," Proceedings, Fourth RILEM International Symposium on Fiber Reinforced Concrete, Ed. Swanny , Chapman and Hall, pp. 12-30.

Tom Paulay
Emeritus Professor of Civil Engineering
University of Canterbury
Private Bag 4800, Christchurch 8020, New Zealand
E-mail: tom.paulay@canterbury.ac.nz

Seismic design of concrete structures

My memorable association with UNAM goes back to the time when the renown icon of earthquake engineering, Emilio Rosenbueth, dazzled us with his immense visions. With irresistible persuasion he recruited Luis Esteva and, among others, my long time colleagues, the late Bob Park, Nigel Priestley, and myself, to contribute to a book (Rosenblueth 1980) addressing the application of the state of the art of earthquake engineering in structural design. With subsequent visits to Mexico and numerous encounters with Luis during our seismic missionary globe trotting, our friendship progressed. My great respect for him and his work, motivated me to look up to him in spite of the fact that he is quite a bit shorter than I am. I was fortunate to work with him within the world wide fraternity of the International Association for Earthquake Engineering. It is pleasing to note that Luis is now completing his term as president of this fraternity. I recall with joy our last encounter with each other, when, while strolling over the colorful streets of Taipei, without comparing our views, we firmly declined to accept the eager offer of a street vendor to sample his steaming snake stew. My good wishes shall accompany him during the coming, undoubtedly very active, years.

THE SEISMIC DISPLACEMENT CAPACITY OF DUAL SYSTEMS

ABSTRACT

To enable acceptable seismic displacement demands imposed by earthquakes to be estimated, the displacement capacity of a structure needs to be known. This is controlled by specific performance criteria. It is postulated that, within sensible limits, the assignment of fractions of the required seismic strength to elements of a system may be arbitrary. This enables the displacement capacity of a structural system to be evaluated without the knowledge of its strength. A redefinition of some traditionally accepted structural properties is a prerequisite of applications. A study of a prototype reinforced concrete mixed frame-wall system was chosen to illustrate rationale, acceptable extents of inevitable approximations and extreme simplicity of application.

Introduction

Traditional techniques, adopted in early seismic code provisions, attempted to provide adequate strength, in terms of lateral force resistance, largely based on the dynamic response of elastic systems. Subsequently it was recognized that for significant but relatively rare seismic events, magnitudes of lateral design forces can be significantly reduced if proper allowance is made for hysteretic damping. Some associated damage was considered inevitable. This presented a major challenges to researchers to identify sources of large deformations in a composite structure, comprising brittle concrete and adequately ductile steel. Astute choices of potential kinematically admissible plastic mechanisms needed to be made. To ensure that only the chosen suitable mechanism could be mobilized during a large earthquake, a quantified hierarchy in the relative strengths of elements and components became imperative. These concepts were embodied in the philosophy of "capacity design" (Park and Paulay 1975, Paulay and Priestley 1992).

More recently emphasize in seismic design strategies was placed world wide on satisfying identifiable performance criteria. Beside providing adequate seismic strength, the paramount importance of realistic estimates of displacement capacities of structural systems, related to specific performance criteria, is presently more widely recognized. To aid simplifications, without which adoption by structural designers of new concepts in seismic design can hardly be expected, deliberate approximations need to be made. These are considered to be compatible with the inevitable crudeness of the prediction of magnitudes of probable earthquake-induced displacement demands.

Certain redefinitions of structural properties, for example the relationship between strength and stiffness, may be viewed by some readers as being controversial.

Terminology Used

In this study of earthquake-imposed displacements on buildings, frequent reference is made to the structural system. A structural system comprises lateral force-resisting elements, generally arranged in orthogonal directions. Typical elements are bents of ductile frames or interconnected walls in the same plane. Due to torsional effects, elements of the system may be subjected to different displacements.

A lateral force-resisting element may comprise several components. Components of elements are assumed to be subjected to compatible displacements associated with the lateral displacement of the element. Typical components are beams, columns, beam-column-joint subassemblages or walls. The latter may be full height cantilevers or coupled walls.

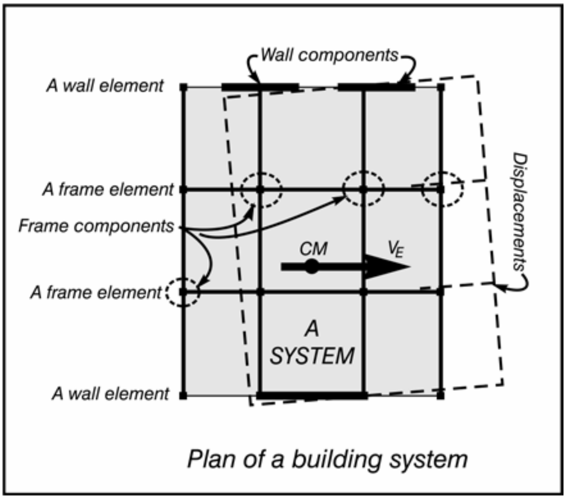

Figure 1. Constituents of a structural system

Figure 1 attempts to clarify these definitions. In the technical literature the terms component and element are often used to describe the same part of the system. To clarify compatibility requirements relevant to lateral displacements, distinct differentiation in the treatment of components and elements needs to be made.

Displacement Limitations

Following currently accepted seismic design aims, maximum displacements imposed on ductile reinforced concrete systems are deemed to be limited by:

- The displacement capacity of critical components of the system corresponding with the adopted, i.e., codified, quality of detailing for construction.
- The magnitude of the story drift, (the angle corresponding with the lateral displacement of a level relative to that of an adjacent level) satisfying the specific performance criterion, distinctly chosen for the building system.
- The more severe limit may then establish the target displacement capacity of the ductile system eventually to be related to the anticipated maximum seismic displacement demand.

The Tools of Displacement Estimates

Traditionally the structural design process starts with experience-based estimates of component dimensions. Once this information, based on architectural and engineering perspectives, is available, with the knowledge of material properties, such as strain limits, displacement estimates, adequate for purposes of seismic design, can be readily made.

Nominal yield curvature

A fundamental property of a structural component is the nominal yield curvature at its critical section or sections. This will characterize its response in the elastic and post-elastic domain of behavior when the element is subjected to monotonically increasing displacements. In reinforced concrete members, it is more realistic to base curvature estimates on quantifiable section properties, rather than on assumed or recommended (Paulay and Priestley 1992) values of flexural rigidity, E_cI_e, where E_c is the modulus of elasticity of the concrete and I_e is the second moment of effective area of the cracked section. In seismic design it may be assumed that extensive cracking will occur over the full length of components. Associated errors are likely to be smaller than those originating from routine neglect of displacements due to causes other than flexure.

Figure 2 shows familiar flexural strength-curvature relationships for a typical structural wall section. With little experience the neutral axis depth associated with the development of steel yield strain at the extreme tension fiber can be readily estimated. As stated, for purposes of seismic design a high degree of precision in the estimation of component properties is not warranted. If necessary, this estimate can be subsequently reviewed, once details of the flexural reinforcement provided are known. For a given steel tensile yield strain, ε_y, and the location of the neutral axis depth, ξD_w, the curvature at the onset of yielding is established as $\phi_y' = \varepsilon_y/(\xi D_w)$, where D_w is the overall depth of a section, or the length, ℓ_w, of a wall. When details of the reinforcement are subsequently known, the associated moment at the onset of yielding at the extreme tension fiber, M_y, may also be evaluated. The need for this will, however, seldom arise. The designer will primarily address the nominal flexural strength, M_n, at a critical section, as constructed, when strength requirements for the components are known.

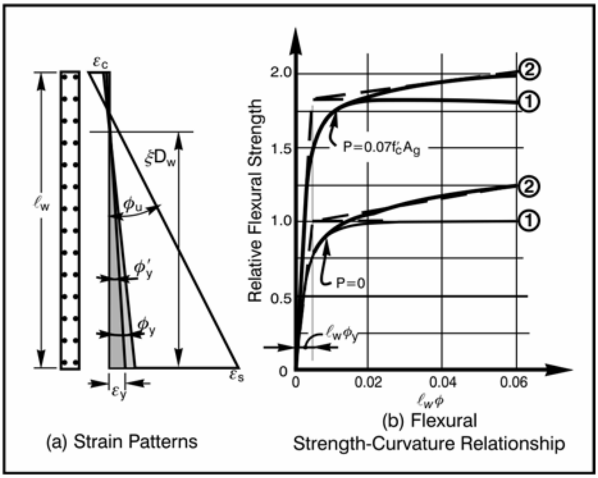

Figure 2. Flexural strength-curvature relationships for a wall section

For seismic design purposes a bilinear simulation of the nonlinear moment-curvature relationship, as shown in Fig. 2(b), is convenient and adequate. With linear extrapolation this leads to the definition of the nominal yield curvature

$$\phi_y = (M_n/M_y)\ \phi_y' = \eta\varepsilon_y/D_w \tag{1}$$

where the coefficient $\eta = (M_n/M_y)/\xi$ recognizes the ratio of the nominal to yield strength in flexure and the relative position of the neutral axis. It enables a benchmark, i.e., reference or nominal, value in bilinear simulation of relationships to be identified. If desired, effects of strain hardening with increasing curvature ductility (Fig. 2(b)) may also be included. These are not considered here.

Extensive studies of a variety of sections, conducted at the University of Canterbury, confirmed previous finding (Priestley-Kowalsky 1998) that for specific types of members, such as walls and beams, the variation of the value of the parameter η is relatively small. The amount of reinforcement used at a section hardly affects nominal yield curvature. As expected, neither do moderate axial compression loads, commonly encountered in structural walls, affect nominal yield curvature to any significance. However, the effect on flexural resistance is significant. Fig. 2(b), where the (cylinder) compression strength of the concrete is denoted as $f_c^{'}$, illustrates this feature.

Nominal yield curvature may be considered like a material property. It is insensitive to, and for design purposes essentially independent of, section flexural strength. The definition presented here contradicts with the widely used terminology, whereby $\phi_y^{'} = M_y/E_cI_e$. The expression implies that, with a commonly assumed constant value of the flexural rigidity, the yield curvature would proportionally increase with the yield moment, M_y.

These relationships are familiar from the study of the behavior of structural members comprising homogeneous isotropic materials, such as steel. For example the nominal yield curvature of a flanged steel section with constant depth, is essentially independent of its strength. The latter is controlled by the width and thickness of the flanges.

Nominal yield displacement

An approach, based on bilinear simulation, similar to that used in defining the nominal yield curvature of a cracked reinforced concrete section, may be utilized. This is illustrated in Fig. 3. The strongly nonlinear response of a component i from the onset of cracking till the development of its nominal strength, V_{in}, is of little interest with respect to estimations of displacements in the elastic range of behavior. The shaded area in Fig. 3 indicates essentially linear response after the occurrence of repeated displacements not exceeding that associated with the yield strength, V_{iy}, and the yield curvature, $\phi_{iy}^{'}$, of the component. Hence the nominal yield displacement, Δ_{iy}, an important reference value, may be based on the nominal yield curvature, ϕ_{iy}, at the critical section. The nominal yield displacement, Δ_{iy}, is also strength-independent!

In this study, only conservatively estimated flexural deformations were considered. If refinements appear to be necessary, other sources of distortions, such as due shear and at anchorages, may be readily included.

Element stiffness

An important conclusion, drawn from the bilinear simulation of the force-displacement relationship for an element, is the definition of its stiffness, k_i, stated in Fig. 3. Because the nominal yield displacement, Δ_{iy}, is not affected by strength, the stiffness of a reinforced concrete element with given dimensions and material properties (ε_y) is proportional to the strength which the designer will eventually assign to it (Paulay, 2001a).

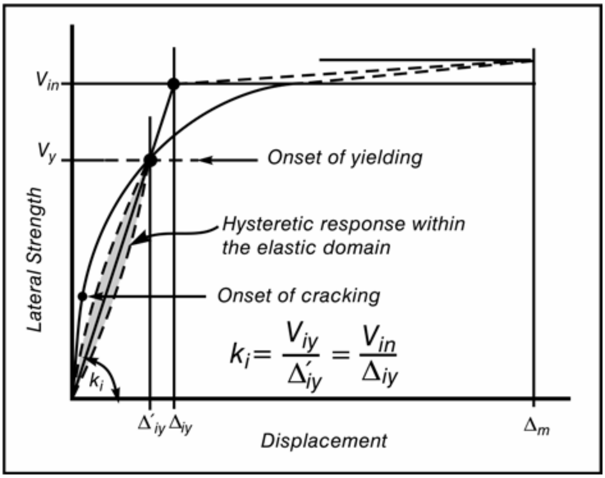

Figure 3. Bilinear simulation of force-displacement relationship

This interpretation of stiffness reveals weaknesses, for example, in the traditional approach to seismic torsional phenomena. These arise from definitions of eccentricities with respect to the center of mass of a system. Perceived detrimental effects of stiffness eccentricities are routinely remedied by redistributing design strengths of elastic elements to eliminate strength eccentricities. The fact that the redistribution of strengths by the designer has altered element stiffness, and hence stiffness eccentricity, is overlooked.

Figure 3 clearly shows the range of strengths, i.e., when $V_{iy}<V_i<V_{in}$, over which stiffness so defined would significantly underestimate displacements. In terms of ductile structural response this transitional range of behavior is in general of little interest.

The bilinear simulation shown in Fig. 3 allows the displacement ductility, applicable to element i, to be more realistically quantified as

$$\mu_{i\Delta} = \Delta_m/\Delta_{iy} \tag{2}$$

The displacement ductility of a system, $\mu_{s\Delta}$, to be defined subsequently, is an essential parameter of current strength- and displacement-based seismic design procedures.

Freedom in the Assignment of Strengths

As stated previously, the nominal yield curvature at the critical section of an element with given dimensions, ϕ_{iy} , and hence its nominal yield displacement, Δ_{iy}, may be considered in seismic design to be independent of its nominal strength. Therefore, the displacement capacity of any element, being a specified multiple of its nominal yield displacement, and hence that of the system, can be estimated with sufficient accuracy already at the preliminary stage of the design. As stated earlier, fractions of the total required nominal strength of a system, to be established subsequently, may be assigned arbitrarily to its elements (Paulay, 2000). Implications of this freedom in assigning element strengths, are thus:

- Irrespective of the strengths assigned to an element, it will commence yielding when the imposed system displacement approaches the nominal yield displacement of that element.

- Simultaneous onset of yielding of geometrically differing elements of a system, such as walls, with different overall depths, is not possible.
- Lateral force-resisting elements of a system with different nominal yield displacements, when subjected to identical translational displacements, will necessarily be subjected to different displacement ductility demands.
- A structural system, comprising elements with different nominal yield displacements, does not exhibit a distinct yield displacement. Existing definitions of the yield displacement of systems are often ambiguous. Hence a redefinition is required.
- To ensure that all elements of a ductile system will perform satisfactorily, the displacement capacity of the system should, in general, be restricted to that of its component with the smallest displacement capacity.

Arbitrariness in strength assignment imparts to the astute designer the ability to chose from a number of possible, viable and appealing solutions. For example, to eliminate possibly detrimental torsional effects (Paulay 2001b), strengths should be assigned to elements so that an acceptably small or no strength eccentricity will result. To illustrate the relevance of the structural features listed above, a somewhat idealized frame-wall system, deliberately made simple, is studied here briefly.

An Example Frame-Wall System

An attractive mode of seismic resistance in medium to high rise buildings may be achieved with the use of interacting cantilever walls and rigid jointed frames, i.e., dual systems, extending over the full height. Before the arrival of computers, these systems represented formidable challenges to the analytical skills of structural engineers. Deformation compatibility in elastic systems necessitates significant changes, via diaphragms, in the lateral force patterns applicable to the walls and the frames. With the appreciation of limitations of the uses of bilinear modeling, generally insignificant within a nonlinear seismic scenario, both required relative strength and real displacement capacity can be readily predicted for each type of element.

This selected example intends to demonstrate how, already at the preliminary stage of the design, such simple, yet rather important, behavior-based predictions can be made, even for such a relatively complex structure. The strategy used exemplifies a deterministic design philosophy, whereby the designer simply 'tells the structure' what it should do in the event of a major earthquake.

Displacement compatibility under lateral force is assumed to be assured by infinitely rigid floor diaphragms. The traditional design approach employing the distribution of seismic strength to different elements of a dual system, based on elastic behavior and still widely used, was extensively studied (Paulay and Priestley 1992). However, issues of displacement estimates, relevant to this type of ductile structures, received then relatively little attention.

The prototype structure

A prototype structure, shown in Fig. 4(b), intends to illustrate several postulated, yet unconventional, design concepts. A symmetrical 12 story reinforced concrete building comprises seven identical frames and two cantilever walls, each with a height, h, to length, D_w, aspect ratio of A_{wr} = 7.1. Dimensions are expressed in terms of the total height, h, of the structure. For modeling purposes the 9 lateral force-resisting elements are condensed into two elements, one comprising 7 frames and the other 2 walls, respectively, as seen in Fig. 4(b). A typical seismic design force pattern, corresponding with a system base shear if $V_b = 1.0$, is shown in Fig. 4(a). These equivalent static forces lead to moment and shear force patterns, applicable to the system, as presented in Figs. 4(c) and (d), respectively. Possibilities for the assignment of lateral forces to the two very different elements, and associated displacement limits, are of prime interest. It is restated that, within rational limits, fractions of the overturning moments, M, and consequently associated story shear forces, V_s, to be sustained by the chosen ductile mechanism of the system, may be assigned to the wall and frame elements in an arbitrary, but sensible, manner.

Chosen mechanisms

The mechanism deliberately chosen for this structure, comprises plastic hinges only at the base of the walls and the columns and at each end of the beams. In accordance with the philosophy of capacity design, other regions of the components will be provided with sufficient reserve strength to ensure that under dynamic actions no inelastic deformations of significance would occur while anticipated target displacements are being developed.

To illustrate principal steps of displacement estimates, familiar simple expressions, reflecting component behavior, will be used. Benchmark deformations are influenced by the pattern of lateral forces, but are independent of strength eventually to be provided. Displacement estimates are based on component dimensions, given here in terms of the height of the building, h, as shown in Fig. 4(b). To design practitioners these are likely to be more meaningful quantities. The symbols D_b, D_c and D_w define overall depths of beams, columns and walls, respectively.

Wall deformations

Capacity designed wall elements, which, with the exception of a plastic hinge at the base, are expected to respond in the elastic domain, will control deformation capacities in dual systems. Therefore, it is best to consider wall deformations first.

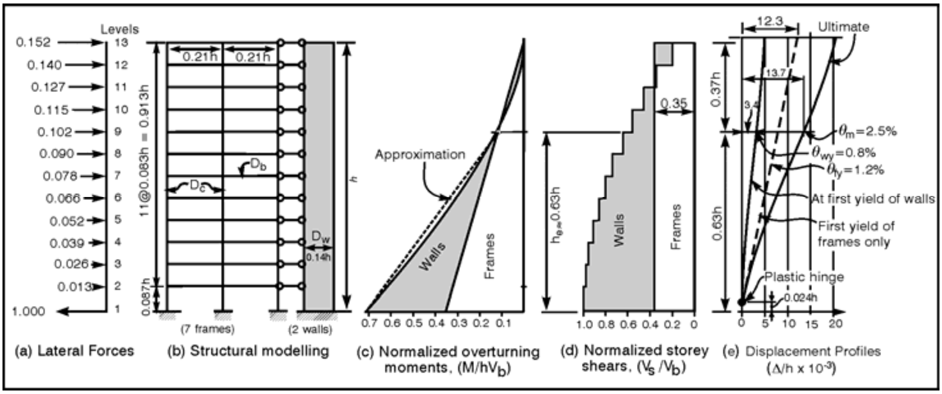

Figure 4. A ductile frame-wall system

The displacement limitations, described earlier, require the assessment of both the displacement ductility capacity of the wall element, $\mu_{w\Delta}$, and the restrictions imposed by specified drift limits. The latter is relevant to the maximum slope of the wall, $\theta_{w,max}$, at some level above the base. Displacement capacities of frame elements will always be larger than those of wall elements. Consequently, displacement demands on the frames can be expected to be moderate. Designers may wish to exploit this feature by relaxing some of the detailing requirements in potential plastic regions of frames. For reasons that will become evident subsequently, the behavior of cantilever walls with a single applied lateral force at the effective height, h_e, are considered in this study.

Estimation of the nominal yield curvature at the wall base, ϕ_{wy}, with Eq.(1), enables the corresponding nominal yield displacement, Δ_{wy}, and the maximum nominal wall yield rotation (slope), θ_{wy}, at the effective height, h_e, to be estimated thus

$$\Delta_{wy} = \phi_{wy} \, h_e^2 / 3 \tag{3}$$

$$\theta_{wy} = \phi_{wy} \, h_e / 2 \tag{4}$$

where the effective height, h_e, eventually selected, is defined in Fig. 4(c).

With appropriate detailing of the potential plastic region at the base of walls, a displacement ductility capacity of $\mu_{w\Delta} = 5$ can be readily achieved. However, this may need to be reduced to satisfy a more restrictive drift criterion. The maximum drift, $\theta_{w,max,}$ at the effective height, including effects of plastic hinge rotations at the base, θ_{wp}, associated with the development of the displacement ductility capacity of the wall element, $\mu_{w\Delta}$, is

$$\theta_{w,max} = \theta_{wy} + \theta_{wp} = \theta_{wy} + (\mu_{w\Delta} - 1)\, \Delta_{wy} / (h_e - 0.5\ell_p) \tag{5}$$

where the length of the equivalent plastic hinge is ℓ_p. The relevant term in Eq.(5) is usually rather small relatively to h_e, and thus it can be ignored. With substitutions from Eq.(1) this expression can then be simplified to

$$\theta_{w,max} = (\mu_{w\Delta} + 0.5)\, \eta \varepsilon_y A_{wr} / 3 \tag{6}$$

Equation (6) relates the chosen drift limit, the wall's displacement capacity and the aspect ratio of the wall element, $A_{wr} = h_e/D_w$, to each other. It enables the contribution to the unit system strength by the two types of elements, satisfying displacement criteria, to be determined. A typical value of the parameter η (Paulay 2002), applicable to rectangular walls with some concentration of the vertical reinforcement in boundary elements, used in subsequent examples, is 1.8. The yield strain of the steel will be taken as $\varepsilon_y = 0.002$.

Assignment of relative element strengths

Consequent to the previously made claim of freedom in the assignment of lateral strength to different elements, an appealing choice may be followed, whereby dimensions of the beams and those of columns of the frames are made identical at all levels. With gravity load being generally the same at all levels the strength and detailing of the beams can also be made identical. Therefore, with identical story shear and story moment capacities, the resistance of the frame element to overturning moments will vary linearly to its maximum at the base. This is shown in Fig. 4(c). The nominal strength of such a frame element is consistent with the application of a single lateral force at level

13. The remainder of the total overturning moments, shown by the shaded area in Fig. 4(c), is then assigned to the wall element.

A few choices of the parameters contained in Eq.(6) are made to enable illustration of applications. The constraints on acceptable system displacements may be a wall's displace-ment capacity corresponding with $\mu_{w\Delta}$ = 4, while limiting the expected maximum drift to $\theta_{w,max}$ = 2.5%. Eq.(6) indicates that this can be achieved if the aspect ratio of the wall element, A_{wr}, does not exceed 4.63. Hence the effective wall length chosen should not be more than h_e = 4.63 x 0.14h = 0.65h. With the assignment of 35% of the system base shear to all stories the frame element (Fig.4(d)) and consequent resistance by the frames of approximately 50% of the total overturning moment at the base, the location of zero wall moment will be in the vicinity of h_e = 0.63h < 0.65h.

Features of interest in this approach to strength assignment are:

- Each of the 7 frames needs to resist 5% of the system base shear in every story. The assignment of element strengths, shown in Figs. 4(c) and (d), could also be used if the maximum acceptable drift is to be reduced to 2%. However, as Eq.(6) dictates, the displacement capacity of the walls would reduce to correspond with $\mu_{w\Delta}$ = 3.2.
- Employing reinforcing steel with say 25% increase of its yield strain, would allow strength assignment, discussed above, also to be used. However, the usable displacement capacity of the walls would need to correspond to a reduction of $\mu_{w\Delta}$ to 2.5. The corresponding diminishing of energy dissipation capacity of the system would negate the possible economic advantages commensurate with the increase of the yield strength of the steel by some 25%.
- A reduction of the target drift limit to say 1.5% and the ductility demand on the walls to 3, would, according to Eq.(6), require an effective height of 0.5h. The story shear strength of the frame element would need to be increased to about 47% of the system base shear, while resisting some 67% of the total base moment.
- Moment patterns applicable to wall elements, seen in Fig. 4(c), enable behavioral modeling with simple cantilevers subjected at the effective height to a single lateral force. However, in accord with capacity deign principles (Paulay and Priestley 1992) appropriate allowances need to be made in the form of design shear magnifications and modified bending moment envelopes to cater for modal effects at the development of the overstrength of such wall elements.

Story deformations of frames

Nominal interstory yield deformations of frames in which the yielding of columns is suppressed by appropriate capacity design procedures, referred to in the introduction, originate primarily from nominal yield curvatures in the potential plastic hinges of beams. Additional elastic deformations will occur due to shear effects in beams, columns and joints, and flexural rotations of columns. Because, compared with nominal yield rotations of beams, the contribution of elastic deformations, listed above, are relatively small, these may be estimated. Details are not given here. It has been shown (Priestley 1998) that a reasonable estimate, particularly for seismic assessments, of the nominal yield drifts, θ_{fy}, of stories in frames, is

$$\theta_{fy} = 0.5\varepsilon_y A_{br} \qquad (7)$$

where A_{br} is the aspect (span/depth) ratio of the beams, in this example taken as 12.3. Hence with $\varepsilon_y = 0.002$, $\theta_{fy} = 0.0123$ rad.

Displacement profiles of elements

Benchmark displacements, relevant to the example structure, are recorded as fractions of the total height, h, in Fig. 4(e). Wall deformation profiles, consistent with the development of the nominal yield displacement and the maximum drift of 2.5% at the effective height, are shown by the full line curves. The nominal yield displacement of the frame elements, associated with the previously estimated identical yield drifts in all stories, is closely approximated by the dashed straight line.

Based on bilinear modeling of element behavior, the force displacement responses of the elements and that of the system are presented in Fig. 5. The displacement capacity of the system, at the level of the effective height, $\Delta_u = 0.0137h$, is that of the wall elements. This is associated with the assumed simultaneous attainment of 2.5% drift and a wall displacement ductility of 4. The corresponding ductility demand imposed on the frames is only in the order of 1.8. Fig. 5, aiding a simple mental pushover exercise, should be sufficient to indicate benchmark displacement magnitudes and ductility relationships. For example the displacement capacity at the effective height of a building with a total height of say 40 m will be, irrespective of its lateral strength, in the order of $\Delta_u = 13.7 \times 40 = 548$ mm. The likely nonlinear monotonic response of the elements and the system is, with neglecting effects of strain hardening, shown by dashed lines in Fig. 5.

The next challenge to the designer, not addressed in this presentation, is to determine the nominal strength which will ensure that, for the local seismic scenario, the imposed displacement demands will not exceed the displacement capacity estimated with this simple procedure.

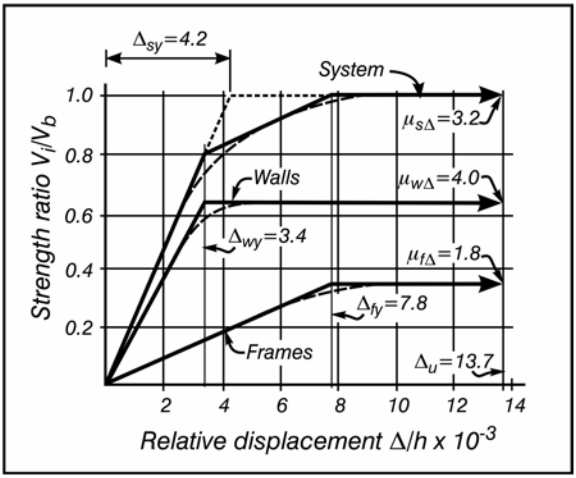

Figure 5. Bilinear modeling of force-displacement relationships in a wall-frame system

Required system strength

In routine design the required lateral strength of a single degree of freedom system, based on its expected dynamic response, is estimated. The basic information required, apart from the total mass, is system stiffness and energy dissipation capacity. The latter may be suitably characterized by the magnitude of the displacement ductility capacity of the system. The final task is thus to estimate for this dual system these two important quantities.

The strength-dependent relative stiffness of the two types of elements of the example structure are obtained, for example from Fig. 5, thus: $k_{wall} = 0.65V_b/(3.4x10^{-3}h) = 191V_b/h$ and $k_{frame} = 0.35V_b/(7.8x10^{-3}h) = 45V_b/h$. Hence the stiffness of the equivalent single degree of freedom system is $k_{system} = \Sigma k_i = 236V_b/h$. A bilinear simulation of the behavior of the equivalent dual system enables its benchmark displacement, that is, nominal yield displacement, to be estimated as $\Delta_{sy} = V_b/\Sigma k_i = 1.0/(236/h) = 4.2x10^{-3}h$. Hence, as Fig. 5 shows, the displacement ductility capacity of the equivalent single degree of freedom system is $\mu_{s\Delta} = 13.7/4.2 = 3.2$. In traditional strength-based seismic design procedures, the two key quantities, k_{system} and $\mu_{s\Delta}$, allow thus the required seismic strength to be established. Using relevant acceleration spectra, a simple trial and error exercise is involved when reconciling the required strength of the system with its strength-dependent stiffness.

In displacement-based design approaches (Priestley 2003) the equivalent displacement capacity-related stiffness (see Fig. 5) of $k_{system} = V_b/\ \Delta_u = 1.0/(13.7x10^{-3}/h) = 73V_b/h$ (i.e., 31% of the stiffness of the elastic system) and damping corresponding with a ductility capacity of 3.2 can be used to establish the required system strength.

Special Features of Frame-Wall Systems

When only cantilever walls provide lateral force resistance their displacement ductility capacity need to be significantly curtailed when aspect ratios, $A_{wr} = h/D_w$, exceed approximately 5.

In ductile frames, exceeding approximately 3 stories, displacement capacities are generally governed by limits on interstory drift, rather then component deformation capacities. Moreover, during the elasto-plastic dynamic response, frame deformations may become sensitive to effects of higher modes of vibrations.

To a large extent these shortcomings of deformation behavior of both walls and frames, may be eliminated when they are coupled within the building by rigid floor diaphragms (Paulay, 2002).

As stated, system deformations are controlled by those of the walls. The nominal flexural strength of the walls provided at levels above the base should be, in accordance with the principles of capacity design, significantly in excess of that indicated in Fig. 4(c). This procedure should ensure that wall sections above the potential plastic region at the base will be subjected, at worse, to very small curvature ductility demands.

When walls, more slender than those shown in Fig. 4(b), are used, for the sake of drift control, the approximate location of zero wall moment must be lowered. This can be achieved by assigning a greater share of the base shear, V_b, to the ductile frames. The designer may thus assign strength to elements to control critical story drift.

The restriction of plastic hinge formation to the base of a wall element should ensure that storey displacements, i.e., story drifts, imposed on frames will be similar over the height, h. However, significant dynamic effects on the elastic portion of the walls should be expected to increase considerably local flexural and shear strength demands, such as recorded in Figs. 4(c) and (d).

Concluding Remarks

This review attempted to highlight some findings relevant to the seismic design of reinforced concrete buildings.

- To satisfy the intents of performance-based seismic structural design, the recognized importance of realistic predictions of target displacement capacities is re-emphasized. For reinforced concrete structures, addressed in this study, such displacement limits can be readily estimated, before any attention is given to required seismic strength. Displacement estimates made during stages of the preliminary design, can immediately draw attention to undesirable seismic features of the contemplated structural system.
- The use of some simple principles, often overlooked or ignored in the design exercise, was demonstrated. These include: (a) The stiffness of a reinforced concrete element should be considered to depend on the strength assigned to it. Therefore, element or system stiffness should not be a priori assumed, as in traditional practice. (b) The nominal yield curvature of a reinforced concrete section, which represents a characteristic strain pattern, and displacements associated with it, are insensitive to the flexural strength of that section.

  (c) Because deformation limits applicable to elements of a ductile system, subjected to typical seismic moment patterns, are insensitive to element strength, the latter may be arbitrarily assigned to them. This enables the astute designer to distribute the total required seismic strength among elements so that more economical and practical solutions, satisfying stipulated displacement limits, could be obtained.
- In the process of evaluating the displacement capacities of elements of a system, the critical one, that with the smallest displacement capacity, needs to be identified. Instead of assuming a global value of the displacement ductility capacity of a system, it should be made dependent on that of its critical element. This criterion can also be established before addressing strength requirements.
- The approach, illustrated with the aid of an example frame-wall structure, can be readily incorporated into existing strength-based seismic design methods. Its major appeal relates, however, to displacement-based seismic design strategies.
- For purposes of the seismic design of ductile systems, bilinear modeling of force-displacement relationships, for both elements and the system, my be considered adequate.
- No attempt was made in this presentation to address displacement demands. It is the designer's responsibility to establish, with the use of force-based or displacement-based design strategies, the level of seismic strength that will ensure that, for a chosen seismic scenario, the established displacement capacity of the system is not likely to be exceeded.
- The concepts presented are design rather than analysis oriented. They are based on very simple principles and are useful tools in the hands of the designer. They enable, even for mixed structural systems considered in this study, more realistic, efficient, practical and simple displacement focused design solutions to be obtained.

Acknowledgement

Information provided in this review has been extracted from previous publications of the author, such as listed in the references.

References

Park, R., and T. Paulay, (1975). *Reinforced Concrete Structures*, John Wiley and Sons, New York.

Paulay, T., and M.J.N. Priestley (1992). *Seismic Design of Reinforced Concrete and Masonry Buildings*, John Wiley and Sons, New York.

Paulay, T. (2000). A simple displacement compatibility-based design strategy for reinforced concrete buildings, *Proceedings of the 12 World Conference on Earthquake Engineering* Paper No. 0062.

Paulay, T. (2001a). A redefinition of stiffness of reinforced concrete elements and its implications in seismic design, *Structural Engineering International* 11 (1), 36-41.

Paulay, T. (2001b). Some design principles relevant to torsional phenomena in ductile buildings, *Journal of Earthquake Engineering* 5 (3), 273-300.

Paulay, T. (2002). An estimation of displacement limits for ductile systems, *Earthquake Engineering and Structural Dynamics* 31, 583-599.

Priestley, M.J.N., and M.J. Kowalsky (1998). Aspects of drift and ductility capacity of rectangular structural walls, *Bulletin of the New Zealand Society for Earthquake Engineering* 31 (2), 73-85.

Priestley, M.J.N. (1988). Brief comments on elastic flexibility of reinforced concrete frames and significance to seismic design, *Bulletin of the New Zealand Society for Earthquake Engineering* 31 (4), 246- 259.

Priestely, M.J.N. (2003). *Myths and Fallacies in Earthquake Engineering, Revisited*, The Mollet Milne Lecture, IUSS Press, Pavia.

Rosenblueth, E. (1980). *Design of earthquake resistant structures*, Pentech Press, London.

Rafael Riddell
Professor of Civil Engineering
Head, Department of Structural and Geotechnical Engineering
Universidad Católica de Chile
Vicuna Mackenna 4860, Santiago, Chile
riddell@ing.puc.cl

Structural Dynamics, Design Spectra, Earthquake Hazard Analysis, Seismic Design

"Seismicity", Chapter 6 in *Seismic Risk and Engineering Decisions*, Elsevier, 1976, was probably the first paper I read authored by Prof. Luis Esteva. This extremely well written paper, which I consider a classic in the discipline, not only introduced me to seismic hazard analysis but strongly influenced my way of thinking on the subject up to now. Although some relationships may have changed and some models evolved in the last thirty years, I still recommend this reference for it provides the fundamental concepts and framework for a rational quantitative description of seismicity. Later on I met him personally, and I followed his lucid presentations in many conferences. I often enjoy asking Luis about other speakers presentations or specific topics of my interest, since his answers are always thorough and clarifying, and I have realized that he knows in much detail almost every subject in the earthquake engineering field.
I take great pleasure in participating in this symposium honoring Prof. Luis Esteva's outstanding and distinguished career in science and engineering.

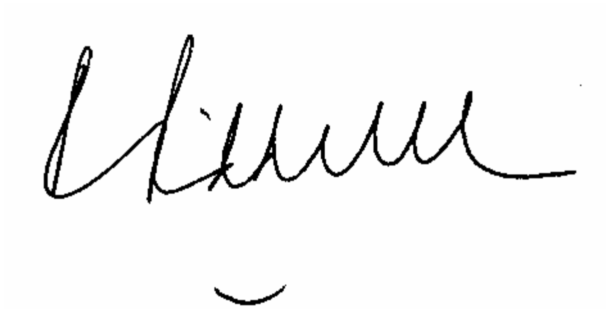

Rafael Riddell,
August, 2005

CORRELATION BETWEEN GROUND MOTION INTENSITY INDICES AND STRUCTURAL RESPONSE TO EARTHQUAKES

ABSTRACT

The characterization of earthquake demands for seismic analysis or design requires the specification of a level of intensity of the ground motion. Response history analyses require scaling of the ground motion records to a specified level of intensity. This study investigates the correlation between twenty-three ground motion intensity indices and four response variables: elastic and inelastic spectral ordinates, input energy and hysteretic energy, based on responses calculated for a set of 52 earthquake records. An essential point of this study is that ground motion indices are relevant as long as they are a sign of the level of structural response. As expected, it is found that no index is satisfactory over the entire frequency range. Indeed, indices based on the ground acceleration history rank better in the acceleration-sensitive region of the spectrum, indices based on ground velocity are better in the velocity sensitive region, and correspondingly occurs in the displacement-controlled region. A rank of indices is presented, according to their correlation with response quantities.

Introduction

The question of how to characterize the strength of ground motions by a simple index has been addressed for long. Housner and Jennings (1982) clearly stated that the difficulties are fundamental: “It is inherently impossible to describe a complex phenomenon by a single number, an a great deal of information is inevitably lost when this is attempted”. Although agreeing with such premise, one is faced with the inexorable demand for a simple specification of the level of intensity of ground motions for seismic analysis and design. Probably the best specification of ground motions one could use in engineering applications is an ensemble of real or synthetic accelerograms with appropriate intensity, duration, frequency characteristics, and consistency with previously recorded motions for a specific site. But, for setting the intensity level of such records, an index is necessary; for example, as customarily done by means of the expected peak acceleration at the site. While using this index is suitable to deal with stiff structures, it can be very inconvenient for the analysis of flexible systems. The same problem arises when the design ground motion is specified by means of a design spectrum; while in some circumstances it may be appropriate to anchor the short-period end of the spectrum to an estimate of the expected peak ground acceleration, in other cases this oversimplification could be unacceptable, and at least two or three parameters are required. Notwithstanding that the latter was proposed about four decades ago by Newmark-Veletsos-Hall (design spectra constructed from peak ground displacement, velocity and acceleration), it is surprising that some standards are still based in only one or two parameters. Although incomplete, the use of two parameters may be acceptable since normally the spectral velocity region is conservatively extended to the low frequency range.

It is apparent from the previous discussion that an index is appropriate as long as it permits to predict or compute a structural response quantity reliably. In other words, one expects an index to be correlated to a response quantity, in such a way that if the index of strength of ground motion increases or decreases, the response quantity does proportionally. For this reason peak ground acceleration (PGA) is not a satisfactory sign of the response of very flexible systems, since these are basically insensitive to acceleration spikes. In turn, this explains why many examples can be found in the literature showing lack of correlation of PGA with observed structural performance during past earthquakes. Indeed, the use of PGA has come under much criticism on the general premise that “it is not adequate to characterize seismic performance of structures”. Such statement is in part right in part wrong, as inferred from the above discussion and as it will be shown below. In fact, the criticism bearing on PGA is extensible to all intensity indices known, for none of them is adequate over the entire frequency range.

The purpose of this study is to evaluate the correlation between various intensity indices with response quantities, in order to rank them according to their quality. It is an extension of the study by Riddell and Garcia (2001) who considered correlations between intensity indices and input and hysteretic energies. For this purpose, the same fifty-two earthquake records considered by Riddell and Garcia were used as input motions, and responses were calculated for elastic and inelastic systems representative of the three characteristic regions of the spectrum. A detailed definition of available intensity indices is given first, then their correlation with response quantities is presented. Finally, the indices are ranked, thus permitting selection of the most appropriate for specific applications. Many references on scaling of ground motion records can be found in a recent paper by Kurama and Farrow (2003).

Ground motion intensity indices

As mentioned above, the intensity of motion can not be satisfactorily characterized by a single parameter. As it will be shown herein, different intensity measures are suitable in the three characteristics spectral regions: short period (acceleration sensitive systems), intermediate period (velocity controlled responses), and long period (displacement sensitive systems). These three spectral regions were first identified by Newmark-Veletsos-Hall in their pioneer work on earthquake response amplification for the derivation of design spectra. In this section, indices related to each of the three mentioned period ranges will be presented.

Acceleration-related indices

The simplest acceleration-related index is the peak value of the ground acceleration history, a_{max}. Quite popular are the indices introduced by Housner and Arias. Housner (1975) argued that a measure of seismic destructiveness could be given by the mean square value of the acceleration history, which he termed “earthquake power index”:

$$P_a = \frac{1}{t_2 - t_1} \int_{t_1}^{t_2} a^2(t)dt \tag{1}$$

where t_1 and t_2 are the limits of the strong portion of motion. To avoid arbitrariness in the selection of t_1 and t_2, the definition of significant duration of motion after Trifunac and Brady (1975) was adopted in this study, i.e., the interval between instants t_5 and t_{95} at which 5% and 95% of the integral in Equation 1 are attained respectively. Arias (1970) proposed as measure of earthquake intensity the integral of the squared acceleration, which he interpreted as the sum of the energies dissipated, per unit of mass, by a population of damped oscillators of all natural frequencies ($o < \omega < \infty$):

$$I_A(\xi) = \frac{\cos^{-1}\xi}{g\sqrt{1-\xi^2}} \int_o^{t_f} a^2(t)dt \tag{2}$$

where ξ is the damping of the oscillator (as a fraction of critical damping), t_f is the total duration of the ground motion and g is the acceleration of gravity. The plain integral of the squared acceleration, its root-mean-square value, and its root-square value have been also considered as potential measures of ground motion intensity:

$$a_{sq} = \int_o^{t_f} a^2(t)dt \tag{3}$$

$$a_{rms} = \sqrt{P_a} \tag{4}$$

$$a_{rs} = \sqrt{a_{sq}} \tag{5}$$

Park et al. (1985) found that the "characteristic intensity" given by

$$I_C = a_{rms}^{1.5}\, t_d^{0.5} \tag{6}$$

that combines the root-mean-square value with the significant duration of the record $t_d = t_{95} - t_5$, was a reasonable representation of destructiveness of ground motions, for it correlated well with structural damage expressed in terms of the damage index after Park and Ang (1985). Riddell and Garcia (2001) found that the following compound index permitted to minimize the dispersion of hysteretic energy-dissipation spectra of inelastic single degree of freedom systems with stiffness degrading force-displacement relationship:

$$I_a = a_{max}\, t_d^{1/3} \tag{7}$$

Araya and Saragoni (1980) defined the "potential destructiveness" of an earthquake as:

$$P_D = \frac{I_A}{\upsilon_o^2} \tag{8}$$

where IA is Arias' intensity (Equation 2) and υo is the number of zero-crossings per unit of time of the accelerogram. The significance of this index is the incorporation of the frequency content of the ground motion through the parameter υo, which modifies its "acceleration-related" character. As υo decreases, the index accounts for shifting of the record damage power to the intermediate and low frequency ranges.

Velocity-related indices

The simplest velocity-related index is the peak value of the ground velocity history, v_{max}. Basic indices similar to the above can be specialized to v(t) the ground velocity history as follows:

$$P_v = \frac{1}{t_{95} - t_5} \int_{t_5}^{t_{95}} v^2(t)dt \tag{9}$$

$$v_{sq} = \int_{o}^{t_f} v^2(t)dt \tag{10}$$

$$v_{rms} = \sqrt{P_v} \tag{11}$$

$$v_{rs} = \sqrt{v_{sq}} \tag{12}$$

Fajfar et al. (1990) proposed the compound index

$$I_F = v_{max}\ t_d^{0.25} \tag{13}$$

as a measure of the ground motion capacity to damage structures with fundamental periods in the intermediate period range. Riddell and Garcia (2001) found that a similar index

$$I_v = v_{max}^{2/3}\ t_d^{1/3} \tag{14}$$

permitted to minimize the dispersion of hysteretic energy dissipation spectra for intermediate frequency inelastic systems. The exponents of v_{max} and t_d varied depending on both the type of force-deformation relationship and the level of ductility; the exponents used in Equation 14 are approximately applicable for any resistance function and for moderate ductility level. Housner's spectral intensity (1952)

$$S_I(\xi) = \int_{0.1}^{2.5} S_v(\xi, T)dT \tag{15}$$

may be also regarded as a velocity related index inasmuch as it weighs preferentially the intermediate period range (approximately 0.5<T<2) against the short period range (T<0.5) and the long period range(T>2). It must be pointed out however that Housner's intensity is a response-related quantity, i.e. an a posteriori index since it is a response quantity itself, in opposition to the other indices presented herein which are of an a priori nature, i.e. they are a direct measure of the ground motion strength.

Displacement-related indices

The simplest index in this case is the peak value of the ground displacement history, d_{max}. Basic indices similar to the above can be specialized to d(t) the ground displacement history as follows:

$$P_d = \frac{1}{t_{95} - t_5} \int_{t_5}^{t_{95}} d^2(t)dt \tag{16}$$

$$d_{sq} = \int_o^{t_f} d^2(t)dt \tag{17}$$

$$d_{rms} = \sqrt{P_d} \tag{18}$$

$$d_{rs} = \sqrt{d_{sq}} \tag{19}$$

In turn, Riddell and Garcia (2001) found that the combined index

$$I_d = d_{max}\ t_d^{1/3} \tag{20}$$

permitted to minimize the dispersion of hysteretic energy dissipation spectra for low frequency inelastic systems.

Correlation between intensity indices and response

The response of simple SDOF systems was considered for this purpose. Elastic systems and inelastic systems with force-displacement relationship given by three nonlinear models were considered: elastoplastic, bilinear, and stiffness degrading. The post yield stiffness of the two latter was 3% of the elastic stiffness. These models cover a broad range of structural behavior. They are intended to represent over-all generic behavior, rather than specific characteristics of individual systems (Riddell and Newmark, 1979). A damping factor ξ=5% of critical was used. SDOF systems associated to three control frequencies 0.2, 1 and 5 cps were chosen as representative of the three characteristic spectral regions. These frequencies are roughly in the middle of the three spectral regions of response amplification.

The fifty-two earthquake records considered by Riddell and Garcia (2001) were used as input ground motions. These records represent moderate to large intensities of motion. They are deemed relevant from the earthquake engineering standpoint since damage was observed near the recording site of many of them. The records satisfy the following intensity condition: peak ground acceleration larger than 0.25g and/or peak ground velocity larger than 25 cm/sec. They represent a variety of conditions regarding tectonic environment, site geology (although most of them on firm ground), Mercalli Intensity, distance to source, or others, thus offering a wide sample regarding frequency content. It is therefore expected that the findings of this study enjoy some generality.

Four response quantities were selected. For elastic systems, two response variables were considered: spectral ordinate (being immaterial which one in particular, since pseudo-acceleration, pseudo-velocity, and maximum displacement are directly related through the frequency factor $\omega=2\pi f$) and input energy per unit of mass E_I supplied to the system by its moving base. The input energy is defined as

$$E_I = -\int_o^u a(t)du = -\int_o^t a(t)\dot{u}(t)dt \tag{21}$$

where u(t) is the relative deformation of the system with respect to the ground. More about this expression and that of EH defined next, as well as about the energy balance equation derived from the equation of motion of the system, are available elsewhere (Kato and Akiyama, 1975; Zahrah and Hall, 1982; Riddell and Garcia, 2001). On the other hand, it has been found that there is an exact functional relationship between the input energy spectrum and the Fourier amplitude spectrum (Ordaz et al, 2003); for this reason, the Fourier spectrum, which is a significant response variable, was not considered in this study.

When Equation 21 is integrated until the ground motion stops (tf) EI is equivalent to the total energy dissipated by damping in the elastic system. It is worth to remark that, according to the previous definition, EI is a response quantity, i.e. it is not a ground motion record attribute. Indeed, the energy input across the spectrum varies, i.e., different amounts of energy is transmitted from the ground to the various systems depending on their natural frequencies. Therefore, one should be cautious about the expression “the earthquake energy input”, since the actual input depends on the system itself. Thus, the quoted term may be misleading, for it may give the wrong impression that there is a fixed amount of energy that the ground forces into every system.

In the case of inelastic systems two response variables were considered: the maximum deformation umax and the hysteretic energy EH dissipated by the oscillator, both of them for a response associated to a displacement response ductility μ=3. The specific value of μ chosen is not a limitation since similar conclusions are reached if other values are used. The total hysteretic energy dissipated per unit of mass is defined as:

$$E_H = \frac{1}{m}\int_o^{t_f} F(u)\dot{u}(t)dt \tag{22}$$

where F(u) is the hysteretic restoring-force history. Energy dissipation is a form of structural damage (Park and Ang, 1985), and thereby plays an important role in the assessment of seismic performance

To visualize the correlation among response quantities and intensity indices, plots like Figures 1, 2, and 3 were made for all indices. In particular, Figure 1 illustrates the relation between peak ground acceleration amax and umax the maximum displacement of inelastic systems with bilinear constitutive rule and response ductility μ=3. Each dot corresponds to the response to each of the 52 earthquake records. It can be seen that amax and umax present excellent correlation (correlation coefficient ρ=0.877 for the functional relationship indicated below) for the high control-frequency (f=5 cps), but they show very poor correlation at intermediate and low frequencies (control-frequencies equal to 1 and 0.2 cps with ρ=0.285 and 0.175 respectively). Figure 2 shows the relation between Housner’ intensity and hysteretic energy EH (for elastoplastic systems with response ductility μ=3); it can be seen that SI and EH present excellent correlation for intermediate frequency systems (f=1 cps, ρ=0.917) and very good correlation for low frequencies (f=0.2 cps, ρ=0.821), but they are un-correlated at high frequencies (f=5 cps, ρ=0.133). Figure 3 relates Riddell-Garcia’s index Id (Equation 20) with hysteretic energy EH for stiffness-degrading systems with response ductility associated to a response ductility factor μ=3; there is no correlation at all at f=5 cps (negativeρ), good correlation at f=1 cps (ρ=0.78), and extremely good correlation at f=0.2 cps (ρ=0.967). To have an objective measure of correlation (as the previously given ρ values), a curve of the form

$$R=\alpha I^{\beta} \tag{23}$$

was fitted to the data, for all possible pairs between the intensity indexes (I) and the response quantities considered (R) at the three control frequencies (f=0.2, 1 and 5 cps), where α and β are the nonlinear regression parameters (or linear regression between the logarithms of the variables). The goodness of fit is quantified by the correlation coefficient given by

$$\rho = \frac{\mathrm{n}\sum(\ell n\mathrm{I}\ \ \ell n\mathrm{R}) - \sum \ell n\mathrm{I}\sum \ell n\mathrm{R}}{\sqrt{(\mathrm{n}\sum(\ell n\mathrm{I})^2 - (\sum \ell n\mathrm{I})^2)(\mathrm{n}\sum(\ell n\mathrm{R})^2 - (\sum \ell n\mathrm{R})^2)}} \tag{24}$$

The correlation coefficients for all response vs. intensity combinations, for the three control frequencies, are summarized in Tables 1 to 5. The indices ranked top-five for each frequency are noted. The correlation coefficient is the same for indices that differ only by a constant or by the exponent (this is the case for example of IA, asq and ars). The main conclusion drawn from the results presented in these tables is that no index shows satisfactory correlation with response in the three spectral regions simultaneously, indeed, acceleration-related indices are the best for rigid systems (5 cps), velocity-related indices are better for intermediate frequency systems (1 cps), and displacement-related indices are better for flexible systems (0.2 cps), although some velocity-related indices do also well in the displacement region. Several specific observations can be made from the mentioned tables as discussed next.

Correlation between intensity indices and spectral ordinates (Tables 1 and 2)

The peak ground motion parameters (amax, vmax, dmax) show very good correlation with elastic and inelastic spectral ordinates, specially in the displacement and acceleration regions where dmax and amax are the best indices. In the velocity region vmax ranks third, after Housner´s intensity (SI) and Fajfar's index (IF). However, averaging the values in Tables 1 and 2, it is found that the correlation coefficient for vmax is only 7.7 % smaller than that for SI, and only 3.2 % smaller than that for IF. Noting that SI is a response variable itself, and hence less appealing as a predictor variable, one comes to realize that vmax is an appropriate intensity index in the velocity region. Considering the previous observation, and recalling that Nau and Hall (1982) tested several of the indices used herein (except PD, IC, IF, Ia, Iv, and Id) to find that none of them provided noteworthy advantage over the peak ground motions to reduce the dispersion of elastic and inelastic spectral ordinates, amax, vmax and dmax must be regarded as significant intensity parameters to characterize the earthquake demand, especially because these indices can be probabilistically predicted for future earthquakes as a function of magnitude, source mechanism, distance and site conditions.

Arias' intensity, which has been widely used as a measure of ground motion severity and as scaling parameter, is essentially and acceleration related index, and therefore appropriate only when the response of acceleration sensitive systems is concerned. In turn, it is not satisfactorily correlated with elastic and inelastic spectral ordinates. Similarly, Housner's intensity is essentially a velocity-related or intermediate frequency index. Although not ranking in the top-five, it is moderately good in the displacement region. It does very poorly with regard to the response of rigid systems.

Correlation between intensity indices and energy responses (Tables 3, 4 and 5)

Housner's intensity ranks first for intermediate frequencies and does fairly well for f=0.2 cps, but it does poorly for rigid systems. In the velocity region SI is closely followed by vsq and vrs, Riddell-Garcia's index (Iv), and Fajfar's index (IF), with all these indices featuring substantially the same correlation coefficients, with differences less than 1%, 3.1% and 3.2% with respect to SI respectively (to facilitate the comparison, the average of the ρ values in Tables 3 to 5 was considered). Peak ground velocity (vmax) comes 15.5% behind SI.

In the acceleration region, Park et al's index is the best (IC), followed closely by Riddell-Garcias's index (Ia) and Arias'intensity (IA), while PGA (amax) does also well particularly regarding hysteretic energy. Their differences on average-ρ with respect to IC are 1%, 1.7% and 7.7% respectively. In the displacement region Riddell-Garcias' index (Id) presents the best correlation with energy responses, followed by the peak ground displacement dmax, the root-square velocity vrs, and the root-square displacement drs (with average-ρ differences of 4%, 7% and 7.8% respectively with respect to Id).

Including td to form compound indices (IC, IF, Ia, Iv, Id) generally results in improved correlation coefficients. For example, in the acceleration region IC is better than arms, in the velocity region IF is better than vmax, and in the displacement region Id is better than dmax. Similarly, the effect of ground motion duration in energy responses is manifested by the fact that root-square values (rs) are always better correlated with energy responses than root-mean-square values do (rms).

Although other indices outperform the peak ground motion parameters, dmax and amax come reasonably close (respectively, only 4% and 7.7% difference in average-ρ with the index ranking top in the corresponding spectral region). Less successful is vmax in the velocity region, with an average-ρ 15.5% smaller than that of the top index.

Summary and conclusions

This study has attempted to contribute to a better understanding of ground motion intensity indices used for specification of design ground motions or for normalizing or scaling ground motions for earthquake response studies. It was found that: a) No index shows satisfactory correlation with response in the three spectral regions simultaneously, indeed, acceleration-related indices are the best for rigid systems, velocity-related indices are better for intermediate frequency systems, and displacement-related indices are better for flexible systems; b) The peak ground motions parameters (amax, vmax, dmax) present very good correlation with elastic and inelastic spectral ordinates in their corresponding frequency ranges. Peak ground acceleration and displacement also present good correlation with input and hysteretic energies in their respective spectral regions, vmax however does only moderately well. Since peak ground motion parameters can be established for future earthquakes with relative ease, on the basis of generally accepted available methodologies for earthquake hazard assessment, they are strongly recommended as intensity indices; c) Housner's intensity is the best index in the velocity region regarding correlation with both spectral ordinates and energy responses. It does moderately well in the displacement region and very poorly in the acceleration region. It should be noted as well that Housner's intensity is a spectral response quantity itself, hence less appealing as a predictor variable; d) Arias' intensity, a widely used measure of ground motion severity, is essentially an acceleration related index, therefore appropriate only when the response of rigid systems is concerned. In the high frequency range it presents good correlation with energy responses, but it is amply outperformed by the peak ground acceleration and other indices with regard to spectral ordinates; e) The duration of motion is effective in increasing the correlation with energy responses when combined with other simple indices in product form. Compound indices proposed by Park et al., Fajfar, and Riddell and Garcia, rise to reach the top or nearly the top rank in their corresponding frequency ranges. In turn, root-square values of the ground motion histories always present better correlation with energy responses than root-mean-square values do, thus reflecting the effect of duration.

Acknowledgements

This study was carried out in the Department of Structural and Geotechnical Engineering at the Universidad Católica de Chile with financial assistance from the National Science and Technology Foundation of Chile (FONDECYT) under grants Nº 1990112 and 1030598.

References

Araya, R. and Saragoni, R., 1980. Capacidad de los movimientos sísmicos de producir daño estructural, *SES I 7/80*, Universidad de Chile, Santiago.

Arias, A., 1970. A measure of earthquake intensity, in Seismic Design for Nuclear Power Plants, R.J. Hansen editor, MIT Press, Cambridge, pp. 438-483.

Fajfar, P., Vidic, T. and Fischinger, M., 1990. A measure of earthquake motion capacity to damage medium-period structures, Soil Dynamics and Earthquake Engineering, Vol. 9, Nº 5.

Housner, G.W., 1952. Spectrum intensities of strong motion earthquakes, Proceedings of the Symposium on Earthquake and Blast Effects on Structures, EERI.

Housner, G.W., 1975. Measures of severity of ground shaking, Proceeding of the US National Conference on Earthquake Engineering, Earthquake Engineering Research Institute, pp. 25-33.

Housner, G.W. and Jennings, P.C., 1982. Earthquake Design Criteria, EERI Monograph.

Kato, B. and Akiyama, H., 1975. Energy input and damages in structures subjected to severe earthquakes, A.I.J, Nº 235.

Kurama, Y.C. and Farrow, K.T., 2003. Ground motion scaling methods for different site conditions and structure characteristics, EESD, Vol. 32, pp. 2423-2450.

Nau, J.M. and Hall, W.J., 1982. An evaluation of scaling methods for earthquake response spectra, Structural Research Series Nº 499, Department of Civil Engineering, University of Illinois, Urbana, Ill., 1982.

Ordaz, M., Huerta, B., and Reinoso, E., 2003. Exact computation of input-energy spectra from Fourier amplitude spectra, EESD, Vol. 32, No.4, pp. 597-605.

Park, Y-J., Ang, A.H-S., and Wen, Y.K., 1985. Seismic damage analysis of reinforced concrete buildings, Journal of Structural Engineering, ASCE, Vol. 111, 4.

Park, Y-J. and Ang, A.H-S., 1985. Mechanistic seismic damage model for reinforced concrete, Journal of Structural Engineering, ASCE, Vol. 111, 4.

Riddell, R. and Garcia, J.E., 2001. Hysteretic energy spectrum and damage control, Earthquake Engineering and Structural Dynamics, Vol. 30, pp. 1791-1816.

Riddell, R. and Newmark, N.M., 1979. Force-deformation models for nonlinear analysis, Journal of the Structural Division, ASCE, Vol. 105, ST12.

Trifunac, M.D. and Brady A.G., 1975. A study on the duration of strong earthquake ground motion, Bulletin of the Seismological Society of America, Vol. 65, 3, pp. 585-626.

Zahrah, T. and Hall, W.H., 1982. Seismic energy absorption in simple structures, Structural Research Series Nº 501, Department of Civil Engineering, University of Illinois, Urbana, Ill.

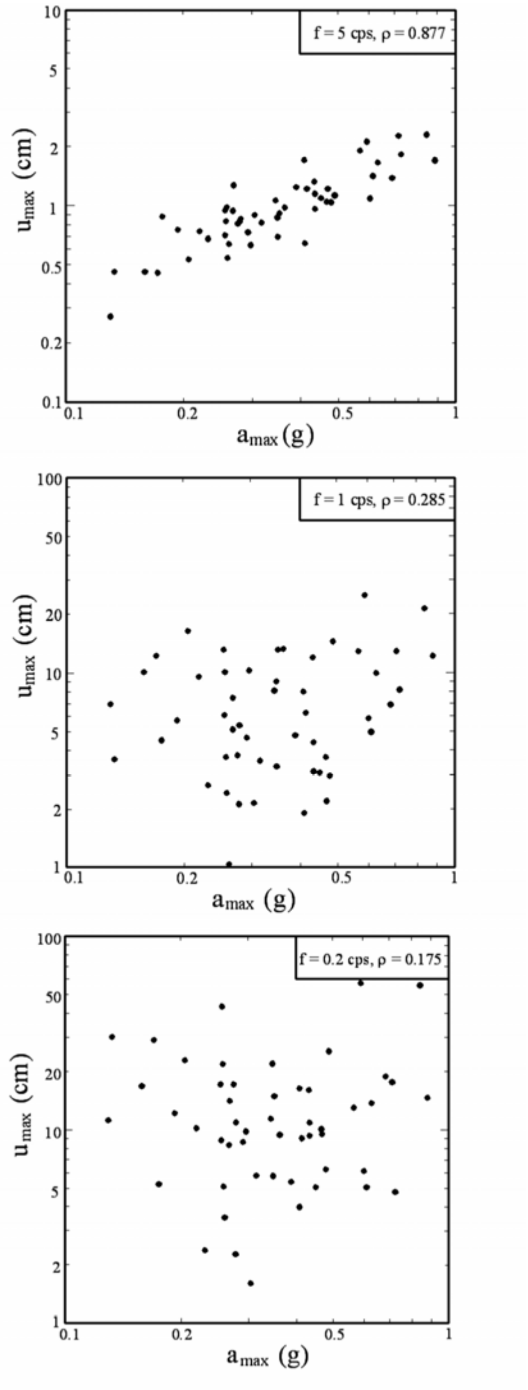

Figure 1. Correlation between peak ground acceleration a_{max} and maximum inelastic displacement u_{max} for bilinear systems with response ductility μ=3

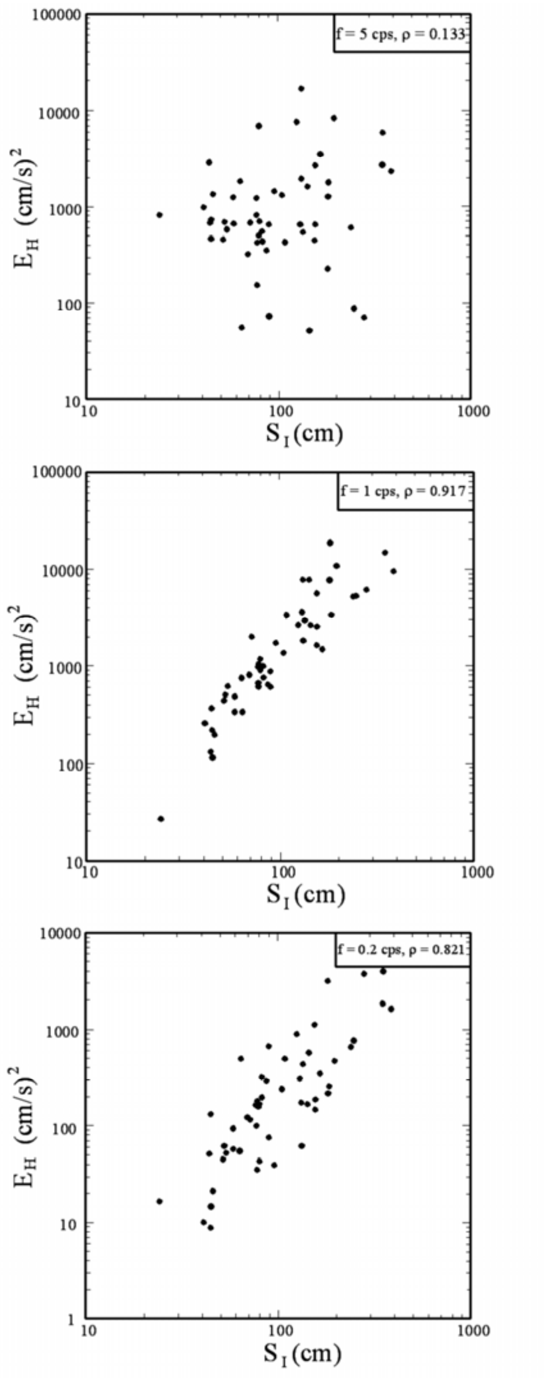

Figure 2. Correlation between Housner´s intensity (S_I) and dissipated energy (E_H) for elastoplastic systems with response ductility μ=3

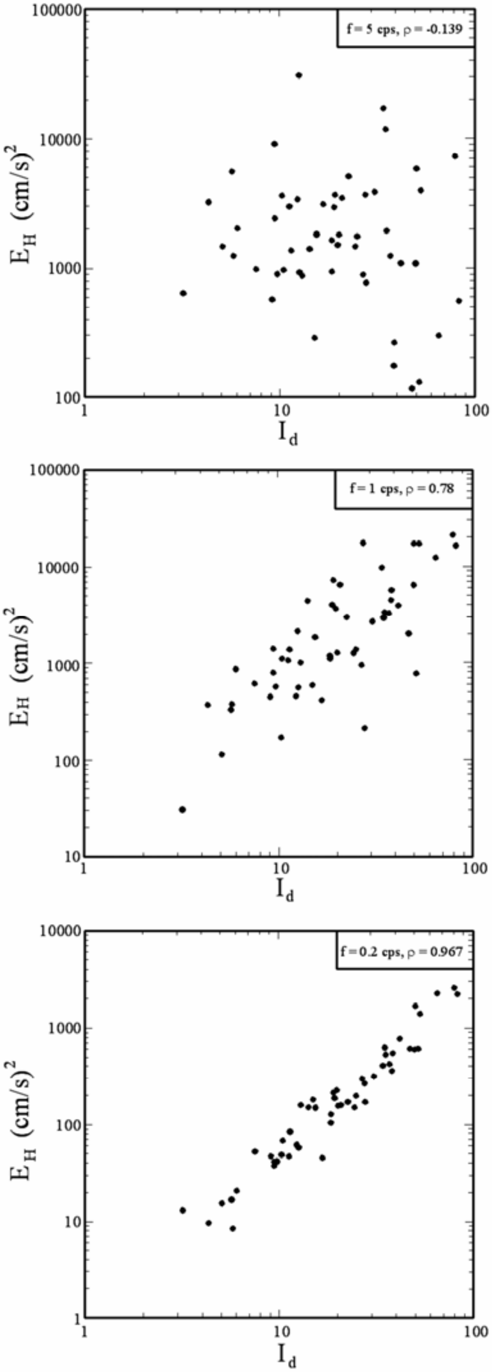

Figure 3. Correlation between Riddell-Garcia's index (I_d) and dissipated energy (E_H) for stiffness degrading systems with response ductility μ=3

TABLE 1. Correlation coefficient ρ between spectral ordinates for elastic systems and various ground motion intensity indices

	f = 0.2 cps		f = 1 cps		f = 5 cps	
	ρ	rank	ρ	rank	ρ	rank
Acceleration-related						
a_{max}	0.186		0.360		0.815	1
I_A and a_{sq} and a_{rs}	0.162		0.455		0.592	5
P_a and a_{rms}	0.202		0.366		0.711	2
P_D	0.542		0.629		-0.051	
I_C	0.192		0.458		0.690	4
I_a	0.142		0.397		0.700	3
Velocity-related						
v_{max}	0.739		0.816	3	0.110	
v_{sq} and v_{rs}	0.748		0.793	4	-0.064	
P_v and v_{rms}	0.788	5	0.756		0.128	
I_F	0.715		0.834	2	0.011	
S_I	0.773		0.883	1	0.071	
I_v	0.612		0.756	5	-0.079	
Displacement-related						
d_{max}	0.938	1	0.629		-0.128	
d_{sq} and d_{rs}	0.868	4	0.488		-0.244	
P_d and d_{rms}	0.900	2	0.516		-0.135	
I_d	0.890	3	0.627		-0.223	

TABLE 2. Correlation coefficient ρ between maximum displacement of bilinear systems with response ductility μ=3 and various ground motion intensity indices

	f = 0.2 cps		f = 1 cps		f = 5 cps	
	ρ	rank	ρ	rank	ρ	rank
Acceleration-related						
a_{max}	0.175		0.285		0.877	1
I_A and a_{sq} and a_{rs}	0.159		0.457		0.660	5
P_a and a_{rms}	0.193		0.326		0.804	2
P_D	0.562		0.701		0.199	
I_C	0.186		0.443		0.773	3
I_a	0.138		0.351		0.738	4
Velocity-related						
v_{max}	0.784		0.871	3	0.443	
v_{sq} and v_{rs}	0.764		0.869	4	0.206	
P_v and v_{rms}	0.805	5	0.801		0.426	
I_F	0.763		0.909	2	0.330	
S_I	0.775		0.945	1	0.377	
I_v	0.658		0.841	5	0.191	
Displacement-related						
d_{max}	0.938	1	0.696		0.118	
d_{sq} and d_{rs}	0.881	4	0.566		-0.026	
P_d and d_{rms}	0.902	2	0.569		0.096	
I_d	0.892	3	0.711		0.003	

TABLE 3. Correlation coefficient ρ between input energy EI for damped elastic systems and various ground motion intensity indices

	f = 0.2 cps		f = 1 cps		f = 5 cps	
	ρ	rank	ρ	rank	ρ	rank
Acceleration-related						
a_{max}	0.127		0.353		0.664	4
I_A and a_{sq} and a_{rs}	0.341		0.612		0.713	2
P_a and a_{rms}	0.139		0.294		0.514	
P_D	0.685		0.553		-0.156	
I_C	0.289		0.536		0.693	3
I_a	0.249		0.546		0.776	1
Velocity-related						
v_{max}	0.736		0.657	5	-0.083	
v_{sq} and v_{rs}	0.905	2	0.785	3	-0.029	
P_v and v_{rms}	0.761		0.574		-0.091	
I_F	0.817	5	0.772	4	-0.039	
S_I	0.842	4	0.792	1	-0.012	
I_v	0.799		0.789	2	0.005	
Displacement-related						
d_{max}	0.862	3	0.469		-0.244	
d_{sq} and d_{rs}	0.811		0.403		-0.216	
P_d and d_{rms}	0.748		0.323		-0.309	
I_d	0.924	1	0.574		-0.196	

TABLE 4. Correlation coefficient ρ between hysteretic energy E_H for elastoplastic systems with response ductility μ=3 and various ground motion intensity indices

	f = 0.2 cps		f = 1 cps		f = 5 cps	
	ρ	rank	ρ	rank	ρ	rank
Acceleration-related						
a_{max}	0.027		0.276		0.817	2
I_A and a_{sq} and a_{rs}	0.175		0.549		0.786	4
P_a and a_{rms}	0.052		0.281		0.751	5
P_D	0.669		0.713		0.044	
I_C	0.140		0.488		0.839	1
I_a	0.101		0.416		0.800	3
Velocity-related						
v_{max}	0.750		0.781	5	0.108	
vsq and vrs	0.871	4	0.901	2	0.050	
Pv and v_{rms}	0.766		0.723		0.140	
I_F	0.804		0.878	3	0.069	
S_I	0.826		0.917	1	0.133	
Iv	0.762		0.867	4	0.026	
Displacement-related						
d_{max}	0.920	2	0.629		-0.163	
d_{sq} and d_{rs}	0.891	3	0.531		-0.249	
P_d and d_{rms}	0.839	5	0.478		-0.201	
I_d	0.948	1	0.703		-0.199	

TABLE 5. Correlation coefficient ρ between hysteretic energy E_H for stiffness-degrading systems with response ductility μ=3 and various ground motion intensity indices

	f = 0.2 cps		f = 1 cps		f = 5 cps	
	ρ	rank	ρ	rank	ρ	rank
Acceleration-related						
a_{max}	0.040		0.187		0.750	4
I_A and a_{sq} and a_{rs}	0.166		0.478		0.878	2
P_a and a_{rms}	0.047		0.190		0.714	5
P_D	0.661		0.763		0.131	
I_C	0.132		0.403		0.887	1
I_a	0.116		0.368		0.820	3
Velocity-related						
v_{max}	0.757		0.806	5	0.127	
vsq and vrs	0.866	4	0.952	1	0.153	
P_v and v_{rms}	0.764		0.744		0.146	
I_F	0.810		0.918	3	0.145	
S_I	0.818		0.946	2	0.187	
Iv	0.766		0.916	4	0.144	
Displacement-related						
d_{max}	0.941	2	0.692		-0.157	
d_{sq} and d_{rs}	0.915	3	0.610		-0.218	
P_d and d_{rms}	0.863	5	0.533		-0.229	
I_d	0.967	1	0.780		-0.139	

Miguel P. Romo
Research Professor
Head of the Geotechnical Department
Institute of Engineering, UNAM
Ciudad Universitaria, México
mromo@pumas.iingen.unam.mx
www.iingen.unam.mx

Geotechnical Earthquake Engineering, Soil Behavior, Soft Computing, Flexible Pavement Systems

Being a research student in soil mechanics at the Institute of Engineering, I became aware of Professor Esteva's high academic profile. However, it was until I took some Earthquake Engineering courses at Stanford and U.C. Berkeley that I fully realized he was not only well known, but also was regarded as one of the world-leading figures in seismology and seismic risk assessment. Indeed, throughout his professional life, he has made long-lasting contributions in these and other related topics.

Over the past twenty five years we have collaborated in a number of engineering projects that involved seismic and earthquake geotechnical matters. Of course, in working meetings, his was the leading voice and often the discussions among peers derived into Luis' lectures that frequently disengaged any controversy. Through these interactions I always benefited from both his original ideas and his natural talent to simplify complex problems. No doubt he is a role model that young researchers should look up to.

It is a privilege to participate in this Symposium to honor Professor Luis Esteva's great accomplishments as engineer, scientist and human being.

A NEUROGENETIC MODEL FOR SYSTEM-PARAMETER IDENTIFICATION AND GROUND RESPONSE ANALYSIS

ABSTRACT

This paper presents a method to solve the complex Geotechnical Earthquake Engineering problem of identifying dynamic soil properties and of predicting responses of layered soil deposits. This procedure makes use of Soft Computer techniques; in this article, Neural Networks are coupled with Genetic Algorithms. The resulting procedure, through the application to a case history, shows its capabilities to carry out the above mentioned tasks. An important finding is that both the dynamic shear modulus and damping ratio are energy-frequency content dependent, aspect seldom known (or admitted) by many members of the profession.

Introduction

As a requirement to understand better the phenomena that control the behavior of engineered structures and ground deposits when subjected to earthquake loading, a great number of seismic instruments have been installed in numerous soil sites and structural systems. As a result, a huge data base has been collected. The information gathered has been mainly used to evaluate (calibrate) existing analytical methods or elaborate new ones.

This data base, spurred up the improvement of computational data analysis aimed at modeling relationships between two domains, *i.e.*, either mapping from cause to effect for estimation and prediction, or inverse mapping from effects to possible causes.

Efficient modeling of engineering systems poses many difficult challenges. Any representation designed for reasoning about models of such systems has to be flexible enough to handle various degrees of complexity and uncertainty, and at the same time be sufficiently powerful to deal with situations in which the input signal may or may not be controllable (Bradley *et al*., 1998).

Mathematically-based models are developed using scientific theories and concepts that apply to specific phenomena. Thus, the core of the model comes from assumptions that for complex systems usually lead to simplifications (perhaps oversimplifications) of the problem phenomena. It is fair to argue that the representativeness of a particular theoretical model largely depends on the degree of comprehension the developer has on the behavior of the actual engineering problem. Predicting natural-phenomena characteristics like those of earthquakes, and thereupon their potential effects at particular sites, certainly belong to a class of problems we do not fully understand. Accordingly, analytical modeling often becomes the bottleneck in the development of more accurate procedures. As a consequence, a strong demand for advanced modeling an identification schemes arises.

This paper shows via the development of a system for the identification of dynamic soil parameters of a clayey deposit in Mexico City, that Soft Computing (SC) techniques –Neural Networks (NNs) and Genetic Algorithms (GAs)- are appealing alternatives for integrated data-driven and theoretical procedures to generate reliable models. This assertion is buttressed using a broad history of seismic events and monitored responses in the accelerometer vertical array of CAO (Central de Abasto Oficinas) site, which is a clayey deposit system.

System identification (SID)

System identification is an important part of the scientific fundament of most natural sciences; it is about building mathematical models for describing an observed physical phenomenon, which may be anything from planetary movements in Astronomy to earthquake response of structural systems in Civil Engineering. In this paper, system models are considered to describe the behavior of natural systems over time as they are influenced from external factors. System identification consists of two subtasks: i) structural identification of the equations in the model *M*, and ii) parameter identification of the model's parameters . A system identification problem can be formulated as an optimization task where the objective is to find a model and a set of parameters that minimize the prediction error between system outputs *y(t)*, *i.e.*, the measured data, and model output *y(t,)* at each time-step *t* (Fig. 1).

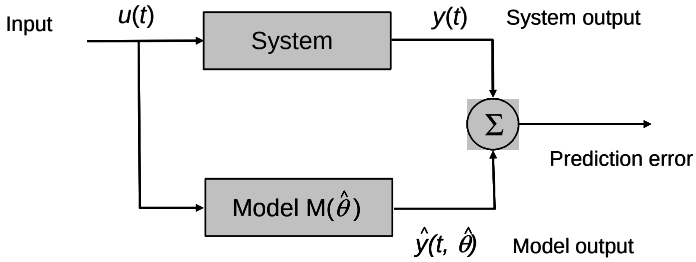

Figure 1. Components of system identification

The data is a vector of system inputs measured at fixed intervals in time, and therefore it is referred to as time-series data. The sum of squared error (SSE) is a commonly used measure of the prediction error.

$$SSE(\hat{y},\hat{\theta}) = \sum_{t=1}^{T} \left(y(t) - \hat{y}(t,\hat{\theta})\right)^2 \qquad (1)$$

Given its practical importance, system identification has derived in a huge research area in engineering. Thus, providing a complete survey is beyond the scope of this work. For an overview of linear identification theory and some non-linear techniques, see (Ljung, 1999). At the present stage, system identification is a well-developed theory for linear systems, but many systems, as geotechnical-earthquake ones, are mainly non-linear and limited theory has been developed to identify adequately this class of problems. For non-linear systems, evolutionary computation -Evolutionary Algorithms, EAs- seems to be a very promising approach, because EAs can readily be combined with a number of other techniques from control engineering, machine learning, and artificial intelligence. Non-linear system identification techniques can generally be grouped into *white box* and *black box* approaches. Table 1 gives an overview of EA-relevant approaches.

In *white box* models, the system is typically described by a set of non-linear differential equations that express the physics behind the system. In *white box* parameter

TABLE 1. Techniques for non-linear identification system. Text within parentheses denotes the part evolved by the EA.

	Parameter identification	Structural identification
White box	Numeric optimization EA (parameters in engineering models)	Unit-typed genetic programming (Equations with correct SID units)
Black box	Neural networks (Weights of the network) Non-linear regression models (Weights of the terms)	Fuzzy logic predictors (Membership functions) Untyped genetic programming (Equations despite of SID units)

identification, the model is derived manually by an engineer. The EA's task is then to determine the model parameters that minimize the prediction error (*e.g.*, Sebag *et al.*, 1998; Haque *et al.*, 1994). *White box* structural identification may also be automated by unit-typed genetic programming, in which differential equations with correct SID units are evolved (*e.g.*, Babovic and Keijzer, 2000).

In contrast, *black box* models are not concerned with the physical soundness of the model, but just to match the system output in the best possible way. *Black box* models usually predict the next system output $\hat{y}(t,\hat{\theta})$ as a function of previously recorded system inputs and outputs, *i.e.*,

$$\hat{y}(t,\hat{\theta}) = f(\varphi(t-1)) \tag{2}$$

where

$$\varphi(t-1) = [u(t-1),...,u(t-n), y(t-1),...y(t-n)] \tag{3}$$

The vector $\varphi(t-1)$ is called a regression vector and the elements of $\varphi(t-1)$ are referred to as regressors. *Black box* approaches include neural networks, regression models, fuzzy logic predictors, and untyped genetic programming. Neural networks and regression models are for parameter identification problems, in which the task is to identify the weights in the network or the terms of the regression model, which is typically a polynomial of the regressors. In *black box* structural identification, fuzzy logic predictors express human readable rules describing the system. The EA's task is to select and design the membership functions for the fuzzy predictor. Another approach is to use untyped genetic programming, which can be seen as a generalization of the regression model technique. For instance, polynomials can be expressed in genetic programming by only using plus and multiplication in the nodes of the expression trees and regressors and constants as the leaves (Rodríguez-Vázquez, 1999). After deriving the model and its parameters, it should be tested to make sure it properly predicts the system behavior. This is usually done by manual verification, performing a whiteness test to see if the residuals are white noise (Ljung, 1999, pp. 511). The residuals, ε(t), are the difference between the measured data and the prediction. Obviously, the model cannot be further improved when the residuals are white noise.

$$\varepsilon(t) = y(t) - \hat{y}(t,\theta) \tag{4}$$

Inferred information about internal system dynamics through SC techniques is developed following an automatic processes (parameter estimation) and empirical knowledge of human experts (structural identification). The aim of this work is building a SC layer to automate the System Identification (SID) process, diagrammed in Fig. 2, around the traditional mathematical techniques and its engineering parameters. This layer automates the high-level stages of the modeling process that are normally performed by a human expert, reasoning from the input-output information to automatically choose, invoke, and interpret the phenomena data and the system results, in order to define parameters most broadly applicable (well formalized) and to generate improvements for models in current use. In this investigation, this layer is constructed using Neural Networks and Genetic Algorithms.

The idea of combining GAs and NNs came up first in the late 80's, and it has generated an intense field of research. Since both are autonomous computing methods, why combine them? The problem with neural networks is that several parameters have to be set before any training can begin. However, there are no clear rules how to set these parameters. Yet these parameters largely determine the success of their training. By combining genetic algorithms with neural networks (GANN), the former is used to find these parameters. The inspiration for this idea comes from nature: in real life, the success of an individual is not only determined by his knowledge and skills, which he gained through experience (equivalent to neural network training), it also depends on his genetic heritage (set by the genetic algorithm). In the following, will be described the basics concepts of NNs and of GAs, as well as the hybrid techniques used in the proposed SC system identification.

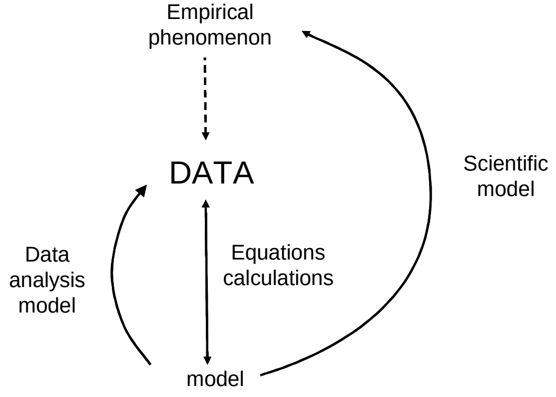

Figure 2. Data analysis and scientific modeling

Neural Networks

A neural network NN, described in purely mathematical terms, is a nonlinear, multidimensional parameterization model. The concept behind developing artificial neural networks is to transfer the idea of parallel processing to the computer, in order to take advantage of some of the human brain's features. NNs were earlier thought to be unsuitable for knowledge discovery because of their inherent *black box* nature. No information was available from them in symbolic form, proper for verification or interpretation by humans. Nowadays, there has been widespread activity aimed at redressing this situation, by extracting the embedded knowledge in trained networks in the form of symbolic rules (*e.g.,* Tickle et al., 1998). This serves to identify the attributes that, either individually or in a combination, are the most significant determinants of the decision, classification or prediction.

There are several neural network models that differ widely in function and applications. In this work, however, only feed-forward networks (FFN) with backpropagation (BP) learning will be examined, because they draw the most attention among researchers, especially in the GANN field. Nonetheless, other algorithm-combinations are being explored.

From the mathematical point of view, a feed-forward neural network is a function that takes an input and produces an output. The input and output are represented by real numbers. The FFN network consists of units (neurons and nodes) and connections. The number attached to each connection is called weight; it indicates the strength of the connection. Connections with a positive weight are called excitatory; the ones with a negative weight are called inhibitory. The constellation of neurons and connections is called the architecture or the topology of the network. In an FFN, the connections are directed in only one way, from top to bottom. There are no loops or circles. It is, however, not a strictly layered network.

In a rigorously layered network, the nodes are arranged in several layers. Connections may only exist to the nodes of the following layer. Yet in our case, there is a connection from the input layer to the output layer. It may be called layered network, because the nodes of each layer are not interconnected. The word “layered”, however, is most often used synonymous with “strictly layered”.

Computation. Fig. 3 illustrates how information is processed through a single node. The node receives the weighted activation of other nodes through its incoming connections. First, these are added up (summation). The result is passed through an activation function; the outcome is the activation of the node. For each of the outgoing connections, this activation value is multiplied with the specific weight and transferred to the next node.

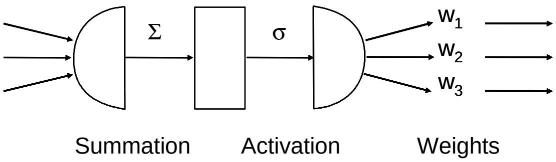

Figure 3. Information processing in a neural network unit

A few different threshold functions are used. It is important that nonlinear threshold function be used; otherwise, a multilayer network is equivalent to a one layer net. The most widely applied - and that has more benefits for BP learning- threshold function is the logistic sigmoid:

$$\sigma(x) = \frac{1}{1+e^{-x}} \tag{5}$$

Back Propagation learning. At the beginning the weights of a network are randomly set or otherwise predefined. However, only little is known about the mathematical properties of neural networks. Especially, for a given problem, it is basically impossible to say which weights have to be assigned to the connections to solve the problem. Since NNs follow the non-declarative programming paradigm, networks are trained by examples usually called patterns. Back-propagation is one method to train the network. It was made popular for neural nets by Rumelhart, Hinten and Williams (Rumelhart, 1986). It is very reliable, although it is a rather slow training strategy. Training is performed by one pattern at a time. The training of all patterns of a training set is called an epoch. The resulting set is a representative collection of input-output examples. BP training is in essence a gradient descent algorithm. It tries to improve the performance of the neural net by reducing its error along its gradient. The error is expressed by the root-mean-square error (RMS), which can be calculated by:

$$E = \frac{1}{2}\sum \left\| t_p - o_p \right\|^{1/2} \tag{6}$$

The error (E) is half the sum of the geometric averages of the difference between projected target (t) and the actual output (o) vector over all patterns (p). In each training step, the weights (w) are adjusted towards the direction of maximum decrease, scaled by some learning rate beta.

$$\begin{aligned} \nabla E &= \left(\frac{\delta E}{\delta w_1}, \frac{\delta E}{\delta w_2}, \ldots, \frac{\delta E}{\delta w_n} \right) \\ w_{new} &= w_{old} - \beta \nabla E \end{aligned} \tag{7}$$

The sigmoid function has the property

$$\frac{d}{dx}\sigma(x) = \sigma(x)(1 - \sigma(x)) \tag{8}$$

That means that the derivative of the sigmoid can be computed by applying simple multiplication and subtraction operators on the results of the sigmoid function itself. This simplifies the computational effort for the back-propagation algorithm. In fact, the equations for weight changes are reduced to:

$$\begin{aligned} \Delta w_{from,to} &= -\beta o_{from} \delta_{to} \\ \delta_{output} &= -\left(t_{output} - o_{output}\right) \\ \delta_{hidden} &= \sigma'\left(s_{hidden}\right) \sum_i \delta_i w_{hidden,i} \end{aligned} \tag{9}$$

There are different functions for connections to hidden and output nodes. The unprocessed sum (, *Fig. 3*) for each neuron has to be stored, before the activation function is applied to it. Then, basic algebra operations like multiplication and subtraction are sufficient to perform the weight changes. These equations describe the basic back-propagation algorithm. There are numerous attempts of its improvement and speed-up. Surveys of these can be found elsewhere (*e.g.*,White, 1993; Schiffmann *et al*., 1992).

Genetic Algorithms

A genetic algorithm (*e.g.*, Golberg, 1989*;* Holland, 1992; Mitchell, 1999) is a random, yet directed search mechanism for an optimal solution to some type of problems. As in biological evolution, we have a population of organisms each having a different set of genes. These genes correspond to the parameters of a given model we wish to optimize, so each organism represents a potential solution to the optimization problem.

For each organism we can determine how well its parameters solve the problem in hand: this determines the 'fitness' of each organism, with better (lower error) solutions corresponding to higher fitness.

The idea behind a genetic algorithm is then to produce new members of the population from members of the current population using various genetic operators. The process of recombination (or crossover) is a means of 'sexual reproduction' in which two 'parents' interchange genes to create two new 'children'. The operation of mutation is a means of 'asexual reproduction' in which an 'offspring' is created from a single 'parent' by randomly changing the value of one of its genes. There are many ways in which these operators can be implemented, but a typical example is shown in Fig. 4. Thus new generations are created iteratively, and at each stage the fitness of each member is a measure of how well each solves the optimization problem.

The goal of this evolutionary approach is to produce diversity within the population and so explore various gene combinations or solutions to the optimization problem. However, this is not a blind search: the probability of reproduction is related to the fitness of the parents, *i.e.*, fitter parents are generally made to produce more children. Nevertheless, not only the fittest individuals produce children. Although that may seem the best strategy, it is similar to only permitting downhill moves in the search for the global minimum of the error function. Such a strategy is prone to getting stuck in local minima. Thus, while less fit members may be produced in the interim, the goal is that, over many generations, the fitness landscape (error surface) is comprehensively explored, and that the population evolves towards a fitter state.

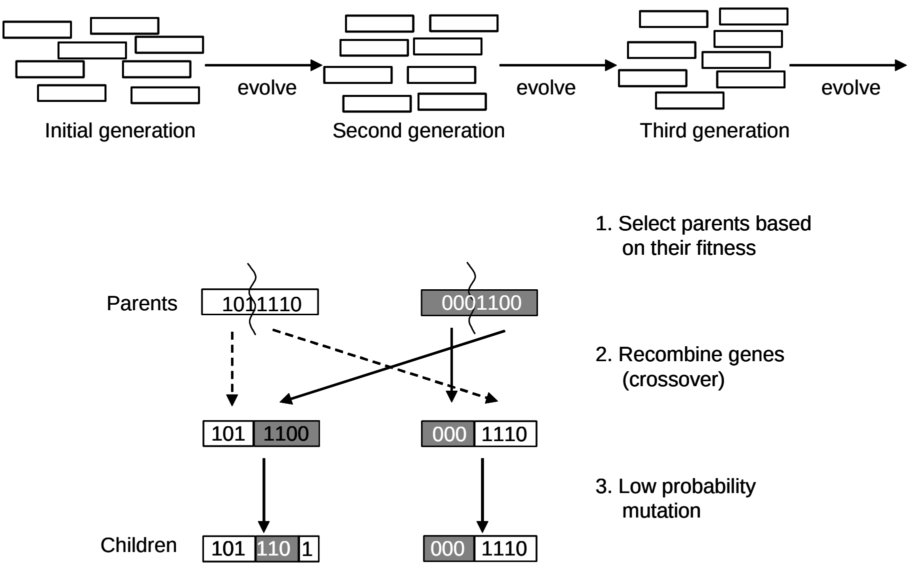

Figure 4. Major functions in a genetic algorithm

An important aspect of genetic algorithms is the encoding of the optimization problem into a genetic formalism. In particular, the parameters of the problem need to be encoded as discrete genes, and the error function expressed as fitness, which can be determined from these genes. For example, a genetic algorithm could be used to determine the optimal weights of a neural network -each weight is represented as a gene- and the fitness is the negative of the error function.

Encoding the network. The general idea of combining GA and NN is illustrated in Fig. 5. Information about the neural network is encoded in the genome of the genetic algorithm. At the beginning, a number of random individuals are generated. The parameter strings have to be evaluated, which means a neural network has to be designed according to the genome information. Its performance can be determined after training with back-propagation. Some GANN strategies rely only on the GA algorithm to find an optimal network; here, no training takes place. Then, they are evaluated and ranked. The fitness evaluation may take into consideration only the performance of the individual. Some approaches consider the network size in order to generate small networks. Finally, after selection takes place, crossover and mutation create new individuals that replace the worst -or all- members of the population. This general procedure is quite straightforward. The problem of combining GA and NN, however, lies in the encoding of the network. The new ideas and concepts of GA and NN bring afresh life into Artificial Intelligence research. But still, we encounter again an old problem: the problem of representation.

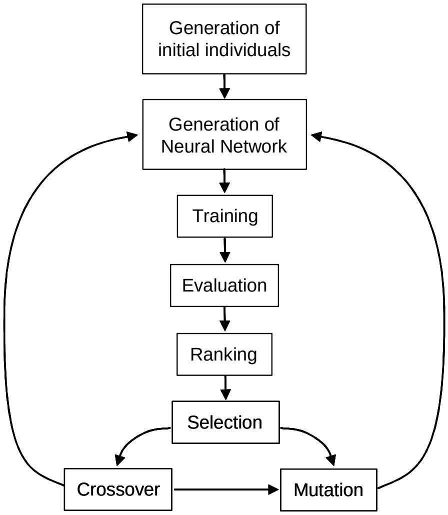

Figure 5. The principle structure of a GANN system

A broad variety of problems have been investigated by different GANN approaches, also, a diversity of different encoding strategies have been implemented. Herein this information is structured focusing on feed-forward networks with back-propagation. It is not emphasized on the complete review of single approaches, it is rather attempted to gather more general information and find general patterns.

The Search for Small Networks. Most of the encoding strategies incorporate the network size in the evaluation function in order to find optimal networks that use fewer neurons and connections. Often, this results in two phases of the search. First, a good network is searched for. Then, the network size of the best individuals is decreased (*e.g.*,White, 1993).

The Problem of Overfitting. One classical problem of neural networks is called overfitting, which occurs especially with noisy data. It has been observed that excessive training results in decreased generalization. Instead of finding general properties of the different input patterns that match to a certain output, the training brings the network closer to each of the given input patterns. This results in less tolerance in dealing with new patterns. For the GANN approach a solution is proposed in (Wong and Wong, 1996). It is suggested to use for the evaluation of the network performance a different set of patterns than those for the training. Hence, only networks that generate the ability to generalize are evaluated high.

Global vs. Local Search. Although GA and NN have in common that they are general search strategies, empirical studies show that they vary in their range (Kitano, 1990). GAs perform a more global search than NN with back-propagation. This point is also stressed in (White, 1993). Fig. 6 illustrates the convergence of the strategies. Back-propagation takes more time to reach the neighborhood of an optimal solution, but then reaches it more precisely. On the other hand, genetic algorithms investigate the entire search space. Hence, they reach faster the region of optimal solutions, but have difficulties to localize the exact point. This happens, because for the final “fine-tuning” of the solution relies almost entirely on mutation.

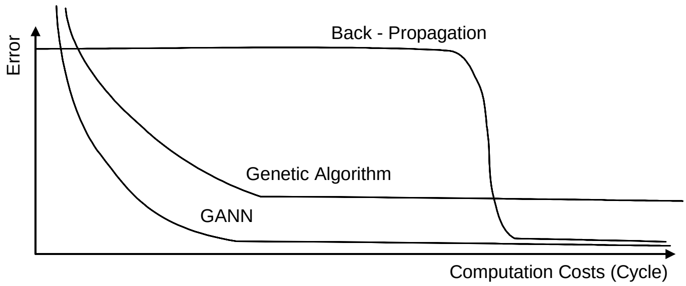

Figure 6. Search speed according to Kitano, 1990

Combining both search strategies seems to be the best thing to do. In addition, as a matter of fact, experiments show that the GANN approach outperforms GA as well as NN in finding a satisfying solution. In the very long run, however, the NN alone seems to be more precise (Kitano, 1990).

Application to a case History

Clayey soil deposit in Mexico City

This analysis is based on the seismic information gathered from a vertical array of accelerometers located in a clayey deposit in Mexico City. The proposed structure consists of (1) establishment of the pattern recognition and parametric identification (inverse analysis) methodology through a GANN topology; (2) model development based on the site information; and (3) validation and assessment of the quality of the model responses in terms of response spectra.

Several inverse analyses for parameter estimation have been introduced by many researchers and they can be classified as time domain procedures, frequency domain procedures and modal analyses (*e.g.*, Zeghal and Abdel-ghaffar, 2001; Zeghal and Oskay, 2001; Glaser and Baise, 2000; Taboada *et al*., 1999; among others). The common aspects of these SID methodologies can be related to Berkey's SID steps (Berkey, 1970): 1) determine the model form and isolate the unknown parameters, 2) select a criterion function for establishing the model results and the actual system responses agreement –error function– and 3) select an algorithm or strategy for system parameters adjustment. This kind of procedures has had a limited success because the methodology for finding the parametric model is strictly directed for stationary signals (Glaser, 1995). The GANN methodology is composed by an adaptable parameter identification subroutine and an identified mathematical structure coded in a second neural environment that ensures efficient-computing responses.

Data Base: CAO site

The CAO (Central de Abasto Oficinas) site is located within the zone of Mexico City soft clay deposits. The stratigraphic profiles and the seismic-instrument vertical-array are depicted in Fig. 7. The soil profile consists of a thick clay layer interbedded by fine sand lenses, underlain by a stiff silty sand layer (locally known as the first hard layer). Then follows a stiffer second clay layer which overlays a thick stiff formation, locally known as the deep deposits, which is composed by partially cemented silty sands, gravels and scattered boulders. CAO down-hole array includes one superficial accelerometer and three more located at 12, 30 y 60 m below the ground surface (Fig. 7). The seismic information that conforms the training and testing sets is summarized in Table 2. M_c, given in column 6, is the maximum earthquake magnitude.

TABLE 2. Data base used for building of the neuro-genetic model

Event	Date dd/mm/aa	Epicenter Depth (km)	Coordinate of epicenter		Magnitude Mc	Type
			LAT. N	LONG. W		
1	24/10/93	19	16.540	98.980	6.5	Test
2	29/07/93	43	17.380	100.650	5.0	Training
3	05/08/93	32	17.080	98.530	5.1	Training
4	04/07/94	31	14.830	97.290	5.9	Training
5	12/10/95	-	18.600	104.100	6.1	Training
6	27/03/96	7	16.21	98.21	4.6	Training
7	21/01/97	18	16.440	98.150	5.0	Training
8	23/03/97	31	17.390	100.880	4.7	Training
9	08/05/97	12	17.320	100.440	4.8	Training
10	10/09/93	20	16.570	98.940	4.8	Training
11	23/02/94	5	17.820	97.300	5.0	Training
12	19/09/85	15	18.081	102.942	8.1	Test
13	14/09/95	22	16.310	98.880	7.3	Test
14	31/05/90	16	17.106	100.893	5.5	Training
15	11/01/97	16	17.910	103.040	6.9	Test
16	23/05/94	23	18.030	100.570	5.6	Test
17	10/12/94	20	18.020	101.560	6.3	Training
18	22/05/97	59	18.410	101.810	6.0	Test

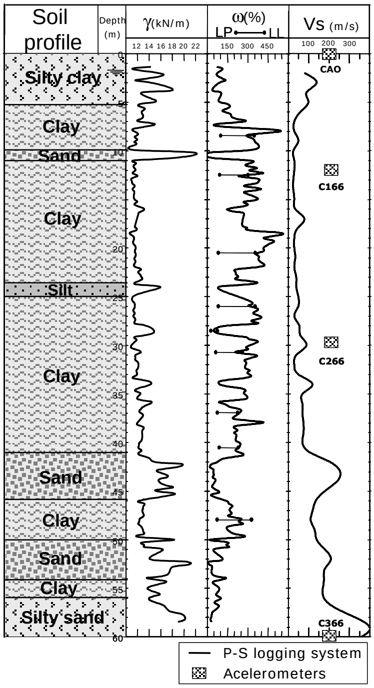

Figure 7. Soil profile of CAO

GANN System. The GANN system presented in this paper was developed to perform in two stages. First, the architecture of a mechanistic neural network (MNN) was designed (this constituted the NN training, also referred to as structural identification in this paper), and then using this MNN the dynamic parameters G and λ that resulted from this first stage were modified following the procedure of continuous GA, until the target spectra of the earthquakes labeled "test" in Table 2 were matched within the specified approximation. This constitutes the parameter identification part of the whole system.

To accomplish the first stage, we proceeded as follows. Using a 1-D wave propagation model a data base of responses was elaborated. The input motions used for this purpose were the time histories recorded at the base of CAO stratigraphy (accelerometer C366 in Fig. 7). Only the motions that are labeled "training" in Table 2 were used. Each analysis was carried out considering the values given by the shear modulus-shear strain and damping ratio-shear strain functions obtained from dynamic laboratory tests on samples retrieved from the CAO site (Romo, 1995). Accordingly, all computed responses included any nonlinear behavior of the soil materials might have developed during shaking. Accordingly, the MNN weights include these nonlinear effects. In addition to the theoretical responses, the input data vector included the description of the CAO site-deposit materials (physical parameters, *i.e.,* plasticity index, natural water content, volumetric unit weight, shear wave velocity, shear modulus and damping ratio's iterated values obtained from 1-D analyses; and geometrical parameters, *i.e.,* layer thickness defined by the distance between input-output motions and depth control) to define the architecture of the mechanistic NN, which consisted of two hidden layers with 50 nodes (computing units) each. The output layer yielded surface ground responses in terms of response spectra.

Fig. 8 compares the responses computed at different depths for various earthquakes with the 1-D wave propagation method and those obtained with the MNN. It may be seen that the analytical responses are well matched by the mechanistic NN responses. However, it is important to comment that none of these procedures were able to match well enough the measured responses. In fact, in some period-intervals the discrepancies were significant (*e.g.*, Correa *et al*., 2004; Correa, 2005).

Once the mechanistic NN was available, it was incorporated (coupled) with the genetic algorithm-module where the dynamic parameters (G and λ) were optimized in the sense that the GANN model could reproduce the "test" (unseen) recorded ground responses.

The convergence criterion used was the root-mean-square error (Eq. 6). Throughout this process it was found that the only manner MNN could match the recorded ground motions (in terms of response spectra) was allowing G and λ varied with the earthquake-energy-frequency content.

The process is schematically described in Fig. 9. The input variables were the same as those used in designing the MNN architecture, but instead of using the ground response computed with the 1-D wave propagation model, the actual responses, labeled "test" in Table 2, were utilized. The GA optimization led to pairs of $G(\omega)$ and $\lambda(\omega)$, for each earthquake, representative of the soil materials underneath the ground response-measuring point. As examples of the results obtained, Fig. 10 clearly shows that both G and λ are frequency (period) dependent. These results conform with several theoretical and experimental results that have shown that the dynamic stiffness and damping parameters are frequency dependent (*e.g.*, Sugito *et al*., 1994; Carvajal et al., 2002; Stokoe., 1999). In this figure are also shown the iterated values of G and λ that resulted from the 1-D analyses, which evidently are constant.

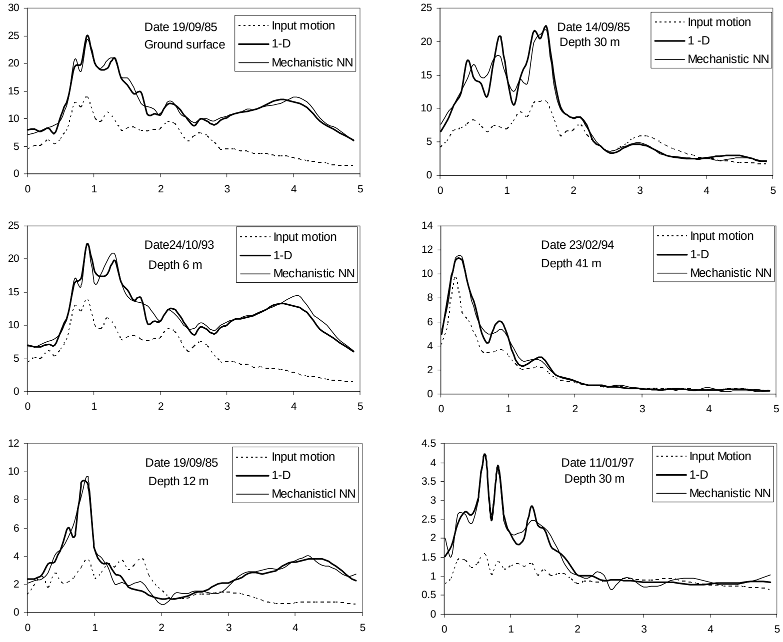

Figure 8. Measured and computed response spectra (5% damping)

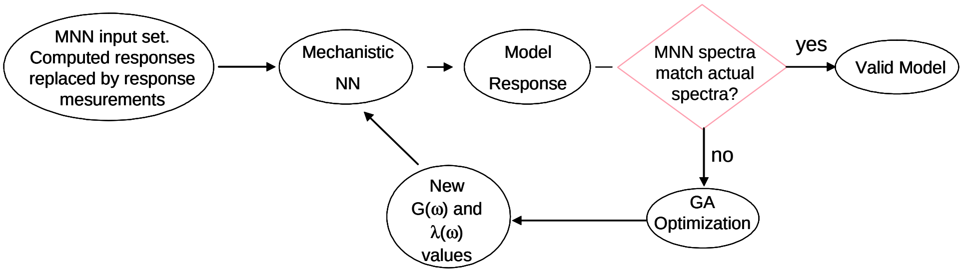

Figure 9. Schematic GANN model

GANN as ground response predictive model. As explained, in the GANN model are defined the values of G(ω) and λ(ω) that optimize the computed response. To this end it is a must to have recorded the response of the soil deposit. This apparently presents a problem to the GANN model for prediction purposes, because predicting implies necessarily not knowing the response.

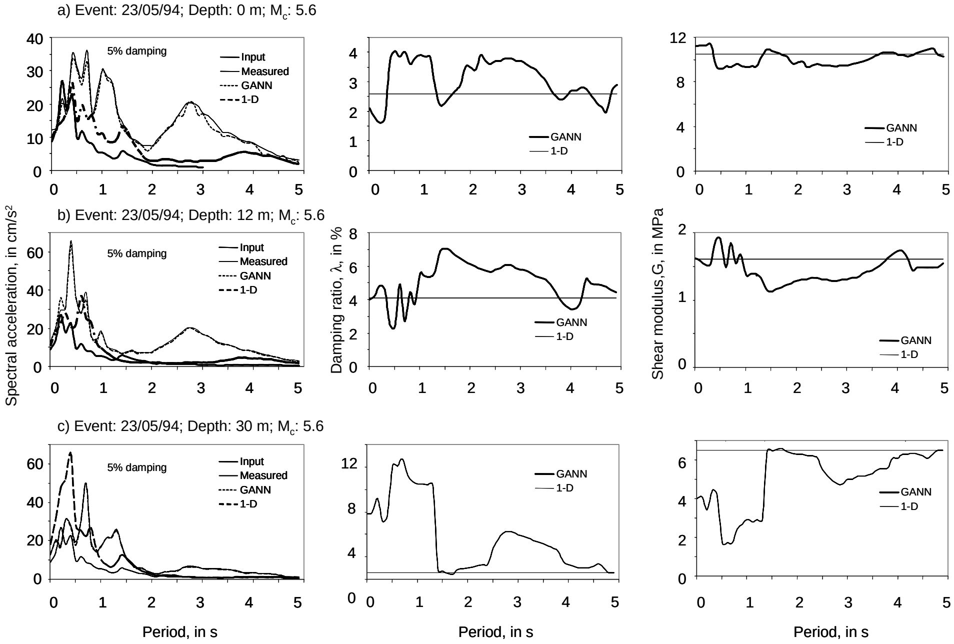

Figure 10. Measured and computed response spectra via GANN and 1-D analytical method

This is obviated in the model in view of the fact that during its training, general patterns of G and λ as a function of the frequency were developed in accordance with the response classified as severe, medium or small. When the GANN model is used for prediction, it automatically selects the appropriate curves G(ω) and λ(ω) corresponding to the severity of the earthquake, and computes the response spectrum.

Since the predicted spectrum highly depends on the G(ω) and λ(ω) functions, this procedure yields responses that might be slightly inaccurate mainly in the neighborhood of sharp peaks, *i.e.*, near predominant frequencies of the soil deposit. Confidence on predictions can be increased as more data is included in the optimization stage. In a research that is going on, alternate procedures are being explored.

Conclusions

Complicated systems thus intricate behaviors (*i.e.*, soil deposits subjected to seismic loading) contaminated by a large amounts of uncertainty -inherent to variables monitoring- are challenging phenomena for designers and scientific professionals who intent to extract knowledge and meaningful conclusions from mathematical functions.

The results included in this paper clearly show that both shear modulus and damping ratio are frequency dependent (strain rate effect). Of special interest is to stress that the shear modulus decreases and, consequently, the damping ratio increases as the spectral amplitudes are higher. This is more noticeably at spectral peaks (higher energy content), which seems to indicate that nonlinear soil behavior develops intermittently in the frequency domain, depending on the energy content. Accordingly, the response of a soil deposit may be linear or nonlinear at different time intervals throughout the duration of the earthquake. This gives the impression of being a misleading conclusion, but it is not because it is backed up by the fact that seismic energy varies from one time interval to another thus causing higher or smaller shear strains. *Ergo*, nonlinearities may evolve now and then while the earthquake lasts. Needless to say that such a behavior has substantial theoretic and practical implications in the design of structural systems.

On the other hand, it becomes evident that Soft Computing evolutionary methods forecasts are more reliable than 1-D analytically-based procedures. Moreover, through the case-history results included in this paper it is demonstrated that the development of hybrid algorithms that are superior to each of their underlying SC components provide the profession with better real-world problem solving tools.

References

Babovic, V., and M. Keijzer (2000). Genetic programming as a model induction engine, *Journal of Hydroinformatics*, 1(2):35–60.

Berkey, G.A. (1970). System identification: An introduction and a survey, *Simulation*, 5(4):151-166.

Bradley, E., A. O'Gallager, and J. Rogers (1998). Global solutions for nonlinear systems using qualitative reasoning, *Annals of Math and Artif. Intel.*, 23:211-228.

Carvajal, J.C., V. M. Taboada-Urtuzuástegui, and M. P. Romo (2002). Influence of earthquake frequency content on soil dynamic properties at CAO site, *Soil Dynamics and Earthquake Engineering*, 22(4):297-308.

Correa, F. J., S. R. Garcia, and M. P. Romo (2004). Sistema de Identificación Inteligente para el análisis de la Respuesta de Sitio, RNMS, Sociedad Mexicana de Mecánica de Suelos, Guadalajara (México).

Correa, F. J. (2005). Identificación de parámetros dinámicos por medio de un sistema neurogenético, *Tesis de Maestría (Mecánica de Suelos)*, División de Estudios de Posgrado, Facultad de Ingeniería, UNAM.

Glaser, S.D. (1995). System identification and its application to estimating soil properties, *Journal of Geotechnical Engineering*, 121(7):553, 60.

Glaser, S.D., and L.G. Baise (2000). System Identification estimation of soil properties at the Lotung site, *Soil Dynamics and Earthquake Engineering*, 19, 521-531.

Goldberg, D. E. (1989). *Genetic algorithm in search, optimization, and machine learning*, Addison-Wesley, Reading, MA, 1989.

Haque, T., R. Nolan II., R. Pillay, and J. Reynaud (1994). Parameter determination for induction motors. In Proceedings of the IEEE SOUTHEASTCON'94, pp 45–49.

Holland, J. H. (1992). *Adaptation in natural and artificial systems* (1st MIT Press Edn), The MIT Press, Cambridge, MA.

Kitano, H. (1990). Empirical studies on the speed of convergence of Neural Networks Training Using Genetic Algorithms. In: Eighth National Conference in Artificial Intelligence (AAAI'90), pages 789–796, Boston, MA, 1990.

Ljung, L. (1999). *System identification: Theory for the user,* Prentice Hall PTR, Second Edition.

Mitchell, M. (1999). *An Introduction to Genetic Algorithms*. MIT Press, Cambridge, MA, USA.

Rodríguez-Vázquez, K. (1999). Multiobjective Evolutionary Algorithms in Non-Linear System Identification. PhD thesis, Department of Automatic Control and Systems Engineering, The University of Sheffield.

Romo, M. P. (1995). Clay behavior, ground response and soil-structure interaction studies in Mexico City, State of the Art paper, Third International Conference on Recent Advances in Geotechnical Earthquake Engineering and Soil Dynamics, St. Louis Missouri, April, 2, 1039-1051.

Rumelhart, D. E., G. E. Hinton, and R. J. Williams (1986). Learning Internal Representations by Error Propagation, in Parallel Distributed Processing, vol. 1, MIT Press, Cambridge, MA.

Schiffmann, W., M. Joost, and R. Werner (1992). Sythesis and performance analysis of multilayer neural network architectures. Technical report 16/1992, University of Koblenz, Institute für Physics, Koblenz, Rheinau 3-4, D-5400.

Sebag, M., M. Schoenauer, and H. Maitournam (1998). Parametric and Non-Parametric Identification of Macro-Mechanical Models. In Quagliarella et al., editors, Genetic Algorithms and Evolution Strategy in Engineering and Computer Science, John Wiley and Sons, 327–340.

Stokoe, K. H., M. B. Darendeli, R. D. Andrés, and L.T. Brown (1999). Dynamic soil properties: laboratory, field and correlation studies, Earthquake Geotechnical Engineering, Seco e Pinto (ed.), pp 811-845, Balkema, Rotterdam.

Sugito, M., N., Aida, and T. Masuda (1994). Frequency dependent equi-linearized technique for seismic response analysis of multi-layered ground, *Journal of Geotechnical Engineering*, Proc. of JSCE, 493:49-58 (in Japanese).

Taboada, V. M., H. Martínez, and M. P. Romo (1999). CAO download array: Evaluation of soil dynamic properties, *Journal of Soils and Foundations*, 39 (6).

Tickle, A. B., R. Andrews, M. Golea, and J. Diederich (1998). The truth will come to light: Directions and challenges in extracting the knowledge embedded within trained artificial neural networks, *IEEE Trans. Neural Networks*, 9, pp. 1057–1068.

White, D., and P. Ligomenides (1993). "GANNet: a genetic algorithm for optimizing topology and weights in neural networks desing", In Proc. of Int'l Workshop on Artificial Neural Networks (IWANN'93), Springer-Verlag, pp 322-327.

Wong, K. P., and S. Y. W. Wong (1996). Combined genetic algorithm/simulated annealing/fuzzy set approach to short-term generation scheduling with take-or-pay fuel contract. *IEEE Transactions on Power Systems*, February, 11(1):128-135.

Zeghal, M., and A. M. Abdel-Ghaffar (2001). Evaluation of the Nonlinear Seismic Response of Earth Dams: I. Pattern Recognition, submitted for Journal publication.

Zeghal, M., and C. Oskay (2001). Local System Identification Analyses of the Dynamic Response of Soil Systems, submitted for Journal publication.

Sonia E. Ruiz
Professor
National University of Mexico
P. O. Box 70-163, Ciudad Universitaria, Coyoacán, 04510
México D. F., México.
sruizg@iingen.unam.mx

Development of reliability- and performance-based seismic design criteria for buildings with energy dissipating devices; analysis and design of special structures (tilted, weak-first-story buildings), and of buildings with seismic isolation and tuned mass dampers; minimum design live loads.

We are sure that the Symposium in the honor of Professor Luis Esteva will be as fruitful (or more) than the one that took place here in Mexico City in 1991, when Prof. Esteva was President of the International Association for Civil Engineering, Reliability and Risk Analysis, and Professor Niels Lind was Past-President.

During the months preceding the Conference (ICASP6) I had the opportunity of learning, following Prof. Esteva, how to organize an international meeting and know to co-edit the conference proceedings. The organizing committee worked very hard; however, I remember that all of us enjoyed it a lot because of the natural leading capacity and the easy way that Prof. Esteva displays when he heads a working group, whether it is scientific or professional.

The same happened when he chaired the XI World Conference on Earthquake Engineering held in Acapulco; however, in the World Conference we had to deal with 1500 abstracts to be reviewed, instead of the 200 that were submitted for ICASP6. Again, the organizing committee worked in the nice and friendly atmosphere that Prof. Esteva normally creates around him, and tries to transmit to his colleagues and students.

I have had the opportunity of sharing that respectful and encouraging environment during more than 25 years at the Institute of Engineering of our National University of Mexico, first as a graduate student and later as his colleague. During that time I have learned from him diverse academic subjects, but what I most appreciate is what I have tried to learn from his **high human quality**; I specially admire the intelligent way in which he always analyzes and solves all problems, and the respect he shows for everybody, in any circumstance.

Congratulations in your 70th anniversary, Doctor Esteva!

Sonia

Sonia E. Ruiz,
January 31, 2005

Photo 1. Opening ceremony ICASP6, Mexico City, 1991.

Photo 2. Professors Emilio Rosenblueth and Luis Esteva.

EVALUATING SEISMIC RELIABILITY OF BUILDING STRUCTURES

ABSTRACT

Modern trends in structural design aim at producing structures characterized by pre-established failure probabilities per unit time for different limit states. This paper addresses the problem of evaluating the reliability implicit in current seismic codes. Several probabilistic design formats are summarized and commented. In order to give information to code writers it is desirable to evaluate the structural reliability implicit in typical designs and different seismic regions; here, the seismic reliability of several buildings designed by engineering firms in accordance with the last version of the Mexico City Building Code is evaluated and discussed. The need of extending this study to other type of buildings and seismic conditions is underlined.

Introduction

Most current seismic design standards are largely based on engineering experience and judgment; and lead to designs with a generally satisfactory behavior; however, the annual failure rate implicit in those designs is *undefined and unknown*. In order to obtain designs with pre-established failure probabilities, several criteria have been proposed in the literature.

In the first part of this paper several probabilistic standard formats proposed in the sixties are reviewed. After that, a description is presented of performance- and reliability-based approaches, including the concepts of seismic hazard analysis and optimization. Comments and limitations related to those formulations are made along the text.

In the second part of the paper, the probabilities of failure per unit time implicit in three office buildings designed by engineering firms in accordance with the Mexico City Building Code (Reglamento de Construcciones para el Distrito Federal, RCDF-2004) are evaluated. It is shown that the reliability levels implicit in those buildings are substantially different. Comments about those differences are presented.

Part I. Review of some probability-based standard formats

Semi-probabilistic format

In an attempt toward consistency in reliabilities, in the sixties several building codes used the following definitions: *characteristic* material strength (R^*) and *characteristic* loads (S^*). The characteristic material strength is defined as a value associated with a small probability (for example 2% or 5%) of not being reached, while the characteristic loads are those values for which there is a small similar probability that the structure will be submitted to a larger load during some arbitrary time interval (50 or 100 years). The *characteristic* load factor of safety factor (SF) is defined as the ratio R^* / S^*.

For reasons of simplicity those codes specify that R^* and S^* were equal to their expected values minus or plus a certain number of their corresponding standard variations. The factor affecting the standard deviations is derived on the assumption that strengths and loads are normally distributed.

This format has several assets but, it has also many limitations. Assets and limitations are discussed in a paper by Rosenblueth (1972).

First-Order Second-Moment format

At the end of the sixties a probability-based structural code format based on first-order second-moment (FOSM) analysis was developed (Cornell 1969, Lind 1969, Ravindra et al 1969).

FOSM format permits the designer to estimate the structural reliability through the reliability index β proposed by Cornell (1969). This index makes use exclusively of the expected values and standard deviations of the effect of loads (S) and strength values (R), and no information is required about the S and R probability density function shapes. It is defined as:

$$\beta = \frac{E(G)}{\sigma(G)} \tag{1}$$

where $G = R - S$. Function G is known as the safety margin, $E(G)$ is the expected value of G, and $\sigma(G)$ is its standard deviation.

The failure probability (p_F) can be obtained by means of the following approximate relation for the case when S and R are independent variables with lognormal density functions (Rosenblueth and Esteva 1971):

$$p_F = 460 \exp(-4.3\beta) \tag{2}$$

The value of β depends on different variables such as: material strength, failure mode, load combinations, etc. For example, the author has compared the reliability inherent in structural elements designed in accordance with two different standards: Mexico City Building Code (RCDF) and ACI-318, and subjected to different types of stresses (flexure, shear, torsion, etc). Her results (Ruiz 1993) indicate that the index value varies from 2.8 to 4.1 for designs made in accordance with the ACI 318 standards, but if the designs are made in accordance with the Mexican Code (RCDF), then the index value varies between 4.25 and 5.57. These differences arise because the codes under study specify different design loads (Ruiz and Soriano 1997) and different partial safety factor values.

Galambos and co-workers (1982) report typical values of β for different loading cases, for different locations in USA, and for concrete and steel beam columns.

Load and resistant factor design format

Using the FOSM procedure with the target values of β, it is possible to compute the resistance factors (ϕ) and the load factors (γ_i, for various loading cases) used in the load and resistance factor design (LRFD) format (Galambos and Ravindra 1973, MacGregor 1983), which is expressed as follows:

$$\phi\ddot{R} \geq \Sigma\gamma_i\ddot{S} \qquad (3)$$

The probability-based LRFD problem is to find appropriate mean resistance ($\ddot{R}$) and load ($\ddot{S}$), and safety factors (ϕ and γ_i) for a prescribed set of β values, load ratios and coefficients of variation of R and S (Ellingwood 1978).

The LRFD format is commonly used around the world in spite that it *does not ensure* that structures with different structural properties will have prescribed levels of safety and performance. Several engineers and researchers have been aware of this problem; therefore, new design methods and probabilistic-based code formats have been proposed.

It is noticed that the studies mentioned up to here refer to reliability of structural *members*, but not of structural *systems*.

Evaluating seismic annual failure rates of multi-story frames

One of the first studies toward evaluating expected seismic annual failure rates of structural *systems* with non-linear behavior, subjected to intense ground motions, was presented by Esteva and Ruiz (1989). The authors took into account uncertainties about mechanical and geometrical properties, as well as about maximum live load and seismic excitations. The expected rate of structural failure (ν_F) was obtained numerically by means of the following integral which is equivalent to that proposed by Esteva and Rosenblueth in 1971:

$$\nu_F = \int_0^\infty -\frac{d\nu_Y(y)}{dy} P(Q \geq 1 | y)dy \qquad (4)$$

where $P(Q \geq 1 | y)$ is the probability of failure given an intensity y, and $Q = S/R$, in that study S is the maximum value of the peak story drift along the height of the building (in what follows this parameter will be just called maximum drift), and R is its ductile deformation capacity. $\nu_Y(u)$ represents the rate of occurrence of any intensity in excess of u.

Esteva and Ruiz (1989) concluded that the expected values of ν_F were very different for the structural frames analyzed (1- , 3- and 9-story frames). Those values ranged from 0.036 x 10^{-3} to 2.61 x 10^{-3}. The authors also concluded that the annual failure structural rate ν_F for the fourteen structural buildings analyzed was very different from the rate of occurrence of intensities higher than the value assumed for seismic design $\nu_Y(y^*)$.

Performance- and reliability-based design formats based on UFR spectra and on seismic hazard analysis

Structural and nonstructural significant failures produced by recent intense earthquakes around the world indicated that *current seismic design approaches have serious deficiencies*. As a consequence, the need appeared to develop new methodologies and criteria for reliability-based design (Fajfar and Krawinkler 1997, Han and Lee 1997, Akiyama et al 1997). With these, the designer should be capable of pre-establishing certain target probability of exceeding a specific maximum response during a given time interval.

Several performance- and reliability-based criteria have been proposed more recently (Collins et al 1995, Cornell 1996, Ellingwood 1999, Wen 2001, Torres and Ruiz 2003). Some of them are reviewed in the following.

Seismic design using uniform failure rate (UFR) spectra

Some of the reliability-based procedures mentioned in the preceding paragraph use uniform hazard spectra or uniform failure rate spectra (Collins et al 1995, Mendoza et al 1995), and "equivalent" single-degree-of-freedom (SDOF) models to estimate the performance of multi-degree-of-freedom structures (MDOF)

The ordinates of uniform failure rate (UFR) spectra are associated with equal annual probabilities of failure in terms of a given damage indicator (i.e.: maximum drift, plastic hinge rotation, normalized dissipated energy, damage index, etc.). Figures 1a and b show examples of response spectra with uniform mean failure rates ν_F corresponding to soft soil in Mexico City (Rivera and Ruiz 2003). The failure criterion of the SDOF systems is defined by the condition that the ductility demand exceeds the available ductility. Curves in Fig. 1 were generated by simulating ground motion time histories with statistical properties similar to those of a record obtained at a specific site (SCT, September 19, 1985) in Mexico City. The vertical axis represents the base shear ratio at yield (C_y), while the nominal period of vibration of the system (T) is represented along the horizontal axis. Each curve corresponds to a given ν_F value. Figures 1a and b show the influence of the design ductility value μ on the UFR spectra. The figure at the left corresponds to μ = 1, and that at the right to μ = 2.

Similar UFR spectra have been obtained for SDOF systems with energy dissipating devices, EDD (Rivera and Ruiz 2003; Rivera 2005). Some examples are shown in Figs. 2a and b, where $\alpha = K_d / K_c$ and $\gamma = d_{yd} / d_{yc}$. Here, K and d_y represent the stiffness and the yield displacement of the structural system, and the sub-indexes d and c correspond to the dissipating system and the conventional structure, respectively. The SDOF model with dissipating system used for the analysis is similar to that proposed by Nakashima et al (1996), and used by Ruiz and Badillo (2001). Figures 2a and b show the influence of the parameter α on the UFR spectra.

Curves like those in Figs. 1 and 2 are useful for the preliminary design of conventional buildings (Collins et al 1995) or for structures with EED's (Rivera and Ruiz 2003). The acceptance condition imposed in the structural systems for the *serviceability* limit state is that the value obtained from the uniform hazard spectral displacement $S_d(T)$ (multiplied by a correction factor that takes into account uncertainties related to the transformation of the maximum response of the SDOF system to that of the MDOF system) should be equal to or smaller than the maximum tolerable drift value stipulated by the code. On the other hand, for the *near-collapse* limit state, the structural design that satisfies the serviceability criterion is checked to ensure that the structure has adequate stiffness and strength to limit the behavior of the structure so that it complies with the maximum drift and the ductility limit. These parameters are supposed to be specified in the design code. Similar acceptance conditions are imposed for buildings designed with energy dissipating devices; however, for this case an additional acceptance condition related to the ductility demand of the dissipating devices should be considered (Rivera 2005).

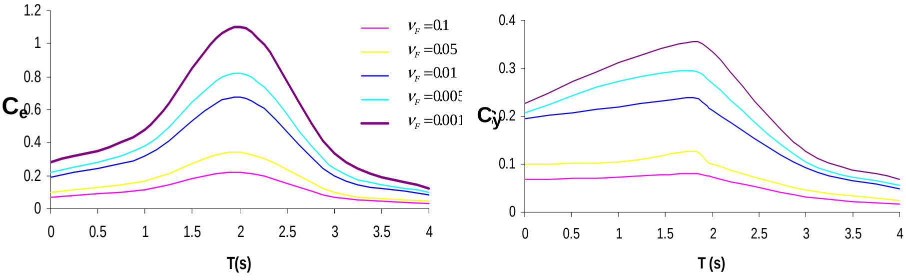

a) $\mu = 1$ b) $\mu = 2$

Figure 1. Uniform failure rate spectra for different ductility capacities

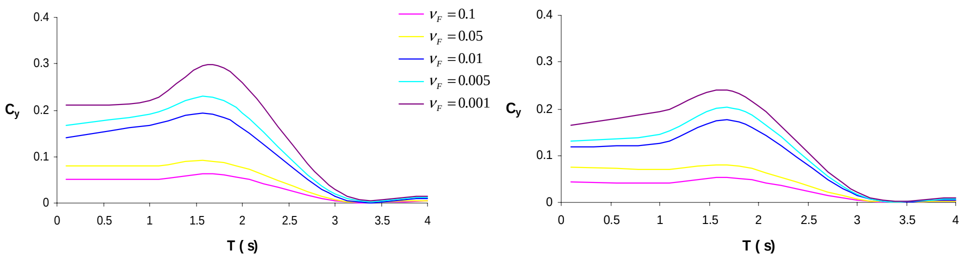

a) $\mu = 2, \alpha = 0.40, \gamma = 0.8$ b) $\mu = 2, \alpha = 0.70, \gamma = 0.8$

Figure 2. Uniform failure rate spectra for $\mu = 2$*, and for different parameters corresponding to energy dissipating devices (EDD's) added in parallel to the SDOF systems*

Transformation functions between the maximum responses of MDOF and "equivalent" SDOF systems

The uncertainties related to the "equivalence" of the response of SDOF and MDOF systems can be taken into account by means of transformation factors of the maximum structural response corresponding to both systems with similar failure probabilities (Inoue and Cornell 1991). Figures 3a and b show examples of maximum story drift hazard values corresponding to a 5- and 10-story regular steel buildings with different structural properties (M1-M3 and M4-M6) and the maximum peak drift hazard values of the "equivalent" SDOF systems (S1-S3 and S4-S6) (Bojórquez et al 2005). The structures are supposed to be built on soft soil (Zone IIIb) in the Valley of Mexico

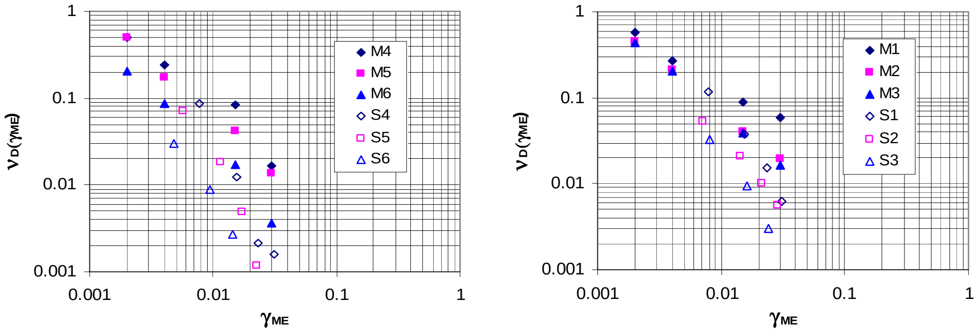

a) 5-story buildings b) 10-story buildings

Figure 3. Demand hazard curves corresponding to six MDOF systems (M1 - M6) and to their "equivalent" SDOF systems (S1 - S6)

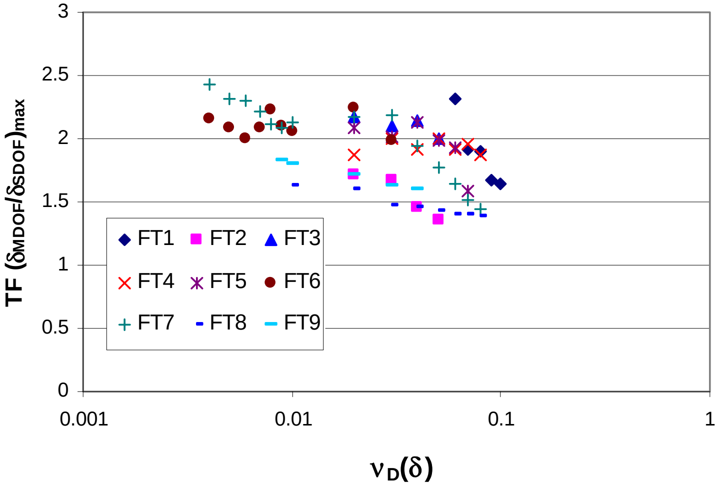

Figure 4. Transformation factor values

Figure 4 shows transformation factors (TF) obtained between the maximum story drifts of the MDOF systems (δ_{MDOF}) and the maximum displacements of the SDOF "equivalent" systems (δ_{SDOF}) for different rates of exceedance, $\nu_D(\delta)$. These factors were obtained from the analysis of nine regular steel frames (six of them correspond to those whose responses are shown in Figure 3) and their corresponding "equivalent" SDOF systems. The ground motions were scaled in accordance with the seismic hazard of the site (Chan et al 2005). Figure 4 gives an idea about the dispersion and the transformation factor values; however, more extensive numerical analysis is needed in this matter.

Seismic hazard analysis based format

Numerical method versus simplified approach

Another way to calculate the annual structural failure rate (ν_F) is by separating the uncertainties concerning structural demands (D) from those of structural capacities (C), as follows:

$$\nu_D(d) = \int -\frac{d\nu_Y(y)}{dy}(P(D \geq d|y))dy \tag{5a}$$

$$\nu_F = \int -\frac{d\nu_D(d)}{dd}P(C \leq d)dd \tag{5b}$$

where $\nu_Y(y)$ represents the seismic hazard function associated with the fundamental period of vibration of the structure, d is the maximum structural response, and y is the seismic intensity. $\nu_D(d)$ represents the demand hazard curve, and C indicates the structural capacity, which is considered as an uncertain variable. This can be obtained through incremental dynamic analysis (Vamvatsikos and Cornell 2002).

Assuming that the seismic hazard curve (represented by ν versus y) is defined by a straight line in a double log graph $\nu = Ky^{-r}$, that the median response $\hat{D}$ is represented by $\hat{D} = ay^b$ (where a and b are parameters that depend on the structural seismic response), and that the maximum response has lognormal distribution, Eqs. 5a and b are transformed into the following simplified formulas (Cornell et al 2002):

$$\nu_D(d) = \nu\left[\left(\frac{d}{a}\right)^{\frac{1}{b}}\right]\exp\left(\frac{1}{2}\frac{r^2}{b^2}\sigma^2_{\ln D}\right) \tag{6a}$$

$$\nu_F = \nu(y^{\hat{C}})\exp\left[\frac{1}{2}\frac{r^2}{b^2}(\sigma^2_{\ln D} + \sigma^2_{\ln C})\right] \tag{6b}$$

where $\sigma^2_{\ln D}$ is the variance of the logarithm of the demand (associated with a given intensity y), and $\sigma^2{}_{\ln C}$ represents the variance of the logarithm of the drift capacity, which is associated with a certain limit state.

Figure 5 compares demand hazard curves ($\nu_D(d)$) obtained by means of Eq. 5a (numerical integration method) and Eq. 6a (simplified approach). The results correspond to reinforced concrete 5- and 10- story buildings designed in accordance with the RCDF-2004 code (Montiel et al 2005).

The curves shown in Figs. 5a and b indicate that the simplified approach gives place to similar results to those of the numerical method for maximum story drifts equal to or smaller than 0.01 and 0.02, for the 5-, and 10-story structures, respectively. For illustration purposes FEMA 273/356 estimates that maximum story drift values for reinforced concrete frame structures of the order of 0.01 and 0.02 may be acceptable for “Inmediate Occupancy” and “Life Safety” performance levels, respectively (Wen et al 2004).

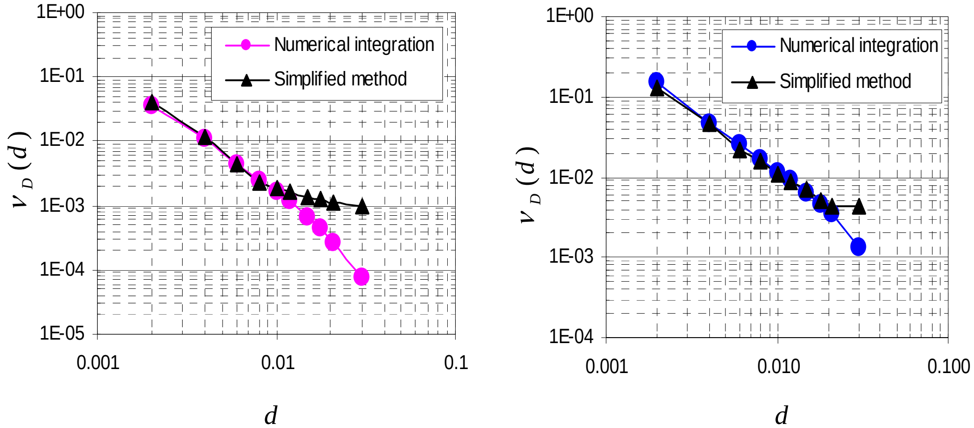

a) 5-story building b) 10-story building

Figure 5. Demand hazard curves obtained by means of two approaches

Displacement-based versus Intensity-based method

An alternative method to calculate the reliability function of a complex structural system in terms of intensity consists in obtaining directly the safety margin with respect to collapse (the ratio of failure intensity to acting intensity) avoiding the need to determine the lateral deformation capacity of the system. This criterion was explored by Esteva (1992) in connection with the response of weak-first-story buildings, including the influence of $P-\Delta$ effects. Facing the impossibility of determining a reasonable value of a deformation capacity under these conditions, he proposed to plot the reciprocal values of the ductility demands of the bottom story of the building ($1/\mu$) for different values of the acting intensities (y). The expected value of the intensity producing collapse was then determined by extrapolating the function $1/\mu$ versus y to its intersection with the y axis.

The intensity-based method can be expressed by the following integral (Shome and Cornell 1999):

$$\nu_F = \int_0^\infty -\frac{d\nu_Y(y)}{dy} P(y \geq S_{a,LS})dy \tag{7}$$

where $S_{a,LS}$ represents the spectral acceleration level at the elastic-first-mode frequency of a structure required to induce certain damage level in that structure (which is generally associated with a given limit sate *LS*).

One advantage of the intensity-based approach (Eq. 7) is that the design and/or assessments are performed in the spectral acceleration ordinates and do not explicitly involve the determination of a displacement capacity. Another advantage is that the method is more direct than the displacement-based method and, as a consequence, the required computational effort is lower.

Due to the reasons mentioned above, several researchers prefer to use the intensity-based method; however, the author of the present paper and her collaborators have found that the failure rate value ν_F corresponding to the near collapse limit state of several structural buildings located at soft soil resulted smaller when ν_F was calculated with Eq. 5b than when Eq. 7 was used. The reason of such differences probably is due to the fact that the structures were excited with *narrow-band* ground motions instead of broad-band motions as used in other studies (i.e., Shome and Cornell 1999). As a consequence of the narrow-band-ness of the ground motions, the standard deviation of the logarithm of the peak story drift capacity resulted smaller than that corresponding to the intensity capacity (Montiel et al 2005).

The use and scaling of *narrow-band* motions (like those recorded during high intensity seismic motions on the soft soil in the Valley of Mexico) is an open question, which needs more study in order to be solved.

Degree of confidence on seismic design

Based on extended versions of Eq. 6b, and assuming that ν_F is equal to a prescribed value ν_0, Cornell and co-workers (2002) obtain an expression for the confidence factor $\lambda_{confidence}$, which is defined as the ratio between the factorized median capacity ($\phi\hat{C}$) and the factorized median demand ($\gamma\hat{D}^{\nu_0}$):

$$\lambda_{confidence} = \frac{\phi\hat{C}}{\gamma\hat{D}^{\nu_0}} \tag{8}$$

where,

$$\phi = \exp\left[-\frac{1}{2}\frac{r}{b}\sigma_{CT}^2\right] \tag{9a}$$

$$\gamma = \exp\left[\frac{1}{2}\frac{r}{b}\sigma_{DT}^2\right] \tag{9b}$$

where $\sigma_{DT}^2 = \sigma_{DR}^2 + \sigma_{DU}^2$ and $\sigma_{CT}^2 = \sigma_{CR}^2 + \sigma_{CU}^2$. The variances σ_{DU}^2 and σ_{CU}^2 are related to the "epistemic" uncertainty implicit in the demand and in the capacity estimations, respectively. The uncertainty is different from the "aleatory" randomness given by σ_{DR}^2 and σ_{CR}^2. The "epistemic" uncertainty of the demand considers, for example, that the properties of the structure are not well defined, and that the method of analysis is not exact. The "epistemic" uncertainty of the capacity is related to the workmanship quality, method of analysis, etc.

The confidence factor $\lambda_{confidence}$ is associated with the level of confidence that the true (but uncertain) annual failure rate is less than the acceptable limit. That quantitative degree of confidence of the design can be evaluated by means of the following equation (Hamburger et al 2003, FEMA 355F):

$$K_x = \left[\frac{1}{2}\frac{r}{b}\sigma_{UT} + \frac{\ln(\lambda_{confidence})}{\sigma_{UT}}\right] \tag{10}$$

where K_x is the standard Gaussian variable (widely tabulated), and σ_{UT} is the total uncertainty calculated as the combined value of the epistemic uncertainties related to demand (D) and capacity (C): $\sigma_{UT} = \sqrt{\sigma_{DU}^2 + \sigma_{CU}^2}$. The other parameters were defined before.

Based on Eq. 10, several design methods (as those contained in FEMA 351) have been proposed for the design of new structural systems and for the rehabilitation of existing structures, including marine platforms.

One of those design approaches was proposed by Montiel and Ruiz (2005) for the rehabilitation of buildings with energy dissipating devices. The approach verifies that the confidence levels (K_x) associated with the serviceability and the ultimate limit states corresponding to a rehabilitated structure are equal to or larger than the confidence levels associated with a similar conventional structure. The idea of establishing the target reliability levels associated with a given limit state in consistency with those implicit in current designs was used by Ellingwood et al (1982).

Optimization-based format

In 1971, Rosenblueth and Esteva described what an ideal code should be. They state that the main purpose of building codes must be to guard the interests of society, which are much wider than a fixed safety level. The authors propose to formulate those codes on the basis of maximizing the expected present value of the benefits derived from the existence of the structure, minus the sum of initial cost and damage, plus maintenance and failure costs (Moses and Kinser 1967). Rosenblueth and Mendoza (1971) and Hasofer (1974) published ideas that later were refined by Roseblueth (1976) related to distinguish between structures that can fail upon construction or never and structures which can fail under rare “disturbances”. Rackwitz (2000) extends those concepts to failures including ultimate limit state failure under normal and extreme conditions, serviceability failure, fatigue and other deterioration, and obsolescence. He demonstrates that failure rates rather than time-dependent failure probabilities are the basis for setting up safety margins.

An overview of the development of methods used in reliability-based structural optimization can be found in Frangopol (1985) and Burns (2002).

Wen (2001) proposes to minimize the following objective function with respect to a design variable vector *X*:

$$U(X,t) = C_o(X) + E\left[\sum_{i=1}^{N(t)}\sum_{j=1}^{k} C_j e^{-\gamma t_i} P_{ij}(X,t_i)\right] + \int_0^t C_m e^{-\gamma\tau} d\tau \qquad (11)$$

where C_o = the initial cost, X = design variable vector, E = the expected value, C_j = cost of jth limit state being reached at time of the loading occurrence, including cost of damage, repair, loss of service, deaths and injuries; $N(t)$= number of severe loading occurrences at time t, t_i = loading occurrence time, $e^{-\gamma\tau}$ = a discount factor, P_{ij} = probability of *j-th* limit state being exceeded given the *i-th* occurrence of a single hazard or joint occurrence of different hazards, k number of limit states under consideration, C_m = operation and maintenance cost per year.

During the last years, seismic design criteria under a life-cycle framework for structures with seismic control have been proposed by several authors (Wen and Shinozuka 1998, Esteva et al 1999, Koh et al 1999, Burns 2002).

Although the optimization-based format is very well understood in theory, it is not practical in every day engineering work. Some authors (Rackwitz 2000) think that code failure rates may be assessed by optimization and, in parallel, by *calibration at present practice*.

Part II. Evaluation of seismic safety of several buildings

Demand hazard curves of three buildings in Mexico City

Most current design standards in the world lead to structural designs with undefined and unknown failure probabilities per unit time. As a consequence, it is desirable to evaluate the reliability that is implicit in those structural designs. Such evaluations would serve to give information to code writers about the probabilities of failure implicit in current designs of typical buildings located at different locations and exposed to different seismic conditions.

The objective of this second part of the paper is to present the reliability implicit in three typical reinforced concrete office buildings designed according to the last version of the Mexican RCDF standard (RCDF-2004). This is the first detailed study about the reliability of buildings designed by engineering firms in Mexico City. The design of the buildings was performed by Alonso (2004), García Jarque (2004), and Granados (2004).

The structures analyzed are 5-, 10- and 15-story reinforced concrete buildings with fundamental vibration periods equal to 0.67s, 1.17s and 1.65s, respectively. The structures are located on soft soil (near the Ministry of Communications and Transportations, SCT building) in Mexico City. The dominant period of the acceleration spectra at that site is about 2s. The variability in seismic and maximum live loads as well as in the material properties were considered by means of Monte Carlo analysis (Montiel 2005).

The reliabilities are expressed in terms of seismic hazard demand curves $\nu_D(d)$ obtained by means of Eq. 5a. Figure 6a shows the story drift hazard curves corresponding to the three structures, and Fig. 6b shows the 50-year probabilities of exceedance of the maximum story drifts. These figures indicate that for the 5-story building the maximum story drift limit of 0.004 will be exceeded with a probability of 41% in the next 50 years (approximately 1 x 10^{-2} per year). The values corresponding to the 10- and to the 15-story buildings are about 90 and 99.9% (4.7 x 10^{-2} and 19 x 10^{-2} per year). The 1.2% limit specified in the RCDF for maximum tolerable drift has a risk of approximately 6%, 37% and 56% of being exceeded in 50 years for the 5-, 10- and 15-story buildings, respectively.

On the other hand, the probability of exceeding a maximum drift value equal to 0.03 in 50 years are equal to 0.40, 6.36 and 1.9% for the 5-, 10- and 15-story buildings, respectively. Here it should be noticed that the 10-story building has a higher probability of exceeding a maximum story drift equal to 0.03 than the 15-story structure. This happens because the response (maximum story drift) increases more rapidly for the 10-story frame than for the 15-story one, as the seismic intensity grows. This occurs because the 10-story structure "*softens*" into the peak of the narrow-band response spectrum, while the 15-story structure does not (Montiel et al 2005).

Figure 6 shows that the reliability implicit in the three buildings is different, even though the structures are located at the same site (SCT), and were designed in accordance with the same seismic code. This study shows the *importance of the frequency content* (narrow-band-ness) of the ground motions on the evaluation of the structural reliability, as well as the significance of the structural vibration period with respect to the period of the spectral peak.

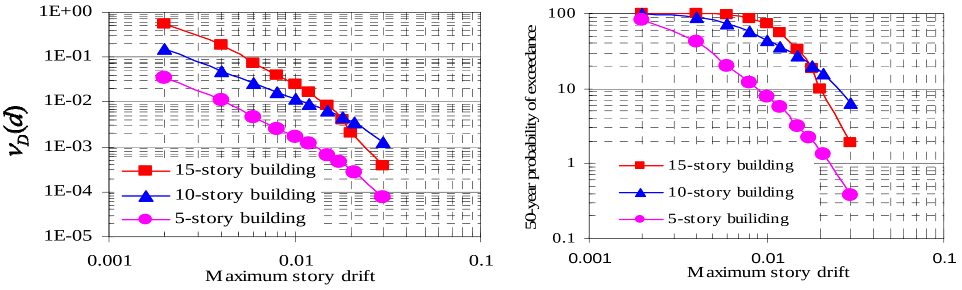

Figure 6. Seismic demand hazard curves of three buildings located on soft soil in Mexico City

Demand hazard curves of other structures

Figure 7 shows the results obtained by Wen (1995) corresponding to two 5-story steel buildings designed with the same code (UBC) and located at two sites. One is 5 km from the Imperial fault at the Imperial Valley and the other is at downtown Los Angeles (LA). The figure shows that, although both sites are in the same zone (Zone 4), the seismic risk is higher at the Imperial Valley (IV) site.

Wen (1995) also presents demand hazard curves for several buildings located in three different countries (5-, 7- and 8-story structures). He found a strong influence of the site seismicity, design philosophy, seismic coefficient values, among other parameters, on the performance curves. He concludes that the annual probability of exccedance equal to 0.004 story drift is of the order of 10^{-2} or lower for the sites studied, and that the corresponding probability of exceeding 0.015 story drift is of the order of 10^{-3}.

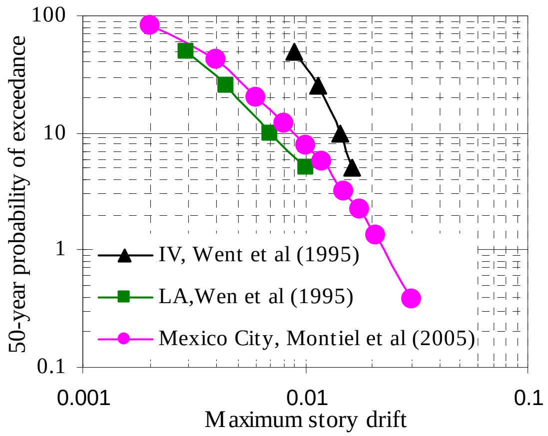

Figure 7. Seismic demand hazard curves for 5-story buildings in Mexico City, Los Angeles (LA) and Imperial Valley (IV)

The values mentioned in the preceding paragraph are in good agreement with those obtained in our study for the 5-story building (see Figure 7); however they *underestimate* the probability of failure for the 10- and 15- story buildings located on soft soil in Mexico City, because the regional seismicity, local soil conditions, frequency content of the ground motions and structural vulnerability in both studies are totally different.

This leads to the following question: which is the annual structural failure rate (for at least two limit states) that the designer should adopt as a target?. From optimization studies it can be seen that it depends on the seismicity of the site, the structural vulnerability, the construction and the failure costs, among other parameters (Esteva 1967, Ang and De Leon 1996). This means that there are not optimum structural failure rate values that we could generalized.

One reasonable strategy consists in fixing a minimum reliability, socially acceptable for the high seismic risk zones, and adopting higher reliabilities, which would increase as the seismic hazard decreases (Esteva and Ordaz 1988, Ordaz 2002).

Final comments

The available literature shows that the theory behind the reliability-based design formats is well developed; in spite of this, most codes around the world base their safety considerations on the FORM methodology, implying that the targets are specified in terms of safety (reliability) indices.

In order to give information to code writers about the reliability implicit in current designs regulations, it is necessary to evaluate the annual failure rates (for at least two different limit states) implicit in typical structures designed with different seismic codes, and located in different seismic regions.

The design of structures characterized with pre-established annual failure rates for different limit states is a matter that will take place gradually after developing simple approaches to facilitate its use, and after introducing educational campaigns for the users of building codes.

Acknowledgments

Thanks are given to the Organizing Committee of the Symposium *Luis Esteva* for inviting the author to write this paper. The author also thanks her students J. L. Rivera, M. A. Montiel and E. Bojórquez for their enthusiastic collaboration.

References

Alonso, J. (2004). *Alonso García & Asociados S. C.*, personal communi-cation.

Akiyama, H., Teshigawara, M., and Fukuyama, H (1997). Outline of a structural performance evaluation system in Japan, *Proceedings*, International workshop on harmonization in performance-based building structural design in countries surrounding Pacific Ocean, Building Research Institute, Tsukuba, Japan.

Ang, A. H-S., and De León, D (1996). Target reliability for structural design based on minimum expected life-cycle cost, *Proceedings*, 7th IFIP WG7.5 Working conference on reliability and optimization of structural systems, 71-84.

Bojórquez, E., Ruiz, S. E., and Esteva, L (2005). Funciones de transforma-ción de respuestas máximas entre marcos estructurales y sus correspondientes S1GDL con probabilidades de falla similares, *Proceedings*, XV Mexican National Conference, Mexico City.

Burns, S. A. Editor (2002). *Recent advances in optimal structural design*, ASCE, USA.

Chan, S., Ruiz, S. E., and Montiel, M. A (2005). Escalamiento de acelerogramas y número mínimo de registros requeridos para el análisis de estructuras, *Revista de Ingeniería Sísmica*, 72, 1-24.

Collins K. R., Wen Y. K., and Foutch D. A (1995). Investigation of alternative seismic design procedures for standard buildings, *Structural Research Series Report 600*, Department of Civil Engineering, University of Illinois at Urbana-Champaign.

Cornell, C. A. (1969). A probability-based structural code, *ACI Journal*, 66 (12), 974-985.

Cornell C. A. (1996). Calculating building seismic performance reliability: a basis for multilevel design norms, *Proceedings*, 11th World Conference on Earthquake Engineering, Paper 2122, 5707-5712.

Cornell, C. A., Jalayer, F., Hamburger, R. O., and Foutch, D. A (2002). The probabilistic basis for the 2000 SAC/FEMA steel moment frame guidelines, *Journal of Structural Engineering*, ASCE, 128 (4), 526-533.

Ellingwood, B. R. (1978). *Reliability basis of load and resistance factors for reinforced concrete design*, NBS Building Science Series 110, U.S. Department of Commerce, National Bureau of Standards, Washington

Ellingwood, B. R. (1999). Probability-based structural design: prospects for acceptable risk bases, Keynote lecture, *Proceedings*, ICASP8, Sydney, Australia.

Ellingwood B. R., Galamabos, T. V., MacGregor, J. G., and Cornell, C. A (1982). Probability-based load criteria: load factors and load combinations, *Journal of Structural Division*, ASCE, 108 (5), 978-997.

Esteva L. (1967). Criterios para la construcción de espectros para diseño por sismo, *Boletín del Instituto de Materiales y Modelos Estructurales*, 19, Universidad Central de Venezuela. Published also in *Proceedings*, XII South American Conference on Structural Engineering, Caracas. Venezuela.

Esteva, L. (1992). Non-linear response of weak-ground-story buildings to narrow-band accerelation time histories, *Report 544*, Institute of Engineering, UNAM (in Spanish).

Esteva, L., and Ordaz, M (1988). Riesgo sísmico y espectros de diseño en la República Mexicana, Mexican Symposium on Building Codes, Guadalajara.

Esteva L., and Rosenblueth E (1971). Use of reliability theory in building codes, *Proceedings*, ICASP1, Hong Kong.

Esteva, L., and Ruiz, S. E (1989). Seismic failure rates of multistory frames, *Journal of Structural Engineering*, ASCE, 115 (2), 268-284.

Esteva, L., Díaz O. and García, J (1999). Life-cycle optimization of structures with seismic energy dissipating devices, Case Studies in Optimal Design and Maintenance of Civil Infrastructure Systems. ASCE, Special Volume, D.M. Frangopol (editor), 57-72.

Fafjar, P., and Krawinkler, H., Editors (1997). *Seismic design methodologies for the next generation of codes*, A. A. Balkema, Rotterdam.

FEMA (2000). Recommended seismic evaluation and upgrade criteria for existing welded steel moment-frame buildings, *Report FEMA-351*, SAC Joint Venture, Federal Emergency Management Agency, Washington, D. C.

FEMA (2000). State of the art report on performance prediction and evaluation of steel moment-frame buildings, *Report FEMA-355F*, SAC Joint Venture, Federal Emergency Management Agency, Washington, D. C.

Frangopol, D. M. (1985). Structural optimization using reliability concepts, *Journal of Sructural Engineering*, ASCE, 111 (11), 2288-2301.

Galambos, T. V., and Ravindra, M. K (1973) Tentative load and resistance factor design criteria for steel buildings, *Research Report 18*, Structural Division, Washington University, St. Louis.

Galambos, T. V., Ellingwood, B. R., MacGregor, J. G., and Cornell, C. A (1982). Probability based load criteria: assessment of current design practice, *Journal of Structural Division*, ASCE, 108 (ST5), 959-977.

García Jarque, F. E. (2004). *García Jarque Ingenieros, S. C.*, personal communication.

Granados R. (2004). *PROYECT S. C.*, personal communication.

Hamburger, R. O., Foutch, D. A., and Cornell, C. A (2003). Translating research to practice: FEMA/SAC performance-based design procedures, *Earthquake Spectra*, 19 (2), 255-268.

Han, S. W., and Lee, L. H (1997). A conceptual performance-based seismic design method for building structures using reliability. *Proceedings*, International workshop on harmonization in performance-based building structural design in countries surrounding Pacific Ocean, Building Research Institute, Tsukuba, Japan.

Hasofer, A. M. (1974). Design for infrequent overloads, *Earthquake Engineering & Structural Dynamics*, 2 (4), 387-388.

Inoue, T., and Cornell, C. A (1991). Seismic hazard analysis of MDOF struc-tures, *Proceedings*, ICASP6, Mexico City, 437-444.

Koh, H M., Kim, J. K., and Ha, D. H (1999). Progress of studies performed in Korea on design rules and cost evaluation in relation to base isolation techniques, *Proceedings*, Post-SMiRT Conference Seminar: Seismic isolation, passive energy dissipation and active control of vibrations of structures, Korea, 1, 209-222.

Lind, N. C. (1969). Deterministic formats for the probabilistic design of structures, in *An Introduction to Structural Optimization*, Solid Mechanics Division, University of Waterloo, Canada.

MacGregor, J. G. (1983). Load and resistance factors for concrete design, *ACI Journal*, 80 (4) 279-287.

Mendoza, E., Díaz, O., and Esteva, L (1995). Consistent-reliability spectra for some nonlinear SDOF systems, *Proceedings*, ICASP, Lemaire, Favre & Mebarki (editors), 417-422.

Montiel M. A. (2005). Confiabilidad implícita en estructuras convencionales como base para establecer criterios para el diseño sísmico de estructuras reforzadas con disipadores de energía. *PhD. Thesis*, in progress, DEPFI, National University of Mexico.

Montiel, M. A., and Ruiz, S. E (2006). Seismic design method for reliability-based rehabilitation of buildings, to be published in *Earthquake Spectra*, February 2006 issue.

Montiel, M. A., Ruiz, S. E. and Rangel, G (2005). Influence of parameter uncertainty on seismic reliability of building structures, submitted for publication in *Earthquake Engineering & Structural Dynamics*.

Moses, F., and Kinser, D. E (1967). Optimum structural design with failure probability constraints, *AIAA Journal*, 5 (6), 1152-1158.

Nakashima, M., Sabuki, K., and Tsuji, B (1996). Energy input and dissipation behaviour of structures with hysteretic dampers, *Earthquake Engineering & Structural Dynamics*, 25, 483-496.

Ordaz, M. (2002) Estado actual y futuro de la normatividad, *Proceedings*, 7th Mexican Symposium on Earthquake Engineering, Cuernavaca.

Ravindra, M. K., Heany, A. C., and Lind, N. C (1969). Probabilistic evaluation of safety factors, *IABSE Symposium*, London, 35-46.

RCDF (2004). *Reglamento de Construcciones del Distrito Federal*, Mexico City Building Code.

Rackwitz, R. (2000). Optimization – the basis of code-making and reliability verification, *Structural Safety*, 22, 27-60.

Rivera, J. L. (2005). Espectros de confiabilidad uniforme para sistemas estructurales con disipadres de energía, *Ph.D. Thesis,* in progress, DEPFI, National University of Mexico.

Rivera, J. L., and Ruiz, S. E (2003). Seismic response spectra having uniform mean failure rates: systems with dissipating devices and without them, *Proceedings*, 13th Wold Conference on Earthquake Engineering, Vancouver.

Rosenblueth, E. (1972). Code specification of safety and serviceability, *Conference Preprints Reports*, International Conference on planning and design of tall buildings, Technical committee 10, Lehigh University, Bethlehem, Pennsylvania, 23-51.

Rosenblueth, E. (1976). Optimum design for infrequent disturbances, *Journal of Structural Division*, ASCE, 102 (ST9), 1807-1825.

Rosenblueth, E., and Esteva, L (1971). Reliability basis for some Mexican codes, *Proceedings*, Annual Convention of the ACI, Denver, Colorado.

Rosenblueth, E., and Mendoza, E (1971). Reliability optimization in isostatic structures, *Journal of Engineering Mech. Division*, ASCE, 97 (EM6), 1625-1642.

Ruiz, S. E. (1993). ACI 318-89 and Mexico City design safety factors, *ACI Structural Journal*, 90 (3), 262-268.

Ruiz, S. E., and Badillo, H (2001). Performance-based design approach for seismic rehabilitation of buildings with displacement-dependent dissipators, *Earthquake Spectra*, 17 (3), 531-548.

Ruiz, S. E., and Soriano, A (1997). Design live loads for office buildings in Mexico and the United States, *Journal of Structural Engineering*, 123 (6), 816-822.

Shome, N., and Cornell, C. A (1999). Probabilistic seismic demand analysis of nonlinear structures, *Report No.RMS-35*, Department of Civil Engineering, Stanford University.

Torres, M. A., and Ruiz, S. E (2003). Design algorithm based on probabilistic seismic demands for buildings rehabilitated with hysteretic energy dissipating devices, *Earthquake Spectra*, 20 (2), 503-521.

Vamvatsikos D., and Cornell C. A (2002). Incremental dynamic analysis, *Earthquake Engineering & Structural Dynamics*, 31, 491-514.

Wen, T. K. (1995). Building reliability and code calibration, *Earthquake Spectra*, 11 (2), 269-296.

Wen, Y. K. (2001). Reliability and performance-based design, *Structural Safety*, 23, 407-428.

Wen, Y. K., and Shinozuka, M (1998). Cost-effectiveness in active structural control, *Engineering Structures*, 20 (3), 216-221.

Wen, Y. K., Ellingwood, B. R. and Bracci, J (2004). Vulnerability function framework for consequence-based engineering, MAE Center *DS-4 Report.*

Francisco J. Sánchez-Sesma
Professor
Instituto de Ingeniería, UNAM
Circuito Escolar s/n
Cd. Universitaria,
Coyocán 04510, México D.F.
MÉXICO
sesma@servidor.unam.mx
Engineering Seismology, Mathematical Modeling of Wave Propagation. Site Effects

My first day as student of UNAM's Engineering Graduate School was March 15th, 1973. I initiated then a Structural Engineering master program. The very same day I entered to the Engineering Institute. My advisor at the time was José Luis Trigos who, after teaching me Strength of Materials, offered me a part-time scholarship-job to follow my courses and help in research activities. For other reasons (mainly economic ones) I was teaching Math and Mechanics for sophomores and had some duties as teaching assistant. Well, I almost forget to mention I was busy writing my the Civil Engineer's Thesis and my English courses. Needless to say, I was overloaded and in practice continued that hectic life for long time (some say this continues so far). Prof. Trigos asked me to plot epicenters in maps and help him in calculations of seismic risk using Luis Esteva's formulae from *Practical considerations for the evaluation of seismic risk*, (I wondered at the time where the "Practical" came from) then I helped Dr. Esteva by computing design coefficients for masonry walls, and work for Roberto Villaverde on the response of appendices in structures. These ideas and many others have been proposed by Dr. Esteva.

The real fact was that my activities were against the rules of the Institute. Beyond our own courses we could have only few hours teaching at the Engineering School. Rafael Aranda and me were in the same condition for almost two years: We were working like dogs and with the fear of being discovered as "illegals" and fired. The day arrived, Dr. Esteva was vice director at the time and called us. Despite our usual discretion, somehow he had some information of our extra load activities, and wanted to talk to us. We went to his office prepared to be fired, as captives going to the Guillotine. He asked why we had so many activities and warned us this is against the rules. We explained him we engaged in many things because personal needs and argued that our work was fine. He says in his soft way "… this cannot continue. This illegality has to stop…" I though "he is going to fire us". Instead, he explained, "You can teach only a course at the Engineering School" and shoot: "Do you want to work for the Institute?" so I said immediately "of course", and we accepted. That was wonderful. We got a job as Research Assistants at the Institute of Engineering. And this was thirty years ago!

Luis Esteva is not only well mannered but patient and with a developed sense of humor. I remember Luis coming to my office asking for a reference and seeing I had a portrait of Gauss, the Prince of mathematics, with a candle I got in a church. He asked why I had a lighted candle and leave surprised and with a big smile, beacuse I answered, "in this office we venerate Gauss" (of course, I was joking).

I worked for Luis Esteva several months in a subject that eventually became center of my research. Later I was assigned to Emilio Rosenblueth who became soon my PhD thesis advisor. Since then Luis Esteva and me have been working in different subjects of earthquake engineering. Along these thirty years Dr. Luis Esteva has been my teacher, a friend to consult, a real reference, always ready to give an advice. Thank you Luis, thank you for your generosity and unselfish advice.

Paco Sánchez-Sesma
September 2, 2005

G. Rodolfo Saragoni
Head Structure – Construction – Geotechnical Division
Department of Civil Engineering – University of Chile
Casilla 228/3 – Santiago - Chile
rsaragon@ing.uchile.cl

Earthquake demand, strong motion accelerogram, earthquake
hazard, soil response, structural dynamics, accelerogram network.

Heidelberg Conversation

The first time I knew about Luis existence was reading in 1967, as engineering student, his paper with Emilio "Earthquake Effects to Moderate and Large Distances", written in 1964. It was an outstanding paper with an integral view of the earthquake engineering.

I met him latter in 1979 in Cordoba, Argentina starting a long friendship that includes our families.

From all our conversations during these years I remember one as the most. We were at Heidelberg in Germany walking around the oldest German University and the riverside of Neka River. Those days were difficult for UNAM closed by a long student strike. We talked for hours about the University roll, the social academic responsibility in developing countries and research. I remember his clever and visionary answers up today.

University of Heidelberg

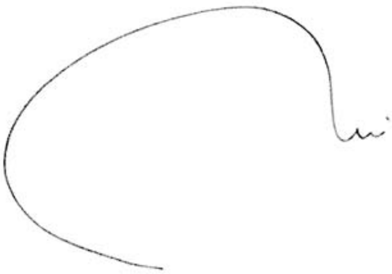

G. Rodolfo Saragoni,
2005 August 10

LARGE EARTHQUAKE SOIL RESPONSE

ABSTRACT

The inconsistency between soil amplification theories and accelerographic measurements for large earthquakes is reviewed. These disagreements become important since they are frequently on the unsafe side of the earthquake design. The analysis of accelerograms by using autocorrelogram, Fourier spectra and particle trajectory are presented. These techniques allow to measure soil higher modes as well as modal damping. Measurement soil fundamental periods are in agreement with 1D elastic soil model. One of the major reasons of the discrepancy of the amplification is due that soil accelerograms are random sequences of episodes of seismic wave arrivals of Rayleigh type alternate with episodes of soil free vibrations. The coupling of vertical and horizontal ground motions for large earthquakes requires that amplification theories include in the future the vertical motion. The presence of one predominant soil period in spectra strongly depends of the frequency content of source seismic waves.

Introduction

The design of structures against earthquakes has become more sophisticated by the use of strong motion accelerograms in recent years. Present aseismic design practice, which incorporate information contained in these strong motions accelerograms, very seldom reconcile the differences in the circumstances under which the accelerograms were recorded with the conditions in which a structure being designed will be located.

One factor involved, which is recognized as being very influential, is the effect of the local soil conditions.

The modification of earthquake motions by the local soil has been observed for a long time by those studying earthquake damage. (Duke 1958). The earliest investigators to quantify the problem were the Japanese, the most prominent Sesawa (Sesawa 1930; Sesawa and Kanai 1935) and Kanai (Kanai and Yoshizawa 1956; Kanai 1957). These researchers obtained algebraic expressions in the frequency domain for the ratio of surface motion to the incident wave for the assumption of vertically propagating, plane SH waves. Their work is limited to one and two horizontal layers of constant velocity for which they included visco-elastic behavior.

In 1932 the world’s first practical accelerograph for seismic applications was introduced in USA (Freeman 1932). In recent years high density arrays have make possible to measure large earthquakes in their epicentral area where structures suffered damage, this new situation also allowed to know the soil response for large earthquakes in that conditions. In this case the earthquake is the full scale experiment for the dynamical soil response and the accelerograms are the experimental measurements.

In the early days of earthquake engineering, in the 1930’s, the theoretical results of Sesawa and Kanai could not verify due to the lack of accelerograms.

The first important accelerograms for earthquake engineering were El Centro 1934 and 1940 records. In USA and the rest of the world these records had a strong influence in the earthquake engineering development. However it must be recognized that for decades there were not available records with high peak ground accelerations. This situation only changed with the 1971 San Fernando earthquake, unfortunately recorded ground motions were not in near source zone condition: i.e. less than 14 Km from the fault.

This scarcity of accelerograms in the early years of the earthquakes engineering of the 1950's allowed that many pioneering computer models proposed to represent the dynamical soil response seems to be robust in test with the very few weak available records by that time. However the most recently accelerogram networks with more records at surface and surface and down holes have shown that most of the proposed theories for soil amplification are unsatisfactory (Faccioli and Reséndiz 1976, Boore 2004).

The unexpected collapse of structures due to soil amplification effects designed following modern seismic codes has motivated the reviewing of soil amplification theories by deploying high density accelerograph arrays to have a better understanding of the phenomenon.

It is matter of fact, during the recent earthquakes of Northridge 1994, Kobe 1995 and Turkey 1999 larger soil amplification than estimated by actual theories were reported on the unsafe side of earthquake engineering design. This situation is maybe due to that most accepted assumption and simplification are incorrect. For instance the common practice to analyze the soil response considering only horizontal components, by assuming mainly incident SH waves, despite the effect that accelerographs in epicentral zone measure vertical components larger than horizontal ones.

In Mexico City, an ideal case, where most common assumptions for soil amplification theory are fulfilled, i.e. strong contrast between soil impedances, almost linear soil behavior and vertical incident shear waves due to the condition of far epicenter of Pacific subduction earthquakes (epicenter distances larger than 400 Km), most accepted amplification theories are partially verified. These theories can only reproduce the natural soil response period but failed to estimate the observed large soil amplification ratios and large durations (Faccioli and Reséndiz 1976, and Gómez 2002).

Saragoni (Saragoni 1968) considered average response spectra of accelerograms to classify soils for the earthquake resistant design Chilean Code for buildings. Japanese researchers (Hayashi et al. 1971) also classified soil using average response spectra. However the most influential is the site dependent spectra for earthquake design proposed by Seed in 1976 (Seed et al. 1976). Nevertheless all these researchers used for their studies accelerogram the database available by that time, characterized by very low peak ground accelerations. Therefore these spectra classification may not represent adequately the soil response during large earthquakes.

Other authors (Seed et al. 1988, and Romo 1995) have compared the observed soil amplification with the ratio between response spectra. These ratios have the advantage to give less soil amplification ratios, however these results are highly sensitive to the viscous damping considered for the family of structures of one degree of freedom. When viscous damping zero is considered large and similar amplification ratios are obtained as from the Fourier spectra ratio considered in the 1D Sesawa model (Gómez and Saragoni 1995).

Most of applications done using SHAKE program also use response spectra to reduce the soil amplification ratios (Seed et al. 1988), which is not necessary guarantee that these reduced ratios will be observed during large earthquakes.

Therefore the important differences between theoretical values and experimental results for large earthquakes look to be consequence of misinterpretation of soil amplification theories. In this paper the soil response will be studied from the interpretation of the accelerographic measurements for large earthquakes in epicentral zone or for large epicentral distances, such as the Mexico City case.

Study of Randomness and Deterministic Components in Accelerograms by UsingAutocorrelation Functions

The first researcher into consider earthquake accelerograms as sample of random processes was Housner (Housner 1947). He assumed that accelerograms can be represented as a series of pulses randomly distributed in time as a white noise process. The Housner's idea does not considered at all any filtering effect due to the soil. His white noise idea had a strong influence in USA and soil response was considered irrelevant for many years in USA earthquake engineering.

On the other hand in Japan Tajimi (Tajimi 1960) based on a Kanai work (Kanai 1957) studies the frequency content of accelerograms. He observed that pulse duration is similar to the natural period of buildings, since Japanese accelerograms has a predominant period less than 0.8 sec.

Based on these observations Tajimi proposed the filtering of an incident random white noise through a one degree of freedom oscillator that represents the soil response. This assumption leads to power spectral density functions with a predominant period. This model proposed by Tajimi has been improved latter by other authors but keeping the two major ideas, i.e. acceleration random process and predominant soil period.

Arias and Petit-Laurent (1963) analyzed the autocorrelograms of accelerograms of USA, Mexico City and Santiago, Chile considered as random process. They found that Mexico City 1962 earthquake accelerograms had deterministic components despite the USA and Chile accelerograms that show a high randomness in a wide band of frequencies. For Arias and Petit-Laurent (1965) the frequency band was a consequence of the soil properties at the site.

The analysis of autocorrelation functions for different accelerograms shows that some of them have an important presence of sine wave components (deterministic). Arias and Petit-Laurent (1963) found that Mexico City autocorrelograms for 1962 Mexico earthquake have a high content of deterministic components. Similar situation is observed for some autocorrelograms of Parkfield 1966 earthquake (Liu 1969), Rumania 1977 and 1986 earthquakes (Lungu at al. 1992) and some Chile earthquake (Ruiz and Saragoni 2004) (See Fig.1).

The shape of these autocorrelograms, i.e. the characteristic period and the attenua-tionconstant, allows to assimilate them to the corresponding deterministic function of the displacement of the free vibration of one degree of freedom oscillator with an initial displacement and zero velocity, i.e.:

$$y(t) = Ae^{-\beta(2\cdot\pi\cdot\frac{t}{T_s})}\cos\left(2\cdot\pi\cdot\frac{t}{T_s}\right) \tag{1}$$

where T_s is the natural period and β the damping ratio.

Making this assumption and choosing adequate values for the natural period and damping ratio of the oscillator both curves coincide (Ruiz and Saragoni 2004).

In Fig.2 the autocorrelogram of San Isidro Longitudinal accelerogram of Chile 1985, M_s = 7.8 earthquake is shown. The autocorrelogram has been normalized by the expected quadratic value. For this autocorrelogram the following T_s and β values were estimated: T_s = 0.34 sec and β = 0.104. Then Eq. (1) is reduced to:

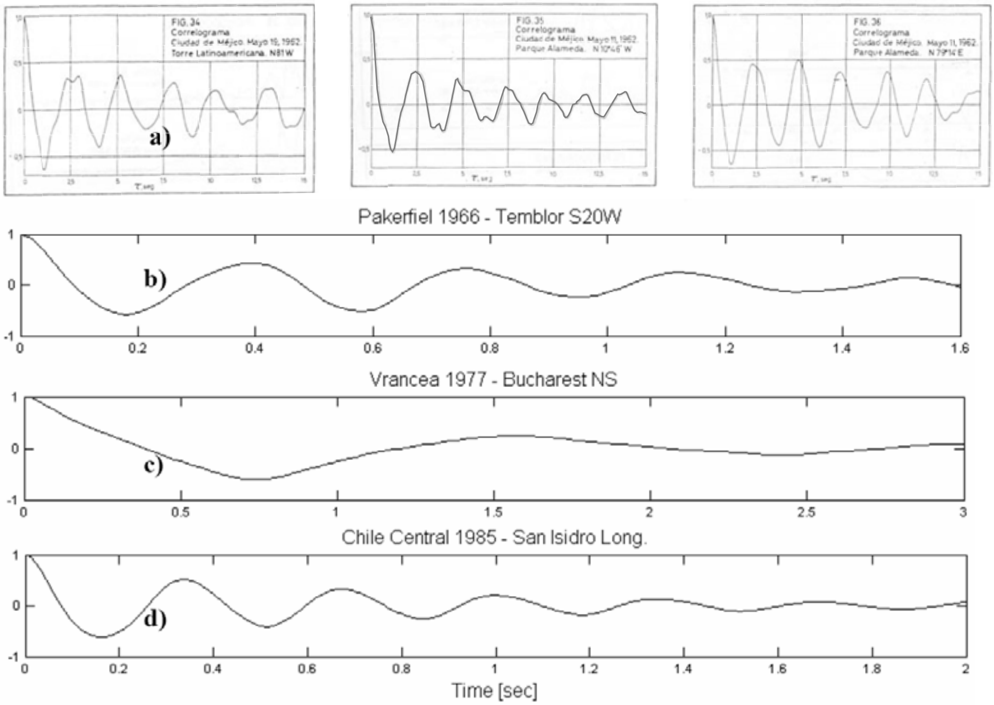

Figure 1a. Autocorrelograms for the accelerograms of Parque Alameda N10W, Mexico 1962 (Arias and Petit-Laurent, 1963). *1b. Temblor S20W, Pakerfield, USA 1966* (Liu, 1969). *1c. Bucharest NS, Rumania 1977*(Lungu et al. 1992). *1d. San Isidro Longitudinal, Central Chile 1985* (Ruiz and Saragoni, 2004). *Autocorrelogram are normalized to the maximum value*

$$y(t) = Ae^{--0.104(2\cdot\pi\cdot\frac{t}{0.34})}\cos\left(2\cdot\pi\cdot\frac{t}{0.34}\right) \tag{2}$$

Fig.2 shows an excellent matching between the function of Eq. (2) and the autocorrelogram of San Isidro Longitudinal. This result suggests that soil at San Isidro Station mainly free vibrated during the 1985 Chile earthquake as a simple damped one of degree of freedom oscillator, despite the large magnitude of the earthquake (M_s = 7.8).

The reason why free vibration happens during large earthquakes, which looks a paradox, is due to the fact that energy released from the source is not permanent continuous on time, there are relax intervals in between without important seismic wave arrivals from the source. Therefore accelerograms can be considered as a random sequence of seismic episodes of seismic wave arrivals and episodes of free soil vibrations.

The estimation of autocorrelation function is usually done by using only one sample accelerogram based on the ergodicity theorem, however the use of this theorem consider random samples, when the samples, as in this analyzed case, have strong deterministic components the estimator is only recognizing the presence of many free

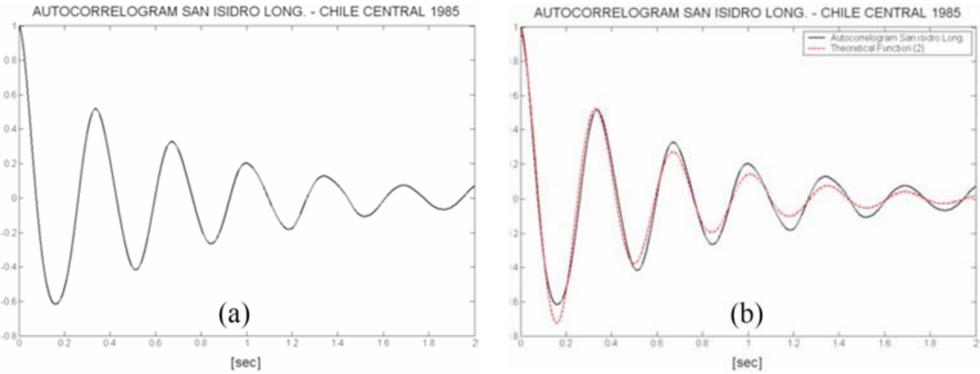

Figure 2a. Autocorrelogram for San Isidro Longitudinal, Chile Central 1985
2b. Comparison between San Isidro Longitudinal, Chile Central 1985, autocorrelogram and the theoretical function $y(t) = Ae^{-0.104(2\cdot\pi\cdot\frac{t}{0.34})}\cos\left(2\cdot\pi\cdot\frac{t}{0.34}\right)$

vibrations due to random initial conditions provoked by intermittent episodes of seismic wave arrivals of short duration.

The free vibration of structure after a forced motion has been used in many fields and in particular to measure the damping of the soil as the random decrement method. The measurement of soil damping in probabilistic way from accelerograms has been also proposed by other authors (Huerta et al. 1998).

These deterministic soil free vibrations are observed in different accelerograms as the ones shown in Fig.3: Tarzana 90, Whittier Narrow 1987 earthquake; Central de Abastos (CDAO NOOE), Mexico 1985 earthquake and San Isidro Longitudinal, Chile 1985 earthquake. All these accelerograms show time windows with a noticeable damping of the acceleration amplitudes, situation which is reflected in their corresponding autocorrelograms. Therefore autocorrelograms in these cases allow to estimate the soil natural period and damping.

In Fig.3., besides the accelerograms, is shown to the right a zoom of a specific region of the accelerogram where the natural period and the damping of the soil can be clearly observed. To the left of the figure the corresponding autocorrelograms are shown with the corresponding period and damping.

This result suggests that accelerograms with harmonic autocorrelograms correspond mainly to episodes of soil free vibrations and deterministic component found in autocorrelograms by other authors in the past are free soil vibrations.

In Fig.4 the corresponding autocorrelograms for the three components of Cauquenes station for 1985 Chile earthquake are shown. In this figure it can be also appreciated that besides the deterministic autocorrelograms for the horizontal components, the vertical autocorrelograms has also the same pattern.

This situation which is not always frequent it can be also appreciated for Tarzana vertical, Northridge 1994 earthquake in the near source region of a large earthquake (PGA ≈ 1[g]). Fig. 5 suggests that in some cases also the vertical mode of vibration of the soil can be estimated from autocorrelograms.

From Fig.4 it can be appreciated that characteristic period of both horizontal autocorrelograms are similar, however vertical autocorrelograms has a period half of the horizontal ones.

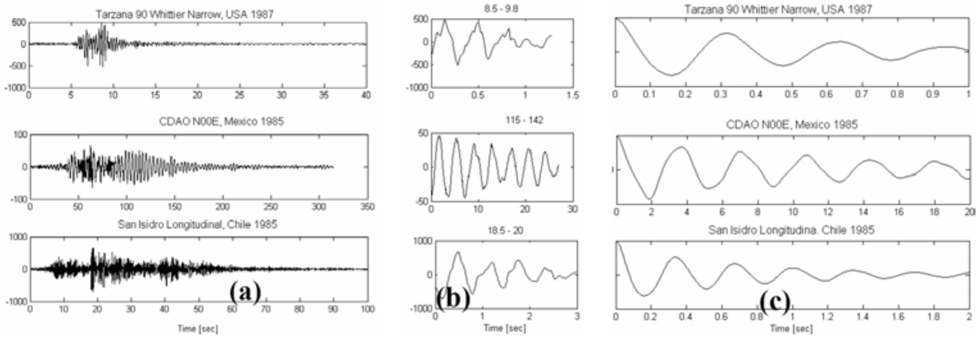

Figure 3a. Different studied accelerogram in [cm/sec²]. 3b. Example of time windows where acceleration amplitudes decay. 3c. Autocorrelogram of the corresponding accelerogram showing that the damping is equal to the observed in the corresponding record

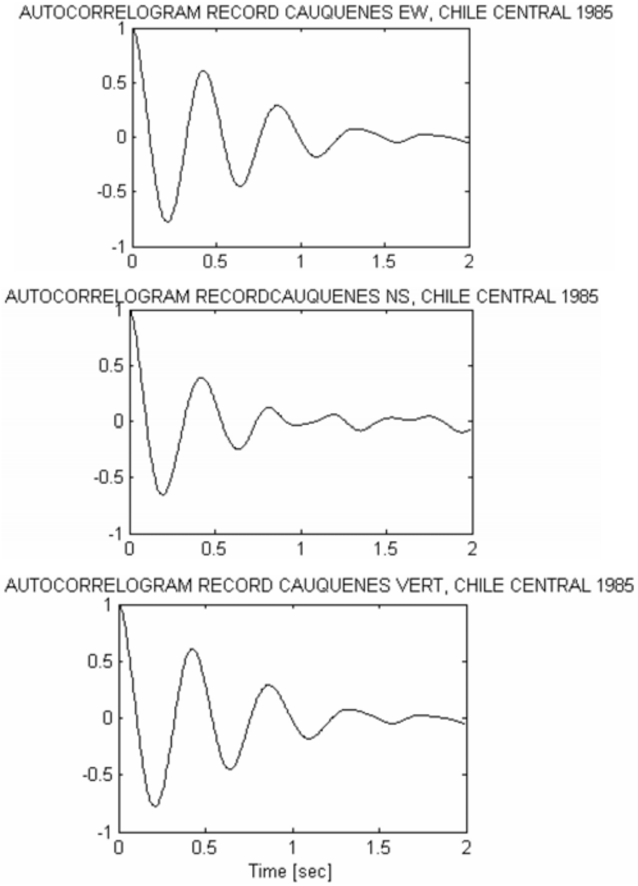

Figure 4. Autocorrelograms for accelerograms of Cauquenes station, Chile Central 1985 earthquake

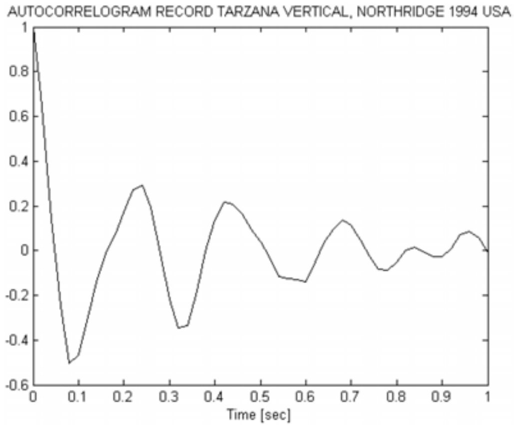

Figure 5. Autocorrelogram for Tarzana Vertical, Northridge 1994 earthquake

$$T = \frac{4H}{V_s} \tag{3}$$

The seismic waves arriving from the source are strongly coupled in the three accelerogram components by high frequency Rayleigh waves (Saragoni and Ruiz 2005) allowingalso episodes of vertical soil free vibrations.

Fundamental Period and Soil Degradation

On September 19, 1985 a large subduction MS = 8.1 earthquake, with epicenter at Pacific Ocean in front Michoacan state, struck Mexico. In the Mexico City, 400 km away, large damages and collapses of modern high rise buildings was observed despite the reduced damages reported at the epicentral zone: Ixtapa, Zihuatanejo and Lazaro Cárdenas (Astroza et al. 1986).

The accelerograms recorded at Mexico City showed again harmonic components with periods between 1 to 4 sec, with important peak ground accelerations and durations.

The Mexico City soils are characterized by outstanding low shear wave velocities for the surface layers (< 100 m/sec) in the lake zone. The bottom of the deep valley of Mexico City is hard soil with a shear wave velocity of 500 m/sec, these values give high impedances for Mexico City, which in addition to the large earthquake epicentral distance let to assume incident seismic shear waves. Both are ideal conditions to obtain the results of the amplification theory (Gómez 2002).

During 1985 Mexico earthquake important accelerograms were recorded at the Mexico City lake zone. In particular the accelerograms recorded at Central de Abastos Oficinas (CDAO) accelerographic station in Mexico City for 4 earthquakes are studied in this paper. The stratigraphic soil of CDAO station is given in Table 1. In addition in Fig.6 the horizontal accelerograms of CDAO station are shown with their corresponding Fourier spectra and normalized autocorrelograms.

The soil fundamental period estimated from the 4 different earthquakes is 3.53 sec (Singh at al. 1988). This value is in agreement with the peaks of the Fourier spectra as well as with the period of the first cycle of the autocorrelograms as it is indicated in Table 2.

TABLE 1. Soil profile of Central de Abasto Oficinas, Mexico City (CDAO). (Seed et al. 1988)

Depth [m]	**Soil Type**	**Shear wave velocity [m/sec]**
0-5	Silty sand	60
5-42	Clay	60
42-52	Sandy silt and silty Clay	110
52-56	Stiff clay	110
	Hard Layer	900

TABLE 2. Soil Period at CDAO, Mexico City station from different Mexican earthquakes estimated from Fourier Spectra and Autecorrelogram techniques

Earthquake	**Magnitude Ms**	**Autocorrelogram Period [sec]** Component		**Fourier Spectra Period [sec]** Component	
		N00E	N90E	N00E	N90E
19 – 09 – 1985	8.1	3.69	3.93	3.62	3.78
21 – 09 - 1985	7.6	3.71	3.62	3.71	3.43
25 – 04 – 1989	6.9	3.29	3.47	3.35	3.46
14 – 09 – 1995	7.4 (Mw)	3.17	2.99	3.13	2.85

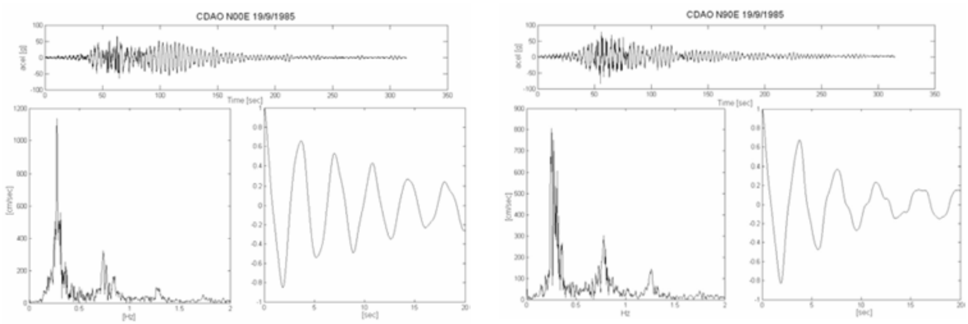

Figure 6. Horizontal components CDAO station, Mexico earthquake 1985 with their corresponding Fourier spectra and autocorrelograms

From Table 2 it can be appreciated that soil natural period obtained from the peak of Fourier spectra coincide with the one from autocorrelograms. In addition these values are in agreement with the results of the following equation of the soil 1D model: where H is the depth of the soil layer and VS is the soil shear wave velocity.

It can be concluded for these cases that Fourier spectra and autocorrelograms represent mainly free vibrations of soils in shear with few episodes of forced seismic wave response.

The soil natural period estimated for CDAO soil for September 19, 1985 earthquake compared with the one corresponding for the aftershock of September 21, 1985 shows a light degradation. The difference between the main event with small events such Guerrero 1989 and Ometepec 1995 earthquakes, may be consequence of soil nonlinearity due to high peak ground accelerations or to that small magnitude earthquake only excite the upper part of the soil stratum. (Saragoni and Ruiz, 2005).

Considering soil natural periods estimated from accelerograms, it is possible, by using Eq. (3), to estimate the soil depth in free vibration. For CDAO station for 1985 Mexico earthquake it is necessary to consider the full depth up to the interface with the hard soil (VS = 900 m/sec), i.e. 60 m depth. Despite this result the soil depth estimated for the Ometepc 1995 earthquake is lower without considers nonlinear soil effects.

However it looks reasonable to assume that for a large magnitude earthquake, even with far epicentral distance, the full soil stratum vibrates up to the bottom of the lake. Similar cases can be observed for Chilean accelerograms (Saragoni and Ruiz 2004).

On March 13, 1985 an earthquake MS = 7.8 struck central part of Chile, this event was recorded by many stations. In particular accelerograms recorded at Iloca station, at a epicentral distance of 200 [km] and with a PGA of 0,2 [g], are studied in detail, in similar way that for CDAO Mexican station.

The period observed in the autocorrelograms and Fourier spectra of Fig. 7 can be easily identified in the accelerograms. Table 3 summarizes the soil natural periods estimated for Iloca station from Fourier spectra and autocorrelograms for 4 aftershocks of the 1985 Chile earthquake.

Table 4 gives the soil profile of Iloca station. Considering the data of this table and the soil natural periods obtained by autocorrelogram and Fourier spectra techniques, it is possible to estimate by using Eq. (3), the soil vibrating depth in 65 m.

The soil periods estimated for Iloca do not show soil degradation for earthquake of different magnitudes. Similar result was obtained for most of the Chilean accelerographic stations with the exception of the ones located on gravel and sand that exhibit light degradation, despite the large magnitude of the earthquake (Saragoni and Ruiz 2004).

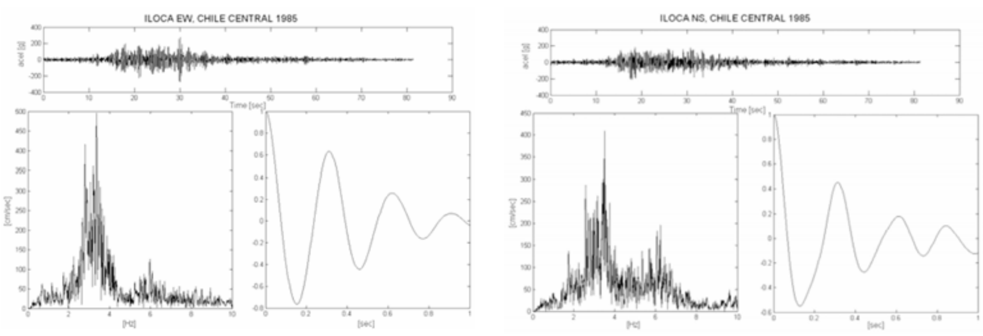

Figure 7. Horizontal components Iloca station, Chile Central 1985 earthquake, showing their corresponding Fourier spectra and autocorrelograms

TABLE 3. Estimation of Soil Natural Period at Iloca, Chile Station considering different earthquakes and using autocorrelogram and Fourier Spectra Technique. (Saragoni and Ruiz, 2004).

Earthquake	**Magnitude Ms**	**Autocorrelogram Period [sec] Component**		**Fourier Spectra Period [sec] Component**	
		EW	NS	EW	NS
03 – 03 – 1985	7.8	0.31	0.32	0.29	0.30
03 – 03 – 1985R	6.4	0.29	0.30	0.30	0.31
25 – 03 – 1985		0.29	0.30	0.29	0.31
03 – 04 – 1985		0.30	---	0.31	0.28
09 – 04 – 1985	7.2	0.30	0.32	0.30	0.33

R = aftershock

TABLE 4. Soil profile Iloca Station. (Araneda and Saragoni, 1994)

Depth [m]	**Shear Wave Velocity [m/sec]**
0 – 4	150
4-12	638
12-95	1210
Basement	2050

When the seismic waves excite the full soil stratum for earthquake of different magnitudes it seems to be that soil degradation is light. However this situation could change when seismic waves only excite the upper part of the soil stratum leading to estimation of lower soil natural periods.

The observed differences between the soil natural periods for both accelerographic components may be due to seismic wave arrivals with strong directivity effect, that soil response attenuates by coupling the motion in both directions. This analysis will be done in next a section.

In soil dynamics is common practice to associate soil degradation with large peak ground accelerations. However this conclusion is not in general truth, for instance the Tarzana 90° record for Northridge 1994 earthquake has a PGA = 1.8 [g] and no important soil degradation was observed. In Fig. 8 the Tarzana 90° record is shown superposed with a sine wave of 0.27 sec period. The sine wave is shown only in 3 parts of the accelerogram showing that the record remains the same characteristic period. Furthermore this soil period will remain invariant for this station for other earthquakes of less magnitude and large epicentral distance such, as the Whittier Narrow 1987 earthquake. This case will be studied in a next section.

In Fig 8 it is also possible to observe in Tarzana 90 accelerogram some time episodes where the soil could present larger periods of vibration. However these larger periods are not due to soil degradation effect, they are consequence of the Rayleigh waves arriving from the source (Saragoni and Ruiz 2005). These Rayleigh waves are shown in Fig 9 for Tarzana 90°, Northridge 1994, obtained from displacement records

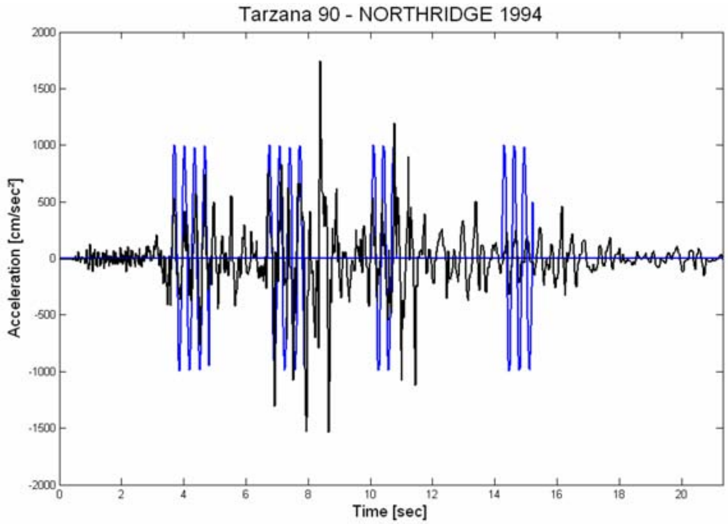

Figure 8. Tarzana 90, component, Northridge 1994 earthquake. Peak ground acceleration 1.8 [g] without observed soil degradation since natural soil period remains constant

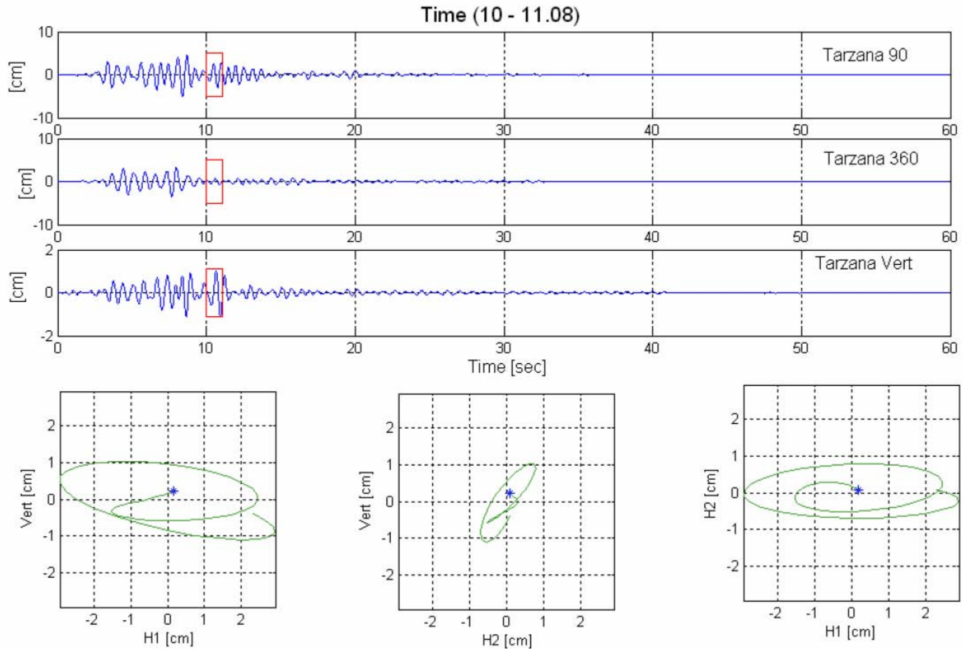

Figure 9. Displacement records of Tarzana, Northridge earthquake 1994, filtered between 1 to 2.5 [Hz] and roted in 45º. Particle motion in three planes: one vertical (Vert) and two horizontals (H1, H2). Showing a Rayleigh wave in the window time between 10 – 11.08 sec

calculated by double integration of the accelerograms and filtering between 1 and 2.5 [HZ]. This Rayleigh wave is observed in the time window between 10 to 11.08 sec. This Rayleigh wave type is more flat that expected from Rayleigh theory due to soil effects. This effect was already noticed by Hanks, who studying these waves for the records of San Fernando 1971 earthquake associated these shapes to soil effect (Hanks 1971). Result that will be confirmed when down hole records of Mexico City will be studied in this paper.

In conclusion, the soil natural period can be observed in accelerograms of large magnitude earthquakes in free soil vibration episodes when seismic wave arrival is negligible. During these episodes the soil response is controlled by 1D shear theory given by Eq. (3). The depth H to be considered in this equation is the full soil stratum height; however this result can change due to the arrival of Rayleigh wave from the seismic source. In general no important soil degradation is observed from changes of soil natural periods for different earthquakes and for the same record for large earthquakes. In a next section the analysis of the upper modes of the soil response will be considered.

Soil Higher Modes

The presence of different modes of vibration of soils in accelerograms can be detected by using Fourier spectra. In Fig 10 the first, second and third horizontal modes of the soil are shown in the Fourier spectra of CDAO NOOE and CDAO N90E accelerograms of Central de Abastos station (CDAO), Mexico City for different Mexican earthquakes and for both components of Ventanas and Almendral, Valparaíso stations for the Chile 1985 earthquake and the corresponding main aftershock.

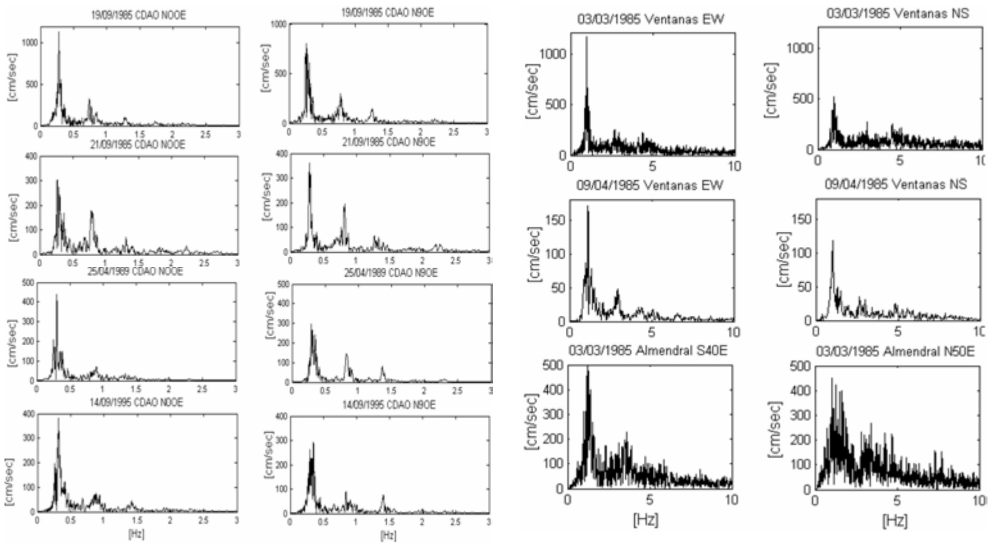

Figure 10. Fourier Spectra from different accelerograms showing the different mode response periods of each soil station. The values are the same for each station for different earthquakes

The frequency values of the different Fourier spectra peaks for the CDAO, Ventanas and Almendral, Valparaíso station are given in Table 5. These values satisfy the approximated relation 1:3:5 indicated in Table 6. Therefore the frequency of the Fourier spectra peaks satisfy the relation, expressed in this case as period:

$$T = \frac{4H}{V_s(n-1)} \tag{4}$$

where n is an integer number that represents the vibration mode and Tn is the natural period of the mode n.

From the analysis of these accelerograms of large earthquakes it can be concluded that upper modes of vibration of soils are observed and they satisfy the shear soil vibration condition given by Eq. (4).

These last results can only be observed when the soil is allowed by the earthquake source to free vibrate in time windows with enough duration to show many cycles of free vibration. These time windows are possible between intermittent wave arrivals. This condition will be studied in a next section.

Soil Natural Periods and Seismic Waves Characteristic Periods

The main participation of the soil second mode happens for the CDAO NOOE 1985 record when an important amount of high frequency seismic waves arrives to the site, this zone corresponds to the strong motion zone of the accelerogram. This condition becomes clearer when the Zacatula SOOE, epicentral record is compared with the CDAO NOOE record in Fig.11. Furthermore in the Fig 12 the spectrogram for CDAO NOOE accelerogram is presented showing that the high frequency content zone occurs between 50 to 100 sec, time when most of the energy is released at the epicenter. In this zone, between 50 to 100 sec, is when the higher soil modes have the strongest participation.

TABLE 5. Natural frequencies of the different modes of vibration of soil estimated from Fourier Spectra peaks

	Soil Mode Natural Frequencies [Hz]					
Earthquake	**1st Mode Component**		**2nd Mode Component**		**3nd Mode Component**	
México CDAO	N00E	N90E	N00E	N90E	N00E	N90E
19 – 09 – 1985	0.28	0.25	0.74	0.78	1.27	1.26
21 – 09 – 1985	0.27	0.29	0.77	0.82	1.31	1.27
25 – 04 – 1989	0.30	0.29	0.90	0.82	1.34	1.36
14 – 09 – 1995	0.32	0.35	0.88	0.84	1.42	1.41
Chile Ventanas	EW	NS	EW	NS	EW	NS
03 – 03 – 1985	1.00	0.99	2.72	3.02	4.38	4.53
09 – 04 – 1985	1.11	1.02	2.93	2.66	4.22	4.84
Chile Almendral	S40E	N50E	S40E	N50E	S40E	N50E
1.21	1.07	3.59	3.44	4.74	4.26	

TABLE 6. Ratio between the Soil Mode Natural Frequency and the First Natural Mode FrequencyEstimated from Fourier Spectra Peak Values

Earthquake	**Ratio Between different Soil Natural Modes [Hz]**					
	1st Mode/1st Mode Component		**2nd Mode/1st Mode Component**		**3nd Mode/1st Mode Component**	
México CDAO	N00E	N90E	N00E	N90E	N00E	N90E
19 – 09 – 1985	1	1	2.6	3.1	4.5	5.0
21 – 09 – 1985	1	1	2.9	2.8	4.9	4.4
25 – 04 – 1989	1	1	3.0	2.8	4.5	4.7
14 – 09 – 1995	1	1	2.8	2.4	4.4	4
Chile Ventanas	EW	NS	EW	NS	EW	NS
03 – 03 – 1985	1	1	2.7	3.1	4.4	4.6
09 – 04 – 1985	1	1	2.6	2.6	3.8 4.7	
Chile Almendral	S40E	N50E	S40E	N50E	S40E	N50E
	1	1	3.0	3.2	3.9	4.0

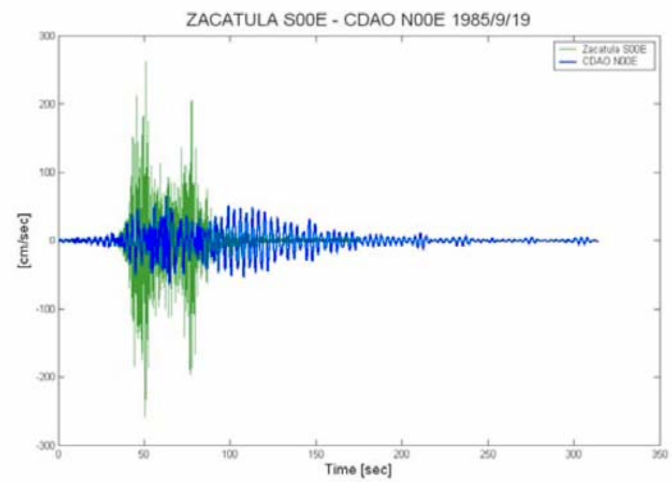

Figure 11. Zacatula S00E, Mexico 1985 accelerogram recorded at epicentral zone compared with CDAO N00E recorded at Mexico City at 400 [km] from the epicenter. The Zacatula accelerogram has been shifted in 30 [sec] from the time origin

In order that soil can vibrate free in its fundamental period it is necessary a time window without important arrival of seismic waves. This situation can be only observed in Mexico City for the 1985 earthquake after the end of the strong motion part (See Fig 12), unless the predominant period of seismic waves coincides with the fundamental period of the soil such is the case of SCT station (Gómez, 2002).

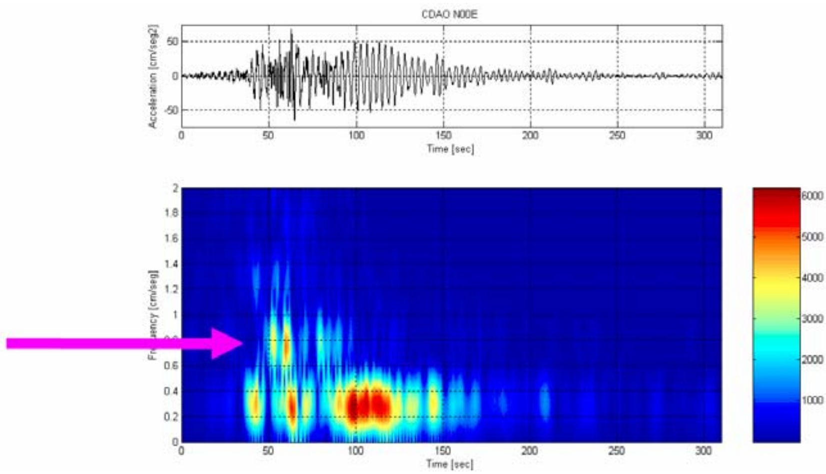

Figure 12. CDAO N00E, 1985 Mexico, frequency spectrogram. The pink arrow indicates the natural frequency of the soil second mode

Due to this reason the fundamental soil period, mainly in epicentral records, can be strongly contaminated by seismic waves arriving from the source, leading to strongly random autocorrelogram, revealing the control of the seismic source on the free soil response.

The strong influence of the seismic source on the characteristic of the Fourier spectra becomes clear in Fig. 13, for Papudo station, Chile for records of different earthquakes. In this Figure it is observed an important peak around 3 [Hz] for all records. However for the inslab subduction Chile earthquake of November 7, 1981 a new situation appears showing two dominant peaks. The first one coincides with the one of the 3 [Hz] presents in all previous earthquakes, but the second one around the 7 [Hz] is only present in the two accelerograms recorded for the inslab earthquake showing unquestionably the effect of the source in the richness of the Fourier spectra frequency content.

Since the inslab earthquake of 1981 was recorded on the hypocenter, an important arrival of seismic waves from the source must be expected, which are Rayleigh wave type. These waves couple the horizontal and vertical components, coupling that stimulates the vertical soil amplification, which it is assumed to happen for the characteristic frequency of 7[Hz].

It is interesting to notice that the corresponding PGA values for Papudo 1981 earthquake records are 0.57 g in the vertical direction and 0.59 g for the S 40°E component.

The peak values of the Fourier spectra for Papudo S 40°E is not in agreement with the expected 1st and 2nd mode since do not satisfy Eq. (4). In this case the frequency of the second mode is double of the first.

The characteristic particle motions and odograms for Papudo 1981 records around the two characteristics main frequencies is given by two typical ground particle motions. The first one are Rayleigh wave type, more flat due to the mentioned soil effect (Hanks 1975), with the wave amplitude increasing with time. The second one are the here call “soil waves”, which have the particular characteristic to couple both horizontal components and without vertical component. These waves are present in the episodes of energy release or radiation corresponding to free vibration of the soil, the amplitude of these waves is attenuated with time but always coupled.

In Fig. 14 both type of waves are shown for Papudo, 1981 Chile earthquake. The first one represents a Rayleigh wave and the second is a soil wave. In Fig. 14 (a) the displacement from the double integration of the accelerogram are presented filtered between 6.8 and 7.8 [Hz] and rotated in 10° for the time window between 10.6 and 11.895 sec. The odogram shows clearly a vertical plane increasing retrograde Rayleigh wave. In Fig. 14 (b) the displacement are presented now filtered between 2.5 and 3.5 [Hz] and rotated in 20° for the time window between 18 to 19.195 sec. Particle trajectory in this case is restricted to the horizontal plane showing a coupled motion which is the characteristic of the soil free vibration episodes.

These results are systematically found for Chilean accelerograms (Luppichini 2004 and Modena 2004), for El Salvador 2001, MS = 7.8 earthquake (Ramírez 2005) and for the Nisqually 2001, USA earthquake (Guerra 2005).

The second peak of the S40°E Papudo Fourier spectra corresponds to Rayleigh wave type coming from the source but in this case it also possible to find an important presence of soil waves releasing energy and corresponding to the soil vertical mode.

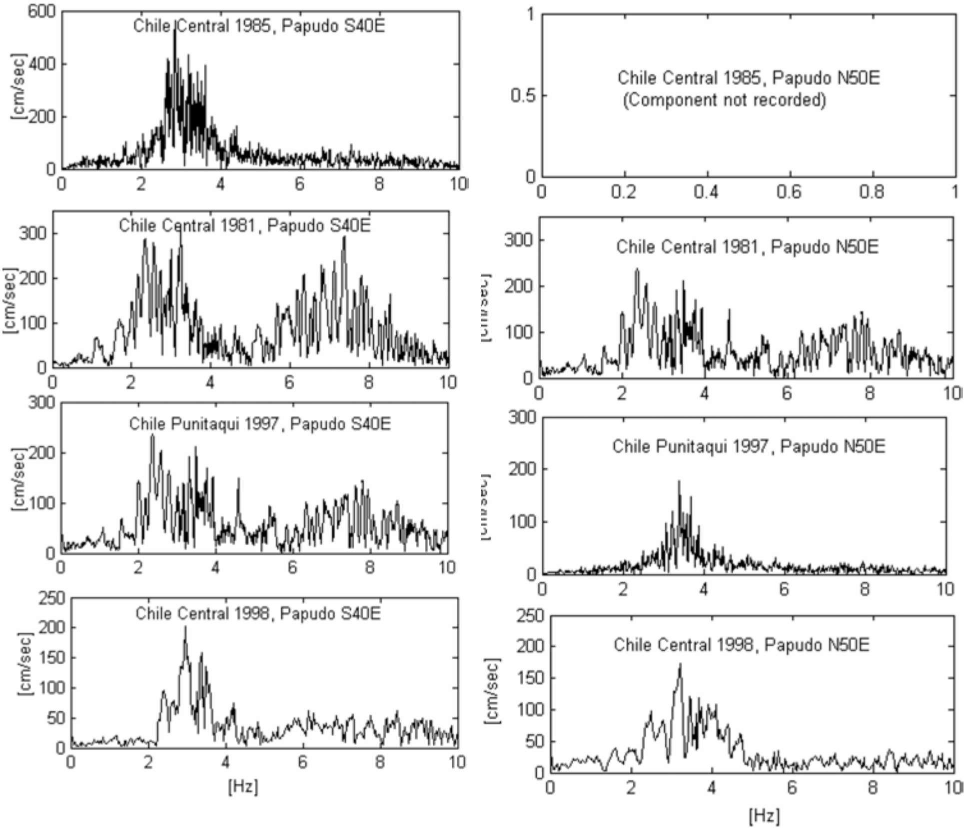

Figure 13. Comparison of Fourier spectra for accelerogram of different earthquakes recorded at Papudo, Chile Station. (The Papudo Component N50E was not recorded for the Chile Central 1985 earthquake)

During the Salvador 2001 earthquake (MS = 7.8) accelerograms were recorded at the surface and down hole at 12 m depth at Relaciones Exteriores station (Foreign Relations), when the Fourier spectra of both vertical records are compared an important soil amplification can be observed around the 11 Hz in Fig. 15.

From these observations it becomes clear that dynamical soil response is controlled by the rupture dynamics of the fault that control the time episodes of energy release (Saragoni and Ruiz 2005), particularly for the long period source waves. In order to illustrate this case the Tarzana station will be considered again. The corresponding Fourier spectra for both horizontal components are shown for the Northridge 1994 earthquake, an aftershock of that earthquake and the Whittier Narrow 1987 earthquake in Fig. 16. For Northridge earthquake as well as for the aftershock the Fourier spectra are of the wide band type due to the superposition of source seismic waves with soil waves. By contrast for the Whittier Narrow earthquake, recorded at 41 Km from the fault, that the spectra in the very narrow.

Free vibrations of the soil at Tarzana station for Northridge 1994 earthquake, recorded at 16.7 Km from the fault, are difficult to appreciate due to important arrivals of source pulses that produce forced vibration, (See Fig 9). However the free vibration of the soil of this station can be easily appreciated for Whittier Narrow 1987 earthquake.

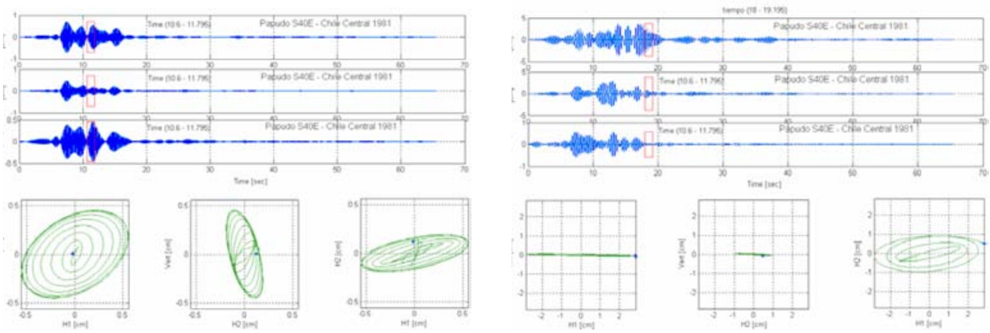

Figure 14. (a) *Rayleigh waves for 1981 Chile earthquake at Papudo Station Filtering between 6.8 and 7.8 [Hz].* (b) *Soil waves for the same records obtained at Papudo Station but filtering between 2.5 and 3.5 [Hz]*

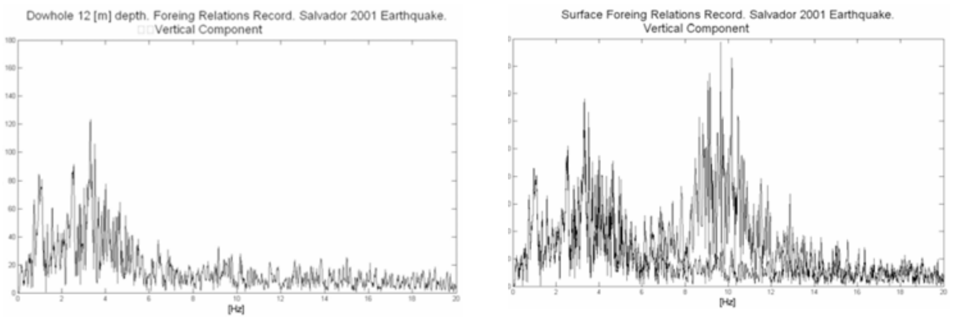

Figure 15. Fourier Spectra for vertical components of Foreign Relation Station, San Salvador at surface and 12 [m] depth down hole, for Salvador 2001 earthquake

Study of Down Hole Soil Response

The accelerographic array with down hole accelerograph allow comparison study of earthquake soil response between surface and depth at the same station. For instance they make possible to verify if observed surface coupled soil free vibrations are really the free vibrations of the full soil column.

For this verification the accelerograms recorded at Colonia Roma, Mexico City for the Ometepec 1995 earthquake with be considered. The array of this station consists of a surface accelerograph (RMCS), one down hole accelerograph at 30 [m] depth (RMC30) and a second down hole accelerograph at 102 [m] depth at the hard soil or rock interface (RMC102).

The stratigraphic soil profile for Colonia Roma station is given in Table 7 (Pérez Cruz, 1988).

The corresponding autocorrelograms for Colonia Roma array accelerograms are shown in Fig. 17. From this figure become clear that the harmonic type autocorrelogram of soil free vibration can be only appreciated clearly at the surface in the N90E direction. The down hole autocorrelograms do not show any predominant period, being essential random.

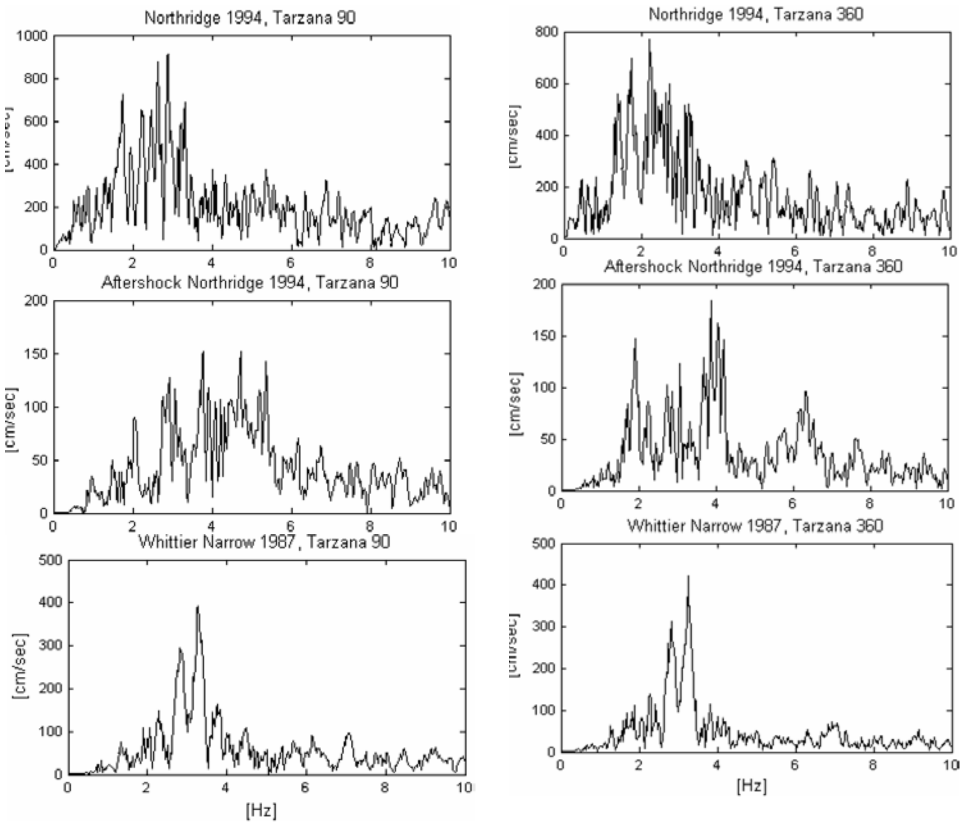

Figure 16. Comparison of Fourier spectra for horizontal accelerograms recorded at Tarzana Station for different USA California earthquakes

TABLE 7. Soil Profile Colonia Roma Station, Mexico City (Pérez Cruz, 1988)

Depth [m]	Shear Wave Velocity [m/sec]
0 - 40	80
40 - 600	700
600 - 1200	1200

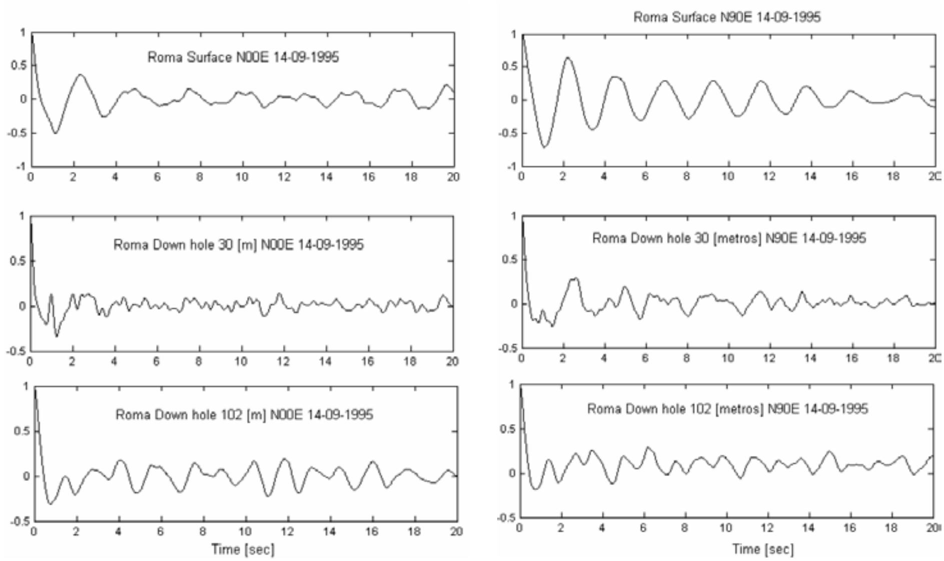

Figure 17. Autocorrelograms for Colonia Roma records of the Ometepec Mexico 1995 earthquake measured at surface and down hole

In Fig. 18 the accelerogram for RMCS N90E (surface), Ometepec 1995 is shown with the corresponding Fourier spectra and autocorrelogram.

Since the period estimated from the first cycle of the autocorrelogram is 2.23 [sec] and from the Fourier spectra is 2.33 [sec], the accelerograms will be filtered between 2 and 3.3 sec to identify the type of wave.

The particle motion for the accelerograms recorded at Colonia Roma filtered between 2 and 3.3 [sec (0.3 and 0.5 [Hz]) and rotated in 45º are shown in Fig. 19. In the same figure are also shown the corresponding odograms at surface and at depth for a time windows between 89 to 95 [sec]. Plane Rayleigh wave are observed at 30 [m] (RMC30) and at 102 [m] (RMC102). However the soil response odogram is diffuse.

However in Fig. 20 it can be appreciated at Colonia Roma Surface (RMC2) the free vibration of the soil in shear. In this figure the accelerograms are also filtered between 2 and 3.3 [sec] (0.3 and 0.5 [Hz]) and rotated in 45º. In this case the wave is a “soil wave” with only a clear plane of horizontal vibrations, without vertical components as the previous analyzed Rayleigh wave case. The considered time window now is between 101 and 109.95 [sec]. In this case since the soil is releasing energy by free vibration the ground motion is amplified at the surface.

The reason why in Fig. 18 the autocorrelogram of RMC2 N00E is more attenuated than RMC2 N90E can be due to the earthquake directivity. In this case the natural period

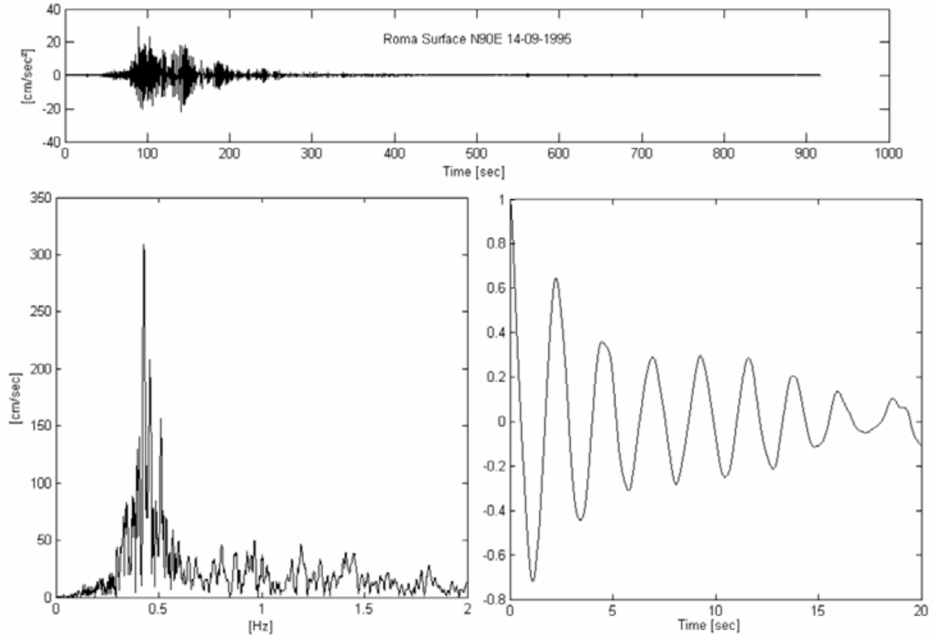

Figure 18. Colonia Roma Surface N90ºE accelerogram for Ometepec 1995, Mexico Earthquake, with the corresponding Fourier spectra and autocorrelogram

of the soil is more easily observed in the components that not receive these seismic waves.

From the analysis of this down hole array it is clear that soil response depends of the type of arriving seismic waves, and in most cases the vertical incident SH wave assumption is not observed, even in this case of far epicentral earthquake such the Ometepec 1995.

Soil Damping

The soil damping has been empirical calculated by using the autocorrelogram technique (Ruiz and Saragoni, 2004) or Random decrement method (RMD) (Huerta et al.1998). Both techniques are approximated due to the superposition of the source waves with the free vibration soil waves. Since soils vibrate in the fundamental and higher modes, the better way to estimate the modal damping is to filtrate the accelero-gram around the fundamental period and then estimate the damping from the corresponding autocorrelograms or particle trajectories, where it can be seen the free coupled vibration attenuating by the soil damping, i.e. a releasing energy episode.

By this assumption that Fourier spectra have a narrow band characteristic, it is possible to filtrate the accelerograms avoiding the influence of the other modes and have a better estimation of the soil modal damping, under large earthquake acceleration, important for seismic design.The filter to be used is Butterworth type of order 4, and the filtered values corresponds to the different Fourier spectra peak frequencies f, in the range $f - f/\sqrt{2}$ and $f + f/\sqrt{2}$. This technique is applied to CDAO N00E 1985 Mexico and Ventanas EW and Almendral, Valparaiso S40E, Chile 1985 accelerograms.

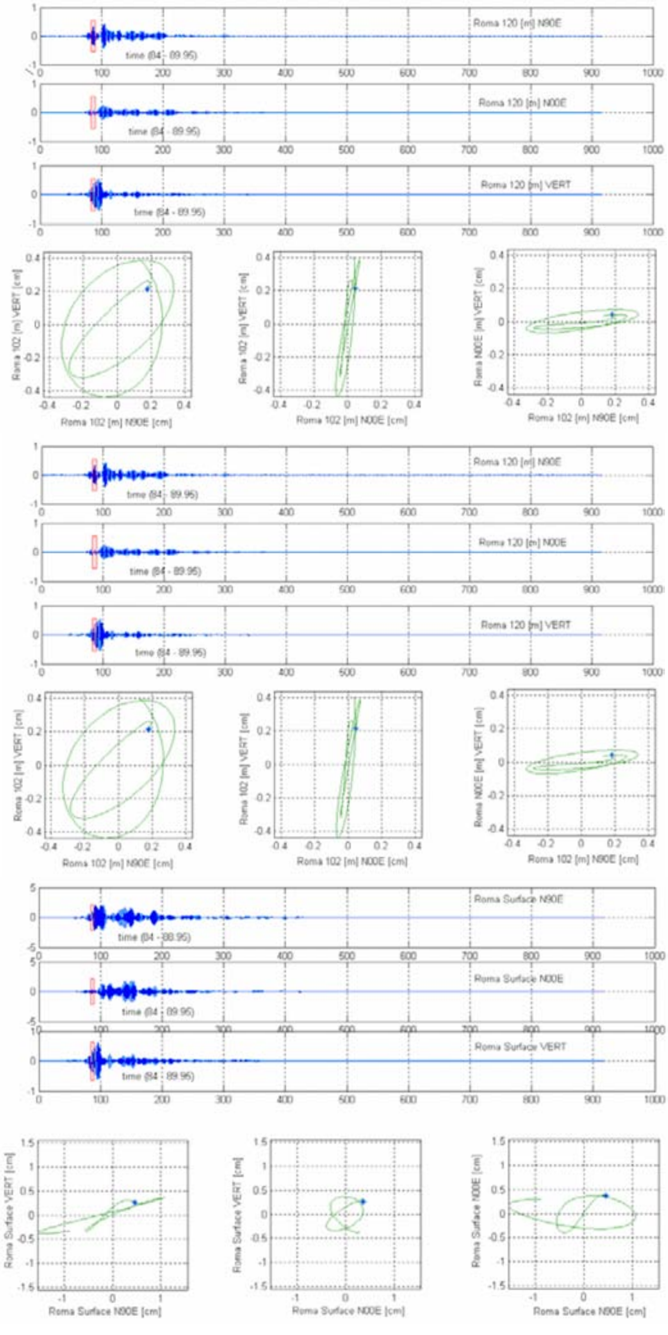

Figure 19. Particle motion and odogram for the Ometepec 1995, Mexico earthquake recorded at Colonia Roma, Mexico City Station. Records are filtered between 0.3 and 0.5 [Hz] and rotated in 45º. Rayleigh wave is only observed in depth accelerograh. Surface wave are plane

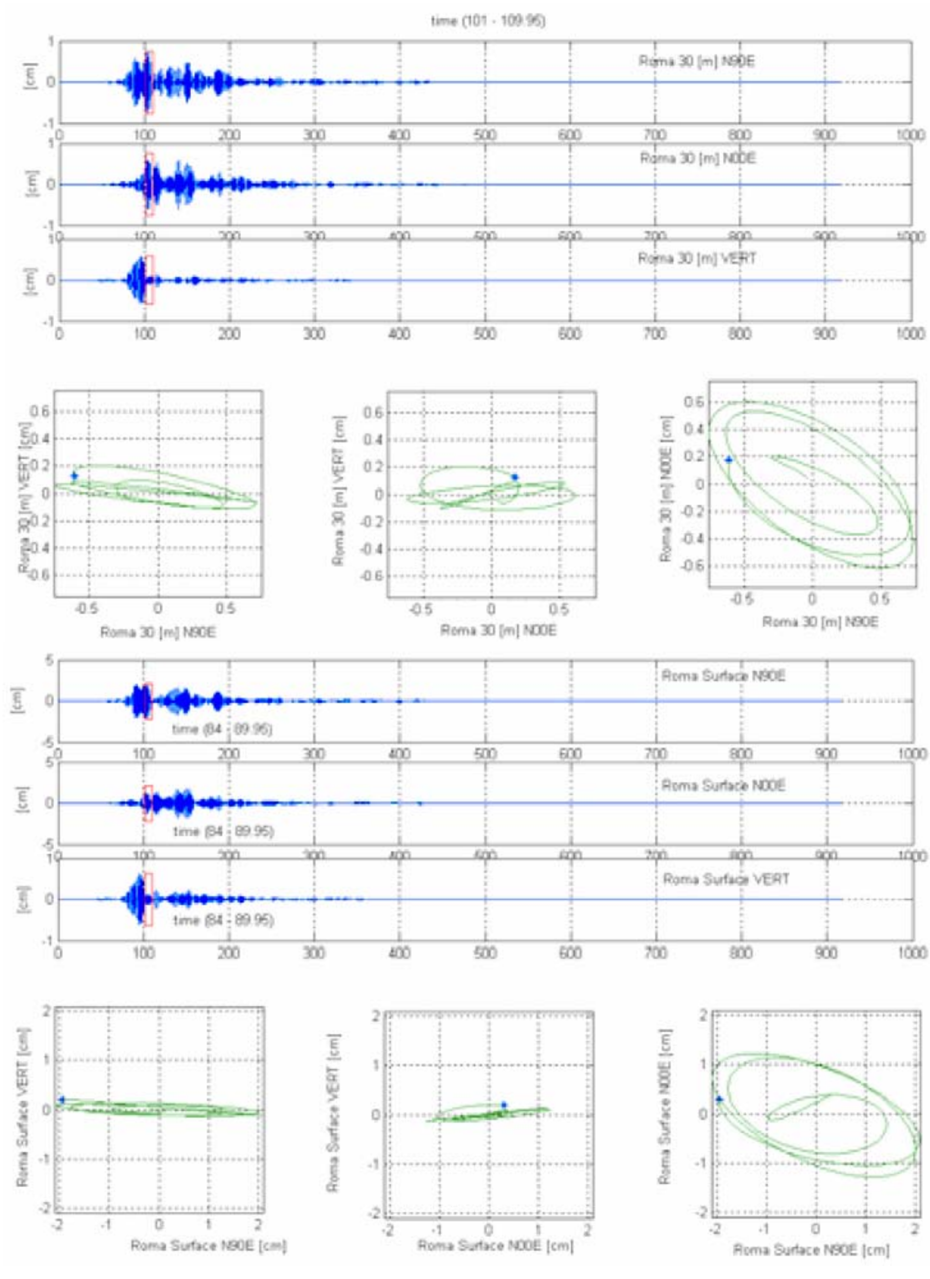

Figure 20. Particle motion and odogram for Colonia Roma, Ometepec 1995 Mexico earthquake, accelerograms. Records are filtered between 0.3 and 0.5 Hz and rotated in 45º. Particle motion of soil waves without vertical component

The CDAO N00E has a first mode period of 3.57 sec, then is filtered between 6.67 and 2.22 [sec], and a second mode period of 1.35 sec, then is filtered between 1.54 and 1.18 sec. In the case of Ventanas EW accelerogram the first mode period is 1 sec, then

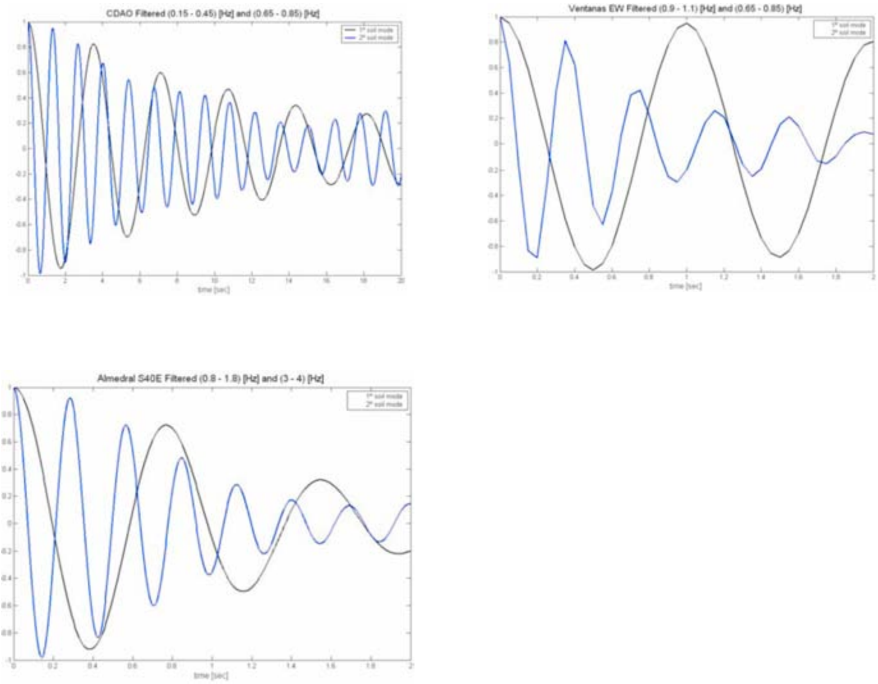

Figure 21. Comparison of autocorrelograms for CDAO N00E 1985 Mexico earthquake accelerogram and for Almendral S40Eº and Ventanas EW, Chile Central 1985 earthquake accelerograms. Showing the natural period and damping of the two first modes of the soil. Records were filtered around the period of the first and second modes of the soil

is filtered between 0.9 and 1.1 sec, and a second mode period of 0.37 sec, then is filtered between 0.29 and 0.42 sec. Finally the Almendral S40E record first mode is 1.21 sec, then is filtered between 0.56 and 1.25 sec, and a second mode period of 0.28 sec, then is filtered between 0.25 and 0.33 sec.

Fig. 21 shows the corresponding autocorrelograms for the filtered accelerograms around the first and second mode periods. It can be appreciated from these figures, that the second mode damping are little greater than the corresponding to the first mode. These results are in agreement with the values which can be appreciated in the Fourier spectra, where a wider band is observed for higher modes (See Fig. 10).

Soil Free Vibration Requirements During Large Earthquakes

The frequency of seismic wave arrivals episodes can be detected by autocorrelograms. Many times it is not possible to have harmonic autocorrelograms due to the permanent arrivals of seismic waves which not allow soil free vibrations. This situation can be appreciated at Gilroy 1 and Gilroy 2 stations for the Loma Prieta 1989 earthquake, the first station located on rock and the second on soil. Since the rock period of Gilroy 1 station is shorter, it is possible to have time windows between seismic wave

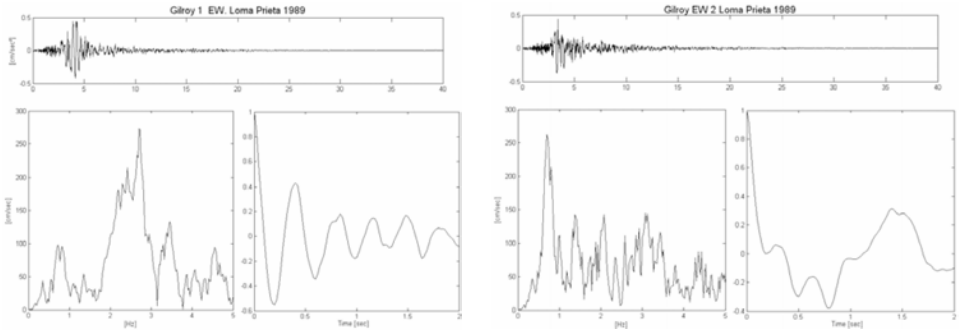

Figure 22. Horizontal accelerograms in the EW direction for Gilroy 1 and Gilroy 2, Loma Prieta 1989 earthquake with their corresponding Fourier Spectra and autocorrelograms

arrival episodes, in which the rock can free vibrate. This condition is not possible for Gilroy 2 station since the natural period of the ground is greater and the time windows are too short to observe the soil free vibration episodes. Therefore the autocorrelograms shown in Fig. 22 for both accelerograms are quite different: harmonic for Gilroy 1 EW and uncorrelated for Gilroy 2 EW.

However uncorrelated autocorrelograms do not necessarily mean that soil are not vibrating in the fundamental mode, it only means that the fundamental mode has a low participation in the soil vibration in these cases.

This participation of the fundamental modes depends of the characteristic of the seismic waves. In general seismic waves are of high frequency during the seismic wave arrival episodes of accelerograms, therefore in these episodes the higher modes have a larger participation.

The detected randomness of accelerograms by autocorrelograms is not only due to the randomness of the accelerogram, it can be also consequence of the participation of higher modes.

After the pass of the larger part of the earthquake energy the soil can free vibrate. This condition can be observed at the end of the accelerograms at CDAO N00E, Mexico 1985, Papudo S40E, Chile 1981 and Ventanas EW, Chile 1985. This situation can be seen in the spectrograms shown in Fig. 23.

Finally in Fig 24 the different durations of the accelerograms recorded in Mexico City in the EW direction for the 1989 Guerrero earthquake are shown. The different durations are consequence of the arrival of seismic waves at the end of the earthquake with different periods that excite soil with similar periods and which are attenuated with the corresponding soil damping. The observed different durations are controlled by the number of cycles of free vibration multiply by the corresponding fundamental period.

Conclusions and Recommendations

The main conclusion of this study is that in general recorded accelerograms on soil should be considered as a random sequence of episodes of seismic wave arrivals alternated with free soil vibrations episodes. The detection of these episodes has been possible by using autocorrelogram and Fourier spectra techniques.

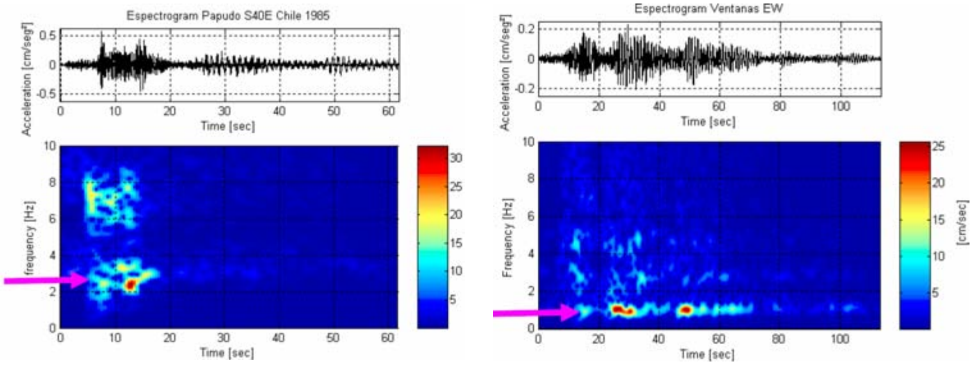

Figure 23. Spectrograms for Papudo S40E, Chile Central 1981 earthquake and Ventanas EW, Chile Central 1985 earthquake. The pink arrow corresponds to the natural frequency of the soil in each case

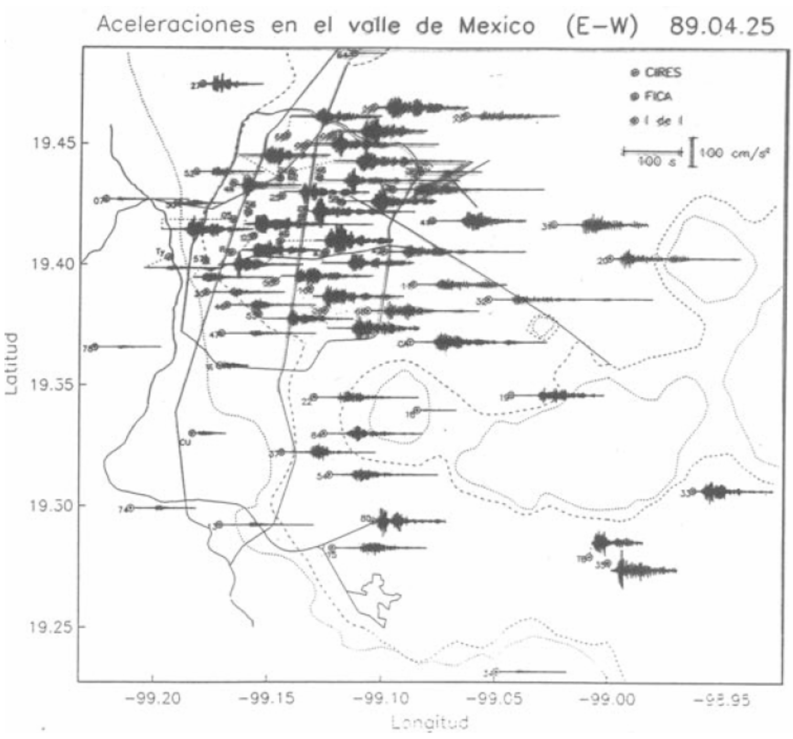

Figure 24. Horizontal accelerograms at Mexico City in the EW direction for the 1989 Guerrero earthquake, showing the different durations due to the presence of the free vibrations of the soil

Using the autocorrelogram technique the fundamental soil period can be measured when free vibration episodes are present in accelerograms. These measurement periods coincide with the one estimated by using Fourier spectra. In these cases the natural period coincide with the estimated from the 1D soil model with the expression $T = 4H / V_s$ however the depth H must be up to the rock interface.

This study has been concentrated in the soil response for large earthquakes either in epicentral zone or for larger epicentral distances. It has been found from the analyzed cases using these techniques that not major soil degradation has been observed.

Using the Fourier spectra technique the soil higher modes were detected with natural periods in agreement with the 1D soil model theory.

Depending of the type of seismic waves some time the soil vertical mode is also excited and important vertical soil amplification has been observed in some large earthquake accelerograms.

The particle soil motion analyses shown strong coupling between horizontal and vertical components, coupling which depend of the type of waves. Important vertical coupling is observed for source wave of Rayleigh type and important horizontal coupling for free vibration soil waves. Therefore it is recommended to do study on soil amplification theories that consider these effects.

The natural period can be easily estimated when the time windows between seismic arrivals episodes allow free soil free vibrations.

Autocorrelograms technique can be also used to estimates modal damping of soil higher modes.

The observation of a soil predominant period depends of the rupture dynamics of the seismic source, some time important seismic waves of Rayleigh type override the presence of the predominant period, and more that one predominant period must be expected which is independent of the soil properties. This situation is particularly important for accelerograms recorded at epicentral zones of large earthquakes.

The effects of these seismic waves are some times misinterpreted as soil degradation.

Future research is recommended to integrate these new detected features of the soil response during large earthquakes which leads to amplification theories in agreement with accelerographic array measurement as well at surface as down hole.

References

Araneda, C., and G. R. Saragoni (1994). Project of geological survey of strong motion site in Central

Chile, Report for: Kajima Institute of Construction Technology of Tokyo, Chile, Santiago.

Arias, A. and Petit-Laurent L., (1963). “Autocorrelation and Power Spectra Function of Strong Motion Accelerogram”, Revista del IDIEM, Vol 3, Nº3; and First Chilean Congress on Seismology and Earthquake Engineering, Santiago, Chile. (In Spanish)

Arias, A. and Petit-Laurent L., (1965). “A Theoretical Model for Strong Motion Accelerograms”, Revista del IDIEM, Vol 4, Nº1; Santiago, Chile. (In Spanish)

Astroza, M; Saragoni, R., and Yañes, F., (1986). “The Mexico Earthquake of September 19 , 1985”. 4th Chilean Congress on Seismology and Earthquake Engineering. Viña del Mar, 1986. (In Spanish) Boore, D., (2004). “Can site response be predicted?”. Journal Earthquake Engineering. Vol. 8, pp. 1-41.

Duke, C. M. (1958). “Effects of Ground on Destructiveness of Large Earthquakes”. Journal of Soil Mechanics and Foundation Division. American Society of Civil Engineerings. 84 (SM3), 1 -23.

Faccioli, E. and Reséndiz, D., (1976). “Soil dynamics: Behavior including liquefaction”. Developments in Geothnical Engineering, by Lomnitz, C y Rosenblueth, E (Editors).

Freeman, J. R., (1932). “Earthquake Engineering and Earthquake Insuarence”. New York, Mc Graw Hill. 1932.

Gomez, B., A., (2002). “Interpretation of Soil Effect at Mexico City Valley Using Accelerograph High Density Arrays”, Ph. D. Thesis. Facultad de Ingeniería, Universidad Autónoma de Mexico, Mexico. (In Spanish).

Guerra, F. (2005). “Accelerogram Interpretation of Nisqually, USA, 2001 Earthquake Considering High Frequency Seismic Waves”. Memoria para optar al título de Ingeniero Civil, Universidad de Chile, Santiago, Chile. (In Spanish)

Hanks, T (1975). “Strong Ground motion of the San Fernando, California, earthquake: Ground Displacements”. Bulletin of the Seismological Society of America, Vol. 65, Nº1, pp. 193-225.

Hayashi, S., Tsuchida, H. and Kurata, E.,1971. “Average response spectra for various subsoil conditions”. Third Joint Meeting, U.S – Japan Panel on Wind and Seismic Effects, UJNR, Tokyo, Japan.

Housner, G. W. (1947). “Characteristics of strong – motion earthquakes”. Bull. Seism. Soc. Am., vol 37, nº1.

Huerta, C. I., Roesset, J. M., and Stokoe, K. H. (1998). “Evaluation of the random decrement method for in-situ soil properties estimation”. Second International Symposium on the effects of Suruface Geology on Seismic Motion. Recent progress and new horizon on ESG study. Yokohama, Japan. Proceeding Vol. II, pp 749-756.

Kanai, K., (1957). “The requisite conditions for the predominant vibration of ground”. Bull. Earthquake Research Institute, Tokio XXXV.

Kanai, K. and S. Yoshizawa (1956). “Relation Between the Amplitude of Earthquake Motions and the Nature of Surface Layer”. IV Bulletin of the Earthquake Research Institute. 34, 168-184.

Liu, S. (1969). “Autocorrelation and Power Spectral Density Functions of the Pakerfield Earthquake of june 27, 1966”. Bulletin of the Seismological Society of America, Vol. 59, Nº4, pp. 1475-1493.

Lungu, D., Demetrio, S. and Cornea, T., (1992). “Frequency bandwith of Vrancea eartquakes and the 1991 edition of seismic Codeo f Romania”. Earthquake Engineering, Tenth World Conference, 1992,

Balkema, Rotterdam. Luppichini, N., (2004). “Interpretation of Chile Central 1985 Earthquake Accelerograms Considering High Frequency Waves”. Memoria para optar al título de Ingeniero Civil, Universidad de Chile, Santiago, Chile. (In Spanish)

Modena, P., (2004). “Interpretation of Chilean Inslab Earthquakes of Intermediate Depth Accelerograms Considering High Frequency Seismic Waves”. Memoria para optar al título de Ingeniero Civil, Universidad de Chile, Santiago, Chile. (In Spanish)

Pérez Cruz, G. A. (1988). “Reflection Seismological Study of Mexico City Soil”. Tesis de maestría. División de Estudios de posgrado, UNAM, México, D.F. (In Spanish)

Ramírez, R. (2005). “Interpretation of Subduction El Salvador 2001 Earthquake Considering High Frequency Waves”. Memoria para optar al título de Ingeniero Civil, Universidad de Chile, Santiago, Chile. (In Spanish)

Ruiz, S. and Saragoni, G. R., (2004). “Experimental Measurement of 1D Soil Dynamic Response by using Autocorrelograms of Accelerograms of Ms = 7.8, 1985 Chile Earthquake”. Proc. 5to Congreso Chileno de Geotecnia, Santiago, Chile. (In Spanish)

Saragoni, G. R and Ruiz, S., (2004), “Elastic 1D Models From the Dynamical Response Analyzed of Central Chile Earthquake Accelerograms ”. Proc. 5to Congreso Chileno de Geotecnia, Chile. (In Spanish)

Saragoni, G. R. and Ruiz, S (2005). To be submitted. “Seismic Wave in Soil Response”. Journal of Earthquake Engineering and Structural Dynamics.

Seed, B., Ugas, C. and Lysmer, J., (1976). “Site dependent spectra for earthquake resistant design”. Bull. Seism. Soc. Am., vol 66, nº1.

Seed H. B., Romo, M. P., Jaime, A and Lysmer, J., 1988. “The Mexico Earthquake of September 19, 1985 Relationships Between Soil Conditions and Earthquake Ground Motions”. Earthquake Spectra, Vol 4, Nº 4, pp 687-729.

Sezawa, K. (1930). “Possibility of the Free – Oscilations of the Surface Layer Excited by the Seismic Waves”. Bull. Earthq. Res. Inst 13, 1 – 12.

Sezawa, K. and Kanai, k., (1935). “Decay Constants of Seismic Vibrations of a Surface Layer”. Bull. Earthq. Res. Inst 13, 251 – 265.

Singh, S, K; Lermo, J; Domínguez, T; Ordaz, M; Espinosa J.M; Mena, E y Quaas R., 1988. “The Mexico Earthquake of September 19, 1985 A study of Amplification of Amplification of Seismic Waves in the Valley of Mexico with Respect o a Hill Zone Site”. Earthquake Spectra, Vol 4, Nº 4, pp 653-673.

Tajimi , H., (1960). “A statistical method of determining the maximum response of a building structure during an earthquake”, Proc, 2nd World Conf. On Earthquake Eng., Tokyo, Japan.

Keh-Chyuan Tsai
Director and Professor
National Center for Research on Earthquake Engineering
200, SECT 3, Xinhai Road, Taipei, 106 Taiwan
kctsai@ncree.org.tw

Research interests: steel structures, earthquake resistant design,
hybrid test method, nonlinear analysis computer code

Prof. Luis Esteva is such an outstanding leader in the international communities of earthquake engineering research and practice. In particular, in the year of 1998, he visited Taiwan and has made a remarkable presentation on the seismic design and optimization of structures provided with energy dissipaters. His work has inspired many Taiwanese scholars and engineers on the research and application of seismic response control technology.

On behalf of NCREE, I would like to take this opportunity to express our highest respect to his dedication in advocating seismic hazard mitigation in Mexico and in the world.

Keh-Chyuan Tsai,
August 10, 2005

PSEUDO DYNAMIC PERFORMANCE OF LARGE SCALE BUCKLING RESTRAINED BRACED FRAMES

ABSTRACT

This paper first evaluates the gusset plate performance of a 3-story 3-bay buckling restrained braced (BRB) composite frame tested in Taiwan National Center for Research on Earthquake Engineering (NCREE). Then, the design of a full scale 2-story single bay BRBF specimen representing a main lateral force resisting frame in the transverse direction of a prototype steel building is described. The 2-story BRB steel frame was tested using the substructure pseudo dynamic test procedures. A general purpose frame responses analysis computer program PISA3D originally developed in the National Taiwan University has been incorporated into the networked hybrid simulation test platform developed in NCREE. The BRBF was subjected to five bi-directional earthquake ground accelerations scaled to three different hazard levels, namely 50%, 10% and 2% chances of exceedance in 50 years, respectively. It is illustrated that the BRBF specimen sustained a total of five pseudo dynamic tests without global stiffness or strength degradation. Finally, two sets of mutually orthogonal, bi-directional cyclic increasing inter-story drifts were imposed until the first story BRB-to-beam and column joint was completely fractured at the second cycle of 0.03 radian. No gusset plate instability was observed throughout the bi-directional hybrid and cyclic tests.

Introduction

In October 2003, a full-scale 3-story 3-bay CFT column and buckling restrained braced composite frame (CFT/BRBF) specimen (Fig. 1) was tested in a Taiwan-US-Japan Cooperative Research Program (Tsai et al. 2004, Chen et al. 2004, Lin et al. 2004). Measuring 12 meters tall and 21 meters long, the specimen is among the largest frame tests of its type ever conducted. The frame was tested using the pseudo-dynamic test procedures applying input ground motions obtained from the 1999 Chi-Chi and 1989 Loma Prieta earthquakes, scaled to represent 50%, 10%, and 2% in 50 years seismic hazard levels. Being the largest and most realistic composite CFT/BRB frame ever tested in a laboratory, the tests have provided a unique data set to verify computer simulation models and seismic performance of CFT/BRB frames. This experiment also provides great opportunities to explore international collaboration and data archiving envisioned for the Networked Earthquake Engineering Simulation (NEES) program and the Internet-based Simulations for Earthquake Engineering (ISEE) (Wang et al. 2005) launched recently in USA and Taiwan, respectively. The two earthquake records are TCU082-EW (from the 1999 ChiChi earthquake) and LP89g04-NS (from the 1989 Loma Prieta earthquake), both of which are considered to represent general motions without near-field directivity effects. The original test plan was to scale these two records in acceleration amplitude to represent four separate pseudo-dynamic loading events, which were sequenced as follow: (1) TCU082 scaled to represent a 50/50 hazard intensity, i.e., with a 50% chance of exceeding in 50 years, (2) LP89g04 scaled to a 10/50 hazard intensity, which represents the design basis earthquake, (3) TCU082 scaled to a 2/50 hazard, and (4) LP89g04 scaled to a 10/50 hazard – identical to loading (2). However, Fig.2 indicates that the actual number of applications of the ground motions in the PDTs for the CFT/BRB frame specimen is six. This is because some unexpected events encountered during the testing. In the Test No. 1, due to the buckling of the gusset plate occurred at the brace to beam connection in the first story (Fig. 3a), the test stopped at the time step of 12.3 second. Then stiffeners were therefore added at the free edges of all the gusset plates underneath the floor beams (Figs. 3 and 4). Then the test resumed using the same ground accelerations as Test No.1 in reversed direction. In test No.4, the PDT test was stopped at the time step of 12.54 second due to the crack on the top of concrete foundation near the gusset plate for the south BRB-to-column joint were observed. After one pair of angles was installed bracing the stiffener to the two anchoring steel blocks, the test resumed again by applying the same earthquake acceleration as that for Test No.4. Thus, a total of six PDTs was conducted. After these six pseudo dynamic tests, all the BRBs were not damaged. Therefore, cyclic increasing story drifts were imposed until the failure of the BRBs. Since the scheduled PDT and cyclic tests were completed with failures only in bracing components including the BRBs, UBs and the gusset plates (but not any beam or column), it was decided that Phase-2 tests be conducted after repairing the damaged components. Due to the buckling to the gusset plates observed in the brace-to-column joints at the end of Phase-1 tests (Fig. 5), additional stiffeners were added at the free edges of the gusset at the two third floor brace-to-column joints after the buckled gussets were heat straightened (Fig. 6). Six new BRBs, two all metal double cored construction for the 1st story, four concrete filled double cored for the 2nd and 3rd stories, were installed. Phase-2 tests not only allowed to make the best use of the 3-story, 3-bay frame but also aimed to investigate the performance of the stiffened gussets plates and the new BRBs. The ground motion accelerations applied in Phase 2 PDTs are also shown in Fig. 2. Details of the observation and discussion for the PDTs are summarized in the reference papers (Tsai et al., 2004; Chen et al., 2004; Lin et al., 2004).

Evaluation of Compressive Gusset Plate Performance

As mentioned above, at the beginning of Test No.1 in Phase 1, the gusset at first story buckled out of plane as shown in Fig. 3a. The test was stopped for inspection, followed by adding stiffeners shown in Fig. 3b to the edges of the gussets (only to the ones underneath the beam bottom flange) from the 1st story to the 3rd story. The situations before and after adding stiffeners are shown in Fig. 4. Stress in the gusset plate is very complex when external load is acting on it, thus some simplified design methods proposed by Whitmore (1952) have been adopted for the design of the gussets. Whitmore suggested that the location of the peak stress can be defined in a “Whitmore Section” where the stresses distributed along a 30 degree angle from the line connecting the first bolt hole to the last bolt hole (Fig. 7). The section within the extended width is called the “Whitmore Section”, and the greatest stress would occur within this section. When the tensile stress on Whitmore Section reaches the yield stress of the gusset F_y, the corresponding brace force defines the tensile capacity of the gusset plate. When the gusset plate is under compression, compressive stress on Whitmore Section may not be able to develop *Fy*. To prevent the gusset plate from buckling, buckling strength should be checked against the design compressive load. Thornton further suggested (Thornton, 1984) that from the midpoint or the two ends of the Whitmore Width along the force direction to the beam or column flanges, the longest length, L_c of three lines L_1, L_2, and L_3 as shown in Fig. 7 can be used to define the most critical effective length. An effective length factor K of 0.65 has been suggested by Thornton. Thus, capacity design criteria of gusset under tension and compression conditions are summarized in Eqs. (1) and (2).

$$P_{y\ Gusset} = F_y b_e t \geq P_{y\ Brace} \quad for\ \ tension \tag{1}$$

$$P_{cr} = \frac{\pi^2 E}{(KL_c / r)^2}\ b_e\ \ t \geq P_{\max} \quad for\ \ compression \tag{2}$$

By examining the failure modes of the gusset plate shown in Figs. 3a and 5, it appears that the buckling shape at the brace-to-gusset joint in the specimen is similar to that shown in Fig. 8c. Therefore, before the edge stiffeners were added, the effective length factor might be appropriate to assume it is about 2.0, instead of 0.65. The results of the calculations are shown in Table 1. It's evident that the critical loads P_{cr} of the gussets become quite small when the effective factor K is 2.0. The critical load P_{cr}, using K=2.0 for the top gusset plate at the first story BRB is about 842kN, closely agree with the experimental buckling load (805*kN*) observed. After adding the edge stiffeners at this gusset and repairing the BRB, the gusset plate (having an effective length factor of 0.65) sustained the rest of all tests. For the bottom gusset at the third story (Fig. 5), the critical load of the gusset plate (without the edge stiffeners, assuming K=2.0) is also very close to the ultimate compressive load P_{max} of the third story BRB. This could be used to explain why the gussets at bottom end of BRBs in 3rd story buckled during the final cyclic loads in the Phase I tests. Further, after stiffening the gussets (Fig. 6), there was no more gusset buckling occurred in the Phase II tests. It appears that after adding edge stiffeners, the boundary condition is closer to that shown in Fig. 8d. Thus, it appears that the effective length factor can be assumed as 0.65 for the capacity design of the gusset only when the gusset plate is stiffened properly. Finite Element Analysis using ABAQUS was further conducted to check the buckling strength of gusset plate. The finite element material model for the gusset plate is the bi-linear strain-hardening using the actual material coupon strength. The FE meshes are shown in Fig. 9a. For the un-stiffen gusset, the FE buckling load is equal to 0.43P_{max}(=750kN) which is close to the experimental buckling load (805kN). After adding stiffeners to the gusset as shown in Fig. 9b, the buckling load of the gusset is increasing to 3.49P_{max}. Evidently, the out-of-plane buckling has been prevented in the Phase II tests.

3D Hybrid Experiment of A 2-story Full Scale Steel BRBF Substructure Subjected to Bi-directional Ground Motions

In order to further investigate the performance of the brace to gusset plate connections subjected to both in-plane and out-of-plane deformational demands, an experiment was launched on a full scale two-story single bay BRBF (Weng et al. 2005, Lin et al. 2005). It also provided another opportunity to verify the performance based design methodology of the BRBF building systems. The prototype of the 2-story building configuration and the BRBF specimen is shown in Fig. 10. In the context of the pseudo dynamic testing, only one BRB frame specimen was tested, the remaining structure was simulated analytically. The bay width and story height of the BRBF are 8m and 4m, respectively. This experimental program consists of two phases. In Phase I, the seismic ground motion records, which was recorded in the 1999 Chi-Chi earthquake, are scaled up to represent 50%, 10%, and 2% probability of exceedance in 50 years (denoted as 50/50, 10/50 and 2/50 events, respectively). The ground motions were applied bi-directionally in the transverse (Y-axis) and longitudinal (X-axis) directions. One of the test objectives in Phase I is to evaluate the performance of various BRB to gusset plate connections (Fig. 11) under the bi-directional seismic load effects (Lin et al., 2005). In Phase II tests, the prototype structure was adjusted to form an asymmetric structure, which has the common experimental BRB frame on Frame Line B. The objective in Phase II is to verify the validity of the simplified procedures in estimating the seismic demands of asymmetric structures (Weng et al. 2005). This experiment also provides great opportunities to further enhance the networked pseudo-dynamic test and data archiving techniques envisioned for the Internet-based Simulations for Earthquake Engineering (ISEE) (Wang et al., 2005) launched in 2002 in Taiwan. This paper compares the key experimental responses with the analytical predictions computed from a general purpose frame response analysis program, PISA3D (Tsai and Lin, 2003). The prototype building was first designed according to the story force distribution prescribed in the 2002 Taiwan Seismic Building Specifications (ABRI, 2002). The beam-to-column joints of the perimeter frame are all moment connections and all the other beam-to-column joints are pin-connected. A double-core BRB (Tsai et al. 2002, Uang et al. 2004), with cement mortar infilled in two rectangular tubes, has been installed in each story of the BRBF specimen (Fig. 10). All beams and columns are wide flange sections. The prototype 2-story building structure is assumed to be located in Chiayi City with Soil Type I (hard rock site) and the occupancy importance factor I is 1.0. The design dead load (DL) and live load (LL) are 6.89kN/m^2 and 2.45kN/m^2, respectively. The steel beams at the perimeter frame are A36 and all other members are A572 Grade 50. Design load combinations include: (1) 1.2DL+0.5LL+1.0EQ, (2) 0.9DL+1.0EQ, and (3) 1.2DL+1.6LL. It should be noted that the design spectra for the 10/50 event (Fig. 12a) are S_{DS}=0.8g and S_{D1} =0.45g, while for the 2/50 event (Fig. 12b), S_{MS}=1.0g and S_{M1} =0.55g. The members sized from the force-based method were compared with those determined from the displacement based procedures described hereafter.

Displacement-based Seismic Design

The design procedures adopted for the prototype building consist of the following steps: 1) select an initial desired displaced shape for the structure, 2) determine the effective displacement by translating the actual MDOF structure to the substituted SDOF structure, 3) estimate system ductility from the properties of BRB members, 4) determine the effective period of the substituted SDOF structure from an inelastic design displacement spectra, 5) compute the effective mass, effective stiffness, and design base shear, 6) Distribute the design base shear over the frame height, 7) design the members for the steel frame. There are some key points in these steps described above. First, the i^{th} yield story drift θ_{yi} corresponds to the brace yielding can be estimated as:

$$\frac{\varepsilon_c}{\varepsilon_{wp}} = \frac{1}{\frac{L_j A_c}{L_{wp} A_j} + \frac{L_t A_c}{L_{wp} A_t} + \alpha_c} = \gamma \tag{3}$$

$$\theta_{yi} = 2 \cdot \varepsilon_{cy} / \gamma \cdot \sin 2\phi \tag{4}$$

where ε_{cy} is the yielding strain of the brace center cross section, γ is the ratio between a specific elastic axial strain of the brace center segment and the corresponding elastic averaged strain of the entire braceε_{wp} (computed from the brace end work-point to work-point length). ψ is the angle between the horizontal beam and the brace. θ is the story drift angle, ε_c is the strain of the brace steel core section and $\alpha_c = L_c / L_{wp}$ (L_c and L_{wp} are defined in Fig. 13). Thus, if θ_{mi} is the target drift of the i^{th} story calculated from the target displacement profile, then the story ductility can be computed from:

$$\mu_i = \theta_{mi} / \theta_{yi} \tag{5}$$

After calculating all the story ductilities from Eq. 5, the average of all story ductilities is taken as the system ductility. Since the BRBs are the primary energy dissipation element under the two levels of earthquakes, the connecting beams and the columns need to be designed considering the capacity design requirements. Typical force versus deformation relationships for A572 Gr.50 steel BRB specimens, is shown with actual yield capacity ($A_c \times F_{y,actual}$) in Fig. 14 (Tsai and Lin 2003). It is evident that the peak compressive force is slightly larger than the peak tensile force under large cyclic increasing strains. In addition, the strain hardening factor of Grade 50 steel is about 1.3. Therefore, the maximum possible brace force can be estimated as follows:

$$P_{\max} = \beta \times \Omega \times \Omega_h \times P_y \tag{6}$$

where P_y is the nominal tensile yield strength, Ω accounts for possible material overstrength, Ω_h represents the effects of strain hardening, and β is about 1.1 considering the 10% difference between the peak compressive and tensile forces. Since the actual yield strength obtained from the tensile coupon tests was employed to adjust the final BRB cross sectional area before fabrication, the material overstrength factor Ω is not included in the capacity design of members or connections for the BRBF specimen. Applying LRFD specifications (AISC, 1999):

$$P_u / (\phi_c P_n) \geq 0.2 \qquad P_u / (\phi_c P_n) + \frac{8}{9} M_u / \left[\left(1 - \frac{P}{P_e} \right) \phi_b M_n \right] \leq 1.0 \tag{7}$$

where $P_n = F_{cr} A_g$, $P_{cr} = \pi^2 EI / (kl)^2$, $\phi_c = 0.75$ $(tension)$ or $0.85(compression)$, $\phi_b = 0.9$. Two hazard levels considered in this study, for the 10/50 and 2/50 events, the inter-story drift limits are set at 0.02 and 0.025 radians, respectively. The actual material test results given in Table 2 can be used to refine the estimations of the ductility demand. With the actual steel core strength and assume the length ratio α_{ci} for braces at 1st- and 2nd- floor as 0.7 and 0.6, respectively, the averaged system ductility demands for the 10/50 and 2/50 events are 5.39 and 6.74, respectively (shown in Table 3). Applying the target displacement profile obtained in the Step 2, the effective displacement δ_{eff} is 0.13 m and 0.17 m for the 10/50 event and 2/50 event, respectively. Intersecting the effective target displacements of 0.13 m and 0.17 m on the inelastic displacement response spectra shown in Fig. 15, the effective first vibration period $(T_{eff})_1$ during the 10/50 and 2/50 events can be found as 1.19 and 1.22 second, respectively. In Fig. 15, the elastic displacement response spectrum (μ=1.0) is also given. Based on the results computed by the aforementioned Steps 5 and 6, the design base shears, 4149.8 kN (=0.24W) and 4509.4 kN (=0.26W) represent the stage of significant system yielding for the two events. It is evident that the 2/50-0.025 hazard/performance criteria govern the design. In the transverse direction (Y-direction), the stiffness ratio (SR) of the BRBF and the MRF is assumed 3, thus the BRBF resists 75% design earthquake force. Using this criterion, the core cross-sectional areas of the A572 Gr.50 steel BRB are $50cm^2$ and $33cm^2$ for the 1^{st}- and 2^{nd}-story, respectively. Using the capacity design principle, more than 14x24-mm diameter A490 bolts would be required for each first story BRB connection. In order to reduce the length of the connection, welded brace-to-gusset connection details are adopted. For the BRB in the second story, bolted details using 10-24mmϕ A490 bolts are adopted at each brace end. After a few iterations, the final dimensions of the braces and other members are selected as shown in Fig.16. In particular, the BRBs will yield in the proximity of the design story shear. The vibration periods are 0.69sec and 0.57sec in the longitudinal (MRF, noted as X-direction) and transverse (BRBF+MRF, noted as Y-direction) directions, respectively.

Scaling Ground Motions and Experimental Program

Based on the IBC2000 provisions (ICC, 2000) and the recommendations provided by Shome et al. (1998), for each pair of (bi-lateral) horizontal ground motion components, the square root of the sum of the square (SRSS) of the 5% damped site-specific spectra of the scaled horizontal components was constructed first. The ground motions were scaled such that the spectral acceleration of the SRSS spectra was not less than 1.4 times the 5% damped smoothed design spectra at the fundamental period of the prototype building in the considered direction. In addition, the scaling factor (denoted as SF) should not exceed 4.0. Two pairs of earthquake records from the 1999 Chi-Chi earthquakes, CHY024 and TCU076 have been chosen as input ground motions. The corresponding spectra representing 10/50 and 2/50 hazard levels and satisfying the above mentioned requirements are shown in Fig. 12. The earthquake scenario, including the earthquake intensities and sequence, for Phase I tests is shown in Fig. 17. Figure 18 shows three earthquake ground accelerations which are 50/50 (CHY024), 10/50 (TCU076), and 2/50 (CHY024) in the longitudinal and transverse directions. The gravity forces for the BRBF specimen are applied by using the post-tension steel rods anchored at the strong floor (Fig. 10) and connected to a cross beam on top of each column. The force responses of the 2-story BRBF were combined with all other finite element forces of the entire structure before solving all the nodal displacements for the next time step. The global target nodal displacements were transformed incorporating the actuators' orientation (Wang et al. 2005). Once the target actuator displacements have been reached, the force responses of the BRBF was measured and incorporated into the complete structural force response for solving next set of nodal displacements. Any difference on the force responses from the analytical BRBF (Fig. 10) and the experimental BRBF specimen will result in the torsional responses of the entire building. Thus, torsional responses were investigated by purposely differentiate the stiffness and strength of the analytical BRBF and the experimental BRBF. The torsional responses of the entire structure have been avoided in the Phase I test by assuming the analytical BRBF's force responses are identical to those of the experimental BRBF.

Analytical Predictions and Key Experimental Responses

Analytical Model

Nonlinear static and dynamic time-history analyses have been conducted using the PISA3D program (Tsai and Lin, 2003). In the PISA3D model, all beams, columns were modeled using the two-surface plastic strain hardening beam-column element. All BRBs were modeled using the two-surface plastic strain hardening truss element. The 2^{nd} order effects developed in the gravity columns are also considered. Analytical predictions of key structural responses, such as floor displacement and story shear time histories were broadcasted through Internet (http://substructure-brbf.ncree.org) along with the experimental responses during the course of each test. Typical Internet plots are shown in Fig. 19.

Phase I Tests

In Phase 1, as noted above, three pairs of earthquake ground accelerations scaled to three different PGAs were applied for the sub-structural PDT of the BRBF specimen. The predicted and experimental distributions of the peak inter-story drifts under the applications of 50/50, 10/50 and 2/50 three earthquake loads are shown in Figs. 20 and 21 for the X and Y directions, respectively. It is shown that the experimental peak inter-story drifts of 1^{st}- and 2^{nd}-story in both directions were satisfactorily predicted. In particular, the design inter-story drift target of 0.025 radian for the 2/50 events, has been reached in the transverse direction. Other test results can be conveniently found in the web site (http://substructure-brbf.ncree.org) during and after the tests.

Phase II Tests and Cyclic Loading Tests

At the end of applying the 50/50, 10/50 and 2/50 earthquake ground accelerations, base metal cracks were observed at the tip of two gusset plate welded joints. In the Phase II tests, the prototype structure was adjusted to form an asymmetric structure, which has the common experimental BRB frame on Frame Line B. Two additional 2/50 hazard level earthquake loads were subsequently applied on the BRBF. Thus, the BRBF was subjected to five bi-directional earthquake ground accelerations scaled to three different hazard levels, namely one 50/50, one10/50 and three 2/50 events. However, it is illustrated that the BRBF specimen sustained these five pseudo dynamic loading without global stiffness or strength degradation. Finally, two sets of mutually orthogonal, bi-directional cyclic increasing inter-story drifts were imposed until the first story BRB-to-beam and column joint was completely fractured at the second cycle of 0.03 radian. No gusset plate instability was observed through out the bi-directional hybrid and cyclic tests.

Conclusions

Based on the 2-story BRBF tests, summary and conclusions are made as follows:

1. The peak story drift has reached 0.025 radian in the transverse direction in Phase I tests after applying the 2/50 design earthquake on the BRBF specimen. Tests suggest that the DSD procedure adopted in the design of the specimen is effective in limiting the ultimate story drift under the design earthquake.
2. The peak story drift has reached 0.015 radian in the longitudinal building (BRBF's out-of-plane) direction in Phase I tests. It appears that all the gusset plates sustained these moderate out-of-plane deformational demands without failure.
3. These tests and ABAQUS analysis confirmed that the stiffeners arranged for the gusset plates are effective, and have made an effective length factor of K=1.0 appropriate in computing the compressive gusset strength.
4. It is illustrated that the real-time webcast of the test results is extremely effective for researchers to understand the responses of the specimen during the tests.

Acknowledgements

The author would like to acknowledge the financial supports of the National Science Council. The technical supports provided by the laboratory at NCREE are gratefully acknowledged. Many NCREE staffs and NTU graduate students made significant contributions to the success of these studies. It includes Wei-Chung Cheng, Po-Chien Hsiao, Yean-Chih Huang, Juin-Wei Lai, Bo-Zhou Lin, Min-Lang Lin, Jui-Liang Lin, Shen-Ling Lin, Cheng-Yu Tsai, Kung-Juin Wang, Yuan-Tao Weng, Chong-Shing Weng and Min-Jie Zhuang. Without their efforts, these research results would not be possible. Valuable suggestions provided by Prof. Stephen Mahin of University of California at Berkeley, Prof. Charles Roeder of University of Washington, Mr. Rafael Sabelli of DASSE Design Inc. on the gusset plate design of the 2-story BRBF are gratefully acknowledged.

References

ABRI, (2002). *Recommended Provisions Updated Draft for Building Seismic Regulations*, Taipei, 2002 (in Chinese).

AISC(American Institute of Steel Construction), (1999). *Seismic Provisions for Structural Steel Buildings*, Chicago, IL, 1997.

Chen, C.H., Hsiao, P.C., Lai, J.W., Lin, M.L., Weng, Y.T., and Tsai K.C. (2004). "Pseudo-Dynamic Test of a Full-Scale CFT/BRB Frame: Part 2 - Construction and Testing." *Proceedings of 13th World Conference on Earthquake Engineering,* Vancouver, B.C., Canada, Paper No. 2175.

Chopra, A.K. and Goel, R. K. (2004)."A modal pushover analysis procedure to estimate seismic demands for unsymmetric-plan buildings. *Earthquake Engineering and Structural Dynamics* 33, 903-927.

ICBO, (2000). *Internal Building Code*, Whittier, CA.

Lin, M.L., Weng, Y.T., Tsai, K.C., Hsiao, P.C., Chen, C.H. and Lai, J.W. (2004). "Pseudo-Dynamic Test of a Full-Scale CFT/BRB Frame: Part 3 - Analysis and

Performance Evaluation." *Proceedings of 13th World Conference on Earthquake Engineering*, Vancouver, Canada. Paper No. 2173.

Lin, M.L., Tsai, K.C., Hsiao, P.C. and Tsai, C.Y., "Compressive behavior of buckling restrained brace gusset connections", First Conference on Advanced in Experimental Structural Engineering (AESE), Nagoya, Japan, 2005.

Mahin, S. A. and Lin, J. (1983). *Construction of Inelastic Response Spectra for Single-Degree-of-Freedom Systems : Computer Program and Applications* (Report No. UCB/EERC-83/17), Earthquake Engineering Research Center, University of California.

Shome, N., Cornell, C. A., Bazzurro, P. and Carballo, J. E. (1998). "Earthquake, records, and nonlinear responses." Earthquake Spectra, Vol.14, No.3, 469-497.

Tsai. C. Y., Lin, M. L., and Tsai, K. C. (2005) "Design of a full scale two-story steel buckling restrained braced substructure for 3D hybrid tests." *Proceeding, The 3rd Annual KKN Student Seminar on Civil Engineering Research*, Cheju-island, Korea.

Tsai, K.C., and Lin, B.Z. (2003a). *User Manual for the Platform and Visualization of Inelastic Structural Analysis of 3D Systems PISA3D and VISA3D* (Report No. CEER/R92-04), Center for Earthquake Engineering Research, National Taiwan University.

Tsai, K.C. and Lin, S.L, (2003b). *A Study of All Metal and Detachable Buckling Restrained Braces* (Report No. CEER/R92-03), Center for Earthquake Engineering Research, National Taiwan University.

Tsai, K.C., Weng, Y.T., Lin, S.L., and Goel, subhash. (2004). "Pseudo-Dynamic Test of a Full-Scale CFT/BRB Frame: Part 1 - Performance Based Specimen Design." *Proceedings of 13th World Conference on Earthquake Engineering,* Vancouver, B.C., Canada, Paper No. 750.

Tsai, K.C., Hwang, Y.C., Weng, C.S, Shirai, T, and Nakamura, H. (2002). "Experimental Tests of Large Scale Buckling Restrained Braces and Frames." *Proceedings, Passive Control Symposium 2002*, Tokyo Institute of Technology, Tokyo.

Thornton, W.A. (1984). "Bracing Connections for Heavy Construction." *Engineering Journal of AISC*, Vol.21, No.3, pp. 139~148.

Uang, C.M., Nakashima, M. and Tsai, K.C. (2004). "Research and Applications of Buckling Restrained Braced Frames." *International Journal of Steel Structures*, 4/2004.

Wang. K. J., Wang, S. J., Cheng, W. C.,Yang, Y. S. and Tsai, K. C. (2005) "A platform for networked collaborative structural experiments." *the First Conference on Advanced in Experimental Structural Engineering (AESE)*, Nagoya, Japan, 2005.

Whitmore, R.E. (1952). *Experimental Investigation of Stresses in Gusset Plates*, Bulletin No.16, Engineering Experiment Station, University of Tennessee.

Weng, Y. T., Lin, J. L., Tsai, C. Y., and Tsai, K. C. (2005). "Analytical assessment of a 2-story BRBF for full-scale 3D sub-structural pseudo-dynamic testing." *the First Conference on Advanced in Experimental Structural Engineering (AESE)*, Nagoya, Japan.

TABLE 1. Capacity check of gusset plates

		Gusset Plate (kN)			BRB (kN)	
		$P_{y\ Gusset}$	P_{cr} (K=2.0)	P_{cr} (K=0.65)	$P_{y\ Brace}$	$P_{\max}$
1F	Top	2287	842	7975	1558	1713
	Bottom	2287	1367	12939	1558	1713
3F	Top	1397	603	5709	686	755
	Bottom	1397	743	7036	686	755

TABLE 2. Material test results

		Positions of Sampling		f_y (MPa)	f_u (MPa)
A572 Gr.50	2FL	BRB2	core steel	367.9	523.9
	1FL	BRB1	core steel	371.8	512.1

TABLE 3. Computation of story ductility and system ductility

Story	α_{ci}	Story Ductility					
		10/50			2/50		
		θ_{yi}	θ_{mi}	μ_i	θ_{yi}	θ_{mi}	μ_i
		unit : 1/1000 rad			unit : 1/1000 rad		
2F	0.70	3.49	20	5.73	3.49	25	7.16
1F	0.60	3.93	20	5.08	3.93	25	6.35
Average		3.71	20	5.39	3.71	25	6.74

TABLE 4. The member sizes and properties of BRB

	α_{ci}	A_c (mm^2)	A_t (mm^2)	A_j (mm^2)	L_c (mm)	L_t (mm)	L_j (mm)	L_{wp} (mm)	γ
BRB1	0.6	5000	8100	11200	6201	520	2081	8802	1.18
BRB2	0.7	3300	6226	9152	5396	450	3101	8947	1.33

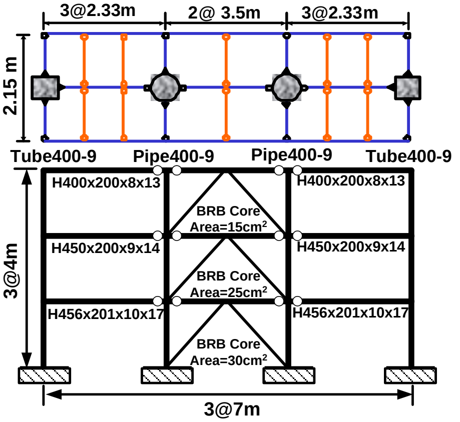

(a)

(b)

Figure 1. (a) *Plan and elevation of the full-scale CFT/BRB composite frame*
(b) *Photo of the CFT/BRB frame specimen*

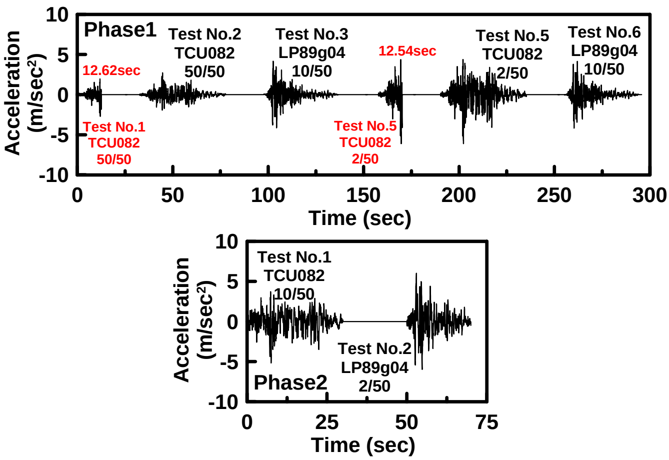

Figure 2. Ground acceleration time history in PDTs

(a)

(b)

Figure 3. (a) *Out-of-plane buckling of the gusset plate* (b) *Gusset plate after adding stiffeners*

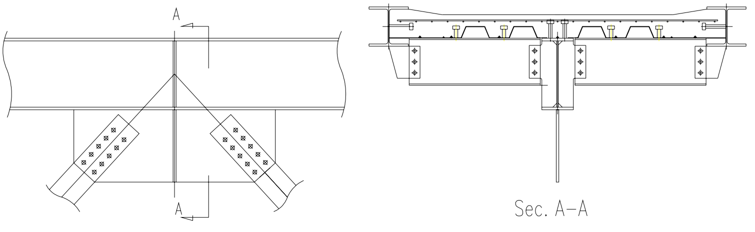

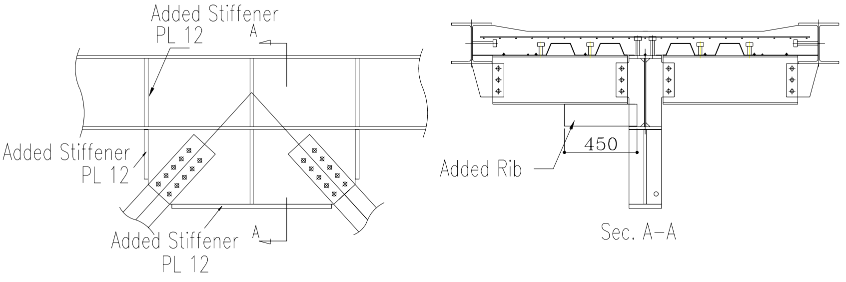

Figure 4. (top two) Original design of the gusset plate (bottom 2) Details of added stiffeners

Figure 5. Buckling of the gusset at the brace to column joint after Phase-1 tests

Figure 6. Added stiffeners at the free edges of the gusset at the brace to column joint before Phase-2 test

S

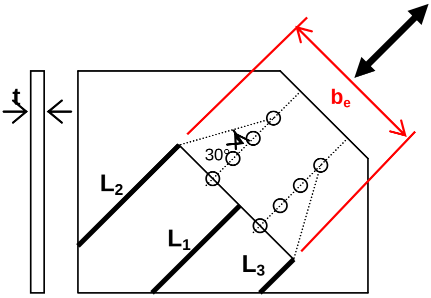

Figure 7. Whitmore's and Thornton's design methodologies

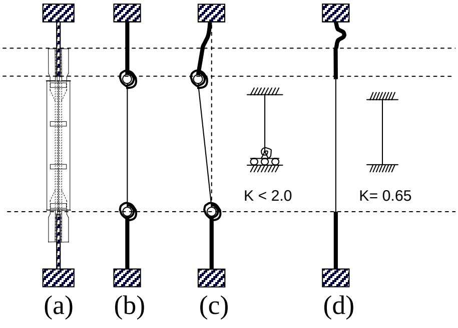

Figure 8. Brace boundary conditions and buckling modes

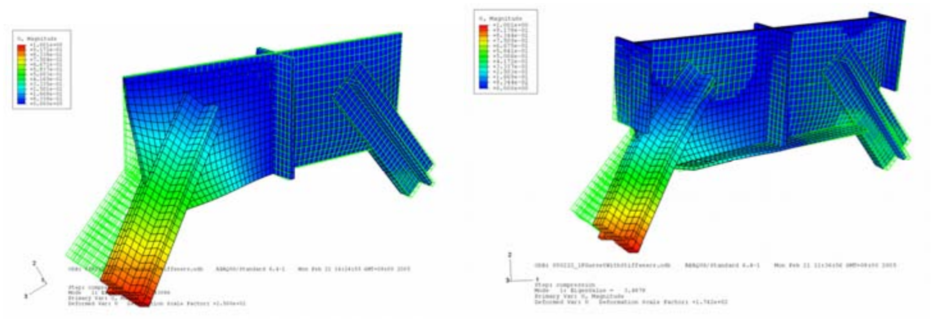

a) b)

Figure 9. (a) *FE Model of un-stiffened gusset plate*
(b) *FE Model of stiffened gusset plate*

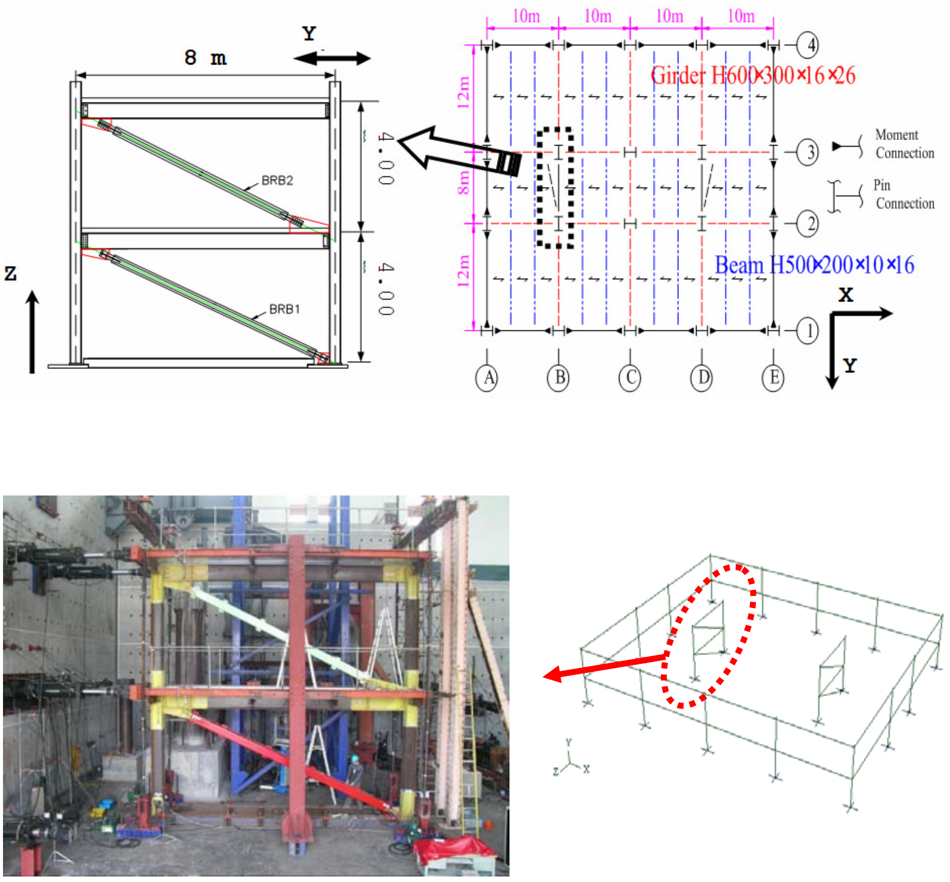

Figure 10. Sub-structural BRBF elevation and floor framing plan of the prototype 3D steel frame

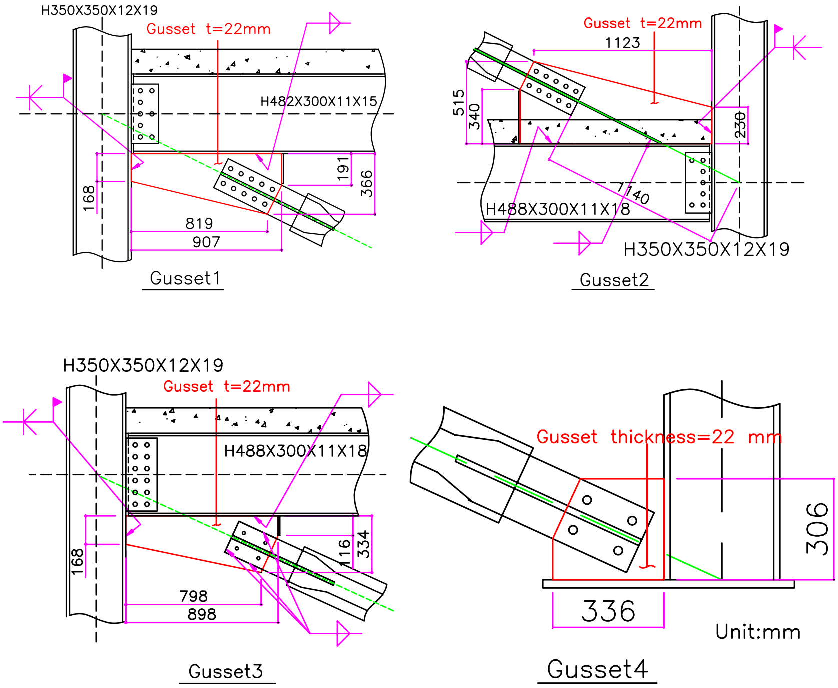

Figure 11. Details at the gusset plate connections

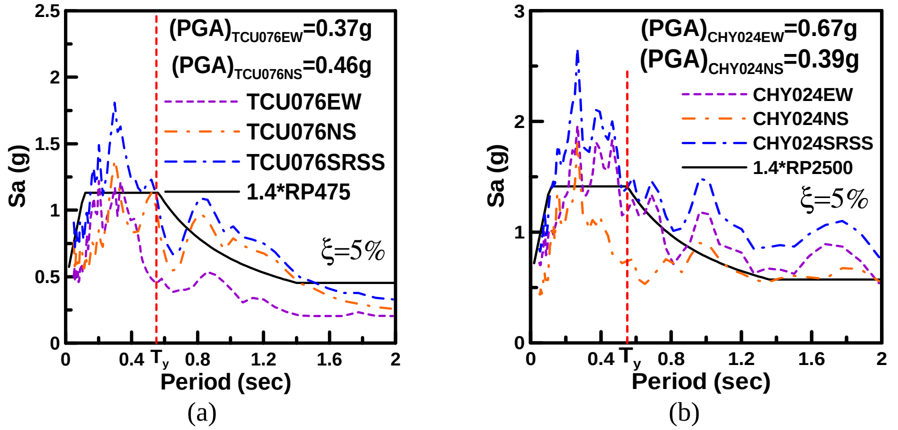

Figure 12 Design acceleration spectra (a)10/50 (b)2/50 hazard level in Phase 1 PDTs

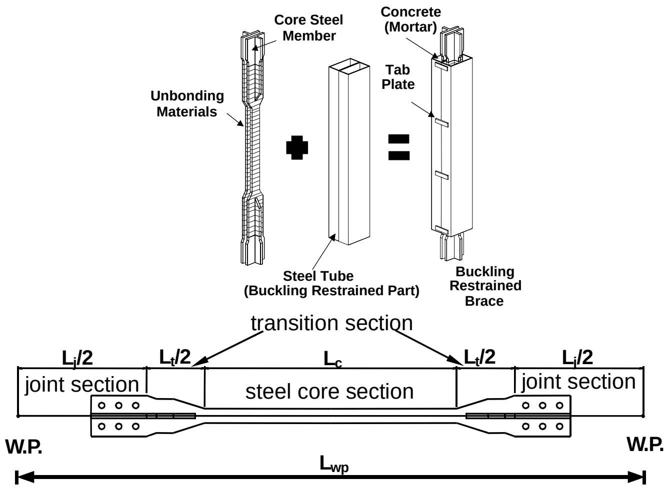

Figure 13. Profiles of core steel in the BRB

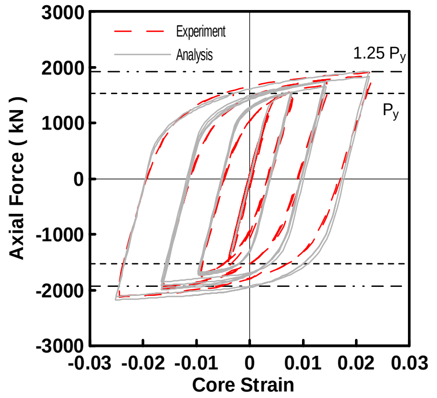

Fig 14. Force versus core strain relationship of BRB using A572 Gr.50 steel

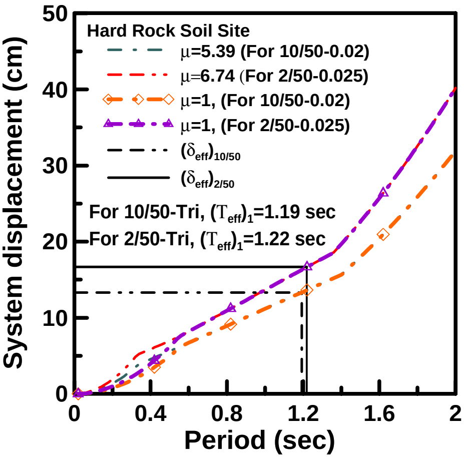

Figure 15. Inelastic design displacement spectra

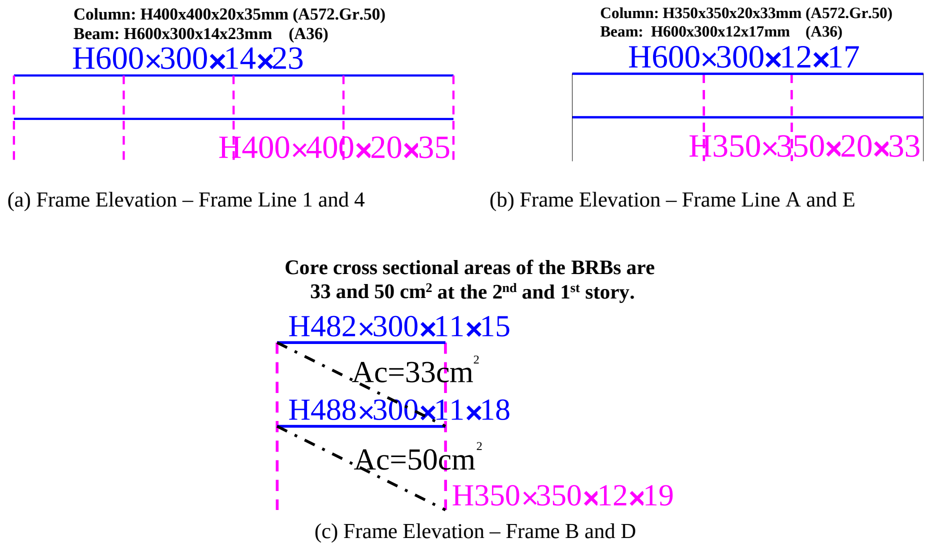

Figure 16. Beam and column sizes in the MRF and BRBF

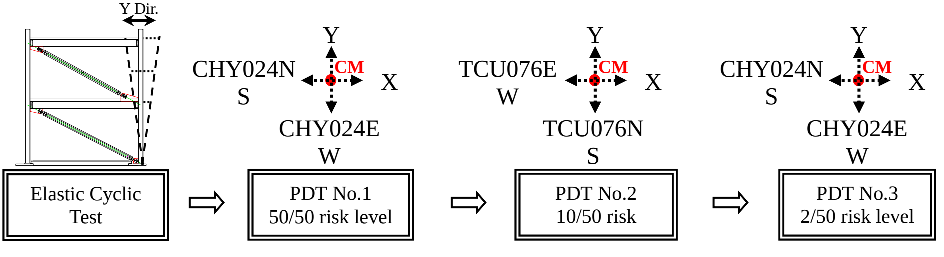

Figure 17. Earthquake scenario for Phase I of test

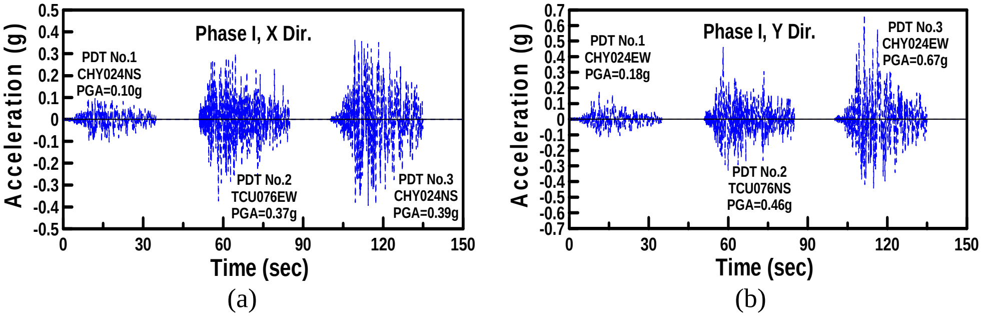

Figure 18. Ground acceleration time history involving three earthquake events for Phase I of test (a) X-Direction (b) Y-Direction

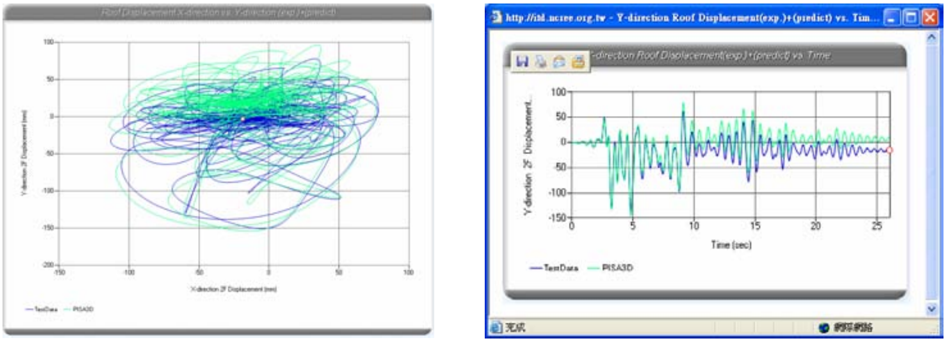

Figure 19. Typical Internet plots of experimental responses and analytical predictions, left: X versus Y roof displacement, right: Y-direction roof displacement time history

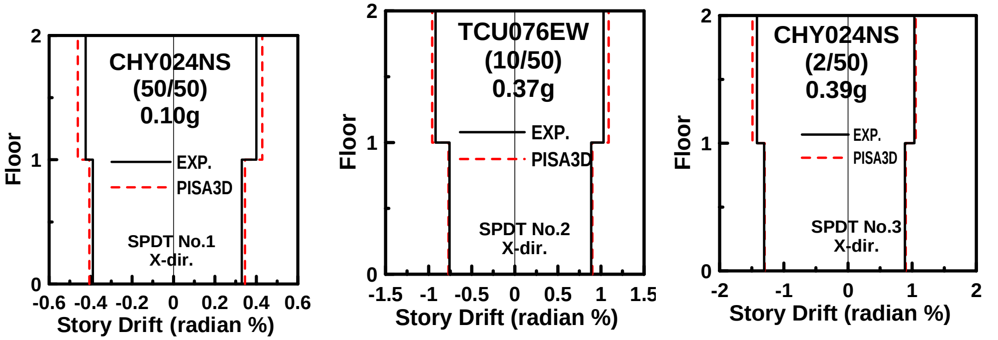

Figure 20. Peak X-direction inter-story drift distribution of BRB frame specimen in three hazard levels

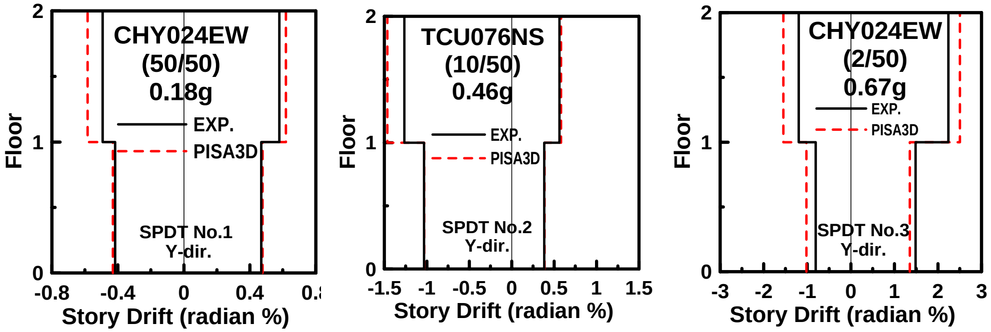

Figure 21. Peak Y-direction inter-story drift distribution of BRB frame specimen in three hazard levels

Roberto Villaverde
Professor Emeritus
University of California, Irvine
Department of Civil Engineering
Irvine, California 92697 USA
E-mail: rvl@eng.uci.edu
Main research interests:
Seismic response of equipment and nonstructural components
Damping and isolating devices for vibration reduction
Dynamic response analysis of nonlinear systems
Collapse analysis of structures

I was fortunate to meet Luis Esteva for the first time back in 1973. I was visiting a former classmate of mine at my alma mater, the National University of Mexico, and was told by this former classmate that Luis was looking for a research assistant. Intrigued by the opportunity to work on research projects, I went to see him and he offered me the position. Soon after that I quit the job I had in an engineering firm at that time and began working for him. We worked together in a couple of interesting projects dealing with seismic risk. A couple of publications came out of this work. It was in this capacity that I had the chance to know Luis well and realize that he is an exceptional individual. He is a man with a great intellectual ability, a vast knowledge of both the theoretical and practical aspects of structural engineering, an unquestioned integrity, an unparalleled generosity, an extraordinary kindness, and, above all, a great sense of humor. It was indeed a privilege and a pleasure to work with him and learn from him. It was also a challenge because it was not always easy to digest the advanced concepts he usually and effortlessly deals with in his research and was not easy to live up to his standards.

Little did I know, however, that crossing paths with Luis Esteva was to change my life radically. For, about a year after I started working for him, he encouraged me and offered me the opportunity to go abroad and study for my Ph. D. Inspired by him and attracted to the idea of pursuing a research career like his, I, needless to say, took the opportunity. The rest, as it is commonly said, is history. Had not he inspired me to become a researcher and had not he unselfishly offered me that encouragement and opportunity, I would not have become what I became and would not be where I am today. I owe to him more than to anybody else what I am professionally. I am grateful, thus, for this opportunity to thank him for the influence he had in my life and for being a role model, a mentor, and a good friend throughout the years.

It is with great pleasure that I join the Engineering Institute of the National University of Mexico and the other symposium participants in honoring Professor Luis Esteva for his magnificent contributions to earthquake engineering and his long and distinguished career.

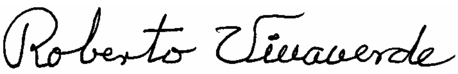

Roberto Villaverde,

CAN WE PREDICT THE SAFETY MARGIN OF STRUCTURES AGAINST AN EARTHQUAKE-INDUCED COLLAPSE?

ABSTRACT

The collapse of engineered buildings during past earthquakes has put into question the adequacy of current seismic provisions to prevent a partial or a total collapse. As is well known, modern seismic provisions rely on a philosophy based on strong column-weak beam designs, story drift limits, and post-elastic energy dissipation to guaranty the survivability of building structures in the event of an unexpectedly severe earthquake. However, this survivability has never been demonstrated analytically, experimentally, or by field studies. On the contrary, the fractures found in modern steel buildings after the 1994 Northridge and 1995 Kobe earthquakes have introduced new doubts into the validity of such an assumption. Past collapses and the unproven adequacy of current design standards to prevent a collapse raise thus questions as to how to determine the collapse safety margin of structures, what is the inherent collapse safety margin in code-designed structures, and how to strengthen structures to effectively augment such margin. It is the purpose of this paper to review the methods that are available to assess the collapse capacity of structures under earthquake ground motions, point out the limitations of these methods, describe past experimental work in which specimens are tested to collapse, and identify what is needed for an accurate evaluation of the collapse capacities of structures and the safety margin against such a collapse. It is contended that (a) there are no established methods to estimate the collapse capacity of structures and the corresponding safety margin; (b) it is not known if currently available collapse assessment methods can reliably predict the collapse capacity of structures; and (c) it is not known what is the inherent safety margin against collapse of code-designed structures. It is also contended that there is a need for experiments with realistic full-scale specimens in which the specimens are tested all the way to collapse as well as studies to evaluate the intrinsic safety margin in current seismic provisions against a structural collapse.

Introduction

Buildings have partially or totally collapsed during many of the earthquakes that have occurred worldwide in the last two decades. Significant building collapses occurred during the earthquakes in Valparaiso, Chile, in 1985 (Wyllie *et al*. 1986; Leiva and Wiegand 1996); Mexico City in 1985 (Osteraas and Krawinkler 1988; Villaverde 1991); Armenia in 1988 (Wyllie and Filson 1989); Luzon, Philippines, in 1990 (Schiff 1991); Guam in 1993 (Comartin 1995); Northridge, California, in 1994 (Hall 1994); Kobe, Japan, in 1985 (Comartin *et al*. 1995; Nakashima *et al*. 1998); Kocaeli, Turkey, in 1999 (Youd *et al*. 2000); Chi-Chi, Taiwan, in 1999 (Jain *et al* 2002; Huang and

Skokan 2002); and Bhuj, India in 2001 (Uzarski and Arnold 2001). Many of these collapses occurred in older buildings designed with what is nowadays considered inadequate design standards. Others have been attributed to shoddy design and construction practices, which undoubtedly was the case in many of them. Several of the collapses, however, took place in buildings that were designed and constructed in accordance with modern seismic design principles (see Fig. 1). A most dramatic example is the 22-story steel frame tower of the Pino Suarez complex in Mexico City, which totally collapsed during the 1985 earthquake there (Osteraas and Krawinkler 1988; Ger *et al* 1993). Therefore, as demonstrated by the fractures observed in the welded connections of modern steel buildings during the 1994 Northridge earthquake (Bertero *et al*. 1994) and the 1995 Hyogoken-Nanbu earthquake (Nakashima *et al*. 1998), it is possible that many of the observed collapses have been the result of deficiencies in our knowledge of the regional seismic hazard, the behavior of structural materials under dynamic loads, and the post-elastic behavior of structural systems.


(a)


(b)


(c)

Figure 1. Collapse of modern multi-story buildings during the (a) 1985 Mexico City earthquake; (b) 1995 Kobe, Japan, earthquake; and (c) 1999 Chi-Chi, Taiwan, earthquake

The collapses observed during past earthquakes have raised many questions regarding the adequacy of current seismic provisions to prevent a partial or total collapse. As is well known, modern seismic provisions rely on a philosophy based on strong column-weak beam designs, story drift limits, and post-elastic energy dissipation to guaranty the survivability of building structures in the event of an unexpectedly severe earthquake. However, this survivability has never been demonstrated analytically, experimentally, or by field studies. In fact, some investigators have put into question the validity of such an assumption. For example, Jennings and Husid

(1968) note that if repeated excursions into the inelastic range of deformation of a structure occur in response to ground shaking, then the accumulated permanent deformations in the structure may render gravity forces the dominant forces and make the structure collapse by lateral instability. This effect, however, is not properly considered in modern design provisions. As noted by Bernal (1987), code provisions account for the P-Δ effect of gravity loads in terms of an inadequate extrapolation of results pertaining to static elastic behavior. In his study of the instability of buildings subjected to earthquakes, Bernal (1992) also notes that the safety of a structure against inelastic dynamic instability cannot be ensured by simply limiting the maximum elastic story drifts of the structure, a finding that has been recently confirmed by Williamson (2003). Similarly, Challa and Hall (1994), in their investigation of the collapse capacity of a 20-story steel frame, observe significant plastic hinging in the structure's columns and a likely collapse of the structure under a severe earthquake ground motion. This despite the fact that, as required by current code provisions, the flexural strength of its columns exceeds that of its beams at all joints. Interestingly enough, that observation has been recently corroborated by Medina and Krawinkler (2005). For, in a study to evaluate the strength demands of a large number of regular moment-resistant frames under different ground motions, they find that the potential for the formation of plastic hinges in columns is high for regular frames designed according to the strong column-weak beam requirements of recent code provisions. In study similar to that of Challa and Hall, Martin and Villaverde (1996) find that a two-story, two-bay frame structure collapses under a moderately strong ground motion even when the structure meets all the requirements from the 1992 AISC seismic provisions (AISC 1992). Likewise, Roeder *et al*. (1993a 1993b) observe in a study performed with an eight-story steel frame that the minimum design criteria required by the 1988 Uniform Building Code (ICBO 1988) are not enough to ensure that the inelastic story drifts of the structure are always below the maximum values considered in its design. It is clear, thus, that structures designed in accordance with modern code provisions may be susceptible to a total or partial collapse if excited by a sufficiently strong earthquake.

The collapses of modern structures during past earthquakes and the inadequacy of current design standards to prevent these collapses brings thus the question as to what is the actual safety margin of structures against an earthquake-induced collapse, a question that has acquired a new importance as a result of the desire of the profession to move towards performance-based designs. As is well known, collapse prevention is one of objectives of a performance-based design, and one of its promises is the assurance of an adequate safety margin against collapse under the expected maximum seismic load. Currently, however, as pointed out by several investigators (Hamburger 1997; Astaneh *et a*l. 1998; Li and Jirsa 1998; Bernal 1998, Griffith *et al*. 2002; Esteva 2002), there are no established methods (other than the collective judgment of code writers) to calculate such a safety margin. Even more, it is not known if the available analytical tools are adequate enough to evaluate it in a reliable way since the process of collapse involves large deformations, significant second-order effects, and a complex material degradation due to localized phenomena such as cracking, local buckling and yielding. What is worse, it appears that not even an established criterion exists to identify when and how a structure collapses under the effect of dynamic loads. The reason is that reaching an unstable condition (i.e., a singular effective stiffness matrix) is not sufficient to infer the collapse of a structure under dynamic loads as unloading right after reaching such an unstable condition may restore the stability of the structure (Araki and Hjelmstad 2000).

The purpose of this paper is to review the methods that are currently available to assess the collapse capacities of structures under earthquake ground motions, point out the limitations of these methods, describe past experimental work in which specimens are tested to collapse, and identify what are the needs and challenges for an accurate evaluation of the aforementioned collapse capacities and the safety margin against such a collapse.

Collapse Assessment Methods

Single-degree-of-freedom Models

Several methods have been suggested or used in research studies in which structures are modeled as single-degree-of-freedom systems to assess their collapse capacity. Takizawa and Jennings (1980) employ an equivalent single-degree-of-freedom system that accounts for the destabilizing effect of gravity forces to examine the ultimate capacity of ductile reinforced concrete frame structures under the combined action of strong ground shaking and gravity loads. The single-degree-of-freedom idealization results from linking the actual structure to an auxiliary rigid frame that makes the structure follow a specified deformation pattern. From the results of their investigation, they find that: (a) short-duration motions have a low destructive capability, even when they have a high peak acceleration; (b) stiff structures have a much larger safety margin between damage and collapse than flexible structures; (c) the conventional single-parameter measures used to characterize ground motions are unsatisfactory to describe their destructive potential; and (d) serious damage and collapse are significantly influenced by ground motion duration. In a similar study, Bernal (1987) proposes an empirical formula in terms of a ductility factor and a stability coefficient that characterizes the influence of gravity loads to compute an amplification factor that accounts for P-Δ effects in inelastic structures subjected to earthquakes. The formula is derived from amplification spectra generated by dividing the inelastic acceleration response spectrum ordinates obtained when gravity effects are included by those determined when these effects are not considered. An elastoplastic single-degree-of-freedom model and an ensemble of four recorded earthquake ground motions are used in the generation of these amplification spectra. Based on the results from his study, he shows that the amplification formulas recommended by seismic codes are unconservative, and that they are increasingly so as the design ductility factor increases. Bernal (1992) also develops a simplified method to check the safety against dynamic instability of two-dimensional buildings. The method is based on the reduction of a multistory structure to an equivalent single-degree-of-freedom system and the derivation of statistical expressions to correlate the minimum base shear coefficient needed to prevent instability with some key structural and ground motion parameters. An ensemble of 24 earthquake records from firm ground sites is used to obtain these statistical correlations. With this method, the safety margin of a structure is estimated by dividing the actual base shear capacity of the structure by such a statistically determined minimum base shear. From the results of this study, Bernal finds that the safety against dynamic instability strongly depends on the shape of the failure mechanism. For buildings with a regular configuration, he identifies this failure mechanism using a static limit analysis with lateral forces proportional to the structure's story weights. Using an approach similar to the one employed by Bernal in his 1987 study and based on the analysis of bilinear oscillators with different post-elastic to elastic stiffness ratios, MacRae (1994) proposes a method for considering P-Δ effects on oscillators with different hysteretic characteristics. From the results of the aforementioned analysis, MacRae observes that the post-elastic to elastic stiffness ratio is a major parameter that affects the unidirectional accumulation of inelastic deformation in a system and, hence, the system's stability.

More recently, Williamson (2003) uses a simple model that explicitly considers the state of damage in a system to determine the response of a number of single-degree-of-freedom systems under various earthquake ground motions and study the role of damage accumulation and *P*-Δ effects on the response of inelastic systems. The earthquake vertical acceleration is considered explicitly in the analysis of the studied systems. He finds that damage accumulation has a significant effect on the behavior of the analyzed systems. He also finds that *P*-Δ effects are important even for small values of the axial force and may lead to responses that are as much as five times greater than in the case when *P*-Δ effects are ignored. In agreement with the findings from other investigators, he observes, in addition, that a system's response is not affected significantly by the earthquake vertical acceleration. Finally, Adam *et al*. (2004) propose a procedure to consider *P*-Δ effects in multi-degree-of-freedom structures through the use of an equivalent single-degree-of-freedom system with properties defined based on the results from a pushover analysis. The underlying assumption in this procedure is that the post-yielding global stiffness obtained from the pushover analysis characterizes the global or local mechanism involved when the actual structure approaches dynamic instability. With it, the collapse capacity of a structure is determined through a series of dynamic analyses of the equivalent single-degree-of-freedom system under progressively increasing ground motion intensities. The basic difference between this procedure and that suggested by Bernal (1992) lies in the way the properties of the equivalent system are determined. To assess the accuracy of the procedure, Adam *et al*. compare the collapse capacities of two single-bay, non-deteriorating, multi-degree-of-freedom frame structures obtained using the proposed procedure to those determined analyzing the actual structures. An ensemble of 40 ground motions is used in this comparative analysis. They conclude that the global *P*-Δ effects of non-deteriorating structures may be predicted with good accuracy with the proposed procedure and that in most cases the predictions err on the conservative side.

Finite Element Models

Several investigators have used finite element models to assess the collapse capacities of building structures. Challa and Hall (1994) investigate the nonlinear response and collapse of moment-resisting plane steel frames under the effect of severe earthquake ground motions. For this purpose, they analyze employing a step-by-step integration procedure a 20-story frame designed to meet the Zone 4 requirements of the 1991 Uniform Building Code (ICBO 1991) under ground motions of two types. One is of the oscillatory type with long period components, and the other is of the impulsive type. Fiber elements are used to model the members of the frame and shear panel elements to model its beam-column joints. In addition, they consider the geometric stiffnesses of the elements and realistic force-deformation relationships for both the element fibers and the panel zones. They also update the deformed configuration of the structure at each time step in the step-by-step analysis of the structure. As such, strain-hardening, axial-flexural yield interaction, residual stresses, spread of yielding, P-Δ effects, and column buckling are accounted for in the analysis. However, stiffness and strength degradation is neglected, as is the effect of torsion and multi-component ground motions. They find that the frame collapses under the oscillatory ground motion as a result of the formation of plastic hinges in the frame's columns and a collapse mechanism involving its lower stories.

In like fashion, Ger *et al.* (1993) investigate the factors that led to the collapse of a 22-story steel building during the 1985 earthquake in Mexico City. To this end, they establish first realistic nonlinear hysteretic constitutive relationships for the individual members of the structure, which consisted of open-web girders, welded box columns, and H-shape diagonal braces. Then, using a three-dimensional finite-element model that includes the geometric stiffness of its structural elements, they analyze the building under the three components of the ground motion recorded at a station near the building's site during the earthquake. From this analysis, they observe that most of the building's longitudinal girders experienced severe inelastic behavior, leading to ductility demands that exceeded the ductility capacities considered in their design. Because of the failed girders, a redistribution of forces takes place and local buckling occurs in the columns of floors 2 to 4. This local buckling, in turn, makes the affected columns loose their load-carrying capacity. In consequence, the building tilts and rotates, experiences significant drifts and P-Δ effects, and eventually collapses. Their results are in agreement with field observations of an almost identical building adjacent to the collapsed one, which was heavily damaged and was at the verge of collapse during the same earthquake. Perhaps a significant conclusion from this study is that it is possible to predict the collapse of a building using simplified models, provided realistic force-deformation relationships are adopted.

In a somewhat different study, Martin and Villaverde (1996) develop a methodology to (a) determine analytically if a structure excited by a given earthquake ground motion will experience a partial or total collapse, and (b) identify the structural elements that fail first and lead in consequence to the collapse of the structure. The method is formulated on the basis of a step-by-step, nonlinear, finite element analysis and the examination at each integration step of the updated effective stiffness matrix of the structure. A partial or total collapse is detected when one or more of the pivots of the triangularized effective stiffness matrix become zero or negative. The part of the structure where the collapse is initiated (i.e., region of local instabilities) is located by identifying the structural nodes that correspond to the found zero or negative pivots. Martin and Villaverde (1996) apply their methodology to a steel cantilever beam and a two-story, three-dimensional steel moment-resisting frame to validate the adequacy of the method.

More recently, Mehanny and Deierlein (2001) propose a methodology to evaluate the likelihood of a structural collapse under earthquake effects using a component damage index developed by them. The methodology involves an inelastic time-history analysis with a finite-element model, the calculation of the aforementioned damage index for each of the components of the structure in accordance with the results of the analysis, the modification of the analytical model according to the calculated damage indices and the corresponding local damage effects, and a second-order analysis of this modified model under gravity loads alone. The ratio of the gravity load under which the structure reaches its global stability limit to the actual gravity load defines a global stability index that correlates collapse capacity to ground motion intensity.

Incremental Dynamic Analyses

Incremental dynamic analyses have recently emerged as a powerful means to study the overall behavior of structures, from their elastic response through yielding and nonlinear response and all the way to global dynamic instability (FEMA 2000). An incremental dynamic analysis involves performing a series of nonlinear dynamic analyses in which the intensity of the ground motion selected for the collapse investigation is incrementally increased until the global collapse capacity of the structure is reached. It also involves plotting a measure of the ground motion intensity (i.e., spectral acceleration at the fundamental natural period of the structure) against a response parameter (demand measure) such as peak story drift ratio. The global collapse capacity is considered reached when the curve in this plot becomes flat. That is, when a small increase in the ground motion intensity generates a large increase in the structural response. As different ground motions lead to different intensity versus response plots, the analysis is repeated under different ground motions to obtain meaningful statistical averages. Incremental dynamic analyses have been proposed as early as 1997 (Bertero 1980) and have been studied extensively lately by several investigators.

Vamvatsikos and Cornell (2002), for example, describe the method in detail, determine intensity–response curves for several structures (a 20-story moment-resisting steel frame, a 5-story braced steel frame, and a 3-story moment-resisting frame with fracturing connections), examine the properties of these response-intensity curves, and propose techniques to perform efficiently an incremental dynamic analysis and summarize the information obtained from the different curves that different ground motions produce. They observe that incremental dynamic analyses are a valuable tool that simultaneously addresses the seismic demands on structures and their global capacities. They also call attention to some unusual properties of the response-intensity curves such as non-monotonic behavior, discontinuities, multiple collapse capacities, and their extreme variability from ground motion to ground motion. Recognizing that a complete incremental dynamic analysis requires an intense computational effort, Vamvatsikos and Cornell (2004) propose a practical method to perform it efficiently, and show, through a detailed example with a nine-story steel moment-resisting frame, how to apply it, how to interpret the results, and how to use these results within the framework of performance-based earthquake engineering. By exploiting the relationship between an incremental dynamic analysis and a static pushover analysis, they also develop (Vamvatsikos and Cornell 2005) a simplified method to estimate the seismic demands and collapse capacities of multi-degree-of-freedom structures through the use of an equivalent single-degree-of-freedom system.

Along the same lines, Ibarra and Krawinkler (2004) propose a methodology to evaluate the global collapse capacity of deteriorating frame structures under earthquake ground motions. The methodology is based on the use of a relative intensity measure, which they define as $S_a(T_1)/\ g/\gamma$, where $S_a(T_1)$ denotes the 5%-damping spectral acceleration at T_1, the fundamental period of the structure; g is the acceleration due to gravity; and γ is a base shear coefficient equal to V_y/W, where V_y is the yield base shear without P-Δ effects and W is the weight of the structure. For structures with no overstrength, this intensity measure is equivalent to the reduction factor used in building codes for the analysis of yielding structures. The methodology is also based on the use of deteriorating hysteretic models to represent the cyclic behavior of the structural components under large inelastic deformations. To evaluate collapse capacity, they increase the intensity measure until the intensity measure versus normalized maximum roof drift curve becomes flat. The relative intensity at which this curve becomes flat is then considered to be the collapse capacity of the structure. The evaluation is made using a probabilistic format to consider the uncertainties in the frequency content of ground motions and the deterioration characteristics of the structural elements. They use the proposed methodology to (a) conduct a parametric study with typical frame structures and study the influence of several parameters on the collapse capacity of structures; (b) develop collapse fragility curves, and (c) determine mean annual frequency curves. The structures considered in the parametric study are stiff and flexible single-bay frames with 3, 6, 9,12,15 and 18 stories with plasticity concentrated at the beam ends and the base of the columns, i.e., plastic hinges are permitted to form only at the beam ends and at the base of the columns. From the parametric study, they find that the two parameters that most influence the collapse of a structure are the slope of the post-yield softening branch in the moment-rotation relationship of the yielding members and the displacement at which this softening begins. In contrast, they also find that cyclic deterioration is an important but not a dominant factor in the collapse of structures.

In a similar study, Ayoub *et al.* (2004) investigate the effect of stiffness and strength degradation on the seismic collapse capacity of structures. To this end, they perform an incremental dynamic analysis of a single-degree-of-freedom structure with a natural period of one second considering three degrading constitutive models that explicitly account for the possibility of collapse. They also develop collapse fragility curves for such a system. The constitutive models take into account strength softening (branch with negative stiffness) and degradation of strength and stiffness under cyclic loading. Collapse occurs when the system looses its full strength. The three constitutive models considered are: a bilinear model, a modified Clough model, and a pinching model. An energy-based criterion is used to define strength softening and stiffness and strength degradation. The study is carried out employing an ensemble of 80 earthquake ground motions and considering different levels of degradation. They find that the collapse rate of systems with low degradation is similar to the one for systems with moderate degradation. In contrast, systems with severe degradation fail at a much faster rate.

Finally, Lee and Foutch (2004) evaluate the performance of 20 steel frame buildings designed according to the recommendations of the 1997 NEHRP provisions (FEMA 1998) and considering pre-qualified post-Northridge beam-column connections. To this end, the buildings are subjected to a nonlinear time-history analysis under an ensemble of 20 earthquake ground motions. For a performance objective of collapse prevention, they scale the ground motions so as to have intensities that have a 2% probability of being exceeded in 50 years. The analytical models used in the analysis account for the ductility of beam-column joints, the panel zone deformations, and the influence of interior gravity frames. The behavior of the beam-column joints is characterized by a gradual strength degradation after a rotation of 0.03 radians. To evaluate the performance of the building for the aforementioned collapse prevention objective, they compare the maximum story drift demands against the drift capacities of the buildings. Local and global drift capacities are considered in this comparison. The local drift capacities are the maximum drift angles the beam-column joints can sustain before losing their gravity load carrying ability. Based on the results from full-scale experiments, they consider a local drift capacity of 0.07 radians. The global drift capacities are determined by performing an incremental dynamic analysis for each of the buildings and plotting the corresponding maximum story drift ratio versus spectral acceleration curves. A building's global drift capacity is considered to be the maximum story drift ratio at which the maximum story drift ratio versus spectral acceleration curve becomes flat, or, alternatively, the maximum story drift ratio at which this curve reaches a slope equal to 20 percent of the slope in the elastic region of the curve. However, if this slope is not reached before a story drift ratio of 0.10 is attained, it is assumed that the global drift capacity is equal to 0.10. Based on the calculated drift demands and assumed local and global capacities, Lee and Foutch conclude that all the buildings considered in the study satisfy the collapse prevention performance objective.

Shake Table Collapse Experiments

Only a few experiments have been conducted in which structural models are tested all the way to collapse. Kato *et al*. (1973) test simple models to collapse, or near collapse, on a shaking table and compare their response with the response obtained analytically considering strain hardening and P-Δ effects. The models are formed with 15-cm high *H* steel columns fixed at both ends and a concentrated mass on top of the columns. They conclude that except for some softening of the hysteresis loops due to Bauschinger effect, the tests results are well predicted by the analytical model. Vian and Bruneau (2003) also test to collapse on a shaking table 15 simple specimens, each built with four steel columns connected to a rigid mass. The column heights range from 91.7 mm to 549.5 mm and are designed to have a slenderness ratio of 100, 150 or 200. The tests are conducted under the N-S component of the 1940 El Centro ground acceleration record, progressively increasing the intensity of the motion until the specimens collapse. From their test results, they observe that the inelastic behavior of the specimens have a high dependence on a stability factor that is used to measure the influence of gravity loads. Specimens with a stability factor of less than 0.1 are able to withstand the ground motions with larger ductility demands and accumulated drifts than those with a stability factor of more than 0.1. They also compare their experimental results against those obtained analytically using a simple hysteretic model. They find that the analytical results do not provide a good match to their experimental data. On a shake table too, Kanvinde (2003) tests to collapse, or near collapse, nineteen simple structures with a story height of 10 inches, a bay width of 24 inches, and a floor plan of 12 by 24 inches. The structures are built with four steel flat columns connected to a rigid 320-lb. steel mass. They are tested under two of the ground motions recorded during the 1994 Northridge earthquake: Obregon Park and Pacoima Dam. The specimens collapse after plastic hinges are formed at the top and bottom of the columns and a story mechanism is formed. Kanvinde also conducts a nonlinear, large displacement, dynamic analysis of the specimens to evaluate the ability of analytical tools to predict their response under very large displacements. For this purpose, he uses the OpenSEES program being developed by the Pacific Earthquake Engineering Research Center (OpenSEES 2005). The hysteretic model used in the analyses is the Giufré-Menegotto-Pinto model, which is characterized by a yield envelope and a nonlinear hardening exponential law. The parameters for this model are determined from monotonic and cyclic tests of the columns used to build the experimental models. By comparing the displacement time histories obtained analytically and experimentally, Kanvinde finds that the analytical simulations predict with an average error of about 15 percent the results from the shake table tests.

Needs and Challenges

It may be inferred from the foregoing literature review that the process to assess the safety margin of a structure against an earthquake-induced collapse is complicated and unreliable. The reason is that many factors are involved and it is difficult to account for many of these factors accurately. Factors that may significantly affect the collapse safety margin of a structure are: (a) the characteristics of the ground motion (intensity, frequency content, and duration) exciting the structure; (b) the dynamic properties of the structure; (c) the geometry of the structure; (d) the post-elastic and post-buckling behavior of its components; (e) the strength and stiffness of these components; (f) the degradation of this strength and stiffness after several loading cycles; (g) the interaction between vertical loads and lateral drifts; (h) the interaction of the structure with its non-structural components; and (i) residual stresses and initial imperfections. Besides, the evaluation of this safety margin is complicated by the fact that it varies significantly from one ground motion to another and the fact that the characteristics of the ground motions that will affect the structure during its lifetime are largely unknown. In principle, therefore, an analytical prediction of such a safety margin is only possible by means of a step-by-step dynamic finite element analysis in which (1) the equations of equilibrium are established on the basis of the deformed configuration of the structure; (2) this deformed configuration is updated at each step; (3) non-linear large-deformation elements are used; (4) the mesh considered is sufficiently fine to accurately account for the spread of plasticity, local and global instabilities, and crack formation; (5) a characteristic response of the structure is monitored to identify a rapid increase in its magnitude; and (6) the analysis is repeated under a sufficiently large number of different ground motions with different characteristics to obtain statistically meaningful averages.

It may also be inferred from the presented literature review that the currently available methods to assess the collapse capacity of a structure are not completely satisfactory. Those based on single-degree-of-freedom models, although simple, are unreliable because, as pointed out by Bernal (1992, 1998), the collapse capacity of a structure strongly depends on the assumed shape of the failure mechanism and this shape cannot be predicted a priori, not even with the help of a pushover analysis. The methods based on finite element models seem to be fine except that to be reliable it is necessary to account properly for the many factors listed above. This renders them computationally demanding and therefore impractical. Likewise, the methods based on an incremental dynamic analysis, besides being also computationally demanding, they are also unreliable because they lead to multiple collapse capacities and depend on the parameter selected to measure the ground motion intensity.

Lastly, it may be observed that (a) the reliability of collapse assessment methods may be affected by the accuracy and convergence problems that are likely to occur due to the high levels of nonlinear behavior and large displacements a structure may experience when it is near collapse; (b) the adequacy of the available collapse assessment methods has not been verified through experimental or field studies; (c) only a few shake table experiments have been carried out to study the collapse of structures and verify the adequacy of collapse assessment methods; (d) realistic models of real structures have never been tested to collapse; (e) little information is currently available about the real capacity of structures to resist a collapse; and (f) little is know about the inherent safety margin against collapse in code-designed structures.

It is clear, thus, that further research is needed before the collapse capacities of structures and the associated safety margin against collapse may be evaluated with confidence. There is a need for experiments with realistic full-scale specimens in which the specimens are tested all the way to collapse. These experiments are needed to (a) advance the understanding of the conditions that lead to a collapse in real, full-scale, three-dimensional structures; (b) evaluate the capability of existing numerical analysis techniques to predict building behavior at the levels of deformation involved when a structure is near collapse; and (c) assess the adequacy of current collapse assessment methods. There is also a need to evaluate the inherent safety margin in current seismic provisions against a structural collapse and establish whether or not this safety margin is adequate enough.

The great challenge for the profession is the development of simplified techniques to estimate in a reliable way the aforementioned collapse capacities and safety margin. These techniques are urgently needed to facilitate (a) the scrutinization of present and future code provisions in regard to their ability to provide an adequate safety margin against collapse; (b) the development of design procedures that explicitly would make structures resist a collapse with a specified safety margin; and (c) the identification and strengthening of weak structural components that may compromise the collapse capacity of a structure. Undoubtedly, the availability of such techniques could help improve the seismic performance of building structures and minimize the number of catastrophic failures during earthquakes.

References

Adam, C., L. F. Ibarra, and H. Krawinkler (2004). Evaluation of P-delta effects in non-deteriorating MDOF structures from equivalent SDOF systems, Paper No. 3407, *Proceedings of the 13th World Conference on Earthquake Engineering*, Vancouver, Canada.

AISC(1992). *Seismic Provisions for Structural Steel Buildings*, American Institute of Steel Construction, Inc., Chicago, Ill.

Araki, Y. and K. D. Hjelmstad (2000). Criteria for assessing dynamic collapse of elastoplastic structural systems, *Earthquake Engineering and Structural Dynamics*, 29(8), 1177-1198.

Astaneh-Asl A. *et al*. (1998). Stability of damaged steel moment frames in Los Angeles, *Engineering Structures*, 20(4-6), 433-446.

Ayoub, A., C. Mijo, and M. Chenouda (2004). Seismic fragility analysis of degrading structural systems. Paper No. 2617, *Proceedings of the 13th World Conference on Earthquake Engineering*, Vancouver, Canada.

Bernal, D. (1987). Amplification factors for inelastic p-Δ effects in earthquake analysis, *Earthquake Engineering and Structural Dynamics*, 15(5), 635-651.

Bernal, D. (1992). Instability of buildings subjected to earthquakes, *Journal of Structural Engineering, ASCE*, 118(8), 2239-2260.

Bernal, D. (1998). Instability of buildings during seismic response, *Engineering Structures*, 20(4-6), 496-502.

Bertero, V. V., J. C. Anderson, and H. Krawinkler (1994). Performance of Steel Building Structures During the Northridge Earthquake, *Report No. UCB/EERC-94/09*, Earthquake Engineering Research Center, University of California, Berkeley, Calif.

Bertero, V. V. (1980). Strength and deformation capacities of buildings under extreme environments, *Structural Engineering and Structural Mechanics*, A Volume Honoring Edgar P. Popov, K. Pister, Ed., Prentice-Hall, Inc., Englewood Cliffs, N.J.

Challa, V.R.M. and J. F. Hall (1994). Earthquake collapse analysis of steel frames, *Earthquake Engineering and Structural Dynamics*, 23(11), 1199-1218.

Comartin, C. D., Ed. (1995). Guam Earthquake of August 8, 1993 Reconnaissance Report, *Earthquake Spectra*, Supplement B to Volume 11.

Comartin, C. D., M. Greene, and S. K. Tubbesing, Eds. (1995). *The Hyogo-Ken Nanbu Earthquake, January 17, 1995*, Preliminary Reconnaissance Report, Earthquake Engineering Research Institute, Oakland, Calif.

Esteva, L. (2003). Optimum damage-control policies for structural systems under seismic risk conditions, *Proceedings of the 3rd World Conferences on Structural Control*, F. Casciati, Ed., John Wiley & Sons, Ltd., Chichester, England, Vol. 1, pp. 33-46.

FEMA (1998). NEHRP Recommended Provisions for Seismic Regulations for New Buildings and Other Structures: Part I-Provisions, 1997 Edition, Federal Emergency Management Agency, Washington, D.C.

FEMA (2000). Recommended Seismic Design Criteria for New Steel Moment Frame Buildings, Report No. FEMA 350, Federal Emergency Management Agency, Washington, D.C.

Ger, J.F., F.Y. Cheng, and L.W. Lu (1993). Collapse behavior of Pino Suarez Building during 1985 Mexico City earthquake, *Journal of Structural Engineering, ASCE*, 119(3), 852-870.

Griffith, M. C., A. Kawano, and R. F. Warner (2002). Towards a direct collapse-load method of design for concrete frames subjected to severe ground motions, *Earthquake Engineering and Structural Dynamics*, 31(10), 1879-1888.

Hall, J. F., Ed. (1994). *Northridge Earthquake January 17, 1994: Preliminary Reconnaissance Report*, Publication No. 94-01, Earthquake Engineering Research Institute, Oakland, Calif.

Hamburger, R. O. (1997). A framework for performance-based earthquake resistive design, The EERC-CUREE Symposium in Honor of Vitelmo V. Bertero, *UCB/EERC Report 97/05*, pp. 101-108.

Huang S. C. and M. J. Skokan (2002). Collapse of the Tungshing building during the 1999 Chi-Chi earthquake in Taiwan, *Proceedings of the 7th U.S. National Conference on Earthquake Engineering*, Boston, Massachusetts.

Ibarra, L. F. and H. Krawinkler (2004). Global collapse of deteriorating mdof systems, Paper No. 116, *Proceedings of the 13th World Conference on Earthquake Engineering*, Vancouver, Canada.

ICBO (1988). *Uniform Building Code*, International Conference of Building Officials, Whittier, Calif.

ICBO (1991). *Uniform Building Code*, International Conference of Building Officials, Whittier, Calif.

Jain, S. K., W. R. Lettis, C. V. R. Murty, and J. P. Bardet, Eds. (2002). Chi-Chi Taiwan, Earthquake of September 21, 1999, Reconnaissance Report, *Earthquake Spectra*, Supplement A to Volume 18.

Jennings P.C. and R. Husid (1968). Collapse of yielding structures during earthquakes, *Journal of Engineering Mechanics Division, ASCE*, 94(EM5), 1045-1065.

Kanvinde, A. M (2003) Methods to evaluate the dynamic stability of structures—Shake table tests and nonlinear dynamic analyses, Winner EERI Annual Student Paper Competition.

Kato, B., H. Akiyama, H. Suzuki, and Y. Fukuzawa (1973). Dynamic collapse tests of steel structural models, Proceedings of the *5th World Conference on Earthquake Engineering*, Rome, Italy.

Lee, K. and D. A. Foutch (2002). Performance evaluation of new steel frame buildings for seismic loads, *Earthquake Engineering and Structural Dynamics*, 31(3), 653-670.

Leiva G. and W. Wiegand (1996). Analysis of a collapsed building using the displacement seismic design approach, Paper No. 1512, *Proceedings of the 11th World Conference on Earthquake Engineering*, Acapulco, Mexico.

Li, Y. R. and J. O. Jirsa (1998). Nonlinear analyses of an instrumented structure damaged in the 1994 Northridge earthquake, *Earthquake Spectra*, 14(2), 265-283.

MacRae, G. A. (1994). P-Δ effects on single-degree-of-freedom structures in earthquakes, *Earthquake Spectra*, 10(3), 539-568.

Martin S. C. and R. Villaverde (1996). Seismic collapse of steel frame structures, Paper No. 475, *Proceedings of the 11th World Conference on Earthquake Engineering*, Acapulco, Mexico.

Medina, R. A. and H. Krawinkler (2005). Strength design issues relevant for the seismic design of moment-resisting frames, *Earthquake Spectra*, 21(2), 415-439.

Mehanny. S. S. F. and G. G. Deierlein (2001). Seismic damage and collapse assessment of composite moment frames, *Journal of Structural Engineering, ASCE*, 127(9), 1045-1053.

Nakashima, M., K. Inoue, and M. Tada (1998). Classification of damage to steel buildings observed in the 1995 Hyogoken-Nanbu earthquake, *Engineering Structures*, 20(4-6), 271-281.

OpenSEES (2005). *Open System for Earthquake Engineering Simulation*, Pacific Earthquake Engineering Research Center, http://opensees.berkeley.edu.

Osteraas J. and H. Krawinkler (1988). The Mexico earthquake of September 19, 1985 - Behavior of steel buildings, *Earthquake Spectra*, 5(1), 51-88.

Roeder, C. W., S. P. Schneider, and J. E. Carpenter (1993a). Seismic behavior of moment-resisting steel frames: Analytical study, *Journal of Structural Engineering, ASCE*, 119(6), 1867-1884.

Roeder, C. W., S. P. Schneider, and J. E. Carpenter (1993b). Seismic behavior of moment-resisting steel frames: Experimental study, *Journal of Structural Engineering, ASCE*, 119(6), 1885-1902.

Schiff, A. J., Ed. (1991). Philippines Earthquake Reconnaissance Report, *Earthquake Spectra*, Supplement A to Volume 7.

Takizawa H. and P.C. Jennings (1980). Collapse of a model for ductile reinforced concrete frames under extreme earthquake motions, *Earthquake Engineering and Structural Dynamics*, 8, 117-144.

Uzarski, J. and C. Arnold, Tech. Eds. (2001). Bhuj, India, Earthquake of January 26, 2001, Reconnaissance Report, *Earthquake Spectra*, Supplement A to Volume 17.

Vamvatsikos, D. and Cornell, C. A (2002). Incremental dynamic analysis, *Earthquake Engineering and Structural Dynamics*, 31(3), 491-514.

Vamvatsikos, D. and C. A. Cornell (2004). Applied incremental dynamic analysis, *Earthquake Spectra*, 20(2), 523-553.

Vamvatsikos, D. and C. A. Cornell (2005). Direct estimation of seismic demand and capacity of multidegree-of-freedom systems through incremental dynamic analysis of single degree of freedom approximation, *Journal of Structural Engineering, ASCE*, 131(4), 589-599.

Vian D. and M. Bruneau (2003). Tests to Structural Collapse of Single Degree of Freedom Frames Subjected to Earthquake Excitations, *Journal of Structural Engineering, ASCE*, 129(12), 1676-1685.

Villaverde, R. (1991). Explanation for the numerous upper floor collapses during the 1985 Mexico City earthquake, *Earthquake Engineering and Structural Dynamics*, 20(3), 223-241.

Williamson, E. B. (2003). Evaluation of damage and P-Δ effects for systems under earthquake excitation," *Journal of Structural Engineering, ASCE*, 129(8), 1036-1046.

Wyllie, L. A. *et al*., (1986). The Chile Earthquake of March 3, 1985, *Earthquake Spectra*, 2(2).

Wyllie, L. A., Jr., and J. R. Filson, Eds. (1989). Armenia Earthquake Reconnaissance Report, *Earthquake Spectra*, Special Supplement.

Youd, T. L., J.P. Bardet, and J. D. Bray, Eds. (2000), Kocaeli, Turkey, Earthquake of August 17, 1999 Reconnaissance Report, *Earthquake Spectra*, Supplement A to Volume 16.

Zifa Wang
Director and Research Professor
Institute of Engineering Mechanics
9 Xuefu Road, Harbin, China, 150080
zifa@iem.net.cn
Research interests: earthquake engineering, earthquake insurance, and information technology

Prof. Luis Esteva has been a long-time friend of China, especially with Institute of Engineering Mechanics (IEM), China Earthquake Administration. He visited IEM and China in early 1980s when China was still in its early stage of opening to the outer world. When I visited Mexico in June, 2004 for his support of China's bid to host 14WCEE, he instantly supported personally our proposal. During 13WCEE in Vancouver, Canada, as the President of IAEE, he was instrumental in organizing the Conference and witnessing China's successful bid (see picture bid.gif). During the closing ceremony, he was also congratulatory to China for its bid, and his genuine friendly altitude toward China has made him largely popular among Chinese researchers on earthquake engineering (see two attached pictures).

In July, 2005, he visited IEM and China again. His lecture on perform-based earthquake engineering has helped young researchers in IEM to understand the frontline research results outside China. His meeting with deputy director general of China Earthquake Administration has been very helpful for us in soliciting supports for organizing 14WCEE in China.

As the secretary general of Chinese Association of Earthquake Engineering and the director of Institute of Engineering Mechanics, I look forward to his continuous advice and support in the future. May health and wealth be with him forever!

Zifa Wang

Zifa Wang
August 18, 2005

EARTHQUAKE DISASTER REDUCTION IN CHINA

ABSTRACT

This paper starts with the broad definition of three major areas of work under China Earthquake Administration for earthquake disaster reduction. The detailed contents and measures for every task, combining with the introduction to China Digital Earthquake Observation Network, is then defined and explained. A mathematical formula, based on economical impact of every factor in earthquake disaster reduction, is proposed to consider the overall effect of every measure for earthquake disaster reduction. Finally, comments toward future direction of earthquake disaster reduction in China are discussed.

Introduction

The first destructive earthquakes since the founding of People's Republic of China occurred on March 8, 1966 in Xingtai, Hebei Province, with a magnitude of 6.8 and 7.2. The quakes killed more than 8,000 people and injured another 38,000. More than 5 million houses collapsed in the two events. Since then, the government started to realize the impacts of earthquakes, and subsequently, China Earthquake Administration (CEA, then called State Seismological Bureau) was established in 1971 to deal with the taunting task of earthquake disaster reduction. Since its formation, CEA has undergone a series of evolution in its short history. The name has changed from State Seismological Bureau to China Seismological Bureau in 1998, and finally to China Earthquake Administration in 2003. The staff team within CEA has grown from a few dozens of members to over 12,000 full-time members, including over 8,000 technical personnel. Every province in China has its provincial branch for earthquake administration, and local branches are also set up under provincial guidance. In addition, there are 5 major research institutes and a number of other administration institutes within CEA. These institutes, together with provincial earthquake administration branches, work under CEA as a large composite team for earthquake disaster reduction in China.

As one of the very few ministry level government agencies worldwide only for earthquake disaster reduction, CEA's focus on earthquake disaster reduction in China has gradually evolved from earthquake observation, monitoring and prediction only to inclusion of preparedness, prevention measures and the recent expansion to emergency response and management. These three areas of work form the foundation for the daily administrational work and the project planning within CEA.

Earthquake observation, monitoring and prediction

Earthquake observation, monitoring and prediction have been one of the top priorities for CEA. With over 30 years of continuous construction, China now has accumulated a network of over 2,000 seismic observation stations. Another network of earthquake precursory observation is also built. With these networks in place, China has the monitoring capacity as defined in the following.

M≥ 4.0 nation wide
M≥ 2.5 50% land areas
M≥ 1.5 provincial capitals and their adjacent areas in the eastern part of China
M≥ 1.0 capital area

On the other hand, earthquake prediction has been one of the unique administration areas in China. There are basically four different types of predictions as defined in the following.

- ✓ Long-term Prediction: a few years to tens of years or longer
- ✓ Mid-term Prediction: a few months to a number of years
- ✓ Short-term Prediction: a few days to a few months
- ✓ Imminent Prediction: within days

Although much progress has been made in earthquake prediction in China, the overall accuracy of earthquake prediction is still in its infancy stage. The historical successful example of predicting the Haicheng Earthquake in 1975 was a combination of empirical experiences and earthquake observation, which is not readily duplicable in other cases. It is said that the success rate of short-term prediction is close to 37% while it is higher for long-term and mid-term predictions. It becomes more difficult to predict imminent occurrence of earthquakes. The current status is that a few types of earthquakes could be predicted under certain conditions, but the prediction relies more on empirical experience than scientific analysis. Earthquake prediction is still a global challenge for earthquake scientists.

Earthquake preparedness and prevention measures

Seismic design for structures

Seismic design codes for structures were completed in China as early as 1964. Since then, a number of improvements have been made, resulting in modified design codes in 1974, 1978, 1989 and 2001. The current seismic design code of buildings is prepared for the purpose of carrying out the policy of giving priority to the prevention of earthquake disasters so that when buildings are made earthquake resistant, damage to buildings, loss of life and economic losses will be minimized. The principles for the design code can be summarized as the following.

When buildings designed based on the code are subjected to the influence of frequently occurring earthquakes with an intensity of less than the fortification intensity of the region, the buildings will not be, or will be only slightly damaged and will continue to be serviceable without repair; When they are subjected to the influence of earthquakes equal to the fortification intensity of the region, they may be damaged but will still be serviceable after ordinary repair or without repair; When they are subjected to the influence of unexpected rare earthquakes with intensity higher than the fortification intensity of the region, they will neither collapse nor incur damage that would endanger human lives.

Raising public awareness of earthquake disaster mitigation

Raising public awareness has been proven to be effective in past earthquakes. For example, during Niigata Chuetsu Earthquake of October 23, 2004, a number of people escaped the disaster because of prior knowledge on how to respond during an earthquake. This verifies the fact that public awareness program is effective in reducing especially casualties during an earthquake. In China, a number of earthquake exhibition halls and special libraries are set up to educate the public. Outreach programs are sometimes incorporated into extension education for both the general public and students in classrooms

Improvement of legislation system

In order to increase the effect of earthquake disaster reduction in China, the People's Congress of People's Republic of China promulgated in 1997 the national Law of the People's Republic of China on Protection against and Mitigating Earthquake Disasters. This national law supports and guarantees the works on earthquake prevention and disaster reduction. Based on this law, a number of local regulations and industry stipulations are also issued to materialize the national law into engineering practice. Some of the examples include "The Protection Act for Facilities of Earthquake Monitoring and Environmental Condition of Earthquake Observation (1994)", "Emergency Response Act for Destructive Earthquakes (1995)", and "Stipulations for Issuing Earthquake Prediction(1998)".

Another set of result issued as national regulation is the national acceleration zonation map for China (2000), as shown in figure 1.

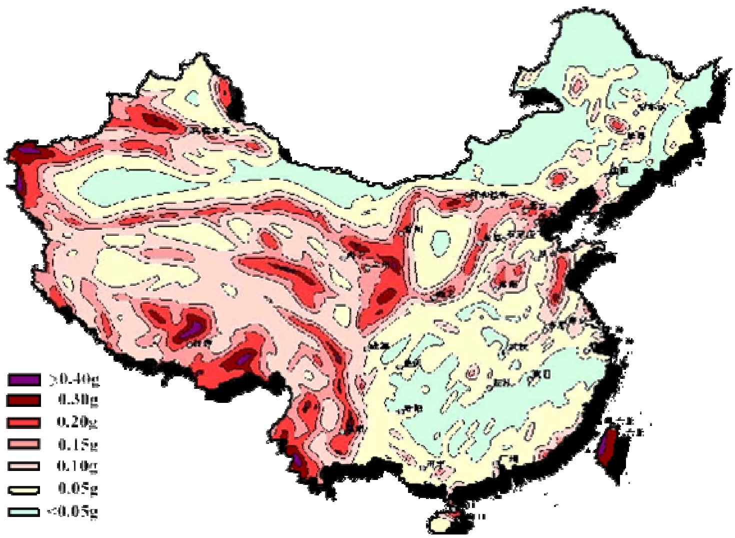

Figure 1. Acceleration zonation map for China (2000) [CEA, 2004]

There are two rules as regard to how to apply the result from this map.

- Ordinary industrial and civil structures can be built in accordance with the above zoning map
- Key construction projects and lifeline works have to be constructed in line with the results from dedicated engineering assessment**.**

Retrofitting the existing structures

There are two reasons why there is a need to retrofit existing structures. One is to fix the weakening of strength due to aging or external damage to the existing structures. Two is to enhance existing structures to be compatible with new design standards. Up to now, retrofitting is performed either to mostly on historical monuments and important structures or to damaged structures during an earthquake. Retrofitting has also been proven to be effective in Taiyuan, Shanxi province. Before Yanggao Earthquake the city of Taiyuan had been retrofitted with the aid from a UN fund. There was obviously light damage in the city for the retrofitted structures, while comparable structures under similar ground motion excitation suffered heavier damage. At this time, gradual and increasing efforts are put forward by both central and local governments as well as private enterprises to retrofit vulnerable structures.

Engineering assessment for key projects

The national law described in 3.3 provides the basis for the need to assess earthquake safety for large and key projects, especially the national key projects such as the Three Gorges Dam and most of the nuclear power plants. The aim of the project is to determine the ground motion level at or surround a given project construction site via sophisticated engineering approaches. The result from this assessment shall be used to design the project accordingly, if it is different from the zonation map. In a good percentage of the cases where there is a need for sophisticated engineering assessment it is found that the ground motion level appears to be different from the zonation map, which stresses the importance of such a complicated study.

Urban Active Faults Detection Projects

Starting from 2003 a new national key project, called China Digital Earthquake Observation Network, is under way for a 5-year construction. Included in this project are three networks (seismic observation, precursory, and strong ground motion), three systems (active fault detection, information, and emergency response and commanding), and a training base for rescue teams. Active fault detection system tries to identify active faults in almost all the major cities in China, including the provincial capitals in the country. When the result from this project is compiled, it will definitely help the preparedness and prevention of earthquake disaster if it happens.

Earthquake loss estimation

Earthquake loss estimation tries to assess the economical impact of an earthquake disaster should it happens. The purpose of this field of work is to identify the most vulnerable spots within a city during an earthquake, and corresponding retrofitting measures are proposed at the same time. For example, in Daqing city of Heilongjiang province, earthquake loss estimation is performed for the whole city as well as the surrounding oil fields, and numerous vulnerable spots are identified for further repair and enhancement. The result can be readily incorporated into city planning.

Earthquake Emergency Response

Earthquake Emergency Pre-plan

In order to better prepare for emergency during an earthquake, the State Council has set up an earthquake disaster relief headquarter within CEA. This headquarter will enact during a destructive earthquake. On April 27, 2001 China International Search and Rescue Team (CISAR) was established with much fanfare. This team is governed by the relief coordinating office within CEA, which is under the administration of State Council of China. There are over 200 members in CISAR with the background of engineering, earthquake science and medicine. CISAR is equipped with advanced tools and communication systems.

Emergency relief and rescue

Ever since its founding, CISAR has played a major role in relief, search and rescue. It was deployed domestically to Bachu-Jiashi Earthquake and Zhaosu Earthquake in Xinjiang Province. Internationally it was deployed to Algiers, Iran in 2003 and it was again deployed to Indonesia after the great Sumatran Earthquake of 2004. The team has won a high fame as a hard working and reliable search and rescue team at the field, thus earn an excellent reputation both domestically and internationally.

The mathematical representation of earthquake disaster reduction in China

Around the world there are few countries like China that have coordinated central governmental efforts in earthquake disaster reduction. There are many reasons to this. One could be that China has suffered heavily during past earthquakes. In 20^{th} century, around half of the casualties of earthquakes occurred in China. Over half of the inland earthquakes also occurred within China. The second reason is that Chinese government places a high priority to the importance of human life. Therefore, in 2004, a national goal for earthquake disaster reduction in 2020 was issued, which states "By 2020 China should be resistant nationally to an M6 class earthquake, or to the current fortification level in design standards. Developed regions and large cities should have comparable earthquake resistance level comparable moderately developed countries". There are at least two problems to this. 1) How to assess the resistance and scientifically define such a goal? 2) How to get there? The second question can be partially answered if the first question is clearly answered. Therefore, we will focus on the first one.

In order to assess earthquake resistance, we need a physical parameter that is a complicated function of many factors. With the existence of such a parameter, the effect of every factor can be studied independently, thus resulting in the identification of most important affecting factors in determining earthquake resistance. Economic loss is proposed to be such a parameter because an earthquake usually only causes damage and loss while creating little benefit. The extent of the damage can be best expressed by the amount of economic loss of the event. Therefore, the 2020 national goal can be expressed via the following formula.

Minimize: Total_Loss = Property_Loss + Derivative_Loss + Human_Loss + Commercial_Loss + Other_Losses,

Where

Casualty <= Target_1
Business_Interruption <= Target_2
Property_Loss <= Target_3
Derivative_Loss <= Target_4

From the above, it is clear that if we convert casualty loss into economic loss this becomes a typical problem in operational research. By studying the amount variation of total loss due to the change in every domain of work in earthquake disaster reduction, we can assess the effect of different measures. With such a formula in place, we can at least derive the results for the following questions.

1) What is the most important affecting factor?
2) What is the most effective measure?
3) Where is the problem?

and many more.

Conclusion

China, with its ministry level government agency China Earthquake Administration, has put into a good amount of efforts into earthquake disaster reduction. Earthquake observation, monitoring and prediction, earthquake preparedness and prevention, and emergency response and rescue are three areas of work in reducing earthquake disaster in China. A number of measures have been taken in China to prepare and prevent earthquake should it happens. Furthermore, a national goal for 2020 has been established requiring extra efforts to realize it. A mathematical formula is proposed to further study the problem.

At this time, China is planning its 11th 5-year plan for earthquake disaster reduction. A long-term plan for year 2020 is also simultaneously happening. In the next five years, China will focus on at least the following areas in order to reduce the impacts of potential destructive earthquakes.

- ✓ Earthquake safety for large cities and major metropolitan areas
- ✓ Earthquake safety for rural areas
- ✓ Emergency response for key infrastructure systems
- ✓ Experimental fields in seismically active regions

For further reduction of earthquake disaster in China, both international and domestic help are needed and a closer international collaboration is expected in the coming years.

References

China Earthquake Administration (2003), *annual report (2003)*

Wang, Z. (2005), Research Report for 11th 5-yearPlan for Earthquake Disaster Reduction, *Recent Developments in World Seismology*, 2005(7), 17-22